

2 June 2006 | \$10

Science



Hayabusa at
Asteroid Itokawa

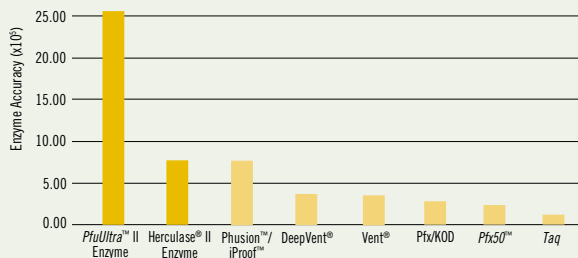


Our new breed is the center of attention.

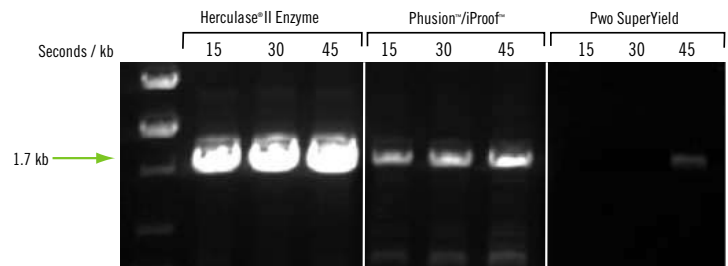
PfuUltra[™] II enzyme for highest fidelity · *Herculase*[®] II enzyme for superior yield

Our next generation of high fidelity *Pfu*-based fusion enzymes sets a new standard in high fidelity PCR performance. Engineered for industry-leading fidelity *plus* 12x enhanced processivity, our new *PfuUltra*[™] II Fusion HS DNA Polymerase and *Herculase*[®] II Fusion DNA Polymerase deliver superior yield, excellent reliability, and faster overall run times.

Our *PfuUltra*[™] II Fusion HS DNA Polymerase offers the highest fidelity.
Error rates were determined by the *lacI* fidelity assay.



Our *Herculase*[®] II Fusion DNA Polymerase produces superior yield in as short as 15 second/kb extension time.



Need More Information? Give Us A Call:

Stratagene USA and Canada

Order: 800-424-5444 x3

Technical Service: 800-894-1304 x2

Stratagene Japan K.K.

Order: 3-5821-8077

Technical Service: 3-5821-8076

Stratagene Europe

Order: 00800-7000-7000

Technical Service: 00800-7400-7400

www.stratagene.com

Ask us about these great products:

PfuUltra[™] II Fusion HS DNA Polymerase 40 rxn 600670

Herculase[®] II Fusion DNA Polymerase 40 rxn 600675

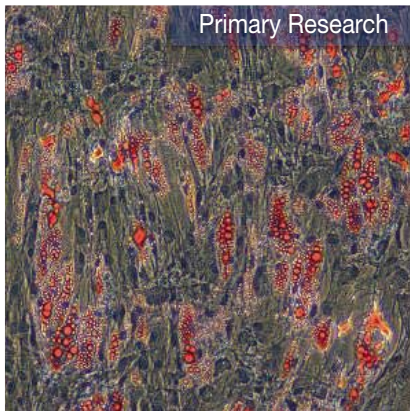
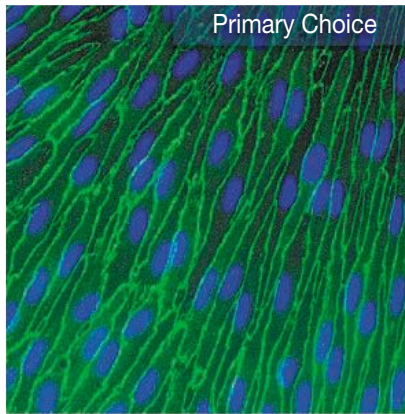
PfuUltra[™] is a trademark of Stratagene in the United States. *Herculase*[®] is a registered trademark of Stratagene in the United States.

Deep Vent[®] and Vent[®] are registered trademarks of New England Biolabs. iProof[™] is a trademark of BioRad Laboratories. Phusion[™] is a trademark of Finnzymes Oy. *Pfx50*[™] is a trademark of Invitrogen.

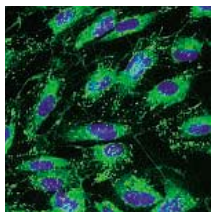
U.S. Patent Nos. 6,734,293, 6,489,150, 6,444,428, 6,379,553, 6,333,165, 6,183,997, 5,948,663, 5,866,395, 5,545,552 and patents pending

Purchase of this product is accompanied by a license under the foreign counterparts of U.S. Patents Nos. 4,683,202, 4,683,195 and 4,965,188 for use in the polymerase chain reaction (PCR) process, where such process is covered by patents, in conjunction with a thermal cycler whose use in the automated performance of the PCR process is covered by the up-front license fee, either by payment to Applied Biosystems or as purchased, i.e., an authorized thermal cycler.





Primary Cells for Pioneering Research



Clonetics® Lung Lymphatic and Blood Endothelial Cells



Lung Lymphatic (LEC) and Lung Blood (BEC) Microvascular Endothelial Cell Systems have a higher purity for better experimental results in your angiogenesis, pulmonary,

vascular and lymphatic research.

- Cells are derived from normal human lung tissue and deliver >90% purity.
- No more mixed endothelial cultures with unknown LEC:BEC ratios.
- Optimal performance guaranteed with existing EGM-2MV media kit.
- Cleaner, more consistent results with less cell variability.



Poietics™ Normal Peripheral Blood Leukopaks



Normal Peripheral Blood Leukopak is a bag of fresh human blood cells collected from normal peripheral blood by automated apheresis. Each leukopak contains a mixture of

monocytes, lymphocytes, platelets, plasma, and red cells.

- Leukopaks are monocyte enriched.
- Standard leukopak contains total white cell count of >60 million per ml and volume is >100 ml.
- All donors are screened for general health, and test negative for HIV-1, hepatitis B & C.
- Leukopaks with special donor characteristics are available, such as tetanus-boosted, CMV negative, diabetic, EBV and PMN enriched.

Cambrex, the source for Clonetics® and Poietics™ Cell Systems, BioWhittaker™ Classical Media, SeaPlaque® and NuSieve® Agarose, and PAGEr® Precast Gels.

For more information contact us at:

www.cambrex.com

U.S. 800-638-8174 | Europe 32 (0) 87 32 16 11

For Research Use Only. Not for Use in Diagnostic Procedures.

Cambrex Bio Science Walkersville, Inc.
8830 Biggs Ford Road | Walkersville, MD 21793



Innovation. Experience. Performance.



Faster protein purification? It's not rocket science.

HiTrap™ columns give you pure proteins with less effort. They come prepacked with the widest choice of media, ensuring results you can depend on in a broad range of applications, and the highest level of convenience.

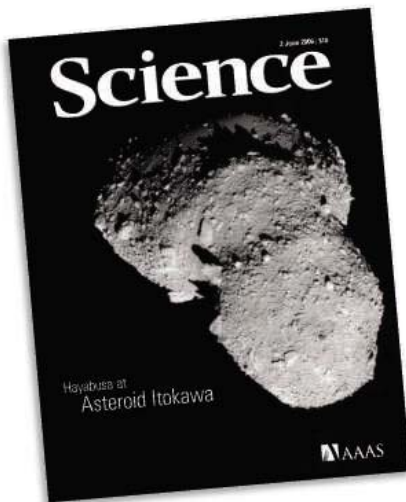
But we're never content to stand still. We constantly strive for new innovations for tomorrow's research and drug development. And thanks to our technological achievements and global presence, we're able to help you turn your scientific ideas into reality – bringing science to life and helping transform healthcare.

We call it Life Science Re-imagined.

Discover how HiTrap columns can help power your protein purification.
Visit www.gehealthcare.com/life



imagination at work



COVER

The near-Earth asteroid 25143 Itokawa as imaged from the Hayabusa spacecraft. The view is from the direction of the longest axis (535 m; the other axes are 294 and 209 m). The surface is covered with a great number of large boulders. See the special section beginning on page 1327.

Image: Japan Aerospace Exploration Agency

DEPARTMENTS

- 1271 *Science Online*
- 1273 *This Week in Science*
- 1279 *Editors' Choice*
- 1282 *Contact Science*
- 1285 *NetWatch*
- 1287 *Random Samples*
- 1307 *Newsmakers*
- 1407 *New Products*
- 1408 *Science Careers*

EDITORIAL

- 1277 *The Billion-Ton Biofuels Vision*
by Chris Somerville

SPECIAL SECTION

Hayabusa at Asteroid Itokawa

INTRODUCTION

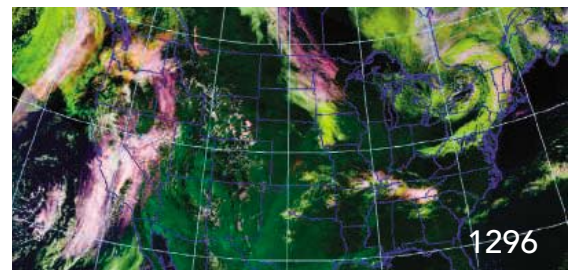
- The Falcon Has Landed 1327

PERSPECTIVE

- Adventures in Near-Earth Object Exploration 1328
E. Asphaug

REPORTS

- The Rubble-Pile Asteroid Itokawa as Observed by Hayabusa 1330
A. Fujiwara et al.
- Near-Infrared Spectral Results of Asteroid Itokawa from the Hayabusa Spacecraft 1334
M. Abe et al.
- X-ray Fluorescence Spectrometry of Asteroid Itokawa by Hayabusa 1338
T. Okada et al.
- Detailed Images of Asteroid 25143 Itokawa from Hayabusa 1341
J. Saito et al.
- Mass and Local Topography Measurements of Itokawa by Hayabusa 1344
S. Abe et al.
- Pole and Global Shape of 25143 Itokawa 1347
H. Demura et al.
- Touchdown of the Hayabusa Spacecraft at the Muses Sea on Itokawa 1350
H. Yano et al.



NEWS OF THE WEEK

- University Bids to Salvage Reputation After Flap Over Logging Paper 1288
- Bristol-Myers Ends No-Strings Grants 1289
- Over Protests, U.K. Union Endorses Boycott of Israeli Academics 1289
- India Opens Universities to More Underprivileged Students 1291
- SCIENCESCOPE 1291
- Ancient Figs Push Back Origin of Plant Cultivation 1292
>> Report p. 1372
- Court Revives Georgia Sticker Case 1292
- Tools Link Indonesian 'Hobbits' to Earlier *Homo* Ancestor 1293
- Spain Aims to Lure Systems Biologists to a Place in the Sun 1295
- Senate Bill Would Boost High-Tech Workforce 1295

NEWS FOCUS

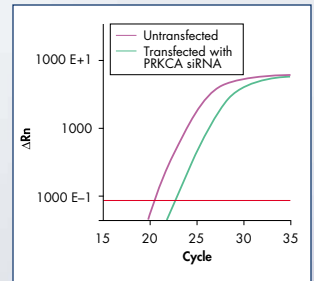
- Stormy Skies for Polar Satellite Program 1296
- South Korea Picks Up the Pieces 1298
- A Surprising Stellar Nursery 1301
- Aging Atom Smasher Runs All Out in Race for Most Coveted Particle 1302
- Genes Commute to Factories Before They Start Work 1304
- Neutrino Hunters Plan a Voyage to the Bottom of the Sea 1305

CONTENTS continued >>

Systems Biology — RNAi and Gene Expression Analysis

GeneGlobe — the world's largest database of matching siRNAs and RT-PCR assays

New



Reliable quantification after knockdown



Visit www.qiagen.com/GeneGlobe

Enter the world of reliable gene silencing and gene expression analysis!

Genomewide solutions from QIAGEN include potent, specific siRNAs and matching, ready-to-use, validated primer sets for SYBR® Green based real-time RT-PCR assays. Benefits include:

- Easy online access to RNAi and gene expression solutions at GeneGlobe
- siRNAs and RT-PCR assays for the entire human, mouse, and rat genomes
- RT-PCR assays for arabidopsis, drosophila, dog, and chicken

For matched siRNAs and real-time RT-PCR assays you can rely on, go to www.qiagen.com/GeneGlobe !

For up-to-date trademarks and disclaimers, see www.qiagen.com . RNAiGEXGeneGlobe0106S1WW © 2006 QIAGEN, all rights reserved.



WWW.QIAGEN.COM

Qs & AAAS



www.sciencedigital.org/subscribe

For just US\$99, you can join AAAS TODAY and start receiving *Science* Digital Edition immediately!

Qs & AAAS



www.sciencedigital.org/subscribe

For just US\$99, you can join AAAS TODAY and start receiving *Science* Digital Edition immediately!



SCIENCE EXPRESS

www.sciencexpress.org

DEVELOPMENTAL BIOLOGY

Hox Control of Organ Size by Regulation of Morphogen Production and Mobility

M. A. Crickmore and R. S. Mann

The small size of the *Drosophila* hindwing results from spatial restriction of the critical morphogen by binding proteins not expressed in the larger forewing.

10.1126/science.1128650

PLANT SCIENCE

Hierarchical Action and Inhibition of Plant Dicer-Like Proteins in Antiviral Defense

A. Deleris et al.

RNA silencing blocks infection and long-distance transport of infecting viruses in *Arabidopsis*.

10.1126/science.1128214

ASTRONOMY

The Spiral Structure of the Outer Milky Way in Hydrogen

E. S. Levine, L. Blitz, C. Heiles

Imaging the distribution and density of atomic hydrogen in the Milky Way shows that our galaxy forms a multi-armed spiral that is not symmetric about its axis.

10.1126/science.1128455

CHEMISTRY

An Octahedral Coordination Complex of Iron(VI)

J. F. Berry et al.

A complex in which iron is in the rare +6 oxidation state and triple bonded to nitrogen is stable to 77 kelvin and can serve as a powerful oxidant upon warming.

10.1126/science.1128506

LETTERS

New Scientific Society in Nicaragua *J. A. Huete-Pérez* 1309

Examining Knowledge of Geometry *K. Wulff;*

R. M. Delson Response *S. Dehaene et al.*

Ecological Revitalization of Chinese Villages *E. C. Ellis*

Stereotype Threat: A Clarification *L. J. Stricker*

Response *D. Lewis*

CORRECTIONS AND CLARIFICATIONS 1312

BOOKS ET AL.

1491 New Revelations of the Americas Before Columbus; 1313

Ancient Americans Rewriting the History of the New World

C. C. Mann, reviewed by D. R. Snow

The Sensory Hand Neural Mechanisms of Somatic 1314

Sensation

V. B. Mountcastle, reviewed by C. G. Gross and A. A. Ghazanfar

POLICY FORUM

Finding Criminals Through DNA of Their Relatives 1315

F. R. Bieber, C. H. Brenner, D. Lazer

PERSPECTIVES

Linking Nutrition and Tissue Growth 1317

P. Léopold and S. Layalle >> Report p. 1385

Unfallen Grains: How Ancient Farmers Turned Weeds 1318

into Crops
J. Doebley >> Report p. 1392

Exploring Other Worlds to Learn More About Our Own 1319

I. C. F. Müller-Wodarg >> Report p. 1366

Align in the Sand 1320

D. Grünbaum >> Report p. 1402

Toward Efficient Hydrogen Production at Surfaces 1322

J. K. Nørskov and C. H. Christensen

Aerosols, Clouds, and Climate 1323

D. Rosenfeld >> Report p. 1375

TECHNICAL COMMENT ABSTRACTS

CELL BIOLOGY

Comment on "HST2 Mediates SIR2-Independent 1312

Life-Span Extension by Calorie Restriction"

M. Kaerberlein et al.

full text at www.sciencemag.org/cgi/content/full/312/5778/1312b

Response to Comment on "HST2 Mediates SIR2-Independent

Life-Span Extension by Calorie Restriction"

D. W. Lamming et al.

full text at www.sciencemag.org/cgi/content/full/312/5778/1312c

BREVIA

MATERIALS SCIENCE

Direct Determination of Local Lattice Polarity 1354

in Crystals

K. A. Mkhoyan, P. E. Batson, J. Cha, W. J. Schaff, J. Silcox

A scanning transmission electron microscope reveals atomic-level columns of nitrogen and their polarity in an aluminum nitride with sub-angstrom resolution.

RESEARCH ARTICLE

NONHUMAN GENETICS

Metagenomic Analysis of the Human Distal 1355

Gut Microbiome

S. R. Gill et al.

Sequencing the trillions of microbes in the human colon identifies genes involved in the digestion of plant carbohydrates, the fermentation of fiber, and vitamin synthesis.

REPORTS

PHYSICS

Conductance Quantization at a Half-Integer 1359

Plateau in a Symmetric GaAs Quantum Wire

R. Crook et al.

Electron spins in a thin gallium-arsenide wire spontaneously organize in the absence of a magnetic field, producing a new ferromagnetic phase useful in spintronics.

CONTENTS continued >>

Assistance!



SCIENCE @ WORK

At Sigma, we're pulling with you

For a change think inside the box and choose the assay kit that truly facilitates your cell biology research. You have better ways to spend your time than developing and validating cell biology assays. With more than 100 kits available, let our assay kits do the work for you.

Inside each kit is everything you need to make assaying simpler than ever before. Plus, we have technical experts on hand worldwide to further assist in getting the very best from your research.

Our assay kits are just one of the many cell biology solutions that we offer to more than a million scientists every day. From the widest selection of products to the best technical support, we're the research partner of choice around the world.

So when you need assistance in finding an easier way to assay, count on Sigma.

sigma.com/assaykits

REPORTS CONTINUED...

APPLIED PHYSICS

Atomic-Scale Coupling of Photons to Single-Molecule Junctions 1362*S. W. Wu, N. Ogawa, W. Ho*

The tip of a scanning tunneling microscope can be used to transfer excited electrons to a molecule, allowing the excited and charged states to be mapped in detail.

PLANETARY SCIENCE

Solar Rotation Effects on the Thermospheres of Mars and Earth 1366*J. M. Forbes, S. Bruinsma, F. G. Lemoine*

Simultaneous satellite measurements of the atmospheric density of Mars and Earth during variable heating by the Sun constrain how carbon dioxide cools upper atmospheric layers.

>> *Perspective p. 1319*

GEOCHEMISTRY

Neodymium Isotope Evidence for a Chondritic Composition of the Moon 1369*K. Rankenburg, A. D. Brandon, C. R. Neal*

The neodymium isotope composition of the Moon resembles that of early meteorites and not Earth's crust, supporting the early differentiation of Earth's mantle.

ANTHROPOLOGY

Early Domesticated Fig in the Jordan Valley 1372*M. E. Kislev, A. Hartmann, O. Bar-Yosef*

Many of the figs found in 11,300-year-old Neolithic sites in the Jordan Valley are unfertilized fruit of planted trees and may represent the first domesticated crop. >> *News story p. 1292*

ATMOSPHERIC SCIENCE

Size Matters More Than Chemistry for Cloud-Nucleating Ability of Aerosol Particles 1375*U. Dusek et al.*

Size matters more than chemistry in controlling which aerosol particles can nucleate water droplets in clouds, potentially simplifying the treatment of aerosols in climate models.

>> *Perspective p. 1323*

EVOLUTION

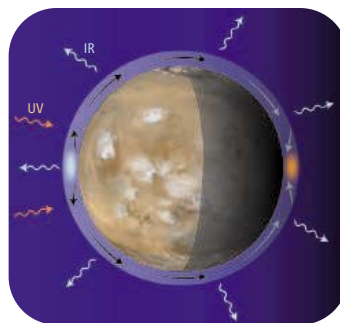
A New Genus of African Monkey, *Rungwecebus*: Morphology, Ecology, and Molecular Phylogenetics 1378*T. R. B. Davenport et al.*

Molecular phylogenetics and morphology indicate that a recently described monkey defines a new extant African primate genus.

CELL BIOLOGY

Checkpoint Proteins Control Survival of the Postmitotic Cells in *Caenorhabditis elegans* 1381*A. Olsen, M. C. Vantipalli, G. J. Lithgow*

In *C. elegans*, a cell cycle protein unexpectedly functions in postmitotic tissues, where it regulates cell survival and stress-related life span.



1319 & 1366

DEVELOPMENTAL BIOLOGY

Juvenile Hormone Is Required to Couple Imaginal Disc Formation with Nutrition in Insects 1385*J. W. Truman et al.*

A hormone permits cells in developing insect larvae to divide when nutrients are available; later its reduction triggers the cells' differentiation into adult phenotypes.

>> *Perspective p. 1317*

MEDICINE

Onset and Progression in Inherited ALS Determined by Motor Neurons and Microglia 1389*S. Boillée et al.*

A gene mutation in mouse motor neurons triggers degeneration typical of ALS (Lou Gehrig's disease) and, when present in surrounding cells, exacerbates disease progression.

PLANT SCIENCE

An SNP Caused Loss of Seed Shattering During Rice Domestication 1392*S. Konishi et al.*

A gene that controls the retention of rice grains on the plant after ripening is from a transcription factor of a different class from that of another recently identified gene for this trait.

>> *Perspective p. 1318*

STRUCTURAL BIOLOGY

Outer Membrane Active Transport: Structure of the BtuB:TonB Complex 1396*D. D. Shultzis, M. D. Purdy, C. N. Banchs, M. C. Wiener***Structure of TonB in Complex with FhuA, *E. coli* Outer Membrane Receptor** 1399*P. D. Pawelek et al.*

Vitamins and iron are transported into bacteria through a pore in the outer membrane, assisted by a protein that induces a strand to form in the plug of the pore.

BEHAVIOR

From Disorder to Order in Marching Locusts 1402*J. Buhl et al.*

As predicted by statistical models, swarms of locusts undergo rapid transitions from disordered to ordered collective motion as their density increases. >> *Perspective p. 1320*



ADVANCING SCIENCE. SERVING SOCIETY

SCIENCE (ISSN 0036-8075) is published weekly on Friday, except the last week in December, by the American Association for the Advancement of Science, 1200 New York Avenue, NW, Washington, DC 20005. Periodicals Mail postage (publication No. 484460) paid at Washington, DC, and additional mailing offices. Copyright © 2006 by the American Association for the Advancement of Science. The title SCIENCE is a registered trademark of the AAAS. Domestic individual membership and subscription (51 issues): \$139 (\$74 allocated to subscription). Domestic institutional subscription (51 issues): \$650; Foreign postage extra: Mexico, Caribbean (surface mail) \$55; other countries (air assist delivery) \$85. First class, airmail, student, and emeritus rates on request. Canadian rates with GST available upon request, GST #1254 88122. Publications Mail Agreement Number 1069624. Printed in the U.S.A.

Change of address: Allow 4 weeks, giving old and new addresses and 8-digit account number. Postmaster: Send change of address to AAAS, P.O. Box 96178, Washington, DC 20090-6178. Single-copy sales: \$10.00 current issue, \$15.00 back issue prepaid includes surface postage; bulk rates on request. Authorization to photocopy material for internal or personal use under circumstances not falling within the fair use provisions of the Copyright Act is granted by AAAS to libraries and other users registered with the Copyright Clearance Center (CCC) Transactional Reporting Service, provided that \$18.00 per article is paid directly to CCC, 222 Rosewood Drive, Danvers, MA 01923. The identification code for Science is 0036-8075. Science is indexed in the Reader's Guide to Periodical Literature and in several specialized indexes.

CONTENTS continued >>

Create!



INNOVATION @ WORK

with Sigma, the new leader in RNAi create your advantage

Faster siRNA manufacturing? 100% transduction efficiency of shRNA constructs? Long and short term silencing? Sigma has developed the most comprehensive array of cutting edge products for every step of your RNAi experimental design – creating for you a real advantage.

- Taking siRNA manufacturing to a new level by providing a rapid turnaround, high throughput and cost effective service that caters to your siRNA needs
- MISSION™ TRC shRNA libraries, comprising 150,000 pre-cloned shRNA constructs targeting 15,000 human genes and 15,000 mouse genes
- Lentiviral shRNA delivery that boasts flexibility of long and short term silencing, 100% transduction efficiency and enables experimentation with difficult to study cell types such as non-dividing or primary cells

So whether you are determining gene function, analyzing signal transduction or screening for potential drug targets, why not discover how you can create your RNAi advantage.

sigma.com/rnai

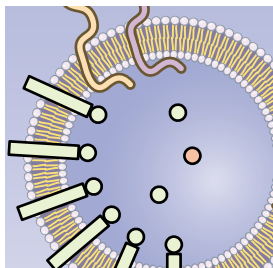
Accelerating Customers' Success through **Leadership in Life Science, High Technology and Service**
SIGMA-ALDRICH CORPORATION • BOX 14508 • ST. LOUIS • MISSOURI 63178 • USA



Member of the RNAi Consortium

MISSION is a trademark belonging to Sigma-Aldrich Co. and its affiliate Sigma-Aldrich Biotechnology LP. The RNAi Consortium shRNA library is produced and distributed under license from the Massachusetts Institute of Technology.

SIGMA®



Selective cytokine secretion.

SCIENCE'S STKE

www.stke.org SIGNAL TRANSDUCTION KNOWLEDGE ENVIRONMENT

PERSPECTIVE: Differential Secretion of Cytokines

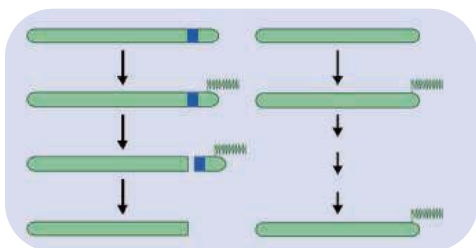
R. Moqbel and J. Coughlin

Localization of the IL-4R α alpha chain to eosinophil granules enables recruitment of IL-4 to secretory vesicles.

TEACHING RESOURCE: Cytokine Receptors and Jak-STAT Signaling

C. Schindler

Prepare a lecture for a graduate-level class describing interferons, their receptors, and Jak-STAT signaling.



Lamin defects cause multiple diseases.

SCIENCE'S SAGE KE

www.sageke.org SCIENCE OF AGING KNOWLEDGE ENVIRONMENT

NEWS FOCUS: Pushing the Envelope

M. Leslie

Research blossoms on rare genetic disorders that might be linked to aging.

CLASSIC PAPER: The Maintenance of the Accuracy of Protein Synthesis and Its Relevance to Aging

L. E. Orgel

The author discusses the "error catastrophe" hypothesis; *Proc. Natl. Acad. Sci. U.S.A.* **49**, 517 (1963).

SCIENCE NOW

www.sciencenow.org DAILY NEWS COVERAGE

Thumbs Up for Leech Therapy

Doctors use bloodsucking worms to alleviate thumb arthritis.

Bye-Bye Birdie

Populations of long-distance European flyers are declining rapidly.

Water, Water Everywhere

Nanomaterial plucks moisture from the air.



A broader perspective on forestry science.

SCIENCE CAREERS

www.sciencecareers.org CAREER RESOURCES FOR SCIENTISTS

US/CANADA: Northern Exposure

B. Benderly

At the University of Ottawa, postdocs are getting the recognition they deserve.

EUROPE: Seeing the Forest and the Trees

E. Pain

Greek forest geneticist Andreas Drouzas brings a broader perspective from his policy work.

US: Baby Talk and Monkey Talk

V. Chase

Jessica Maye studies why babies are better at acquiring language than monkeys or human adults.

GRANTSNET: June 2006 Funding News

J. Fernandez

Learn about new research funding, scholarships, fellowships, and internships.

Separate individual or institutional subscriptions to these products may be required for full-text access.








yield of dreams.

Taq DNA Polymerase from New England Biolabs

HIGH YIELD, ROBUST AND RELIABLE PCR REACTIONS IN CONVENIENT FORMATS

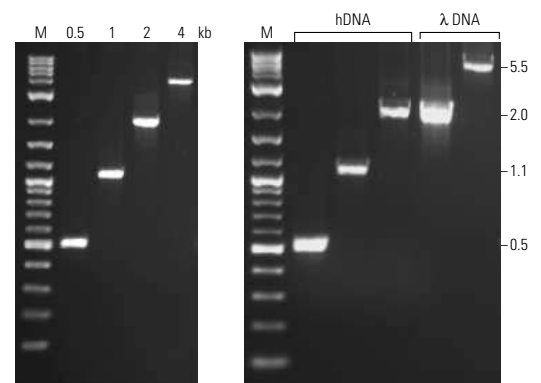
Looking for the right solution for your high yield PCR? Choose recombinant *Taq* DNA Polymerase from New England Biolabs. As the leader in enzyme technology, New England Biolabs provides the highest quality recombinant *Taq* at exceptional value. Our expanded selection of *Taq* based products includes kits, master mixes, and a choice of reaction buffers. Choose *Taq* DNA polymerase from NEB for guaranteed Performance, Convenience and Results.

- **Taq with Standard Buffer**  **M0273S/L**
Compatible with existing assay systems and high throughput applications, is always detergent free and available with or without MgCl₂
- **Taq with ThermoPol Buffer**  **M0267S/L**
Promotes high yields under demanding conditions, available with or without MgSO₄ and detergent
- **Taq 2X Master Mix**  **M0270S/L**
Just add template and primers
- **NEW Quick-Load™**
Taq 2X Master Mix  **M0271S/L**
Load PCR products directly onto agarose gels
- **Taq PCR Kits**  **E5000S/E5100S**
Contains reagents for 200 PCR reactions, available with or without controls

 = Recombinant

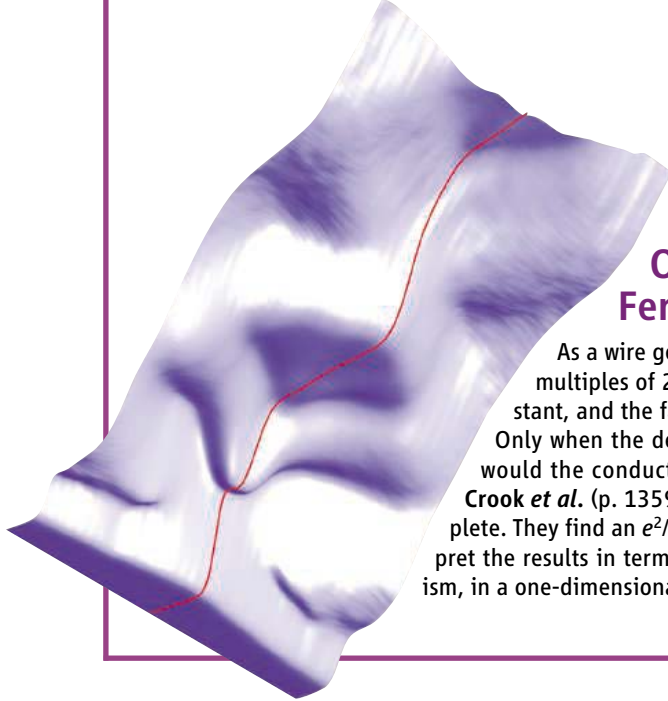
For more information and international distribution network, please visit www.neb.com

- **New England Biolabs Inc.** 240 County Road, Ipswich, MA 01938 USA 1-800-NEB-LABS Tel. (978) 927-5054 Fax (978) 921-1350 info@neb.com
- **Canada** Tel. (800) 387-1095 info@ca.neb.com
- **Germany** Tel. 0800/246 5227 info@de.neb.com
- **UK** Tel. (0800) 318486 info@uk.neb.com
- **China** Tel. 010-82378266 beijing@neb-china.com



Selective and specific PCR amplification from Human Genomic DNA:
Specific amplicons of 0.5, 1, 2, and 4 kb from human genomic DNA were amplified by *Taq* DNA Polymerase with Standard Buffer for 30 cycles. Marker (M) shown is 2-Log DNA Ladder (NEB #N3200).

Versatility of the Taq 2X Master Mix:
30 ng human genomic DNA (hDNA) or 0.1 ng lambda DNA (λ DNA) was amplified in the presence of 200 nM primers in a 25 μ l volume. Marker (M) shown is 2-Log DNA Ladder (NEB #N3200).



One-Dimensional Ferromagnetism?

As a wire gets narrower, its conductance can become quantized in multiples of $2e^2/h$, where e is the electron charge, h is Planck's constant, and the factor of 2 accounts for the two possible spin channels. Only when the degeneracy is lifted, for example, by a magnetic field, would the conductance be expected to show a value of e^2/h . However, **Crook *et al.*** (p. 1359) present evidence that this scenario may not be complete. They find an e^2/h plateau without applying a magnetic field and interpret the results in terms of a spontaneous spin polarization, or ferromagnetism, in a one-dimensional GaAs wire.

Sizing Up Aerosols

Determining which aerosol particles will act as cloud condensation nuclei (CCN) is vital for understanding the interaction of aerosols and clouds and the resulting climatic impacts. However, the formation of CCN is thought to occur through a complex series of processes that includes many chemical and physical pathways, and has always been difficult for models to parameterize. **Dusek *et al.*** (p. 1375; see the Perspective by **Rosenfeld**) show that measured CCN concentrations can be approximated quite well for a number of classes of aerosols by using mainly size-distribution measurements and only a crude parameterization of the chemical effects on CCN activation. This result, if general, has important implications for the fields of cloud and climate modeling in that it would greatly simplify the treatment of aerosol effects on cloud physics in regional and global models and allow CCN abundances to be estimated from remote-sensing data.

Beats of Heat

The Sun's atmosphere rotates with a period of about 25 days near the equator and 35 days near the poles, and the resulting twist of magnetic field lines causes the output of solar energy pulses on similar time scales. The extreme ultraviolet radiation from the Sun is the heat source for the upper atmospheres, or thermospheres, of planets, and **Forbes *et al.*** (p. 1366; see the Perspective by **Müller-Wodarg**) have spotted a 27-day periodic fluctuation in Mars' thermosphere, which they compared with simultaneous measurements at Earth. The beating of Earth's upper-atmosphere temperature changes is twice as strong as the signal for Mars; the difference

arises from a combination of distance from the Sun and the effects of cooling by CO_2 . These joint observations constrain CO_2 cooling rates in basic models of planetary atmospheres.

Firing Photoelectrons from STM Tips

The high spatial resolution afforded by the scanning tunneling microscope (STM) has been used to transfer a photoexcited electron from the STM tip to a molecule. **Wu *et al.*** (p. 1362, published online 20 April) adsorbed magnesium porphine on a thin oxide film grown on a metal and then varied the incident radiation at a nearby STM tip from near-infrared to green. The molecules accept the electron through a two-step, photon-assisted resonance tunneling pathway. This method allows the excited and charged states to be mapped out as a function of position and photon energy.

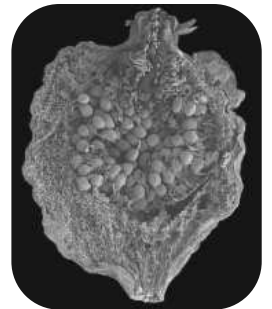
Daughter Confirmation of Early Differentiation

The short-lived isotope ^{142}Nd can be used to date events in the first 50 million years of the history of the solar system. Samples from Earth evidently have a different $^{142}\text{Nd}/^{144}\text{Nd}$ ratio from that of early meteorites, implying that there was an early differentiation event in Earth's mantle that removed a complementary reservoir from later geological processes that we can sample. **Rankenburger *et al.*** (p. 1369) show that samples from the Moon are isotopically like meteorites and not Earth. This result supports the interpretation of an early differentiation on Earth and implies that widespread melting of the Moon

may have persisted to about 220 million years after formation of the solar system.

Recognizing a Good Thing Growing

Remains of figs appear in several archaeological sites in the Jordan Valley as early as about 11,400 years ago. **Kislev *et al.*** (p. 1372; see the news story by **Gibbons**) describe these samples and show that they represent a variety of fig in which the fruit forms and ripens without pollination. This mutation arises on some fig trees, but the abundance of the remains implies that humans recognized these rare trees and propagated them by planting branches. Evidence of such activity may mark one of the earliest forms of agriculture.



Getting to Grips with Gut Flora

At least 10 trillion microorganisms inhabit our lower intestinal tract; without them, we could not process the bulk of our food, and we would be vulnerable to the damaging effects of ingested toxins. **Gill *et al.*** (p. 1355) present a detailed metagenomic analysis of human intestinal microflora. Colonic bacteria and archaea not only help to keep the gut wall intact and healthy;

Continued on page 1275



www.roche-applied-science.com

Universal ProbeLibrary

Simplify array validation and gene knockdown quantification



Use the online assay design center and Universal ProbeLibrary probes to generate over 2.6 million assays for multiple transcriptomes.

"All real-time PCR assays worked in the first run"

— Neven Zoric, TATAA Biocenter, Sweden

Increase lab productivity

Design custom assays online in 30 seconds and perform qPCR assays without optimization.

Obtain the benefits of probes at near-SYBR Green I prices

Use prevalidated Universal ProbeLibrary probes to detect specific amplicons – not primer-dimers or nonspecific products.

Benefit from complete assay sequence information

Obtain primer, probe, and amplicon sequences from the free, online ProbeFinder assay design software.

To learn more, and to design your next assay, visit

www.universalprobelibrary.com

This product is a Licensed Probe. Its use with an Authorized Core Kit and Authorized Thermal Cycler provides a license for the purchaser's own internal research and development under the 5' nuclease patents and basic PCR patents of Roche Molecular Systems, Inc. and F. Hoffmann-La Roche Ltd. No real-time apparatus or system patent rights or any other patent rights owned by Applied Biosystems, Inc. and no rights for any other application, including any *in vitro* diagnostic application under patents owned by Roche Molecular Systems, Inc. and F. Hoffmann-La Roche Ltd claiming homogeneous or real-time amplification and detection methods, are conveyed expressly, by implication or by estoppel.

PROBELIBRARY is a registered trademark of Exiqon A/S, Vedbaek, Denmark. Other brands or product names are trademarks of their respective holders. © 2006 Roche Diagnostics GmbH. All rights reserved.



Diagnostics

Roche Diagnostics GmbH
Roche Applied Science
68298 Mannheim
Germany

Continued from page 1273

they supply us with a suite of glycoside hydrolases to digest plant carbohydrates, trophic chains of organisms for fermentation of fiber to short chain fatty acids, methanogenesis for hydrogen scrubbing, the means to synthesize amino acids and vitamins, and pathways for the transformation of xenobiotic compounds from plant phenolics to tetrachloroethene.

More on the Highland Mangabey

In 2005, a description of the highland mangabey *Lophocebus kipunji* from southwest Tanzania was published. At that stage, the species was known only from photographs. More recently, a specimen became available that enabled an assessment of a range of morphological and molecular parameters. **Davenport et al.** (p. 1378, published online 11 May) provide molecular and morphological evidence that *kipunji* is actually more closely related to *Papio* than it is to *Lophocebus*. Thus, they name and describe *Rungwecebus*, Africa's first new extant genus of primate in 83 years, and provide results from ecological studies carried out on this endangered monkey.

Development, Stress, and Life Span

Cell-cycle checkpoint proteins arrest cell division in response to genomic damage and are important in development, but in nondividing cells, these proteins may play a further role in cell maintenance. **Olsen et al.** (p. 1381) show that decreased function of checkpoint proteins in postmitotic, somatic cells of the adult worm triggered increased expression of genes that allow the organism to resist stress. This adaptive response increased organism survival and extended life span by up to 25%. Thus, checkpoint proteins may control whole organism susceptibility to stress, survival, and normal aging.

The Making of an Insect

In insects, imaginal discs control the transition from larva to adult. The discs must grow and differentiate in order to form an adult of reasonable size with all of its normal legs and wings. **Truman et al.** (p. 1385; see the Perspective by **Léopold and Layalle**) now analyze the processes controlling disc growth and differentiation in the *Manduca* larva. Cellular proliferation in the discs depends on how well fed the larva was, whereas differentiation into adult structures is managed by juvenile hormone, the presence of which represses differentiation.



Getting Across the Membrane

Bacteria obtain essential nutrients such as vitamin B₁₂ and iron through a family of outer membrane proteins that sequester these compounds and transport them into the periplasmic (intermembrane) space. The members of this family all adopt a barrel-like architecture and have one domain that serves as a plug. How the nutrient is moved through the barrel is unclear, although an inner membrane protein called TonB is known to participate and to supply the energy to unplug the transporter. **Shultis et al.** (p. 1396) and **Pawelek et al.** (p. 1399) have determined the structures of the complexes formed by the vitamin transporter BtuB and the iron transporter FhuA, respectively, with the C-terminal domain of TonB. In both cases, TonB induces a portion of the plug to form a β strand, which is then co-opted into a β sheet.

March of the Locusts

Locust swarms can invade large areas of Earth's land surface and are estimated to affect the livelihood of one in ten people on the planet. The key to effective management of locust outbreaks is early detection of the marching juveniles (bands), because control of flying swarms is costly and ineffective. **Buhl et al.** (p. 1402; see the Perspective by **Grünbaum**) reveal that there is a critical density at which locusts will begin collective motion. The onset of this behavior is characterized by a sudden switch from disordered movement of individuals in the group to highly aligned collective motion. The nonlinearity of this transition means that small increases in density can result in abrupt changes in collective motion. The results match predictions from models of phase transitions from disorder to order in statistical physics. These models can permit scaling from laboratory experiments to large populations in the field and hence inform plans for controlling locust outbreaks.

CREDIT: TRUMAN ET AL.

Optical O₂ Sensors

From Tissue Analysis ...



Visit oceanoptics.com/photowinners2nd.asp for details on this application.

... to Food & Beverage Monitoring

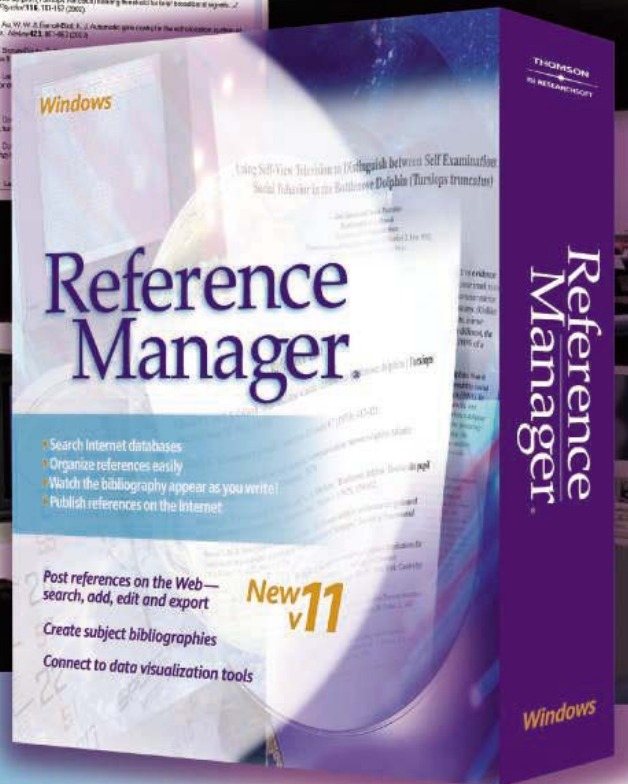


Ocean Optics optical sensors consist of transducer materials that are trapped in a sol-gel matrix and placed at the tip of a fiber. These materials change optical properties in response to specific analytes. Materials also can be coated on flat substrates. Applications include DO monitoring in biological samples, headspace gases, cosmetics, foods and liquids.



Visit OceanOptics.com
 Info@OceanOptics.com
 U.S.: 727.733.2447
 Europe: 31 (0) 26 319 0500

BIBLIOGRAPHY CENTRAL



Your High-Tech Command and Control Center for References.

Introducing Reference Manager 11—a powerful upgrade to the bibliographic software that streamlines research, writing and publishing.

Reference Manager has served corporate, government and academic researchers worldwide for over 20 years. And now version 11 delivers new ways to share and view your reference collections: Post your databases to the Web. Collaborate with colleagues over a network. Link to full text pdf files.

These are just some of the powerful features that await you. Reference Manager is your command and control center for all things reference related.

What's new in v11:

- Publish Reference Manager databases to the Web or intranet
- Create subject bibliographies instantly
- Access new and updated content files at www.refman.com
- Share traveling libraries with colleagues
- Connect to data visualization tools

Put innovation into action. Order or upgrade today.
Available for Windows in a single-user and network edition.
Phone: 800-722-1227 • 760-438-5526 • info@isiresearchsoft.com

Download a Free Demo Today
www.refman.com

THOMSON
ISI RESEARCHSOFT

© Copyright 2004 Thomson. Reference Manager is a registered trademark of Thomson. All other trademarks are the property of their respective companies.



Chris Somerville is director of the Department of Plant Biology, Carnegie Institution, and a professor at Stanford University. His research concerns plant cell and molecular biology.

The Billion-Ton Biofuels Vision

IN 1895, SWEDISH CHEMIST SVANTE ARRHENIUS PRESENTED A PAPER TO THE STOCKHOLM Physical Society titled *On the Influence of Carbonic Acid in the Air upon the Temperature of the Ground*, in which he argued that the combustion of fossil fuel would lead to global warming. He was right, so we must deal with the consequences of global climate change and somehow meet our expanding energy needs while limiting greenhouse gas emissions. Earth receives approximately 4000 times more energy from the Sun each year than humans are projected to use in 2050. Some of that energy can be captured through a variety of “renewable” sources, but the only form of solar energy harvesting that can contribute substantially to transportation fuel needs at costs competitive with fossil fuel is that captured by photosynthesis and stored in biomass.

Brazil now obtains a quarter of its ground transportation fuel from ethanol produced by the fermentation of sugarcane sugar, and in the United States, approximately 90 corn grain-to-ethanol refineries produce about 4.5 billion gallons of ethanol annually. The U.S. Energy Policy Act of 2005 would increase that production to 7.5 billion gallons by 2012, but the United States currently uses about 140 billion gallons of ground transportation fuel per year. To replace 30% of that amount with ethanol of equivalent energy content, as proposed recently by the Secretary of Energy, will require about 60 billion gallons of ethanol. A recent analysis* concluded that the United States could produce about 1.3 billion dry tons of biomass each year in addition to present agricultural and forestry production. Because it is theoretically possible to obtain about 100 gallons of ethanol from a ton of cellulosic biomass (such as corn stover, the stalks remaining after corn has been harvested), the United States could sustainably produce about 130 billion gallons of fuel ethanol from biomass. In addition to a positive effect on the release of greenhouse gases, a biofuels program on this scale would have substantial economic and strategic advantages.

The creation of a new industry on that scale will require much basic and applied work on methods for converting plant lignocellulose to fuels, because several significant problems must be overcome to make the process ready for large-scale use. For example, cellulose is a recalcitrant substrate for bioconversion, and unacceptably large amounts of enzymes are required to produce sugar. Lignin occludes polysaccharides and inhibits enzymatic hydrolysis of these carbohydrates; energetically expensive and corrosive chemical pretreatments are required for its removal. The yeast currently used in large-scale ethanol production cannot efficiently ferment sugars other than glucose. And relatively low concentrations of ethanol kill microorganisms, requiring an expensive separation of the product from large volumes of yeast growth medium.

These and other technical issues associated with this emerging industry have potential solutions, and many incremental advances can be envisioned. However, substantial public and private investment will be needed to meet the nation's goals. For instance, competitive funding for basic research in plant biology by all federal agencies totals only about 1% of the National Institutes of Health's budget. Small wonder that we do not know basic things such as the composition of the enzyme complex that synthesizes cellulose. Hopefully, a new U.S. Department of Energy (DOE) report† that outlines the scientific issues will help set the direction for increased funding in this area.

A national biofuels strategy will ultimately depend on massive support for basic curiosity-driven research in many aspects of nonmedical microbiology, plant biology, and chemical engineering. A fivefold increase in federal support during the next decade could readily be justified by the projected economic gains from the accelerated development of a cellulosic biofuel industry. To ensure parallel progress on the many different components of a biofuels strategy, it may be necessary to create a mission-oriented project similar to the Manhattan Project. Indeed, several of the national laboratories that were founded during the Manhattan era also pioneered some aspects of biofuel technology and could be a powerful source of relevant scientific and engineering expertise.

– Chris Somerville

10.1126/science.1130034

*R. D. Perlack *et al.*, *Biomass as Feedstock for a Bioenergy and Bioproducts Industry: The Technical Feasibility of a Billion-Ton Annual Supply* (DOE/GO-102005-2135, Oak Ridge National Laboratory, Oak Ridge, TN, 2005). †U.S. DOE, *Breaking the Biological Barriers to Cellulosic Ethanol: A Joint Research Agenda* (U.S. DOE Office of Science and Office of Energy Efficiency and Renewable Energy, 2006) (available at www.doe.gov/energyefficiency/biofuels/).





HUMAN FRONTIER SCIENCE PROGRAM

12 Quai Saint-Jean, 67080 Strasbourg Cedex, FRANCE
Phone: +33 (0)3 88 21 51 27/34 Fax: +33 (0)3 88 32 88 97
E-mail: fellow@hfsp.org Web site: <http://www.hfsp.org>

POSTDOCTORAL OPPORTUNITIES FOR INTERDISCIPLINARY RESEARCH IN THE LIFE SCIENCES

The Human Frontier Science Program (HFSP) supports basic research in the life sciences with emphasis on **novel, innovative, and interdisciplinary** approaches that involve scientific exchange across national and disciplinary boundaries. Recent developments in emerging fields at the interface of biological and physical sciences open up new approaches to understand the mechanisms of living organisms. This indicates a clear need for participation of scientists from outside the life sciences to reveal the structures and networks that characterize the living state. Therefore the HFSP supports postdoctoral investigators who explore new areas within the life sciences or who use their expertise in chemistry, physics, mathematics, computer science, or engineering to bear on a biological question. Initially the program provides **fellowships for training of postdoctoral researchers** in another country (~150K USD over 3 years). HFSP fellows returning to their home country may then apply for a Career Development Award (300K USD over 3 years) to start their independent research program.

Nationals from one of the HFSP supporting countries can apply to work in any other country, while other nationals can apply for training only in a supporting country. Current supporting members are: *Australia, Canada, the European Union, France, Germany, Italy, Japan, the Republic of Korea, New Zealand, Switzerland, the United Kingdom, and the United States of America.*

Important fellowship deadlines for award year 2007:
Compulsory pre-registration for password: **24 August 2006**
Submission of applications: **31 August 2006**

Long-Term Fellowships

Long-Term Fellowships are intended for applicants with a Ph.D. degree in the life sciences who are expected to **broaden their horizon and to move into a new research area that is different from their doctoral studies or previous postdoctoral training.** Applicants that propose a significant departure from their previous research are viewed favorably.

Cross-Disciplinary Fellowships

Cross-Disciplinary Fellowships are intended for applicants with a Ph.D. degree in physics, chemistry, mathematics, engineering, or computer sciences who wish to **gain research experience in the life sciences in proposing a significant change in discipline.** Those with some experience in the life sciences are expected to move into a new research area.

Fellows receive support for up to 3 years of training in an outstanding laboratory of their choice in another country. The final year can be used to return to the home country. As a rule, fellows who choose to return to their home country can defer their final year for up to two years for extended research training while being funded through other sources. HFSP fellows who return to their home country are **invited to apply for a Career Development Award** to establish themselves as independent young investigators.

The online submission system will become available in summer 2006 on the HFSP web site.

Short-Term Fellowships

Short-Term Fellowships are intended for researchers early in their careers and provide up to 3 months of support to **learn techniques in a new area of research or establish new collaborations in another country.** Applications are accepted throughout the year.

Application guidelines with more details are available on the HFSP web site (www.hfsp.org).

HIGHLIGHTS OF THE RECENT LITERATURE

ECOLOGY/EVOLUTION

Butterfly Population Dynamics

Population dynamics of animals are generally considered to be governed by environmental influences and demographic processes. The potential influence of genetic variation on population dynamics, however, has received much less attention. In a study of the Glanville fritillary butterfly in Finland, Hanski and Saccheri provide evidence that allelic variation in the glycolytic enzyme phosphoglucose isomerase (Pgi), which affects metabolic rate and flight performance, also affects population growth. The butterflies inhabit discrete habitat patches, which vary in size and degree of connectivity to other patches. The strength and nature of the Pgi effect on population growth depended on the ecological context. In larger patches, selection favored genotypes with a slower maturation rate, but the opposite was true in smaller patches, where a faster maturation rate would allow efficient exploitation of limited resources. This integration of detailed field study and molecular genetics promises to open new avenues in the study of population dynamics. — AMS

PLoS Biol. 4, e129 (2006).



The Glanville fritillary butterfly.

APPLIED PHYSICS

Streams Traced by Speckle

Particle-imaging velocimetry (PIV), a common technique for studying the flow of fluids, involves seeding a fluid with tracer particles such as dyes or photoluminescent beads, and then tracking their motion over time. In many applications, there is a growing need to understand the flow pattern in all three spatial dimensions. However, the optics involved in PIV generally limit the sampling volume to a thin two-dimensional (2D) sheet within the bulk flowing system.

Alaimo *et al.* present a simple technique to address this shortcoming. After directing a coherent probe beam through the flowing particle suspension, they detect and analyze the speckle pattern that results from the interference of the weak portion of light scattered by the seed particles with the intense transmitted portion. Because the speckle pattern arises from particles distributed throughout the whole fluid volume, 3D flow dynamics can be extracted from the 2D velocity mapping data acquired in real time. The authors demonstrate the method using an aqueous suspension of 300-nm-diameter latex spheres. — ISO
Appl. Phys. Lett. 88, 191101 (2006).

MICROBIOLOGY

The Social Life of Bacteria

We know relatively little about the population biology of bacteria in natural environments such as the soil; it is unclear, in particular,

whether strains compete or whether the diversity observed is functional. Vos and Velicer investigated genetic diversity in *Myxococcus xanthus*, a remarkable social bacterium that indulges in swarming, social predation, and, in the face of starvation, can differentiate to form multi-cellular fruiting bodies. Multilocus sequence typing was used to study the evolutionary relationships among isolates sampled from a 16-x-16-cm patch of soil. More than 20 unique genotypes were found that appeared to have evolved clonally. Most were closely related, but there were rare divergent strains that had perhaps blown in as spores. This type of population structure does

not resemble the epidemic populations of pathogens, nor does it resemble the emerging picture for marine bacteria, which seem to accumulate neutral mutations that are not regularly purged. Perhaps the spatially structured soil habitat offers clones protection from selective sweeps, or sympatric genotypes may come into contact when swarming or if the soil is disturbed. In the lab, clone pairs of *Myxococcus* are known to be highly antagonistic; it will be interesting to see how more closely related strains interact under natural conditions. — CA

Appl. Environ. Microbiol. 72, 3615 (2006).



Fruiting bodies.

ASTROPHYSICS

Silicon Seeding

Why should planets form around some stars but not others? One clue has been that planets are more common around stars rich in iron. However, the role of iron in planetary growth remains unclear. Robinson *et al.* show that planet-hosting stars are enriched not only with iron but also with silicon and nickel.

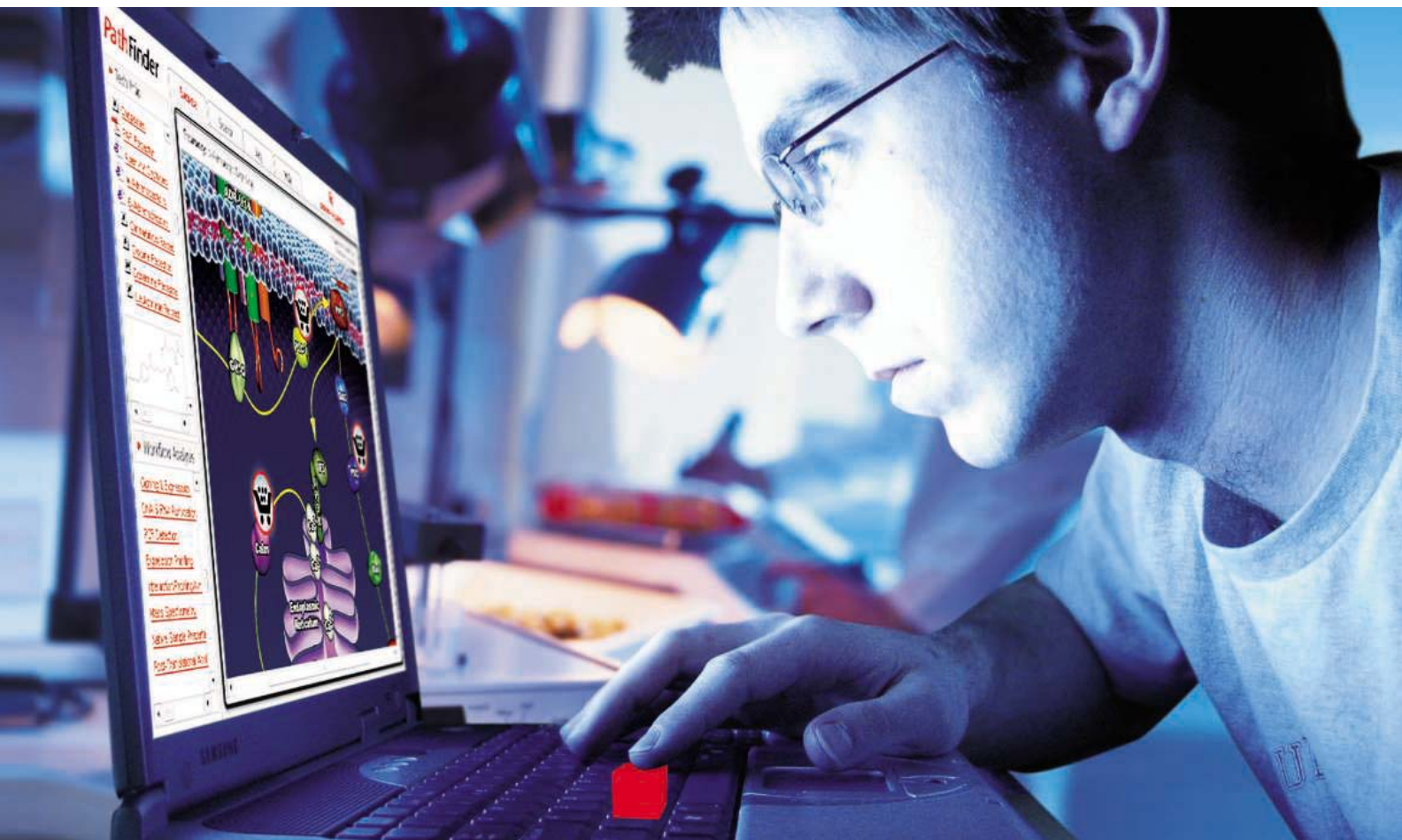
Silicon, in particular, may be a key player in the process. Initially, silicon is created from the fusion of oxygen nuclei inside the star, perhaps suggesting that planet-ringed stars should also be high in oxygen. Abundant silicon and oxygen could facilitate formation of a disk of solid debris around the star—indeed, silica and silicates are basic building blocks of most large planetary bodies in our own solar system.

The observed abundance of silicon also supports the core accretion model of the formation of large gas planets, such as Jupiter and Saturn. The hard cores of gas giants must grow rapidly, so that they can sweep in their gas atmospheres before the disk dissipates. To form a planet, the density of solid material in the disk must be high enough for the solids to clump together quickly. High silicon abundance would increase the likelihood of reaching this density threshold, perhaps helped by the presence of nickel and other heavy metals. — JB

Astrophys. J. 643, 484 (2006).

Continued on page 1281

PathFinder



INNOVATION @ WORK

Discover Your Path to Innovation

On your path to innovation, Sigma is with you every step of the way. PathFinder is an online collection of interactive, interconnected maps showing biological signaling and metabolic pathways. For you to explore the relationships between different pathway elements, individual components are linked with related high-quality products.

You know your destination. PathFinder will get you there.

With Sigma's broad range of products, you will discover that we offer everything from small molecules to antibodies and enzymes. You will also be able to use PathFinder to locate qPCR components and siRNAs for gene knockdown. A valuable resource, PathFinder provides fast and accurate information on numerous levels, all in one place – and all linked to the important products that are key to the success of your research. In addition to products and services, you'll have immediate access to these helpful tools:

- Specific workflow analysis
- Detailed product descriptions
- In-depth technical information
- Relevant technical articles

Learn how PathFinder can help you discover your path to innovation by visiting us at:

sigma-aldrich.com/pathfinder

Accelerating Customers' success through Leadership in Life Science, High Technology and Service
SIGMA-ALDRICH CORPORATION • BOX 14508 • ST. LOUIS • MISSOURI 63178 • USA

SIGMA[®]

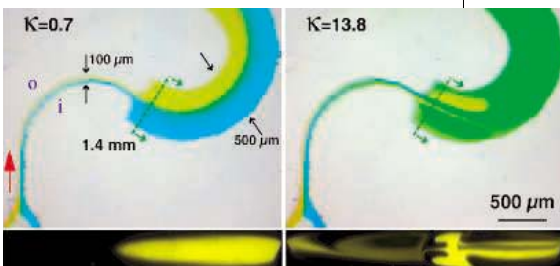
Continued from page 1279

MICROFLUIDICS

Streams Swirled by Dean

In microfluidic systems, mixing of the low-volume fluid streams is hindered by slow diffusion rates and smooth flow behavior. Although mixing can be enhanced using external energy, passive approaches that rely on the channel geometries are often preferred for sensitive materials. However, such passive strategies can require complex, expensive channel fabrication, such as elaborate three-dimensional (3D) networks and incorporation of groove or ridge features in the channels.

Sudarsan and Ugaz present an easily fabricated passive design, composed of simple 2D smooth-walled channels. The mixing enhancement arises from Dean flow: the trans-



Raising flow rate (left to right) enhances mixing in both horizontal (upper panels) and vertical dimensions.

verse flow field induced in curved channels by the interplay of centrifugal effects and inertial axial motion. A planar split-and-recombine arrangement generated alternating layers of different fluids. When two colored streams moved through the curve, counterrotating Dean vortices caused them to flow through one another and exchange position. In a second device, the authors incorporated an abrupt increase in the

channel cross-sectional area, which induced expansion vortices that enhanced mixing in the horizontal dimension. At the same time, vertical mixing occurred through Dean flows brought on by an asymmetric serpentine geometry. — MSL

Proc. Natl. Acad. Sci. U.S.A. **103**, 7228 (2006).

ECOLOGY/EVOLUTION

A Fishy Tale of Diversity

The lifestyle of the mangrove killifish *Kryptolebias marmoratus* is a solitary one, in which the fish inhabits areas around red mangrove forests. Populations are generally made up of self-fertilizing hermaphrodites that are homozygous; however, high genetic diversity is observed among lineages. This diversity has been attributed to a high rate of mutation, migration, and genetic drift among populations. Mackiewicz *et al.* have surveyed 35 microsatellite loci in individual wild-caught fish from Florida. Based on the genotypes of these animals, the authors propose that genotypic diversity results, instead, from outcrossing. This represents a mixed-mating strategy—

something that has been observed previously in hermaphroditic plants and invertebrates, but such extensive interspecimen genetic variation in vertebrates with negligible heterozygosity has not been observed. The outcrossing events provide inbred lines with a burst of genetic heterozygosity for subsequent generation of new recombinant inbred lines after self-fertilization resumes. The mixed-mating strategy is likely to provide an adaptive advantage for the harsh environment in which the killifish reside. — BAP

Proc. R. Soc. London Ser. B
10.1098/rspb.2006.3594 (2006).



www.stke.org

<< Women See Friends, Men See Foes

Gender differences in social behavior are well known. Thompson *et al.* now show that arginine vasopressin (AVP), which is known to influence the behavior of other mammals, influences social behaviors in humans in a gender-specific manner. AVP or saline was administered intranasally, and various responses to faces of the same sex with happy, neutral, or angry expressions were recorded. Differences in the activity of a muscle in the brow, the contraction of which is associated with anger or threat, were increased in men exposed to AVP and then shown neutral faces, whereas women exposed to AVP showed a decrease in the activity of this muscle in response to happy or angry faces. Although AVP-treated individuals of both sexes exhibited increased anxiety, men reported a decrease in the perceived friendliness or approachability of people with happy expressions, whereas women reported an increase in the approachability or friendliness of people with neutral expressions. The results may provide a molecular mechanism for the evolution of gender-specific responses to stress. — NG

Proc. Natl. Acad. Sci. U.S.A. **103**, 7889 (2006).

Institutional Site
License Available

Q

What can *Science*
STKE give me?



A

The definitive
resource on cellular
regulation

STKE – Signal Transduction
Knowledge Environment offers:

- A weekly electronic journal
- Information management tools
- A lab manual to help you organize your research
- An interactive database of signaling pathways

STKE gives you essential tools to power your understanding of cell signaling. It is also a vibrant virtual community, where researchers from around the world come together to exchange information and ideas. For more information go to www.stke.org

To sign up today, visit promo.aaas.org/stkeas

Sitewide access is available for institutions. To find out more e-mail stkelicense@aaas.org



1200 New York Avenue, NW
Washington, DC 20005

Editorial: 202-326-6550, FAX 202-289-7562
News: 202-326-6500, FAX 202-371-9227

Bateman House, 82-88 Hills Road
Cambridge, UK CB2 1LQ

+44 (0) 1223 326500, FAX +44 (0) 1223 326501

SUBSCRIPTION SERVICES For change of address, missing issues, new orders and renewals, and payment questions: 866-434-AAAS (2227) or 202-326-6417, FAX 202-642-1065. Mailing addresses: AAAS, P.O. Box 96178, Washington, DC 20090-6178 or AAAS Member Services, 1200 New York Avenue, NW, Washington, DC 20005

INSTITUTIONAL SITE LICENSES please call 202-326-6755 for any questions or information

REPRINTS: Author Inquiries 800-635-7181
Commercial Inquiries 803-359-4578
Corrections 202-326-6501

PERMISSIONS 202-326-7074, FAX 202-682-0816
MEMBER BENEFITS Bookstore: AAAS/BarnesandNoble.com bookstore www.aaas.org/bn; Car purchase discount: Subaru VIP Program 202-326-6417; Credit Card: MBNA 800-847-7378; Car Rentals: Hertz 800-654-2200 CDP#343457, Dollar 800-800-4000 #AA11115; AAAS Travels: Betchart Expeditions 800-252-4910; Life Insurance: Seabury & Smith 800-424-9883; Other Benefits: AAAS Member Services 202-326-6417 or www.aaasmember.org.

science_editors@aaas.org (for general editorial queries)
science_letters@aaas.org (for queries about letters)
science_reviews@aaas.org (for returning manuscript reviews)
science_bookrevs@aaas.org (for book review queries)

Published by the American Association for the Advancement of Science (AAAS), *Science* serves its readers as a forum for the presentation and discussion of important issues related to the advancement of science, including the presentation of minority or conflicting points of view, rather than by publishing only material on which a consensus has been reached. Accordingly, all articles published in *Science*—including editorials, news and comment, and book reviews—are signed and reflect the individual views of the authors and not official points of view adopted by the AAAS or the institutions with which the authors are affiliated.

AAAS was founded in 1848 and incorporated in 1874. Its mission is to advance science and innovation throughout the world for the benefit of all people. The goals of the association are to: foster communication among scientists, engineers and the public; enhance international cooperation in science and its applications; promote the responsible conduct and use of science and technology; foster education in science and technology for everyone; enhance the science and technology workforce and infrastructure; increase public understanding and appreciation of science and technology; and strengthen support for the science and technology enterprise.

INFORMATION FOR CONTRIBUTORS

See pages 102 and 103 of the 6 January 2006 issue or access www.sciencemag.org/feature/contribinfo/home.shtml

SENIOR EDITORIAL BOARD

John I. Brauman, *Chair, Stanford Univ.*
Richard Lesick, *Harvard Univ.*
Robert May, *Univ. of Oxford*
Marcia McNutt, *Monterey Bay Aquarium Research Inst.*
Linda Partridge, *Univ. College London*
Vera C. Rubin, *Carnegie Institution of Washington*
Christopher R. Somerville, *Carnegie Institution*
George M. Whitesides, *Harvard University*

BOARD OF REVIEWING EDITORS

Joanna Aizenberg, *Bell Labs/Lucent*
R. McNeill Alexander, *Leeds Univ.*
David Altshuler, *Broad Institute*
Arturo Alvarez-Buylla, *Univ. of California, San Francisco*
Richard Amadio, *Univ. of Wisconsin, Madison*
Meinrat O. Andreae, *Max Planck Inst., Mainz*
Kristi S. Anseth, *Univ. of Colorado*
Cornelia I. Bargmann, *Rockefeller Univ.*
Brenda Bass, *Univ. of Utah*
Ray H. Baughman, *Univ. of Texas, Dallas*
Stephen J. Benkovic, *Pennsylvania St. Univ.*
Michael J. Bevan, *Univ. of Washington*
Ton Bisseling, *Wageningen Univ.*
Pina Bissell, *Lawrence Berkeley National Lab*
Peter Bork, *EMBL*
Dennis Bray, *Univ. of Cambridge*
Stephen Buratowski, *Harvard Medical School*
Jillian M. Buriak, *Univ. of Alberta*
Joseph A. Burns, *Cornell Univ.*
William P. Butz, *Population Reference Bureau*
Doreen Cantrell, *Univ. of Dundee*
Peter Carmeliet, *Univ. of Leuven, VIB*
Gerhard Ceder, *MIT*
Mildred Cho, *Stanford Univ.*
David Clapham, *Children's Hospital, Boston*
David Clary, *Oxford University*
J. M. Claverie, *CNRS, Marseille*

Jonathan D. Cohen, *Princeton Univ.*
F. Fleming Crim, *Univ. of Wisconsin*
William Cumberland, *UCLA*
George O. Daley, *Children's Hospital, Boston*
Caroline Dean, *John Innes Centre*
Judy DeLoache, *Univ. of Virginia*
Edward DeLong, *MIT*
Robert Desimone, *MIT*
Dennis Discher, *Univ. of Pennsylvania*
Julian Downward, *Cancer Research UK*
Denis Duboule, *Univ. of Geneva*
Christopher Dye, *WHO*
Richard Ellis, *Cal Tech*
Gerhard Ertl, *Fritz-Haber-Institut, Berlin*
Douglas H. Erwin, *Smithsonian Institution*
Paul Everitt, *Univ. of Cambridge*
Barry G. Falkowski, *Rutgers Univ.*
Ernst Fehr, *Univ. of Zurich*
Tom Fenchel, *Univ. of Copenhagen*
Alain Fischer, *INSEEM*
Jeffrey S. Flier, *Harvard Medical School*
Chris D. Frith, *Univ. College London*
R. Gadagkar, *Indian Inst. of Science*
John Gearhart, *Johns Hopkins Univ.*
Jennifer M. Graves, *Australian National Univ.*
Christian Haass, *Ludwig Maximilians Univ.*
Dennis L. Hartmann, *Univ. of Washington*
Chris Hawkesworth, *Univ. of Bristol*
Martin Heimann, *Max Planck Inst., Jena*
James A. Hendler, *Univ. of Maryland*
Ary A. Hoffmann, *La Trobe Univ.*
Evelyn L. Hu, *Univ. of California, SB*
Olli Ikkala, *Helsinki Univ. of Technology*
Meyer B. Jackson, *Univ. of Wisconsin Med. School*
Stephen Jackson, *Univ. of Cambridge*
Daniel Kahne, *Harvard Univ.*
Bernhard Keimer, *Max Planck Inst., Stuttgart*
Elizabeth A. Kellog, *Univ. of Missouri, St. Louis*
Alan B. Krueger, *Princeton Univ.*
Lee Kump, *Penn State*
Virginia Lee, *Univ. of Pennsylvania*

Anthony J. Leggett, *Univ. of Illinois, Urbana-Champaign*
Michael Lenoir, *NIAID, NIH*
Norman L. Letwin, *Beth Israel Deaconess Medical Center*
Olle Lindvall, *Univ. Hospital, Lund*
Richard Losick, *Harvard Univ.*
Ke Lu, *Chinese Acad. of Sciences*
Andrew P. MacKenzie, *Univ. of St. Andrews*
Raul Madariaga, *Ecole Normale Supérieure, Paris*
Rick Matzeis, *Univ. of Edinburgh*
Michael Malim, *King's College, London*
Eve Marder, *Branis Univ.*
George M. Martin, *Univ. of Washington*
William McGinnis, *Univ. of California, San Diego*
Virginia Miller, *Washington Univ.*
H. Yasushi Miyashita, *Univ. of Tokyo*
Edvard Moser, *Norwegian Univ. of Science and Technology*
Andrew Murray, *Harvard Univ.*
Naoto Nagasa, *Univ. of Tokyo*
James Northrup, *Stanford Univ. School of Med.*
Roeland Noels, *Univ. of Maastricht*
Helle Nowotny, *European Research Advisory Board*
Eric N. Olson, *Univ. of Texas, SW*
Erin O'Shea, *Univ. of California, SF*
Elinor Ostrom, *Indiana Univ.*
Jonathan T. Overpeck, *Univ. of Arizona*
John Pendry, *Imperial College*
Philippe Poulin, *CNRS*
Mary Power, *Univ. of California, Berkeley*
David J. Read, *Univ. of Sheffield*
Les Real, *Emory Univ.*
Colin Renfrew, *Univ. of Cambridge*
Trevor Robbins, *Univ. of Cambridge*
Nancy Ross, *Virginia Tech*
Edward M. Rubin, *Lawrence Berkeley National Lab*
Gary Ruvkun, *Mass. General Hospital*
J. Roy Sambles, *Univ. of Exeter*
David S. Schimel, *National Center for Atmospheric Research*
Georg Schulz, *Albert-Ludwigs-Universität*
Paul Schulze-Lefert, *Max Planck Inst., Cologne*
Terrence J. Sejnowski, *The Salk Institute*
David Sibley, *Washington Univ.*

George Somero, *Stanford Univ.*
Christopher R. Somerville, *Carnegie Institution*
John Steitz, *Yale Univ.*
Edward I. Stiefel, *Princeton Univ.*
Thomas Stocker, *Univ. of Bern*
Jerome Strauss, *Univ. of Pennsylvania Med. Center*
Tomoyuki Takahashi, *Univ. of Tokyo*
Mara Taira, *Brown Univ.*
Glenn Telling, *Univ. of Kentucky*
Marc Tessier-Lavigne, *Genentech*
Craig B. Thompson, *Univ. of Pennsylvania*
Michiel van der Klis, *Astronomical Inst. of Amsterdam*
Bert van der Kooy, *Univ. of Toronto*
Derek Vogelstein, *Johns Hopkins*
Christopher A. Walsh, *Harvard Medical School*
Christopher T. Walsh, *Harvard Medical School*
Graham Warren, *Yale Univ. School of Med.*
Colin Watts, *Univ. of Dundee*
Julia R. Weertman, *Northwestern Univ.*
Daniel M. Wegner, *Harvard University*
Ellen D. Williams, *Univ. of Maryland*
R. Sanders Williams, *Duke University*
Ian A. Wilson, *The Scripps Res. Inst.*
Jerry Workman, *Stowers Inst. for Medical Research*
John R. Yates III, *The Scripps Res. Inst.*
Martin Zatz, *NIMH, NIH*
Walter Ziegler-Schäfer, *Max Planck Inst., Munich*
Huda Zoghbi, *Baylor College of Medicine*
Marta Zuber, *MIT*

BOOK REVIEW BOARD

John Aldrich, *Duke Univ.*
David Bloom, *Harvard Univ.*
Linda Schiebigler, *Stanford Univ.*
Richard Sweder, *Univ. of Chicago*
Ed Wasserman, *DuPont*
Lewis Wolpert, *Univ. College, London*

FULFILLMENT & MEMBERSHIP SERVICES (membership@aaas.org) DIRECTOR Marlene Zendeck; MANAGER Waylon Butler; SYSTEMS SPECIALIST Andrew Vargo; CUSTOMER SERVICE SUPERVISOR Pat Butler; SPECIALISTS Laurie Baker, Tamara Alfson, Karena Smith, Vicki Linton; CIRCULATION ASSOCIATE Christopher Refice; DATA ENTRY SUPERVISOR Cynthia Johnson

BUSINESS OPERATIONS AND ADMINISTRATION DIRECTOR Deborah Rivera-Wienhold; BUSINESS MANAGER Randy Yi; SENIOR BUSINESS ANALYST Lisa Donovan; BUSINESS ANALYST Jessica Tierney; FINANCIAL ANALYST Michael LoBue, Farida Yeasmin; RIGHTS AND PERMISSIONS: ADMINISTRATOR Emilie David; ASSOCIATE Elizabeth Sandler; MARKETING: DIRECTOR John Meyers; MARKETING MANAGERS Darryl Walter, Allison Pritchard; MARKETING ASSOCIATES Julianne Weigel, Mary Ellen Crowley, Catherine Featherston, Alison Chandler, Lauren Lamoureux; INTERNATIONAL MARKETING MANAGER Wendy Sturley; MARKETING/MEMBER SERVICES EXECUTIVE: Linda Rusk; JAPAN SALES Jason Hannaford; SITE LICENSE SALES: DIRECTOR Tom Ryan; SALES AND CUSTOMER SERVICE Mehan Dossani, Kiki Forsythe, Catherine Holland, Wendy Wise; ELECTRONIC MEDIA: MANAGER Lizbeth Harman; PRODUCTION ASSOCIATES Sheila Mackall, Amanda K. Skelton, Lisa Stanford, Nichole Johnston; APPLICATIONS DEVELOPER Carl Saffell

ADVERTISING DIRECTOR WORLDWIDE AD SALES Bill Moran

PRODUCT (science_advertising@aaas.org); MIDWEST Rick Bongiovanni: 330-405-7080, FAX 330-405-7081 • WEST COAST/UK/TEOLA Teola Young: 650-964-2266 EAST COAST/ CANADA Christopher Breslin: 443-512-0330, FAX 443-512-1607 • UK/EUROPE/ASIA Tracey Peers (Associate Director): +44 (0) 1782 752531, FAX +44 (0) 1782 752531 JAPAN Mashy Yoshikawa: +81 (0) 33235 5961, FAX +81 (0) 33235 5852 TRAFFIC MANAGER Carol Maddox; SALES COORDINATOR Deandra Simms

CLASSIFIED (advertise@sciencereaders.org); U.S.: SALES DIRECTOR Gabrielle Boguslawski: 718-491-1637, FAX 202-289-6742; INSIDE SALES MANAGER Daryl Anderson: 202-326-6543; WEST COAST/MIDWEST Kristine von Zedlitz: 415-956-2531; EAST COAST Jill Downing: 631-580-2445; CANADA, MEETINGS AND ANNOUNCEMENTS Kathleen Clark: 510-271-8349; LINE AD SALES Emmet Tesfaye: 202-326-6740; SALES COORDINATORS Erika Bryant, Rohan Edmondson Christopher Normile, Joyce Scott, Shirley Young; INTERNATIONAL SALES MANAGER Tracy Holmes: +44 (0) 1223 326525, FAX +44 (0) 1223 326532; SALES CHRISTINA Harrison, Svetlana Barnes; SALES ASSISTANT Helen Moroney; JAPAN: Jason Hannaford: +81 (0) 52 789 1860, FAX +81 (0) 52 789 1861; PRODUCTION: MANAGER Jennifer Rankin; ASSISTANT MANAGER Deborah Tompkins; ASSOCIATES Christine Hall; Amy Hardcastle; PUBLICATIONS ASSISTANTS Robert Buck; Mary Lagnouai

AAAS BOARD OF DIRECTORS RETIRING PRESIDENT, CHAIR Gilbert S. Omenn; PRESIDENT John P. Holdren; PRESIDENT-ELECT David Baltimore; TREASURER David E. Shaw; CHIEF EXECUTIVE OFFICER Alan I. Leshner; BOARD ROSINA M. Bierbaum; JOHN E. DOWLING; LYNN W. ENQUIST; SUSAN M. FITZPATRICK; ALICE GAST; THOMAS POLLARD; PETER J. STANG; KATHRYN D. SULLIVAN



ADVANCING SCIENCE. SERVING SOCIETY

val' i · da' tion



It's a synonym for TaqMan® Gene Expression Assays.

Your single easiest solution

TaqMan® Gene Expression Assays deliver accurate real-time PCR results to validate your microarray discoveries. TaqMan® Assays are designed to run under universal thermal cycling conditions and are formulated into a single 20X solution—less pipetting means less chance of error.

**NOW
AVAILABLE**
Arabidopsis and
Drosophila
Assays!

>600,000 assays, and all very affordable

Virtually every gene and every transcript for human, mouse, rat, Arabidopsis and Drosophila is covered—with no time, reagents or effort spent on design and optimization, you save money on every experiment.

The gold standard in quantitative gene expression analysis

TaqMan Assays provide unmatched sensitivity, specificity and reliability for true gene expression validation—you can publish your data with confidence.

To learn more about TaqMan Gene Expression Assays and how they can help you validate your research, visit www.allgenes.com.

AB Applied Biosystems



For Research Use Only. Not for use in diagnostic procedures. The PCR process and 5' nuclease process are covered by patent owned by Roche Molecular Systems, Inc. and F. Hoffmann-La Roche Ltd, and by patents owned by or licensed to Applera Corporation. Further information on purchasing licenses may be obtained from the Director of Licensing, Applied Biosystems, 850 Lincoln Centre Drive, Foster City, California 94404, USA. Applied Biosystems is a registered trademark and AB (Design) is a trademark of Applera Corporation or its subsidiaries in the US and/or certain other countries. TaqMan is a registered trademark of Roche Molecular Systems, Inc. © 2006 Applied Biosystems. All rights reserved.

DATABASES

Bug Genealogy

Ribosomal RNA genes, which code for part of the cell's protein-producing machinery, have changed little over time, and researchers use them to tease out the relationships among bacterial species. The recently upgraded Ribosomal Database Project, hosted by Michigan State University in East Lansing, houses more than 200,000 partial and complete gene sequences for the small subunit of the 16S ribosomal RNA. You can search the sequences by size, strain, and the organism's source. If you've got a gene to analyze, tools can help you find out where your bug fits on the bacterial evolutionary tree and identify its closest kin. >>

rdp.cme.msu.edu

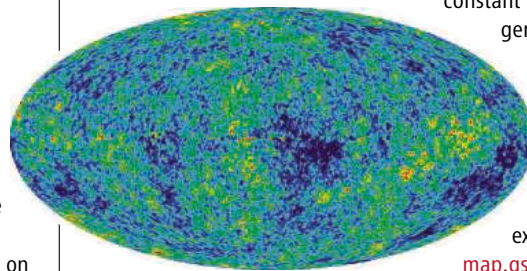
EDUCATION

From the Beginning

What do the latest measurements of remnant radiation from the big bang indicate about the universe's fate? Why do some astronomers want to resurrect an idea Einstein dubbed his biggest mistake? Find answers to these and many other questions about the universe at this NASA cosmology primer. Aimed at students and the public, the tutorial is part of the Web site for the Wilkinson Microwave Anisotropy Probe, which is mapping the energy left over from the big bang more than 13 billion years ago (below). Eighteen chapters tackle big bang basics and recent extensions of the theory. For example, to keep the universe stable,

Einstein penciled a factor called the cosmological constant into his formulation of general relativity—and later regretted it. However, some cosmologists now advocate reviving the constant to explain observations that suggest the universe's expansion is speeding up. >>

map.gsfc.nasa.gov/m_uni.html

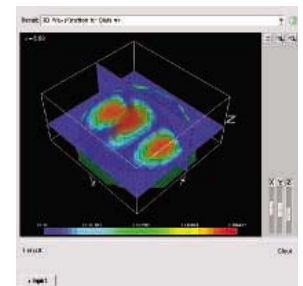


EDUCATION

School of the Small >>

A slew of nanotechnology products has already hit the market, and future advances might someday give us quantum computers or allow doctors to rehabilitate cancer cells rather than kill them. Students and researchers can plug into the fast-expanding field at nanoHUB from the Network for Computational Nanotechnology, a consortium of scientists at seven U.S. universities. The site's centerpiece is a collection of simulators for exploring the physics behind nanotech. One model lets users design quantum dots, blobs of electrons that might eventually replace conventional semiconductors (above). The site also offers audio lectures at undergraduate and advanced levels. Visitors must complete the free registration. >>

www.nanohub.org



Send site suggestions to >> netwatch@aaas.org

Archive: www.sciencemag.org/netwatch



RESOURCES

TAKE THE PLUNGE

Anyone intrigued by ocean life can hook plenty of information at MarineBio.org. Founded by geoscientist David Campbell of Houston, Texas, the site holds a multimedia encyclopedia that describes more than 200 species, with accounts on another 800 in the works. Visitors can cue up audio snippets of blue whale songs or read about the dining habits of the bearded fireworm (*Hermodice carunculata*; above), a bristly relative of earthworms that slurps up reef-building coral animals. Galleries let you tag along on expeditions to havens such as Bonaire in the Caribbean and the coast of Honduras. At the Plankton Forums, browse the latest marine science headlines or discuss newly discovered deep-sea critters with scientists and other ocean fans. The site also features backgrounders on conservation issues such as sustainable fishing and invasive species. >>

marinebio.org

RESOURCES

Call for Writers

If you know a thing or two about animal behavior, remote sensing, pollution, or related topics, you might want to contribute a chapter to the nascent Encyclopedia of Earth. Bucking the trend toward user-written—but sometimes inaccurate—content, the environmental reference will feature some 1000 peer-reviewed articles penned by experts. Sponsored by the nonprofit National Council for Science and the Environment, the project seeks writers and editors. >>

www.earthportal.net/about/steward

Hot Performance

Finnzymes' New **Phusion™ Hot Start** The Number One DNA Polymerase



Accuracy

The highest fidelity of any available thermostable polymerase

Speed

Increased processivity allows reaction times to be reduced dramatically

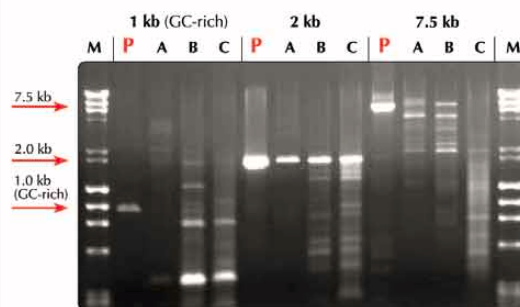
Specificity

Reduces non-specific amplification and primer degradation

Robustness

Reduces reaction failures and minimizes optimization

Phusion - Extreme Performance



The following fragments were amplified from human genomic DNA: 1 kb from CEBPB gene (GC-rich), 2 kb and 7.5 kb from human β -globin gene. Hot start high-fidelity DNA polymerases (P, A, B, C) were used according to suppliers' recommendations:

- P) Phusion™ Hot Start High-Fidelity DNA Polymerase
- A) novel *Pfu*-based fusion DNA polymerase
- B) modified *Pfu* DNA polymerase
- C) *T. kodakaraensis* DNA polymerase

Distributed in the US and Canada by New England Biolabs. For other countries visit www.finnzymes.com. PCR license notice: These products are sold under licensing arrangements of Finnzymes Oy with F. Hoffman-La Roche Ltd. The purchase of these products is accompanied by a limited license to use them in the Polymerase Chain Reaction (PCR) process in conjunction with a thermal cycler whose use in the automated performance of the PCR process is covered by the up-front fee, either by payment to Applied Biosystems or as purchased, i.e. an authorized thermal cycler.





SENATE PRESSURED ON STEM CELLS

On the first anniversary of the vote on HR. 810, passed 24 May 2005 by the U.S. House of Representatives to loosen

presidentially imposed restrictions on federally funded stem cell research, biomedical lobby groups and their congressional supporters held a press conference to pressure the Senate to pass an identical measure. Senators may have other issues—such as immigration—on their minds, but public support continues to rise, noted Sean Tipton, president of the Coalition for the Advancement of Medical Research in Washington, D.C. According to the group's latest poll, 70% of respondents want the Senate to get moving on the bill, S. 471.

Discussions are reportedly continuing with Senate Majority Leader Bill Frist (R-TN), who announced last July that he favors the bill and has repeatedly promised to schedule a vote. A staffer for Senator Tom Harkin (D-IA) (pictured above), cosponsor of S. 471, says the current plan is to buffer it with two other measures—one calling for research on “alternatives” to destruction of fertilized eggs, the other banning “embryo farming”—that could make it more palatable to conservatives.

MALES ON SPEED

Men have higher rates of addiction than do women to most substances. Now researchers may have discovered one reason why: Male brains release up to three times as much dopamine—the “pleasure molecule”—as women do in response to amphetamine use.

Neuroendocrinologist Gary Wand and colleagues at Johns Hopkins University in Baltimore, Maryland, gave 28 men and 15 women doses of amphetamine comparable to what a user might take. Although they found no sex difference in dopamine-receptor density, males showed larger dopamine releases in three of four regions of the striatum, ranging from 50% to 200% greater than the average female release, the team reports in the 15 May issue of *Biological Psychiatry*. Men also ranked the positive effects of the drug higher than women.

A difference in dopamine release may help explain the sex disparity not only in addictions but in dopamine-related diseases such as Parkinson's, Tourette syndrome, and schizophrenia, which hit males harder than women, says Wand. The findings mirror sex discrepancies in dopamine release observed in mice, says neuroendocrinologist Dean Dluzen of Northeastern Ohio Universities College of Medicine in Rootstown. His studies of Parkinson's disease in mice have revealed greater neurodegeneration in males, and he believes the new study “makes for a strong case” that this is true in humans as well.

\$15K Butterfly

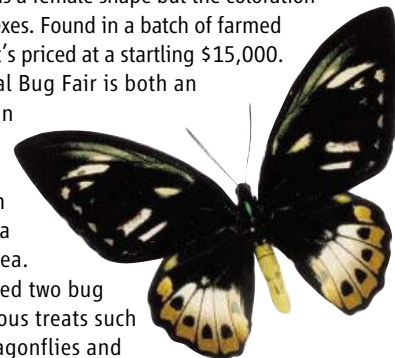
Bugs are booming, judging by a sprawling bazaar held last weekend at the Natural History Museum of Los Angeles County and attended by 10,000 people—more than half of them children—and millions of insects and arachnids.

One of the stars was this gynandromorph *Ornithoptera priamus poseidon* that has a female shape but the coloration and patterning of both sexes. Found in a batch of farmed New Guinea butterflies, it's priced at a startling \$15,000.

The museum's annual Bug Fair is both an educational event and an outlet for commercial insect farms, dozens of which have sprung up in tropical areas from Costa Rica to Papua New Guinea.

Other attractions included two bug chefs, who offered dubious treats such as tempura-battered dragonflies and pesto-drizzled tarantulas.

“If more scientists would go to a bug fair,” says neurobiologist Ronald Hoy of Cornell University, “it would change the way they read the [biology] literature. You can't help but be inspired by seeing nature up close and personal.”



EGYPT DEMANDS MASK BACK

Egypt's chief of antiquities plans to sue the Saint Louis Art Museum in Missouri for the return of an allegedly looted funeral mask.

Zahi Hawass, secretary general of Egypt's Supreme Council of Antiquities, charged last month that the 3200-year-old mask was stolen from a storage facility in the 1950s after it was uncovered in Saqqara, the ancient burial ground of kings south of Cairo. He demanded its immediate return.

Director Brent Benjamin says the museum has proper documentation from the Swiss dealer who sold it to the museum in 1998 and that the museum checked with both Interpol and the Art Loss Register to be sure the mask was legit. In a 12 May statement, Benjamin said that “although Dr. Hawass has challenged the integrity of the Saint Louis Art Museum, he has not provided conclusive evidence to support his claim.” Hawass responded that Egypt will sue for the mask's return in a St. Louis court and provide proof of ownership to Interpol. Museum officials said last week that there's no such proof in the material they've received from Hawass so far.



Hawass in recent years has been aggressive in trying to win back Egyptian treasures from abroad. He suggested earlier this year that New York City return its famous obelisk, Cleopatra's Needle, even though it was a 19th century gift from the Egyptian government.



Fruits of earliest cultivation?

1292



Lineage of hobbit tools

1293

ACADEMIC CONDUCT

University Bids to Salvage Reputation After Flap Over Logging Paper

Five tumultuous months after controversy erupted over industry influence and academic freedom, a leading U.S. academic forestry program is struggling to restore harmony and reestablish its credibility. A faculty report issued last week describes deep divisions within the College of Forestry at Oregon State University (OSU), Corvallis, in the aftermath of a paper by graduate student Dan Donato and colleagues on the ecological effects of salvage logging: the practice of removing timber after a major fire. The college's dean, Hal Salwasser, has agreed to adopt some reforms, but fallout over the paper continues and Salwasser himself may face a no-confidence vote later this month.



Salvage logging is seen by the forest industry as a good way to encourage regrowth and reduce fire risk. But a paper, published online by this journal on 5 January, found that the heavy equipment used to remove dead trees in one southern Oregon forest had killed seedlings and left woody debris that increased fire hazard. The paper attracted national attention when other OSU researchers claimed the work was deeply flawed and asked *Science* to delay its print publication. That request was widely perceived as an attempt at censorship (*Science*, 10 February, p. 761).

Observers say the conflagration has exposed a deep divide between departments with different perspectives on forest management. Last week's report by a faculty committee on academic freedom criticized Salwasser for "significant failures of leadership" that it says worsened those divisions. The committee suggests several ways to improve governance and collegiality, including a faculty code of ethics. But observers see those as first steps on

a long road to recovery. "It's a really tough situation," says forest ecologist Jerry Franklin of the University of Washington, Seattle.

Historically, colleges of forestry have been dominated by departments that favor active management to increase harvests and spur regeneration after fires, including salvage logging. That includes OSU's, which derives 12% of its budget from taxes on the logging industry in a state with highly productive forests. During the 1980s and 1990s, however, OSU and other colleges also increased their emphasis on biodiversity conservation.

But that tension isn't confined to academic circles. Responding to the *Science* paper, the U.S. House of Representatives' Committee on Resources held a field hearing in Medford,



Under fire. Dean Hal Salwasser (inset) of Oregon State University has been criticized for his leadership during the controversy over research by graduate student Dan Donato, who was called to testify before a congressional hearing.

Oregon, on 24 February on a bill to facilitate salvage logging. Two of the bill's sponsors grilled Donato on his research, subjecting him to what the OSU committee's report labels "intense, sometimes hostile, questioning." Meanwhile, memos critical of the Donato article—"some quite personal in their attacks," according to the report—were anonymously posted around the College of Forestry building.

The dispute intensified in April, after a state senator subpoenaed e-mails from Salwasser's

office. Those e-mails depicted the dean collaborating closely with industry to minimize the political fallout of the Donato paper. "It showed all of them working together to squash this *Science* article," says Denise Lach, an OSU sociologist on the academic freedom committee.

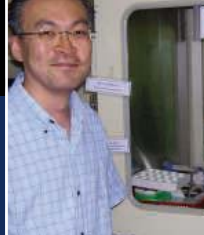
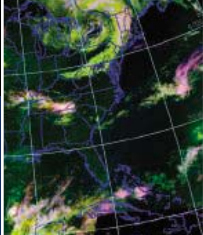
Salwasser says his goal was to protect students from the attacks. In other e-mails, however, Salwasser expressed contempt for environmental activists, calling them "goons" and comparing their protests to Mafia extortion. Salwasser says he now regrets those e-mails, which he calls "stupid, unthinking, unkind."

The committee agrees. It concludes that Salwasser's actions have "fostered the divisions within the college" and that the college's leadership council is too narrowly focused on industry interests. To improve the situation, the committee recommends a more diversified governing body, more transparent decision-making, a faculty code of conduct, and a possible reorganization of the college.

Although these suggestions have been greeted favorably, few expect them to resolve the underlying tension within the college. Beverly Law, Donato's adviser, says she worries that a code of conduct doesn't address the problem of bullying by some faculty members. Forest modeler John Sessions, one of the faculty members who lobbied *Science* to delay publication, says he wants access to both the field site and the data that were collected to understand the context of the study and its conclusions. But Law says that's out of the question. "It's my student's thesis, and [Sessions] is infringing on his ability to produce papers," she says, adding that plot locations are often not disclosed until a study is completed. "There has been a history of sabotaged research plots in this region." Replies Sessions, "The only thing that will satisfy me is full disclosure."

That lack of collegiality lies at the heart of the problem, according to the faculty committee. "In many ways, what we're trying to deal with is an interpersonal problem," says Lach. She and others hope that more conversations can help. But as Law notes wistfully, "I still think we have a long ways to go." A no-confidence vote is scheduled for 5 June, although the academic freedom committee has yet to decide who gets to vote.

—ERIK STOKSTAD



BIOMEDICAL RESEARCH

Bristol-Myers Ends No-Strings Grants

Scientists are mourning the cancellation of a long-running research grants program funded by a major drug company. The Bristol-Myers Squibb (BMS) Freedom to Discover program, begun in 1977, only supports about 50 biomedical scientists at a time. But the grants, about \$6 million a year recently, come with no strings attached. That feature, which allows for high-risk research, is particularly welcome at a time when U.S. funding for biomedical research is tightening. Some scientists are troubled that the company is pulling the plug in part because of the growing global debate over the ethics of corporate payments to academic physicians. “I think they’ve gone overboard and are tanking a wonderful program,” says grantee Carl June, a cancer researcher at the University of Pennsylvania.

BMS says that Freedom to Discover is the largest corporate-funded, unrestricted research grants program in the world. Scientists can’t just bid for the grants, however. Instead, BMS scientists identify potential recipients doing work of interest to the company in six biomedical fields and invite them to compete. The winners, chosen largely based on their track records, receive \$100,000 a year for 5 years. The grantees also meet annually to choose a distinguished scientist to

receive a \$50,000 lifetime achievement award considered to be among the most prestigious in their fields.

The resulting flexibility to follow one’s hunches is extremely rare, says Johns Hopkins University neuroscientist Michela Gallagher. She says her search for neurobiological markers that explain why some rats remain mentally sharp into old age might be seen as a “fishing expedition” by a U.S. National Institutes of Health study section. Others have used the company’s money to support postdocs until they get their first grant or to collect chimp fecal samples in Africa for an HIV study. BMS makes no claim to any of the findings. “There’s lots of payola within the pharmaceutical industry, but this is one of the few programs that is really squeaky clean,” says immunologist W. Allan Walker of Harvard Medical School in Boston, who is also a recipient.

Earlier this year, the company began telling grantees, many of whom are not physicians, that



Fishing license. Michela Gallagher says a BMS grant lets her explore promising ideas.

it was changing some rules to avoid the perception of any conflict of interest. Spouses could no longer attend the awards selection meeting for free, for example, and grantees were asked to sign an agreement saying they were consultants to BMS.

BMS spokesperson Rebecca Taylor says the program was killed in order to expand efforts such as a \$150 million, multi-year program that funds pediatric AIDS clinics in Africa. But “an increase in compliance regulations affecting the global pharmaceutical industry” is a contributing factor, she adds. Some recipients say they were told that BMS lawyers felt the company could run afoul of new, restrictive regulations in Europe on corporate gifts to physicians.

—JOCELYN KAISER

ACADEMIC POLITICS

Over Protests, U.K. Union Endorses Boycott of Israeli Academics

Rejecting the advice of its own executive officer, Britain’s largest university union endorsed a motion this week calling on its members “to consider the appropriateness of a boycott” of individuals and institutions “that do not publicly dissociate themselves” from Israel’s policies toward Palestinians. Scientific leaders around the world strongly condemned the union’s action.

The resolution, which denounces Israel’s “apartheid policies, including construction of the exclusion wall,” may not carry much formal weight: The 67,000-strong National Association of Teachers in Further and Higher Education (NATFHE), which approved it at its annual meeting on 29 May, was scheduled to go out of business on 1 June after merging into a new organization, the University and College Lecturers’ Union. The boycott resolution will only be “advis-

ory” to the new organization, according to a spokesperson. But critics are concerned that it may encourage a “gray boycott.” Warns Jonathan Rynhold of Bar-Ilan University in Ramat Gan, Israel, which was targeted by an earlier boycott attempt, academics could be judged not on merit but “according to their nationality and political opinions.”

Even before it passed, the proposal drew heavy criticism from within the union and outside. NATFHE General Secretary Paul Mackney, although a supporter of the Palestinian cause, urged members not to endorse the boycott because it had not been vetted within the union, a NATFHE spokesperson says. Several thousand U.S. and Israeli academics made public their objections in May, as did several Nobel Prize winners, including physicist Steven Weinberg of the University of Texas, Austin. The board of AAAS (publisher of

Science) last week called the NATFHE proposal “antithetical to the role of free scientific inquiry” and asked that it be withdrawn.

After the vote, astronomer Martin Rees, president of the U.K.’s Royal Society, issued a statement deploring the action, saying that “NATFHE members ... should remember that boycotts of scientists at Israeli universities grossly violate the principles set out by the International Human Rights Network of Academies and Scholarly Societies.” Those guidelines rule out attempts to block the free expression of ideas and opinions. Scientific leaders drafted the policy 4 years ago in response to an earlier boycott petition—a move that failed. Last year, the U.K. Association of University Teachers, a smaller union, endorsed a boycott but rescinded it when faced with legal objections.

—ELIOT MARSHALL

All truths are easy to understand once they are discovered; the point is to discover them.

Galileo Galilei

Italian physicist, astronomer, philosopher (1564-1642)

Shimadzu transcends modern assumptions and limits to shine a beam of light on yet undiscovered scientific truths. Shimadzu believes in the value of science to transform society for the better. For more than a century, we have led the way in the development of cutting-edge technology to help measure, analyze, diagnose and solve problems. The solutions we develop find applications in areas ranging from life sciences and medicine to flat-panel displays. We have learned much in the past hundred years. Expect a lot more.

www.shimadzu.com



Quota quarrels. A plan to boost university enrollment of underprivileged students has sparked weeks of protests.



HIGHER EDUCATION

India Opens Universities to More Underprivileged Students

NEW DELHI—Defying countrywide protests, India's government last week approved a radical expansion of affirmative action programs for helping millions of disadvantaged citizens attend university. The changes will spur a "massive expansion" of India's higher education system, promises Prime Minister Manmohan Singh.

Experts concur that India's higher education system, with 9.2 million students, includes far too few of the socially disadvantaged. "Many Indian geniuses are still hidden in the dust, and if we can't find them, as a country we won't go really far in our development," says astronomer Yash Pal, former chair of the University Grants Commission in New Delhi.

But that's where the consensus ends. "We can either move forward and create centers of academic excellence, or go along with the demands of identity politics based on caste and community, but we cannot do both," says Andre Béteille, a sociologist at the University of Delhi, who earlier this week resigned in protest from a panel advising Singh on how to transform India into a knowledge economy. Even Singh's chief science adviser, C.N.R. Rao, claims he was not consulted before the government announced the reforms. It's a "stupendous task," Rao says, that is "being presented in a highly oversimplified fashion."

Despite its emergence as a regional power, India is still divided along caste lines, with several groups by tradition performing menial jobs and manual labor. To erode this social stratification, India has long set promotion quotas for "scheduled" castes and tribes, including the untouchables, which guarantee them 22.5% of places in higher education and jobs in the public sector. The new amendment to the Indian constitution, approved unanimously by Parliament, will reserve another 27% of placements for the Dalits, or "other backward castes."

The prospect of nearly half of all current

university places being set aside for disadvantaged castes has sparked furious protests among young people of privileged castes, who argue that merit will be overlooked to make amends for historical social injustices. Over the past 3 weeks, medical and engineering students have staged strikes across the country, crippling the public health system and sparking several brutal clashes with police. As *Science* went to press, student leaders were weighing whether to continue the protests.

To take the sting out of the quota increase, the government has promised to dramatically expand enrollment at public higher education institutions. Among those included under the new policy, to take effect next year, are the seven Indian Institutes of Technology (IIT), which together enrolled 5444 students in 2006; the Indian Institute of Science (IISc) and its 2000 students; and 18 federally funded universities with an annual enrollment of about 180,000 students. The University of Delhi alone would need to increase from 40,000 students in 2006 to 60,000 next year. To further boost capacity, two new Indian Institutes of Science Education and Research, at a cost of \$250 million, are expected to open in Pune and Kolkata by year's end.

The government plans to support the expansion by injecting \$2 billion this year into the higher education system—almost double the annual expenditure. Some worry whether the money will be well spent. Rao, a former IISc director, says the technology institutes are a case in point. A rapid doubling of enrollment will be "very difficult," he says. "Where will you get the trained faculty to teach these additional students?" Even today, a quarter of IIT faculty slots are vacant. Staffing decisions, Rao says, require "very careful selection, which can't be done overnight." Their still time to devise a workable strategy, he says—if cooler heads prevail.

—PALLAVA BAGLA

House Boosts Energy Science

The White House's plan for a 10-year doubling of the research budgets at three important agencies passed its first hurdle last week after the U.S. House of Representatives met the president's request to boost funding next year for the Office of Science at the Department of Energy by 14%, to \$4.1 billion. That office, which supports most U.S. fundamental physics, is part of the American Competitiveness Initiative, which includes the National Science Foundation and the in-house labs of the National Institute of Standards and Technology, whose 2007 budgets have yet to be drafted. Research lobbyists now turn to the Senate, where expectations are high.

—ELI KINTISCH

A French Twist in Pasadena

A French-born civil engineer is the new president of the California Institute of Technology. Jean-Lou Chameau, 53, has helped transform the Georgia Institute of Technology into a powerhouse of engineering research as provost and vice president of academic affairs.



This fall, he will succeed Nobelist David Baltimore, who is stepping down after 9 years.

At Georgia Tech, Chameau led a sizable expansion of its research portfolio, forged closer links with industry, and helped establish a satellite presence in France, Ireland, and Singapore. "He is an excellent businessman in the scientific arena," says Georgia Tech physicist Uzi Landman. That makes Chameau "well-suited to the challenges and opportunities of the Caltech presidency," says Baltimore.

—YUDHJIT BHATTACHARJEE

Vitamins for Chinese Pharma

China's burgeoning pharmaceutical industry got a boost last week from U.K.-based AstraZeneca, which announced a 3-year, \$100 million research investment. The firm has conducted clinical research in China since 2001 (*Science*, 29 July 2005, p. 735). Most of the new money will increase efforts to apply basic discoveries to clinical practice, including, by 2009, a so-called Innovation Center at a site to be decided later. The company also plans to expand in-country collaborations, including its partnership with researchers at Shanghai Jiao Tong University on the genetics of schizophrenia.

—DENNIS NORMILE

ARCHAEOLOGY

Ancient Figs Push Back Origin of Plant Cultivation

Scientists seeking to date the origins of agriculture have been following the trail of wheat, barley, and other grains at archaeological sites in the Near East for decades. They recently concluded that cultivation of annual cereal crops started about 10,500 years ago (*Science*, 31 March, p. 1886). But a new study suggests that fruit rather than grains may yield the earliest evidence of purposeful planting.

On page 1372, a team of Israeli researchers reports the discovery of domesticated figs stored in an ancient house in the Lower Jordan Valley. They painstakingly show that the carbonized figs were a cultivated variety that differed from wild figs. Based on radiocarbon dating of the village, this cultivation occurred about 11,400 years ago, Mordechai E. Kislev, an archaeobotanist at Bar-Ilan University in Ramat-Gan, Israel, and his colleagues conclude. That pushes back the age of the first known cultivated plant by about 1000 years and also indicates that humans must have been experimenting with agriculture on a small scale hundreds of years before that. “This is the oldest evidence for deliberate planting of a food-producing plant, as opposed to just gathering food in the wild,” says archaeologist Peter Bellwood of the Australian National University in Canberra.

This evidence sat ignored for several decades. Nine dried figs and hundreds of fig drupelets—the pulpy sections of a fruit—were collected in the 1970s and 1980s during an excavation of a pristine house in the Neolithic village of Gilgal in the Lower Jordan Valley, about 12 kilometers north of Jericho. After the Israeli archaeologist who led the excavation died, the figs were forgotten until the Israel Museum, Jerusalem, invited Harvard University archaeologist Ofer Bar-Yosef and others to study the finds from the excavation. The figs were sent to Kislev, who eventually analyzed them with a graduate student, Anat Hartmann. They realized that the figs were a sterile but soft and edible variety that required human selection and planting to grow.

Kislev says humans must have been cultivating figs for hundreds of years, because it would have taken centuries for the wild fruit to have evolved the genetic and morphological changes that resulted in the variety of



Fruitful find. Mordechai Kislev studies figs for clues about the origins of agriculture. This ancient fig (*inset*), wrapped in gold for imaging, was cultivated 11,400 years ago.

figs found at Gilgal. This gradual domestication of figs is similar to the speed with which wild cereals were domesticated; cereals crops, first cultivated in southern Turkey and northern Syria 11,500 years ago, are thought to have taken about 1000 years to domesticate from wild grains in the area. Kislev is now asking archaeologists to search for figs

in even older excavations to pinpoint when the cultivation of the fruit began.

The purposeful planting of figs shows that settlers in the Jordan Valley were auditioning a variety of foods to see what they could grow, says archaeologist Bruce Smith of the National Museum of Natural History in Washington, D.C. The development of early agriculture, he notes, was a slow process that took place on a small scale in different areas, through trial and error with different plants. It would take another 2000 years before humans were such adept farmers that half of their calories came from crops. The discovery of dried cultivated figs, however, makes it clear that 11,000 years ago, more than meat, cereals, and wild nuts and berries were on the menu. “Humans cannot live on steak alone,” says Bar-Yosef. “They wanted condiments and all kinds of things that tasted good.”

—ANN GIBBONS

TEACHING EVOLUTION

Court Revives Georgia Sticker Case

The fight over antievolution stickers in U.S. public school biology textbooks took a new twist last week when a federal appeals court told a lower court to try again.

In its 25 May ruling, a three-judge panel in Atlanta, Georgia, vacated a January 2005 District Court ruling ordering the Cobb County school board to remove a sticker from 35,000 textbooks warning students that evolution is “a theory, not a fact.” The District Court called the policy unconstitutional because it mingled government with religion (*Science*, 21 January 2005, p. 334). But Judge Ed Carnes of the 11th Circuit Court of Appeals wrote that the record lacked proof that the board acted with religious intent and actually reflected “rampant confusion” over the evidence. Carnes said the court must either “flesh out” the record or, preferably, conduct “a completely new trial.”

Both sides seem pleased with the decision. It’s “a victory as it throws out the problematic ruling [made by] the trial court,” says Casey Luskin, a lawyer at The Discovery Institute, creationism’s main think tank in Seattle, Washington. Evolution defender

Sarah Pallas, a biologist at Georgia State University in Atlanta, says, “We think this is a good thing” because the appellate judges are not known to be sympathetic to evolution and “could have reversed instead of remanding.” Eugenie Scott of the National Center for Science Education in Oakland, California, says the case will be bolstered by a recent Dover, Pennsylvania, decision (*Science*, 6 January, p. 34) that shot down intelligent design and the strategy of labeling evolution “theory, not fact.”

Carnes wrote that the do-over is necessary because “key” documents were missing that would show the board’s sticker policy was driven by religious rather than educational concerns. The main one is a 2300-signature petition calling for a textbook disclaimer that a parent, Marjorie Rogers, submitted to the board prior to its March 2002 decision.

Board vice president Curtis Johnson says, “We are awaiting instructions from [District Court] Judge Cooper” before deciding whether to defend the stickers, which were removed last year.

—CONSTANCE HOLDEN

CREDITS: ANAT HARTMANN; (INSET) JONATHAN REIF

PALEOANTHROPOLOGY

Tools Link Indonesian 'Hobbits' to Earlier *Homo* Ancestor

The battle of the hobbits is heating up. Two weeks ago, skeptics argued that fossils found on the island of Flores in Indonesia were simply diseased modern humans (www.sciencemag.org/cgi/content/full/312/5776/999b) rather than a dwarf species evolved from an early *Homo* ancestor, as its discoverers had claimed. Now the discovery team fires back. In this week's issue of *Nature*, they argue that stone tools associated with *Homo floresiensis* resemble newly discovered tools from a much more ancient nearby site, suggesting cultural continuity over hundreds of thousands of years.

The tool data "establish an independent source of evidence linking late Pleistocene *Homo floresiensis* with an early Pleistocene progenitor," says Russell Ciochon of the University of Iowa in Iowa City. But some caution that the tools are so simple that inferences of cultural continuity may not be warranted, and a few skeptics question the dates.

The ancient tools come from Mata Menge, 50 kilometers from the Liang Bua cave on Flores where *H. floresiensis* bones and tools were found by an Indonesian-Australian team including Michael Morwood of the University of New England (UNE) in Armidale, Australia. Researchers had previously uncovered stone tools at Mata Menge and dated the artifact-bearing layers to between 800,000 and 880,000 years ago using fission-track dating on volcanic tuffs.

In 2004 and 2005, Fachroel Aziz of the Geological Research and Development Centre in Bandung re-excavated Mata Menge and invited Australian colleagues including Morwood and first author Adam Brumm of Australian National University in Canberra. They found a bonanza of artifacts: 507 small, well-shaped pieces made from volcanic cobbles, with a few chert pieces.

The team then compared the Mata Menge tools to the much younger artifacts from the Liang Bua cave, dated from 95,000 to 12,000 years ago—and found a match in both the types of artifacts and the methods used to create them. At both sites, hominids produced elongated flakes by rotating cores and striking downward; they also created "perforators," pointed tools with retouched edges. "All of the techniques at Mata Menge are also at Liang Bua," says co-author Mark Moore of UNE. "These are quite common approaches to reducing stone."

They are also simple approaches. That's in contrast to the team's original publication, which described a few Liang Bua tools as much more sophisticated. That led some researchers to claim that the tools must have been made by modern humans, not a hominid with a brain the size of a grapefruit. But Moore now says that although

some elongated flakes resemble "blades" used by modern humans, that may simply be coincidence. Richard Potts of the Smithsonian Institution in Washington, D.C., agrees: "Yes, [the Liang Bua hominids] are making what people have called 'blades,' but that doesn't imply that you have to have a certain number of neurons," he says. Morwood is more emphatic: "Some of our critics have claimed that these Liang Bua artifacts are so



Toolmaking tradition? Tools from an ancient site on Flores (top row), including a "perforator" (left column), resemble those found near hobbit bones (bottom).

sophisticated that they must have been made by modern humans. The [new] evidence shows that the basis of that argument is just plain wrong."

Morwood adds that the team now considers the hobbits' most likely ancestor to be a small early *Homo* species, smaller than the classic *H. erectus* found in nearby Java but perhaps similar to fossils found in Africa and Dmanisi, Georgia.

However, Kathy Schick and Nicholas Toth, knapping experts at Indiana University, Bloomington, caution that the technology is so simple that different kinds of hominids might converge upon it. And James Phillips of the University of Illinois, Chicago, a co-author of the critique published in *Science*, thinks that the tools may be out of sequence.

Morwood points out that many hominid species were first greeted with skepticism. The type specimen of *H. erectus*—uncovered in 1891 on Java—was described at the time as a "microcephalic idiot, of an unusually elongated type," in a review in *Nature*. —ELIZABETH CULOTTA

New Archaeology Fund

A new grants program for young archaeologists in Indonesia and East Timor has made its first awards, notwithstanding the current devastation and turmoil in the archipelago. A three-person team from Makassar, Indonesia, and an archaeologist from Yogyakarta, the ancient city near the recent quake's epicenter, will each receive \$3800 for prehistory research from the Anthony F. Granucci Fund. The fund is endowed from the estate of the late lawyer, who had a passion for Indonesian culture.

"Most students [in the region] are forced to work on government-sponsored projects designed by someone else," says archaeologist John Miksic of the National University of Singapore. He says the grants "should lead to a lot more innovative research topics and strategies" by encouraging students to pursue their own ideas.

—RICHARD STONE

A Climate of Change?

Although they aren't likely to pass any legislation this year related to climate change, U.S. lawmakers seem to be warming to the issue. Senator James Inhofe (R-OK), despite viewing controls as a "hoax" based on the "supposed threat of global warming," last week convened a closed meeting that included oil and gas business leaders and environmentalists to promote "a better understanding of the technologies that drive emission reductions." Inhofe chairs the Environment and Public Works Committee. The same day, the Senate Foreign Relations Committee called on the government to reengage in the United Nations Framework Convention on Climate Change process with an eye toward "minimiz[ing] the cost."

Supporters of climate change measures also noted three other developments last week. The Government Accountability Office, the watchdog for Congress, reported that federal voluntary carbon-cutting programs touted by the Bush Administration account for less than one-half of U.S. emissions, and that there are few administrative controls to track company participation. A poll found that 70% of a national sample of hunters and sport fishers believe that warming poses a "serious threat" to humans. "There's a shift going on in ... the political dialogue," says David Doniger of the Natural Resources Defense Council. He and other activists also hope for a boost from *An Inconvenient Truth*, a documentary on former vice president Al Gore's antiwarming crusade.

—ELI KINTISCH



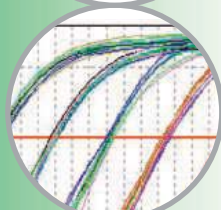
- Mastercycler ep® *realplex* real-time PCR System



- epMotion® 5070 automated pipetting system



- Highly precise pipetting tools



- Comprehensive software for optimized data analysis



Automated real-time PCR that pays for itself

Precision pipetting · Reproducible results · Affordable automation

Eppendorf Automation and real-time Systems (ARTS™) combine the most accurate and reproducible pipetting with the fastest and most sensitive real-time cycling.

That means you get highly consistent and reproducible results within and across experiments. You can even perform reactions in lower volumes—and with fewer replicates, so you will also save significantly on reagents!

Visit: www.epMotion.info or www.realplex.com

Mastercycler ep *realplex*:

- Real-time PCR in less than 30 minutes
- User-friendly software
- Highly sensitive optical system

epMotion 5070 automated pipetting system

- Easy operation via control panel or PC
- Preinstalled, validated applications/consumables
- High-precision pipetting from 1 µl to 1.000 µl



www.eppendorf.com · Email: info@eppendorf.com · Application support: 516-515-2258

In the U.S.: Eppendorf North America, Inc. 800-645-3050 · In Canada: Eppendorf Canada Ltd. 800-263-8715

Your local distributor: www.eppendorf.com/worldwide · Application support: Phone +49 180 366 67 89

Practice of the patented polymerase chain reaction (PCR) process requires a license. The Eppendorf [or appropriate trademark] Thermal Cycler is an Authorized Thermal Cycler and may be used with PCR licenses available from Applied Biosystems. Its use with Authorized Reagents also provides a limited PCR license in accordance with the label rights accompanying such reagents. This is a Licensed Real-Time Thermal Cycler under Applera's United States Patent No. 6,814,934 and corresponding claims in non-U.S. counterparts thereof, for use in research and for all other applied fields except human in vitro diagnostics. No right is conveyed expressly, by implication or by estoppel under any other patent claim.

RESEARCH FACILITIES

Spain Aims to Lure Systems Biologists to a Place in the Sun

BARCELONA—In a stylish marriage, the European Molecular Biology Laboratory (EMBL) is teaming up with the Spanish government to create a new center for the development of mathematical models of living systems. The venture, funded by Spain, will be based at a beachfront research park that opened here last month. The partnership creates a new southern outpost of the Heidelberg-based EMBL, in partnership with Barcelona's new Center for Genomic Regulation (CRG).

Spain has agreed to invest \$16.5 million over the next 9 years to support six research groups in systems biology as part of a broader push to boost Barcelona's scientific profile. The systems biologists will join hundreds of other researchers in the Barcelona Biomedical Research Park (BBRP), which will house up to 80 research groups studying topics as diverse as embryonic stem cells, genetic sequencing, and the effects of environmental pollutants.

"With BBRP, we want Barcelona to become a big capital of knowledge in southern Europe," says pharmacologist Jordi Camí, the park's general director and former head of Barcelona's Municipal Institute of Medical Research (IMIM). In addition to the EMBL offshoot, the park will house IMIM and its respected department of environmental epidemiology, a 400-bed hospital, the Pompeu Fabra University Experimental and Health Sciences Department, a

Center of Regenerative Medicine, and the CRG, which will support research on genomics, proteomics, and bioinformatics, as well as systems biology. A new Institute of High Technology will provide access to sophisticated imaging with a cyclotron and two positron emission scanners.

At the helm of the EMBL/CRG unit will be Luis Serrano, currently coordinator of the EMBL Structural and Computational Biology Unit in Heidelberg. The EMBL/CRG groups will work with a variety of systems, including RNA interference, biochemical networks, and mouse development. Serrano says all groups will be working to develop "a quantitative understanding of biological systems that allows you to make testable predictions." Two principal investigators have been appointed, and the mixed EMBL/CRG search committee has plans to hire three more.

Like their counterparts at EMBL, the researchers will receive 5-year contracts, renewable for an additional 4 years. Serrano says he hopes the system will encourage "a spirit of rotation and the removal of the 'position for life' philosophy" that is prevalent in Spanish science. Organizers also hope the EMBL brand name will



Hot area. Barcelona launched a new biomedical park in May.

help the unit attract international talent.

Ben Lehner, an RNA interference scientist at Wellcome Trust Sanger Institute in Cambridge, U.K., has been hired to lead one of the research groups at the Systems Biology unit. He says he's impressed by "how serious the Catalan government is about turning Barcelona into an international hub for biomedical research." He thinks it may be a "golden" time for recruiting talent back to Europe in light of "the current crisis in science funding that we are seeing in the United States."

—XAVIER BOSCH AND GRETCHEN VOGEL

Xavier Bosch is a science writer based in Barcelona.

U.S. IMMIGRATION REFORM

Senate Bill Would Boost High-Tech Workforce

Business leaders and U.S. academic institutions are applauding some of the provisions in the immigration reform bill approved last week by the Senate. And although the overall measure is at odds with a version passed last fall by the House of Representatives, which focuses more on reducing rather than regulating immigration, scientists don't expect those provisions to be bargaining chips as the two bodies try to reach a compromise.

The Senate bill retains several provisions from last month's abortive agreement (*Science*, 14 April, p. 177), including hiring more high-tech foreign workers and granting permanent residency to foreign students graduating with advanced degrees in science and engineering from U.S. universities. It also would modify a program that annually awards 50,000 visas by lottery to applicants from low-immigration countries—poor nations such as Bangladesh and Angola as well as wealthier ones such as Australia and Germany. Current rules allow applications from anyone who has

finished high school and worked for 2 years. The amendment would reserve two-thirds of these visas for applicants with advanced science and engineering degrees. "Rather than have a lottery system which says to the unemployed cab driver in Kiev, 'You should have a chance to come to America,' we are going to have a lottery system that says to the physicist in Kiev, 'You have a shot at coming to America,'" explained Senator Judd Gregg (R-NH) as he offered the amendment.

Sandra Boyd of the National Association of Manufacturers welcomes the change, although she says the immediate benefits may be slight. "The countries that qualify for the diversity visa program are not the ones where U.S. companies go looking for talent in the first place," she explains. The amendment even makes sense to Jack Martin of the Federation of American Immigration Reform (FAIR), which opposes opening U.S. borders. "Having a higher degree requirement for the lottery would certainly be in keeping with the needs of the economy," he says.

Higher education lobbyists are heartened by the Senate's support of a proposal to grant automatic permanent residency, or "green cards," to foreign students graduating from U.S. institutions with master's degrees and Ph.D.s in science and engineering fields. The legislators also raised the H-1B visa cap from the existing 65,000 to 115,000 a year, with an automatic 20% boost each year if the ceiling is reached, and increased the annual employment-based green card ceiling from 140,000 to 290,000.

None of these measures is expected to figure prominently in upcoming discussions between the House and Senate, however, although the House version of the bill would eliminate the diversity program. "The principal issues of contention will be the amnesty and guest worker provisions," says Martin. President George W. Bush has supported immigration reform but must walk a fine line to avoid alienating conservatives who prefer the House version.

—YUDHIJIT BHATTACHARJEE

Budget, technical, and administrative problems continue to plague a fleet of U.S. polar satellites being built for the military, weather forecasters, and climate researchers

Stormy Skies for Polar Satellite Program

WITH MORE USES THAN A SWISS ARMY knife, the National Polar-Orbiting Operational Environmental Satellite System (NPOESS) was supposed to be the world's most sophisticated series of weather satellites. But somewhere in its 12-year history, the multibillion-dollar NPOESS has also become one of the country's most troubled technology projects. Next week, the Pentagon will issue binding plans on how to fix a project now behind schedule and massively over budget. The expected overhaul could shape for decades how well U.S. forces prepare for battle, civilian authorities anticipate killer storms, and scientists understand Earth's ever-changing climate.

Since the 1960s, the U.S. Department of Defense and the National Oceanic and Atmospheric Administration (NOAA) have used separate north-south orbiting satellite systems to provide daily global weather coverage and crucial multiday forecast data. In 1994, President Bill Clinton proposed to merge those systems in a \$6.5 billion project that was to save an estimated \$1.8 billion over its lifetime. The system would pack 14 sensors—half of them new—onto six 7-meter-long crafts, with three flying at a time until 2018. Sounders would probe the air column, sensors would look through clouds as well as watch for space weather, and the crafts' capabilities would be a quantum leap over decades-old NOAA and Pentagon polar systems. "We have made major strides to converge military and civil weather requirements," Air Force Maj. Gen. Robert Dickman told Congress in 1995.

But now, more than a decade later, technical problems on one of the sensors have rippled through the program and pushed estimated cost overruns into the billions of dollars. As currently configured, the system is as much as 3 years behind schedule and carries, by the Pentagon's latest estimate, a lifetime price tag

of \$14 billion (see graph). The overrun triggered an automatic top-to-bottom review, which the Secretary of Defense is set to present to lawmakers next week.

The delay could leave U.S. forces without the best data on sandstorms or ocean currents, military planners worry, not to mention a possible weakening of civilian weather coverage if there are problems with a NOAA satellite scheduled to be launched in 2007. What the Government Accountability Office (GAO) calls a "program in crisis" is really the "fleecing of America," according to Representative Bart Gordon (D-TN), ranking Democrat on the House Science Committee, who wants NOAA Administrator Conrad Lautenbacher to resign for ignoring what Gordon says were clear warn-

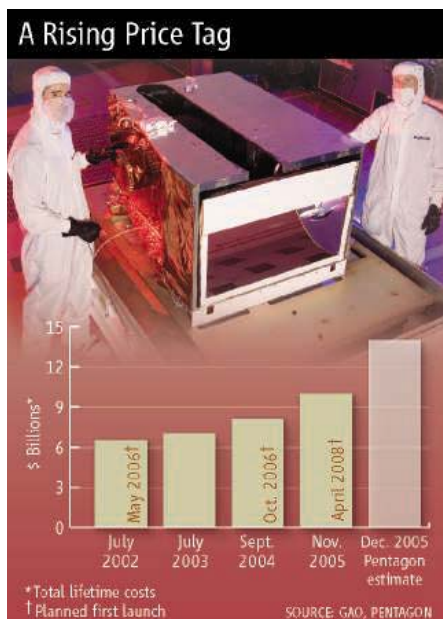
ing signs about NPOESS. "This is a program that is dangling by a thread," says one congressional staffer who follows the project.

NPOESSing a challenge

Polar satellites are wonderfully useful because their 100-minute orbits provide coverage of nearly every point on Earth. But their attractiveness didn't forge an automatic alliance between defense and research bureaucrats operating in two different cultures. "NOAA looked at the Air Force and said, 'Huh, goose-stepping fascists.'" And the Air Force looked at NOAA and said, 'Fish-kissing tree huggers,'" said former program manager John Cunningham at a 2003 briefing on the project.

Their needs were different as well: The Pentagon wanted sensors with high resolution and speedy delivery of the data, whereas NOAA sought instruments with a multitude of spectral bands for weather research. NASA agreed to join in, canceling planned follow-ons for environmental missions while adding environmental and climate sensors to the NPOESS fleet after its scientists lusted after the chance to use systems whose sequential platforms will stay aloft for 20 years rather than the usual 5-year window. "I thought [NPOESS] was the right thing to do, and in some ways, the only way to do it," says biogeochemical modeler Berrien Moore of the University of New Hampshire, Durham, who has long advised the government on behalf of the climate community.

The initial cooperation went "surprisingly well," says the Navy's Robert Winokur, then head of NOAA's satellite program. The package would include everything from an ozone detector to a device for aerosol studies (see graphic, p. 1297). The microwave imager would provide more channels for detailed moisture profiles than existing instruments. And the Visible/Infrared Imager Radiometer



Skyward. The Pentagon's estimate for the program is much higher than what NPOESS staff assume.

◀ **Eagle eye.** Planners say NPOESS will allow more accurate weather forecasts.

Suite (VIIRS) of instruments was designed to capture everything from quarter-kilometer-resolution ground detail to surface-water temperature and movement of ice floes.

But despite passing a critical review early on, VIIRS has turned out to be the program's Achilles' heel. Progress reports to agency brass show that the strain appeared soon after defense giant Northrop was awarded the NPOESS contract in mid-2002. In July 2003, NOAA official Greg Withee told congressional overseers that early sensor problems were "getting under control." But only 2 months later, an internal report called VIIRS "our problem child" and confessed that the "work was more difficult than estimated."

The challenges included electronics not processing data correctly and protective doors that broke during vibration tests. After costs grew by tens of millions, outside experts were asked to find out why the subcontractor, Raytheon, was having so much trouble building an instrument based on a sensor currently flying on NASA satellites. "I believe these problems must have existed then but were masked by the very, very strong in-house NASA support," a NOAA program manager wrote his boss in 2004—2 months before problems with the cooling system cropped up. Soon after, Raytheon replaced most of its technical team, and Northrop told the government that problems with VIIRS would push back a preliminary testing mission by more than a year. Last summer, NPOESS program manager John Cunningham, as a congressional staffer put it, "took the bullet" and resigned as part of a series of management changes.

Following the ripples

Experts disagree on whether problems with VIIRS could have been foreseen. Some, such as former NOAA director James Baker, say it's "not surprising" that such a complex endeavor could have run up such an unexpected tab. "It's a great program, [it] just got into trouble," he says now.

Critics say project managers should have worked harder to prevent initial delays from having a domino effect on the entire project. It didn't help the situation when, in 2003, Congress approved a Bush Administration request for a \$50 million cut in the program. The lower request was triggered by the reduced sense of urgency after the launch of a defense weather satellite was delayed. That 1-year tightening of the fiscal spigot led to a huge bump-up in NPOESS's price tag, however, from \$6.5 billion to \$8.1 billion, due to new plans, a longer production schedule, and more staffing.

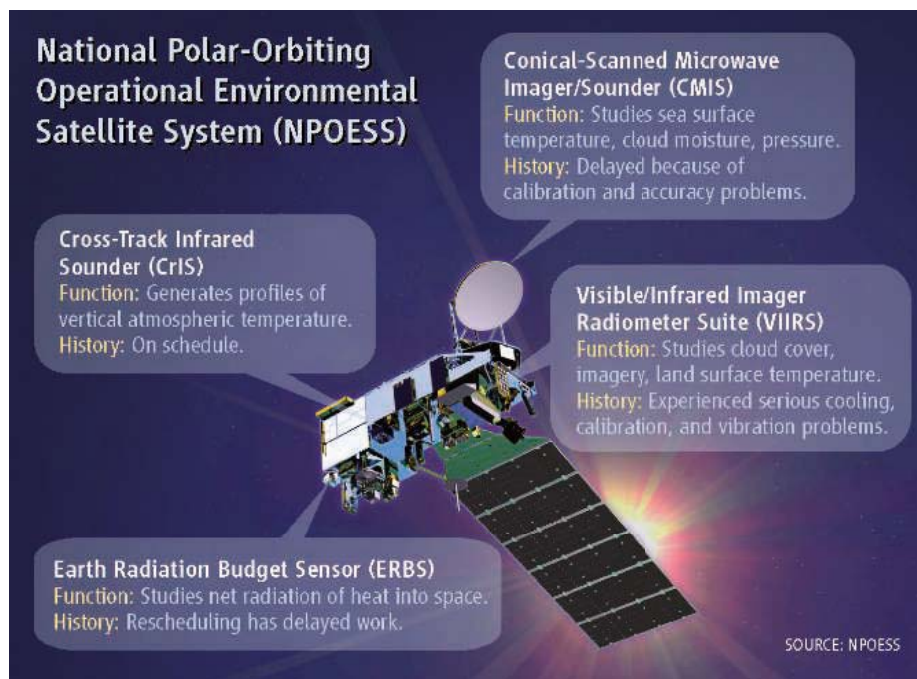
What Cunningham's goodbye letter calls "triagency hassles" also appear to have played a role in the rising costs and delays. "Everyone—contractors, government, and scientists—misjudged the difficulty that was inherent by

both the [military-civilian] convergence and [adding] the environmental mission" to the weather one, says Moore, who says the errors show contractors have "lost capability" in building new instruments. It wasn't the "mission creep" that often plagues big programs, he adds; the complexity of the whole endeavor made a tough job even harder.

Storms ahead?

The top priority in the pending Pentagon review is continuity of weather sensing. That fear is grounded in the fact that several cur-

their already third-class status on the craft. NOAA's Withee told *Science* 2 years ago that NPOESS's sensors would give climate science "a nice ride" with plenty of data. But from the beginning, calibration work—crucial to making nuanced measurements needed to detect a shifting climate—has taken a far back seat to weather operations. Work on a radiation surveyor, meant to give scientists a continuous measurement of Earth's electromagnetic radiation budget, has been rescheduled while precious program dollars have been plunged into fixing VIIRS.



Under the weather. The VIIRS instrument has been the most troubled piece of the state-of-the-art weather satellite system under construction.

rent systems could fail in the near future. NOAA and the Pentagon each have two polar satellites in orbit. Augmented by coverage from foreign partners, they ensure that weather data anywhere on Earth is no more than 6 hours old. The Air Force has the last satellite ready to replace the polar DMSP orbiter that NPOESS will eventually replace, although it wants the upgrades in NPOESS. NOAA's long-planned weather satellite POES is further behind schedule—it is now scheduled for launch in 2007. The fear is that if POES fails and NPOESS is further delayed, weather forecasters and scientists would be left in the lurch. A mission to test key NPOESS sensors and fill potential gaps in NASA atmospheric data-gathering was originally to launch this year. That date has been pushed back to as late as 2008, and the belated test data from that launch will mean further NPOESS delays and costs.

Climate researchers fear that the Pentagon will recommend changes that will degrade

Pointing to a recent program revamp, NPOESS officials say they've done their best to cope with what they believe is a series of bad breaks, although they wouldn't comment on the program's future pending the Pentagon's review. Northrop program manager David Ryan says an interim plan written in December has the program "ahead of schedule, on budget" with VIIRS problems resolved as the instrument undergoes thermal testing. (Government managers are waiting for test results.)

When former vice president Al Gore announced the program in 1994, he said NPOESS would "cut costs and eliminate duplication." The result, said Gore, would "[take] the nation's space-based environmental monitoring program into the next century." But climate researchers are worried that they could be left with 20th century tools if military officials decide that the continuing cost of the wars in Iraq and Afghanistan force them to build a less-capable NPOESS.

—ELI KINTISCH

STEM CELL RESEARCH

South Korea Picks Up the Pieces

Korean scientists are moving beyond the Hwang scandal with a new strategy for the country's stem cell research

SEOUL—Woo Suk Hwang, the would-be stem cell pioneer, is leaving an ironic legacy: South Korea is more determined than ever to become a force in worldwide stem cell research, and he won't be playing a role. Over the last several months, as public prosecutors were unraveling how Hwang and his team at Seoul National University (SNU) fabricated data to make it look as though they had created patient-specific stem cells, a task force of scientists and public officials has been working on a strategic plan to guide the country's future stem cell efforts. The plan's bold goal is for the government to spend \$454 million over the next 10 years in the hope of having Korea emerge as one of the top three global leaders in stem cell research.

Commissioned by the government and due to be unveiled in Seoul this week, the plan calls for developing a stem cell research infrastructure, attracting more scientists to the field, and providing even more money than what had been promised when the country's hopes and funding were centered on Hwang. (According to media reports, Korea's Ministry of Science and Technology budgeted \$28 million for stem cell research last year.) "It's a national plan to do stem cell research more effectively and systematically," says Dong-Wook Kim, a stem cell researcher at Yonsei University in Seoul, who led the task force. The funds will likely be spread in a more balanced way across institutions and between research on both embryonic stem cells—the focus of Hwang's efforts—and adult stem cells, which have been tested in a Korean clinic for treating heart attack patients and are envisioned here for possible use in treating neurological and other disorders.

In contrast to the breathless anticipation that surrounded Hwang's work, the plan will have

"a long-term perspective, not a focus on short-term results," says Youngsook Son, a Seoul researcher working with adult stem cells at the Korea Institute of Radiological and Medical Sciences, who was among the 50 scientists on the task force. The researchers hope to convince the Korean public of the value of continuing an aggressive research program even while giving a more sober assessment of the potential benefits of stem cell therapies and when they will reach the clinic, as well as Korea's place in global stem cell research efforts. And most important, "we will forget Hwang, and we will move on," declares Il-Hoan Oh, another task force member at the Catholic University of Korea in Seoul.

Taking stock

The task force's first job was a realistic assessment of Korea's strengths and weaknesses in stem cell research, irrespective of Hwang's claims. Kye-Seong Kim of Hanyang University in Seoul, who headed a subgroup on human embryonic stem cells (hESCs), says there was no question about the coun-



Bright spot. Kye-Seong Kim is one of a small number of Korean researchers studying the basic biology of human embryonic stem cells (above).

try's greatest strength. "Maintaining and establishing stem cells is where Korea is competitive," he says.

Korean researchers got off to an early start, thanks to a rivalry among Korean fertility clinics. In 1998, James Thomson and colleagues at the University of Wisconsin, Madison, reported the first stem cell line derived from human embryos (*Science*, 6 November 1998, p. 1145). Within less than 3 years, four Korean groups, all affiliated with fertility clinics, had duplicated the feat. "We were all competing but still cooperating, sharing information for producing human embryonic stem cells," recalls Hyung Min Chung, a cell biologist at Pochon CHA University College of Medicine, which is affiliated with one of Korea's largest obstetrics and gynecology hospital chains. Rival MizMedi Hospital, which produced hESC lines by the end of 2000, subsequently got a grant from the U.S. National Institutes of Health (NIH) to prepare those lines for worldwide distribution, says MizMedi chair Sung-il Roh. Those two groups, plus the Seoul-based Maria Biotech Co., are among the 15 groups on NIH's Human Embryonic Stem Cell Registry, which lists stem cell lines created before August 2001 and thus eligible for use in federally funded research in the United States. A group led by in vitro fertilization specialist Shin Yong Moon at SNU Hospital derived its own hESC lines in September 2001.

These clinics are continuing to push their advantage. For example, Chung says Pochon CHA has 1000 donated human embryos, left over from in vitro fertilization treatments, and scientists there plan to derive 100 hESC lines over the next 10 years. Unlike the original hESC lines, these will not be grown on animal feeder cells and thus should be suitable for clinical use, he says.

Progress has been slowed, however, by the Hwang debacle, as two of the original labs are

now under a cloud. Hwang recruited both Moon and MizMedi to his team for the stem cell know-how he needed to attempt therapeutic cloning. Earlier this year, SNU suspended Moon for 3 months for "failing to uphold the principles of academic honesty and integrity," according to an SNU press release; Seoul public prosecutors later cleared him of any legal wrongdoing. Then last month, the prosecutors charged that one of the MizMedi researchers seconded to Hwang's team, Sun Jong Kim, was heavily involved in the fraud and indicted him for destroying evidence and obstructing research work. Roh says he is rethinking the direction of their research; Moon could not be reached for comment.

The task force also concluded that Korean researchers have an edge in somatic cell nuclear transfer (SCNT), or cloning—Hwang's specialty. Hwang attributed much of his success in cloning cows and Snuppy, a dog, to a technique that involved gently squeezing rather than sucking the nucleus out of cells. An investigation into Hwang's research by SNU concluded that he did not develop this technique, but that he had refined it; a half-dozen other Korean institutions have used it to clone dozens of pigs and cows.

Korean researchers are also competitive in research on adult stem cells, the task force concluded. Although they are less malleable than embryonic stem cells, adult stem cells, found in many tissues and organs throughout the human body, can renew themselves as well as differentiate into the specialized cells of those tissues and organs. Bone marrow has long been a source of stem cells for therapies for blood diseases and certain cancers. Recently, groups throughout the world have been experimenting with other adult stem cell therapies in humans.

In 2003, SNU cardiologist Hyo-Soo Kim led what is so far the country's only large randomized adult stem cell clinical trial. He treated heart attack patients with their own peripheral blood stem cells to try to promote the growth of new blood vessels and heart muscle. A group in Germany had done a similar trial using bone marrow stem cells, and Kim's group wanted to try something less invasive. The team first used a drug called G-CSF to induce the patient's bone marrow to overproduce peripheral blood stem cells, which they harvested and then injected into the patients' hearts.

The trial was halted early because 7 of the 10 patients treated with G-CSF suffered a renarrowing of previously blocked arteries in the area around an inserted stent. Kim is optimistic that the side effect can be minimized, and he notes that patients treated with stem cells showed a measurable, although minor, improvement in heart function. The team published a brief report on the trial in *The Lancet* in 2004, and a more complete paper is now being prepared. "We believe that only a small percentage of the stem cells clung to the heart tissue," says Kim, who is trying to "prime" cells with chemicals and proteins so that a greater percentage will

lodge in the heart and, he hopes, grow into replacement tissue.

The task force highlighted one major weakness of the Korean research community: its limited expertise in cell, molecular, and developmental biology. This hinders efforts to understand and ultimately exploit stem cells'



Uncertain legacy. Construction has stopped on the building once intended for disgraced cloner Woo Suk Hwang (*bottom*); the space intended for his Stem Cell Hub (*above*) will be used for gene therapy.

magical ability to both self-renew and differentiate into all the specialized cells of the body. "Japan, the U.S., the U.K., and other countries in Europe are leading in this field," admits Hanyang's Kim, whose own work is one of the bright spots. He led a team that recently identified 36 novel microRNAs apparently involved in regulating hESC development. Their report in *Developmental Biology* in May 2004 was among the journal's top 10 most frequently downloaded papers for the past 2 years. "I'm really proud," he says. He's now working on elucidating the functions of these microRNAs.

A fresh start

The task force spelled out a new research agenda that aims to capitalize on the country's strengths and take advantage of new opportunities, says Yonsei's Kim. All grants will be competitively reviewed to avoid "concentrating funding on one person," says Catholic University's Oh. Priority areas include:

- characterizing stem cells and directing differentiation,
- improving techniques to isolate and expand adult stem cells,
- developing new culture methods suitable for clinical use,
- exploring alternatives to SCNT for producing patient-specific stem cells,
- verifying the safety and efficacy of transplanted stem cells in animals and humans, and
- applying stem cells to drug development.

The plan also calls for establishing common-use facilities such as a stem cell bank, sponsoring international collaborations, and strengthening training programs. Kim expects the government to implement these recommendations in 2007.

In the aftermath of the Hwang scandal, the task force, which included bioethicists, also called for "a heightened awareness of ethical issues," says Oh. For instance, the group urges more stringent requirements to confirm the efficiency of therapies in animals before trying them in humans. Meanwhile, research on human therapeutic cloning is on indefinite hold, Hanyang's Kim notes, although not because of this report. He explains that groups attempting therapeutic cloning will need permission from the national bioethics review board set up last year, which has yet to decide the criteria for granting permission.

Finally, the task force recommends frank communication between researchers and the public. "Many people in Korea and probably even most of the young officials in the government really believed that Korea was one of the most prominent and leading countries in the world in stem cell research," says Hanyang's Kim. Instead, "we were leading in a small part of stem cell research," he says. Researchers here say the public and patients alike must be given realistic assessments of the expected results of experimental stem cell therapies. SNU's Kim says the goal for his stem cell therapy for heart attack patients is to improve damaged heart function by 10% over what it would be without treatment. "That would be noticeable by patients," he says, but still far short of fully restoring their hearts.

Stem cells are "not a miracle cure; only God can make miracles," says Kook In Park, a stem cell biologist at Yonsei University. It may help get his message across that the Hwang-inspired postage stamp showing a patient rising from a wheelchair thanks to stem cell therapy is no longer on sale.

—DENNIS NORMILE

With reporting by D. Yvette Wohn in Seoul.

Research Corporation proudly announces the 2006 Cottrell Scholar Awards

The Cottrell Scholar Award, \$100,000 in discretionary funds, is designed to identify early-career faculty who show promise to be future leaders in research, and who are committed to making significant contributions to teaching, especially at the undergraduate level.

"The drive to become a Cottrell Scholar made me think deeply on issues of undergraduate education... [this] made me realize how much I enjoyed teaching and working with undergraduate students, and taught me how to excel in both research and education. My involvement in undergraduate education has continued until today, many years after I received the Cottrell Scholar award." - Yi Lu, Professor of Chemistry, University of Illinois, Urbana-Champaign and Howard Hughes Medical Institute Professor



If you'd like additional information,
please visit our website,
www.rescorp.org

Research Corporation

*a foundation for the
advancement of science*

Mu-Hyun Baik
Indiana University at Bloomington, Department of Chemistry
Towards a quantitative understanding of diastereoselective carbocyclizations through quantum chemical modeling

Jeffrey W. Bode
University of California, Santa Barbara,
Department of Chemistry and Biochemistry
New ligation reactions for the synthesis of biomolecules and biomaterials

Erica W. Carlson
Purdue University, Department of Physics
Quantum soft matter

David S. Ginger
University of Washington, Department of Chemistry
Probing optoelectronic processes in conjugated polymer blends

Darren W. Johnson
University of Oregon, Department of Chemistry
Supramolecular arsenic coordination chemistry

Masaru K. Kuno
University of Notre Dame, Department of Chemistry and Biochemistry
Disorder induced optical heterogeneity in solution-based straight/branched semiconductor nanowires

Adam Leibovich
University of Pittsburgh, Department of Physics
Particle physics calculations using effective field theories

Thorsten Ritz
University of California, Irvine, Department of Physics and Astronomy
*Weak magnetic field effects on blue-light signaling in Arabidopsis thaliana:
A model system for geomagnetic field detection*

Justine P. Roth
Johns Hopkins University
How do intra-protein redox reactions control the activities of enzymes involved in oxidative stress?

Melanie S. Sanford
University of Michigan, Ann Arbor, Department of Chemistry
Transition metal-catalyzed carbon-fluorine bond-forming reactions

Jairo Sinova
Texas A&M University, Department of Physics
Spin-Hall effect in semiconductors and related phenomena in nano-spintronics

Keivan Guadalupe Stassun
Vanderbilt University, Department of Physics and Astronomy
A systemic approach to problems in star formation and minority representation

Joseph C. Weingartner
George Mason University, Department of Physics and Astronomy
The alignment of grains with the interstellar magnetic field

ASTRONOMY

A Surprising Stellar Nursery

By sharpening their view of the Milky Way's core, astronomers have deduced that stars can arise close to the giant black hole there

CAMBRIDGE, MASSACHUSETTS—As astronomers peer through their looking glasses at the crowded heart of our galaxy, their view becomes curiously and curiously. For years, stars darting close to the core have pointed to a fearsome black hole hidden there, pulling with the gravity of nearly 4 million suns. But with ever-clearer vision, telescopes revealed that the true mystery was not the black hole but the youthful stars around it. Gas in that wild setting seemed too churned up to create stars, so where did they come from?

The likeliest answer, described here at a recent meeting,* is both delightful and unsettling. Every few million years, gas gathers around the black hole into a disk that gets squeezed by the hole's intense influence. This fragments the disk into dense clumps that spawn giant stars in planetlike orbits, trapped by the hole's sway like motes in a whirlpool.

It's the antithesis of calm star birth elsewhere in the Milky Way. "It's like moving the maternity ward into the emergency room," says Roger Blandford, director of the Kavli Institute for Particle Astrophysics and Cosmology at Stanford University in California. And it could happen at the centers of all galaxies, the realms where black holes apparently reign supreme.

Evidence for this picture comes from deep studies of the Milky Way's core by competing teams in Germany and the United States. The astronomers use infrared light, which penetrates veils of dust, to resolve hundreds of stars in the innermost light-year around the black hole, known as Sagittarius A* (pronounced "A-star") (*Science*, 30 May 2003, p. 1356). In recent years, the teams have tracked fainter stars by using adaptive optics to smooth the blurring of

Earth's atmosphere. And in a new advance, spectrographs that capture light from dozens of stars at once have enabled each team to deduce the motions, sizes, and ages of the core's residents.

The results are glaring, says Reinhard Genzel of the Max Planck Institute for Extraterrestrial Physics in Garching, leader of the German team. "There is a spectacular concentration of young, massive stars in the central light-month," he says, jammed into a space just 1/50 as wide as the gulf between our sun and the nearest star. Team member Thibaut Paumard and colleagues found that more than half of the central stars revolve within a single plane, clockwise to our line of sight.

The stars are just 6 million years old on average—too young to have migrated from

thousands of suns born within 10 light-years of the galaxy's core. Models suggested that such clusters could sink quickly toward a luminous self-destruction near the black hole.

But that scenario has problems, says astrophysicist Sergei Nayakshin of the University of Leicester, U.K. "A disrupted cluster should leave behind a trail of stars, but the observed disks have outer edges," he says. What's more, the cluster's debris should include thousands of active lower-mass stars, he notes. Ground-based telescopes can't see those stars, but the orbiting Chandra X-ray Observatory should spot their flares. "They clearly aren't there," Nayakshin says.

Advocates of doomed clusters argue that their scenario still has merit. A knot of at least seven massive stars, called IRS 13, shines a fraction of a light-year away from Sagittarius A*. The group couldn't persist in that perilous spot without the binding force of a moderate black hole of its own, says astrophysicist Simon Portegies Zwart of the University of Amsterdam, the Netherlands. Such midsize holes could shepherd big stars deep into the galaxy's maw, he maintains.

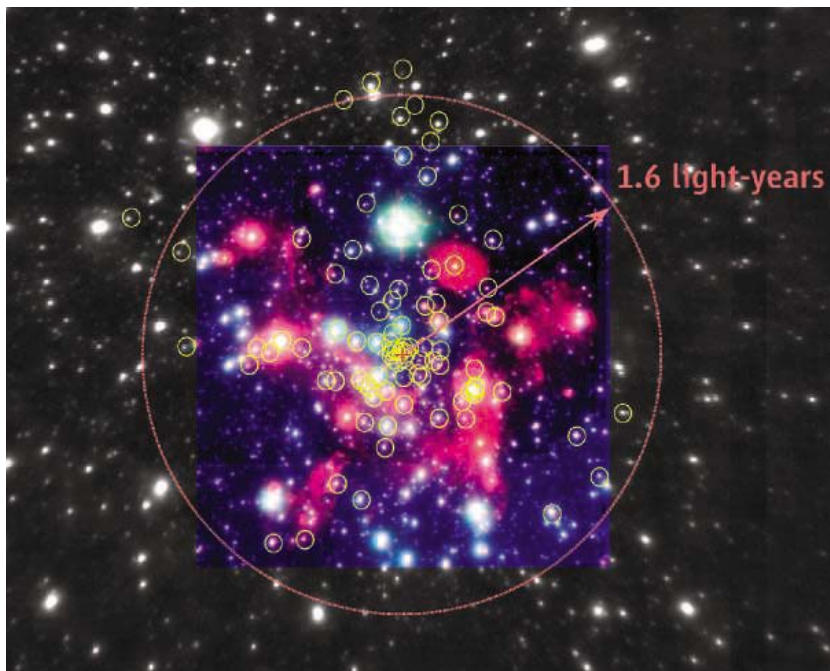
"Honestly, I think both things are going on," including star formation in a disk, Portegies Zwart says. "The clusters are there, and there is enough evidence that they spiral in and do these tricks," such as perturbing some stars into cigar-shaped orbits around the black hole. As Ghez noted at the meeting, such wacky orbits exist—and they seem inconsistent with star birth solely within a Frisbee-like disk of gas.

Today, little gas envelops Sagittarius A*. But theorists believe the galaxy feeds its core with gas in surges that take millions of years to unfold. "I think it's gas from normal stellar evolution, periodically falling into the center and triggering starbursts," says astrophysicist Jeremiah Ostriker of Princeton University. Other galaxies show signs of star-forming

wombs at their cores, Ostriker notes—such as NGC 4258, which emits dazzling beacons of microwaves from dense clouds swirling within 0.3 light-years of its central black hole.

Closer to home, astronomers await the closest stellar passage to the Milky Way's black hole yet seen. This summer, a star may dip within 7 billion kilometers of the center, about the distance of Pluto from our sun. It will race at 3% the speed of light, Ghez observes. For a globe of gas fully 10 times the sun's mass, that's a blazing clip.

—ROBERT IRION



Flirting with danger. Nearly 100 young, massive stars (yellow circles) dash within close confines around a prodigious black hole (red cross) at the Milky Way's center.

calmer nurseries farther out in the galaxy. Rather, the team believes they were born right there in a long-vanished disk that girdled the black hole just as planet-forming disks swaddle embryonic stars.

This research, along with similar conclusions presented by U.S. team leader Andrea Ghez of the University of California, Los Angeles, impressed theorists at the meeting. Until recently, another origin for the young stars was in the running: not gas but stars deposited by the breakup of tight clusters of

* Fourth Harvard-Smithsonian Conference on Theoretical Astrophysics, 15–18 May, Cambridge, Massachusetts.



Roaring back. The Tevatron (far ring) is finally producing data at a copious rate.

High expectations and low luminosity

To make a comeback, first you have to fall behind. And that's what the Tevatron did in 2001, when it started up after a 5-year overhaul in which physicists replaced the accelerator that feeds the collider protons and antiprotons. Experimenters had hoped the Tevatron would pump out collisions 10 to 20 times faster than it had before the upgrade. But 2 years into "Run II," it was producing collisions at only twice the previous rate. To spot the Higgs, experimenters needed a torrent of data. They got a trickle.

The key problems lay not with the new main injector but with the system to produce antiprotons, says Roger Dixon, head of the accelerator division at Fermilab. To generate antiprotons, the machine fires protons into a metal target, and an accelerator known as the accumulator collects the bits of antimatter that result. Physicists had hoped to pass the particles into yet another accelerator known as the recycler to cool them and pack them into tight bunches before passing them to the main injector and into the Tevatron. But the recycler wouldn't cooperate, and accelerator physicists had to bypass it entirely.

Fermilab threw everything it had at the Tevatron and even called on other labs for help. Then-director Michael Witherell shook up the lab's accelerator division. In 2003, the new management set a timetable for improving various parts of the facility and increasing the rate at which the Tevatron produces collisions, a quantity that is known as the luminosity and is measured in inverse femtobarns. Since then, researchers have stayed on schedule, says Fermilab accelerator physicist David McGinnis. In June 2004, they brought the recycler on line and last August implemented a bold scheme to cool antiprotons in it with electrons. The Tevatron now produces as much data in 6 weeks as it did in all of Run I, from 1992 through 1996.

In retrospect, some of the angst over the Tevatron's performance early in Run II stemmed from unrealistic expectations, some say. "Everyone in the trenches knew this was going to be a marathon, not a sprint, and that it was going to be slow going at the start," McGinnis says. "I don't think that message got through to the experimenters." The Tevatron is on pace to log a total of 8 inverse femtobarns by the end of 2009, maybe just enough to snare the Higgs, the linchpin of the standard model of particle physics.

Whence mass?

The standard model marries the electromagnetic force, which accounts for all of electricity and magnetism, and the weak nuclear force, which produces a kind of radioactive decay. Since the 1970s, physicists have known that the two are different manifestations of the same thing,

HIGH-ENERGY PHYSICS

Aging Atom Smasher Runs All Out In Race for Most Coveted Particle

After years of frustration, Fermilab's Tevatron collider is running well. Researchers say they have a shot at spotting the Higgs boson—if there's time

In autumn 2004, Boston's beloved baseball team, the Red Sox, spotted the archrival New York Yankees a three-games-to-none lead in the best-of-seven American League Championship Series. The plucky Sox then whipped the Yankees in four straight and went on to win the World Series for the first time in 86 years. Now, physicists at Fermi National Accelerator Laboratory (Fermilab) in Batavia, Illinois, hope to pull off a similarly dramatic comeback and bag particle physics' biggest prize, the long-sought Higgs boson.

Four years ago, physicists wrung their hands as Fermilab's Tevatron collider faltered after a major upgrade (*Science*, 8 February 2002, p. 942). The revamped machine failed to smash protons into antiprotons at the rate researchers had counted on. As a result, many thought the 6-kilometer-long Tevatron had no chance of making a major discovery before a more powerful particle smasher—the 27-kilometer-long Large Hadron Collider (LHC) under construction at the European particle physics laboratory, CERN, near Geneva, Switzerland—came to life, as it is supposed to do next year.

But after a reshuffling of personnel and much hard work, the Tevatron is now cranking out data at a prodigious rate. And experimenters at Fermilab are cautiously optimistic that, if nature cooperates, they have a shot at seeing the Higgs boson, the particle thought to give other particles their mass. The Tevatron hasn't recovered completely from its missteps; if the

machine continues to improve, by 2009 it will produce slightly more than half the data researchers once hoped for. But that may be just enough to spot the Higgs.

"Two or three years ago, we couldn't foresee having enough data to have a fair chance," says Jacobo Konigsberg, an experimenter at the University of Florida, Gainesville, and co-spokesperson for CDF, one of two large particle-detector experiments fed by the Tevatron. "Now the picture has changed tremendously." If the Higgs is light, no more than about 130 times as massive as a proton, then Fermilab researchers might be able to spot it, says Gerald Blazey, an experimenter at Northern Illinois University in DeKalb and co-spokesperson for DZero, the other particle-detector experiment.

That's if the Tevatron runs through 2009 as planned. The U.S. Department of Energy (DOE) could unplug the machine a year earlier to free up money for future projects—in particular, the proposed International Linear Collider, a 30-kilometer-long straight-shot behemoth that would map the conceptual terrain opened by the LHC (*Science*, 21 February 2003, p. 1171). In a year, a DOE advisory panel will evaluate the Tevatron's performance and recommend whether to shutter it early. "They've turned that machine around remarkably," says Lyn Evans, a physicist at CERN, who is directing construction of the LHC. "It's a tough call whether to run the Tevatron in 2009, that's for sure."

although they aren't exactly interchangeable. The electromagnetic force works at lengths as long as lightning; the weak force reaches only across an atomic nucleus. That's because the photons that convey the electromagnetic force are massless particles, whereas the particles that carry the weak force, the W and Z bosons, weigh far more than a proton.

But there's a catch. If theorists simply assign masses to the W, Z, and other particles, the standard model goes haywire mathematically. To "break the symmetry" between the forces, mass must originate somehow through the interactions of particles that are otherwise massless themselves.

That's where the Higgs comes in. Theorists assume that empty space is filled with a Higgs field, which vaguely resembles an electric field. The field drags on other particles, giving them inertia or mass. Like all fields, the Higgs field consists of hidden "virtual" particles that can pop into existence in sufficiently violent collisions.

The standard model does not predict the mass of the Higgs, but the theory is so tightly interconnected that precise measurements of familiar particles limit the possibilities. Measurements of the mass of the W, the mass of a particle called the top quark, and other particle properties suggest that the Higgs is light and possibly within the Tevatron's grasp, says Volker Buescher, a member of the DZero team from the University of Freiburg in Germany. Physicists measure masses and energies in electron volts; the Tevatron smashes particles with an energy of 1.96 trillion electron volts, or TeV. That's enough to generate new particles with masses of a few hundred billion electron volts, or GeV.

However, the standard model also enables physicists to estimate how often a Higgs of a particular mass will emerge and how hard it will be to detect as it decays into other particles. With those effects taken into account, the Tevatron should be able to unearth evidence of the Higgs if the particle's mass is less than 125 GeV. "While a Higgs search up to 125 GeV may sound limited, that's exactly the range where we would expect to find it," Buescher says. With 8 inverse femtobarns of data, researchers should be able to spot solid evidence, if not incontrovertible proof, of a Higgs in that range—if it's there.

Of course, the standard model explains "electroweak symmetry breaking" in only the

simplest and most ad hoc way. Nature could play by richer and more complicated rules. For example, a theory called supersymmetry posits an undiscovered "superpartner" for every known particle. The theory helps solve conceptual problems with the standard model, and it requires at least two Higgs fields and five Higgs particles, the lightest of which resembles the standard model Higgs. That particle might be harder to find, says Marcela Carena, a theorist at Fermilab. On the other hand, measurements at

Panel (P5) will weigh several factors next spring when considering whether to stop the machine early, says panel chair Abraham Seiden of the University of California, Santa Cruz.

Most important will be the performance of the Tevatron and its CDF and DZero detectors. Experimenters say the detectors are running in top form, and accelerator physicists are just now completing the last upgrades that should get the Tevatron to a full 8 inverse femtobarns. But even if all the machinery runs perfectly, Fermilab faces a problem: Half of all experimenters may leave for the LHC by 2009. Having studied the issue, Fermilab officials are confident they can keep the experiments running, says Fermilab experimenter Joel Butler. "The real issue is can the data be analyzed in a timely fashion? Because of the LHC, it has a shelf life," he says. But even on that account, he's optimistic: "If there is a real shot to get the Higgs, people will stay to do the analysis."

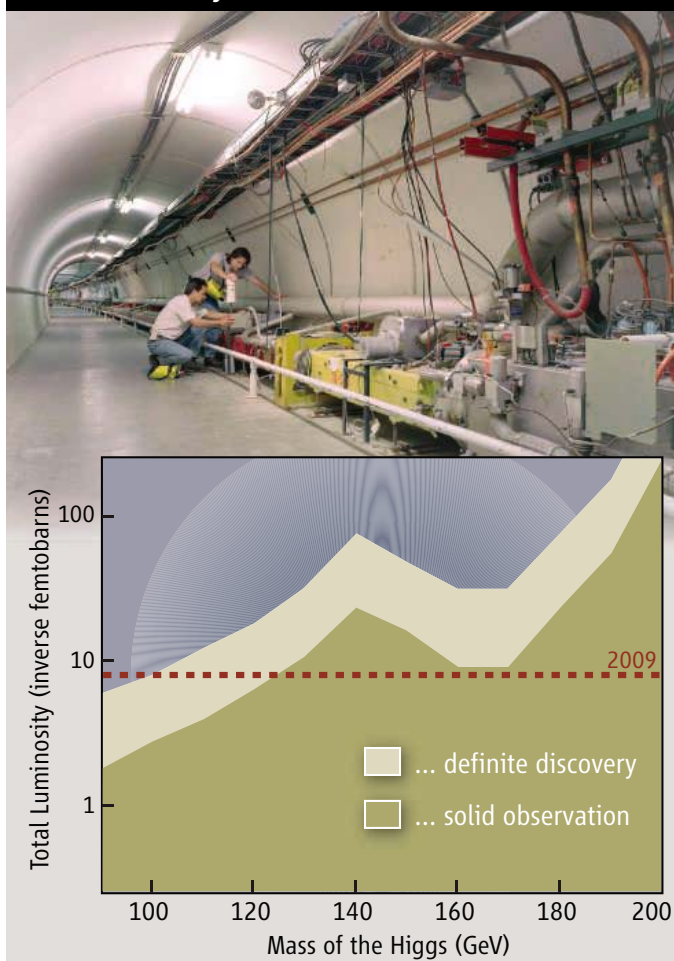
P5 will also consider progress on the LHC, which should turn on next autumn and take its first data the following spring. The LHC, which will crash protons into protons at a whopping 14 TeV, will come on slowly, says CERN's Evans. That's because it will pack so many protons and so much energy into its beams that should a beam accidentally strike the accelerator itself, it could blast a crippling hole in it. "The speed with which we bring up the luminosity will be limited by our ability to protect the machine," Evans says. But, he adds, "certainly in 2009 we'll be up to 50% of luminosity and completely swamping the Tevatron."

Ultimately, whether the Tevatron runs through 2009 may depend on whether researchers catch a whiff of something in the next year, Seiden says. "The main thing will be the Tevatron data itself," he says. "If it looks interesting, that's a really important plus. If it looks unlikely [to yield a discovery], you might want to think of ending earlier."

Only time will tell what nature has in store. So for the moment, physicists at Fermilab continue to push to improve the performance of the Tevatron and their detectors. In the competition for the Higgs, they've entered the late innings and are down a couple of runs—or inverse femtobarns. But they can feel their fortunes turning and hope for one last shot at triumph. As they say in baseball, it's not over till it's over.

—ADRIAN CHO

Total Luminosity Needed for ...

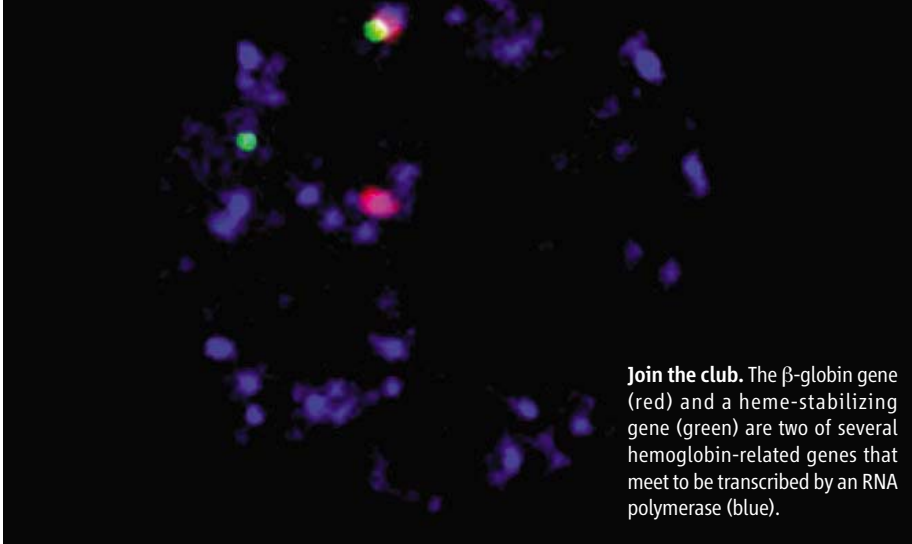


Just enough? The Tevatron could pump out 8 inverse femtobarns of data by the end of 2009. That should allow researchers to glimpse the Higgs boson if its mass is less than roughly 125 GeV, as other data suggest.

the Tevatron may significantly limit the parameters of supersymmetry. "One way or the other," Carena says, "the Tevatron will shape our understanding of physics beyond the standard model in the next 2 or 3 years."

An early exit?

All of this depends on the Tevatron's logging as much data as possible. But researchers would get at most 6 inverse femtobarns of luminosity if the Tevatron shuts down at the end of 2008. DOE's Particle Physics Project Prioritization



Join the club. The β -globin gene (red) and a heme-stabilizing gene (green) are two of several hemoglobin-related genes that meet to be transcribed by an RNA polymerase (blue).

MOLECULAR BIOLOGY

Genes Commute to Factories Before They Start Work

A new study suggests that genes whose proteins work together move to the same transcription site

The more researchers learn about gene regulation, the more complicated the story gets. First there were transcription factors, proteins that bind DNA to turn genes on. Then molecular biologists figured out that each transcription factor can either stimulate or repress gene activity, depending on which specific DNA sequence it targets. Now, another layer of control is drawing increased scrutiny, says Peter Fraser, a molecular biologist at the Babraham Institute in Cambridge, U.K.

Each nucleus contains discrete sites dubbed transcription factories, where DNA's code is copied into strands of messenger RNA. Growing evidence indicates that when a gene becomes active, its DNA moves to one of those factories. For genes, "where you are in the nucleus may be extremely important for your potential to become expressed," says Mark Groudine, a molecular biologist at the University of Washington School of Medicine and the Fred Hutchinson Cancer Research Center in Seattle. Earlier this month at a genome meeting,* Fraser added the latest twist to this emerging story: Genes whose proteins work together travel long distances within the nucleus to meet up in the same factories.

Transcriptional factories first came to light some 20 years ago, when Dean Jackson and Peter Cook, while at Oxford University, found that activated RNA polymerase II, the enzyme that transcribes DNA into messenger RNA, occurs in discrete clusters scattered throughout the nucleus. Cook, a biochemist, and Jackson, a molecular cell biologist, coined the term factories for these clusters, which their experiments suggested were at fixed spots in the

nucleus. "Everything you need to make a productive RNA is located [there]," says Jackson, who is now at the University of Manchester, U.K. Factories "provide an environment where transcription can occur with high efficiency."

Cook and Jackson suggested that genes move into such factories to be transcribed instead of recruiting transcriptional machinery to where they are. It was a heretical notion. Most researchers thought RNA polymerase II moves along stationary DNA during transcription, but the factory concept challenged that theory, suggesting that DNA is the more mobile component.

Researchers skeptical of Cook and Jackson's interpretation worried that the techniques used to study what was happening inside the nucleus corrupt the organelle's organization and lead to spurious results. Recently, however, Fraser and a half-dozen other researchers have worked out new visualization procedures that are much gentler on the nucleus. That has let them see more clearly what's happening with factories, even in three dimensions.

Fraser, for example, has studied genes key to production of hemoglobin, observing those genes moving into position at the factories. In 2002, he showed that a chromosome could flex and move crucial regulatory DNA, which is 50,000 bases from the β -globin gene it regulates, toward a factory. This DNA sequence, called a locus control region, "increases the gene's residency in the factories," thereby encouraging more gene activity, says Fraser. In a manner that's still not clear, the β -globin gene actually needs the locus control region to find its way to a factory, Groudine will report in the June issue of *Genes and Development*.

Fraser subsequently discovered that other genes involved in the synthesis of hemoglobin, ones on the same chromosome as β -globin but quite far away, also converge on the same factories. For example, an alpha-hemoglobin stabilizing gene is some 24 million bases away from the β -globin gene, yet it spends about 40% of its time in factories with this distant neighbor. "Nobody had thought that genes so far away could come together," says Fraser.

Even more impressive is the ability of genes on different chromosomes to congregate at a factory. Several recent studies have demonstrated this phenomenon. Last month, a team led by Andrew Hoffman of Stanford University in California described a role for the DNA-binding protein CTCF in helping the insulin-like growth factor 2 gene on chromosome 7 come together with another gene located on chromosome 11, allowing the genes to regulate one another's expression (*Science*, 14 April, p. 269). And in the 2 June 2005 issue of *Nature*, Richard Flavell of Yale University School of Medicine and his colleagues reported that the regulatory regions of genes involved in the fate of T helper cells positioned themselves side by side, possibly at factories, in anticipation of transcription—even though the regions and the genes were on different chromosomes. They observed this by adding formaldehyde to the nucleus to cause cross-linking of adjacent DNA. "These genes are finding each other at pretty high frequencies," says Fraser.

Groups of genes may be drawn to particular factories because they have transcription factors in common. But Fraser is finding that the strongest attraction for genes to a particular factory may instead be having a common goal, such as building hemoglobin. By fluorescently labeling forming mRNA sequences, he and his colleagues looked at the positioning in the nucleus of 30 genes undergoing transcription. "Physiologically related genes are coming into the same factory," he concludes. Such an arrangement makes sense, says Kelly Frazer, a genomicist at Perlegen Sciences in Mountain View, California, because transcribing a network of genes together should help maintain a proper balance of the genes' products.

Not everyone agrees with Peter Fraser's view of the nuclear landscape. Ana Pombo of the MRC Clinical Sciences Center at Imperial College London says her work indicates that factories are not stably located and that genes from different chromosomes are interacting all the time, both inside and outside factories. Nonetheless, other gene-regulation researchers are impressed by the latest finding from Fraser and his colleagues. "It's extraordinarily surprising that pairs of genes go through these maneuvers to be cotranscribed," says Peter Little of the University of New South Wales in Sydney, Australia. Adds Perlegen's Frazer, "It represents a paradigm shift in our way of thinking."

—ELIZABETH PENNISI

* The Biology of Genomes meeting, 10–14 May, Cold Spring Harbor, New York.

HIGH-ENERGY PHYSICS

Neutrino Hunters Plan a Voyage To the Bottom of the Sea

European researchers hope detectors deep in the Mediterranean will nab high-energy particles from the center of our galaxy

Astronomers will scale high mountains to get a clear view of the heavens, but a team of European researchers is taking the opposite tack. They are drawing up plans to build an observatory 3 kilometers down at the bottom of the Mediterranean Sea, looking downward.

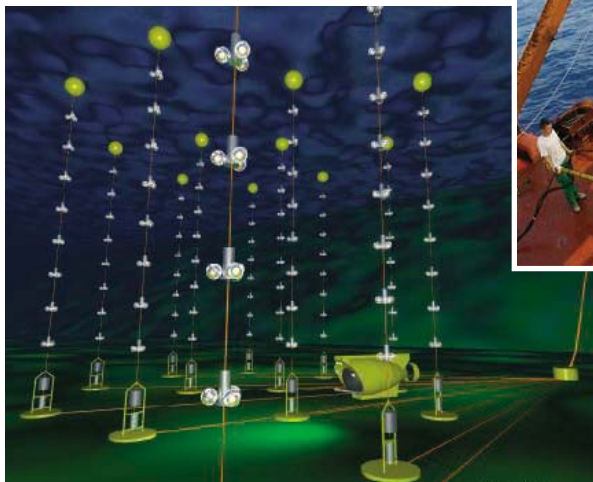
The team is not aiming to detect light or radio waves, but neutrinos—minuscule particles with virtually no mass that are created in the nuclear furnaces of stars and in violent events such as supernovas. Neutrinos rarely interact with normal matter—about 5×10^{34} of them pass through Earth every day—but every so often, one will collide with an atom and produce a brief flash of light. In the pitch dark of the sea floor, sensitive light detectors will be able to detect the flashes from neutrinos that have passed through Earth and will calculate where they came from. “It’s a totally different way of looking at the universe,” says John Carr of the Centre for Particle Physics of Marseilles in France.

The roots of this burgeoning field of neutrino astronomy lie in efforts beginning 4 decades ago to study neutrinos from the sun. Researchers built their neutrino traps—enormous tanks of fluid, such as perchloroethylene—deep below ground in mines, where overlying rock and the great bulk of Earth itself would shield them from particles such as cosmic rays. Two decades later, when several of these detectors picked up neutrinos that obviously came from supernova 1987A, astronomers started to get interested. Most neutrino telescopes now use water as the detection medium. Whenever a neutrino hits a nucleus in the water it produces muons, particles that streak along at more than the speed of light in water, shedding energy called Cerenkov radiation that is picked up by sensitive detectors called photomultipliers.

U.S. researchers led the way with an attempt at building a detector off Hawaii by anchoring arrays of detectors to the seabed and co-opting a large volume of seawater as the detection medium. But Dumand, as it was called, was abandoned in 1995 because of the difficulty and expense of installing sensitive detectors in deep open water. Instead, U.S. researchers took a dif-

ferent tack with a telescope called Amanda buried deep in the ice below the National Science Foundation’s base at the South Pole. In its 2 years of data collecting, Amanda has spotted thousands of neutrinos. But physicists think they are all local products created by cosmic rays bombarding Earth’s upper atmosphere—not visitors from deep space. A Russian-German team has adopted yet another approach: They drive onto the frozen surface of Siberia’s Lake Baikal during the winter and lower strings of detectors through holes into the murky depths.

Meanwhile, three European teams—one French, one Italian, and one Greek—have persisted with experiments to attach detectors to the seabed. The French team is the most advanced and is in the process of constructing a full observatory, called



Into the abyss. Researchers with the Antares project are putting anchors (above, right) on the seabed and attaching strings of detectors. They hope to install 12 by the end of 2007.

Antares, off the coast near Toulon. Carr, who is the spokesperson for the Antares project, thinks that after it is completed in 2007, it may have more luck than Amanda. Amanda’s Antarctic location, he explains, forces it to look outward from the galaxy, so any sources would be very distant. A Mediterranean observatory, by contrast, has most of our galaxy, including the center, in its field of view. “We can hope to see something that has not been seen before,” Carr says.

But neutrino researchers have already got bigger things on their minds. Kilometer-scale instruments are needed to really see astro-

physical sources,” says Uli Katz of the University of Erlangen in Germany.

Existing telescopes, researchers say, were based on theoretical estimates of the number of neutrinos produced by sources such as supernovas, gamma ray bursts, and active galactic nuclei. But in the past few years, data from a new generation of gamma ray telescopes, such as HESS in Namibia (*Science*, 3 September 2004, p. 1393)—which look at radiation from similar high-energy objects—show that the early estimates were too optimistic. Researchers working on Amanda now calculate that a detector needs a cubic kilometer of ice to thoroughly study astrophysical neutrinos. For the past 2 years, they’ve been building such a telescope, dubbed IceCube, also at the South Pole. Project director James Yeck of the University of Wisconsin, Madison, says they have drilled nine out of 70 planned boreholes and inserted strings of photodetectors. The project should be completed by 2011, he says.

European researchers are a few years behind, but the three separate Mediterranean projects decided a couple of years ago to combine their efforts. Earlier this year, they received €9 million from the European Union for a 3-year design study, led by Katz, and boosted by a similar amount from national funders. Team members say the project, known as the Kilometer Cubed Neutrino Telescope (KM3NeT), may cost about €200 million and could be completed by 2013. Only the design study has been funded so far, and no site has been chosen yet.

If the planned detector is built, researchers hope the neutrinos it captures will give insights into what is happening inside energetic sources and may shed light on high-energy particles called cosmic rays, whose source has been a mystery for decades. Some also hope to detect exotic dark matter, the mysterious stuff that makes up about a quarter of the mass of the universe. Some theories suggest that dark matter particles may accumulate in the core of bodies such as the galactic nucleus, or even inside stars such as our sun. When the particles annihilate each other, they produce neutrinos. Detecting them would be “a smoking gun for a dark matter population in the core of the sun,” says Lee Thompson of the University of Sheffield, U.K. project scientist for KM3NeT.

Carr believes that the unique nature of neutrinos will lead to unexpected discoveries. “Past history, such as with the gamma ray telescopes, has shown that many new objects can be found with a new type of instrument,” he says.

—DANIEL CLERY



“The Digital Library”

Vinton G. Cerf
Vice President and Chief Internet Evangelist
Google



“Online Books and Courses”

Amy Wu
Computer Science Student
Stanford University



“Publications”

Benjamin Mako Hill
Research Assistant
MIT Media Laboratory



“Conferences”

Maria Klawe
Dean of Engineering
Princeton University

ACM: KNOWLEDGE, COLLABORATION & INNOVATION IN COMPUTING

Uniting the world's computing professionals, researchers and educators to inspire dialogue, share resources and address the computing field's challenges in the 21st Century.



Association for Computing Machinery
Advancing Computing as a Science & Profession
www.acm.org/learnmore



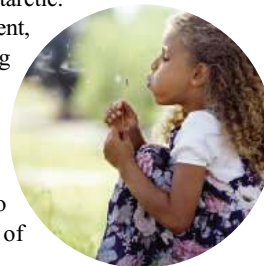
Politics

DON'T CITE MY WORK. Remote-sensing specialist Curt Davis was prepared for his 15 minutes of fame after this magazine published his article on the snowfall-driven growth of East Antarctic ice (*Science*, 24 June 2005, p. 1898). But it took nearly a year to attract serious media attention, and the inquiries were not what he expected: Global warming skeptics had made it the centerpiece of a new ad campaign.

"It was a complete misuse of what I was doing," says the University of Missouri, Columbia, researcher. "And I felt I had to respond."

The 60-second ad put out by the Washington, D.C.-based Competitive Enterprise Institute (CEI) shows Davis's paper as the narrator explains that "The Antarctic ice sheet is getting thicker, not thinner" (streams.cei.org). Not exactly, says Davis. His data can only show that the ice is growing in the interior of the East Antarctic. Emerging evidence suggests net shrinkage for the entire continent, he notes. Davis responded with a university press release refuting the ad—which also makes the point that CO₂ is life (right)—and this magazine criticized the ad for "selective referencing" that "misrepresents" the paper. A CEI press release then countered that Davis misunderstood his paper's bottom line.

"You know where they're coming from," says Davis, so "there's no point arguing with these people. There's a sense of futility; I can't say it's been pleasant."



MONEY MATTERS

PROLIFIC BUT HOMELESS. Scientists are protesting a decision to close the lab of a renowned pharmacologist at the National Institutes of Health as part of a budget-cutting exercise.

John Daly, a member of the U.S. National Academy of Sciences, has discovered hundreds of bioactive alkaloids in the skin of poisonous frogs, such as epibatidine, a potent painkiller. Daly retired in 2003 at age 69 but continues to work with two staff scientists at the National Institute of Diabetes and Digestive and Kidney Diseases (NIDDK). Despite working without pay, Daly co-authored 13 papers in the past year.

But last month, NIDDK Scientific Director Marvin Gershengorn decided to shutter Daly's program as part of a possible 20% cut in the NIDDK intramural operating budget for fiscal year 2007. Gershengorn declined comment, but NIDDK spokesperson Elizabeth Singer says an emeritus scientist with lab "privileges" is "unusual." The institute is closing at least two other labs, including that of chemist Donald Jerina.

More than two dozen scientists from around the world have urged NIH to keep Daly's lab open. "He's active as hell," says Cornell University chemical ecologist Thomas Eisner. "It's shortsighted." Singer says "options ... are being explored" for Daly to continue his research at NIH.

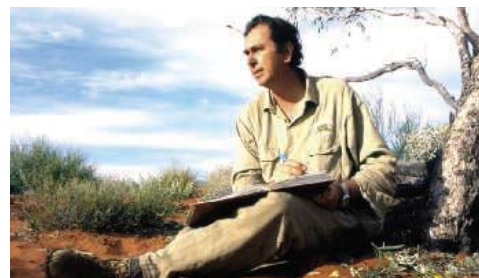


CREDITS (TOP TO BOTTOM): UNIVERSITY OF MISSOURI, COLUMBIA; GETTY; STEPHEN SCOURFIELD; JOHN DALY

They Said It

"We need to put the engineering back into the Army Corps of Engineers."

—Robert Bea, a civil engineering professor at the University of California, Berkeley, releasing the findings of a National Science Foundation-funded study last week on why the levees in New Orleans collapsed during last summer's devastating Hurricane Katrina. The study cites technical and institutional problems within the U.S. Army Corps of Engineers, which was responsible for building and maintaining the levees.



Movers >>

CROSSING HEMISPHERES. An expert on evolution and conservation biology in the world's oldest landscapes has been named director of the U.K.'s Royal Botanic Gardens, Kew. Stephen Hopper, a professor of plant conservation biology at the University of Western Australia in Perth, will succeed Peter Crane in October (*Science*, 25 November 2005, p. 1275).

Hopper, 54, has done research in southwest Australia, South Africa's Cape region, and the Venezuela-Guiana highlands and is former chief of Kings Park and Botanic Garden in Perth. Calling Kew's 250-year-old collection of 7 million specimens an "unparalleled library and herbarium," Hopper says he's eager to expand Kew's international work on biodiversity, including a project to store germ plasm from 10% of Earth's flora. He also hopes to increase public access to the collections.

Got a tip for this page? E-mail people@aaas.org

Call for Sustainability Science papers

PNAS is pleased to announce the launch of a section on Sustainability Science, a vibrant area encompassing fundamental research on interactions between human and environmental systems, as well as sustainability challenges relating to agriculture, biodiversity, cities, energy, health, and water.

Why Submit to PNAS?

- **Premier multidisciplinary science journal**
- **Fast online submission and peer review**
- **No need for Academy Member sponsorship**
- **Worldwide authors and readers**



Submit your manuscript today

Contact Dr. Jennifer Byers at jbyers@nas.edu
for more information.

www.pnas.org/misc/sustainability.shtml

PNAS

Proceedings of the National Academy of Sciences of the United States of America

Qs & AAAS



www.sciencedigital.org/subscribe

For just US\$99, you can join AAAS TODAY and start receiving *Science* Digital Edition immediately!

Qs & AAAS



www.sciencedigital.org/subscribe

For just US\$99, you can join AAAS TODAY and start receiving *Science* Digital Edition immediately!

The Americas BC

1313



DNA databases and criminal justice

1315



Hormone as food sensor

1317



LETTERS | BOOKS | POLICY FORUM | EDUCATION FORUM | PERSPECTIVES

LETTERS

edited by Etta Kavanagh

New Scientific Society in Nicaragua

IN MARCH OF THIS YEAR, *SCIENCE* PUBLISHED AN Editorial entitled “Fighting tropical diseases” (J. D. Sachs and P. J. Hotez, 17 Mar., p. 1521) discussing science-based approaches to address the UN Millennium Development Goals. Additionally, in the past few months, *Science* has reported on recent efforts to improve Africa’s capacity in science, including the creation of science academies in various African countries. Because the motivation behind all these efforts is, in part, the urgent need to address extreme poverty, other low-income countries such as Nicaragua could benefit from similar initiatives.

Within Latin America, Nicaragua is a latecomer in promoting the use of science as a tool for economic development. Although scientific councils were created in most countries in the 1960s, in Nicaragua, it wasn’t until 2002 that such a council (CONICYT) was first established. Even so, the lack of funding and working ties with the scientific community has rendered the council ineffective.

“The organized engagement of scientists to make their voices heard could **finally put science on Nicaragua’s national agenda.**”

—Huete-Pérez

Despite these difficulties, Nicaragua is currently experiencing a rapid period of scientific growth, particularly in the health sciences and biotechnology research. A recent report (1) by various members of the InterAmerican Network of Academies of Sciences (IANAS) praises the scientific achievements of Universidad Centroamericana and other Nicaraguan universities, but stresses that national planning and coordination are necessary for a stronger scientific enterprise.

In light of these recommendations and in an effort to build on this momentum, leading scientists have organized the Nicaraguan Society for Science as an essential step toward the creation of a Nicaraguan Academy of Sciences. In addition to providing independent advice to the government, such an academy would be able to help prepare a strategy to support science-based economic development.

For this effort to make headway, decision-makers will need to be persuaded of its value and be determined to allocate financial support. The organized engagement of scientists to make their voices heard could finally put science on Nicaragua’s national agenda.

JORGE A. HUETE-PÉREZ

Director, Molecular Biology Center, Universidad Centroamericana, UCA, Apartado 69, Managua, Nicaragua. E-mail: huete@ns.uca.edu.ni

Reference

1. H. Alper, M. Clegg, H. Ramkissoon, Report on the Inter American Network of Academies of Science (IANAS) visit to the Universidad Centroamericana, 16 to 18 Feb. 2006 (unpublished report).

Examining Knowledge of Geometry

IN THEIR REPORT “CORE KNOWLEDGE OF GEOMETRY in an Amazonian indigene group” (20 Jan., p. 381), S. Dehaene *et al.* present evidence that an isolated Amazonian group, the Mundurukú, are able to understand geometric concepts. They state that geometry constitutes “a core set of intuitions present in all humans.” I disagree with the basic concept of this investigation.

The central feature of Euclidean geometry is its demonstrative character and its logical structure, rather than graphical pictures of triangles, circles, etc. This logical system is built upon two pillars: (i) the concept of the “theoretical object,” e.g., the abstract metaphysical idea of a circle, rather than a real constructed circle; and (ii) the deductive mathematical proof, based purely on axioms and postulates.

Other civilizations dealt with geometrical

figures in a more intuitive way, and their activities cannot be characterized as geometry in the Euclidean sense. Ancient civilizations other than the Greeks did not develop a demonstrative geometry. For example, the ancient Chinese never developed a theoretical geometry (1–3).

The topic being investigated by Dehaene *et al.* is simply pattern recognition. It is by no means surprising that the people tested recognized different geometric figures, since they can recognize, e.g., human faces and identify different species of tree by their silhouettes.

KARL WULFF

Geschamp 15, D-29640 Schneverdingen, Germany. E-mail: karl.ah.wulff@t-online.de

References

1. J. Needham, *Science and Civilisation in China*, vol. 3, *Mathematics and the Science of the Heavens and the Earth* (Cambridge University Press, Cambridge, 1959), p. 91.
2. G. F. Leibniz, *Novissima Sinica* (ed. 2, 1699), section 9.
3. C. Cullen, *Astronomy and Mathematics in Ancient China: The Zhoubi Suanjing* (Cambridge University Press, Cambridge, 1996), pp. 77, 219.

IN THEIR REPORT “CORE KNOWLEDGE OF GEOMETRY in an Amazonian indigene group” (20 Jan., p. 381), S. Dehaene *et al.* present research documenting the Brazilian Mundurukú Indians’ ability to understand concepts of geometry and to orient themselves spatially. This team, as well as the scholars mentioned in C. Holden’s article “Hunter-gatherers grasp geometry” (News of the Week, 20 Jan., p. 317), might be interested to learn that over 200 years ago, the great Brazilian naturalist Alexandre Rodrigues Ferreira also observed this innate ability of indigenes. In his memoirs of Amazonian zoology and botany [published collectively as the *Viagem Filosófica* (1)], he posed the question “what would a European, brought up like an Indian and ignorant of geometry, geog-



Amazonian Mundurukú villager reading a map to identify a hidden object.

raphy and hydrology, do if asked about a river's direction, branching and neighboring villages?" (p. 93, my loose translation). Anticipating Dehaene *et al.*, Ferreira conducted an experiment and asked this question of a Tapuio Indian, who by tying together several cords was able to create an approximate map of the local river and its tributaries, as well as point out the location of Indian villages. Further, Ferreira wrote that a Macuxí Indian he encountered not only drew an intelligible map of local river patterns and scaled hut outlines using a stick to trace lines in sand, but when presented with a pen and ink rendered the same idea on paper. Clearly, the naturalist understood native Brazilians not only to be reasoning individually, but capable of understanding geometric and geographic concepts. Thus, on the basis of his own experiments, Ferreira would have agreed with Dehaene *et al.*'s conclusion that "geometrical knowledge arises in humans independently of instruction, experience with maps or measurement devices, or mastery of a sophisticated geometrical language."

ROBERTA M. DELSON

Division of Anthropology, American Museum of Natural History, New York, NY 10024, USA, and Department of History, Drew University, Madison, NJ 07940, USA.

Reference

1. A. R. Ferreira, *Viagem Filosófica pelas capitânicas do Grão Pará, Rio Negro, Mato Grosso e Cuiabá*, vol. 2, *Memórias zoológica e botânica* [manuscript 1783–1792] (reprinted by the Conselho Federal de Cultura, Rio de Janeiro, Brazil, 1974).

Response

WULFF CONTRASTS PROCESSES OF DEDUCTIVE reasoning based on the axioms and postulates of Euclidean geometry with processes of visual pattern recognition, and he suggests that the latter processes underlie performance on our tests of geometrical categorization and map use. Our tasks were designed to assess geometrical concepts at a higher level of representation. Recognition of visual patterns is orientation-specific (*I*), yet both our tasks required that the Mundurukú abstract geometrical relations from figures that varied in orientation. The Mundurukú's globally high performance, particularly in the map task which requires a transformation from two to three dimensions, cannot plausibly be attributed to low-level processes of visual pattern recognition and implies extraction of genuine geometrical invariants.

Our tasks also do not depend on processes of deductive reasoning. Although geometry now appears as a beautiful logical construction, logic and deduction are neither necessary nor sufficient to account for core human geometrical concepts and intuitions. The central intuitions of Euclidean geometry cannot be deduced from simpler axioms, as the history of mathematics and physics attests (2): Absent the problematic and unprovable parallel postulate, Euclid's axioms and postulates support an infinite family of geometries at odds

with human intuition. Geometrical intuitions nevertheless come naturally to the human mind and continue to guide commonsense reasoning about space, even in scientists who have come to believe, by deduction and experiment, that the classical three-dimensional view of space fails to capture the structure of the universe (3).

We thank Delson for drawing our attention to Alexandre Rodrigues Ferreira's report. His informal observations on map-making appear to antedate ours by two centuries. Insofar as his observations were found to be general, they would confirm that the capacity to understand maps predates the most serious intrusions of Western culture. Caution is required in evaluating such ancient reports, but both Ferreira's report and our research suggest that all human cultures share an approximate arithmetic and intuitive geometry, which are highly stable over variations in education, language, and intercultural contact. On this point, we distance ourselves from claims of a radical "incommensurability" of cognitive functions in other cultures such as the Pirahã (4, 5), which are sometimes lumped together with our own views.

Research on core knowledge of geometry is at an early stage. How do geometrical concepts emerge in children? Are these concepts unique to humans or shared by other animals? What accounts for the distinctive profile of geometrical abilities shown both by indigenous tribes and by urban Americans? Converging studies across species, ages, and cultures, using methods of psychology and neuroscience, can begin to address these questions.

STANISLAS DEHAENE,^{1,2*} VÉRONIQUE IZARD,^{1,4}
PIERRE PICA,³ ELIZABETH SPELKE⁴

¹INSERM-CEA Cognitive Neuroimaging Unit, Service Hospitalier Frédéric Joliot, Commissariat à l'Énergie Atomique, 91401 Orsay Cedex, France. ²Collège de France, 11, place Marcelin Berthelot, 75231 Paris Cedex 05, France. ³Unité Mixte de Recherche 7023 "Formal Structure of Language," CNRS and Paris VIII University, Paris, France. ⁴Psychology Department, Harvard University, Cambridge, MA 02139, USA.

*To whom correspondence should be addressed. E-mail: dehaene@shfj.cea.fr

References

1. I. Rock, *Orientation and Form* (Academic Press, New York, 1973).
2. G. Hatfield, *The Natural and the Normative* (MIT Press, Cambridge, MA, 1990).
3. L. Randall, *Warped Passages* (Ecco, New York, 2005).
4. D. Everett, *Curr. Anthropol.* **46**, 621 (2005).
5. P. Gordon, *Science* **306**, 496 (2004).

Ecological Revitalization of Chinese Villages

I READ R. STONE'S ARTICLE "VILLAGERS DRAFTED into China's model of 'sustainability'" (News of the Week, 7 Apr., p. 36) with great interest. In my 16 years investigating long-term ecological

changes in rural China, I have witnessed numerous governmental programs aiming to link improved rural livelihoods with ecological revitalization of village landscapes (1–3). Energy self-sufficiency and improved land management have been central to all of these programs, which have combined national and provincial policy and organizational efforts with demonstration villages, townships, counties, and even provinces. Although often only modestly successful, China's efforts to improve rural environments are an absolute triumph when compared with those of most rural developing countries and compare well with those of many developed countries during their own industrial transition.

The convergence of national and international environmental agendas on a single rural village will inevitably cause conflict. And Huangbaiyu will probably end up as have other village experiments: Temporary improvements will ultimately be dwarfed by the needs of local people to adapt to the developments going on around them. Although local demonstration projects might therefore be avoided, these can help to highlight and fix problems before more extensive programs are implemented. Regardless, the failings of a single village experiment should be presented as a minor part of the main story. China and the Chinese continue to make major efforts, by many means, to make the best of what is arguably the greatest environmental challenge any human population has ever faced (4).

ERLE C. ELLIS

Department of Geography and Environmental Systems, University of Maryland, Baltimore County, 211 Sondheim Hall, 1000 Hilltop Circle, Baltimore, MD 21250, USA.

References

1. X. Cheng, C. R. Han, D. C. Taylor, *World Dev.* **20**, 1127 (1992).
2. T. Shi, *Ecol. Econ.* **42**, 359 (2002).
3. "Opinion: Document shows determination to build a new countryside," *People's Daily Online*, 23 Feb. 2006 (http://english.people.com.cn/200602/23/eng20060223_245370.html).
4. V. Smil, *China's Environmental Crisis, an Inquiry into the Limits of National Development* (M.E. Sharpe, New York, 1993).

Stereotype Threat: A Clarification

THE REVIEW BY D. LEWIS (24 JUNE 2005, P. 1871) of the book *Gender Differences in Mathematics (I)* inadvertently perpetuates misinformation that has appeared elsewhere (2–4) about a key finding in our study of stereotype threat on an Advanced Placement calculus test (5, 6).

The study investigated whether asking women to record their gender immediately before taking the test elicited stereotype threat and thereby adversely affected their test performance. A quote in the review from a chapter in the book (4) cites an erroneous statistic from our initial technical

Letters to the Editor

Letters (~300 words) discuss material published in *Science* in the previous 6 months or issues of general interest. They can be submitted through the Web (www.submit2science.org) or by regular mail (1200 New York Ave., NW, Washington, DC 20005, USA). Letters are not acknowledged upon receipt, nor are authors generally consulted before publication. Whether published in full or in part, letters are subject to editing for clarity and space.

report (5), corrected in our subsequent article (6), that women asked their gender before the test scored significantly lower than those asked afterward. In fact, the mean difference between the two groups of women was not statistically significant. Another quote from the same chapter repeats an estimate (made by a referee in a privileged review of a draft of our article) that “as many as 2837 additional women per year” (about 47,000 took the test at the time of the study) would pass the test, earning advanced credit for calculus, if they were asked about their gender after the test rather than before it. This estimate is unreliable. It is based on rough calculations and extrapolations from the atypical sample of test takers in the study.

In short, this study of actual test taking, in common with our replication that examined community college students being given place-

ment tests for algebra and arithmetic (6), found no evidence of the deleterious effects of stereotype threat on the performance of women on quantitative tests that have been observed in laboratory experiments (4).

LAWRENCE J. STRICKER*

Educational Testing Service, Princeton, NJ 08541, USA.

*Any opinions expressed in this letter are those of the author and not necessarily of Educational Testing Service.

References

1. A. M. Gallagher, J. C. Kaufman, Eds., *Gender Differences in Mathematics* (Cambridge Univ. Press, Cambridge, 2005).
2. J. Aronson, in *Improving Academic Achievement*, J. Aronson, Ed. (Academic Press, San Diego, CA, 2002), pp. 279–301.
3. C. M. Steele, S. J. Spencer, J. Aronson, in *Advances in Experimental Social Psychology*, vol. 34, M. Zanna, Ed. (Academic Press, San Diego, CA, 2002), pp. 379–440.
4. P. G. Davies, S. J. Spencer, in (1), pp. 172–188.
5. L. J. Stricker, *Inquiring About Examinees' Ethnicity and Sex: Effects in AP Calculus AB Examination Performance* (College Board Report No. 98-1, ETS RR No. 98-5, College Entrance Examination Board, New York, 1998).
6. L. J. Stricker, W. C. Ward, *J. Applied Soc. Psychol.* **34**, 665 (2004).

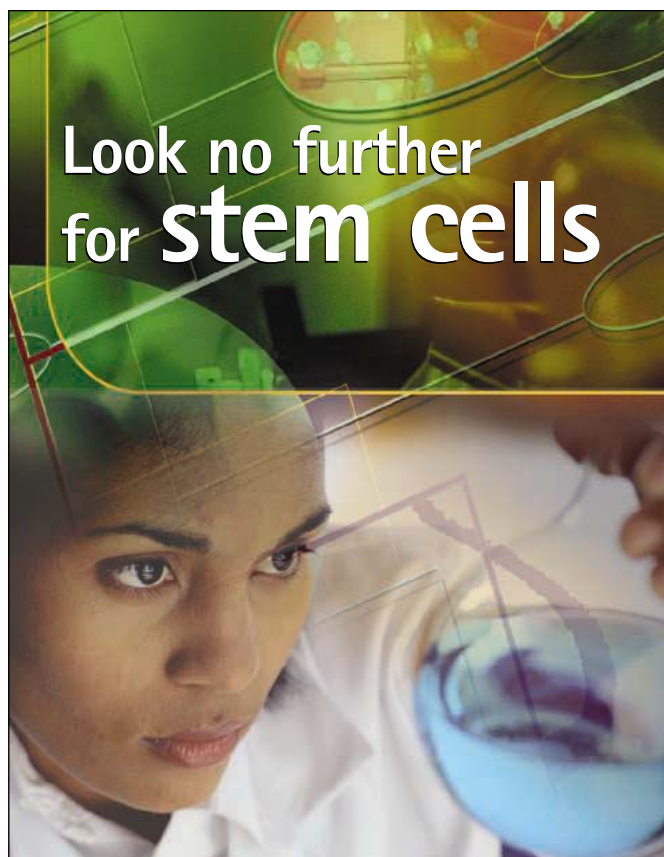
Response

MY USE OF A QUOTATION INCLUDING “SIGNIFICANTLY” WITHOUT qualification or explanation was indeed ambiguous and open to misinterpretation. Neither gender alone nor the interac-

tion of gender and the experimental–control (E-C) conditions was found to have a sufficiently large effect on AP grades to meet the standard of practical significance used by Stricker and Ward (1). However, the difference in the mean grades for the experimental and control groups of girls does meet a widely accepted standard of statistical significance, whether the means (2.62 and 2.41) reported in the original report (2) or those (2.61 and 2.41) reported in (1) are used.

Assuming normal means, the mean difference in boys' and girls' grades within the experimental group has the 95% confidence interval (3) 0.16 ± 0.18 , while the mean difference within the control group is 0.51 ± 0.17 . The mean difference for the experimental and control groups of girls is 0.20 ± 0.18 ; that for boys is -0.15 ± 0.16 . (If the stereotype threat/lift hypothesis is correct, the experimental conditions should improve girls' performance and degrade boys'.) By way of comparison, note that in the introduction to their paper, Stricker and Ward describe the mean difference of 0.31 for boys and girls taking the exam in 1995 as substantial [(1), p. 669].

As regards the AP exam, practical significance seems to be the appropriate measure—the costs and possible unintended consequences of attempting to neutralize a very small



Stem cells, bone marrow, cord blood, placenta and umbilical cord products

- Bone marrow, fresh and cryopreserved
- CD34⁺ cells from bone marrow
- CD34⁺ depleted bone marrow
- CD34⁺ cells from cord blood
- CD31⁺ / CD45 - endothelial progenitor cells
- Multiple expanded cell lines
- Placenta
- Umbilical cords

Full quality assurance data supplied.

For more information or to place an order call NDRI at 800-222-6374 or email us at cells@ndriresource.org

Visit NDRI online at www.ndriresource.org to apply for human tissues, organs and derivatives.

NDRI is The National Resource Center serving scientists throughout the nation for more than twenty-five years with human tissues, organs and derivatives.

- Not-for-profit
- Funded by the National Institutes of Health



N A T I O N A L D I S E A S E R E S E A R C H I N T E R C H A N G E

effect don't seem justified. However, given the inherent limitations of laboratory tests of stereotype threat—the stress and motivation associated with the AP, SAT, and GRE exams presumably aren't easily reproduced in the lab—and the obvious ethical and practical restrictions on experimentation with the actual exams, small but statistically significant differences resulting from apparently subtle changes in the exams may merit consideration as experimental results and as reality checks. If something as seemingly innocuous as filling in the appropriate gender bubble can have an effect on mathematical performance comparable in size to the effect of gender itself, we should think carefully about just how big the gender gap in mathematics really is, and what the effects of the popularization of that gap may be.

DEBRA LEWIS

Institute for Mathematics and Its Application, University of Minnesota, 40 Lind Hall, 207 Church Street, SE, Minneapolis, MN 55455, USA.

References and Notes

1. L. J. Stricker, W. C. Ward, *J. Appl. Soc. Psychol.* **34** (no. 4), 665 (2004).
2. L. J. Stricker, *Inquiring About Examinees' Ethnicity and Sex: Effects in AP Calculus AB Examination Performance* (College Board Report No. 98-1, ETS RR No. 98-5, College Entrance Examination Board, New York, 1998).

3. Given two samples of size n_1 and mean μ_j , $j = 1, 2$, with common standard deviation SD , the 95% probability confidence interval of the mean difference (assuming normal means) is approximately

$$\mu_1 - \mu_2 \pm 1.96 SD \sqrt{\frac{1}{n_1} + \frac{1}{n_2}}$$

The means are considered different if the interval does not contain the origin. See, e.g., (4).

4. "Multiple Comparisons: Comparison of Normal Means," in *Encyclopedia of Statistical Sciences* (Wiley, New York, 2005) (online version).

CORRECTIONS AND CLARIFICATIONS

Policy Forum: "Incidental findings in brain imaging research" by J. Illes *et al.* (10 Feb., p. 783). On page 784, the DOI is incorrect; it should be 10.1126/science.1124665. The DOI is correct in the online version.

Reports: "Freezing as a path to build complex composites" by S. Deville *et al.* (27 Jan., p. 515). The symbols for author attributes were incorrect. S. Deville is the author to whom correspondence should be addressed (e-mail: sdeville@lbl.gov), and the present address for R. K. Nalla is Intel Corporation, 5000 West Chandler Boulevard, Chandler, AZ 85226, USA.

TECHNICAL COMMENT ABSTRACTS

Comment on "HST2 Mediates SIR2-Independent Life-Span Extension by Calorie Restriction"

Matt Kaerberlein, Kristan K. Steffen, Di Hu, Nick Dang, Emily O. Kerr, Mitsuhiro Tsuchiya, Stanley Fields, Brian K. Kennedy

Calorie restriction (CR) increases life span in yeast independently of Sir2. Lamming *et al.* (Reports, 16 September 2005, p. 1861) recently proposed that Sir2-independent life-span extension by CR is mediated by the Sir2 paralogs Hst1 and Hst2. Contradictory to this, we find that CR greatly increases life span in cells lacking Sir2, Hst1, and Hst2, which suggests that CR is not mediated by Sir2, Hst2, or Hst1.

Full text at www.sciencemag.org/cgi/content/full/312/5778/1312b

Response to Comment on "HST2 Mediates SIR2-Independent Life-Span Extension by Calorie Restriction"

Dudley W. Lamming, Magda Latorre-Esteves, Oliver Medvedik, Stacy N. Wong, Felicia A. Tsang, Chen Wang, Su-Ju Lin, David A. Sinclair

Our two labs and others have shown that SIR2 controls the life span of diverse species, including *Saccharomyces cerevisiae* and *Drosophila melanogaster*, and that deleting SIR2 blocks life-span extension by calorie restriction. The methods of Kaerberlein *et al.* allow yeast to bypass the requirement for SIR2 and its homologs, which brings into question their suitability for modeling the physiology of more complex organisms.

Full text at www.sciencemag.org/cgi/content/full/312/5778/1312c

NUDE MOUSE MODELS AND SERVICES



CD-1[®] nude
BALB/c nude
NIH-bg-nu-xid
NU/NU

Excellent availability of immunodeficient models from Charles River provides customers with high quality nude mice for their research and supports our expanded preclinical xenograft services.

US: 1.877.CRIVER.1
Europe: info@eu.crl.com
WWW.CRIVER.COM


CHARLES RIVER
LABORATORIES
Research Models and Services

cystic fibrosis foundation
THERAPEUTICS inc.

Enabling Technologies for CF Therapies

Cystic Fibrosis Foundation Therapeutics, Inc. (CFFT), a non-profit affiliate of the Cystic Fibrosis Foundation, announces a new award program to support application of emerging technologies toward restoring function to the genetically defective protein responsible for cystic fibrosis (CF) in patients. The most common mutation in the cystic fibrosis transmembrane conductance regulator (CFTR) protein lacks phenylalanine 508 ($\Delta F508$ CFTR) and undergoes premature degradation at the endoplasmic reticulum, leading to production of fewer folded CFTR proteins. The $\Delta F508$ CFTR proteins that do reach the airway epithelial cell surface have compromised chloride channel activity. Over the years, CFFT and the Cystic Fibrosis Foundation have focused on identifying and taking advantage of leading edge technologies to expand understanding of CF with the aim of giving insight into potential new therapies. Our efforts in high throughput screening, structural genomics, and more recently, siRNA, have expanded our therapeutic pipeline and the understanding of the basic defect in CF. We are now searching for new and/or complementary approaches that will facilitate the identification and evaluation of novel compounds and new drug target pathways in the $\Delta F508$ CFTR processing pathway. CFFT will provide as much as \$1,000,000 annually for up to three years in support of research directed at these problems. Established investigators within academic institutions or biopharmaceutical companies with a potentially applicable technology or therapeutic hypothesis are strongly encouraged to apply, irrespective of expertise in CF biology or physiology.

Persons interested in this opportunity should contact **Chris Penland, Ph.D.** at (301) 907-2520 or cpenland@cfft.org for programmatic information. A letter of intent, due by **July 1, 2006** will be required and should be sent to CFFTawards@cffttherapeutics.org.

ANTHROPOLOGY

Picturing the Pre-Columbian Americas

Dean R. Snow

American Indians have inhabited the continents of the Western Hemisphere for fourteen, give or take a couple, millennia, having arrived from northeastern Asia as very small, biologically modern human populations. At the time, humans everywhere lived in simple hunter-gatherer societies, although their languages and intellectual capabilities were equivalent to those of anyone living today. The subsequent cultural evolution of American Indians took many of them along developmental paths to tribes, chiefdoms, states, and empires that paralleled cultural developments on most of the other inhabited continents. Farming, writing, music, arts, crafts, politics, war, and all the other traits that make up human culture were as much a part of this process in the Americas as anywhere else. Still, everything changed for them with the advent of globalization, for which 1492 is a convenient benchmark.

The long history of the American Indians from their first arrival to the first voyage of Columbus is important to their living descendants because it is their heritage. It is inherently important to other modern Americans because it is embedded in the landscape we all share. And it is important to science because in 1491 the societies of the Americas, from the simplest to the most complex, were remarkably like those of what we still like to call the Old World, despite their virtually complete mutual isolation since well before the end of the Pleistocene. Were it not for the American Indians, we could never be quite sure that things like urbanism, state religion, literacy, and empire were all elements of universal but latent human potential back when nobody had so much as dreamed of any of them.

Native Americans were at an adaptive disadvantage in their collision with European, African, and Asian cultures in what Columbus called the "Other World." The Americans lacked the wide range of grains, vehicles, domesticated animals, and (ironically) the diseases that gave Europeans the edge. Epidemics

decimated the Americans ahead of the inexorable European conquest, a process so pervasive that many modern Americans are unaware of what Native Americans were like before 1492. It is this ignorance that Charles Mann has sought to rectify with *1491: New Revelations of the Americas Before Columbus*.

That is a noble purpose, and Mann (a contributing correspondent for *Science*) is an able writer, but there are potential pitfalls. Most of the long history of American Indians is known mainly through the incomplete record of archaeology—with epigraphy, genetics, historical linguistics, oral traditions, and a few other subjects providing additional lines of evidence. Scientific inference from these clues entails its own hazards, and in a popular book

there is the additional constant risk of overstatement when one's purpose is to convince the reader that credit has not been given where it was due. There is also the temptation to proffer as "new revelations" findings that have been known and written about for decades. Mann has sidestepped some, but not all, of these pitfalls.

The author's approach is anecdotal, covering subjects that interest him and about which he has acquired a reasonably deep knowledge. His chapters touch on New England, Peru, Mexico, eastern Brazil, the Mississippi Basin, Guatemala, the Amazon lowlands, and the lower Great Lakes, sometimes repeatedly and in no particular order.

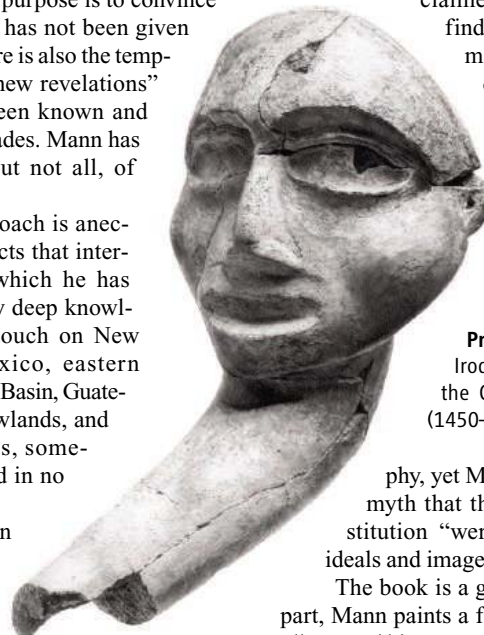
Along the way, Mann shoots down popular misconceptions that have been previously refuted by various authorities. I will cite just a few. Tisquantum (Squanto) was a skilled and well-traveled politician, not an innocent dupe of the New England Pilgrims. Surprisingly simple hunting societies encountered in interior South America were the scattered remnants of more complex societies that had been devastated by epidemics, not pristine survivors from the stone age. Pizarro and Cortés

defeated American Indian empires because they had guns, cavalry, and germs on their side, not because the Incas and Aztecs were hobbled by superstition and other forms of inferiority. The American landscape was an anthropogenic one for millennia, which reverted temporarily to wilderness between the epidemic decline in Indian populations and resettlement by expanding Europeans. Deep anthropogenic soils and other archaeological evidence in the Amazon lowlands indicate that before 1492 Indian populations were much larger there than previously suspected. The last finding was particularly inspiring for the author.

Unfortunately the book also contains overstatements, errors, and speculations of the kinds that creep in when an author's purpose is to make a strong case for a thesis. Again, I will cite just a few. It is unnecessary to argue that Europeans were "unbearably dirty" to make the case that Indians were not filthy savages or to repeat Henry Dobyns's wildly inflated population estimates to make the case that colonial era epidemics were unprecedented in their devastation—everybody was smelly in 1491, and 60% mortality is horrendous no matter what the absolute size of the population. Older is better in popular books, and Brazil's Lagoa Santa skeletons are dusted off again. But none

of the surprisingly early dates claimed for these and other finds in eastern Brazil meet minimum scientific standards for reliability. The Great Law of the Iroquois is very different from the U.S. Constitution. The framers of the latter were inspired mainly by European philoso-

Pre-contact pipe. A Mohawk Iroquois effigy pipe found at the Ostungo, New York, site (1450–1525).



phy, yet Mann repeats the modern myth that the framers of the Constitution "were pervaded by Indian ideals and images of liberty."

The book is a good read. For the most part, Mann paints a fair picture of American Indians, and his account is largely free of fawning political correctness. But readers who know the subject well will question the polemics, erratic organization, and various factual statements. Critical readers should use *1491* only as a starting point, following the author's excellent notes and bibliography to explore more specific topics in the vast literature pertaining to Columbus's Other World.

10.1126/science.1128736

1491

New Revelations of the Americas Before Columbus

by Charles C. Mann

Knopf, New York, 2005. 478 pp. \$30, C\$40. ISBN 1-4000-4006-X.

Ancient Americans

Rewriting the History of the New World

Granta, London, 2005. £20. ISBN 1-86207-617-0.

The reviewer is at the Department of Anthropology, Pennsylvania State University, 409 Carpenter Building, University Park, PA 16802, USA. E-mail: drs17@psu.edu

NEUROSCIENCE

A Mostly Sure-Footed Account of the Hand

Charles G. Gross and Asif A. Ghazanfar

In one of the first systematic attempts to describe the differences between primates and other mammals, Thomas Huxley argued that the former are distinguished by virtue of their adaptation to arboreal life (1). Central to this arboreal life is the grasping hand. Indeed, the primate hand is so fundamental to how we define ourselves that some, including Friedrich Engels (2), have claimed that hand use (particularly with tools) was the driving force that gave rise to our sophisticated cognitive abilities. Though this idea is an overstatement, our hands do represent a masterpiece of Darwinian evolution; its elegant design is on a par with the eyes and ears.

What is so special about primate hands? Few, if any, are more qualified to answer this question than Vernon Mountcastle. He and his colleagues have been the leading students of somatic sensibility (“somesthesia”) in primates for over half a century. In *The Sensory Hand*, he offers an overview of a lifetime of influential, and sometimes controversial, research. The massive treatise begins with a review of the evolution and structure of the human hand. Mountcastle then ventures forth on a journey from manual behavior to tactile receptors all the way to the cerebral cortex. Through sixteen lengthy chapters, he reviews each level of the somatosensory pathway in rich detail. To give a sense of scale: there are chapters devoted to “Large-Fibered Peripheral Interface,” “Ascending Spinal Cord Systems of Intrinsic Origin,” “Postcentral Somatic Sensory Cortical Areas in Primates,” and the “Parietal Frontal Sensory–Motor Transition.”

Although the book is large and comprehensive, its intended audience is unclear. Is it meant to serve as a textbook, a critical review, or a theoretical statement? As a textbook, it provides a valuable summary of many aspects of somesthesia. The chapter on the various uses of somatosensory stimulation as a substitute for vision is a particularly welcome treat. However, unlike most modern textbooks, the illustrations are generally poor, usually appropriated, sometimes marginally legible and without adequate legends, and replete with unnecessary and unexplained detail. Some crucial figures—such as one showing the basic features of the hand

(e.g., phalanges, metacarpals, and saddle joint)—are entirely absent. In another puzzling aspect of the production, the lengthy reference list includes a number of papers that we could not find mentioned in the text as well as a number of misspellings of author names. Lastly, there is essentially no mention of subjects of great interest to contemporary students (beginning or advanced), such as handedness, gestures, and tool manufacture. Surely handedness is directly relevant to the sensorimotor processing of tactile inputs, given that there is a direct link between lateralized hand use and sensorimotor skill in both humans and chimpanzees and, further, a putative link between these skills and the size of motor cortex. Such a discussion would have played nicely into an otherwise outstanding chapter on cortical plasticity.

As a critical review of exciting developments in the field today or as a theoretical statement, the book is even more deficient. One of the most important recent developments is the discovery by Giacomo Rizzolatti and his colleagues of “mirror neurons,” which respond both when a subject performs an action and when the subject observes the same action performed by another individual. These actions are often specific to particular types of grasping. Existing in humans and nonhuman primates, they are thought to be a neural link in understanding the social intentions of others and, perhaps, imitation and speech perception in humans. Although Mountcastle deals with the anatomy of the premotor area in which these neurons are found (“area F5”) and lists several papers by Rizzolatti’s group on mirror neurons in the references, he never mentions the phenomenon in the text.

In the past, Mountcastle has made strong claims for the existence of “command neurons” in parietal cortex that underlie reaching for visual targets. He hypothesized that these neurons receive afferent signals descriptive of the position and movement of the body in space and contain a “command apparatus” for operation of the hands, limbs, and eyes within extrapersonal space. He argued that these neurons encode behavioral goals, not the details of their execution. Curiously, Mountcastle does not discuss these earlier claims or the controversy surrounding them, although several of his papers on this subject appear in the reference list. This is unfortunate, because recent work by Rizzolatti and his colleagues (3)—perhaps unavailable when the book went to press—support Mountcastle’s idea, at least in part. Their findings confirm that some parietal neurons have motor functions and

encode behavioral goals. However, unlike Mountcastle’s claims, their and others’ results indicate that these parietal cells provide representations of potential actions rather than commands to move.

Another topic currently of major interest is multisensory integration, the phenomenon where neurons respond to more than a single sensory modality. For example, cells in the ventral intraparietal area and ventral premotor cortex respond to both somatosensory and visual stimulation. They have visual receptive fields “attached” to tactile receptive fields on the hand and thus move in space as the hand moves even when the eyes remain stationary. Even in primary somatosensory cortex, neurons can respond to visual stimuli and receive connections from the visual cortex, including the middle temporal (MT) area. Furthermore, tactile object recognition (haptics) by normal human subjects activates a large swath of extrastriate visual cortex. A discussion of these tactile-visual interactions

would have led naturally to the last chapter on the haptic sense as a substitute for vision. As presented, readers may incorrectly infer that haptic-visual interactions are solely an adaptive by-product of blindness.

Despite our dismay at the absence or inadequate treatment of certain topics, we find the tome is an otherwise comprehensive compendium of a voluminous amount of data. For the most part, Mountcastle does a masterful job integrating the basics of what we know about how sensory information travels from the hand to the highest regions of the brain. Although there are a few excellent books on the evolution of the hands and how we use them, this is the only sophisticated book on the neural basis of how the hand works. Even with its excessive neuroanatomical detail, *The Sensory Hand* can serve as a reference for systems neuroscientists in fields outside of somesthesia. As Engels pointed out, “Man alone has succeeded in impressing his stamp on nature ... and he has accomplished this primarily and essentially by means of the hand ... step by step, with the development of the hand went that of the brain. ...” (2). Mountcastle’s book shows us how we are beginning to understand this process.

References

1. T. H. Huxley, *Evidence as to Man’s Place in Nature* (Williams and Norgate, London, 1863).
2. F. Engels, *Dialectics of Nature*, C. Dutt, Transl. and Ed., preface and notes by J. B. S. Haldane (International, New York, 1940).
3. L. Fogassi et al., *Science* **308**, 662 (2005).

The Sensory Hand Neural Mechanisms of Somatic Sensation

by Vernon B. Mountcastle

Harvard University Press,
Cambridge, MA, 2005. 630
pp. \$85, £53.95, €78.30.
ISBN 0-674-01974-1.

The reviewers are in the Program in Neuroscience, Department of Psychology, Princeton University, Princeton, NJ 08540, USA. E-mail: cggross@princeton.edu; asifg@princeton.edu

HUMAN GENETICS

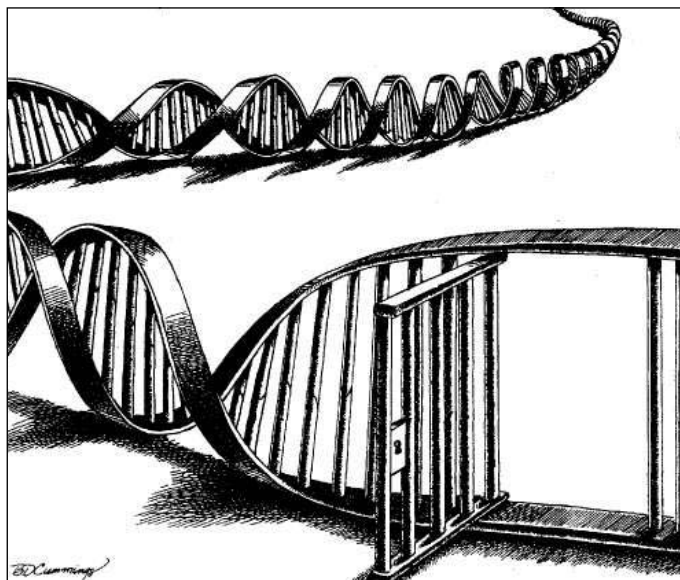
Finding Criminals Through DNA of Their Relatives

Frederick R. Bieber,^{1*} Charles H. Brenner,² David Lazer³

DNA methods are now widely used for many forensic purposes, including routine investigation of serious crimes and for identification of persons killed in mass disasters or wars (1–4). DNA databases of convicted offenders are maintained by every U.S. state and nearly every industrialized country, allowing comparison of crime scene DNA profiles to one another and to known offenders (5). The policy in the United Kingdom stipulates that almost any collision with law enforcement results in the collection of DNA (6). Following the U.K. lead, the United States has shifted steadily toward inclusion of all felons, and federal and six U.S. state laws now include some provision for those arrested or indicted. At present, there are over 3 million samples in the U.S. offender/arrestee state and federal DNA databases (7). Statutes governing the use of such samples and protection against misuse vary from state to state (8).

Although direct comparisons of DNA profiles of known individuals and unknown biological evidence are most common, indirect genetic kinship analyses, using the DNA of biological relatives, are often necessary for humanitarian mass disaster and missing person identifications (1, 2, 9). Such methods could potentially be applied to searches of the convicted offender/arrestee DNA databases. When crime scene samples do not match anyone in a search of forensic databases, the application of indirect methods could identify individuals in the database who are close relatives of the potential suspects. This raises compelling policy questions about the balance between collective security and individual privacy (10).

To date, searching DNA databases to identify close relatives of potential suspects has been used in only a small number of cases, if some-



times to dramatic effect. For example, the brutal 1988 murder of 16-year-old Lynette White, in Cardiff, Wales, was finally solved in 2003. A search of the U.K. National DNA Database for individuals with a specific single rare allele found in the crime scene evidence that identified a 14-year-old boy with a similar overall DNA profile. This led police to his paternal uncle, Jeffrey Gafoor (11). Investigation of the 1984 murder of Deborah Sykes revealed a close, but not perfect, match to a man in the North Carolina DNA offender database, which led investigators to his brother, Willard Brown (12). Both Gafoor and Brown matched the DNA from the respective crime scenes, confessed, and were convicted.

Although all individuals have some genetic similarity, close relatives have very similar DNA profiles because of shared ancestry. We demonstrate the potential value of kinship analysis for identifying promising leads in forensic investigations on a much wider scale than has been used to date.

Let us assume that a sample from a crime scene has been obtained that is not an exact match to the profile of anyone in current DNA databases. Using Monte Carlo simulations (13, 14), we investigated the chances of successfully identifying a biological relative of someone whose profile is in the DNA database as a possible source of crime scene evidence (15). Each Monte Carlo trial simulates a database of known offenders, a sample found

Analyses of the DNA databases maintained by criminal justice systems might enable criminals to be caught by recognizing their kin, but this raises civil liberties issues.

at a crime scene, and a search. The search compares the crime sample with each catalogued offender in turn by computing likelihood ratios (LRs) that assess the likelihood of parent-child or of sibling relationships (1, 16). We used published data on allele frequencies of the 13 short tandem repeat (STR) loci on which U.S. offender databases are based and basic genetic principles (17–19). A high LR is characteristic of related individuals and is an unusual but possible coincidence for unrelated individuals. The analysis of each simulation therefore assumes that investigators would follow these leads in priority order, starting with those in the offender database with the highest LR for being closely related to the owner of the

crime scene DNA sample.

Our simulations demonstrate that kinship analysis would be valuable now for detecting potential suspects who are the parents, children, or siblings of those whose profiles are in forensic databases. For example, assume that the unknown sample is from the biological child of one of the 50,000 offenders in a typical-sized state database. Of the 50,000 LRs comparing the “unknown” sample to each registered offender in the database, the child corresponds to the largest LR about half the time, and has a 99% chance of appearing among the 100 largest LRs (see chart). An analysis of potential sibling relationships produced a similar curve (13).

These results could be refined by additional data—for example, large numbers of single-nucleotide polymorphisms (SNPs). Better and immediately practical, a seven-locus Y-STR haplotype analysis on the crime scene and the list of database leads would eliminate 99% of those not related by male lineage (20). Determining (vital records, genealogical and geographical data) for the existence of suitable suspects related to the leads can also help to refine the list.

The potential for improving effectiveness of DNA database searches is large. Consider a hypothetical state in which the “cold-hit” rate—the chance of finding a match between a crime scene sample and someone in the offender database—is 10%. Suppose that

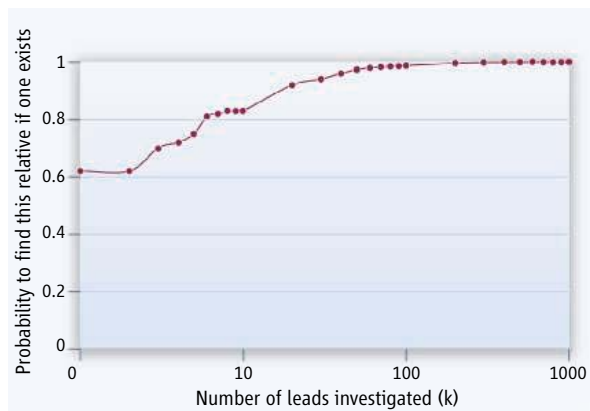
¹Department of Pathology, Brigham and Women’s Hospital and Harvard Medical School, Boston, MA 02115, USA. ²DNA-VIEW, Oakland, CA 94611, and School of Public Health, University of California, Berkeley, CA 94720, USA. ³John F. Kennedy School of Government, Harvard University, Cambridge, MA 02138, USA.

Authors are alphabetized to reflect equal contributions. Comments and ideas expressed herein are their own.

*Author for correspondence. E-mail: fbieber@partners.org

among criminals who are not (yet) in the database themselves, even 5% of them have a close (parent/child or sibling) relative who is. From our projections that up to 80% (counting the 10 best leads) of those 5% could be indirectly identified, it follows that the kinship analyses we describe could increase a 10% cold-hit rate to 14%—that is, by 40%. There have been 30,000 cold hits in the United States up to now (5). Kinship searching has the potential for thousands more.

Success of kinship searching depends most saliently on a close relative of the perpetrator actually being in the offender database. Studies clearly indicate a strong probabilistic depend-



Finding the genetic needle in a large haystack. The probability of identifying a close relative (i.e., parent/child) of a known offender by kinship searching is shown. Crime scene evidence would be searched against each profile in a simulated offender DNA database. A parent/child would be identified 62% of the time as the very first lead, and 99% of the time among the first 100 leads. Although these familial searching methods do not invariably distinguish parent/child from siblings, they have a high chance of identifying close relatives, if they exist, among the database samples with the highest LRs.

ency between the chances of conviction of parents and their children, as well as among siblings (21). Consistent with these studies, in a U.S. Department of Justice survey, 46% of jail inmates indicated that they had at least one close relative who had been incarcerated (22). Such observations do not define or delineate the possible complex roles of genetics, environment, and society in criminal behavior.

The widespread implementation of genetic kinship analysis for indirect database searches would represent a critical shift in the use of government forensic data banks, as they could identify, as potential suspects, not just those in the database, but their close relatives as well. Genetic surveillance would thus shift from the individual to the family.

Challenges to forensic DNA data banking have been based largely on claims of U.S. constitutional protections from unreasonable search and seizure. Such challenges have not prevailed, as the courts have ruled that the interests of public safety outweigh individual privacy interests

(23, 24). These DNA collections have sparked considerable controversy, especially in light of recent trends to expand collections to arrestees and those convicted of minor crimes and misdemeanors (25). Although use of retained samples for other purposes is prohibited by federal and several state laws, sample retention also has been a controversial practice.

Debates on the expansion of the scope of DNA collections for offender and arrestee databases, as well as collections of volunteer samples, e.g., through DNA dragnets, have concentrated on the balance between society's interests in security and privacy interests of individuals who might be included in the database and on the fairness and equity of including some in the databases but not others (26, 27). Privacy interests include genetic privacy [as DNA samples can yield medical and other information (28)] and locational privacy (where the contributor has been and left DNA). As with any investigative technique, these DNA matching strategies will lead to investigation of the innocent.

Existing state and federal statutes do not specifically address familial searches, and it is unlikely such search strategies were even considered at the time original statutes were written. Use of familial searching methods described herein could raise new legal challenges, as a new category of people effectively would be placed under lifetime genetic surveillance. Its composition would reflect existing demographic disparities in the criminal justice system, in which arrests and convictions differ widely based on race, ethnicity, geographic location, and social class. Familial searching potentially amplifies these existing disparities. These issues need to be confronted, as widespread use of various familial searching tools, including formal kinship analysis, is foreseeable. The de facto inclusion of kin into DNA data banks may lead some to oppose familial searching. It may lead others to support calls for a universal DNA database (29), which to date have been rejected. Other options include limiting familial searching methods to investigation of the most serious crimes and defining statistical thresholds that minimize intrusions on innocent parties (30).

The rapid proliferation and expansion of DNA collections along with the results of our analyses require careful consideration of the implications of familial searching methods. Every agency or country considering such

methods should evaluate attendant policy, ethical, and legal implications, in addition to their valuable investigatory potential.

References and Notes

1. C. H. Brenner, B. S. Weir, *Theor. Popul. Biol.* **63**, 173 (2003).
2. C. H. Brenner, *Forensic Sci. Int.* **157**, 172 (2006).
3. F. R. Bieber, in *DNA and the Criminal Justice System*, D. Lazer, Ed. (MIT Press, Cambridge, MA, 2004), pp. 23–72.
4. L. Biasecker *et al.*, *Science* **310**, 1122 (2005).
5. F. Bieber, *J. Law Med. Ethics* **34**, 222 (2006).
6. U.K. Criminal Justice Act, 2003 (www.opsi.gov.uk/acts/en2003/2003en44.htm).
7. See (www.fbi.gov/hq/lab/codis/index1.htm).
8. For a summary of DNA database legislation in the United States, see (www.aslme.org).
9. B. Budowle, F. R. Bieber, A. Eisenberg, *Legal Med.* **7**, 230 (2005).
10. D. Lazer, M. Meyer, in *DNA and the Criminal Justice System*, D. Lazer, Ed. (MIT Press, Cambridge, MA, 2004), pp. 357–390.
11. BBC News, "How police found Gafoor," 4 July 2003 (<http://news.bbc.co.uk/1/hi/wales/3038138.stm>).
12. R. Willing, *USA Today*, 7 June 2005, p. 1 (www.usatoday.com/news/nation/2005-06-07-dna-cover_x.htm).
13. Materials and methods are available as supporting material on *Science Online*.
14. N. Metropolis, S. Ulam, *J. Am. Stat. Assoc.* **44**, 335 (1949).
15. In the simulations, we made a variety of simplifying assumptions (e.g., regarding random mating, mutation rates). These results are thus, of course, approximations that will need experimental validation.
16. C. C. Li, L. Sacks, *Biometrics* **10**, 347 (1954).
17. B. Budowle *et al.*, *J. Forensic Sci.* **44**, 1277 (1999).
18. J. Butler, *Forensic DNA Typing* (Elsevier Academic Press, Burlington, MA, ed. 2, 2005).
19. A. J. F. Griffiths *et al.*, *An Introduction to Genetic Analysis* (Freeman, New York, ed. 2, 2004).
20. Data from Y-Chromosome Haplotype Reference STR database (YHRD), see (www.yhrd.org).
21. C. Smith, D. Farrington, *J. Child Psychol. Psychiatr.* **45**, 230 (2004).
22. U.S. Bureau of Justice Statistics, *Correctional Populations in the United States, 1996* (NJC 170013, U.S. Department of Justice, Washington, DC, April 1999), p. 62 (www.ojp.usdoj.gov/bjs/pub/pdf/cpius964.pdf).
23. See *United States v. Kincaid*, 379 F. 3d 813 (9th Cir. 2004) (en banc).
24. *State v. Raines*, 875 A. 2d 19 (Md. 2004) (collecting cases).
25. D. Cardwell, *New York Times*, 4 May 2006.
26. A. Etzioni, in *DNA and the Criminal Justice System*, D. Lazer, Ed. (MIT Press, Cambridge, MA, 2004), pp. 197–224.
27. D. Lazer, V. Mayer-Schoenberger, *J. Law Med. Ethics* **34**, 366 (2006).
28. D. Altschuler, A. G. Clark, *Science* **307**, 1052 (2005).
29. D. H. Kaye, M. S. Smith, in *DNA and the Criminal Justice System*, D. Lazer, Ed. (MIT Press, Cambridge, MA, 2004), pp. 247–284.
30. R. Williams, P. Johnson, *J. Law Med. Ethics* **33**, 545 (2005).
31. We gratefully acknowledge the American Society of Law, Medicine and Ethics, through NIH grant 1R01HG2836-01, and the NSF (grant 0131923 to D.L.) for partial support. We thank E. Smith for research assistance.

Supporting Online Material

www.sciencemag.org/cgi/content/full/1122655/DC1

Published online 11 May 2006; 10.1126/science.1122655
Include this information when citing this paper.

10.1126/science.1122655

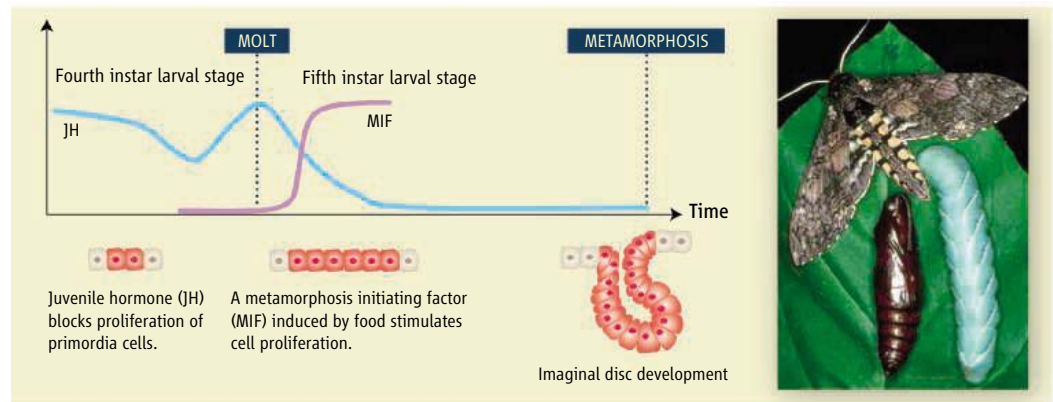
DEVELOPMENT BIOLOGY

Linking Nutrition and Tissue Growth

Pierre Léopold and Sophie Layalle

Complex organisms must be able to adapt their developmental programs to ever-changing environmental conditions. One important way to coordinate this is through the use of hormones, regulatory molecules that exert diverse biological effects on multiple and remote target tissues. In this context, juvenile hormone has fascinated insect endocrinologists for decades. This factor, present in insects that undergo metamorphic changes during development, has many functions in orchestrating the insect life cycle, and thus provides an illuminating example of the kinds of pleiotropic effects that hormones can have. Although it is known mostly for controlling (together with the steroid hormone ecdysone) molting during insect development, juvenile hormone also regulates organ morphogenesis, female fertility, adult behavior, diapause, and longevity (1, 2). On page 1385 of this issue, Truman *et al.* (3) add a new, key function to this list: relaying nutritional information to developing tissues during insect development. Using the tobacco hornworm model *Manduca sexta*, the authors provide compelling evidence that juvenile hormone prevents the growth and development of future adult tissues in response to nutrient shortages during larval life.

M. sexta, a pest for tobacco farmers, is a longtime lab star in the world of insect physiologists. As in all holometabolous insects, the adult organism, a moth, is produced from the transformation of larval tissues called imaginal discs (4). Imaginal discs are relatively simple structures that have served as a paradigm for understanding fundamental principles of development, such as the action of morphogenetic molecules in establishing tissue polarity, as well as the mechanisms coordinating patterning during tissue growth and differentiation. Previous studies have found that imaginal tissue growth is controlled by two primary factors: the patterning activity of morphogens, diffusible proteins that organize fields of cells into distinct territories and define final tissue shapes; and environmental cues like nutrition, which are conveyed



Coordinating nutrition and hormone influence on tissue development. In the tobacco hornworm *M. sexta*, imaginal disc tissue forms from primordia tissue late in larval development, after the fifth larval molt. This process is initiated by a signal of unknown nature called metamorphosis initiation factor, which is itself triggered by feeding. Shortly afterward, there is a decrease in the amount of circulating juvenile hormone.

to the discs via circulating systemic factors such as insulin-like molecules and steroids (5).

To enable the rapid increase in tissue mass that occurs during larval growth, larvae undergo a series of molts in which the cuticle is replaced. These molts follow peaks of ecdysone production that occur in the context of high concentrations of juvenile hormone. During the last larval stage (the fifth instar), however, the concentration of juvenile hormone drops, and the next molt changes from a larva-to-larva to a larva-to-pupa transition (see the figure). Also, shortly before this, in the primordia tissue that develops late into imaginal discs, cells commit to metamorphosis and undergo marked cell proliferation. This commitment requires feeding, because complete starvation of the animals during this period suppresses disc formation (6). Interestingly, juvenile hormone does not decline during the last larval stage in starved animals, suggesting that sustained amounts of this hormone might be linked to the starvation-induced inhibition of disc formation. In a key experiment, Truman and collaborators suppressed juvenile hormone production in developing larvae by ablating their secretory gland. In these animals, imaginal discs still formed, even under starvation conditions. Furthermore, locally treating the primordia of these larvae with pyriproxifen, a compound that mimics the effects of juvenile hormone, efficiently restored growth inhibition of imaginal disc tissue, showing that the hormone acts as a signal for starvation-induced growth inhibition and that it does not need to be relayed by a systemic growth-activating molecule like insulin.

Environmental cues affect the course of an organism's development. For example, in some insects, scarce nutrients induce a hormone to block tissue formation.

Interestingly, the normal persistence of juvenile hormone during the first day of the last larval instar stage in fed animals does not prevent commitment of cells in the primordia to form late discs, suggesting that during the early period of the fifth instar larva, the growth-inhibitory effects of juvenile hormone are overridden by feeding. Indeed, locally applied pyriproxifen does not affect disc growth in feeding late larvae. However, the dominance of feeding over juvenile hormone appears to be restricted to the last larval instar, because the hormone does block disc formation in younger feeding animals. Thus, a nutrition-induced dominance factor appears to be produced early in the last larval instar, allowing the imaginal disc primordia cells to commit to metamorphosis despite the persistence of circulating juvenile hormone.

As is often the case with novel and insightful findings, the Truman *et al.* work raises many new questions. The local effect of juvenile hormone-induced growth inhibition suggests that the hormone might act cell autonomously on target tissues, directly affecting growth or proliferation in the cells of forming discs. The authors provide evidence to support this, showing that subnanomolar concentrations of pyriproxifen inhibit primordia cell proliferation. Further deciphering the relevant molecular interactions might be tricky though, because the signaling pathways downstream of juvenile hormone are poorly understood.

It will be equally important to determine how the nutritional sensing mechanism operates in *Manduca* larvae. The simplest mechanism could

involve a nutrition-induced signal that would render each individual primordia cell insensitive to juvenile hormone-induced growth inhibition. This would not explain, however, why the same primordia cells are sensitive to juvenile hormone in early-stage feeding larvae but become resistant in the last instar. Alternatively, a signal that is dominant over juvenile hormone and that is triggered by nutrition at this specific stage could do the job. The existence of such a “metamorphosis initiating factor” is suggested both by Truman *et al.* and by another recent study (7). Its nature and the mechanisms leading to its specific activation by nutrition at the start of the last-instar larva remain to be identified.

Finally, the sustained presence of juvenile hormone in starved animals suggests that the endocrine tissue that produces this hormone might respond to nutrition and modulate its pro-

duction or secretion accordingly. During food deprivation and in the absence of a metamorphosis initiating factor, juvenile hormone would prevent disc formation. Another possibility comes from recent studies in *Manduca*'s cousin, the fruit fly *Drosophila melanogaster*, that implicate a larval tissue called the fat body (the equivalent of both vertebrate liver and fat tissue) in orchestrating nutritional responses (8, 9). The larval fat body is an important source of juvenile hormone esterase, an enzyme that degrades the hormone to control its circulating levels. One possible scenario is that the fat body, acting as a nutrition sensor, modulates circulating amounts of juvenile hormone by producing the esterase and thereby directs imaginal disc development. The temporal control of this process is an intriguing issue that also needs to be addressed. Possible answers to these questions may come by extending these

results to the genetically amenable *Drosophila* model, where new roles for juvenile hormone in development, growth, and morphogenesis are prime for exploration.

References

1. T. Flatt, M. P. Tu, M. Tatar, *Bioessays* **27**, 999 (2005).
2. L. I. Gilbert, N. A. Granger, R. M. Roe, *Insect Biochem. Mol. Biol.* **30**, 617 (2000).
3. J. W. Truman *et al.*, *Science* **312**, 1385 (2006).
4. J. W. Truman, L. M. Riddiford, *Nature* **401**, 447 (1999).
5. S. J. Day, P. A. Lawrence, *Development* **127**, 2977 (2000).
6. S. G. MacWhinnie *et al.*, *Dev. Biol.* **285**, 285 (2005).
7. J. P. Allee, C. L. Pelletier, E. K. Fergusson, D. T. Champlin, *J. Insect Physiol.* **52**, 450 (2006).
8. J. S. Britton, B. A. Edgar, *Development* **125**, 2149 (1998).
9. J. Colombani *et al.*, *Cell* **114**, 739 (2003).

10.1126/science.1128343

PLANT SCIENCE

Unfallen Grains: How Ancient Farmers Turned Weeds into Crops

John Doebley

Some 10,000 years ago during the agricultural revolution, ancient farmers bred hundreds of wild species into the domesticated crops on which humans are dependent today. During this process, these ancient peoples saved seeds from plants with favored traits to form each subsequent generation, and over time they converted slender and unpromising wild species into reliable, bountiful crops. Variants or mutants of genes that conferred favorable phenotypes rose in frequency over time, while variants that best adapted plants to life in the wild were removed by selection from the domesticated population.

Foremost among the creations of ancient plant breeders are the cereals—rice, wheat, and maize, a triumvirate that provides more than 50% of the calories consumed by humans. As compared to their progenitors, these cereals have more and larger grains, thicker stalks, seed that thresh freely from the chaff, and improved flavor. The cereals, and most other crops, share one additional feature that is central to domestication: Their grains remain attached to the plant for harvest by humans rather than falling (shattering) from the plant, as required for wild species to produce their next generation. Although quantitative trait locus (QTL) mapping (1) has convincingly shown that the evolution of domestication traits



Gathering grain. Two agricultural workers harvesting rice in Yangshuo, Guangxi Province, China.

such as the loss of shattering arose through a relatively small number of gene changes, the nature of these genes and the molecular changes within them is not well understood.

In research published in *Science* earlier this year (2) and on page 1392 of this issue (3), groups in the United States and Japan take two

Cereals are the world's primary food, but if they are to be harvested grains must remain on the plant. Two of the genetic changes responsible for this essential trait for domestication have been identified.

big steps toward bridging the gap between domestication QTLs and domestication genes. Li *et al.* (2) cloned *shattering4* (*sh4*), a gene first identified by this group as a major QTL controlling 69% of the variance for shattering in crosses of wild and cultivated *indica* rice. This team was able to localize the causative difference to a 1700-base pair region, and then to demonstrate that a single amino acid change is principally responsible for the loss of shattering. An extraordinary feature of the cultivated allele of *sh4* is that it severely weakens but does not eliminate shattering. Thus, the grains are retained on the plants long enough for harvest, but then they can be removed easily by threshing.

Konishi *et al.* (3) identified a second major shattering QTL (*qSH1*) in a cross of the two independently domesticated forms of rice, *indica* and *japonica*. This QTL controls 68% of the variation for shattering in this hybrid population, and the authors cloned the gene and mapped the causative difference to a single nucleotide change. An absolutely exquisite result is that this single nucleotide change in cultivated rice obliterates a cis-regulatory element required for the expression of *qSH1* in the abscission layer, which is needed for the grain to break away from the plant. Other cis-regulatory elements in *qSH1* are conserved between wild and cultivated rice, and thus *qSH1* still fulfills its other functions in the inflorescence of cultivated rice.

These two rice genes join the growing number of plant domestication QTLs cloned to date.

The author is in the Laboratory of Genetics, University of Wisconsin, Madison, WI 53706, USA. E-mail: jdoebley@wisc.edu

In 1997, the maize gene *tb1* was reported as the first domestication QTL to be cloned (4). *tb1* controls the complex differences in plant architecture between maize and its progenitor, teosinte. In 2000, a major QTL (*fw2.2*) contributing to the massive increase in fruit size that was a central feature of tomato domestication was cloned (5). In 2005, the maize domestication QTL *tga1*, which provides naked grains to maize (as opposed to the covered grains of teosinte), was cloned (6). And thus far in 2006, in addition to the two rice shattering genes, cloning of the wheat *Q* gene was reported (7). *Q* controls the compaction and fragility of the ear of wheat and also the ease with which the grain can be separated from the chaff.

A notable feature of this list of six domestication genes is that five of the six encode transcription factors that regulate other (target) genes by directly binding to their DNA. Transcription factors represent only about 5% of genes in plant genomes (8, 9) but 83% of the domestication genes listed above. Interestingly, the five domestication transcription factors belong to five separate families: TCP (*tb1*), SBP (*tga1*), AP2 (*Q*), MYB3 (*sh4*), and HOX (*qSH1*). This suggests that the exaggerated proportion of transcription factors among domestication genes is the product of some general feature of transcription fac-

tors and not of one particular class of transcription factors. The predominant role of transcription factors in domestication mirrors their equally large role in controlling plant development (10), which supports the view that they have properties that predispose them to become the major genes contributing to morphological evolution in plants (11).

Another remarkable feature of this list is that the domesticated alleles of all six genes are functional. If domestication involved the crippling of precisely tuned wild species, one might have expected domestication genes to have null or loss-of-function alleles. Rather, domestication has involved a mix of changes in protein function and gene expression. As a consequence of domestication, *sh4* shows changes in protein function and expression level (2), *qSH1* shows a change in the spatial pattern of its expression (3), *tb1* shows increased expression (4), *tga1* shows a change in protein stability or protein function (6), *fw2.2* shows a heterochronic shift in its expression (5), and *Q* shows changes in protein function and gene expression (7). Given that the cultivated allele of not one of these six domestication genes is a null, a more appropriate model than “crippling” seems to be adaptation to a novel ecological niche—the cultivated field. Tinkering and not disassembling is the order of

the day in domestication as in natural evolution, and Darwin’s use of domestication as a proxy for evolution under natural selection was, not surprisingly, right on the mark.

A consequential question now is whether modern plant breeders might borrow from the playbook of their Neolithic predecessors. Might one tinker with the expression patterns or protein functions of known domestication genes to create superior alleles? Can every transcription factor in the genome be manipulated in a systematic manner to generate a pool of new trait variation? Knowledge of past successes should help to intelligently guide future crop improvement.

References

1. A. Paterson, *New Phytol.* **154**, 591 (2002).
2. C. Li, A. Zhou, T. Sang, *Science* **311**, 1936 (2006); published online 8 March 2006 (10.1126/science.1123604).
3. S. Konishi *et al.*, *Science* **312**, 1392 (2006).
4. J. Doebley, A. Stec, L. Hubbard, *Nature* **386**, 485 (1997).
5. A. Frary *et al.*, *Science* **289**, 85 (2000).
6. H. Wang *et al.*, *Nature* **436**, 714 (2005).
7. K. J. Simons *et al.*, *Genetics* **172**, 547 (2006).
8. Y. Xiong *et al.*, *Plant Mol. Biol.* **59**, 191 (2005).
9. S. H. Shiu, M. C. Shih, W. H. Li, *Plant Physiol.* **139**, 18 (2005).
10. J. Doebley, L. Lukens, *Plant Cell* **10**, 1075 (1998).
11. J. Doebley, *Curr. Opin. Genet. Dev.* **3**, 865 (1993).

10.1126/science.1128836

PLANETARY SCIENCE

Exploring Other Worlds to Learn More About Our Own

Ingo C. F. Müller-Wodarg

The exploration of our solar system was originally driven primarily by curiosity and the search for answers to the eternal question: Are we alone? As the first spacecraft began to visit our neighboring planets in the solar system, hopes of finding life quickly faded and instead the focus began to shift toward gaining a more scientific understanding of their nature and history. After a generation of exploratory robotic spacecraft missions from the 1960s through the 1980s, it became clear that most planets—except Mercury—and some moons had permanent and substantial atmospheres. These atmospheres can be subdivided into three large families: those composed primarily of nitrogen (Earth, Titan, Triton, Pluto), carbon dioxide (Venus, Mars), and hydrogen/helium (Jupiter, Saturn, Uranus, Neptune). On page 1366 of this issue, Forbes *et*

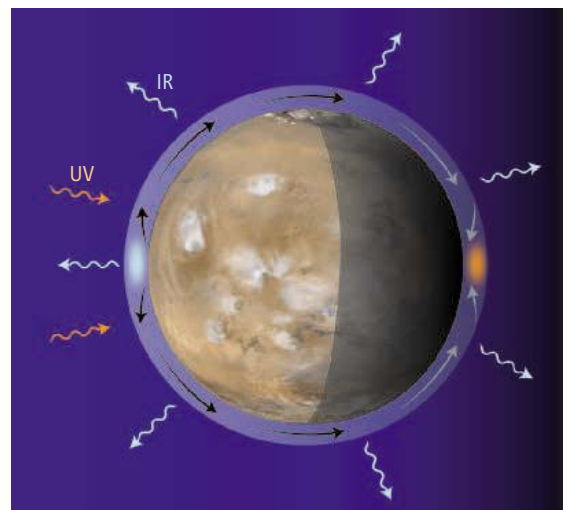
al. (1) provide fresh insights into the effects of variations in solar radiation intensity on the upper atmospheres of Mars and Earth, which have now been simultaneously observed.

Numerous space missions, along with Earth-based observations and theoretical models, have given us an unprecedented understanding of planetary atmospheres. Yet some of their fundamental prop-

Energy flow on Mars. Solar ultraviolet radiation heats the dayside to 300 K; winds transport some of this energy toward the nightside, where temperatures are typically lower by 100 K. On the dayside, vertical conduction and adiabatic cooling offset solar heating, whereas the nightside temperatures are raised by adiabatic heating. A portion of the solar energy is radiated back into space through infrared cooling by CO₂.

Simultaneous observations of the drag of satellites through the upper atmospheres of Mars and Earth reveal how carbon dioxide is differentially cooling their upper atmospheres.

erties are still poorly understood, including the atmospheric energy balance (see the figure). What are the sources of energy incident upon an atmosphere, how is this energy redistributed



internally, and how much of it is lost back into space? The key common source of energy in our solar system is the Sun, and this energy is distributed either through radiation or via the solar wind. Since the time of formation of our solar system, some energy has been stored internally in the planetary bodies as thermal, chemical, or rotational energy. Energy also reaches us from outside our solar system in the form of cosmic radiation, in particular gamma rays.

The high-energy ultraviolet portion of radiation from the Sun is absorbed in Earth's upper atmosphere by the principal gases nitrogen (N₂) and oxygen, both molecular and atomic (O₂, O). Most of the absorbed energy is thermally conducted to lower altitudes. Near 90 km (the mesopause region), CO₂ and other radiating molecules are abundant enough to emit a large portion of the energy back to space through infrared radiation. At high latitudes, energetic particles precipitating from the magnetosphere interact with the atmosphere, leading to substantial heating as well as spectacular auroral emissions. Electrical currents between the magnetosphere and the atmosphere can also heat the atmospheric gases at high latitudes, particularly during geomagnetic disturbances.

In essence, most of the physical processes that control Earth's energy balance are also acting on other planets. On Venus and Mars, the large abundances of CO₂ lead to effective radiative cooling of their upper atmospheres. The heating processes at auroral latitudes on Jupiter and Saturn may exceed solar heating rates because of the larger distances from the Sun. Another likely heat source on the gas giants is the transfer of energy from inside the planets to their outer atmospheres via waves.

The exploration of other bodies in our solar system also helps us understand our own planet far better. Cooling by CO₂, which dominates Venus and Mars, is also acting on Earth and turns out to be one of the keys to understanding the evolution of our atmosphere as well as climate change. Major uncertainties, however, pertain to Earth's CO₂ cooling rate, which is controlled by the excitation of CO₂ through collisions with atomic oxygen. It turns out that observing Mars or Venus simultaneously with Earth can help us better determine this rate, but such observations are challenging and have not been made until recently.

Now, analyses by Forbes *et al.* of the atmospheric drag on satellites orbiting Earth and Mars have yielded measurements of how variations in solar radiation intensity affect atmospheric densities. At any given altitude, heating of the atmosphere will result in an enhancement of densities and stronger atmospheric drag on a satellite. Measuring these drag variations allows derivation of atmospheric temperature changes, and thereby of the effects of solar forcing. Mars is found to be half as responsive as Earth to changes in solar forcing, but is estimated to be

four to seven times as responsive as Venus. These numbers are corrected for distances from the Sun; thus, the differences are primarily due to the varying CO₂ cooling efficiencies, which have so far remained poorly understood. This study, in helping us to improve our knowledge of the CO₂ cooling efficiencies, is a prime example of how we can use other planets in our solar system as laboratories to better understand the complexity of our own atmosphere, and thereby improve our predictions of changes, including those due to anthropogenic effects.

Previous simultaneous observations of planets had focused on comparing solar forcing of the ionized portions of the atmospheres on Earth and Mars (2–4) and the propagation of interplanetary shocks through the solar system. Interplanetary shocks are triggered by violent solar eruptions and cause compression of magnetospheres around planets. Such compressions lead to increased levels of energetic particle precipitation into upper atmospheres, and thereby enhanced auroral brightness. Only recently, observations have followed an interplanetary shock as it propagated from the Sun to Earth, Jupiter, and Saturn and successively caused enhanced brightness of their aurorae (5), confirming the effects of solar forcing on planetary magnetic

and plasma environments and atmospheres. These comparative space weather observations have highlighted important differences between the ionospheres and magnetospheres of planets, again helping us to better understand Earth and its space environment.

The examples illustrate that comparative studies of planets are far more effective than examining each body individually. Knowledge of Earth's atmosphere and environment helps us understand aspects of other planets, but we can only understand the evolution of our own atmosphere by studying those of other planets. Ultimately, the lessons learned within our solar system can also be applicable to the exploration of planets orbiting stars far from our solar system.

References

1. J. M. Forbes, S. Bruinsma, F. G. Lemoine, *Science* **312**, 1366 (2006).
2. M. Mendillo, S. Smith, J. Wroten, H. Rishbeth, *J. Geophys. Res.* **108**, 10.1029/2003JA009961 (2003).
3. H. Rishbeth, M. Mendillo, *Planet. Space Sci.* **52**, 849 (2003).
4. M. Mendillo, P. Withers, D. Hinson, H. Rishbeth, B. Reinisch, *Science* **311**, 1135 (2006).
5. R. Prangé *et al.*, *Nature* **432**, 78 (2004).

10.1126/science.1128497

BEHAVIOR

Align in the Sand

Daniel Grünbaum

Many animal species form large organized groups, but how information is shared within swarms, flocks, and herds is not clear. Studies of locust swarms reveal distinct transitions from disordered to ordered phases.

Large, coordinated animal groups such as swarms, herds, schools, and flocks are widespread phenomena that strongly affect many biological systems (1). High population densities often bring negative consequences (increased competition for resources, disease transmission, and attention from predators), but species that take advantage of dense populations to form organized groups may benefit by more effective foraging, reproduction, migration, and escape from predators. The analysis by Buhl *et al.* of coordinated movement in juvenile desert locusts on page 1402 of this issue presents the most detailed description yet of the behavioral mechanisms enabling social animals to form and maintain coherent, large-scale groups (2).

Locust plagues can contain 10⁹ individuals and are among the most spectacular and consequential of animal aggregations (3). Seemingly

spontaneous appearances of multitudes of hungry locusts, which fill the air and carpet the ground as each eats its own weight per day of natural and agricultural vegetation, have caused ecological, economic, and (after these locusts die and putrefy) epidemiological catastrophes of historic proportions (4). All of this devastation originates with a profound transition by immature, nonflying locusts from a relatively innocuous solitary phase, in which they actively avoid each other, to a behaviorally and physiologically distinct gregarious phase, in which they seek each other out (5). When this happens, the locusts form massive, coherent, and highly mobile foraging groups (see the figure). Desert locusts almost completely destroy plant material as they go, and they go a long way; migrations routinely carry these insects thousands of kilometers across Africa and have reached as far as Europe and the New World (6).

"The locusts have no King, yet all of them march in rank," observed an insightful ancient naturalist (7), capturing the enduring mystery of

The author is in the School of Oceanography, University of Washington, Seattle, WA 98195, USA. E-mail: grunbaum@ocean.washington.edu

animal aggregations: How do they do it? Coordinated motion by locusts and other large animal groups is remarkable, because these groups lack centralized leadership and each individual can interact with only a few nearby neighbors. Group members have no direct means of assessing overall group characteristics, such as size and direction of travel. For these groups to remain intact, behavioral interactions among members must somehow propagate directional information from the large scale—in the case of locusts, millions of individuals distributed across tens of kilometers—down to a neighborhood on the scale of a few centimeters surrounding each individual member.

This information is of no small value. In dense locust populations, the only undepleted resources are ahead of the traveling aggregation. Each member's access to food depends on its ability to at least occasionally anticipate the group's direction of travel and to beat the masses to virgin fodder.

What behavioral mechanisms are involved in this information transfer in locusts and other animal groups? This is the core question addressed in the Buhl *et al.* study. Despite the wide diversity of animal aggregations, there are likely far fewer fundamentally different types of grouping behaviors. By understanding one group, we will probably also understand many others. However, it has proven difficult to identify the precise behaviors used by grouping animals. One obstacle is the difficulty in accurately quantifying movements by entire neighborhoods of animals in the midst of large mobile groups. Another is that most mathematical tools for analyzing biological movement are designed to infer movement characteristics from known interaction rules (8). These tools do not work in reverse; they do not extract interaction rules from observed movements.

Buhl *et al.* solved the tracking problem by studying immature, flightless locusts, and they used computerized motion analysis to obtain high-resolution, two-dimensional positions and orientations of all individuals within an annular experimental enclosure. Their study's first key message is that two distinct transitions in group-level directionality occur as locusts become increasingly crowded. At low population density, locusts tend to have random orientations and do not align with one another. Because locusts interact only over relatively short distances, neighbors who are not aligned move quickly

apart and thereafter have little effect on each other. The first transition occurs at intermediate density, when locusts begin to align in neighborhoods to form coherent traveling groups. However, these groups' movement directions are not persistent; they undergo frequent directional changes that are spontaneous and unpredictable. As density increases still further, a second transition occurs in which locust groups that are already aligned acquire the high directional persistence that is characteristic of locust migrations in nature.



Getting a move on. An aligned group of desert locusts, *Schistocerca gregaria*, in Mauritania.

Buhl *et al.* addressed the lack of deductive tools for behavior analysis by showing a detailed correspondence between alignment transitions in locusts and those in an idealized mathematical model of animal grouping. Since the 1920s, the standard hypothesis for organized movements of biological groups has been that group members move toward and align with neighbors within specific ranges of relative positions (9, 10). Neighbors outside these attraction and alignment zones are either too distant to provoke a reaction, or may be so close that they induce an anticrowding avoidance response. Most grouping models also include a stochastic movement component, representing intrinsic behavioral randomness or responses to environmental noise. Behavioral randomness tends to break down ordered arrangements among neighboring individuals. Thus, in these models, the key dynamic process that determines the timing and extent of biologi-

cal grouping is a competition between the tendency of social interactions to induce directional order and the opposing tendency of behavioral randomness to induce disorder.

Buhl *et al.* analyzed a simplified version of this grouping model—the self-propelled particle (SPP) model—that includes alignment among neighbors but omits attraction and repulsion (11, 12). This model predicts that as local population density goes up, social interactions increase in frequency and so too do their order-inducing effects. Behavioral randomness does not in-

crease with density. The result is a shift in the order/disorder balance: In sparse populations, organized groups are unstable and transient. However, when density increases to a critical level, a transition occurs in which coherent aligned groups become stable. As these groups move, they encounter and entrain previously unaligned individuals. These traveling groups convey directional information rapidly over large distances, so that eventually the entire population adopts a uniform and persistent migratory direction. Thus, the second key message of Buhl *et al.* is a demonstration of remarkable agreement between this theory and their observed alignment transitions, which they suggest is strong evidence that locusts use SPP-like grouping mechanisms.

The SPP model is general and not tailored to any particular animal species. A model that is simple, quantitatively accurate, and potentially

broadly applicable opens a number of doors to better theoretical and practical understanding of group dynamics. From an evolutionary perspective, the costs and benefits of behavioral choices in groups change dramatically depending on how other group members respond, and they can be deciphered only through quantitative models of behavioral cause and effect. Furthermore, if the organizational transitions seen in locusts are as fundamental as the SPP model suggests, then their presence is not the result of selective fine tuning; for better or worse, these and perhaps other features may be evolutionarily unavoidable aspects of grouping. In applied terms, intelligent management of natural resources depends on

understanding grouping transitions not only in desert locusts, where we may want to derail collective motion, but also in cases such as overexploited migratory fish stocks, where we need to avoid collapse of reproductive aggregations to prevent catastrophic population declines.

References and Notes

1. J. K. Parrish, L. Edelman-Keshet, *Science* **284**, 99 (1999).
2. J. Buhl *et al.*, *Science* **312**, 1402 (2006).
3. R. C. Rainey, *Migration and Meteorology: Flight Behavior and the Atmospheric Environment of Locust and Other Migrant Pests* (Oxford Science, Oxford, 1989).
4. S. Baron, *The Desert Locust* (Charles Scribner's Sons, New York, 1972).
5. S. J. Simpson, E. Despland, B. F. Hagele, T. Dodgson,

6. N. R. Lovejoy *et al.*, *Proc. R. Soc. London Ser. B* **273**, 767 (2006).
7. Proverbs 30:20, The Holy Bible, English Standard Version (Crossway Bibles, Good News Publishers, 2001).
8. V. Kumar, N. Leonard, A. S. Morse, Eds., *Cooperative Control, Lecture Notes in Control and Information Sciences* (Springer-Verlag, Berlin, 2005), vol. 309.
9. A. E. Parr, *Occasional Papers of the Bingham Oceanography College* **1**, 1 (1927).
10. A. Okubo, S. A. Levin, *Diffusion and Ecological Problems: Modern Perspectives* (Springer-Verlag, New York, 2001).
11. A. Czirok, A. Barabasi, T. Vicsek, *Phys. Rev. Lett.* **82**, 209 (1999).
12. T. Vicsek *et al.*, *Phys. Rev. Lett.* **75**, 1226 (1995).
13. The author thanks the NSF for support through grant CCR0313250.

10.1126/science.1127548

CHEMISTRY

Toward Efficient Hydrogen Production at Surfaces

Jens K. Norskov and Claus H. Christensen

Hydrogen is considered by many to be a promising energy currency, particularly for the transportation sector and for mobile devices (1). The combustion of hydrogen yields water as its only waste product, and hydrogen is a perfect fuel for fuel cells. In most hydrogen-producing technologies, a solid surface catalyzes the required chemical reactions. Higher efficiencies require the development of better catalysts. Recent studies have raised hopes that combined computational and experimental surface studies can aid the design of new catalysts.

In most steam-reforming processes, this energy is provided as heat (2), whereas water splitting is usually performed electrochemically

or photochemically (3). These processes require bonds to be broken and new bonds to be made, chemical transformations that are activated and typically catalyzed by solid surfaces. Today, the development and optimization of catalytic surfaces is usually based on an intuitive trial-and-error approach. Rational catalyst development strategies would be greatly facilitated by an improved molecular-level knowledge of how chemical reactions proceed on solid surfaces. Recently, new detailed insights have been provided by density functional theory calculations.

Industrial steam reforming of natural gas—that is, $\text{CH}_4 + 2\text{H}_2\text{O} \rightarrow \text{CO}_2 + 4\text{H}_2$ —is conducted with nickel catalysts at temperatures of $\sim 800^\circ\text{C}$ and provides a convenient and cost-effective method for hydrogen production. Ideally, four hydrogen molecules are formed per methane molecule when the methane reacts with water. Today, compact hydrogen-production facilities with capacities of more than 250,000 $\text{m}^3 \text{H}_2$ per hour can be designed (2).

Calculations are providing a molecular picture of hydrogen production on catalytic surfaces and within enzymes, knowledge that may guide the design of new, more efficient catalysts for the hydrogen economy.

Steam reforming of renewable bioresources is also a viable route to large-scale hydrogen production. Glucose can be reformed in water at surprisingly mild conditions, producing more than six hydrogen molecules for each glucose molecule (4). Ethanol, available for example through fermentation of biomass, can also be steam-reformed in the presence of oxygen. The required heat is supplied directly by combusting some of the hydrogen produced; such an autothermal process yields five hydrogen molecules for each ethanol molecule (5).

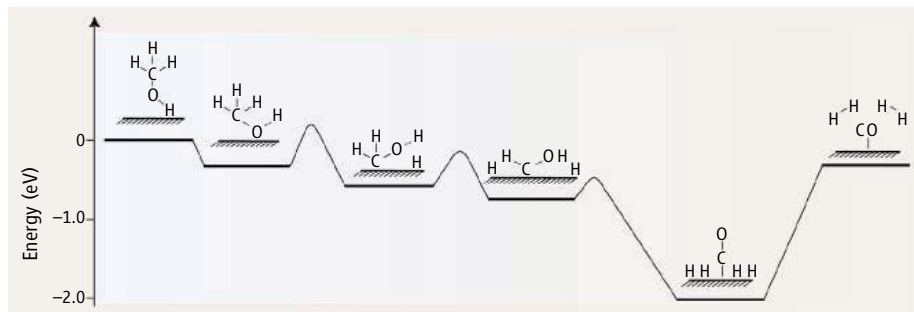
The catalytic conversion of alkanes, alcohols, or carbohydrates with water into hydrogen and carbon dioxide are complex multistep chemical reactions. It is not possible to pinpoint a priori why one catalytic surface performs better than another. For even the simplest alcohol—methanol—the number of elementary reactions associated with its decomposition and the subsequent formation of molecular hydrogen is large (6). However, calculated potential-energy dia-

Enhanced online at
www.sciencemag.org/cgi/content/full/312/5778/1322

To realize a hydrogen-based fuel economy, hydrogen must be produced in an efficient and sustainable manner. Today, most hydrogen is produced from fossil resources by steam reforming, a process in which steam reacts with hydrocarbons in the presence of a metal-based catalyst. Sustainable alternatives include biological or catalytic degradation of biomass and electrochemical or photochemical splitting of water. But irrespective of how the hydrogen is produced, the process is endothermic and requires a considerable amount of energy input.

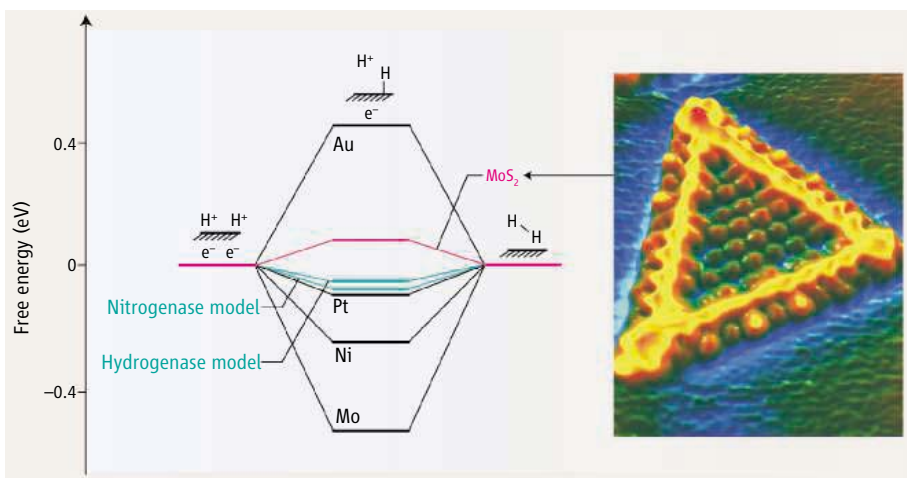
In most steam-reforming processes, this energy is provided as heat (2), whereas water splitting is usually performed electrochemically

J. K. Norskov is in the Department of Physics, Technical University of Denmark, 2800 Lyngby, Denmark. E-mail: norskov@fysik.dtu.dk C. H. Christensen is in the Department of Chemistry, Technical University of Denmark, 2800 Lyngby, Denmark. E-mail: chc@kemi.dtu.dk



Understanding catalyst activity. This calculated potential-energy diagram (6) shows one way in which methanol decomposes into molecular H_2 and adsorbed CO over a platinum surface. Elucidating this and other competing pathways for decomposition may help to devise new catalysts.

CREDIT: ADAPTED FROM (6)



Aiming for a shallow well. This calculated free-energy diagram for electrochemical H_2 formation (9) shows that some metal surfaces bind hydrogen too strongly to make hydrogen evolution likely at room temperature, whereas others bind it too weakly to allow hydrogen adsorption at all. The aim is a shallow well that allows both adsorption and evolution. (**Inset**) Scanning tunneling microscopy image of MoS_2 nanoparticles (12), showing the edges where hydrogen can adsorb and H_2 evolve.

grams (see the first figure) can provide a direct identification of the highest activation barriers, providing information on which reaction intermediates need to be stabilized to improve the overall reaction rate. With this knowledge, one can attempt to modify the surface structure or composition in a search for more active catalysts.

There is also renewed interest in the interaction of water with surfaces and in the electrochemical splitting of water into molecular oxygen and hydrogen (7, 8). For the hydrogen evolution reaction, $2(H^+ + e^-) \rightarrow H_2$, a molecular picture of hydrogen evolution has been proposed to explain why platinum is an outstanding catalyst for this reaction, whereas other metals close to platinum in the periodic table (such as nickel or gold) are not (9). Free-energy diagrams calcu-

lated with density functional theory show that hydrogen adsorption on platinum surfaces is associated with the smallest free-energy change (see the second figure) (9).

Similar calculations have modeled the interaction of atomic hydrogen with the catalytically active sites of two classes of enzymes—hydrogenases (10) and nitrogenases (9)—which catalyze hydrogen evolution. The results indicate that the enzymes have hydrogen adsorption properties very similar to those of platinum (see the second figure). The catalytic sites in these enzymes contain no noble metals but rather sulfur complexes of nickel, iron, and molybdenum. Nature seems to have found an inexpensive way of imitating platinum for this purpose.

These calculations open up the possibility of designing surfaces with nanometer-scale structure that share some of the enzyme properties. One promising material involves nanometer-scale MoS_2 particles (see the second figure, inset). This system yields reasonable hydrogen evolution rates (9), but is not as active as platinum. The biological examples indicate that there may be other metal sulfides that are better catalysts than MoS_2 , but very little research has been done, either theoretically or experimentally, in this direction.

More efficient hydrogen production methods will require more efficient catalysts. The challenge is to find inexpensive, active, and stable nanostructured materials designed for optimal performance, be it in the production of hydrogen from bioresources or via electrochemical or photochemical routes. The emerging molecular-level picture of surface reactions may soon allow us to design such catalytic surfaces on the basis of insight (11).

References

1. M. Z. Jacobson, W. G. Colella, D. M. Golden, *Science* **308**, 1901 (2005).
2. J. R. Rostrup-Nielsen, *Catal. Rev.* **46**, 247 (2004).
3. M. Grätzel, *Nature* **414**, 338 (2001).
4. R. D. Corthright, R. R. Davda, J. A. Dumesic, *Nature* **418**, 964 (2002).
5. G. A. Deluga *et al.*, *Science* **303**, 993 (2004).
6. J. Greeley, M. Mavrikakis, *J. Am. Chem. Soc.* **126**, 3910 (2004).
7. H. Ogasawara *et al.*, *Phys. Rev. Lett.* **89**, 276102 (2002).
8. J. S. Filhol, M. Neurock, *Angew. Chem. Int. Ed.* **45**, 402 (2006).
9. B. Hinnemann *et al.*, *J. Am. Chem. Soc.* **127**, 5308 (2005).
10. P. E. M. Siegbahn, *Adv. Inorg. Chem.* **56**, 101 (2004).
11. M. P. Andersson *et al.*, *J. Catal.* **239**, 501 (2006).
12. J. V. Lauritsen, R. T. Vang, F. Besenbacher, *Cat. Today* **111**, 34 (2006).

10.1126/science.1127180

ATMOSPHERE

Aerosols, Clouds, and Climate

Daniel Rosenfeld

The power of greenhouse gases to warm the planet may have been underestimated, because much of it has been masked by the cooling effects of aerosols from combustion and other pollution sources (1). Aerosols also reduce vital water resources in densely populated semi-arid regions by suppressing precipitation (2). Because pollution aerosols act as cloud condensation nuclei, clouds forming in a more polluted atmosphere contain a larger number of

smaller drops that are slower to merge and fall as precipitation. As a result, the clouds are brighter, thicker, longer-lived, and more extensive, thus reflecting more sunlight back into space and partially mitigating global warming.

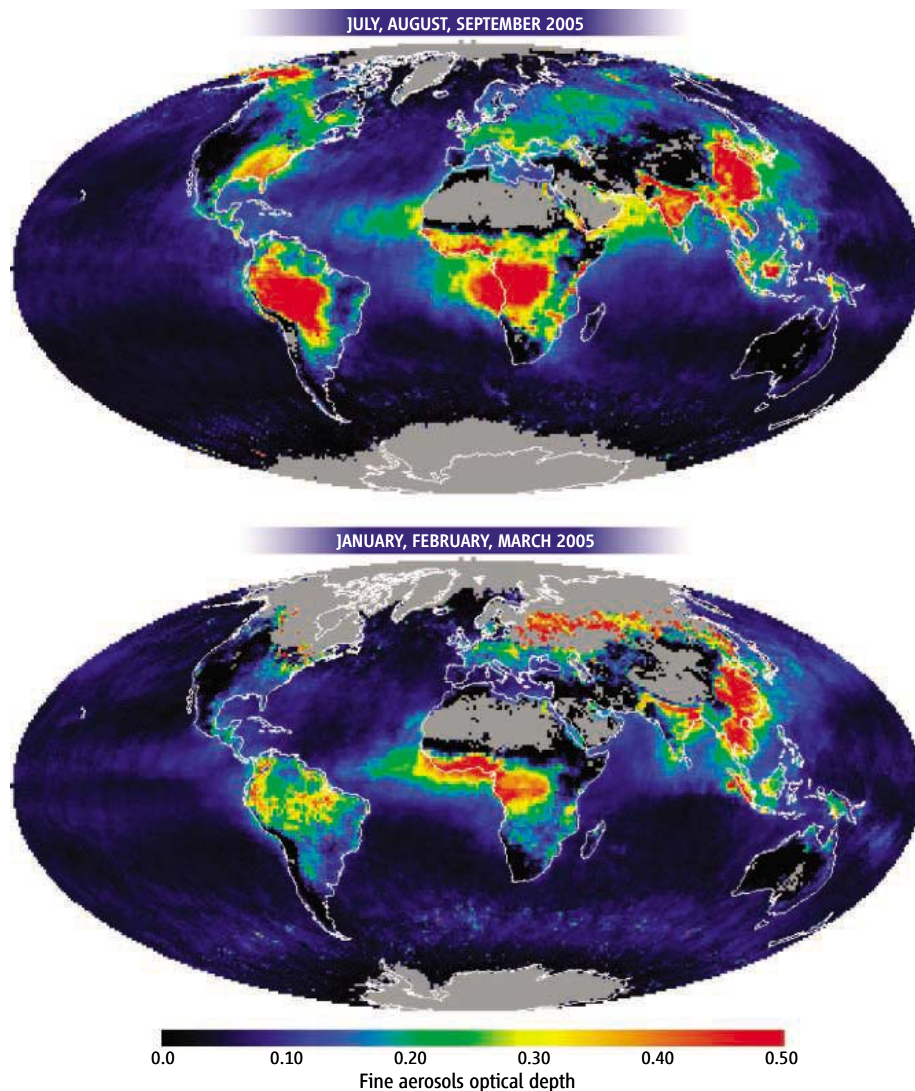
These aerosol effects are poorly quantified and represent the greatest uncertainty in our understanding of the climate system. The chemical composition of an aerosol particle is crucial to its ability to nucleate a new cloud droplet, yet measuring the chemical composition of aerosol populations on climatologically meaningful scales is very difficult. But on page 1375 of this issue, Dusek *et al.* (3) show that the size distribu-

The chemical composition of aerosol particles is much less important than their size in determining their ability to nucleate clouds, a result that will clarify aerosol effects on climate.

tion of such aerosol populations—a property that is easier to measure than chemical composition—can explain most of the variability in their cloud drop nucleating activity. This result should make it easier to quantify the effects of aerosols on clouds and hence on climate.

The cloud drop nucleating activity of an aerosol particle is determined mainly by how many water-soluble molecules and ions it can release into a newly nucleated droplet. Chemistry determines the number of soluble molecules and ions per unit mass of aerosol. This number, multiplied by the mass of the particle, determines its cloud drop nucleating activity. This is how size

The author is at the Institute of Earth Sciences, The Hebrew University of Jerusalem, Jerusalem, 91904 Israel. E-mail: daniel.rosenfeld@huji.ac.il



Toward estimating global cloud drop nucleation. MODIS measurements of the average optical depth of fine aerosols (5) during July, August, and September (top) and January, February, and March (bottom) of 2005. Dusek *et al.* show that these measurements are related more closely to the concentrations of cloud condensation nuclei than was considered previously. The large optical depth over densely populated areas is due to air pollution, and that over the tropical regions is mainly due to forest fires and agricultural burning. No measurements are made over the bright surface areas of the deserts and ice sheets. The very low values at the fringes of the deserts are caused by masking of the fine aerosols by the coarse desert dust that is dominant there (5).

comes into play. Under atmospheric conditions, particles that are at least 3 hours old always contain a significant fraction of soluble material (4). This diminishes the relative role of chemistry compared to that of size, as now substantiated and quantified by Dusek *et al.*

Assessing cloud-mediated impacts of aerosols on temperature and water resources requires measurements of aerosol cloud drop nucleating activity at both regional and global scales. Ideally, global measurements should be done by remote sensing from space. To date, most such measurements come from the Moderate Resolution Imaging Spectrometer (MODIS), which has orbited and imaged the globe since 1999. These data allow the optical depth (rep-

resenting the aerosol amount) of coarse and fine (radius $< 0.5 \mu\text{m}$) aerosols to be quantified over most of the globe (5) (see the figure). Coarse aerosols are mostly of natural origin, such as sea salt and desert dust, whereas pollution dominates the fine aerosols. The effective radius of the latter can be measured by MODIS over the dark background of the ocean. The radius of the smallest aerosols detectable by MODIS approaches $0.05 \mu\text{m}$, which is fortuitously also the most probable minimum size for aerosols to act as cloud drop nuclei (3).

Now, thanks to Dusek *et al.*, it has become easier to convert the sizes and amounts of aerosols into concentrations of particles that can nucleate cloud drops. However, measuring the aerosol

effective radius by MODIS is not quite enough to determine the concentrations of cloud condensation nuclei, for two reasons. First, at high relative humidity aerosols often expand by absorbing water, whereas we need to know their smaller dry size to calculate their cloud drop nucleating activity. Second, knowledge of the shape of the aerosol size distribution is needed to calculate the concentration of particles larger than the minimal size shown by Dusek *et al.* to have cloud drop nucleating ability. Therefore, the concentrations of cloud drop nuclei calculated from MODIS data over the ocean (5) have large error bars. Over the land, even that information is missing.

The extent of aerosol expansion due to water uptake can be partially addressed by the POLDER (Polarization and Directionality of the Earth's Reflectances) instrument onboard the Parasol mission (6) that was launched in December 2004. POLDER measures the same area simultaneously at several polarizations and extracts additional information on the size of the submicrometer aerosols and their index of refraction, a property that is closely related to the amount of water uptake by the aerosols. More accurate data on aerosol size distribution and water uptake will come from NASA's Glory mission (7), which is scheduled to be launched at the end of 2008. In addition, the Cloud-Aerosol Lidar and Infrared Pathfinder Satellite Observation (CALIPSO), launched on 28 April 2006, has started taking measurements of the vertical distribution of aerosols in the atmosphere (8). This information is essential, because aerosols must be at the level of the clouds to be able to interact with them.

MODIS, POLDER, and CALIPSO already orbit Earth as parts of a constellation of research satellites that follow each other over the same ground track, called the "A-Train." The CLOUDSAT (8) satellite, which recently joined the A-Train, measures the clouds that are potentially affected by the aerosols characterized by the other satellites. Glory is planned to join the A-Train. The collocated and synchronized measurements of aerosol and cloud properties by the satellite constellation are opening a new era in our understanding of the impact of aerosols on clouds, precipitation, and climate.

References

1. M. O. Andreae, C. D. Jones, P. M. Cox, *Nature* **435**, 1187 (2005).
2. A. Givati, D. Rosenfeld, *J. Appl. Meteorol.* **43**, 1038 (2004).
3. U. Dusek *et al.*, *Science* **312**, 1375 (2006).
4. B. Ervens G. Feingold, S. M. Kreidenweis, *J. Geophys. Res.* **110**, D18211 (2005).
5. L. A. Remer *et al.*, *J. Atmos. Sci.* **62**, 947, 2005.
6. O. Boucher, D. Tanré, *Geophys. Res. Lett.* **27**, 1103 (2000).
7. M. I. Mishchenko *et al.*, *J. Quant. Spectrosc. Radiat. Transfer* **88**, 149 (2004).
8. G. L. Stephens *et al.*, *Bull. Am. Meteorol. Soc.* **83**, 1771 (2002).



Play **Spot the Ball** with **physicsworld**

Let's see how good you are at applying physics to soccer!
Go to www.physicsweb.org/spot-the-ball today to enter our game.

Coming up... June 2006

Physics World gets in the mood for this summer's World Cup in Germany with a look at the science behind one of the key aspects of the game of soccer – the throw-in.

Dr Nick Linthorne, Lecturer in Sports Biomechanics at Brunel University, reveals how new research is proving that players can throw a ball furthest from a throw-in if they release it at 30 degrees to the horizontal, rather than 45 degrees as was previously suspected.

If you need some help with the **Spot the Ball** game, you can read this article online now.

www.physicsweb.org/spot-the-ball

Institute of **Physics** PUBLISHING



Big News

AAAS Science Journalism Awards Call for Entries

The AAAS Science Journalism Awards honor distinguished reporting on science by professional journalists. The awards are an internationally recognized measure of excellence in science reporting for a general audience. They go to individuals (rather than institutions, publishers or employers) for coverage of the sciences, engineering and mathematics.

U.S. CATEGORIES

Awards will be presented for U.S. submissions in the following categories:

- ▶ Large Newspaper
- ▶ Magazine
- ▶ Television
- ▶ Small Newspaper
- ▶ Online
- ▶ Radio

INTERNATIONAL CATEGORY

Open to journalists worldwide, across all news media.

- ▶ Children's Science News

Deadline: August 1, 2006
www.aaas.org/SJAwards



SPONSORED BY
Johnson & Johnson
PHARMACEUTICAL RESEARCH
& DEVELOPMENT, L.L.C.

AAAS
ADVANCING SCIENCE. SERVING SOCIETY

Isn't it time science discovered you?

GE & Science Prize for Young Life Scientists was established in 1995, and is presented by *Science*/AAAS and GE Healthcare. The prize was established to help bring science to life by recognizing outstanding PhDs from around the world and reward their research in the field of molecular biology.

This is your chance to gain international acclaim and recognition for yourself and your faculty, as well as to turn your scientific ideas into reality. If you were awarded your PhD in molecular biology* during 2005, describe your work in a 1,000-word essay. Then submit it for the 2006 GE & Science Prize for Young Life Scientists. Your essay will be reviewed by a panel of distinguished scientists who will select one grand prizewinner and four regional winners.

The grand prizewinner will get his or her essay published in *Science*, receive US\$25,000, and be flown to the awards ceremony in Stockholm, Sweden. Entries should be received by **July 15, 2006**.

GE & Science Prize for Young Life Scientists: Life Science Re-imagined.

For more information on how to enter, go to www.gehealthcare.com/science



Dr. Ahmet Yildiz

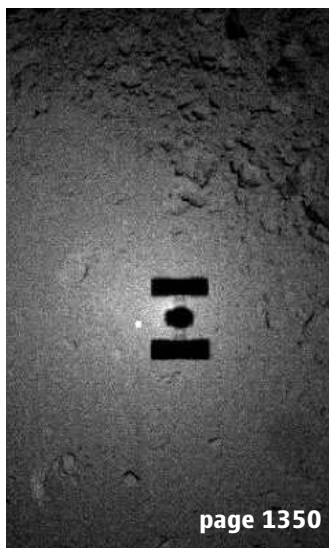
Grand prizewinner 2005 for his essay,
"Elucidating the Mechanism of
Molecular Motor Movement."



Established and presented by:



* For the purpose of this prize, molecular biology is defined as "that part of biology which attempts to interpret biological events in terms of the physico-chemical properties of molecules in a cell" (McGraw-Hill Dictionary of Scientific and Technical Terms, 4th Edition).



INTRODUCTION

The Falcon Has Landed

KILLER ASTEROIDS ARE THE STUFF OF SCIENCE FICTION MOVIES, BUT THE THREAT FROM near-Earth asteroids, at least in the long term, is real. Asteroids are small solid bodies, hundreds of meters to many kilometers in size, with rocky, perhaps icy, surfaces. Understanding of what and how they are built may not only someday help us deflect or destroy one on a collision course with Earth, but tell us how Earth was formed. Asteroids preserve within them detritus left over from the debris disk out of which the planets grew some 4.5 billion years ago. Since then, most asteroids have suffered collisions and impacts and often show the scars. Some can even be linked to collected meteorites that were ejected as a result.

Enough has been learned about asteroids to group and classify them, but basic questions about their formation remain. Overall chemical compositions can be determined from spectroscopy with ground-based telescopes and compared with meteorite samples, but morphological information requires a closer look. The first close-up pictures of lumpy asteroids Ida and Gaspra were snapped by Galileo on its way to Jupiter, and Eros' weathered surface was probed by NASA's Near Earth Asteroid Rendezvous (NEAR) Shoemaker spacecraft in 2001.

The next step requires technically challenging missions designed to land on and return samples from a variety of asteroids. The Japanese Hayabusa mission is the trailblazer. Launched in May 2003 and propelled by an ion-drive engine, in September 2005 Hayabusa reached asteroid Itokawa, a tiny rocky asteroid just 500 m across, whose elliptical orbit crosses the paths of both Earth and Mars.

The Hayabusa spacecraft ("hayabusa" means falcon) hovered 20 km above the asteroid and, in November 2005, swooped down to perch for about 30 min on its surface. Whether it managed to grasp any rocks in its robotic talon is not yet known, as the mission scientists had to wrestle hard to pull off the maneuver. Nevertheless, Hayabusa, low on fuel, is now gliding slowly back to Earth, where it may drop its cargo capsule into the Australian desert in 2010.

Whether or not Hayabusa makes it back to Earth, the papers in this issue show that it has already enlarged our view of asteroids. Unlike solid Eros, Itokawa turned out to be a strange rubble world of loose-packed rocks held together by its own tenuous gravity. Its shape suggests that two unequal lumps were squashed together in an earlier collision. Yet few craters are seen on the rocky surface, perhaps because any impacts shake the rubble pile and erase indentations. Fine gravel "seas" also cover several regions where the local gravity is weak. Infrared and x-ray spectrometers carried by Hayabusa show that Itokawa's composition is chondritic and so is typical of many other asteroids.

Hayabusa's hard-won success may yet be crowned by the return of a sample in 2010. But even now, this imaginative mission shows us that rubble-pile asteroids are weird worlds indeed.

—JOANNE BAKER

Hayabusa at Asteroid Itokawa

CONTENTS

Perspective

- 1328 Adventures in Near-Earth Object Exploration
E. Asphaug

Reports

- 1330 The Rubble-Pile Asteroid Itokawa as Observed by Hayabusa
A. Fujiwara et al.
- 1334 Near-Infrared Spectral Results of Asteroid Itokawa from the Hayabusa Spacecraft
M. Abe et al.
- 1338 X-ray Fluorescence Spectrometry of Asteroid Itokawa by Hayabusa
T. Okada et al.
- 1341 Detailed Images of Asteroid 25143 Itokawa from Hayabusa
J. Saito et al.
- 1344 Mass and Local Topography Measurements of Itokawa by Hayabusa
S. Abe et al.
- 1347 Pole and Global Shape of 25143 Itokawa
H. Demura et al.
- 1350 Touchdown of the Hayabusa Spacecraft at the Muses Sea of Itokawa
H. Yano et al.

PERSPECTIVE

Adventures in Near-Earth Object Exploration

Erik Asphaug

Asteroids, because of the hazard they pose to Earth, are compelling targets for robotic and human space exploration. Yet because of their exotic low-gravity environment, simply landing on an asteroid appears to be much more challenging than we had appreciated 5 or 10 years ago. Thanks to a bold new mission from Japan that has made the first asteroid sample return attempt, this goal is now within our reach.

Calling upon the poetry of Yeats to describe the near-failure of the risky Hayabusa mission at asteroid 25143 Itokawa might seem overly dramatic, but his words seemed all too appropriate late last year: “The falcon cannot hear the falconer; / Things fall apart.” Hayabusa (Falcon) had lost communication with Deep Space Control at ISAS, the Institute of Space and Astronautical Sciences of the Japan Aerospace Exploration Agency (JAXA). Its hydrazine had leaked away shortly after the second sample collection attempt. Two of the reaction wheels had failed and the battery was dead. Adding insult to injury, Minerva—intended to be the first asteroid surface robot—had been released during an unexpected maneuver and was lost to space. “The centre cannot hold.” Yet despite these heartbreaking setbacks, Hayabusa has been a stunning success both for asteroid science and for deep space concept testing, as reported in an exciting set of mission reports in this issue. These are the rewards of heroic efforts to make things go right in the face of multiple setbacks.

Failures are not uncommon in deep space, and in this case ingenuity and perseverance have paid off in remarkable ways. Hayabusa is the first spacecraft to visit one of the small (diameter ~300 m) asteroids that regularly come whizzing past Earth; it has returned startlingly clear images of Itokawa’s rubble surface and made the most important asteroid mass and compositional determinations since NEAR [NASA’s Near Earth Asteroid Rendezvous mission (*J*)] mapped the asteroid 433 Eros. The Hayabusa mission has also been a trial by fire of what works and does not work in spacecraft engineering and mission planning. The key instruments that performed well (the imaging camera, laser altimeter, near-infrared spectrometer, and x-ray fluorescence spectrometer) have delivered a treasure trove of knowledge that enhances our understanding of

near-Earth objects (NEOs). NEOs are not only important scientifically—our planet formed from them—but have also become political hot potatoes, given the growing pressure to “do something” to mitigate the risks they may pose to Earth.

Asteroid Itokawa is by all accounts as typical as they come—an elongate rocky body a few hundred meters across, spinning a couple of times a day, and belonging to the common S spectroscopic class of rocky asteroids. There are literally thousands of asteroids just like it on Earth-crossing orbits, many of them battered fragments from larger common parent bodies. It is remarkable that it took half a century of spaceflight to achieve reconnaissance with one of them. Itokawa is among the easiest asteroids to visit, requiring low launch velocity. It crosses

the orbits of Earth and Mars (Fig. 1) in its 1.5-year orbit around the Sun.

The Hayabusa results indicate that Itokawa is probably a chondritic rubble pile. Chondritic meteorites are the original space rocks that never underwent differentiation into core and mantle. S-type asteroids appear to be composed of the undifferentiated “raw stuff” of planet formation: olivine, pyroxene, metallic iron, plagioclase, and sulfides. The primary source region for S asteroids—along with presumably more primitive carbonaceous C types, metallic M types, igneous V types, and others—is the main belt between Mars and Jupiter. From here, asteroids get scattered by gravitational and thermal forces. The rocks of Itokawa have been battered for millions of years, or billions if you count its existence as part of a larger (but never melted) parent body that dates back to the beginning of solar system time.

After making detailed analyses of Itokawa’s incredibly blocky and complex surface, Hayabusa descended for a sample collection campaign described by Yano *et al.* (2). Site selection was a major challenge: There was no bedrock *per se* to sample, and around the largest massifs there were too many spacecraft-sized rocks. Looking for something reasonably flat, the sample return team selected an area equivalent to a gravelly beach, the Muses Sea (Fig. 2). It is unknown whether any samples actually made it into the belly of the spacecraft.

This is an exhilarating first taste of surface operations at an asteroid. From the touch-



Fig. 1. This orbital diagram, which can be generated at <http://neo.jpl.nasa.gov/orbits>, shows asteroid Itokawa along with the terrestrial planets. Positions are plotted for 17 September 2008; planets revolve counterclockwise. Itokawa regularly crosses the orbits of Mars and Earth, making its long-term orbital evolution chaotic. Earth-crossing asteroids like Itokawa are potentially hazardous but may also someday serve as ferryboats between the planets.

down sites we see with high resolution the textures of asteroid surface materials: fine gravels in the very smoothest areas (not the fine powders that were found on Eros) and boulders that are imbricated, possibly a relic of past metamorphic layering. Saito *et al.* (3) discuss the plethora of boulders and absence of craters—features that, in combination, suggest that impact reverberations (4) might be erasing the craters and sorting out the boulders [e.g., (5)].

Most asteroid scientists had not expected to find Itokawa to be a rubble pile; its gravity, smaller than that of Earth by five orders of magnitude, was thought too small to hold it together. It is not even clear why Itokawa is there at all, given that you just have to shake it gently at about 10 cm/s (escape velocity) for it to fly apart. But Itokawa hangs on to its pieces. It seems to be nothing but pieces: a sediment-world governed by ballistic mobilization and pulverization, seismic shaking by impact, vibrational size sorting, low strain rate flow of charged granules, complex gravitational dynamics, dust levitation by photoionization, and solar wind winnowing of lofted dust. Weird stuff. Impact craters are resurfaced as quickly as they form, and smooth deep gravel beds (“seas”) are found. One cannot help but wonder how an asteroid will respond to an astronaut’s first footprint. Will it be crunchy? Will she sink? Will clouds of dust rise up?

The infrared (6) and x-ray fluorescence (7) spectroscopy experiments onboard the orbiting spacecraft have determined that Itokawa is probably chondritic in composition. This is in concordance with the NEAR spectroscopic investigation of Eros (8), another S-type asteroid.

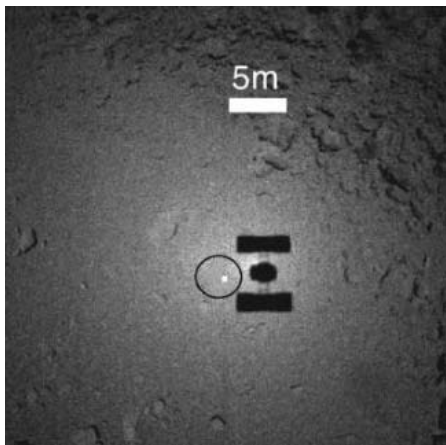


Fig. 2. Pictures from the landing on Itokawa show Hayabusa’s shadow on the Muses Sea and the bright target marker dropped onto the surface, into which 880,000 names of supporters from 149 countries are etched. The marker was used for touchdown autonavigation. [Image: ISAS/JAXA]

The density of an ordinary chondrite meteorite is around 3 to 3.5 g/cm³. Abe *et al.* (9) use laser altimetry and spacecraft telemetry to derive the mass of Itokawa (3.5×10^{10} kg), giving a density value (1.9 g/cm³). If chondritic, it must have a porosity around 40%, which is greater than the porosity of sand and about as loose as you can possibly pack a rock pile. Itokawa would have to be extremely loose rubble all the way down (10). This is consistent with spacecraft measurements and what we know of the impact evolution of asteroids, but the true test awaits a mission devoted to interior exploration that may include, for example, penetrating radar, seismological, and cratering experiments.

From afar, Itokawa looks like a potato; close up, it is a crystalline sea otter. The lumpy oblong shape (11) is common to small asteroids and may arise from gravitational instabilities where mass is shifted under repeated peppering by meteoroids. Alternatively, asteroids may take on a lumpy shape the way an old bar of soap does, by wearing down unevenly, or they may consist of reagggregated matter from a bigger impact that broke up a much larger parent body, or from a catastrophic tidal passage near Earth. How about the merger of two asteroids from the same family that collided at relatively low velocity? Hypotheses for Itokawa’s origin and a careful elucidation of the physics pertaining to these curious whirling mountains are found in Fujiwara *et al.* (10).

With no thrusters for fine control, Hayabusa no longer remains under the subtle gravitational influence of Itokawa and instead orbits the Sun. Communication has been reestablished. Late next year, its seemingly tireless solar electric propulsion system will fire up for a long-shot attempt to limp home with a return capsule that may or may not contain some grams of surface material. But engineers must first bake off the leaked hydrazine condensations, lest they torque the spacecraft during cruise. Then the engines, star trackers, and attitude control systems must all check out. And finally, reentry through Earth’s atmosphere must succeed in 2010 with no possibility of late-course correction.

If the account of Hayabusa sounds worthy of a novel, the European Space Agency (ESA) has come up with Don Quijote, a dual-spacecraft mission designed to tilt at these windmills of rock and ice. The first of the duo, Sancho, will enter orbit early and place a surface payload, including seismometers, on an asteroid not yet selected. The second spacecraft, Hidalgo, arrives at much higher speed a year later. It will make a big crater in the manner of NASA’s Deep Impact mission to comet 9P/Tempel 1 (12). This time, though, in situ instruments will characterize the impact, the formation of an al-

most natural new crater, the aftermath of seismic shaking, landslides, erasure of prior craters, and even satellite formation. You could easily spend US\$700 million on Don Quijote; the budget indicated by ESA is substantially less. Perhaps given budgetary realities, NEOs—which belong to everyone—are destined to be probed in partnership. Europe, Japan, the United States, Russia, China, and other nations bring complementary interests, resources, and technologies to the table.

NASA has taken a leadership role in asteroid exploration: NEAR was the first asteroid mission, and Galileo acquired the first spacecraft images of an asteroid. Yet NASA has not committed to a spacecraft exploration strategy for NEOs. Unlike lunar and Mars exploration, which are being pushed from the top, NEO missions are pushed from below, in principal investigator-led competition. No new NASA Discovery missions were selected in the last round, which included a handful of proposals to fly to NEOs. NASA has budgets and timelines for outer solar system exploration, for Mars exploration, and for the Moon; where is the plan and the timeline for these objects that come closest to Earth, that strike Earth, and from which Earth originally coalesced?

If we are seeking a new vision for human exploration in space, it should be emphasized that astronauts could visit a small NEO without developing a lot of new space hardware. Veteran astronaut Jones and his colleagues (13) have put forward a mission concept where a modified Soyuz crew vehicle, refueled and docked to the International Space Station (ISS), takes astronauts on a several-month “vacation” to rendezvous with an Earth-approaching asteroid, returning to the ISS for stories of adventure to be told around the galley. Perhaps asteroids are the logical, achievable first focus for human rocketry beyond the Moon; if so, then missions such as Hayabusa are paving the way.

References

1. J. Veverka *et al.*, *Science* **289**, 2088 (2000).
2. H. Yano *et al.*, *Science* **312**, 1350 (2006).
3. J. Saito *et al.*, *Science* **312**, 1341 (2006).
4. J. E. Richardson, H. J. Melosh, R. Greenberg, *Science* **306**, 1526 (2004).
5. E. Asphaug, P. J. King, M. R. Swift, M. R. Merrifield, *Lunar Planet. Sci. Conf.* **32**, abstract 1708 (2001).
6. M. Abe *et al.*, *Science* **312**, 1334 (2006).
7. T. Okada *et al.*, *Science* **312**, 1338 (2006).
8. J. I. Trombka *et al.*, *Science* **289**, 2101 (2000).
9. S. Abe *et al.*, *Science* **312**, 1344 (2006).
10. A. Fujiwara *et al.*, *Science* **312**, 1330 (2006).
11. H. Demura *et al.*, *Science* **312**, 1347 (2006).
12. M. F. A’Hearn *et al.*, *Science* **310**, 258 (2005).
13. T. D. Jones *et al.*, in *The Future of Solar System Exploration, 2003–2013*, M. V. Sykes, Ed. (ASP Conference Series, vol. 272) (Astronomical Society of the Pacific, San Francisco, 2002), pp. 141–154.

10.1126/science.1128496

REPORT

The Rubble-Pile Asteroid Itokawa as Observed by Hayabusa

A. Fujiwara,^{1*} J. Kawaguchi,¹ D. K. Yeomans,² M. Abe,¹ T. Mukai,³ T. Okada,¹ J. Saito,¹ H. Yano,¹ M. Yoshikawa,¹ D. J. Scheeres,⁴ O. Barnouin-Jha,⁵ A. F. Cheng,⁵ H. Demura,⁶ R. W. Gaskell,² N. Hirata,³ H. Ikeda,¹ T. Kominato,⁷ H. Miyamoto,⁸ A. M. Nakamura,³ R. Nakamura,⁹ S. Sasaki,¹⁰ K. Uesugi¹

During the interval from September through early December 2005, the Hayabusa spacecraft was in close proximity to near-Earth asteroid 25143 Itokawa, and a variety of data were taken on its shape, mass, and surface topography as well as its mineralogic and elemental abundances. The asteroid's orthogonal axes are 535, 294, and 209 meters, the mass is 3.51×10^{10} kilograms, and the estimated bulk density is 1.9 ± 0.13 grams per cubic centimeter. The correspondence between the smooth areas on the surface (Muses Sea and Sagami-hara) and the gravitationally low regions suggests mass movement and an effective resurfacing process by impact jolting. Itokawa is considered to be a rubble-pile body because of its low bulk density, high porosity, boulder-rich appearance, and shape. The existence of very large boulders and pillars suggests an early collisional breakup of a preexisting parent asteroid followed by a re-agglomeration into a rubble-pile object.

The Hayabusa (the original code name was MUSES-C) engineering spacecraft, launched by the fifth Mu V launch vehicle on 9 May 2003 [hereafter universal time coordinated (UTC) times are noted], was designed to acquire samples from the surface of near-Earth asteroid 25143 Itokawa (1998 SF36) and return them to Earth. The main objectives of the mission were to demonstrate the performance of various technical items such as ion engines, autonomous navigation, sampling of the asteroid's surface, and high-speed reentry into the Earth's atmosphere (1). In addition, important scientific results were expected from this mission.

Primitive asteroids are key objects in the research of the early planetary system evolution process. Spectroscopic observations of asteroids have resulted in about a dozen spectral classes. To draw a first-order big picture for the whole asteroid region, we need to know the physical properties of

asteroids of each spectral class and to assign each class to a corresponding meteorite group. This is possible by sending a small number of spacecraft to well-selected asteroids that are individual representatives of the major spectral types. Once this is achieved, we can make maximum use of the abundant meteorite data to understand the origin and the evolution of the corresponding spectral class of asteroids. This sample return mission was intended to initiate this program.

¹Institute of Space and Astronautical Science (ISAS), Japan Aerospace Exploration Agency (JAXA), 3-1-1 Yoshinodai, Sagami-hara, Kanagawa 229-8510, Japan. ²Jet Propulsion Laboratory, California Institute of Technology, Pasadena, CA 91109, USA. ³Graduate School of Science and Technology, Kobe University, 1-1 Rokkodai-cho, Nada, Kobe, Hyogo 657-8501, Japan. ⁴Department of Aerospace Engineering, University of Michigan, Ann Arbor, MI 48109-2140, USA. ⁵Applied Physics Laboratory, Johns Hopkins University, Laurel, MD 20723, USA. ⁶School of Computer Science and Engineering, Aizu University, Ikki-machi, Aizu, Fukushima 965-8580, Japan. ⁷NEC Aerospace Systems Limited, 4206 Ikebe, Tsuzuki, Yokohama, Kanagawa, 224-0053, Japan. ⁸Department of Geosystem Engineering, University of Tokyo, Tokyo 113-8656, Japan. ⁹Grid Technology Research Center (GTRC), National Institute of Advanced Industrial Science and Technology (AIST), Umezono 1-1-1, Tsukuba 305-8568, Japan. ¹⁰Mizusawa Astrodynamics Observatory, National Astronomical Observatory of Japan, 2-12 Hoshigaoka, Mizusawa, Iwate 023-0861, Japan.

*To whom correspondence should be addressed. E-mail: fujiwara@planeta.sci.isas.jaxa.jp

Before the final selection of Itokawa, the target asteroid was changed twice because of changes in mission scenarios and a delay in the spacecraft launch schedule. Itokawa, an Apollo asteroid discovered in 1998, follows its orbital path from 0.9530 astronomical units (AU) just inside the Earth's orbit to 1.6947 AU just outside of the orbit of Mars. Its orbit allows close encounters with the Earth, a circumstance that provides frequent opportunities for ground-based observations. Photometric observations (2, 3) and radar observation (4) provided the initial shape models; the rotational period was found to be 12.1 hours, the rotation axis is almost perpendicular to the ecliptic plane, and the rotation direction is retrograde. Spectrally, Itokawa is classified as an S-type asteroid, a type common in the inner portion of the asteroid belt. The surface mineralogy is apparently dominated by silicates (pyroxene and olivine) and Fe metal (5). Hence, spectral observations of Itokawa were expected to form baseline measurements representative of these common asteroids. However, this asteroid was selected primarily because it is one of the most accessible targets for the low-energy launch vehicle.

One crucial issue in the current asteroid research is the puzzle of the rubble-pile structure. Although some asteroid researchers have supposed that most of the asteroids larger than about 1 km in size should be rubble piles, there has been no definite evidence of the rubble-pile structure for any of the asteroids observed to date by spacecraft.

Hayabusa's trajectory to the asteroid is illustrated in Fig. 1A. After cruising with nearly

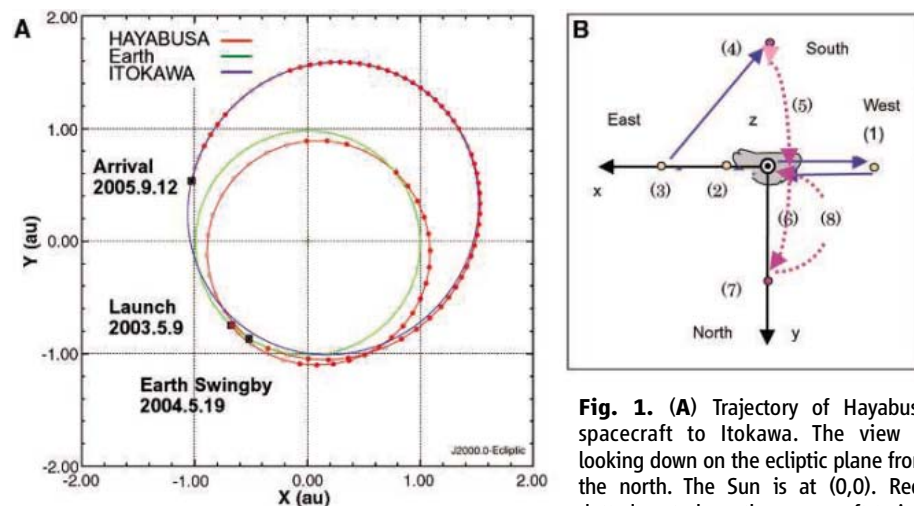


Fig. 1. (A) Trajectory of Hayabusa spacecraft to Itokawa. The view is looking down on the ecliptic plane from the north. The Sun is at (0,0). Red-dotted part along the spacecraft trajectory denotes the thrust direction of ion engines is northward, while other southward. (B) The spacecraft undertook a tour near the asteroid after achieving the home position observation. The view is from the Sun. The asteroid and the home position are overlapped at the origin. Arrows indicate the sequential path of the spacecraft. Dots show the hovering sites. Each spacecraft position indicated by the number in the figure corresponds to the dates that follow: position (1), 8 to 10 October, westward, high phase angle; (2), 12 and 13 October, zero solar phase angle; (3), 15 October, east side high, phase-angle; (4), 17 and 18 October, south pole; (5), 20 October, south pole, low altitude (~4 km); (6), 22 October, north pole, low altitude (~4 km); (7), 23 and 24 October, north pole; (8), 27 and 28 October, low altitude observation (~3 km). Dashed lines include low-altitude observation.

continuous operation of the ion engines and an Earth swingby on 19 May 2004, the spacecraft arrived at an altitude of about 20 km (Gate position) near the sub-Earth point on 12 September 2005 (Fig. 1A). After a period of reconnaissance operation, the spacecraft transferred to the nominal hovering position (Home position) on 30 September 2005, at an altitude of about 7 km from the asteroid's surface and near the sub-Earth point.

Observational instruments onboard the Hayabusa spacecraft include a telescopic imaging camera (AMICA) with both a wide band-pass filter and seven narrowband filters, a near-infrared spectrometer (NIRS), a laser ranging instrument (LIDAR), and an x-ray fluorescence spectrometer (XRS). Specifications of these instruments are given in the following reports in this issue (6–9). A microrover named MINERVA (micro/nano experimental robot vehicle for asteroid), carrying a pair of stereoscopic imaging cameras, one short focal length camera, and thermal probes was released, but its landing onto the asteroid's surface was unsuccessful.

During 8 to 28 October 2005, the spacecraft left the home position and made tours to various altitudes and solar phase angles to access the polar regions and make high resolution topographic images under differing lighting conditions (Fig. 1B). On the basis of topographic and spectroscopic data, a surface sampling location on a smooth terrain called Muses Sea was selected. The touchdown, the 30-min stay on the asteroid surface, and the liftoff were performed on 19 and 25 November.

At the time of the second touchdown, a small pellet should have been fired into the surface to get the ejected surface sample, but subsequent spacecraft telemetry suggests that the ignition for this shooting may not have occurred. In the first touchdown, however, there is a possibility that some surface material was flicked by the tip of the sampler and captured during the stay on the asteroid's surface. The return of the spacecraft and the sample capsule to Earth is now expected in June 2010, postponed from the original time of June 2007 because of problems with the chemical propulsion system.

Itokawa's fundamental parameters are summarized in Table 1. The pre-arrival results from ground-based observations (2–5) were all confirmed by the Hayabusa data within the observational uncertainties. The pole position was solved by tracking the ground control points on an AMICA image. There was no apparent short-term precession of the spin pole.

The mass of Itokawa was estimated from the Hayabusa tracking and navigation data by using different methods and data intervals. Initially, the mass was estimated by using range and Doppler data when Hayabusa moved from the gate position to home position (from 12 September to the beginning of October 2005). The estimated value was 3.51×10^{10} kg with an uncertainty of 15%. The mass determination undertaken at this time suffered somewhat from errors because the effect of the radiation pressure was much larger than Itokawa's gravity. Therefore, we expected that we would be able to estimate the mass of Itokawa more accurately when Hayabusa approached

Itokawa much more closely. However the second reaction wheel had a problem at the beginning of October 2005. After that, the chemical thrusters were used frequently to control the altitude, and this compromised subsequent mass determination attempts. On 21 and 22 October 2005, at a distance about 3 km from Itokawa, we intentionally stopped the altitude maneuvers and tried to estimate the mass of Itokawa by using Doppler, range, LIDAR, and optical data. The estimated mass was 3.43×10^{10} kg with an uncertainty of 5%. The mass of Itokawa was also obtained on 12 November 2005, when the spacecraft approached Itokawa within a distance of 100 m. By using LIDAR data (6) as well as the navigation data and by considering the effects of attitude maneuvers, we estimated the mass of Itokawa during two orbit spans of this approach; the distances from Itokawa were 1400 to 800 m and 800 to 100 m. The estimated masses for these two spans were 3.58×10^{10} kg with an uncertainty of 5% and 3.54×10^{10} kg with an uncertainty of 6%, respectively. Therefore we have four separate estimations of Itokawa's mass, which are consistent within each estimation error. Calculating the weighted mean, we take the value of 3.51×10^{10} kg as the most probable mass estimate. The uncertainty of this value is 3%.

The volume of Itokawa was estimated on the basis of the three-dimensional shape models created by the following three independent methods: (i) The limb profiling method, which integrates the outlines of images. This result is obtained most quickly and easily, but it cannot reproduce the concave surface areas. (ii) Stereogrammetry (multi-viewpoints' epipolar method). This model is constructed by using the stereometric views of representative points selected from the surface. The result depends on how the representative points can be appropriately extracted. (iii) Shaping from shading (photoclinometry). This model is constructed from the information on the surface brightness slopes, assuming the scattering properties of the surface are known. The volume adopted here is $1.84 \pm 0.092 \times 10^7$ m³ (5% uncertainty) (10). Thus, the bulk density of Itokawa is 1.9 ± 0.13 g cm⁻³.

Itokawa's shape resembles a sea otter (Fig. 2). It is composed of two parts; one is named the otter's "head" (smaller one) and the other is the otter's "body" (larger one) from their appearance (referred to hereafter as head and body). Both parts are not angular, like asteroid 951 Gaspra, but rather rounded. The appearance of the surface from the home position is, at first look, somewhat similar to the image of 433 Eros' surface at the same scale, but even in these images Itokawa's surface is still rougher and more boulder-rich. The Eros surface is globally covered with a thick regolith layer (11).

The surface of Itokawa is divided into rough terrain, mostly consisting of numerous boulders and smooth terrain (Muses Sea extending around the "neck" area between the head and body and

Table 1. Parameters for 25143 Itokawa. Osculating orbital elements are calculated from position and velocity at the specified time (Epoch – 2006 March 6.0 TDB, where TDB is barycentric dynamical time, TDB – UT = 65.2 seconds). These are from ground-based observations where a , e , q , Q , Ω , ω , i , and T are the semi-major axis, eccentricity, perihelion distance, aphelion distance, longitude of the ascending node, argument of perihelion, and the perihelion passage time, respectively. β , λ and RA, DEC are right ascension and declination in space and on the body, respectively.

Property	Value
Osculating orbital elements	$a = 1.3238$ AU $e = 0.2801$ $\Omega = 69.0949^\circ$ $\omega = 162.7526^\circ$ $i = 1.6223^\circ$ $q = 0.9530$ AU $Q = 1.6947$ AU $T = 2005$ November 27.2169 TDB S(IV) (5)
Spectral type	
Size (diameter)	
Major axes	$x = 535$ m, $y = 294$ m, $z = 209$ m (± 1 m)
Osculating box size	550 m by 298 m by 224 m (± 1 m)
Rotational properties	
Period	12.1324 ± 0.0001 hours (31)
Pole position in the space	$[\beta, \lambda] = [-75^\circ \pm 12^\circ, 320^\circ \pm 30^\circ]$ (3) $[-84^\circ \pm 5^\circ, 355^\circ]$ (2) $[\beta, \lambda] = [128.5, -89.66]$ (J2000 ecliptic) retrograde ($\pm 6.9^\circ$)
on the body	$[RA, DEC] = [90.53, -66.30]$ ($\pm 6.9^\circ$) (J2000 equator)
Volume	$1.84 \times 10^7 \pm 0.092 \times 10^7$ m ³
Mass	$3.51 \times 10^{10} \pm 0.105 \times 10^{10}$ kg
Density	1.9 ± 0.13 g cm ⁻³

Sagamihara around the north polar region). The smooth region is apparently similar to the Eros pond in the low resolution image, but it was found to be composed of fragmental debris with grain sizes of cm to mm scales from close-up images (12).

The largest boulder, Yoshinodai, is located near the end of the body and several boulders with sizes larger than a few tens of meters were found on the western side (180° to 360°E), whereas large boulders are less abundant on the eastern side. A black boulder exists at the end of the head and this feature marks the body's prime meridian. Large pinnacles are seen in the neck region on the western side associated with landslide-like topography (7). There is no substantial difference in mineralogical composition over the whole asteroid's surface in spite of the bifurcated appearance of Itokawa's shape (8, 9).

The surface slopes, potential, and accelerations were computed by combining a polyhedral model of the Itokawa shape and the total estimated mass of the body. Assuming a constant density, the gravity field potential and acceleration at the surface can be evaluated analytically (13) and combined with the centripetal potential and acceleration to compute the amended potential, total acceleration, surface slope, and other dynamical quantities of interest (14). Figure 3 presents two such computations, the relative potential over the surface of the body and the surface slope over the body. It is noted that toward both end regions the potential becomes higher whereas low potential regions exist near the neck and northern areas on the body. There are two regional areas where the surface consistently has slopes less than 8°: an isolated region about the north pole and the Muses Sea area. In these regions, smooth terrain was observed and maintains its smoothness down to at least cm to mm sizes. A surface region with near-zero slopes can be considered locally to be an energetically relaxed shape, because the surface normal and the net acceleration acting at the region are approximately aligned with each other. This would be consistent with a loose granular layer in these regions that has been allowed to seek out its minimum energy. Hence, the accumulation of small grains could be explained by secondary movement of these grains on the surface through seismic shaking induced by impacts (15), shifting tidal loads from close planetary flybys, or perhaps electrostatic levitation for the finest sub-mm components if they exist (16). The existence of a thermally insulating layer consisting of gravels (12) in the smooth terrain and boulders in the rough terrain on the surface of Itokawa is also suggested by recent ground-based thermal inertia measurements (17). Itokawa's thermal inertia of $750 \text{ J m}^{-2} \text{ s}^{-0.5} \text{ K}^{-1}$ is more than an order of magnitude higher than that for large main-belt asteroids (5 to $25 \text{ J m}^{-2} \text{ s}^{-0.5} \text{ K}^{-1}$) and for the Moon ($50 \text{ J m}^{-2} \text{ s}^{-0.5} \text{ K}^{-1}$).

Past impacts by interplanetary projectiles would have repeatedly fragmented and ejected Itokawa's surface material. Most of the finest ejecta particles would have velocities much higher than 10 to 20 cm s^{-1} and would have easily escaped from Itokawa's surface. In impact experiments, the fragments having velocities less than this escape velocity are limited to a very small number of the largest fragments, with ejection being less effective for granular targets (18, 19). Hence, one could suppose that finer particles are gradually lost as a result of impacts and the surface becomes covered with an abundance of larger boulders.

However, cm- to mm-sized regolith does exist on Itokawa's surface. One probable scenario is that such grains existed from the initial formation of the head and body and have been gradually depleted through cratering. Perhaps grains may be continuously produced if Itokawa is composed of boulder aggregates of various sizes with considerable macroporosity, at least near the surface. This structure would not only reduce the shock effect during impacts but also produce fine fragments in the shallow interior, if the characteristic size of the aggregate boulders is roughly comparable with the projectile sizes. Thus, a considerable amount of grains will be retained within the interior of the asteroid, and the fine particles can easily migrate through the larger boulders toward the low-potential regions like Muses Sea.

There is an empirical relationship between the size of a crater and the maximum size of the ejected fragment (20), which can well explain the relation of the largest boulder and the largest crater found on Eros (21). Following this empirical relationship, the size of the crater that would have produced the largest boulder, Yoshinodai, and some others actually exceeds the size of the largest craters found on Itokawa. Hence, these boulders are the likely relics

formed in some cataclysmic event related to the formation of Itokawa's rough current shape.

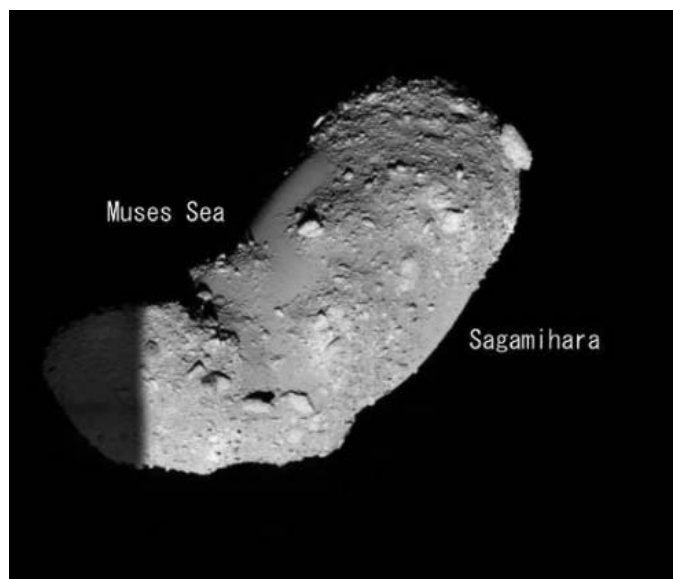
Itokawa's bulk density of 1.9 g cm^{-3} is considerably lower than the $\sim 2.6 \text{ g cm}^{-3}$ determined for other S-type asteroids with well-determined bulk densities (21). Assuming that LL ordinary chondrites are reasonable analogs for Itokawa's composition (8) and a typical value for their bulk density is 3.2 g cm^{-3} (22), the macroporosity of Itokawa is estimated to be $\sim 41\%$. This value is substantially higher than the average value of $\sim 30\%$ for S-type asteroids, including Eros. Although it is not clear what the relative micro- and macroporosity values are, it is clear that Itokawa contains considerable void space in its interior. At least in terrestrial geology, porosities larger than 30% usually indicate loose soils or rubble (22).

The head and body are round in shape, rather than irregular as is typical for a monolithic fragment. This is also suggestive of the configuration that a rubble pile would preferentially evolve toward over long time intervals.

There are no conspicuous long linear structures extending nearly the entire length of the asteroid like the long ridge found on Eros (23), and this, coupled with the existence of some faint local facets with scales of at most several tens of meters, suggests that Itokawa is not a single consolidated, coherent body but rather an aggregate of rubble with sizes ranging up to about 50 m . It seems very likely that Itokawa has a rubble pile structure.

Careful observation of the head and body shows these surfaces are composed of many facets (7). In particular, the shape of the head looks like a polyhedron composed of many facets. Because the floors of craters formed on convex surfaces become flatter or even convex as the surface convexity increases (24), some of the facets observed on Itokawa could be of impact origin. The typical

Fig. 2. Image of Itokawa taken at 7-km altitude taken from 6 km on 18 October (western side as seen from neighbor of south pole). Width of sight is 600 m.



example of this type is Little Woomera, a circular structure of diameter about 150 m extending around the end of the body (180°E). There is, however, a possibility that some facets could be the exposed surfaces of large fragments embedded near the asteroid's surface [for example, see the lateral side of the body in figure 2 in (10)].

If Itokawa was once a coherent body, it might have experienced collisional disruption followed by re-agglomeration. Hence, Itokawa could be either a young object or a loosely consolidated body, or both. Few asteroids as large as, or larger than, Itokawa are fast rotators, and this evidence has been used to argue that most asteroids larger than about 150 m may be rubble piles (25).

The existence of large facets and many boulders implies that Itokawa has experienced a number of large impacts (paucity of craters is due to shaking, and this does not deny many past impacts). If the asteroid is a gravitationally aggregated body and has large macroporosity, impact shocks should not be transmitted effectively (26), which would suppress further impact disruptions.

Landslide-like deposits at the base of the head are observed (10), and this region has slopes in excess of 35° (Fig. 2B). On Itokawa, most angular grain materials have an angle of repose on the order of 32° to 35°, and slope angles in excess of this height cannot be maintained unless there is cohesion. The observation of the candidate landslide, and the fact that the steep slopes on the head measure up to near 50°, may suggest that at least this region resulted from an angular rubble pile that collapsed.

Itokawa looks to be composed of two parts, the head and the body. There are plausible origin scenarios to produce such a bifurcated configuration.

The first scenario is the contacted bodies hypothesis: Originally the head and body could have formed separately and later come into contact at a slow relative speed, and, almost retaining the original shape of both bodies but with some mass movement, the present shape of Itokawa was formed. Between the head and body, a depressed neck zone is observed, and in this region there is a high-slope region (expressed as yellow in Fig. 3B) that suggests that the head was once an independent body and that the material has not yet completely relaxed into the neck region. The prominent ridge in Muses Sea near the south side of the neck may have originated from the collision of the head and the body. The different orientations of the principal axes of the head and body (7) also imply these bodies were originally separate and were produced by a slow collision between the head and body. The likely scenarios for the origin of the contacted body would include the following: (i) Formation by capture of two independent asteroids. This is in fact unlikely because of the low probability of encounters at relative velocities lower than the crushing velocity, and there is no hard evidence that strongly suggests that the head and body originated from two independent asteroids. (ii) Mutual capture of two fragments after catastrophic disruption of a larger parent body, which might be possible, as indicated by numerical modeling

results (26). However, capture scenarios may have difficulty accounting for the ellipsoidal shapes of the head and the body. (iii) Mutual agglomeration after a catastrophic breakup of the parent body. The flying fragments agglomerated (27), forming some rubble-pile bodies, two of which may have co-orbited around one another and, after development of the ellipsoidal shapes, then came into contact as a result of some unknown event, for example, after a close planetary encounter (28). (iv) Rotational fission due to an excessive spin rate, which however is not consistent with the currently observed spin rate. (v) Mass shedding resulting from tidal disruption during a close planetary encounter.

Another possible scenario for the formation of the depressed neck region includes it being formed by a large impact. In this scenario, the body originally existed as a single entity and a large impact formed the depression presently seen at the neck region on Itokawa. Impact experiments suggest that a large impact on the lateral side of an elongated body could produce a saddle-like depression (24). It is plausible that an impact could cause a large breakage at the neck region or perhaps separate the body into two parts (body and head). Then both bodies could have settled back together, forming the present shape of Itokawa.

The properties of Itokawa found by Hayabusa, such as its being boulder-rich and with a rubble pile structure, may be common for small S-type asteroids because Itokawa does not belong to any special category with respect to parameters such as spectra, rotational period, and orbital

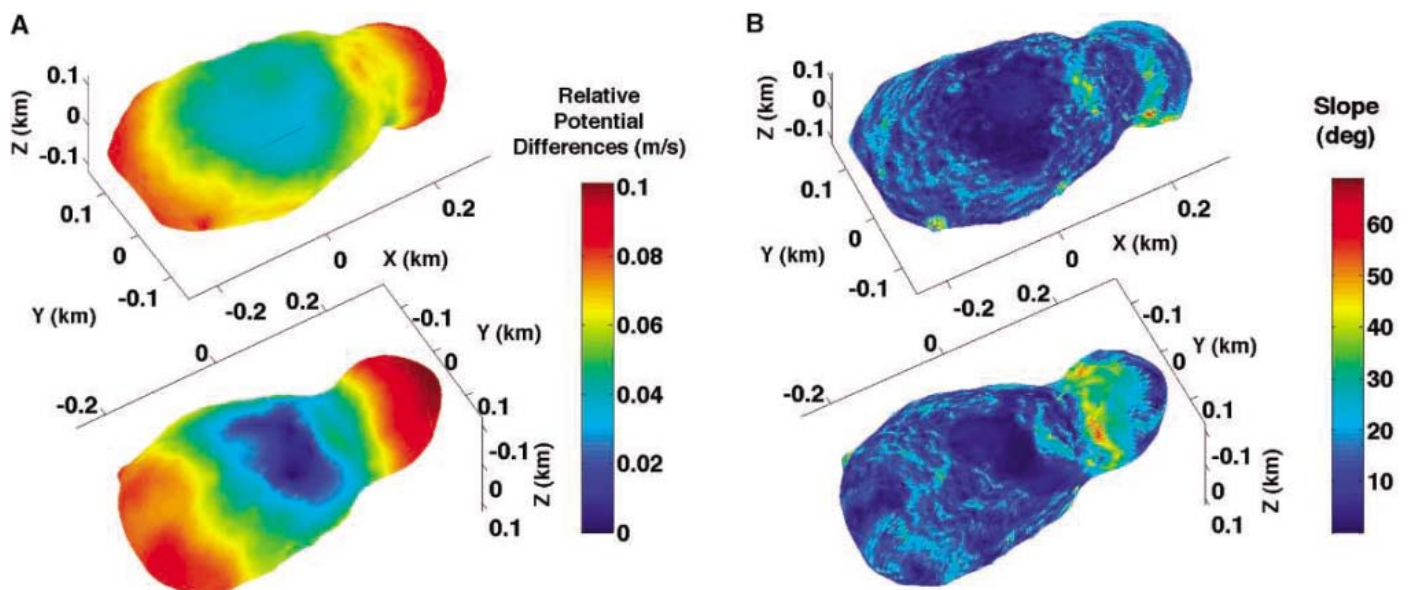


Fig. 3. (A) Relative gravitational and rotational potential mapped onto an Itokawa shape model. This plot measures the speed needed to energetically transition from the lowest potential point on Itokawa to any other region (30). Conversely, it measures the speed a particle dropped with zero speed at that location if it fell unimpeded to the lowest potential point on Itokawa, which is situated within the Muses Sea region. Top and bottom

views show the northern and southern hemisphere, respectively. **(B)** Surface slopes mapped onto an Itokawa shape model. The slopes are defined as the angle between the local surface normal and the total gravitational and rotational acceleration acting on a particle at that surface location (14). Upper and lower views show northern and southern hemispheres, respectively.

elements. Moreover, it should also be noted that elongated asteroids and binary asteroids are numerous among the near-Earth asteroid population (29) and that these characteristics are consistent with these objects evolving into contact binary systems. In this sense, the Hayabusa results provide a benchmark for understanding general properties of small asteroids.

References and Notes

- J. Kawaguchi *et al.*, *Acta Astronaut.* **52**, 117 (2003).
- M. Kaasalainen *et al.*, *Astron. Astrophys.* **405**, L29 (2003).
- Y. Ohba *et al.*, *Earth Planets Space* **55**, 341 (2003).
- S. J. Ostro *et al.*, *Meteorit. Planet. Sci.* **39**, 407 (2004).
- R. J. Binzel *et al.*, *Meteorit. Planet. Sci.* **36**, 1167 (2001).
- S. Abe *et al.*, *Science* **312**, 1344 (2006).
- J. Saito *et al.*, *Science* **312**, 1341 (2006).
- M. Abe *et al.*, *Science* **312**, 1334 (2006).
- T. Okada *et al.*, *Science* **312**, 1338 (2006).
- H. Demura *et al.*, *Science* **312**, 1347 (2006).
- C. R. Chapman *et al.*, *Icarus* **155**, 104 (2002).
- H. Yano *et al.*, *Science* **312**, 1350 (2006).
- R. A. Werner, D. J. Scheeres, *Celestial Mech. Dyn. Astron.* **65**, 313 (1997).
- D. J. Scheeres, S. J. Ostro, R. S. Hudson, R. A. Werner, *Icarus* **121**, 67 (1996).
- A. F. Cheng *et al.*, *Meteor. Planet. Sci.* **37**, 1095 (2002).
- P. Lee *et al.*, *Icarus* **124**, 181 (1996).
- T. G. Mueller *et al.*, *Astron. Astrophys.* **443**, 347 (2005).
- A. Nakamura *et al.*, *Icarus* **92**, 132 (1991).
- E. Asphaug *et al.*, in *Asteroids III*, W. F. Bottke Jr., A. Cellino, P. Paolicchi, R. P. Binzel, Eds. (Univ. Arizona Press, Tucson, AZ, 2002), pp. 463–484.
- D. E. Gault *et al.*, *NASA Technical Document TND-1767*, 39 (1963).
- P. C. Thomas *et al.*, *Nature* **413**, 394 (2001).
- D. T. Britt *et al.*, in *Asteroids III*, W. F. Bottke Jr., A. Cellino, P. Paolicchi, R. P. Binzel, Eds. (Univ. Arizona Press, Tucson, AZ, 2002), pp. 485–500.
- J. Verweke *et al.*, *Science* **278**, 2109 (1997).
- A. Fujiwara *et al.*, *Icarus* **105**, 345 (1993).
- R. J. Whitely *et al.*, *Icarus* **157**, 157 (2002).
- E. Asphaug *et al.*, *Nature* **393**, 437 (1998).
- P. Michel *et al.*, *Nature* **421**, 608 (2003).
- P. Michel *et al.*, *Icarus* **179**, 291 (2005).
- W. J. Merline *et al.*, in *Asteroids III*, W. F. Bottke Jr., A. Cellino, P. Paolicchi, R. P. Binzel, Eds. (Univ. Arizona Press, Tucson, AZ, 2002), pp. 289–312.
- The gravitational plus rotational potential is defined by the Jacobi integral of the system: $J = V^2/2 - U(r)$, where U is the gravitational plus centripetal force potential, r defines a location on the surface of the body, and V is the speed of a particle relative to the rotating body frame (14). The gravitational plus rotational potential is defined as the value of J evaluated for zero speed or the value of $-U(r)$ over the surface of the body. The speed necessary to have sufficient energy to travel from the lowest point of the potential [largest value of $U(r)$ at location r^*] to any other point r on the surface of the body is then $\sqrt{2[U(r^*) - U(r)]}$, which is plotted in the figure.
- S. Nishihara *et al.*, *Lunar Planet. Sci. Conf. XXXVI*, abstr. 1833 (2005).
- We thank the mission operation and spacecraft team of the Hayabusa project at ISAS/JAXA for their efforts that resulted in making Hayabusa the first Japanese spacecraft rendezvoused and landed at the asteroid. This research was supported by ISAS/JAXA, NASA, Kobe University through the 21st Century COE Program of the Origin and Evolution of Planetary Systems, and University of Aizu. A portion of the research reported in this paper was performed at the Jet Propulsion Laboratory, California Institute of Technology, under a contract with NASA.

6 February 2006; accepted 6 April 2006
10.1126/science.1125841

REPORT

Near-Infrared Spectral Results of Asteroid Itokawa from the Hayabusa Spacecraft

M. Abe,¹ Y. Takagi,² K. Kitazato,^{1,3} S. Abe,⁴ T. Hiroi,⁵ F. Vilas,⁶ B. E. Clark,⁷ P. A. Abell,⁸ S. M. Lederer,⁹ K. S. Jarvis,^{8,10} T. Nimura,^{1,3} Y. Ueda,³ A. Fujiwara¹

The near-infrared spectrometer on board the Japanese Hayabusa spacecraft found a variation of more than 10% in albedo and absorption band depth in the surface reflectance of asteroid 25143 Itokawa. Spectral shape over the 1-micrometer absorption band indicates that the surface of this body has an olivine-rich mineral assemblage potentially similar to that of LL5 or LL6 chondrites. Diversity in the physical condition of Itokawa's surface appears to be larger than for other S-type asteroids previously explored by spacecraft, such as 433 Eros.

Visible and near-infrared spectroscopic observations (from 0.3 to 3.3 μm) have been used extensively to study the mineralogy and physical properties of asteroid surfaces. These data are compared with similar

laboratory measurements of meteorites from asteroids to determine the geologic history of the asteroid regions. Because most of the asteroids have not experienced major mineralogical alteration since the formation of the solar system, study of their chemical and physical properties tells us about the earliest epochs of planet formation. Asteroid 25143 Itokawa (previously 1998 SF36) has been observed unresolved from ground-based telescopes at mineralogically diagnostic wavelengths (1, 2) and has been found to be similar to ordinary chondrite and/or primitive achondrite meteorites. Here, we report spectral observations of Itokawa at high spatial resolution and place them in the context of their geologic interpretation.

The near-infrared spectrometer (NIRS) onboard the Japanese Hayabusa spacecraft (also known as MUSES-C) obtained more than 80,000 spectra of asteroid Itokawa during mapping operations at the asteroid from September

to November 2005. NIRS has a 64-channel InGaAs photodiode array detector and a grism (a diffraction grating combined with a prism). The dispersion per pixel is 23.6 nm. Spectra were collected from 0.76 to 2.1 μm (3). The NIRS field of view ($0.1^\circ \times 0.1^\circ$) was aligned with the LIDAR (Light Detection and Ranging) and the AMICA (Asteroid Multiband Imaging Camera) fields of view before launch. During the cruising and mapping phases, this colignment was verified multiple times.

The first spectrum from Itokawa was obtained by NIRS on 10 September 2005 at a distance of 50 km from the asteroid. NIRS spectra were obtained at solar phase angles ranging from near 0° to 38° and at footprint sizes ranging from 6 to 90 m^2 (not including the touchdown phase of the mission). Most spectra were obtained between 7° and 11° solar phase angle during the first mapping phase of the mission in September.

During this mapping phase, while the spacecraft was 7 to 20 km from the asteroid, an equatorial scan was performed using only the rotation of the asteroid to shift the pointing of NIRS. During the second mapping phase in October 2005, a two-dimensional scan was obtained by slewing the attitude of the spacecraft in the direction of the rotational axis of the asteroid. The spacecraft hovered at a distance of 3.5 to 7 km above the asteroid during this time. The position of the spacecraft was limited to near 0° Earth phase angle during the first mapping phase, but after arriving at a distance of 7 km from the asteroid's surface, the spacecraft was moved off the Earth-asteroid line to vary the solar phase angle and aspect angle while observations were performed.

Itokawa's phase curve (brightness as a function of varying solar phase angle) at NIRS wavelengths can be compared to phase curves of

¹Institute of Space and Astronautical Science, Japan Aerospace Exploration Agency, 3-1-1 Yoshinodai, Sagami-hara, Kanagawa 229-8510, Japan. ²Toho Gakuen University, 3-11 Heiwagaoka, Meito, Nagoya, Aichi 465-8515, Japan. ³University of Tokyo, 7-3-1 Hongo, Bunkyo, Tokyo 113-0033, Japan. ⁴Graduate School of Science and Technology, Kobe University, 1-1 Rokkodai, Nada, Kobe, Hyogo 657-8501, Japan. ⁵Department of Geological Science, Brown University, Providence, RI 02912, USA. ⁶MMT Observatory, Post Office Box 210065, University of Arizona, Tucson, AZ 85721, USA. ⁷Department of Physics, Ithaca College, Ithaca, NY 14850, USA. ⁸National Aeronautics and Space Administration, Lyndon B. Johnson Space Center, Houston, TX 77058, USA. ⁹Department of Physics, California State University, 5500 University Parkway, San Bernardino, CA 92407, USA. ¹⁰ESC Group/Hamilton Sundstrand, 2224 Bay Area Boulevard, Houston, TX 77058, USA.

similar asteroids at similar wavelengths. There are differences in reflectance at the same phase angle (Fig. 1A), because the incidence and

emission angles within the NIRS' footprint vary. To compare Itokawa to other asteroids, we binned the data with respect to phase angle and selected

spectra with maximum reflectance within a 0.2° phase angle bin and fitted a Hapke five-parameter shadow-hiding model photometric function (4). Overplotted on the data is the fitted phase curve for asteroid 433 Eros at 950 nm (5). Itokawa appears to have an opposition surge (nonlinear brightening near zero phase) with a lower amplitude and narrower angular width than Eros. In theory, this would indicate that the average particle on Eros is more opaque than the average particle on Itokawa, and/or that Eros has a lower surface porosity than Itokawa. This is consistent with the data that so far indicate a brighter geometric albedo (at $0.55 \mu\text{m}$) for Itokawa ($\sim 30\%$) (6–9) than for Eros ($\sim 25\%$) (5, 10). However, we hesitate to use phase curves to predict other surface characteristics (such as grain sizes) of Itokawa and Eros on the basis of the information available because of the following factors: (i) The Itokawa data have a limited phase angle range (0° to 38°), (ii) the five-parameter photometric model is not accurate to the level required, and (iii) the viewing angles of the Itokawa spectra are preliminary.

Itokawa is observed to spectrally redden with increasing phase angle (Fig. 1B). Phase reddening has been observed in laboratory studies of particulate media (11) and was predicted to occur on asteroids; the Near Earth Asteroid Rendezvous (NEAR) spacecraft made the first such actual observation at Eros (5, 12). The physical mechanism for the effect is still unclear [e.g., (13)]. However, it has been suggested that the single-scattering albedo, and hence multiple scattering, are more important controls of phase reddening than is the single-particle phase function (13). We find the long-wavelength reflectance to be up to 9% higher at 38° phase angle than at 0° phase angle. This is consistent with the phase reddening detected by NEAR at Eros (5).

During the mapping phase, we performed several equatorial scans. Throughout each equatorial scan, the footprint of NIRS was fixed at the image center. A comparison between the spectrum obtained near 8° phase angle and that obtained near 30° phase angle reveals a phase reddening of $\sim 6\%$ across the wavelength range of 1.0 to $1.6 \mu\text{m}$ (Fig. 2). The 30° spectrum was redder than the 8° spectrum.

An average NIRS spectrum of Itokawa over a large range of incidence and emission angles compares well with the ground-based disk-integrated spectra (1, 2). The largest discrepancy occurs at wavelengths less than $0.9 \mu\text{m}$. At these wavelengths, the apparent reflectance of Itokawa is lower in the NIRS spectra than in the ground-based data. In part this discrepancy is due to the difference of the viewing geometry and the footprint size. Although the discrepancy may also be partly due to calibration error, we cannot confirm this until we can compare our results to the calibrated AMICA data at 0.86 and $0.96 \mu\text{m}$; AMICA data are not yet available for analysis.

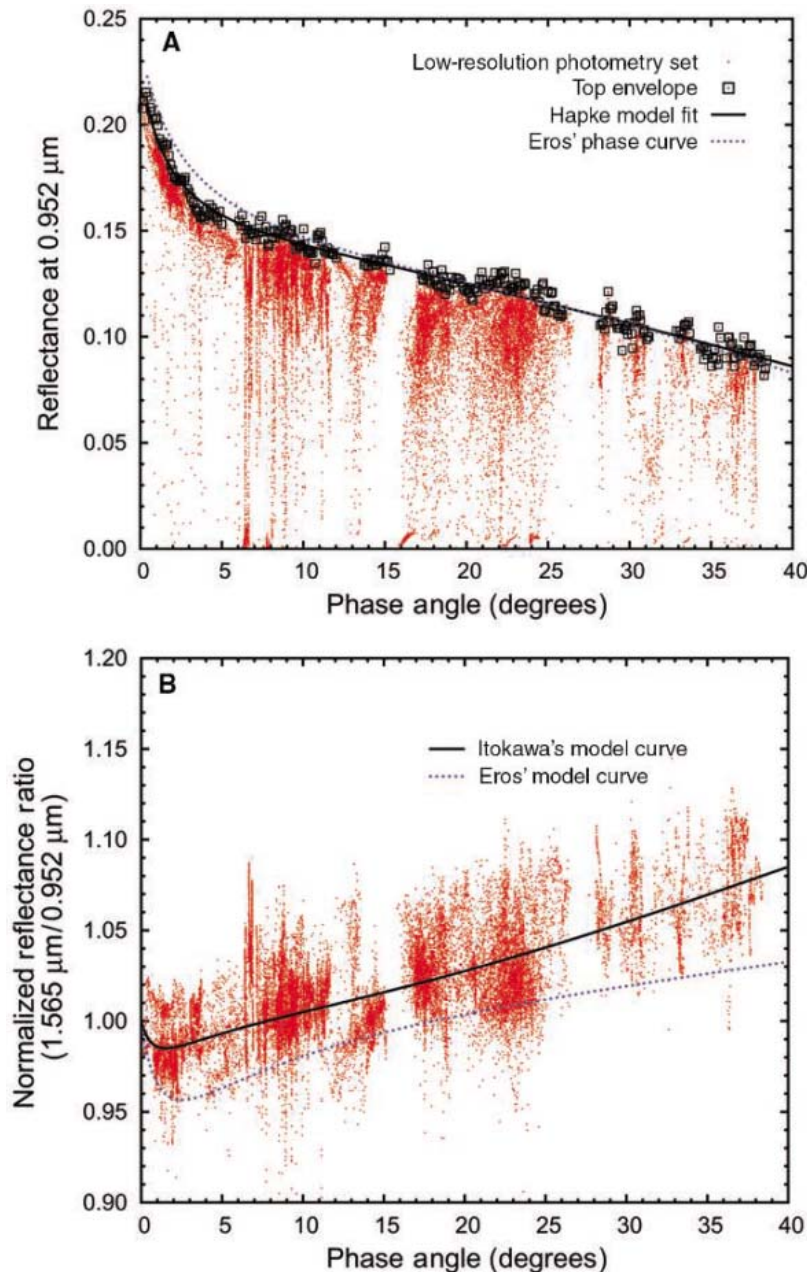


Fig. 1. (A) Reflectance at 952 nm as a function of solar phase angle. Data shown are those observed at a distance of 4 to 11 km from the surface, at an average resolution of $12 \text{ m} \times 12 \text{ m}$. Data points in boxes denote the top of the envelope for each 0.2° phase angle bin. The top envelope is used in generating a photometric model for two reasons: It restricts the size of the data set and allows more tractable computation time in fitting five free parameters, and it selects the data with the highest signal-to-noise ratio. Use of a selection of the data is defensible if no biases are introduced. For example, if the top envelope consisted only of the lowest emission angle (or lowest incident angle) data at a given phase angle, then it would not be a representative sample of the data. We carefully checked the range in incidence angles (0° to 80°) and emission angles (0° to 80°) of the top envelope and found no evidence for restriction in these angles. The fitted phase curve of Itokawa (solid line) is plotted with that of Eros (dashed line) at similar wavelengths (5). (B) Ratio of the reflectance at 1565 nm to that at 952 nm , plotted as a function of phase angle. The fitted model curve of Itokawa (solid line) is plotted with that of Eros (dashed line) at similar wavelengths.

The NIRS spectra shown in Fig. 2 are replotted in Fig. 3 with the background continuum removed in the natural logarithmic scale. The wavelength range of NIRS does not completely span the 1- μm absorption band, so we used the shortest wavelength of NIRS as one of the contact points to define the 1- μm band continuum background. Because NIRS data do not cover the entire 2- μm band, the 2- μm band continuum background is assumed to be a constant (horizontal line). After continuum removal and further adjustment to the vertical scale by a factor of 0.5, both NIRS spectra are consistent with the spectrum of an Alta'ameem (14) LL5 chondrite sample with particle sizes of $<125\ \mu\text{m}$ measured at 30° incidence and 0° emergence angles by the RELAB spectrometer (15). The 2- μm band center of the NIRS spectra may not match that of Alta'ameem, which suggests mineralogical differences that are not yet understood.

NIRS data points were calculated by deriving the relative band strength values from each of the spectra measured and obtaining the daily average and standard deviation (Fig. 4). Key wavelength positions for characterizing the 1- μm absorption bands of pyroxene and olivine are located at 0.95, 1.05, and 1.25 μm (16, 17). We compared Itokawa data points with those for Eros (18), ordinary chondrites, and some primitive achondrites on the basis of their reflectance spectra measured at RELAB (Fig. 4). In addition, we plotted data points for tricomponent mixtures of olivine, pyroxene, and plagioclase (19). Note that the continua of NIRS data may be different from those for the meteorite samples used in Fig. 4 because of their incomplete coverage of the 1- μm band. The 0.95- μm pyroxene band strength may be underestimated for this same reason. Therefore, the actual NIRS data points would probably shift to the lower left, toward the LL5 (Alta'ameem) points (Fig. 3).

Itokawa NIRS data points appear to have an olivine-rich mineral assemblage similar to LL5 or LL6 chondrites. More specifically, this plot suggests that the olivine/(olivine + pyroxene) ratio of the average surface material of Itokawa is about 70 to 80%. This range represents the uncertainty of the estimate of the continuum based on the shortest wavelength of NIRS. In contrast, Eros is plotted closer to the L chondrite region. This result suggests that Itokawa may be more olivine-rich than Eros, which is estimated to have a surface composed of 50 to 80% olivine (16, 20, 21). Elemental investigation by the x-ray fluorescence spectrometer also supports this result (22).

Spectra of several distinct areas on Itokawa were obtained (Fig. 5, A and B): boulder-rich areas, high-albedo areas (so-called brighter areas), and the Muses Sea. The spectrum footprint within each area was verified with AMICA imaging (Fig. 5, C to E). The spectra were obtained at phase angles near 22° , incidence angles near 25° , and emission angles near 30° . Comparison of these

three areas shows that the albedo and absorption band depth of the reflectance spectrum varies by more than 10% (Fig. 5, A and B). The spectral

properties of these distinct areas indicate that the high-albedo areas have deeper 1- μm features than the other two terrains. These spectral trends are

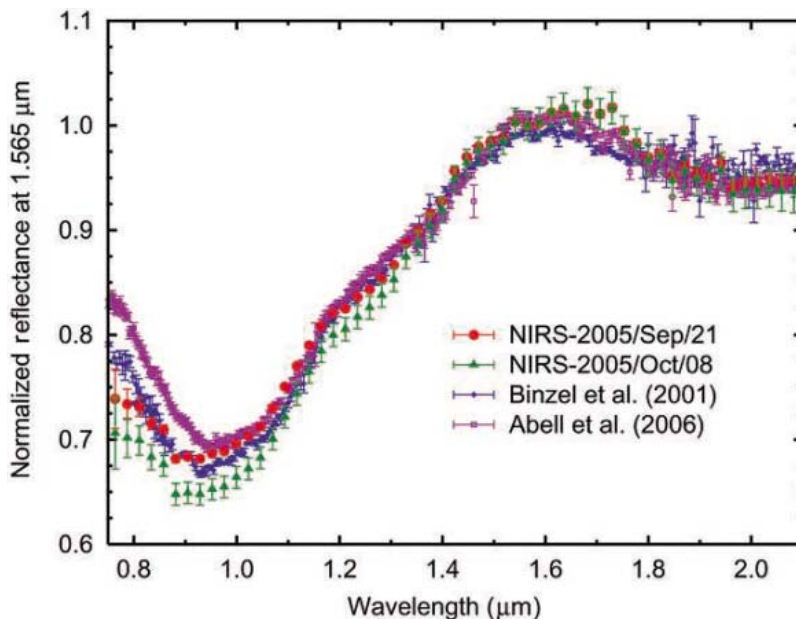


Fig. 2. Equatorial averaged NIRS spectra of Itokawa observed on 21 September 2005 (red circles) and 8 October 2005 (green triangles). The distance from the asteroid is 18 km and 11 km, respectively, for these dates; the solar phase angles are 8° and 30° , respectively. The difference in error bars for each spectrum is mainly due to the difference in the number of individual spectra stacked together to produce an average spectrum for that particular date. Also plotted are two independent ground-based disk-integrated spectra [blue diamonds (1) and purple squares (2)]. All reflectance spectra are normalized at 1565 nm.

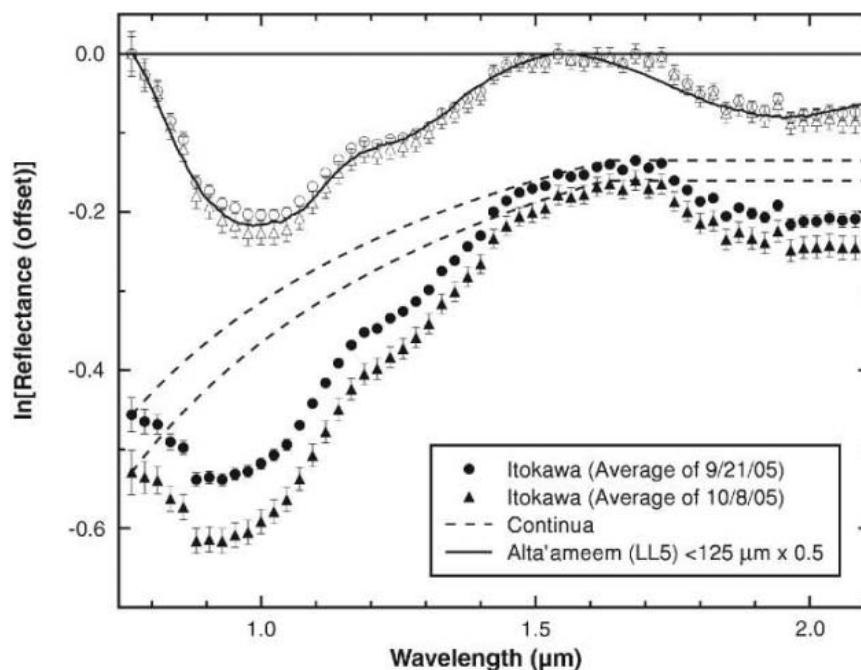


Fig. 3. Natural log average reflectance spectra of Itokawa observed by NIRS on 21 September 2005 (solid circles) and 8 October 2005 (solid triangles). Background continua (broken curves) are subtracted from them and they are replotted (open circles and triangles) together with the scaled, continuum-removed spectrum of an Alta'ameem LL5 chondrite sample (solid line).

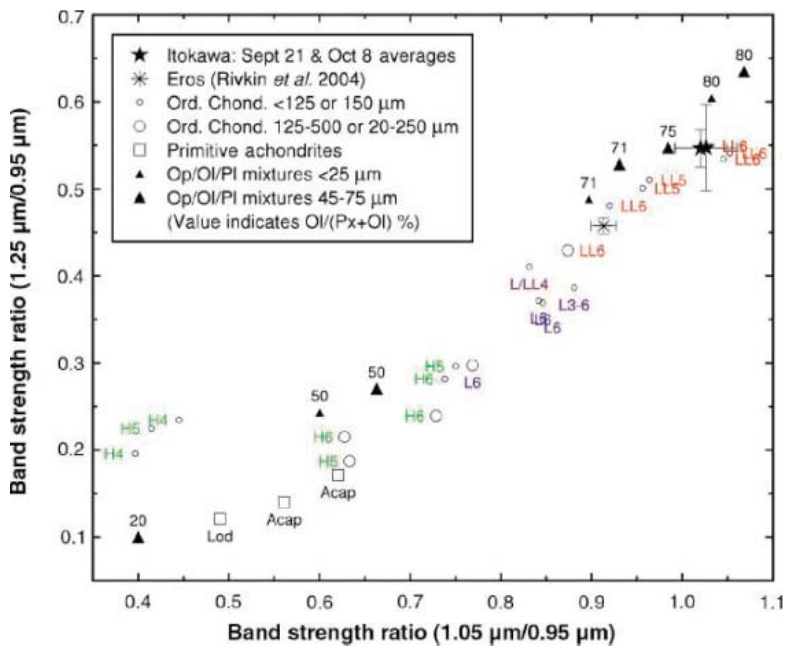


Fig. 4. Natural log absorption strengths at 1.05 and 1.25 μm relative to that at 0.95 μm of average Itokawa spectra acquired by NIRS on 21 September and 8 October 2005 in comparison with Eros (18), powder samples of ordinary chondrites, primitive achondrites [acapulcoites (Acap) and lodranites (Lod)], and orthopyroxene-olivine-plagioclase mixtures (15). This figure indicates that Itokawa has an olivine-rich mineral assemblage similar to LL5 and LL6 chondrites.

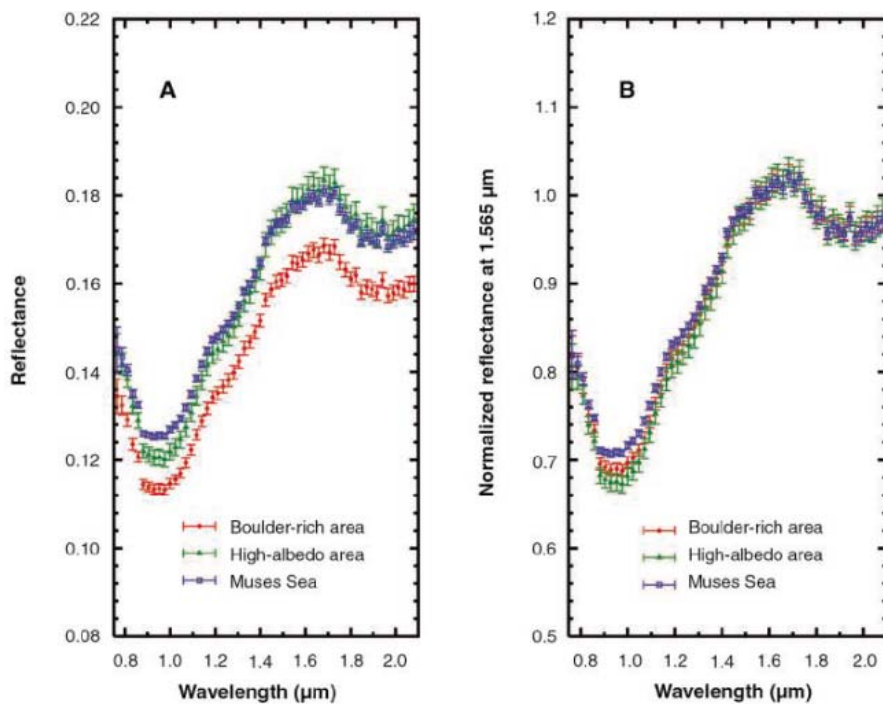
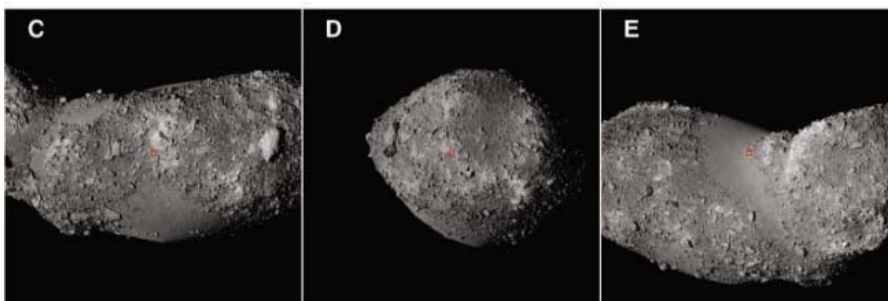


Fig. 5. (A) Reflectance spectra of three typical areas on Itokawa. A boulder-rich area (red), a high-albedo area (green), and Muses Sea (blue) are plotted. (B) Replotted spectra are normalized at 1565 nm. (C) The footprint for observing the boulder-rich area is denoted by a small red square at the center of the simultaneously obtained AMICA image. (D) Same as (C) for the observed high-albedo area. (E) Same as (C) for the Muses Sea area.



inconsistent with differences resulting from photometric viewing geometry, but they may be consistent with differences in optical freshness and/or particle size. These spectral trends were confirmed in imaging and spectral comparisons obtained at 4°, 6°, and 15° phase angle.

The boulder-rich areas have lower albedos than the other two areas and shallower 1- μm bands than the high-albedo areas. Surface roughness and/or space weathering may explain why the boulder-rich areas have a low albedo and shallow absorption features (23).

Muses Sea is one of the smooth terrains discussed in the AMICA report (23). This area shows a shallower 1- μm absorption band than the other two terrains, but is not as reddened as the high-albedo area. These spectral trends suggest that the smooth terrain may consist of a different range of particle sizes than that of the high-albedo areas (24), because powders with very large particle sizes may have bluer colors and shallower absorption band depths (25). Close-up images by AMICA show that Muses Sea is densely filled with size-sorted gravels from millimeter to centimeter scales (26). This finding supports the above interpretation, although fine particles may also exist in Muses Sea.

In conclusion, NIRS confirms that Itokawa has a spectrum characteristic of S-class asteroids with absorption bands of pyroxene and olivine. NIRS data suggest that Itokawa has an olivine-

rich mineral assemblage similar to LL5 and LL6 chondrites. Given the general decrease in olivine abundance with heliocentric distance (27), the most probable source region of Itokawa is the inner part of the main belt (28). On the surface of Itokawa there are differences in the absorption band depth, color, and albedo. It is likely that such diversity is a result of combinations of different degrees of space weathering and different grain sizes (physical properties).

References and Notes

- R. P. Binzel, A. S. Rivkin, S. J. Bus, J. M. Sunshine, T. H. Burbine, *Meteorit. Planet. Sci.* **36**, 1167 (2001).
- P. A. Abell, F. Vilas, K. S. Jarvis, M. J. Gaffey, M. S. Kelley, in preparation.
- Observation wavelength and pixel number of the detector are related by the following expression:
$$\text{Wavelength (nm)} = 2271.44 - [23.56 \times (\text{pixel number})]$$

The observational limit at the long-wavelength end was determined by the cutoff wavelength of the InGaAs photodiode array to be ~ 2100 nm. The short-wavelength cutoff is 763.60 nm.
- B. W. Hapke, *Icarus* **67**, 264 (1986).
- B. E. Clark *et al.*, *Icarus* **155**, 189 (2002).
- T. Sekiguchi *et al.*, *Astron. Astrophys.* **397**, 325 (2003).
- M. Ishiguro *et al.*, *Pub. Astron. Soc. Jpn.* **55**, 691 (2003).
- S. M. Lederer *et al.*, *Icarus* **173**, 153 (2005).
- T. G. Müller, T. Sekiguchi, M. Kaasalinen, M. Abe, S. Hasegawa, *Astron. Astrophys.* **443**, 347 (2005).
- J. Li, M. F. A'Hearn, L. A. McFadden, *Icarus* **172**, 415 (2004).
- J. Gradie, J. Veverka, B. Buratti, *Proc. Lunar Planet. Sci. Conf.* **11**, 799 (1980).
- B. E. Clark *et al.*, *Meteorit. Planet. Sci.* **36**, 1617 (2001).
- K. Muinonen, J. Piironen, Y. Shkuratov, A. Ovcharenko, B. E. Clark, in *Asteroids III*, W. F. Bottke Jr., A. Cellino, P. Paolucchi, R. P. Binzel, Eds. (Univ. of Arizona Press, Tucson, AZ, 2002), pp. 123–138.
- K. S. Al-Bassam, *Meteoritics* **13**, 257 (1978).
- C. M. Pieters, T. Hiroi, *Lunar Planet. Sci. Conf. XXXV*, 1720 (2004).
- J. B. Adams, *J. Geophys. Res.* **79**, 4829 (1974).
- J. M. Sunshine, C. M. Pieters, *J. Geophys. Res.* **103**, 13675 (1994).
- A. S. Rivkin *et al.*, *Icarus* **172**, 408 (2004).
- T. Hiroi, C. M. Pieters, *J. Geophys. Res.* **99**, 10867 (1994).
- L. A. McFadden *et al.*, *Meteorit. Planet. Sci.* **36**, 1711 (2001).
- N. R. Izenberg *et al.*, *Meteorit. Planet. Sci.* **38**, 1053 (2003).
- T. Okada *et al.*, *Science* **312**, 1338 (2006).
- J. Saito *et al.*, *Science* **312**, 1341 (2006).
- B. E. Clark, *J. Geophys. Res.* **100**, 14443 (1995).
- Y. Shkuratov, L. Starukhina, *Icarus* **137**, 235 (1999).
- H. Yano *et al.*, *Science* **312**, 1350 (2006).
- M. J. Gaffey, J. F. Bell, R. H. Brown, T. Burbine, *Lunar Planet. Sci. Conf. XXI*, 399 (1990).
- P. Michel, M. Yoshikawa, *Astron. Astrophys.* **449**, 817 (2006).
- Some of the meteorite samples were loaned by the Field Museum and the National Museum of Natural History, and their reflectance spectra were measured at RELAB, Brown University. RELAB is a multiuser facility operated under NASA grant NAG5-13609. We thank the mission operations and spacecraft team of the Hayabusa project at ISAS/JAXA for their efforts that resulted in making Hayabusa the first Japanese spacecraft to rendezvous and land at the asteroid; M. Wadhwa, C. Nunez, and T. McCoy for their assistance; and R. Binzel and an anonymous referee for helpful and constructive reviews. Supported by ISAS/JAXA and NASA.

2 February 2006; accepted 13 April 2006
10.1126/science.1125718

REPORT

X-ray Fluorescence Spectrometry of Asteroid Itokawa by Hayabusa

Tatsuaki Okada,^{1,2*} Kei Shirai,¹ Yukio Yamamoto,¹ Takehiko Arai,^{1,3} Kazunori Ogawa,^{1,4} Kouze Hosono,^{1,2} Manabu Kato^{1,2,4}

X-ray fluorescence spectrometry of asteroid 25143 Itokawa was performed by the x-ray spectrometer onboard Hayabusa during the first touchdown on 19 November 2005. We selected those data observed during relatively enhanced solar activity and determined average elemental mass ratios of $\text{Mg/Si} = 0.78 \pm 0.09$ and $\text{Al/Si} = 0.07 \pm 0.03$. Our preliminary results suggest that Itokawa has a composition consistent with that of ordinary chondrites, but primitive achondrites cannot be ruled out. Among ordinary chondrites, LL- or L-chondrites appear to be more likely than H-chondrites. No substantial regional difference was found on the asteroid surface, indicating its homogeneity in composition.

Understanding the relation between asteroids and meteorites is a long-standing problem in asteroid science, and a relation between S-class asteroids and ordinary chondrites might be constrained with new evidence provided by the Hayabusa x-ray fluorescence (XRF) spectrometer. Near-Earth asteroid 25143 Itokawa is classified spectroscopically as an S (IV)-type asteroid, and ground-based observations suggest that Itokawa has an LL-

chondrite composition [e.g., (1)]. Indeed, a likely correlation between ordinary chondrites and S (IV) class asteroids has been suggested [e.g., (2)], but direct evidence to support this is lacking. Understanding the material composition of Itokawa and its origin is a key scientific objective of the Hayabusa mission (3, 4). XRF spectrometry by the x-ray spectrometer (XRS) was conducted to obtain a major-elemental analysis of the asteroid's surface in order to classify its

rock type (or meteoritic class) and survey any regional variation (5, 6). Here we report preliminary results of the XRS observations during the first touchdown of Hayabusa on the surface of Itokawa, when sample collection was attempted.

XRF is a well-established technique for major-elemental analysis in the laboratory. In space, however, the excitation source is solar x-rays so the analysis is complicated by features in the solar spectrum and flux variations. As was shown in previous planetary missions (7–9), XRF can be used to determine the major-element composition of the uppermost several tens of micrometers of atmosphere-free planetary bodies such as the Moon, Mercury, and asteroids (5, 7–12).

The XRS is an advanced XRF spectrometer (5, 6) with a light-weight (1.5 kg) sensor unit based on a charge-coupled device (CCD) x-ray detector (13); this is the first time a CCD has been used

¹Institute of Space and Astronautical Science, Japan Aerospace Exploration Agency, Sagami-hara, Kanagawa 229-8510, Japan. ²Department of Earth and Planetary Science, University of Tokyo, Hongo, Tokyo 113-0033, Japan. ³Department of Space and Astronautical Science, Graduate University for Advanced Studies, Sagami-hara, Kanagawa 229-8510, Japan. ⁴Department of Earth and Planetary Sciences, Tokyo Institute of Technology, Ookayama, Tokyo 152-8550, Japan.

*To whom correspondence should be addressed. E-mail: okada@planeta.sci.isas.jaxa.jp

Table 1. Elemental composition of Itokawa derived at six sites from the XRS observations on 19 November 2005. Errors are 2σ uncertainties. SSP, XRF, and Norm denote the standard sample plate, x-ray fluorescence, and normalized intensities, respectively.

TIME (UTC)	Longitude (°) region	SSP XRF		Itokawa XRF		Norm XRF		Itokawa composition (wt%)			
		Mg/Si	Al/Si	Mg/Si	Al/Si	Mg/Si	Al/Si	Mg/Si	Al/Si	Mg	Si
01:19	40	1.16	0.49	2.01	0.15	1.73	0.31	0.76	0.06	15.1	19.8
	“Neck” (Pencil boulder)	± 0.07	± 0.08	± 0.05	± 0.08	± 0.15	± 0.17	± 0.08	± 0.03	± 2.3	± 3.0
09:27	285	1.11	0.58	1.97	0.18	1.77	0.31	0.78	0.07	15.2	19.4
	Muses Sea	± 0.06	± 0.06	± 0.07	± 0.06	± 0.11	± 0.12	± 0.07	± 0.03	± 2.0	± 2.5
12:10	5	0.88	0.47	1.63	0.16	1.85	0.34	0.82	0.08	15.5	19.0
	“Head” region	± 0.06	± 0.10	± 0.07	± 0.09	± 0.16	± 0.16	± 0.10	± 0.03	± 2.3	± 2.8
15:12	96	1.35	0.76	2.31	0.17	1.71	0.22	0.75	0.06	15.0	19.9
	Tsukuba	± 0.11	± 0.20	± 0.10	± 0.10	± 0.17	± 0.12	± 0.10	± 0.03	± 2.9	± 3.3
16:02	120	0.95	0.47	1.66	0.19	1.75	0.40	0.77	0.09	14.9	19.4
	A rough terrain	± 0.07	± 0.15	± 0.08	± 0.10	± 0.16	± 0.22	± 0.09	± 0.04	± 2.3	± 2.8
16:34	136	0.92	0.49	1.70	0.12	1.85	0.24	0.81	0.06	15.6	19.2
	Yoshinodai	± 0.07	± 0.08	± 0.07	± 0.07	± 0.14	± 0.14	± 0.08	± 0.03	± 2.0	± 2.8
Average								0.78	0.07	15.22	19.46
								± 0.09	± 0.03	± 2.3	± 2.8

for such a purpose on a planetary mission. The CCD has an energy resolution of 160 eV at 5.9 keV when cooled, which is much higher than that of the proportional counters used in previous planetary missions (14, 15). In addition, the XRS has a standard sample plate (SSP) for concurrently calibrating the XRF when it is excited by the Sun. The SSP is a glassy plate whose composition is intermediate between those of chondrites and basalts (table S1). By comparing x-ray spectra from the asteroid and from the SSP, quantitative elemental analysis can be achieved, although the intensities and spectral profiles of solar x-rays change over time. In-flight performance of the XRS was confirmed by observations of x-rays from the SSP (16), x-ray-emitting bodies such as Kepler’s supernova remnants (17), and x-rays from the far side of the Moon shortly before the Earth swing-by on 17 May 2004 (18).

After arrival at Itokawa on 12 September 2005, Hayabusa began scientific observations. Initially, the solar activity (19) was very faint and unfavorable for XRS observations. However, it became relatively brighter late in November 2005.

Under quiescent conditions, solar x-rays are produced in the solar coronal regions with typical temperatures of 1×10^6 to 4×10^6 K and have steeply decreasing spectra with energy. Under such conditions, K- α line spectra of lighter rock-forming elements such as Mg (1.25 keV), Al (1.49 keV), and Si (1.74 keV) are readily observed. Heavier elements such as Ca (3.69 keV) and Fe (6.40 keV) are detectable only during solar flares, when solar x-rays become more intense and relatively stronger at high energies. S (2.37 keV) is at the lower limit of detection, due to instrumental noise and the relatively low signal-to-background ratios obtained during that time. Therefore, our analy-

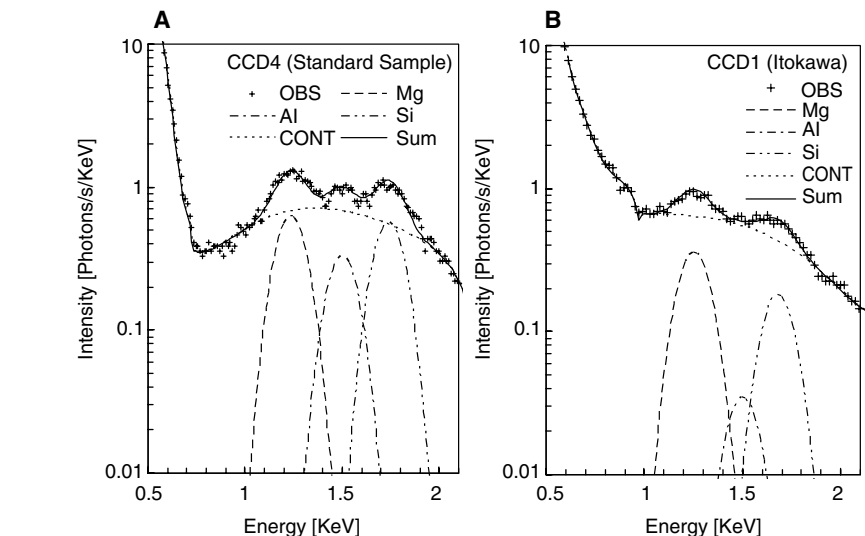


Fig. 1. X-ray spectra of the onboard standard sample (A) and asteroid Itokawa (B) were simultaneously observed by the XRS at 9:27 UTC on 19 November 2005. The observed spectra (OBS) are fitted by Gaussian profiles to K- α lines of major elements (Mg, Al, and Si) and by a background continuum component (CONT).

sis is concentrated on three elements that play important roles in rock type classification and that serve as indicators of evolutionary processes.

Hayabusa began its descent for the first touchdown early on 19 November 2005, staying 1.4 km earthward of Itokawa. The earthward direction was chosen because it allowed scientific instruments on Hayabusa to point toward the asteroid and maintain continuous communication with Earth through the high-gain antenna of the spacecraft. During the descent, the solar phase angle—that is, the angle between the Sun, Itokawa, and Hayabusa—was between 5° and 10° . This small phase angle is favorable for performing XRF spectrometry. At larger phase angles, shadows on the rough surface terrain can interfere with the elemental analysis [e.g., (20)].

Itokawa rotates once every 12.1 hours (21), and it rotated more than once by the time of touchdown. During descent, the XRS continued x-ray spectrometry of Itokawa, and the SSP simultaneously excited by the Sun, so that the entire asteroid surface was observed in a longitudinal direction due to its rotation.

The effective field of view of the XRS is 3.5° by 3.5° (5, 6), corresponding to a “footprint” size of 87 m by 87 m at an altitude of 1.4 km, which became proportionally smaller as Hayabusa descended. Consequently, the XRS observed local areas of Itokawa 550 m by 298 m by 244 m in size (22). XRS observations were sometimes affected by background radiation from space (x-rays and energetic particles) because the footprint was not centered on the

Fig. 2. (A) Elemental ratios of Itokawa (shaded area) plotted as Mg/Si versus Al/Si, together with typical compositions of stony and stony iron meteorites. (B) Enlargement of shaded area in (A). The dashed and dotted lines in (A) denote the best-fit values and their 2σ uncertainties, respectively.

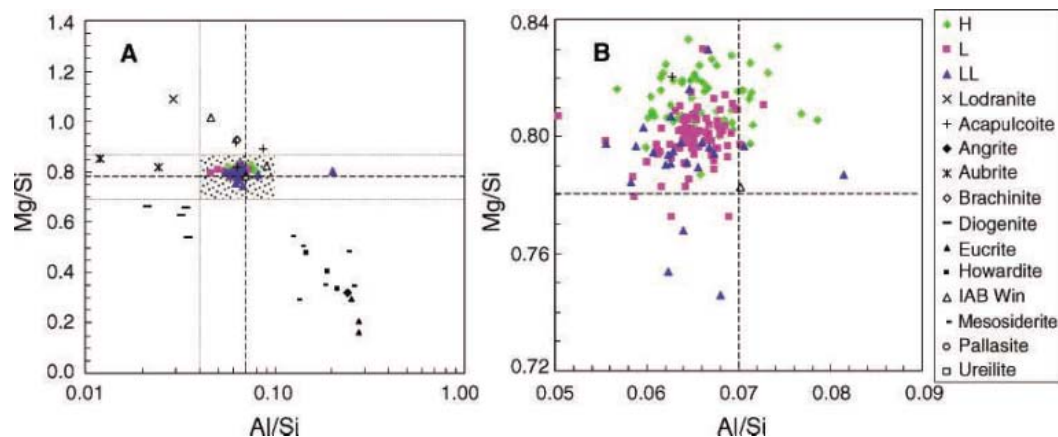
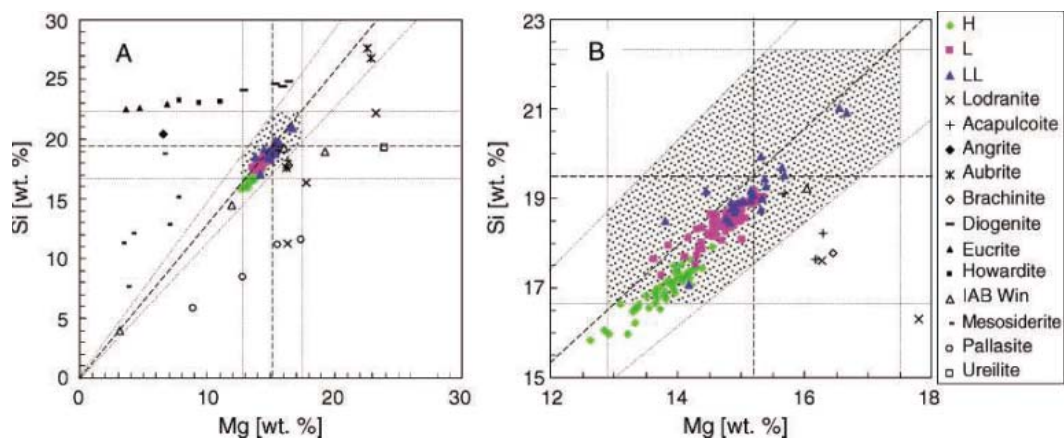


Fig. 3. (A) Elemental composition of Itokawa (Si/Mg) plotted as in Fig. 2. (B) Enlargement of the shaded area in (A). Ordinary chondrites, acapulcoites, and IAB winonaites appear closest in composition, and Itokawa appears to be more like an LL- or L-chondrite in composition than an H-chondrite.



asteroid, due to the rotation of the irregularly shaped asteroid and instability of the spacecraft's attitude control that resulted from the failure of two of the three reaction wheels.

The XRS produced a set of x-ray energy spectra of Itokawa and the SSP, after onboard processing of data from each CCD (6), every 5 min. Much of the data could not be analyzed due to unfavorable solar activity, but six data sets with good signal-to-background ratios—observed during periods of relatively enhanced solar activity—were selected (Table 1). The names of footprint regions on the asteroid (23) are also listed in Table 1, including the touchdown site, Muses Sea. X-ray spectra of the SSP and of Itokawa are shown (Fig. 1, A and B, respectively). Line spectra due to the XRF of Mg, Al, and Si were best-fit with Gaussian profiles, superimposed on background continuum components (Fig. 1, A and B). The errors shown in Table 1 are mainly caused by the background extraction procedure and are almost equal to the uncertainties obtained by least-squares fitting.

The K- α line spectra of Mg, Al, and Si from the SSP are clearly distinguished (Fig. 1A). The continuum component at 1 to 2 keV is dominated by scattered solar x-rays. In contrast, the K- α line spectra of Mg and Si from Itokawa are clearly seen, but that of Al is relatively faint (Fig. 1B). The spectral profile with relatively

higher Mg/Si and lower Al/Si indicates that Itokawa is more chondritic in composition than the SSP. The relatively large continuum strength at lower energy may be due to irradiation of cosmic x-rays and energetic particles, because at times one-third to one-half of the XRS's field of view was occupied by background space.

Table 1 shows the intensity ratios of Mg/Si and Al/Si for the SSP and Itokawa at each observed time. The ratios of Mg/Si and Al/Si for the asteroid normalized by those of the SSP are also shown. A small variation of 10% is found among the sites. Based on the elemental-analysis method using the SSP (24), the elemental ratios of the asteroid surface normalized by those of the SSP are almost proportional to the normalized intensity ratios within the uncertainties of several percent. We then estimated the elemental ratios for each of the six sites and derived average compositions of Mg/Si = 0.78 ± 0.09 and Al/Si = 0.07 ± 0.03 , respectively (Table 1). The derived elemental ratios of Mg/Si are 0.3 to 0.4 of the intensity ratios of Mg/Si, in good agreement with a previous numerical study of chondritic material (25).

The average elemental ratios of Mg/Si and Al/Si are plotted (Fig. 2) along with those for other stony and stony-iron meteorites (table S2), which are considered candidate materials of S-class asteroids (25, 26). Ordinary chondrite

compositions, including those of LL-, L-, and H-chondrites, are likely for Itokawa, within 1σ uncertainties for both Mg/Si and Al/Si. Some primitive achondrites such as acapulcoites cannot be ruled out. IAB-winonaites, a kind of primitive achondrite, and the related silicated IAB iron meteorites, appear closest in composition, although the composition may be diverse.

We also estimated the absolute abundance of Si (and also Mg from Mg/Si) for each site (Table 1), under the assumptions that all minerals have a stoichiometric composition and there is no abundant water on the surface. Such information should take into account the instrumental characteristics including detection area, detection efficiency and field of view (or solid angle of the target), the intensity and spectral profile of the primary x-ray source, and the physical parameters such as fluorescence yield of each element. In this study, they are all given or canceled by using the compared method. Then we calculated the average abundances of Mg = 15.2 ± 2.3 wt. % and Si = 19.5 ± 2.8 wt. %, respectively. This estimate is valid under the assumption that the intensity of the continuum component at Si-K α is dominated by solar-scattered x-rays.

The derived abundances of Mg and Si are also plotted (Fig. 3). LL- or L-chondrites appear most likely within 1σ uncertainty, although

H-chondrites are also possible within 2σ uncertainty. Some primitive achondrites remain possible candidates and cannot be ruled out. Analysis of 1- μm band absorption with near-infrared spectroscopy also suggests that olivine-rich LL-chondrites are preferred and other achondrites are possible although less likely (27). In contrast, analysis of the 2- μm band shows more olivine-enriched features than any known meteorite types, suggesting the possibility of a primitive achondrite whose parent body is probably an LL- or L-chondrite (28).

The target of the Near-Earth-Asteroid-Rendezvous (NEAR)-Shoemaker mission, 433 Eros, is also an S (IV)-class asteroid and is the only other asteroid analyzed by XRF spectrometry (8, 25). Its composition is best described by that of H-chondrites by XRF spectrometry, whereas L- or LL-chondrites are more consistent with γ -ray spectra and visible-to-near-infrared observations. But the conclusion that Eros is more like an ordinary chondrite is nevertheless consistent with the findings for Itokawa, although some melting cannot be ruled out (8, 25, 29). For both Eros and Itokawa, it is significant that the compositions derived by remote spacecraft observations in close proximity to the asteroid seem consistent with those found using Earth-based spectroscopy (1), which is applicable to a large number of asteroids.

As mentioned above, the normalized elemental ratios of Mg/Si and Al/Si are found to

be almost constant within 10% among the sites. A homogeneous composition of Itokawa is likely when observed at a spatial resolution of several tens to a hundred meters. This homogeneity implies that Itokawa probably has a uniform rock type across the asteroid. It also shows that there is no evidence of either local evolution processes or that two bodies of different composition were involved if Itokawa has a contact binary origin (4). At a smaller scale, some regional variation of color and albedo has been found in visible-to-near-infrared wavelength data (22, 27). But the XRS results cannot currently constrain elemental ratios at that scale.

References and Notes

- R. P. Binzel, A. S. Rivkin, S. J. Bus, J. M. Sunshine, T. H. Burbine, *Meteorit. Planet. Sci.* **36**, 1167 (2001).
- M. J. Gaffey *et al.*, *Icarus* **106**, 573 (1993).
- J. Kawaguchi, H. Kuninaka, A. Fujiwara, K. T. Uesugi, *Proc. 5th IAA Int. Conf. Low-Cost Planetary Missions*, Noordwijk, Netherlands, 24 to 26 September 2003, ESA SP-542 25 (2003).
- A. Fujiwara *et al.*, *Science* **312**, 1330 (2006).
- T. Okada, M. Kato, A. Fujimura, H. Tsunemi, S. Kitamoto, *Adv. Space Res.* **23**, 345 (1999).
- T. Okada *et al.*, *Adv. Geosci.*, in press.
- I. J. Adler, J. I. Trombka, *Phys. Chem. Earth* **10**, 10 (1977).
- J. I. Trombka *et al.*, *Science* **289**, 2101 (2000).
- M. Grande *et al.*, *Planet. Space Sci.* **51**, 427 (2003).
- T. Okada, M. Kato, A. Fujimura, H. Tsunemi, S. Kitamoto, *Adv. Space Res.* **25**, 1833 (2000).
- S. Solomon *et al.*, *Planet. Space Sci.* **49**, 1445 (2001).
- R. Grard, A. Balogh, *Planet. Space Sci.* **49**, 1395 (2001).
- K. Miyaguchi *et al.*, *Nucl. Instrum. Methods* **A436**, 24 (1999).
- I. J. Adler, J. I. Trombka, P. Gorenstein, *Anal. Chem.* **44**, 28a (1972).
- J. I. Trombka *et al.*, *J. Geophys. Res.* **102**, 23729 (1997).
- Y. Yamamoto, T. Arai, T. Okada, K. Shirai, M. Kato, *Proc. ISAS Lunar Planet. Symp.* **36**, 286 (2003).
- T. Arai, Y. Yamamoto, T. Okada, K. Shirai, M. Kato, *Proc. ISAS Lunar Planet. Symp.* **36**, 282 (2003).
- T. Okada *et al.*, *Lunar Planet. Sci. Conf.* **36**, 1175 (2005).
- The solar geophysical database (www.sec.noaa.gov/ftpmenu/plots.html) shows that the solar x-ray flux was faint, classified as "very low," from mid-September to early November. During almost all of that period, it was equal to or below the lower limit of detection.
- Y. Kuwada, T. Okada, H. Mizutani, *Proc. 30th ISAS Lunar Planet. Symp.* **30**, 212 (1997).
- M. Kaasalainen *et al.*, *Astron. Astrophys.* **405**, L29 (2003).
- J. Saito *et al.*, *Science* **312**, 1341 (2006).
- H. Demura *et al.*, *Science* **312**, 1347 (2006).
- E. Masuda, thesis, Tokyo Institute of Technology (2002).
- L. Nittler *et al.*, *Meteorit. Planet. Sci.* **36**, 1673 (2001).
- E. Jarosewich, *Meteorit. Planet. Sci.* **25**, 332 (1990).
- M. Abe *et al.*, *Science* **312**, 1334 (2006).
- P. A. Abell, F. Vilas, K. S. Jarvis, M. J. Gaffey, M. S. Kelley, *Lunar Planet. Sci. Conf.* **37**, 1513 (2006).
- T. J. McCoy *et al.*, *Meteorit. Planet. Sci.* **36**, 1661 (2001).
- We thank R. P. Binzel and the anonymous reviewer for constructive comments and fruitful discussions. The Hayabusa mission was organized by the Institute of Space and Astronautical Sciences, Japan Aerospace Exploration Agency. The XRS was manufactured by Meisei Electric Co. in Japan.

Supporting Online Material

www.sciencemag.org/cgi/content/full/312/5778/1338/DC1
Tables S1 and S2

2 February 2006; accepted 20 April 2006
10.1126/science.1125731

REPORT

Detailed Images of Asteroid 25143 Itokawa from Hayabusa

J. Saito,^{1,2*} H. Miyamoto,^{3,4} R. Nakamura,⁵ M. Ishiguro,⁶ T. Michikami,⁷ A. M. Nakamura,⁸ H. Demura,⁹ S. Sasaki,¹⁰ N. Hirata,^{8,9} C. Honda,⁶ A. Yamamoto,¹¹ Y. Yokota,⁶ T. Fuse,¹² F. Yoshida,¹³ D. J. Tholen,¹⁴ R. W. Gaskell,¹⁵ T. Hashimoto,¹⁶ T. Kubota,¹⁶ Y. Higuchi,¹⁷ T. Nakamura,¹³ P. Smith,¹⁷ K. Hiraoka,⁸ T. Honda,⁸ S. Kobayashi,⁹ M. Furuya,⁹ N. Matsumoto,⁹ E. Nemoto,⁹ A. Yukishita,⁹ K. Kitazato,⁶ B. Dermawan,¹⁸ A. Sogame,² J. Terazono,¹⁹ C. Shinohara,¹⁷ H. Akiyama²⁰

Rendezvous of the Japanese spacecraft Hayabusa with the near-Earth asteroid 25143 Itokawa took place during the interval September through November 2005. The onboard camera imaged the solid surface of this tiny asteroid (535 meters by 294 meters by 209 meters) with a spatial resolution of 70 centimeters per pixel, revealing diverse surface morphologies. Unlike previously explored asteroids, the surface of Itokawa reveals both rough and smooth terrains. Craters generally show unclear morphologies. Numerous boulders on Itokawa's surface suggest a rubble-pile structure.

On 12 September 2005, the Hayabusa spacecraft arrived at the near-Earth asteroid 25143 Itokawa (1). Itokawa is categorized as an S (IV)- or Q-type asteroid, which are thought to be similar to ordinary chondrite meteorites through ground-based observations (2, 3). Hayabusa carries the telescopic Optical

Navigation Camera (ONC-T), which is also called Asteroid Multiband Imaging Camera (AMICA) when used for scientific observations (4). AMICA has both a wide-bandpass filter and seven narrowband filters, the central wavelengths of which are nearly equivalent to those of the Eight Color Asteroid Survey (ECAS) system (5) as

follows: 380 (ul), 430 (b), 550 (v), 700 (w), 860 (x), 960 (p), and 1010 nm (zs). AMICA imaged the entire surface of Itokawa with a solar phase angle of $\sim 10^\circ$ at the home position (HP), the altitude of which is ~ 7 km (1). Because the angular resolution is $0.0057^\circ/\text{pixel}$ (99.3 microrad/pixel), the nominal spatial resolution is 70 cm/pixel at the HP. Four position-angle glass polarizers were mounted on an edge of the 1024 pixel by 1024 pixel charge-coupled device chip (6). In addition to the nominal observations at the HP (Fig. 1), we obtained images for specific purposes (7), including images of the polar regions and some with very high resolution.

The size of Itokawa is 535 m by 294 m by 209 m, within a 1-m margin of error [see (1) for more details about the size and global characteristics]. Because the shape of Itokawa is somewhat reminiscent of a sea otter (Fig. 1), we use "head" (smaller part), "body" (larger part), and "neck" (junction between head and body) to denote position on the asteroid (1). The surface of Itokawa shows a variety of features that suggest a complex evolutionary history. A notable example is the existence of "the black boulder," which is a small boulder with extremely low albedo (Fig. 1). Facets have been identified at both ends of the elongated body of Itokawa; most of them are likely the results of impacts. Although several grooves exist, we have not been able to identify

global-scale ones, such as those found on the martian moon Phobos and asteroid 433 Eros (8). This may suggest the lack of a global-scale internal structure, although surface manifestations of internal structures might be obscured by numerous boulders (1).

Two types of terrains (rough and smooth) are observed on the surface of Itokawa. The rough terrain occupies ~80% of the surface. Numerous boulders exist on the rough terrains; these vary widely in size (from a few meters to ~50 m) and shape (Fig. 1). Here, we loosely define boulders as (i) apparently rootless rocks and (ii) features with distinctive positive relief that are larger than a few meters in size. The largest boulder on Itokawa is named Yoshinodai (Fig. 1), with dimensions of ~50 m by 30 m by 20 m. It is 1/10 the size of Itokawa itself. Another conspicuous boulder is called Pencil, which shows distinctive positive relief as if it were embedded in the local terrain (Fig. 1). Boulders have a wide range of angularity and aspect ratio.

The cumulative size distribution of boulders larger than 5 m on the entire surface is shown in Fig. 2. The total number of boulders larger than 5 m exceeds 500. The existence of decameter-sized boulders on Itokawa, as well as the abundance of meter-sized boulders, cannot be explained by simple impact-cratering processes (1, 9). Thus, the boulders might have been produced when Itokawa was generated by a catastrophic disruption, which is consistent with the possible rubble-pile structure of Itokawa (1).

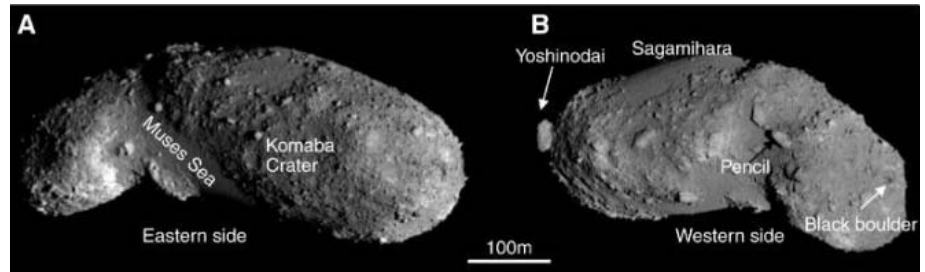


Fig. 1. Global images of Itokawa. (A) Image no. ST2448357351 and (B) ST2426418029. “ST” denotes “science mode imaging” and “ONC-T image”; numbers are the time counter values. The surface of Itokawa is covered by numerous boulders, including the conspicuous ones indicated in the figure (Yoshinodai, Pencil, and Black boulder). Also shown is the Komaba crater. Smooth terrains (e.g., Muses Sea and Sagami-hara) are distinctive because they lack boulders.

The log-log slope of the cumulative number of boulders on Itokawa’s surface (10) is ~-2.8 (Fig. 2), which is shallower than that of previously studied small bodies, including Eros and Phobos (and even the Moon) (11–13). For example, Eros shows a slope as steep as -3.2 for boulder sizes between 15 and 80 m (11). The shallower slope obtained for Itokawa implies that the boulders experienced less processing, including breaking, sorting, and transporting (11). Other probable reasons for the shallow slope may include mass dependencies both in boulder-ejection processes related to the lower gravity of Itokawa and in boulder-transport processes such as impact-induced shaking (14).

The smooth terrains are distinguished from the surrounding rough terrains (Fig. 1) by both a lack of boulders and the featureless smooth surfaces with apparently similar brightness. These characteristics are consistent with the view that the smooth terrain is covered by finer materials (1). The origin of the boulders on the smooth terrains seems to be complicated: Some boulders are surrounded by shallow depressions, whereas most others are not. The depressions (Fig. 3A) may indicate that these boulders were softly landed after the formation of the terrain; however, dynamical interactions between the boulder and fine particles during the resurfacing processes, such as seismic shaking, remain a possible origin.

As noted by Fujiwara *et al.* (1), the low-gravitational potential regions coincide with the smooth terrains (Muses Sea and Sagami-hara) (Fig. 1), which suggests gravitational movement of the finer materials after the formation of the asteroid. The evolution of the smooth terrains likely involves processes for grain-size sorting and dynamical interactions between regolith and boulders, although the transport and deposition mechanisms are not well understood at present. The movements of the regolith materials on the surface of the asteroid are also suggested by a range of surface morphologies; for example, some craters are almost perfectly covered by regolith, which implies the emplacements of deposited materials.

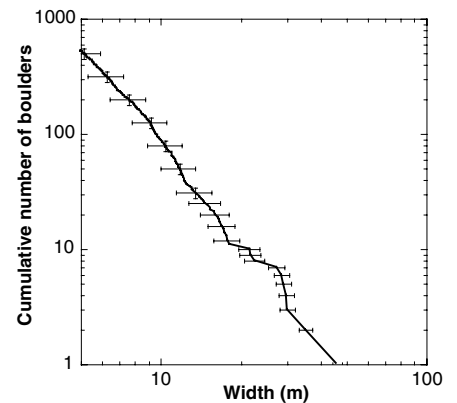


Fig. 2. Cumulative boulder size distribution on the surface of Itokawa. Horizontal axis shows the width (in meters) of the boulder, where the width is defined as the maximum size of the boulder. Vertical axis shows the number of boulders larger than a particular width. Data were collected from the six images of ST2482160259, ST2484352917, ST2485860275, ST2492225173, ST2492513077, and ST2493031594 at an altitude of 3.779 to 4.913 km.

In contrast to the asteroids previously explored by spacecraft, craters on Itokawa are generally indistinct. Several circular depressions, which are interpreted as craters, are seen (Figs. 1 and 3). Some of the circular depressions on rough terrains have floors apparently filled with finer particles (for example, Komaba in Fig. 3A), which are surrounded by brighter rims. As discussed below, the brighter albedo could be related to the fresh materials, which were exposed to the surface by the recent impact and/or downslope motions of possibly weathered materials on a steep slope. The circular and depressed shape of the Little Woomera region (Fig. 3B) suggests that it is the remnant of a large impact, which might be true for some of the other large circular depressions and facets on Itokawa.

The total number of craters on Itokawa is small: Even if we include all of the indefinite crater candidates, the total number of possible craters is less than 100. Because we can detect

¹Hayabusa Project Team, Institute of Space and Astronautical Sciences (ISAS), Japan Aerospace Exploration Agency (JAXA), 3-1-1 Yoshinodai, Sagami-hara, Kanagawa 229-8510, Japan. ²School of Engineering, Tokai University, Kanagawa 259-1292, Japan. ³Department of Geosystem Engineering, University of Tokyo, Tokyo 113-8656, Japan. ⁴Planetary Science Institute, 1700 East Ft. Lowell Road, Suite 106, Tucson, AZ 85719, USA. ⁵National Institute of Advanced Industrial Science and Technology, Tsukuba 305-8568, Japan. ⁶Planetary Science Department, ISAS, JAXA, 3-1-1 Yoshinodai, Sagami-hara, Kanagawa 229-8510, Japan. ⁷Fukushima National College of Technology, Iwaki 970-8034, Japan. ⁸Graduate School of Science and Technology, Kobe University, Kobe 657-8501, Japan. ⁹School of Computer Science and Engineering, University of Aizu, Fukushima 965-8580, Japan. ¹⁰Mizusawa Astrogeodynamics Observatory, National Astronomical Observatory of Japan (NAOJ), Oshu, Iwate 023-0861, Japan. ¹¹Remote Sensing Technology Center of Japan, Roppongi, Tokyo 106-0032, Japan. ¹²Subaru Telescope, NAOJ, Hilo, HI 96720, USA. ¹³Optical and Infrared Astronomy Division, NAOJ, Osawa, Tokyo 181-8588, Japan. ¹⁴Institute for Astronomy, University of Hawaii, Woodlawn Drive, Honolulu, HI 96822, USA. ¹⁵Jet Propulsion Laboratory, California Institute of Technology, Pasadena, CA 91109, USA. ¹⁶Department of Spacecraft Engineering, ISAS, JAXA, 3-1-1 Yoshinodai, Sagami-hara, Kanagawa 229-8510, Japan. ¹⁷Lunar and Planetary Laboratory, University of Arizona, Tucson, AZ 85705-6643, USA. ¹⁸Department of Astronomy and Bosscha Observatory, Bandung Institute of Technology Bandung 40132, Indonesia. ¹⁹Public Affairs Department, JAXA, Tokyo 100-8260, Japan. ²⁰Faculty of Engineering and Resource Science, Akita University, Akita 010-8502, Japan.

*To whom correspondence should be addressed. E-mail: saitoj@planetna.sci.isas.jaxa.jp

Fig. 3. (A) Muses Sea, with the Shirakami area composing the southern part of the “neck” region (ST2474731509). Small white arrows near Yatsugatake indicate the thin, boulder-rich layer similar to landslide deposits. Depressions in Muses Sea are marked by long gray arrows. The Komaba crater and some crater candidates are also indicated. (B) The darker depressed region in Little Woomera (ST2498167622), which is one of the largest facets, is surrounded by a brighter rim. (Inset) A high-resolution image of the northern rim of Little Woomera (ST2516321279). Note the stronger brightness contrast in the inset.

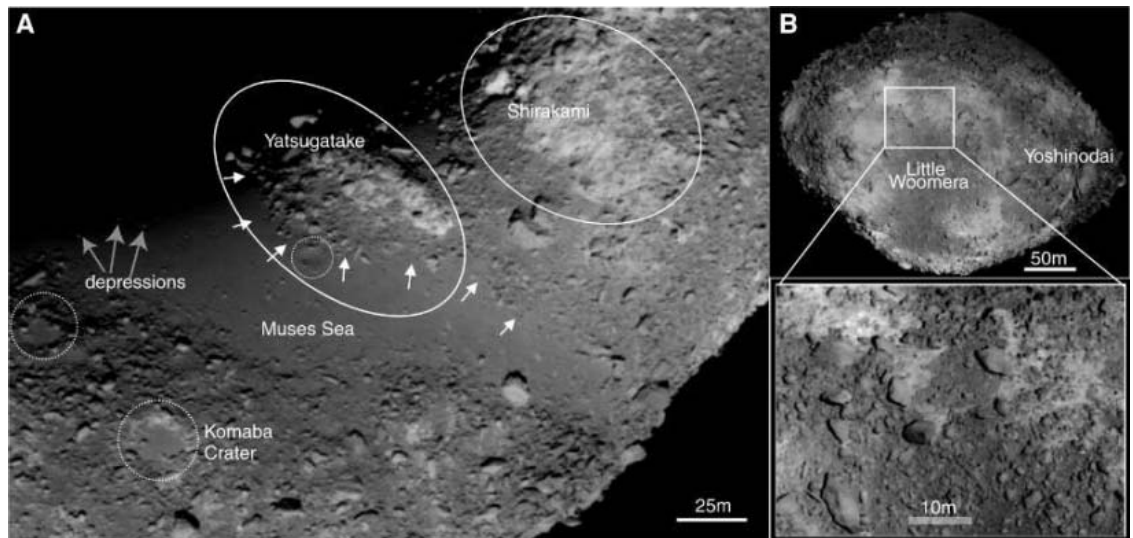
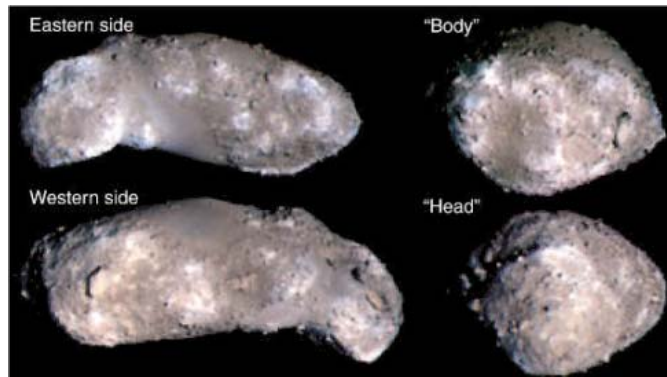


Fig. 4. Composite color images constructed from b-, v-, and w-band data. The contrast adjustment was done in each image to enhance the color variation.



boulders as small as a few meters in the 70-cm-resolution images obtained at the HP, similar-sized craters could be recognized under proper illumination conditions. Therefore, future detailed studies of crater statistics will not drastically increase the total number of craters. The limited total number of craters and their generally obscure morphologies might be attributed to resurfacing processes, such as seismic shaking (14), armoring by numerous boulders (15), or the paucity of smaller impactors (15); alternatively, Itokawa could have been generated by a relatively recent impact in the main belt and then transferred to its current orbit.

Among the most intriguing characteristics of Itokawa are the heterogeneities in color (Fig. 4) and albedo, which are unusual because no previously observed asteroid bodies show large variations in both of these characteristics (16–19). We found a variation of more than 30% in v-band albedo, as compared with only ~15% variation in the w-band/b-band color ratio. There appears to be a correlation between color and albedo on Itokawa; in general, brighter areas are bluer, whereas darker areas

are redder. These variations might be due to the space weathering process (20–23), but other possibilities, such as heterogeneities in mineralogical composition and grain size of surface materials (24), cannot be ruled out.

Brighter areas are mostly found in (i) areas with steeper slopes (Fig. 3A); (ii) areas of local high terrain, including edges of facets; and (iii) apparently eroded areas, such as crater rims. The brighter area in Shirakami (Fig. 3A) has a slope angle that is steeper than a typical angle of repose of granular materials. This situation indicates that most boulders in this area could be gravitationally unstable, which may explain the limited number of boulders there. The notable difference in the number of boulders between the brighter area in Shirakami and the proximal darker area implies the rearrangements of boulders. Thus, the brighter area may have been formed by the removal of the superposed boulders, which exposed the inner bright materials (25). Both the boulders and eroded material may have been deposited at the break of the slope and formed a thin, boulder-rich layer at the base of Shirakami and

Yatsugatake. Although this process can explain the consistencies in both sizes and angularities of the materials in the layer, the lack of flow front and talus features may imply further complexities.

Another example of the brighter area is in the Little Woomera region on the edge of the Otter’s body (Fig. 3B). Little Woomera is a relatively darker depressed region surrounded by rimlike features, which are about 10% brighter when viewed from HP. However, images with higher spatial resolution reveal that the 10% brighter features are composed of the combinations of both darker and 20 to 30% brighter materials (Fig. 3B); that is, the real brightness contrasts are not resolved by lower spatial resolution images. A few darker areas apparently overlap the brighter area, showing relatively sharp boundaries. This dichotomy may indicate that a part of the dark and boulder-rich surfaces was removed by shaking caused by impacts or planetary encounters, leading to exposure of the underlying relatively bright area.

References and Notes

1. A. Fujiwara *et al.*, *Science* **312**, 1330 (2006).
2. R. P. Binzel, A. S. Rivkin, S. J. Bus, J. M. Sunshine, T. H. Burbine, *Meteorit. Planet. Sci.* **36**, 1167 (2001).
3. A. Cellino *et al.*, *Icarus* **179**, 297 (2005).
4. T. Nakamura *et al.*, *Earth Planets Space* **53**, 1047 (2001).
5. E. F. Tedesco, D. J. Tholen, B. Zellner, *Astron. J.* **87**, 1585 (1982).
6. A test polarimetric observation at a solar phase angle of $\sim 10^\circ$ was conducted during the earlier rendezvous phase; however, subsequent observations were canceled because of problems with the system’s attitude control.
7. A search for Itokawa’s satellites was performed at a distance of about 1000 km. The field-of-view of AMICA was about 100 km by 100 km around Itokawa, and it fully covered the Hill sphere (~ 40 km in radius). The limiting V-magnitude was about 9.5, corresponding to objects of less than ~ 1 m in diameter. Preliminary analysis showed no bright satellite candidate.

8. L. Prockter *et al.*, *Icarus* **155**, 75 (2002).
 9. T. Michikami, K. Moriguchi, R. Nakamura, *36th Lunar Planet. Sci. Conf.*, abstr. 1729 (2005).
 10. The slope of the bulk population would be somewhat steeper (0.2 to 0.3) than that of the surface population. See (26).
 11. P. C. Thomas, J. Veveřka, M. S. Robinson, S. Murchie, *Nature* **413**, 394 (2001).
 12. P. C. Thomas *et al.*, *J. Geophys. Res.* **105**, 15091 (2000).
 13. M. J. Cintala, J. B. Garvin, S. J. Wetzel, *Proc. Lunar Planet. Sci. Conf.* **13**, 100 (1982).
 14. J. E. Richardson, E. James, H. J. Melosh, R. J. Greenberg, D. P. O'Brien, *Icarus* **179**, 325 (2005).
 15. C. R. Chapman *et al.*, *Icarus* **155**, 104 (2002).
 16. S. Murchie *et al.*, *Icarus* **155**, 145 (2002).
 17. P. Helfenstein *et al.*, *Icarus* **120**, 48 (1996).
 18. J. Veveřka *et al.*, *Icarus* **120**, 66 (1996).
 19. P. Helfenstein *et al.*, *Icarus* **107**, 37 (1994).
 20. C. R. Chapman, *Meteorit. Planet. Sci.* **31**, 699 (1996).
 21. S. Sasaki, K. Nakamura, Y. Hamabe, E. Kurahashi, T. Hiroi, *Nature* **410**, 555 (2001).
 22. T. Hiroi, S. Sasaki, *Meteorit. Planet. Sci.* **36**, 1587 (2001).
 23. B. E. Clark, B. Hapke, C. Pieters, D. Britt, in *Asteroids III*, W. Bottke *et al.*, Eds. (Univ. of Arizona Press, Tucson, 2002), pp. 585–599.
 24. T. Hiroi, C. M. Pieters, H. Takeda, *Meteoritics* **29**, 394 (1994).
 25. Gravitational sliding of regolith materials with different brightnesses was also observed on Eros. See (27).
 26. W. K. Hartmann, *Icarus* **10**, 201 (1969).
 27. P. C. Thomas *et al.*, *Icarus* **155**, 18 (2002).
 28. We thank the mission operation and spacecraft team of the Hayabusa project at ISAS/JAXA for their efforts that led to Hayabusa being the first Japanese spacecraft to rendezvous with and land on the asteroid. This research was supported by ISAS/JAXA, NASA, Kobe University through "The 21st Century Center of Excellence Program of the Origin and Evolution of Planetary Systems," and the University of Aizu.

2 February 2006; accepted 20 April 2006
 10.1126/science.1125722

REPORT

Mass and Local Topography Measurements of Itokawa by Hayabusa

Shinsuke Abe,^{1*} Tadashi Mukai,¹ Naru Hirata,^{1,3} Olivier S. Barnouin-Jha,² Andrew F. Cheng,² Hirohide Demura,³ Robert W. Gaskell,⁴ Tatsuaki Hashimoto,⁵ Kensuke Hiraoka,¹ Takayuki Honda,¹ Takashi Kubota,⁵ Masatoshi Matsuoka,⁶ Takahide Mizuno,⁵ Ryosuke Nakamura,⁷ Daniel J. Scheeres,⁸ Makoto Yoshikawa⁵

The ranging instrument aboard the Hayabusa spacecraft measured the surface topography of asteroid 25143 Itokawa and its mass. A typical rough area is similar in roughness to debris located on the interior wall of a large crater on asteroid 433 Eros, which suggests a surface structure on Itokawa similar to crater ejecta on Eros. The mass of Itokawa was estimated as $(3.58 \pm 0.18) \times 10^{10}$ kilograms, implying a bulk density of (1.95 ± 0.14) grams per cubic centimeter for a volume of $(1.84 \pm 0.09) \times 10^7$ cubic meters and a bulk porosity of ~40%, which is similar to that of angular sands, when assuming an LL (low iron chondritic) meteorite composition. Combined with surface observations, these data indicate that Itokawa is the first subkilometer-sized small asteroid showing a rubble-pile body rather than a solid monolithic asteroid.

The light detection and ranging instrument (LIDAR) aboard the Hayabusa spacecraft, described in (1–4), provided information on the shape, surface topography, and mass of the near-Earth asteroid 25143 Itokawa. The LIDAR measures distance by determining the time of flight for laser light to travel from the spacecraft to the asteroid and return. The stop time measured by the LIDAR is obtained by filtering a pulse received from the surface and measuring its time of peak intensity. In this manner, the LIDAR averages the topography within the LIDAR footprint on the surface of the asteroid, which approximates 5 by 12 m at a 7-km altitude for normal incidence. It was found that this pulse-detection technique permits identifying features smaller than the LIDAR footprint.

The LIDAR operated from September 10, 2005, at a distance of 49 km from the target, through November 25; a total of 4,107,104 shots were fired, and 1,665,548 returns were detected. The numbers of returns reduced significantly after October 2 when spacecraft pointing was less accurate because of failures in two of the three on-board reaction wheels.

When the spacecraft arrived at Itokawa, we used two methods to confirm the accuracy of LIDAR ranging obtained from ground calibration of the LIDAR instrument (3) (± 1 m from a distance of 50 m and ± 10 m from 50 km). In one approach, the size of the spacecraft shadow that was cast on the asteroid surface at the center of opposition point in a navigation image equaled that expected given the LIDAR-measured range measured by the spacecraft. In another approach, the height of the largest boulder on Itokawa, namely Yoshinodai, was found to be ~20 m when using independent measurements obtained from the LIDAR and the narrow angle imager [Asteroid Multiband Imaging Camera (AMICA)].

The LIDAR beamwidth is 0.04° by 0.097° , and the boresight is coaligned with that of the near-infrared spectrometer (NIRS) with its 0.1° by 0.1° field of view. The NIRS alignments relative to the Hayabusa spacecraft, to AMICA, and to the wide-angle optical navigation camera (ONC-W) used for determination of the spacecraft position relative to the asteroid (2), were determined from in-flight star field calibrations. The coalignment between

the LIDAR and NIRS was confirmed when NIRS detected the reflected 1064-nm yttrium-aluminum-garnet–Nd (YAG–Nd) laser light from LIDAR (Fig. 1) and when changes in LIDAR ranges were found to correspond with expected changes in topography seen in AMICA data.

To measure the mass of Itokawa and its surface topography, the position of the Hayabusa spacecraft relative to Itokawa must be determined. We developed a new method (Fig. 2) to estimate this spacecraft position by combining a shape model (5) of the asteroid determined primarily from images, ONC-W information on the direction to the center-of-light from the asteroid, and LIDAR ranging data. With these data, a first guess at the spacecraft trajectory is made. Often, substantial discontinuities are observed that cannot be explained by thrusting. By least-squares fitting of a smooth function to the initial spacecraft trajectory, a more realistic smooth approximation is obtained, from which a cloud of LIDAR points sitting on the Itokawa surface can be determined. Checks with the actual location of the LIDAR spot in simultaneous AMICA images show that this method provides accurate spacecraft locations as well as good surface topography.

An example of the detailed surface topography that can be obtained from the LIDAR using this methodology is shown (Fig. 3) for data obtained from ~7-km range. In this Tsukuba area (5), located on the eastern side of Itokawa and representative of the rough regions on the asteroid, blocks from 3- to 10-m elevation are visible. These data contrast significantly with results obtained

¹Graduate School of Science and Technology, Kobe University, Nada, Kobe 657-8501, Japan. ²Johns Hopkins University Applied Physics Laboratory, Laurel, MD 20723–6099, USA. ³Department of Computer Software, University of Aizu, Aizuwakamatsu, Fukushima 965-8580, Japan. ⁴Jet Propulsion Laboratory, California Institute of Technology, Pasadena, CA 91109, USA. ⁵Institute of Space and Astronautical Science (ISAS), Japan Aerospace Exploration Agency (JAXA), Yoshinodai, Sagami-hara, Kanagawa 229-8510, Japan. ⁶NEC Aerospace Systems Co. Ltd., Fuchu, Tokyo 181-8551, Japan. ⁷National Institute of Advanced Industrial Science and Technology, Tsukuba 305-8568, Japan. ⁸Department of Aerospace Engineering, University of Michigan, Ann Arbor, MI 48109–2140, USA.

*To whom correspondence should be addressed. E-mail: avell@kobe-u.ac.jp

from the Muses Sea, which is representative of smooth regions on Itokawa (6) where small-scale fluctuations in the elevation are observed that are comparable to the digitization of the LIDAR.

From such topographic data, the fractal roughness of the surface can be measured (7, 8) as the root mean square deviation σ of the height differences along a given baseline. For a 20-m baseline, which exceeds the LIDAR footprint, the Tsukuba region is characterized by a σ value of 2.2 m. This is in contrast to Muses Sea, where σ equals 0.6 m. Comparison of σ on Itokawa and Eros indicates that the rough Tsukuba region of Itokawa has a roughness on 20-m baselines similar to that measured in the interior, near the rim, of the large crater Psyche on Eros (8). This region in Psyche primarily consists of disrupted materials, strewn boulders, and coarse talus typ-

ical of crater ejecta. The similarity in roughness suggests that the near-surface of Itokawa resembles a rubble pile, which AMICA confirms (1, 6). To investigate the interior structure of Itokawa, we also measured the mass of Itokawa to determine its density. We used the best data available to us that the LIDAR acquired during the rehearsal descent phase on November 11, 2005.

The Hayabusa was designed as a simple spacecraft, with fixed antennas on the upper panel perpendicular to the +Z direction and fixed instruments on the base panel faced toward the -Z direction (toward the asteroid during in situ observations). On November 11, 2005, the Hayabusa spacecraft made a descent for the asteroid Itokawa along an Earth-Hayabusa-Itokawa line so as to allow both high-rate communication with Earth and in situ

observations of the asteroid. The solar phase angle, defined as a Sun-Itokawa-Hayabusa angle, was about 8° during the descent.

We estimated the acceleration term F of the spacecraft motion by using the descent data from 17:51:17 to 19:35:49 UT on November 11 (Fig. 4A) at distances from the center of Itokawa from 1427 to 825 m. We subtracted the effects of solar radiation pressure and thruster forces from the acceleration to estimate asteroid gravity. The thruster forces depend on injector temperature, and this contribution is presented as a function of thruster-injection rate when the maneuver uses only $\pm Z$ thrusters. The following relationship was derived from maneuver data obtained in mid-October about 10 km from Itokawa: F_{10} (cm/s²) = $0.1603 \times (\text{thruster ratio}) + 1.5695 \times 10^{-5}$, where thruster ratio is defined as a ratio of an integrated time of thruster burn to the total time of interest, and the acceleration due to solar radiation is calculated as 1.3303×10^{-5} cm/s².

During the above period of the descent, the thrusters were operated in only $\pm Z$ directions with a constant temperature of 35°C, and the total number of thruster injections was 136. Because the duration time of each thruster is 19.53 msec, the thruster ratio becomes 4.2348×10^{-4} , and the resulting F_{10} value is 8.3594×10^{-5} cm/s². We assumed that the acceleration caused by solar radiation force and thruster effect is constant during the descent. As an initial condition, we subtract the above F_{10} value from the total acceleration term. Then, to investigate the gravity potential, we adopted a polyhedron method that was well suited to evaluate the gravitational field of an irregularly shaped body such as Itokawa (9), where we assumed a constant-density interior of the asteroid.

By least-squares fitting of the spacecraft orbit during descent to calculated orbits obtained with the Itokawa's polyhedron model, we estimate the gravitational potential GM of

Fig. 1. LIDAR spectrum observed by NIRS. The 0.1° by 0.1° square-shaped field of view of NIRS was coaligned with that of LIDAR (a 0.04° by 0.097° ellipse). LIDAR spectra reflected by Itokawa were detected by NIRS during the descent. Figure shows a LIDAR spectrum obtained by NIRS from an altitude of 900 m at 01:02:22 UT on November 12, 2005. Dotted line indicates observed LIDAR spectrum after subtracting a spectrum of the asteroid Itokawa. A preflight spectrum of LIDAR measured by NIRS is shown as a solid line for comparison with the one measured in flight. NIRS has a 64-channel InGaAs photodiode array detector corresponding to 764 to 2248 nm, which includes the reflected 1064 nm YAG-Nd laser light from LIDAR. The LIDAR signal detected by NIRS confirmed that LIDAR and NIRS instruments were coaligned within the field of view accuracy, i.e., 1.7 m at a distance of 1 km.

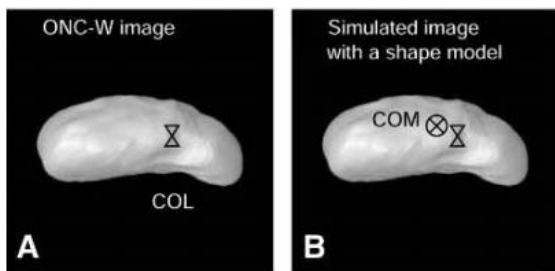
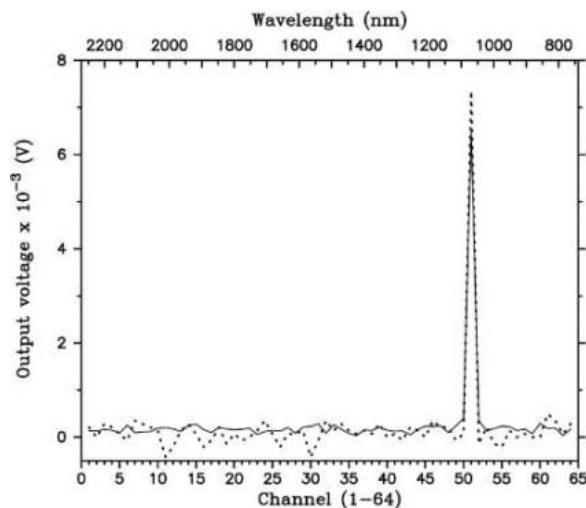
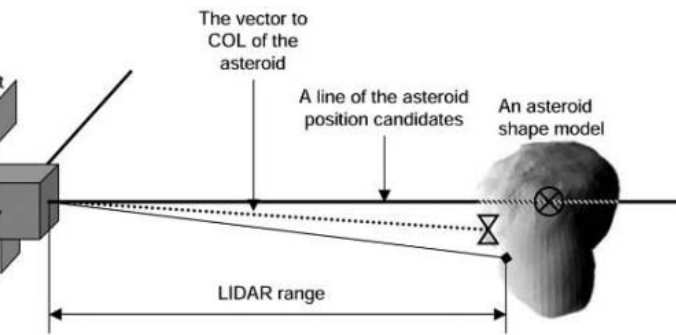


Fig. 2. Conceptual drawings of the method to estimate the position of the spacecraft. (A) ONC-W takes images of the asteroid every 128 s, and the onboard computer calculates the center of light (COL) of the asteroid image. The pixel coordination of COL in the camera detector is included in the telemetry. (B) With a shape model of the asteroid determined primarily from images (although any approximate shape model can be used), an artificial camera image of the asteroid is simulated. Even though this image is nonscaled, two vectors from the spacecraft to the COL and to the shape/mass center (COM) of the asteroid are obtained. (C) From COM



information and the simulated image, the location of the asteroid relative to the spacecraft is estimated with one degree of freedom on a line along the spacecraft-COM vector. Finally, the distance to the asteroid is obtained from an actual ranging data of LIDAR and the shape model. Through iterations, a very accurate spacecraft location can be found. This procedure was carried out on all pairs of the LIDAR ranging data and COL telemetry.

HAYABUSA AT ASTEROID ITOKAWA

Itokawa, where G is the gravitational constant and M denotes the mass of the asteroid (Fig. 4B). The resulting value of GM leads to the gravitational acceleration at a 10-km altitude, which is then also subtracted from the initial F_{10} to obtain an improved estimate of the solar radiation and thruster force. We then iterated the trajectory fit to the descent data to derive a revised value of GM using the modified F_{10} value and find a best estimate of GM equal to $(2.39 \pm 0.12) \times 10^{-9} \text{ km}^3/\text{s}^2$. The gravitational acceleration at the distance of 10 km from Itokawa is $\sim 0.2392 \times 10^{-5} \text{ cm/s}^2$, and it is about 3% of the acceleration term there.

Our GM value finds the mass of Itokawa to be $3.58 \times 10^{10} \text{ kg}$ with an uncertainty of 5%. The shape model of Itokawa constructed with AMICA images indicates that the volume is $1.84 \times 10^7 \text{ m}^3$ within 5% uncertainty (1). Consequently, the bulk density of asteroid Itokawa measures 1.95 g/cm^3 with 7% uncertainty. Our error in mass estimation is significantly larger than that obtained by the laser rangefinder aboard the Near Earth Asteroid Rendezvous mission (10), because Hayabusa did not orbit the asteroid, and the mass of Eros is 190,000 times that of Itokawa, producing greater uncertainty in the determination of spacecraft position.

Hayabusa NIRS reported that the Itokawa spectrum near the 1- μm absorption band is similar to those of LL-type chondrites (11). Considering the bulk density of LL ordinary chondrites of 3.19 g/cm^3 (12), our bulk density of asteroid Itokawa indicates a high porosity of about 40%, similar to that found for freshly formed coarse angular sands. Such a high porosity of Itokawa is noted in (1). It is known that the porosity of five S-type asteroids studied to date does not exceed about 20% (12), whereas two M-type asteroids have larger porosity of about 70%, and the average porosity of four C-type asteroids is about 28%. Our porosity for Itokawa is consistent with identification as a

Fig. 3. Location and elevation of LIDAR spot near Tsukuba region. (A) AMICA image ST2420994934 showing 17 predicted locations of LIDAR spot. (B) Simple cylindrical projection of the transect in meters North and East. (C) Relative elevation (m) along the LIDAR profile where the distance along the path is measured along the transect as if it were completely unwound. This elevation e is computed relative to a reference geoid as done in (7, 8): A ball would roll downhill from a high e to low e . The digitization error in these data are about $\pm 1.5 \text{ m}$. Data points in (B) are color coded by relative elevation according to (C). The letters in the lower two panels correspond to the circles seen in (A), going right to left. Panels (A) and (B) show how the location of the LIDAR spot fluctuates with time because of spacecraft pointing oscillations and the horizontal size of the order of the LIDAR spot are shown as sudden increases in elevation at locations D and G in (C). A jump at point J seen in elevation of about 5 m, and 10 to 15 m horizontally, corresponds to the central Tsukuba feature in (A).

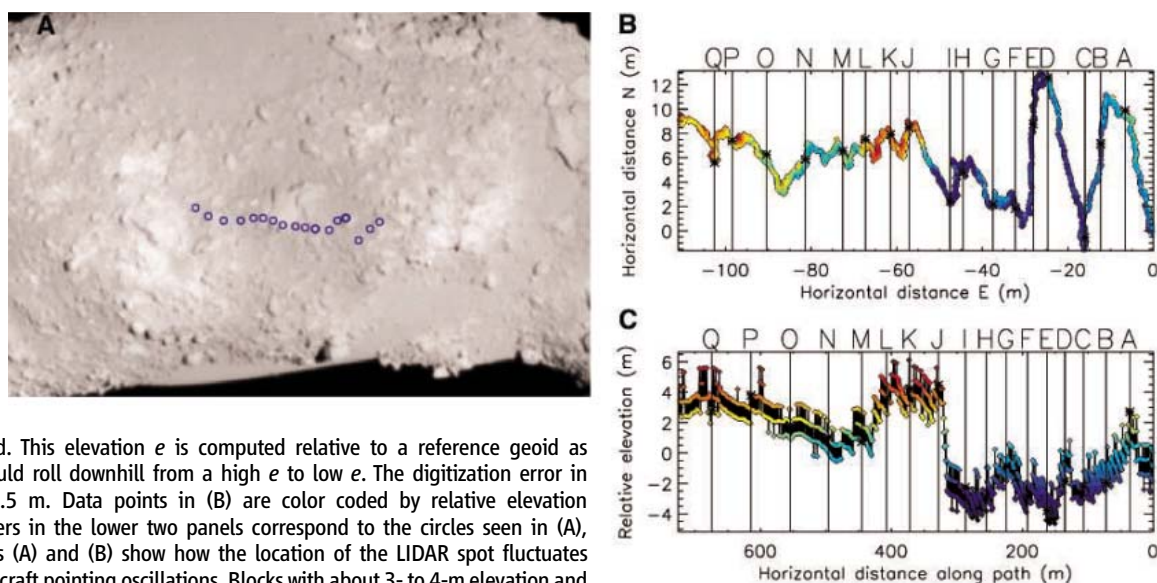
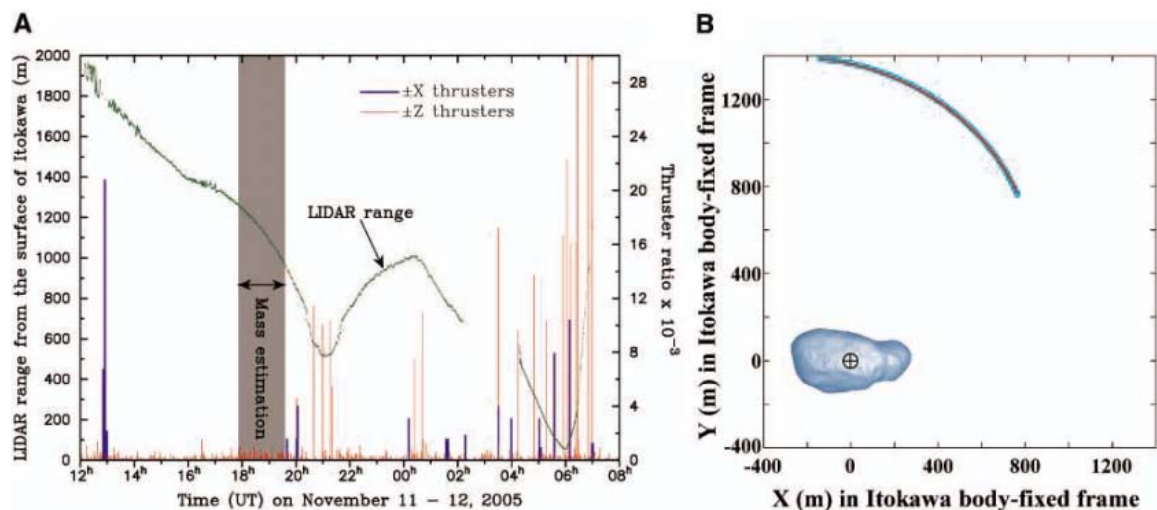


Fig. 4. (A) LIDAR range and thruster ratio during the rehearsal descent of November 11, 2005. LIDAR missed the surface during 2:20 to 4:17 UT. The period of 105 min for the mass estimation shows no abrupt changes and is very smooth relative to the other periods; moreover, the effect of thrusters in the direction of $\pm Z$ could be accurately estimated. (B) The position of Hayabusa spacecraft relative to its computed trajectory. The position of Hayabusa in body-fixed frame (thick blue curve) was determined by LIDAR ranging data with images from the (ONC-W). This approach phase has a good opportunity to measure the gravitational field because the gravitational acceleration of Itokawa is about 18 times stronger than the acceleration as a result of solar radiation pressure at the distance of 1 km from



Itokawa. The red curve on the thick blue curve shows the computed trajectory of the Hayabusa spacecraft for the best fitted GM of $2.39 \times 10^{-9} \text{ km}^3/\text{s}^2$. The adopted shape model (5) for this computation is shown, with ellipsoidal diameters of 535 (X) by 294 (Y) by 209 (Z) m, respectively.

“loosely consolidated (rubble-pile) asteroid” (13). Itokawa is the first S-type asteroid showing such high porosity, and the first subkilometer-sized small asteroid showing a rubble-pile structure rather than a solid monolithic structure.

Two distinct types of terrain are found on Itokawa, rough terrain with numerous boulders and smooth terrain covered with regolith layer (6), which suggests a complex history but does not predicate a heterogeneous composition. In addition, no clear regional difference in the normalized x-ray intensity ratios of Mg/Si and Al/Si has been found on the surface of asteroid Itokawa (14), indicating homogeneous composition. NIRS reported olivine-rich mineral assemblages similar to LL5 and LL6 chondrites, with variations in albedo and absorption band depth more than 10%, but this diversity may be consistent with differences in freshness and/or particle size (11), and it does not suggest the presence of unusual inhomogeneous materials.

As noted in (15, 16), the size of the asteroid, 150 to 1000 m in radius, may be a transition size between monolithic structure and rubble-pile structure. The large porosity of ~40% and the roughness of the surface found on Itokawa strongly

suggest a rubble-pile structure. The 12.1324-hour spin period of Itokawa (I) is far above the critical value of 2 hours, where a rubble-pile structure cannot withstand centrifugal forces [e.g., (17)], and is also consistent with a rubble-pile structure.

The internal structure of the asteroid Itokawa gives us a hint of its origin. It is predicted, on the basis of the numerical simulation of orbital evolution of asteroid Itokawa, that the most probable source region of asteroid Itokawa is the inner part of the main belt (18). High porosity in asteroid Itokawa may be the result of gravitational aggregation of the collision fragments.

References and Notes

1. A. Fujiwara *et al.*, *Science* **312**, 1330 (2006).
2. T. Hashimoto, T. Kubota, T. Mizuno, *Acta Astronaut.* **52**, 381 (2003).
3. T. Mukai *et al.*, *Adv. Space Res.* **29**, 1231 (2002).
4. T. Mukai, A. M. Nakamura, T. Sakai, *Adv. Space Res.* **37**, 138 (2006).
5. H. Demura *et al.*, *Science* **312**, 1347 (2006).
6. J. Saito *et al.*, *Science* **312**, 1341 (2006).
7. A. F. Cheng *et al.*, *Science* **292**, 488 (2001).
8. A. F. Cheng *et al.*, *Icarus* **155**, 51 (2002).
9. R. A. Werner, D. J. Scheeres, *Celest. Mech. Dyn. Astron.* **65**, 313 (1997).
10. M. T. Zuber *et al.*, *Science* **289**, 2097 (2000).
11. M. Abe *et al.*, *Science* **312**, 1334 (2006).

12. D. T. Britt, D. Yeomans, K. Housen, G. Consolmagno, in *Asteroids III*, W. F. Bottke, P. Paolicchi, R. P. Binzel, A. Cellino, Eds. (Univ. Arizona Press, Tucson, AZ, 2002), pp. 485–500.
13. D. C. Richardson, Z. M. Leinhardt, H. J. Melosh, W. F. Bottke Jr., E. Asphaug, in *Asteroids III*, W. F. Bottke, P. Paolicchi, R. P. Binzel, A. Cellino, Eds. (Univ. Arizona Press, Tucson, AZ, 2002), pp. 501–515.
14. T. Okada *et al.*, *Science* **312**, 1338 (2006).
15. W. Benz, E. Asphaug, *Icarus* **142**, 5 (1999).
16. E. Asphaug, E. V. Ryan, M. T. Zuber, in *Asteroids III*, W. F. Bottke, P. Paolicchi, R. P. Binzel, A. Cellino, Eds. (Univ. Arizona Press, Tucson, AZ, 2002), pp. 463–484.
17. P. Pravec, A. W. Harris, T. Michalowski, in *Asteroids III*, W. F. Bottke, P. Paolicchi, R. P. Binzel, A. Cellino, Eds. (Univ. Arizona Press, Tucson, AZ, 2002), pp. 113–122.
18. P. Michel, M. Yoshikawa, *Astron. Astrophys.* **449**, 817 (2006).
19. Supported by ISAS/JAXA through the Hayabusa mission. We are extremely grateful for the numerous engineers and supporting scientists who were critical to the successful development and execution of the first mission that rendezvoused with and landed on an asteroid. We thank E. Okumura and K. Tsuno (NEC Toshiba Space Systems, Ltd.) for their great efforts to develop the LIDAR. This work is partly supported by the 21st Century COE Program “Origin and Evolution of Planetary Systems” under the Ministry of Education, Culture, Sports, Science, and Technology (MEXT).

15 February 2006; accepted 21 April 2006
10.1126/science.1126272

REPORT

Pole and Global Shape of 25143 Itokawa

Hirohide Demura,¹ Shingo Kobayashi,¹ Etsuko Nemoto,¹ Naoya Matsumoto,¹ Motohiro Furuya,¹ Akira Yukishita,¹ Noboru Muranaka,² Hideo Morita,³ Ken Shirakawa,³ Makoto Maruya,⁴ Hiroshi Ohyama,⁴ Masashi Uo,⁴ Takashi Kubota,⁵ Tatsuaki Hashimoto,⁵ Jun'ichiro Kawaguchi,⁵ Akira Fujiwara,⁵ Jun Saito,⁵ Sho Sasaki,⁶ Hideaki Miyamoto,^{7,8} Naru Hirata^{1,9}

The locations of the pole and rotation axis of asteroid 25143 Itokawa were derived from Asteroid Multiband Imaging Camera data on the Hayabusa spacecraft. The retrograde pole orientation had a right ascension of 90.53° and a declination of –66.30° (52000 equinox) or equivalently 128.5° and –89.66° in ecliptic coordinates with a 3.9° margin of error. The surface area is 0.393 square kilometers, the volume is 0.018378 cubic kilometers with a 5% margin of error, and the three axis lengths are 535 meters by 294 meters by 209 meters. The global Itokawa revealed a boomerang-shaped appearance composed of two distinct parts with partly faceted regions and a constricted ring structure.

A telescopic camera on Hayabusa, the Asteroid Multiband Imaging Camera (AMICA) (I), provided about 1400 pictures of Itokawa during its rendezvous phase (2). Members from the AMICA science team and the Guidance and Navigation Control (GNC) team formed a special task force to investigate Itokawa's shape and properties, based on images from AMICA. The task force derived the pole orientation and rotation axis and then formed a global shape model of Itokawa based on a subset of AMICA images. At the beginning of the rendezvous phase, Itokawa was scanned circularly by AMICA. This generated side views, whose mean

interval was about 2°, as well as two polar views. The total number of images was 212, and their resolution ranged from 0.7 to 0.3 m per pixel.

Itokawa's pole orientation was determined by optically tracking feature points, called ground control points (GCPs). The final pole orientation showed retrograde behavior; a right ascension of 90.53° and a celestial declination of –66.30°, or ecliptically as 128.5° and –89.66° with a 3.9° margin of error. The latest ground-based results confirmed the retrograde behavior of Itokawa and its rotation axis, which is almost perpendicular to the ecliptic plane (3–5). Because Itokawa's rotation axis is perpendicular to the ecliptic plane,

AMICA enabled global coverage without polar night regions during a rendezvous that lasted less than half of the orbital time of Itokawa. The north direction (+z) of Itokawa was defined by the International Astronomical Union's right-hand-rule of its own rotation (6), and the +z axis was set to the minimum principal axis of inertia. The direction of the prime meridian (+x) was defined by a GCP, the Black Boulder. The rest of the +y was fixed. This coordinate system was rotated 180° around the z axis with that of previous shape models (4, 7, 8).

The global shape of Itokawa was reconstructed with image-based modeling that integrated limb profiles and stereogrammetric procedures (9). The total number of automatically selected feature points for three-dimensional shape modeling was 308,205, which were related to boulders rather than small distinct craters. Spacing of the points was not ordered, and smooth terrains revealed an absence of such

¹Department of Computer Software, University of Aizu, Ikki-machi, Aizu-Wakamatsu City, Fukushima 965-8580, Japan. ²CosmoLogic, 3-5-7, Kirigaoka, Midori-ku, Yokohama 226-0016 Japan. ³NEC Aerospace Systems, 1-10 Nissincho, Fuchu, Tokyo, 183-8551 Japan. ⁴NEC-TOSHIBA Space Systems, 1-10 Nissincho, Fuchu, Tokyo, 183-8551 Japan. ⁵Institute of Space and Astronautical Science/Japan Aerospace Exploration Agency, 3-1-1, Yoshinodai, Sagami-hara, 229-8510 Japan. ⁶National Astronomical Observatory of Japan, 2-12 Hoshigaoka, Mizusawa, Oshu 023-0861, Japan. ⁷Department of Geosystem Engineering, University of Tokyo, Tokyo 113-8656, Japan. ⁸Planetary Science Institute, 1700E Fort Lowell, Suite 106, Tucson, AZ 85719, USA. ⁹Graduate School of Science and Technology, Kobe University, Kobe 657-8501, Japan.

boulders. These points were converted to a polygon model with about 3° of resolution (Fig. 1). The total number of polygons was 4285. The model revealed the following shape properties: a surface area of 0.393 km^2 ; a volume of $1.84 \times 10^{-2} \text{ km}^3$ with a 5% margin of error; the size along three axes of 535, 294, and 209 m with a 1-m margin of error; and a bounding box size shown to be $550 \times 298 \times 244 \text{ m}$ with a 1-m margin of error. The spin period of Itokawa was 12.132 hours. The volume precision of Itokawa was controlled by ambiguity of perspective, and those of other parameters were controlled by measuring the lengths on the images. The shape model was formed mainly with stereogrammetry. Previous shapes of Itokawa's envelope are consistent with AMICA images, but detailed features such as the boomerang-shaped bending were hard to identify before the rendezvous. Predictions from previous research with ground-based observations proved to be consistent with this result except for the length of z , the minimum principal axis (5, 7–9), with the most accurate estimations observed by a satellite with a thermal infrared surveyor (10).

One of the most remarkable features of the global shape seems to be two parts, a small "head" with a large "body." These two parts show a boomerang-shaped figure that seems to be separated by a constricted "neck" region, which has a concave ring feature (Figs. 1 and 2). The northern depression of the ring is 20 m in depth and 60 to 120 m in width. The steep slope on the head side of the depression has landslide materials at the bottom (Fig. 2). The southeastern part of the neck is buried with regolith materials that form part of the Muses Sea, but the steep slope of the head side is continuous to the Shirakami region (Fig. 3). Angles between the long axes of both parts show 24° around the z axis and 26° around the y axis. Itokawa has a considerable concave area, which cannot be projected to the spherical coordinates of geocentric longitude and latitude. The size of the ellipsoid fitted to the body shows $490 \times 310 \times 260 \text{ m}$, and that to the head shows $230 \times 200 \times 180 \text{ m}$ with a 10-m margin of error. A normal vector of the ring's plane to the x axis shows rotations of 7° around the z axis and -20° around the y axis. This constricted ring structure with related features implies that Itokawa may have been formed from the collision of two asteroids (Figs. 2 and 3) (2).

The surface of Itokawa was classified via stereogrammetric observation of images obtained mostly from an altitude of 7 km and a resolution of 0.7 m per pixel [home position (2)]. Stereogrammetrically derived surface textures with reliefs enabled geologic classification and region splitting in Fig. 3, as well as the identification of rough/smooth terrains and facets, large boulders, and major depressed areas. Characteristics of the boulders and rough/smooth terrains are discussed

in (11). Here we primarily discuss the presence and distribution of facets on Itokawa.

The surface of Itokawa appears to have a polyhedral angular structure, with each face of the angular structure called a facet, although their scales ($<100 \text{ m}$) are much smaller than those observed on other asteroids (12). Most facets are relatively flat, although a few have shallow concavity. These facets are divided by gently elevated boundary zones consisting of polyhedron edges (12). Figure 3 shows the boundaries of the facets and large blocks as broken lines. Although the facets are distributed globally on Itokawa, they are more abundant at both ends of the long axis (the head and tail of the body). The most remarkable feature of the head is its completely faceted surface. At the end of the body is the largest facet named "Little Woomera." Although we may include the faceted area as part of the rough terrain, the abundance of large boulders 10 or more meters in diameter showed that the Little Woomera facet has fewer boulders than found on other rough terrains. Traditional facets show the same behavior (13). Some facet boundaries are brighter in reflectance as well (11). The rim of the Little Woomera, which probably resulted from an impact, is one of the most distinct bright zones on Itokawa.

Each polyhedral, angular, and relatively flat structure revealed a shallow concave-like shape. Because this structure was especially distinctive in the shape model, we specifically use the term facet for the polyhedral angular structure, as is often used to describe similar structures on asteroids (Fig. 3). This kind of structure is difficult to recognize only from a single image, mostly because of the randomly-distributed boulders of various sizes. However, circular depressions, most of which would be impact craters, can be identified as specific and isolated patterns. The process that created these facets seem different from that which made the craters. If facets are craters, their sequential order of impacts can be reconstructed by observing the relationship among their emplacements. The appearance of a craterlike and isolated feature, such as the Little Woomera, shows the most recent impact feature. Although the head is entirely covered with facets, all of these facets are distinguishable from obvious craters or circular depressions. On the other hand, all facets adjoining the two smooth terrains, Sagami-hara, and the Muses Sea, are separated abruptly like coast lines, which are boundaries between rough and smooth terrains. This relationship suggests that the smooth terrains may be regolithic extensions over the rough

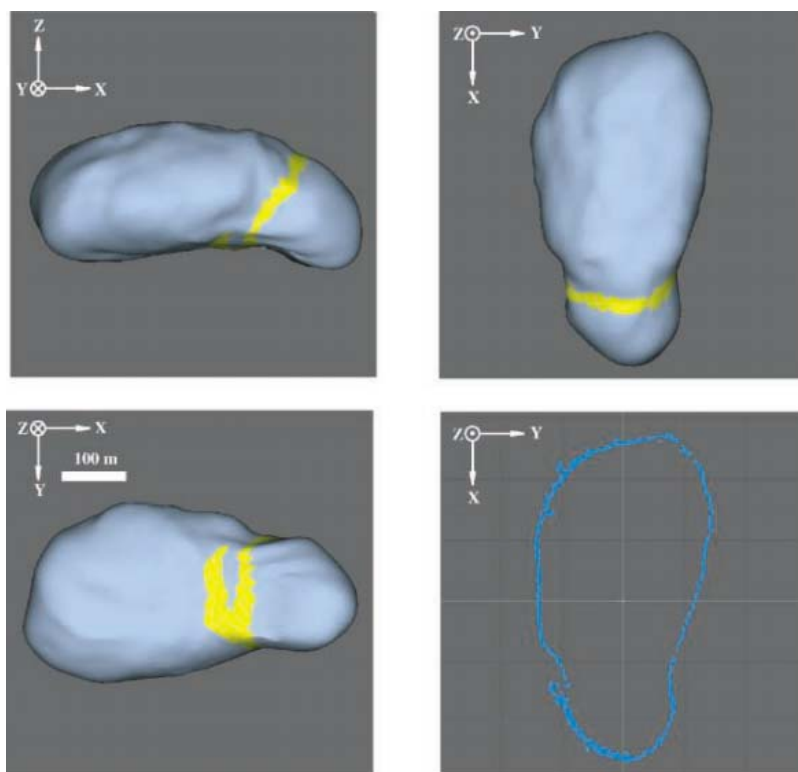


Fig. 1. Three views of Itokawa's shape model and a detailed cross section along the equator. The z direction is north of Itokawa, and the x direction is the prime meridian. The most substantial structure is two pieces (head and body) separated by a circular concave structure (neck). To help guide the eye, a headward slope of the neck is colored in yellow; this region is defined by surface texture of deposits and mass movements derived from the head. A quasi-eyeballed feature of southern polar region shows a local hill (named Yatsugatake in Fig. 3) surrounded by the deposits, but the hill might be an emplacement.

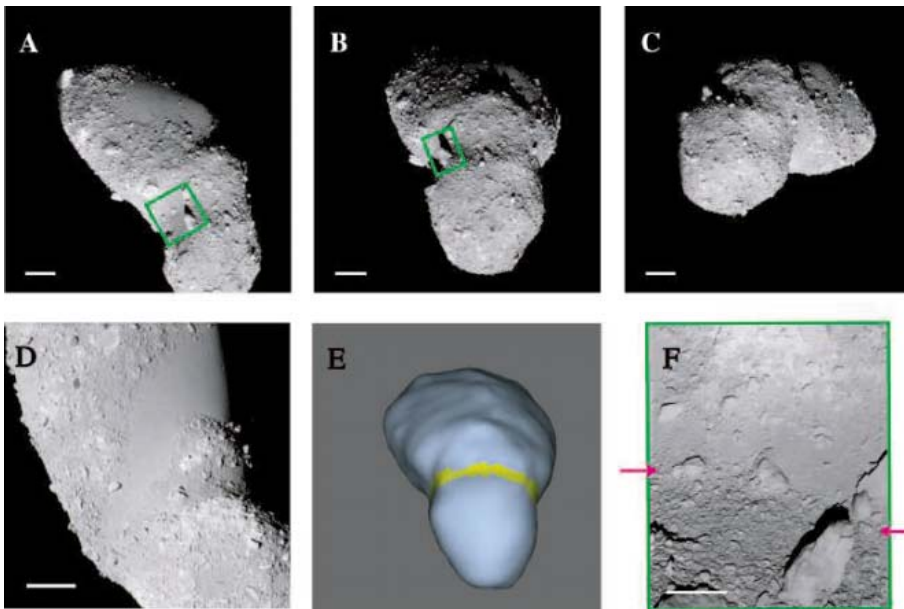


Fig. 2. Views of the neck structure. (A) Northwestern view with image identification code ST_2485860275. (B) Headward north view with ST_2482160259. (C) Northwest view with ST_2485070948. (D) Southeast view with ST_2474846738. (E) Shape model with the same view of the green rectangle in (B). (F) Close-up view (ST_2559003068) of the green rectangle of the neck in (A) and (B). (A) to (C) and (E) show a clear concave ring structure: the neck. (D) shows the southern neck. A brighter local hill is surrounded by gray, rough materials, which underwent a landslide, as shown in yellow in Fig. 1. This hill is called Yatsugatake in Fig. 3. (F) is a close-up of landslides from the head. The red arrow shows its front. Scale bars in (A) to (D), 50 m; in (F), 20 m.

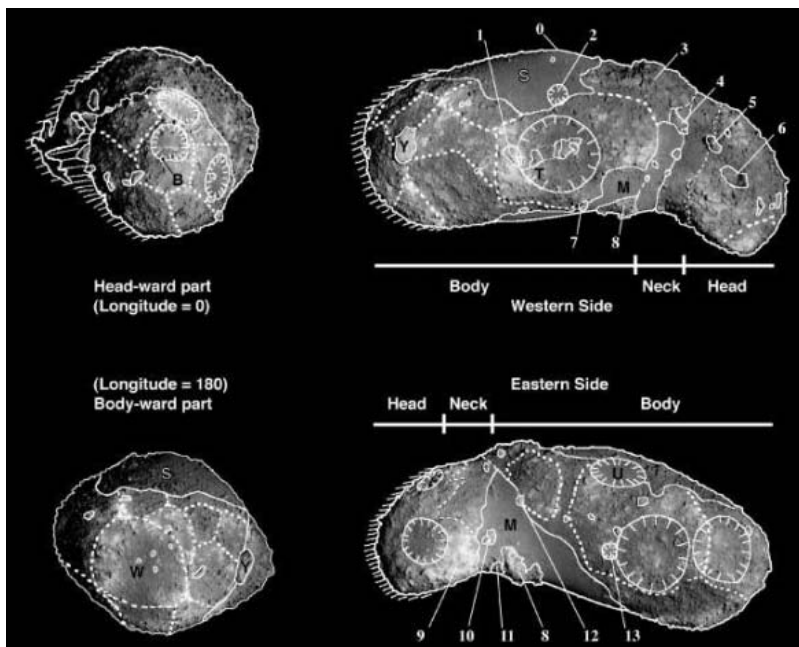


Fig. 3. Facets and nomenclature of Itokawa. Solid lines are boundaries of rough/smooth terrains (11), outlines of Itokawa, and major boulders. Broken lines are boundaries of facets or pedestal blocks. Circular features with spikes are concave features. Hatched regions of left outlines are shadows near the boundaries between day and night. (Image IDs: ST_2423460670, ST_2421011334, ST_2424157005, ST_2417520833.) The following IDs show major landmarks: B, the Black Boulder as the landmark of the prime meridian; Y, Yoshinodai boulder; T, Tsukuba Region; M, Muses Sea Planitia; S, Sagami-hara Planitia; W, Little Woomera Region; U, Uchinoura Region; O, the north vertex (+z pole); 1, Kakuta boulder; 2, Fuchinobe crater; 3, Sanriku ridge; 4, Kokubunji boulder; 5, Pencil boulder; 6, M-V boulder; 7, Hilo boulder; 8, Yatsugatake ridge; 9, Shirakami slope; 10, Mountainview boulders; 11, Noshiro smooth terrain; 12, Usuda boulder; and 13, Komaba crater.

terrains. Some facets show gaps at their boundaries, which are different from other plane polygons. These pedestal facets or “blocks” are found on both sides of the body. These appear to be a large pile of rubble. Apparently, Itokawa experienced about 20 or more substantial impacts, which pockmarked the surface. It is not certain whether the facet formation took place before or after the collision of the two larger elements, which currently comprise the head and the body. The neck zone of Itokawa seemingly lacks a faceted structure, which may have been erased at the time of collision between the head and the body. However, the local steep slope, as well as the transported regolithic materials, probably modified the surface structure of the neck zone recently.

Some implied impact structures are found, but little evidence of a global system of groove structures is observed on Itokawa. Although other suspicious short grooves are observed, these are faint features that are hardly separated from the sequential patterns of the boulders. We observed no long, distinct grooves or lineaments on Itokawa like those on Eros (14). This may imply that Itokawa is not a globally coherent body. However, the layer of scattered boulders on the surface might have obscured the presence of underlying grooves or lineaments.

Itokawa has revealed itself as a boomerang-shaped asteroid, covered with many polygonal facets. Formed by the collision of two large masses, Itokawa not only rotates more slowly than other subkilometer asteroids, but it may also be composed of rubble held together by gravity instead of being one monolithic whole. To better understand Itokawa, future research will require investigation of the facets and craters to clarify Itokawa’s collisional history, as well as investigation of the potential existence of hidden grooves to reveal more about Itokawa’s interior structure.

References and Notes

1. T. Nakamura *et al.*, *Earth Planets Space* **53**, 1047 (2001).
2. A. Fujiwara *et al.*, *Science* **312**, 1330 (2006).
3. M. Kaasalainen *et al.*, *Proc. Hayabusa Symposium* (in press) (2004).
4. S. J. Ostro *et al.*, *Proc. Hayabusa Symposium* (in press) (2004).
5. M. Kaasalainen *et al.*, *Astron. Astrophys.* **405**, L29 (2003).
6. P. K. Seidelman *et al.*, *Celestial Mechanics and Dynamical Astronomy* **91**, 203 (2003).
7. S. J. Ostro *et al.*, *Meteorit. Planet. Sci.* **39**, 407 (2004).
8. S. J. Ostro *et al.*, *Meteorit. Planet. Sci.* **40**, 1563 (2005).
9. R. Hartley, A. Zisserman, *Multiple View Geometry* (Cambridge Univ. Press, Cambridge, 2003).
10. T. G. Muller *et al.*, *Astron. Astrophys.* **443**, 347 (2005).
11. J. Saito *et al.*, *Science* **312**, 1341 (2006).
12. R. J. Sullivan *et al.*, Part III in *Asteroid III*, W. Bottke *et al.*, Eds. (Univ. of Arizona Press, Tucson, 2002).
13. P. C. Thomas *et al.*, *Icarus* **107**, 23 (1994).
14. M. S. Robinson *et al.*, *Meteorit. Planet. Sci.* **37**, 1651 (2002).
15. This research was supported by Japanese Grant-in Aid for Scientific Research 15740278, FY2003-2005.

10.1126/science.1126574

REPORT

Touchdown of the Hayabusa Spacecraft at the Muses Sea on Itokawa

Hajime Yano,^{1*} T. Kubota,¹ H. Miyamoto,² T. Okada,¹ D. Scheeres,³ Y. Takagi,⁴ K. Yoshida,⁵ M. Abe,¹ S. Abe,⁶ O. Barnouin-Jha,⁷ A. Fujiwara,¹ S. Hasegawa,¹ T. Hashimoto,¹ M. Ishiguro,⁸ M. Kato,¹ J. Kawaguchi,¹ T. Mukai,⁶ J. Saito,¹ S. Sasaki,⁹ M. Yoshikawa¹

After global observations of asteroid 25143 Itokawa by the Hayabusa spacecraft, we selected the smooth terrain of the Muses Sea for two touchdowns carried out on 19 and 25 November 2005 UTC for the first asteroid sample collection with an impact sampling mechanism. Here, we report initial findings about geological features, surface condition, regolith grain size, compositional variation, and constraints on the physical properties of this site by using both scientific and housekeeping data during the descent sequence of the first touchdown. Close-up images revealed the first touchdown site as a regolith field densely filled with size-sorted, millimeter- to centimeter-sized grains.

The most challenging engineering demonstration, as well as the most important scientific goal of the Hayabusa spacecraft (originally called MUSES-C) is the sampling of surface materials of the Apollo-type, near-Earth asteroid 25143 Itokawa (previously 1998 SF36). To maximize scientific promises of laboratory analyses of the returned samples, it is necessary to characterize physical and geological contexts of sampling sites as much as possible by using both onboard science instruments and housekeeping data of the spacecraft.

The Hayabusa spacecraft arrived at the asteroid hovering at a 20-km altitude (gate position) on 12 September 2005 UTC (1, 2). At altitudes of 7 to ~20 km above Itokawa's surface, Hayabusa spent 6 weeks performing global remote-sensing measurements (3–5) that revealed a clear dichotomy between boulder-rich rough terrains and low-potential smooth terrains of the asteroid. Shape models show that Itokawa is 550 m by 298 m by 224 m in its circumscribed box size (2).

After completion of the scientific observation phase, the Hayabusa team chose two sampling-site candidates on the basis of sci-

tific merits, judged mainly from optical images and light detection and ranging (LIDAR) topography, as well as technical constraints such as guidance-navigation-control (GNC) accuracy and operational safety during the touchdown sequence (Fig. 1A). These sites were (i) the largest smooth terrain area in the Muses Sea, a part of the adjacent “neck” region between the “head” and “body” parts, which is as wide as ~60 m from the head to the body and ~100 m from north to south and (ii) the largest facet of the rough terrain of the body called Little Woomera (2, 3). Both areas are in the local dayside of the equatorial region during the real-time telemetry coverage from ground stations. They also have relatively flat plains with few obstacles as large as the spacecraft itself (6) and show shallow local surface inclinations such that both high solar-power production and broad telecommunication to Earth are available during all touchdown sequences at a solar angle of ~10°.

The operation team performed two touchdown rehearsals on 4 and 12 November and two imaging navigation tests on 9 November. High spatial resolution images of both candidate sites also were acquired from altitudes

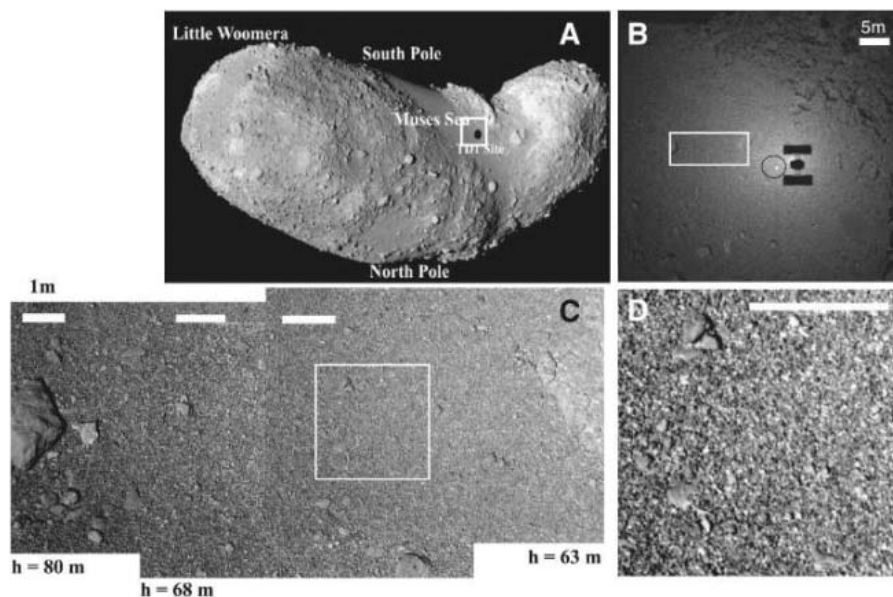


Fig. 1. Location of the Muses Sea smooth terrain, including the first touchdown site on Itokawa. All images were taken in v-band (3). The square in (A) indicates the size of (B); the rectangle in (B) indicates the size of (C); the rectangle in (C) indicates the size of (D). Scale bars in (C) and (D), 1 m. (A) Itokawa is 550 m by 298 m by 224 m in its circumscribed box size (2). (B) Taken by the wide-field optical navigation camera (ONC-W) from ~32-m altitude at 20:33 UTC. The circle next to Hayabusa's shadow shows the target marker that landed on the Muses Sea at TD1. (C) A composite of three close-up images of ST2563511720, ST2563537820, and ST2563607030, which were taken from 80-m, 68-m, and 63-m altitudes, respectively, according to LIDAR measurements. The spatial resolutions are 0.8 to ~0.6 cm/pixel. Contrasts in (C) are arbitrary and stretched to make the apparent brightness of the three images continuous, whereas the gray-scale brightness of (D) is stretched about five times that of the original image. The Muses Sea is composed of numerous, size-sorted granular materials ranging from several centimeters to subcentimeter scales. Rocks larger than tens of centimeters in size often exhibit brighter and/or darker spots on their surfaces than do smaller regolith grains.

¹Department of Planetary Science, Institute of Space and Astronautical Science, Japan Aerospace Exploration Agency, 3-1-1 Yoshinodai, Sagami-hara, Kanagawa 229-8510 Japan.

²Department of Geosystem Engineering, University of Tokyo, Hongo, Tokyo, 113-8656 Japan. ³University of Michigan, Ann Arbor, MI 48109–2140, USA. ⁴Toho Gakuen University, 3-11 Heiwagaoka, Meito, Nagoya, 465-8515 Japan. ⁵Department of Aerospace Engineering, Tohoku University, Sendai, Miyagi, 980-8579 Japan. ⁶Department of Earth and Planetary Science, Kobe University, Kobe, Hyogo, 657-8501 Japan. ⁷Applied Physics Laboratory, Johns Hopkins University, Laurel, MD 20723, USA. ⁸Seoul National University, Seoul, 151-742 Korea. ⁹National Astronomical Observatory of Japan, Mizusawa, Iwate, 023-0861 Japan.

*To whom correspondence should be addressed: E-mail: yano@isas.jaxa.jp

below 7 km, with the telescopic optical navigation camera (ONC-T) equipped with a 1024 by 1024 charge-coupled device of 20 arc sec/pixel resolution and a v-band filter with a central wavelength of 550 nm (3) during each descent [ONC-T is also called Asteroid Multi-band Imaging Camera (AMICA) when it is used for scientific observations (3)]. With these images, the operations team concluded that the Little Woomera area still held too many meter-sized boulders within the GNC accuracy circle of 60-m diameter to conduct a safe descent (7). Thus, the second rehearsal and both of the two actual touchdown attempts on 20 and 26 November 2005 were performed at the Muses Sea area (Fig. 1B).

The smooth terrains cover roughly 20% of the total surface area of Itokawa and mainly concentrate in two areas: the northern polar region and a larger area including the southern polar region and the Muses Sea. These terrains are easily recognized even in low-resolution images because they appear smooth with relatively small brightness contrast. This implies that these terrains are covered with small regolith particles whose grain-size distribution does not vary greatly.

No regional variations were found within spatial resolutions of either the x-ray fluorescence spectrometer (XRS) detecting elements such as Mg, Al, and Si, which were consistent with those of LL or L ordinary chondrites (5), or

the near-infrared spectrometer (NIRS), which was able to measure spectra at 800- to ~2100-nm wavelengths (4) with an ~8-m footprint from a 4.5-km altitude and an ~7-cm footprint during the first touchdown.

Close-up images taken with the ONC-T from altitudes of 80 to 63 m above the touchdown sites provided the highest resolution of ~6 mm/pixel (Fig. 1C). Although grain sizes vary from subcentimeter to ~3 m in this region, it is clear that the Muses Sea is densely filled with size-sorted regolith of similar brightness, mostly ranging from millimeter to centimeter scales, a coarse size that can be classified as “gravel” in the geological term (Fig. 1D). This is far larger than submillimeter regolith powders filling in ponds on 433 Eros (8, 9).

The Muses Sea holds a few boulders larger than several meters across, some of which are surrounded by dips or depressions. The boundary with the body rough terrain has a “transition zone” where boulders appear to exhibit imbrications. Also evident is a gradual decrease of both the average size of regolith particles and the spatial density of large rocks from the transition zone to the center of the Muses Sea. There, these rocks, tens of centimeters in size, often have rounded corners, have flat sides facing down, and tend to collect together. All of the smooth terrains are concentrated in local lows of gravity-centrifugal potential, and the Muses Sea has the minimum

potential over the entire surface of Itokawa (2). These facts suggest a possible comminution and transportation process of regolith materials between the surrounding rough terrains and the Muses Sea smooth terrain, a process that may still be occurring (10, 11).

If the resurfacing process of the Muses Sea is still in progress, both large rocks and sub-surface undulations might have been embedded by regolith that accumulated to similar depth. In this case, the thickness of this region is likely to be more than several meters, which is the typical roughness observed in rough terrains. Nevertheless, possible energy sources for block-regolith interaction/transportation may include electrostatic levitation (mainly for the finest submillimeter components below the best spatial resolution of the ONC-T close-up images) (12), planetary tides during close encounters (13), extreme thermal cycles, impact excavation, and seismic shaking (14).

Hayabusa’s “impact sampler” was designed as a single collection mechanism suitable for a diverse range of target surfaces (15, 16), because surface conditions of Itokawa could not be fully documented from ground observations before the development of the spacecraft. The sampler can operate on targets ranging from metal-silicate hard bedrock to regolith layers with gravel to microparticles. Impact experiments were performed (15) with this sampling system onto various analog materials such as heat-resistant bricks, 200- μ m glass beads, and lunar regolith simulants, at a normal impact incident angle unless otherwise specified both in 1g and in reduced gravity levels ($>10^{-5}g$), by using a 140-m-tall vacuum drop tower at the Micro-Gravity Laboratory (MGLAB) in Gifu, Japan. From the result, the expected amount of the collection mass in the Hayabusa sampler model from 1g and micro-gravity impacts for both bedrocks and regolith were several hundred milligrams to several grams per shot, except oblique impacts at $>45^\circ$, where the collection mass was <100 mg per shot. Additionally, we performed impact tests onto targets consisting of 3- to ~10-mm natural coarse grains and glass balls, which were equivalent in size to the Ta projectiles in the vacuum at 1g. Because of the limit of the experimental setup, we measured only the total ejected mass without using the sampler model. We estimated the collection mass of coarse grain impacts, which were the most likely result of impact sampling at the Muses Sea, to fit values between monolith (i.e., bedrock) and fine regolith (i.e., dust) targets (Fig. 2).

On 19 November UTC (20 November JST), the first touchdown (TD1) resulted in a canceled projectile firing, because the fan beam sensor apparently detected an obstacle, and an avoidance maneuver was conducted. The emergency ascent was autonomously canceled, and the spacecraft continued to free-fall to

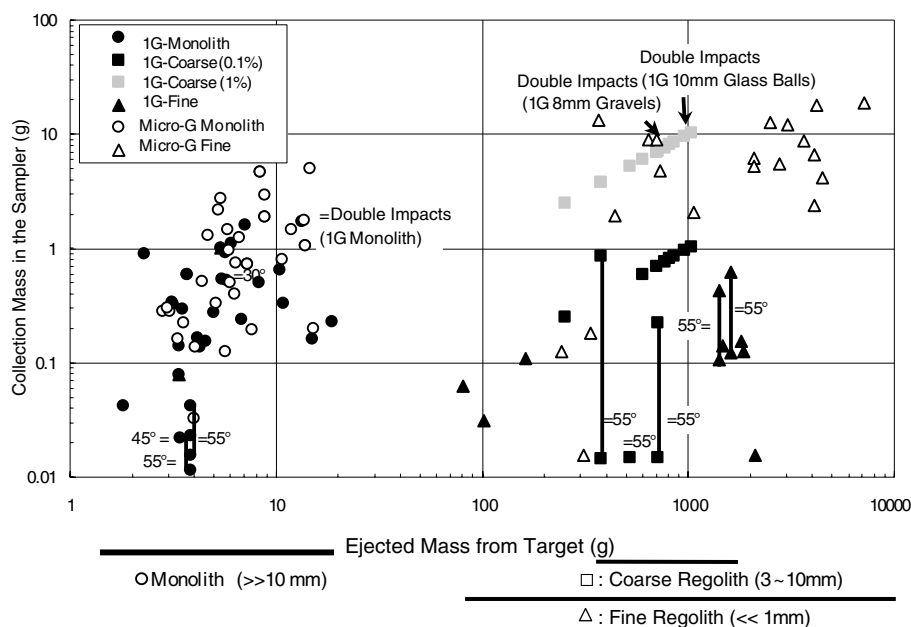


Fig. 2. Collection mass obtained in the Hayabusa impact sampler from impact ejecta mass of bedrocks (monolith) and coarse and fine grains (regolith) in vacuum. Filled shapes are experimental data in 1g, and open shapes are data in microgravity ($10^{-5}g$) using the MGLAB drop tower. Impact angles are normal unless otherwise specified. Inclined impacts at 55° from normal have data ranges between impact ejecta reached to the sampler canister as the maximum and those reached only inside the sampler horn. Shaded legends are coarse-grain impacts in 1g, with 1% collection efficiency assumed. Double impacts indicate the sum of the total sample mass collected by two projectiles that impacted at the same point on the target.

Itokawa's surface. At 21:10 UTC, the sampler horn touched and then rebounded on the asteroid surface near where the target marker landed at 6°S latitude and 39°E longitude in the head side of the Muses Sea. The second bounce occurred at 21:30 UTC. At 21:41 to 22:15 UTC, the spacecraft landed on the southwest of the Muses Sea region, closer to the head part than to the body, until the manual command for an emergency ascent thrust was conducted. Some slow regolith grains (below escape velocity of ~20 cm/s) might have been lifted up by the tip of the horn, and they might have reached the sample canister during the TD1 landing that lasted more than half an hour. Therefore, the hatch of the canister was closed to secure potentially collected samples.

At the second touchdown (TD2) on 25 November UTC (26 November JST), the whole sequence went as planned and the touchdown was detected by measuring deformation of the foldable sampler horn by the laser rangefinder (LRF)-S2 at 22:07 UTC (17). The spacecraft autonomously commanded the firing of two projectiles with a 0.2-s interval and then ascended by using the thrusting reaction control systems. However, after receiving data from the onboard recorder, it was found that the spacecraft might have issued a safeguard command for the projectiles ~4 min before the touchdown (18), which would have overridden the fire

command. At this stage, it remains unclear whether samples were collected during TD2, but the canister was closed to enable its insertion into the return capsule.

Surface characteristics of the Muses Sea area were estimated from altitudes from the center of the spacecraft mass—which were derived by measurements from four beams of LRF-S1 during the TD1 sequence and from stiffness and deformation test results of the prototype and flight model sampler horn in the laboratory (19, 20)—and from bounce time and velocities at the moment of touchdown. In this analysis, we set conditions such that all the LRF-S1 data best approximated to free-fall parabolic curves by least-square fitting in a temporal-altitude plot (Fig. 3A), and the first and second bounces shared a common contact time of 21:09:32 UTC at the asteroid surface. Then, numerical simulation on motion dynamics of the spacecraft was performed to obtain a set of possible surface characteristics satisfying the identified velocity conditions. This simulation was based on the multibody model of the spacecraft, where the sampler horn was modeled as an articulated lumped-mass system connected by compliant hinges (20). By applying Hertz's model and Coulomb's model to the asteroid surface—assumed as a flat, solid plate—the contact force and kinetic friction coefficient were calculated (21–23).

We then estimated the approaching vertical velocity of the spacecraft to the asteroid surface immediately before contact (V_z) as about -6.9×10^{-2} m/s and the bouncing velocity right after the contact (V_z') as about 5.8×10^{-2} m/s. Thus, the coefficient of restitution of the TD1 site is $\epsilon \sim 0.84$, which is far larger than the value measured for unconsolidated quartz sand targets impacted at 1 to ~100 cm/s (i.e., ~0.01 order) in microgravity (24). Although there was no direct measurement available for the relative horizontal velocity to the surface at the moment of the touchdown (V_x), it is inferred to be greater than 4.5×10^{-2} m/s toward the opposite direction of the attachment position of the sampler horn. Otherwise, the spacecraft cannot have $V_z' \sim 5.8 \times 10^{-2}$ m/s. This is due to asymmetric design of the spacecraft with respect to its center of mass (I). The tumbling motion induced during the surface contact becomes very different depending on such horizontal velocity at the moment of touchdown. If $5.0 \times 10^{-2} > V_x > 4.5 \times 10^{-2}$ m/s for this direction, the value of the friction coefficient of the touchdown surface as the solid plate is estimated as $\mu > 0.8$, or even greater than 1. In such a case, the tip of the sampler horn might have scratched rough but deformable surface materials, or possibly pushed and removed some quantity of them. This view is consistent with the regolith field imaged by

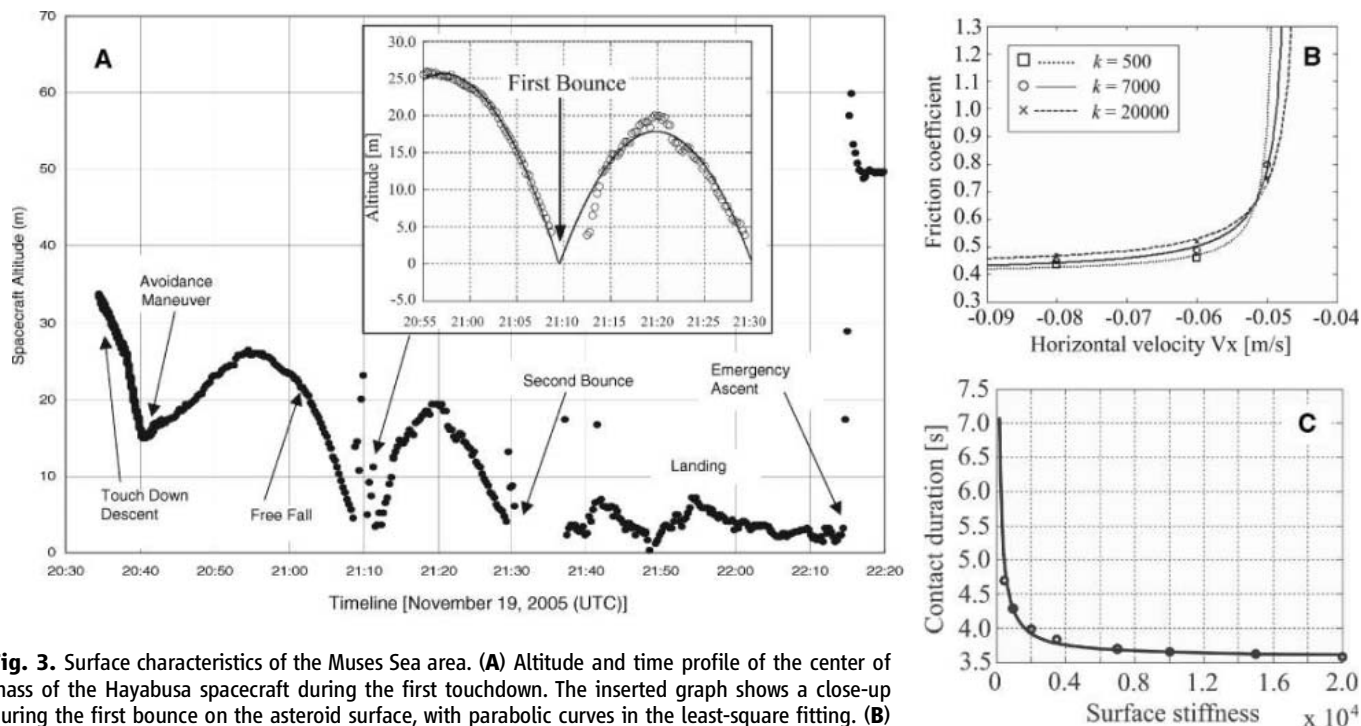


Fig. 3. Surface characteristics of the Muses Sea area. **(A)** Altitude and time profile of the center of mass of the Hayabusa spacecraft during the first touchdown. The inserted graph shows a close-up during the first bounce on the asteroid surface, with parabolic curves in the least-square fitting. **(B)** Simulation results of the friction coefficient (μ) of the asteroid surface, assumed to be a flat, solid plate, and the relative horizontal velocity (m/s), with negative values indicating the opposite direction from the sampler horn with respect to the center of the spacecraft mass at the moment of the first bounce. **(C)** Simulation results of the stiffness ($\text{N/m}^{-1.5}$) of the surface, assumed to be a flat plate, as a function of the contact time(s) during the first bounce in TD1. The surface stiffness is insensitive to the vertical velocity but sensitive to the contact time.

the ONC-T rather than loosely bonded dust layers (25). In this analysis, the result was not as sensitive to the stiffness of the surface as the solid plate (Fig. 3B). It is more sensitive to the time duration of the surface contact, which we do not have in the measured data. The contact duration would have been ~ 3.6 s with $k = 2 \times 10^4$ N/m $^{-1.5}$ and ~ 4.7 s with $k = 5 \times 10^2$ (Fig. 3C).

These first-order estimates still give us the sense that the Muses Sea regolith was not a fluffy, powdery pond in which the tip of the horn would have been embedded but, rather, that the spacecraft would bounce during the touchdown. This insight is important for engineering design constraints of both future sample-return missions and microgravity rovers on asteroids of sizes similar to Itokawa's. It also tells us that a major portion of samples returned to ground laboratories will most likely be coarse-grained regolith and their fragments rather than powdery, submillimeter particles.

A temperature profile from the XRS thermal radiator was also monitored during the TD1 phase (Fig. 4) (26, 27). Its temperature increased by thermal emission from the asteroid surface as the spacecraft descended, but it stopped increasing at 28 ± 2 m altitude above the Muses Sea, when the spacecraft hovered as a result of autonomous obstacle detection and avoidance maneuvers. About 20:53 to $\sim 20:57$ UTC [Fig. 4, part (1)], the radiator temperature almost reached thermal equilibrium, so that the emission temperature

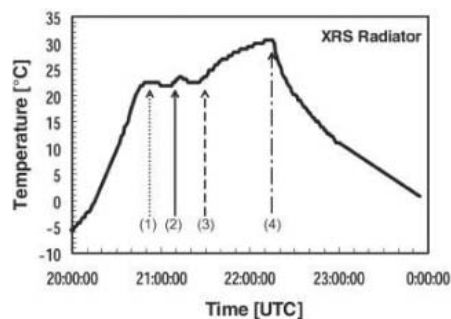


Fig. 4. Direct reading of temperature profile of the XRS radiator during the TD1 sequence before correction with ground calibration data. (1) Its temperature increased until the spacecraft descended to 28 ± 2 m altitude, where an obstacle was detected and the spacecraft conducted avoidance maneuvers. There, the radiator appears to reach a temporal thermal equilibrium. (2) The spacecraft autonomously decided not to escape and finally touched down at the surface at 21:10. (3) After the first bounce, the spacecraft landed on the surface and stayed there for about 40 min, showing a gradual temperature increase. (4) The spacecraft escaped by ground commands with rapid decrease in temperature. The Muses Sea surface temperature is estimated at about 310 ± 10 K, after the calibration with ground test data, in order to equilibrate with the XRS radiator at the period of (1).

from the Muses Sea area below the spacecraft was estimated at 310 ± 10 K, which was equivalent to $+23^\circ\text{C}$ in direct reading (Fig. 4) before the correction with ground calibration data (26, 27). At a solar distance of ~ 1 astronomical unit during the rendezvous with Itokawa, this result favors brecciated rocks and/or a coarse-grain-filled surface with a thermal inertia ($\Gamma = 10^2$ to $\sim 10^3$ Jm $^{-2}$ s $^{-0.5}$ K $^{-1}$) between that of monolithic rocks (e.g., $\Gamma = 4000$ Jm $^{-2}$ s $^{-0.5}$ K $^{-1}$, in which case the surface temperature is expected to be 280 K) and powdery surface like lunar regolith (e.g., $\Gamma = 40$ Jm $^{-2}$ s $^{-0.5}$ K $^{-1}$, the corresponding surface temperature for which is 370 K). This is also supported by the ground-based infrared spectrophotometry of Itokawa [$\Gamma = 750$ Jm $^{-2}$ s $^{-0.5}$ K $^{-1}$ (28)]. This view is consistent with the regolith field images of the Muses Sea. Other possible explanations for the low temperature of the Muses Sea regolith are that the TD1 site might be located at a higher latitude than estimated or that the Muses Sea area had not yet reached the maximum temperature, even at high noon, during TD1 because the area was so concave that duration of daytime was much shorter than in other areas, such as the head and body parts.

Hayabusa represents the first attempt to sample an asteroid surface. If the spacecraft comes back to Earth successfully in June 2010, the samples we have obtained will be surface materials from the Muses Sea. Therefore, understanding their characteristics in structure and composition through both remote sensing measurements and laboratory analyses (29) is vital in bridging current inferences based separately on meteoritic analyses and the ground-observation database of S-type asteroids.

References and Notes

- J. Kawaguchi *et al.*, *Acta Astronaut.* **52**, 117 (2003).
- A. Fujiwara *et al.*, *Science* **312**, 1330 (2006).
- J. Saito *et al.*, *Science* **312**, 1341 (2006).
- M. Abe *et al.*, *Science* **312**, 1334 (2006).
- T. Okada *et al.*, *Science* **312**, 1338 (2006).
- The size of the Hayabusa spacecraft with fully extended solar arrays is ~ 6.0 m (width) by ~ 4.4 m (length) by ~ 2.9 m (height), whereas the spacecraft bus structure is ~ 1 m (width) by ~ 1.6 m (length) by ~ 1.1 m (height).
- This accuracy is estimated by a combination of the target marker landing dispersion of 40 m for the nominal spacecraft capability, with additional instability due to malfunction of two axes of reaction wheels. For details, see (30).
- J. Veverka *et al.*, *Nature* **413**, 390 (2001).
- J. Veverka *et al.*, *Science* **292**, 484 (2001).
- G. D'Anna *et al.*, *Nature* **424**, 909 (2003).
- F. Horz, M. Cintala, *Meteor. Planet. Sci.* **32**, 179 (1997).
- P. Lee, *Icarus* **124**, 181 (1996).
- P. Michel, M. Yoshikawa, *Icarus* **179**, 291 (2005).
- A. F. Cheng, N. Izenberg, C. R. Chapman, M. T. Zuber, *Meteor. Planet. Sci.* **37**, 1095 (2002).
- H. Yano, S. Hasegawa, M. Abe, A. Fujiwara, *Proc. Asteroids, Comets, Meteors 2002 ESA-SP500*, 103 (2003).
- The 1-m sampler horn comprises an Al metal cylindrical horn of 15-cm diameter at the tip, a deformable cylindrical union, and an Al metal conical horn directed to the sample chamber, all connected by

double-helical springs. The sampling mechanism inside the spacecraft consists of a sample catcher canister, a transfer mechanism to the reentry capsule, and three projectile launchers.

- In the final sequence of the touchdown, the Hayabusa spacecraft would have (i) synchronized inertial velocity with the asteroid surface by canceling two-dimensional, horizontal velocities with respect to the target marker landing point, (ii) aligned to the local surface slope measured by four LRF-51 beams, (iii) detected the contact with the surface by the tip of the sampler horn attached on the anti-Sun face at ~ 10 cm/s of free-fall vertical velocity, (iv) fired a pair of 5-g Ta projectiles at ~ 300 m/s, (v) fractured surface materials, (vi) collected ejected rock fragments and/or regolith particles, which are concentrated through the conical horn toward the sample canister inside the spacecraft, and (vii) ascended again within a few seconds.
- A record of the pyrotechnics control device for the projectors did not indicate the completion of firing. However, this report may be faulty as a result of the system power reset that occurred soon after the TD2 ascent due to a temporal attitude control loss by reaction control systems (RCS) fuel leakage.
- The stiffness of the sampler horn is governed by the double-helical springs, and its laboratory data was obtained by NIPPI Corporation before spacecraft integration.
- K. Yoshida, T. Kubota, S. Sawai, A. Fujiwara, M. Uo, *Adv. Astronautical Sci.* **108**, Part 1, 481-490, AAS 01-135, (2001).
- H. Hertz, in *Miscellaneous Papers by H. Hertz*, Jones and Schott, Eds., (London, UK, 1896).
- G. Gilardi, I. Sharf, *Mechanism Machine Theory* **37**, 1213 (2002).
- The contact force F_n generated in the surface normal direction is computed by $F_n = k\delta^n$, where k is the stiffness of the surface assumed as a flat plate, δ is a penetration depth of the end tip of the sampler horn into the surface, and $n = 1.5$ is a constant. The friction force was estimated by Coulomb's model as $F_t = \mu F_n$, where F_t is the friction force generated in the surface tangent direction and μ is the kinetic friction coefficient.
- J. E. Colwell, *Icarus* **164**, 188 (2003).
- This does not mean that the relative horizontal velocity of the spacecraft (V_x) to the surface is constant for the whole period after the target marker tracking. If that were the case, the spacecraft could have traversed the whole Muses Sea area during the final descent, but that was not what actually occurred. Instead, this result tells us that the residual horizontal velocity was accumulated during the attitude-control maneuvers by the RCS in the final descent, including obstacle avoidance.
- T. Matsuda, thesis, Tokyo Institute of Technology, Japan (2001).
- T. Okada *et al.*, *Adv. in Geoscience* **3**, 119 (2006).
- T. G. Müller, T. Sekiguchi, M. Kaasalainen, M. Abe, S. Hasegawa, *Astro. Astrophys.* **443**, 347 (2005).
- I. Kushiro, A. Fujiwara, H. Yano (Eds.), *The First Competition for the MUSES-C Asteroidal Sample Preliminary Examination Team*, **ISAS-SP-16**, ISAS, Japan (2003).
- T. Kubota *et al.*, *Proc. of 11th Astrodynamics Symp.*, ISAS, Japan, 294, (2001).
- We thank M. Uo and T. Okudaira of NEC TOSHIBA Space System, H. Morita and K. Shirakawa of NEC Aerospace Systems, S. Yajima of Sumitomo Heavy Industries, T. Takami of Mitsubishi Heavy Industries, and K. Higuchi of JAXA/ISAS for providing the engineering data for the touchdown sequences. We also thank K. Teramoto of the University of Tokyo and C. Honda of JAXA/ISAS for assisting in impact sampling experiments at JAXA/ISAS, and G. Gilardi of Tohoku University for performing simulation analysis of the sampler dynamics. This work is partly supported by the Japan Space Forum Ground-Based Research Grant.

13 February 2006; accepted 10 May 2006
10.1126/science.1126164

Direct Determination of Local Lattice Polarity in Crystals

K. A. Mkhoyan,^{1*} P. E. Batson,² J. Cha,¹ W. J. Schaff,¹ J. Silcox¹

Materials with the wurtzite structure, such as CdSe quantum dots and rods, GaN-AlN quantum wells, and nanowires, play an increasingly important role in nanoscale science. For some, like the III-V nitrides, the existence of directional polarization is the driving force behind technical applications. Hexagonal crystals with the wurtzite (AB) structure exhibit physical and chemical properties that are different when they are parallel and antiparallel to the *c* axis. This difference is a result of particular stacking of A and B atomic layers, i.e. lattice polarity, along the [0001] direction (Fig. 1A). For a long time, atomic-level determination of the local lattice polarity was not possible. Early methods were based on differences in the surface properties of bulk crystals. Later, microscopic analysis relied on diffraction data recorded by conventional transmission electron microscopy (TEM) (1) or on a statistical analysis of scanning TEM (STEM) images (2).

Unfortunately, these techniques cannot reveal local, atomic-level polarity in nanoscale structures, because they lack the required lateral spatial resolution or are limited to thick samples, where extensive analysis of dynamical diffraction is needed. Demonstration of polarity at the atomic level would allow for understanding and control of phenomena occurring in nanoscale objects, such as selective growth of PbSe with a rock-salt structure on the tips of wurtzite colloidal nanorods (3) and the bonding of zincblende CdTe cores with wurtzite CdTe/CdSe branches in nanocrystals (4). Recent developments in TEM analysis techniques (5) and aberration correction in the TEM (6) and in the STEM (7), where an electron probe smaller than 1 Å has been achieved (8, 9), potentially allow for atomic-level determination of local polarity. TEM analysis has

been successful in improving the effective resolution from 1.7 Å (experimental) to ~0.8 to 0.9 Å with computational analysis using many experimental images (5). We show here that annular dark field (ADF) imaging in an aberration-corrected STEM can provide direct quantitative discrimination during observation in real time without extensive analysis.

Figure 1B shows an ADF image of a small area of wurtzite AlN in the $[\bar{2}110]$ projection, recorded using a VG HB-501 dedicated STEM equipped with an aberration corrector at an energy of 120 keV. Operation at this low energy is important to minimize irradiation damage from direct electron impact. This instrument has demonstrated a 0.75 Å probe in systematic tests (8). ADF imaging in crystals uses large-angle

elastic scattering to locate individual atoms and projected atomic columns, with good sensitivity to atomic number *Z* but with minor dependence on focusing conditions or specimen thickness. The challenge in this case is to image low-*Z* atoms, such as N, located in close proximity to very strongly scattering high-*Z* atoms. In the $[\bar{2}110]$ orientation, the smallest projected spacing between Al and N columns is 1.1 Å, requiring a very small electron probe for discrimination. In Fig. 1B, the N columns are seen as elongations of the column images alternately pointing diagonally up and down. This image represents the local polarity in AlN but also, for the first time, the identification of the single column of N atoms near the Al. In Fig. 1C, the visibility of N is enhanced by removal of the Al column signal. Because the column signal should be azimuthally symmetric, we measured the Al profile in the direction perpendicular to the line joining it with N (Fig. 1B, yellow line), and then subtracted to obtain the N profile.

Fig. 1D shows an example of the use of this technique for a strained AlN/GaN/AlN quantum well, where we can easily pick out the polarity of the AlN substrate and cap. In the quantum well, the much stronger Ga scattering makes direct polarity determination there difficult, but establishing the lattice position and polarity in the AlN matrix allows comparisons of the positions of Ga columns with image calculations (Fig. 1D, inset) to obtain the polarity in the quantum well. This particular structure is unfaulted and carries the substrate polarity through the well to the capping material.

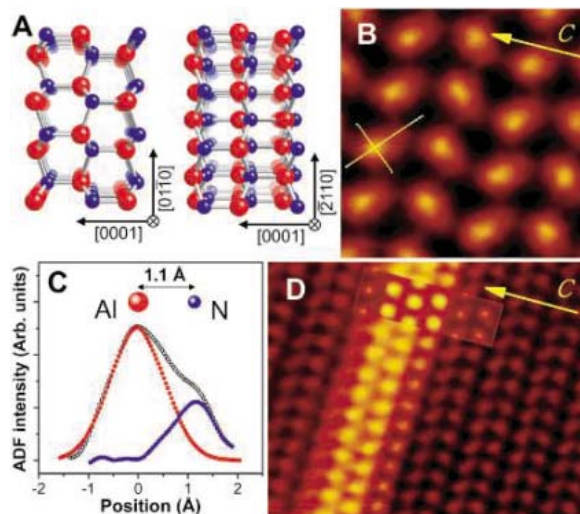


Fig. 1. (A) The wurtzite crystal in the two major projections perpendicular to the *c* axis. The left image shows the $[\bar{2}110]$ projection and the right image shows $[01\bar{1}0]$. These models have B-face polarity, because of ABABAB... stacking along the [0001] direction, where A is the blue and B is the red atom. (B) ADF-STEM image of AlN in the $[\bar{2}110]$ projection. To reduce instrumental noise, this image was filtered with a 0.65 Å⁻¹ low-pass Gaussian filter. (C) The N column is revealed when the Al column profile is removed from the total. These intensities were obtained from line scans whose positions are indicated in (B) by yellow lines. (D) ADF image of a GaN quantum well inside the AlN. The inset shows a calculation for a three-layer well to verify the polarity from the Ga positions.

References and Notes

1. J. Taftø, J. C. H. Spence, *J. Appl. Cryst.* **15**, 60 (1982).
2. A. J. McGibbon *et al.*, *Science* **269**, 519 (1995).
3. S. Kudera *et al.*, *Nano Lett.* **5**, 445 (2005).
4. D. J. Milliron *et al.*, *Nature* **430**, 190 (2004).
5. C. Kisielowski *et al.*, *Ultramicroscopy* **89**, 243 (2001).
6. M. Haider *et al.*, *Nature* **392**, 768 (1998).
7. O. L. Krivanek *et al.*, *Proc. EMAG97, Inst. Phys. Conf. Ser.* **153** (IOP Publishing Ltd., Bristol, 1997), pp. 35–40.
8. P. E. Batson *et al.*, *Nature* **418**, 617 (2002).
9. P. D. Nellist *et al.*, *Science* **305**, 1741 (2004).
10. This work was partially supported by the Nanoscale Science and Engineering Initiative of the NSF grant no. EEC-0117770 and by the New York Office of Science, Technology, and Academic Research grant no. C020071.

Supporting Online Material

www.sciencemag.org/cgi/content/full/312/5778/1354/DC1
Materials and Methods
Figs. S1 to S3
References

3 January 2006; accepted 31 March 2006
10.1126/science.1124511

¹School of Applied and Engineering Physics, Cornell University, Ithaca, NY 14853, USA. ²IBM Thomas J. Watson Research Center, Yorktown Heights, NY 10598, USA.

*To whom correspondence should be addressed. E-mail: kam55@cornell.edu

Metagenomic Analysis of the Human Distal Gut Microbiome

Steven R. Gill,^{1*} Mihai Pop,^{1†} Robert T. DeBoy,¹ Paul B. Eckburg,^{2,3,4}
Peter J. Turnbaugh,⁵ Buck S. Samuel,⁵ Jeffrey I. Gordon,⁵ David A. Relman,^{2,3,4}
Claire M. Fraser-Liggett,^{1,6} Karen E. Nelson¹

The human intestinal microbiota is composed of 10^{13} to 10^{14} microorganisms whose collective genome ("microbiome") contains at least 100 times as many genes as our own genome. We analyzed ~78 million base pairs of unique DNA sequence and 2062 polymerase chain reaction–amplified 16S ribosomal DNA sequences obtained from the fecal DNAs of two healthy adults. Using metabolic function analyses of identified genes, we compared our human genome with the average content of previously sequenced microbial genomes. Our microbiome has significantly enriched metabolism of glycans, amino acids, and xenobiotics; methanogenesis; and 2-methyl-D-erythritol 4-phosphate pathway–mediated biosynthesis of vitamins and isoprenoids. Thus, humans are superorganisms whose metabolism represents an amalgamation of microbial and human attributes.

Our body surfaces are home to microbial communities whose aggregate membership outnumbers our human somatic and germ cells by at least an order of magnitude. The vast majority of these microbes (10 to 100 trillion) inhabit our gastrointestinal tract, with the greatest number residing in the distal gut, where they synthesize essential amino acids and vitamins and process components of otherwise indigestible contributions to our diet such as plant polysaccharides (1). The most comprehensive 16S ribosomal DNA (rDNA) sequence-based enumeration of the distal gut and fecal microbiota published to date underscores its highly selected nature. Among the 70 divisions (deep evolutionary lineages) of Bacteria and 13 divisions of Archaea described to date, the distal gut and fecal microbiota of the three healthy adults surveyed was dominated by just two bacterial divisions, the Bacteroidetes and the Firmicutes, which made up >99% of the identified phylogenetic types (phylotypes), and by one prominent methanogenic archaeon, *Methanobrevibacter smithii* (2). The human distal gut microbiome is estimated to contain

≥100 times as many genes as our 2.85-billion base pair (bp) human genome (1). Therefore, a superorganismal view of our genetic landscape should include genes embedded in our human genome and the genes in our affiliated microbiome, whereas a comprehensive view of our metabolome would encompass the metabolic networks based in our microbial communities.

Progress made with 16S rDNA-based enumerations has disclosed significant differences in community membership between healthy adults (2, 3), differences that may contribute to variations in normal physiology between individuals or that may predispose to disease. For example, studies of humans and gnotobiotic mouse models indicate that our mutualistic relations with the gut microbiota influence maturation of the immune system (4), modulate responses to epithelial cell injury (5), affect energy balance (6), and support biotransformations that we are ill-equipped to perform on our own, including processing of xenobiotics (7). However, we are limited by our continued inability to cultivate the majority of our indigenous microbial community members, biases introduced by preferential polymerase chain reaction (PCR) amplification of 16S rDNA genes and by our limited ability to infer organismal function from these gene sequences.

As with soil (8) and ocean (9), metagenomic analysis of complex communities offers an opportunity to examine in a comprehensive manner how ecosystems respond to environmental perturbations, and in the case of humans, how our microbial ecosystems contribute to health and disease. In the current study, we use a metagenomics approach to reveal microbial genomic and genetic diversity and to identify some of the distinctive functional attributes encoded in our distal gut microbiome.

Sequencing the microbiome. Although whole-genome shotgun sequencing and assembly have historically been applied to the study

of single organisms, recent reports from Venter *et al.* (9) and Baker *et al.* (10) have demonstrated the utility of this approach for studying mixed microbial communities. Variations in the relative abundance of each member of the microbial community and their respective genome sizes determine the final depth of sequence coverage for any organism at a particular level of sequencing. This means that the genome sequences of abundant species will be well represented in a set of random shotgun reads, whereas lower abundance species may be represented by a small number of sequences. In fact, the size and depth of coverage (computed as the ratio between the total length of the reads placed into contigs and the total size of the contigs) of genome assemblies generated from a metagenomics project can provide information on relative species abundance.

A total of 65,059 and 74,462 high-quality sequence reads were generated from random DNA libraries created with fecal specimens of two healthy humans (subjects 7 and 8). These two subjects, ages 28 and 37, female and male, respectively, had not used antibiotics or any other medications during the year before specimen collection (11). The combined sequenced distal gut "microbiome" of subjects 7 and 8 consisted of 17,668 contigs that assembled into 14,572 scaffolds, totaling 33,753,108 bp. The scaffolds ranged in size from 1000 to 57,894 bp and the contigs from 92 to 44,747 bp. The average depth of sequence coverage in contigs was 2.13-fold. Forty percent of the reads (56,292 total) could not be assembled into contigs, most likely because of a combination of low depth of coverage and low abundance of some organisms within the specimens. Together, these singletons accounted for an additional 45,078,063 bp of DNA.

A total of 50,164 open reading frames (ORFs) were predicted from the data set (25,077 for subject 7 and 25,087 for subject 8). These ORFs correspond to 19,866 unique database matches (13,293 for subject 7; 12,273 for subject 8; 5700 that were present in both). ORF-based alignments against public databases identified 259 contigs in subject 7 and 330 in subject 8 that could be assigned to members of Archaea, plus 5992 contigs from subject 7 and 7138 from subject 8 assignable to members of Bacteria (table S1). The remaining contigs either did not match any known ORFs or were ambiguously assigned.

Insight into the diversity within our samples was obtained by comparison of a subset of the shotgun reads to the completed sequence of *Bifidobacterium longum*, a member of the lactic acid bacteria present in the distal gut of healthy humans (12). A total of 1965 reads from the combined data set from subjects 7 and 8 could be aligned to the genome sequence of *B. longum*. These reads represented a total of 1,617,706 bp of DNA sequence, which corre-

¹The Institute for Genomic Research, 9712 Medical Center Drive, Rockville, MD 20850, USA. ²Department of Medicine, Stanford University School of Medicine, Stanford, CA 94305, USA. ³Department of Microbiology and Immunology, 299 Campus Drive, Stanford University, Stanford, CA 94305, USA. ⁴Veterans Affairs Palo Alto Health Care System, Palo Alto, CA 94304, USA. ⁵Center for Genome Sciences, Washington University School of Medicine, St. Louis, MO 63108, USA. ⁶Departments of Pharmacology and Physiology and Microbiology and Tropical Diseases, George Washington University School of Medicine, Washington, DC 20037, USA.

*Present address: Department of Oral Biology, The State University of New York at Buffalo, Buffalo, NY 14214, USA.

†Present address: Center for Bioinformatics and Computational Biology, University of Maryland, College Park, MD 20742, USA.

‡To whom correspondence should be addressed. E-mail: srgill@buffalo.edu

sponds to ~0.7-fold coverage of the *B. longum* genome. There was a great deal of heterogeneity in nucleotide sequence in the 1965 reads that aligned with the *B. longum* genome sequence (80 to 100% identity) with 52% of the reads aligned at less than 95% identity (Fig. 1A). These data suggest that these reads are not derived from a single discrete strain of *B. longum* in subjects 7 and 8, but instead, reflect the presence of multiple strains, as well as other Bifidobacterium phylotypes in the distal gut microbiota.

Previous work (2) has shown that archaeal species, in particular *M. smithii*, are also major players in the human distal gut ecosystem. *M. smithii* was represented in our data set at ~3.5-fold coverage, as indicated by the 7955 shotgun reads that matched this draft assembly (Fig. 1B). The presence of *M. smithii* is also supported by the identification of eight partial-length 16S rDNA sequences with 99.65 to 100% identity to *M. smithii*. Unlike *B. longum*, the majority (89%) of alignments to *M. smithii* had 95% or better sequence identity to the draft assembly, indicating low divergence between *Methanobrevibacter* strains present in our samples. More than half of the archaeal contigs in our data set had significant similarity to *M. smithii*: 145 of 259 archaeal contigs in subject 7 and 174 of 330 archaeal contigs from subject 8 had matches ≥ 100 bases, and $\geq 80\%$ identity to a deep draft assembly of this genome (13), consistent with previous reports on the abundance of this species in the human gut.

Identifying phylotypes. We explored bacterial diversity in both stool samples with analysis of 16S rDNA sequences from the random shotgun assemblies and from libraries of cloned, PCR-amplified 16S rDNA. Phylogenetic assessments of the local microbial community census provide a benchmark for interpreting the functional predictions from metagenomic data. Of the 237 partial bacterial-length 16S rDNA sequences identified in the shotgun assemblies, we selected 132 bacterial sequences for further analysis (2, 11). Using a 97% minimum pairwise similarity definition, 72 bacterial phylotypes were identified. Only one archaeal phylotype was identified (i.e., *M. smithii*). Sixteen bacterial phylotypes (22.2%) were novel, and 60 (83.3%) represented uncultivated species. The bacterial phylotypes were assigned to only two divisions, the *Firmicutes* (62 phylotypes, 105 sequences) and the *Actinobacteria* (10 phylotypes, 27 sequences). Sixty of the *Firmicute* phylotypes belonged to the class *Clostridia*, including *Clostridia* cluster XIV and *Faecalibacteria*. Analysis of 2062 near-full-length PCR-amplified 16S rDNA sequences (1024 from subject 7 and 1038 from subject 8) revealed a similar phylogenetic distribution among higher-order taxa, but a more diverse population at the species level. Using a $\geq 97\%$ similarity phylotype threshold, 151 phylotypes were identified (23% novel; 150 *Firmicutes*; 1

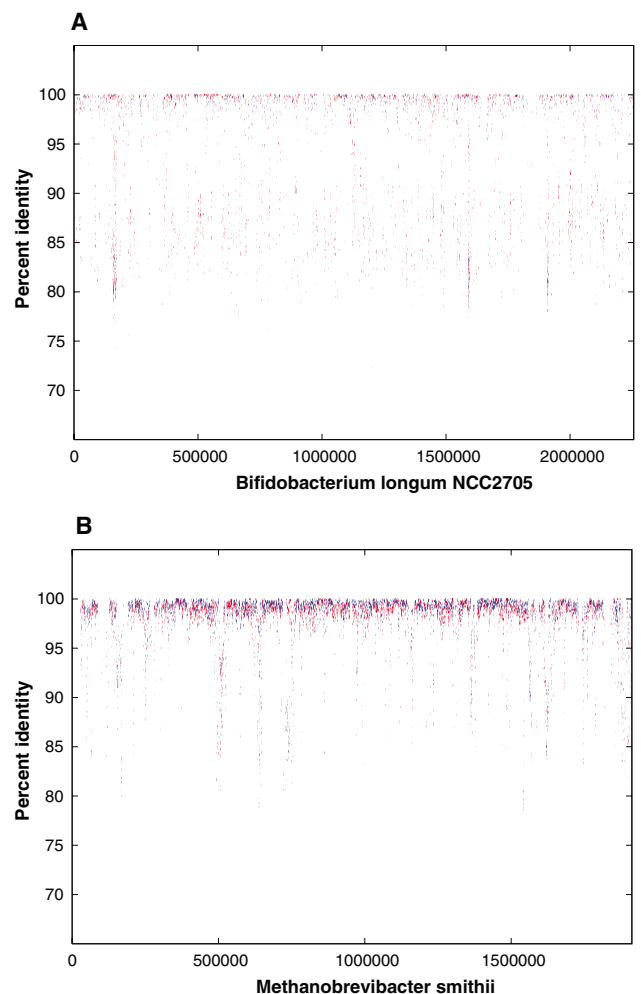
Actinobacteria) (fig. S1A). Similar analyses based on a $\geq 99\%$ similarity threshold are provided (11).

Although there were no *Bacteroidetes* 16S rDNA sequences identified in the random assemblies and clone libraries, amplification with species-specific 16S rDNA primers yielded sequences from *Bacteroides fragilis* and *Bacteroides uniformis*. This relative paucity of *Bacteroidetes* sequences is in conflict with data from other studies (2, 3). This discrepancy may have been caused by the known biases associated with the fecal lysis and DNA extraction methods used in the current study with respect to *Bacteroides* spp. (14); although less likely, it is also possible that members of the *Bacteroidetes* division are less abundant in the feces of subjects 7 and 8. In addition, with respect to the PCR-amplified 16S rDNA sequence data, there may be biases associated with the primers or PCR reaction conditions. Similar arguments may apply to other underrepresented taxa as well, such as the *Actinobacteria* and *Proteobacteria* phyla. Estimates of diversity indicated that at least 300 unique bacterial phylotypes would be

detected with continued sequencing from these stool samples (fig. S1, B to D).

Comparative functional analysis of the distal gut microbiome. To delineate how the human distal gut microbiome endows us with physiological properties that we have not had to evolve on our own, we explored the metabolic potential of the microbiota in subjects 7 and 8 using KEGG (Kyoto Encyclopedia of Genes and Genomes, version 37) pathways and COGs (Clusters of Orthologous Groups) (15, 16). Both annotation schemes contain categories of metabolic functions organized in multiple hierarchical levels: KEGG analysis maps enzymes onto known metabolic pathways; COG analysis uses evolutionary relations (orthologs) to group functionally related genes. Odds ratios were used to rank the relative enrichment or underrepresentation of COG and KEGG categories. An odds ratio of one indicates that the community DNA has the same proportion of hits to a given category as the comparison data set; an odds ratio greater than one indicates enrichment (more hits to a given category than expected), whereas an odds ratio less than one indicates underrepresent-

Fig. 1. Comparison of random metagenome reads with completed genome of *Bifidobacterium longum* and *Methanobrevibacter smithii*. (A) Percent identity plot (PIP) of alignments of shotgun reads along the genome of *B. longum* strain NCC2705. The x axis represents the coordinate along the genome, and the y axis represents the percent identity of the match. (B) Percent identity plot (PIP) of the alignment of shotgun reads along the draft genome of *M. smithii*. The x axis represents the coordinate along a pseudomolecule formed by concatenating all contigs in the *M. smithii* draft assembly. The y axis represents the percent identity of the match. The variation in the percent identity of the matches between the shotgun reads from subjects 7 and 8 as compared with the genome sequences of *B. longum* NCC2705 suggests considerable diversity among Bifidobacterium-like organisms within our samples. Alignments of the reads to the draft genome of *M. smithii* exhibit a much narrower range of percent identity (89% of alignments were at 95% or better identity as compared with 48% for *B. longum*), consistent with lower levels of diversity among archaeal members of the gastrointestinal tract.



tation (fewer hits to a given category than expected). Odds ratios for the KEGG pathway involved in biosynthesis of peptidoglycan (table S3), a major component of the bacterial cell wall, are consistent with expectations: The human gut microbiome is highly enriched relative to the human genome (77.88), similar to all sequenced bacteria (1.83), and moderately enriched relative to all sequenced Archaea (7.06).

Because we have not obtained saturation (see below), we cannot be confident that a given COG or KEGG pathway component is not present in the human distal gut microbiome. Therefore, we have focused our analysis on identified functional categories that are enriched relative to previously sequenced genomes.

BLAST comparisons of all sequences yielded 62,036 hits to the COG database, corresponding to 2407 unique COGs. ACE and Chao1 estimates of community richness were 2558 and 2553 COGs, respectively. This observed degree of community COG diversity is greater than that described for an acid mine drainage (1824 COGs), but less than that described for whale fall (3332), soil (3394), and Sargasso Sea samples (3714) (17). The number of KEGG pathways and COG terms enriched in the human distal gut microbiomes of subjects 7 and 8 is listed in table S2. KEGG maps and COG assignments can be found at (11, 18, 19).

The metabolome of the human distal gut microbiota. Both human subjects showed similar patterns of enrichment for each COG (Fig. 2) and KEGG (Fig. 3) category involved in metabolism. However, compared with subject 7, subject 8 was enriched for energy production and conversion; carbohydrate transport and metabolism; amino acid transport and metabolism; coenzyme transport and metabolism; and secondary metabolites biosynthesis, transport, and catabolism (Fig. 2). At this time, it is not clear whether these differences reflect limited coverage of their microbiomes or other factors such as host diet, genotype, and life-style. The analysis presented below combines the genes identified in the fecal microbiotas of both subjects to create an aggregate “human distal gut microbiome.”

The plant polysaccharides that we commonly consume are rich in xylan-, pectin-, and arabinose-containing carbohydrate structures. The human genome lacks most of the enzymes required for degrading these glycans (20). However, the distal gut microbiome provides us with this capacity (1) (Fig. 3 and tables S3 and S4). The human gut microbiome is enriched for genes involved in starch and sucrose metabolism (fig. S2) plus the metabolism of glucose, galactose, fructose, arabinose, mannose, and xylose (table S4). At least 81 different glycoside hydrolase families are represented in the microbiome, many of which are not present in the human “glycobiome” (table S5).

Host mucus provides a consistent reservoir of glycans for the microbiota and thus, in principle, can serve to mitigate the effects of marked changes in the availability of dietary polysaccharides (1). Gnotobiotic mouse models of the human

gut microbiota have indicated that α -linked terminal fucose in host glycans is an attractive and accessible source of energy for members of the microbiota such as the Bacteroidetes (1, 6). Several COGs responsible for fucose utilization are

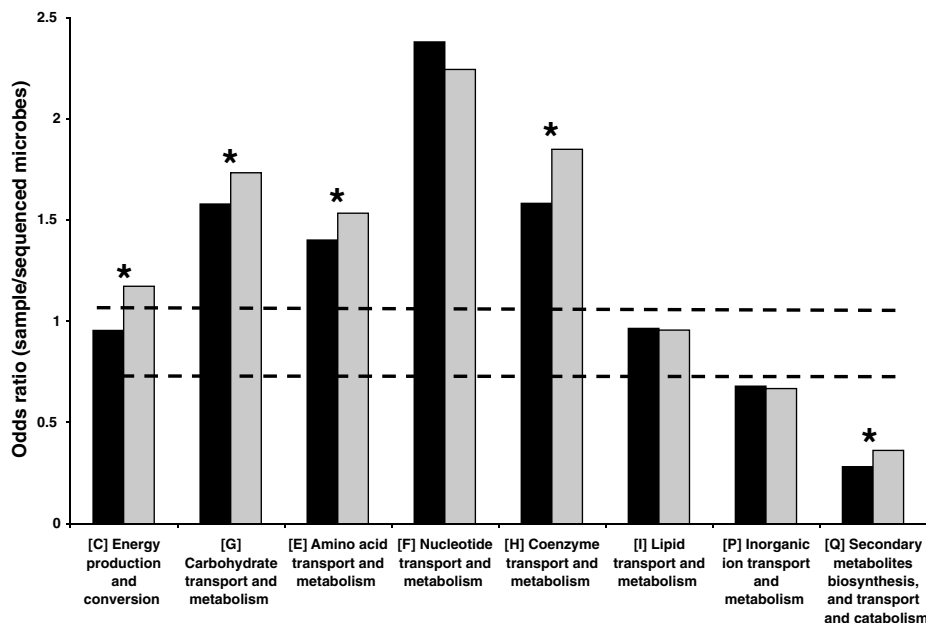


Fig. 2. COG analysis reveals metabolic functions that are enriched or underrepresented in the human distal gut microbiome (relative to all sequenced microbes). Color code: black, subject 7; gray, subject 8. Bars above both dashed lines indicate enrichment, and bars below both lines indicate underrepresentation ($P < 0.05$). Asterisks indicate categories that are significantly different between the two subjects ($P < 0.05$). Secondary metabolites biosynthesis includes antibiotics, pigments, and nonribosomal peptides. Inorganic ion transport and metabolism includes phosphate, sulfate, and various cation transporters.

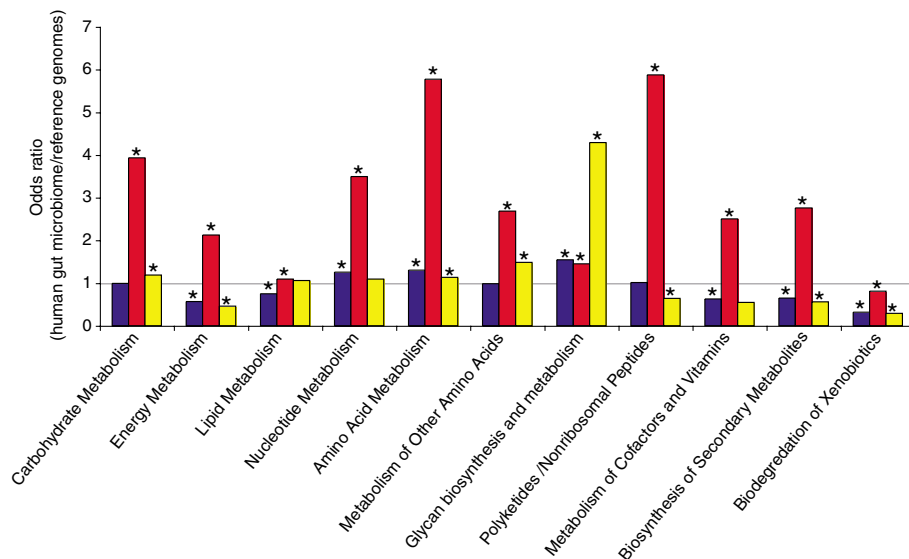


Fig. 3. KEGG pathway reconstructions reveal metabolic functions that are enriched or underrepresented in the human distal gut microbiome as follows: both samples compared with all sequenced bacterial genomes in KEGG (blue), the human genome (red), and all sequenced archaeal genomes in KEGG (yellow). Asterisks indicate enrichment (odds ratio > 1 , $P < 0.05$) or underrepresentation (odds ratio < 1 , $P < 0.05$). The KEGG category, “metabolism of other amino acids,” includes amino acids that are not incorporated into proteins, such as β -alanine, taurine, and glutathione. Odds ratios are a measure of relative gene content based on the number of independent hits to enzymes present in a given KEGG category.

enriched in the human gut microbiome relative to all microbial genomes (table S4).

Fermentation of dietary fiber or host-derived glycans requires cooperation of groups of microorganisms linked in a trophic chain. Primary fermenters process glycans to short-chain fatty acids (SCFAs), mainly acetate, propionate, and butyrate, plus gases (i.e., H_2 and CO_2). The bulk of SCFAs are absorbed by the host. Together, they account for ~10% of calories extracted from a Western diet each day (21). COG analyses demonstrated enrichment of key genes involved in generating acetate, butyrate, lactate, and succinate in the gut microbiome compared with all microbial genomes in the COG database (table S6). The most enriched COG was related to butyrate kinase (odds ratio of 9.30), an enzyme that facilitates formation of butyryl-coenzyme A by phosphorylating butyrate. This enrichment underscores the important commitment of the distal gut microbiota to generating this biologically significant SCFA, which serves as the principal energy source for colonocytes and may fortify the intestinal mucosal barrier by stimulating their growth (22).

Accumulation of H_2 , an end product of bacterial fermentation, reduces the efficiency of processing of dietary polysaccharides (23). Production of methane by mesophilic methanogenic archaeons is a major pathway for removing H_2 from the human distal gut (23), although sulfate reduction and homoacetogenesis serve

as alternate pathways. Enhancement of bacterial growth rates, fermentation of polysaccharides, and SCFA production have been observed when bacteria (e.g., *Fibrobacter succinogenes* and *Ruminococcus flavefaciens*) are cocultured with a *Methanobrevibacter* species (24). The distal gut microbiome is enriched for many COGs representing key genes in the methanogenic pathway (Fig. 4, C and D), consistent with the importance of H_2 removal from the distal gut ecosystem via methanogenesis.

The distal gut microbiome is enriched for a variety of COGs involved in synthesis of essential amino acids and vitamins (tables S7 and S8). COGs representing enzymes in the MEP (2-methyl-D-erythritol 4-phosphate) pathway, used for biosynthesis of deoxyxylulose 5-phosphate (DXP) and isopentenyl pyrophosphate (IPP), are notably enriched ($P < 0.0001$; relative to all sequenced microbes) (Fig. 4, A and B). DXP is a precursor in the biosynthesis of vitamins essential for human health, including B_1 (thiamine) and B_6 (pyridoxal form) (25). IPP is found in all known prokaryotic and eukaryotic cells and can give rise to at least 25,000 known derivatives, including archaeal membrane lipids (26), carotenoids (27), and cholesterol (28). Together, these results indicate that the MEP pathway is much better represented in the distal human gut microbiome than was previously known. The MEP pathway has been proposed as a target for developing new antibiotics,

because some pathogenic bacteria use the MEP pathway instead of the mevalonate pathway for IPP biosynthesis (29). However, our metagenomic study indicates that this approach may be detrimental to the microbiota and, in turn, the host.

Detoxification of xenobiotics could impact the host in a variety of ways, ranging from susceptibility to cancer to the efficiency of drug metabolism. Dietary plant-derived phenolics, such as flavonoids and cinnamates, have pronounced effects on mammalian cells (30–32). Hydrolysis of phenolic glycosidic or ester linkages occurs in the distal gut by microbial β -glucosidases, β -rhamnosidases, and esterases (33). The human distal gut microbiome is enriched for β -glucosidase (COG1472, COG2723 in table S4; $P < 0.0005$; glycosidase families GH3 and GH9 in table S5). Glucuronide conjugates of xenobiotics and bile salts induce microbial β -glucuronidase activity (34). The microbiome is enriched in this enzyme activity (i.e., COG3250; table S4). KEGG analysis also indicates enrichment for pathways involved in degradation of tetrachloroethene, dichloroethane, caprolactam, and benzoate (table S3).

Conclusion. This metagenomics analysis begins to define the gene content and encoded functional attributes of the gut microbiome in healthy humans. Future studies are needed to provide deeper coverage of the microbiome and to assess the effects of age, diet, and pathologic states (e.g., inflammatory bowel diseases, obe-

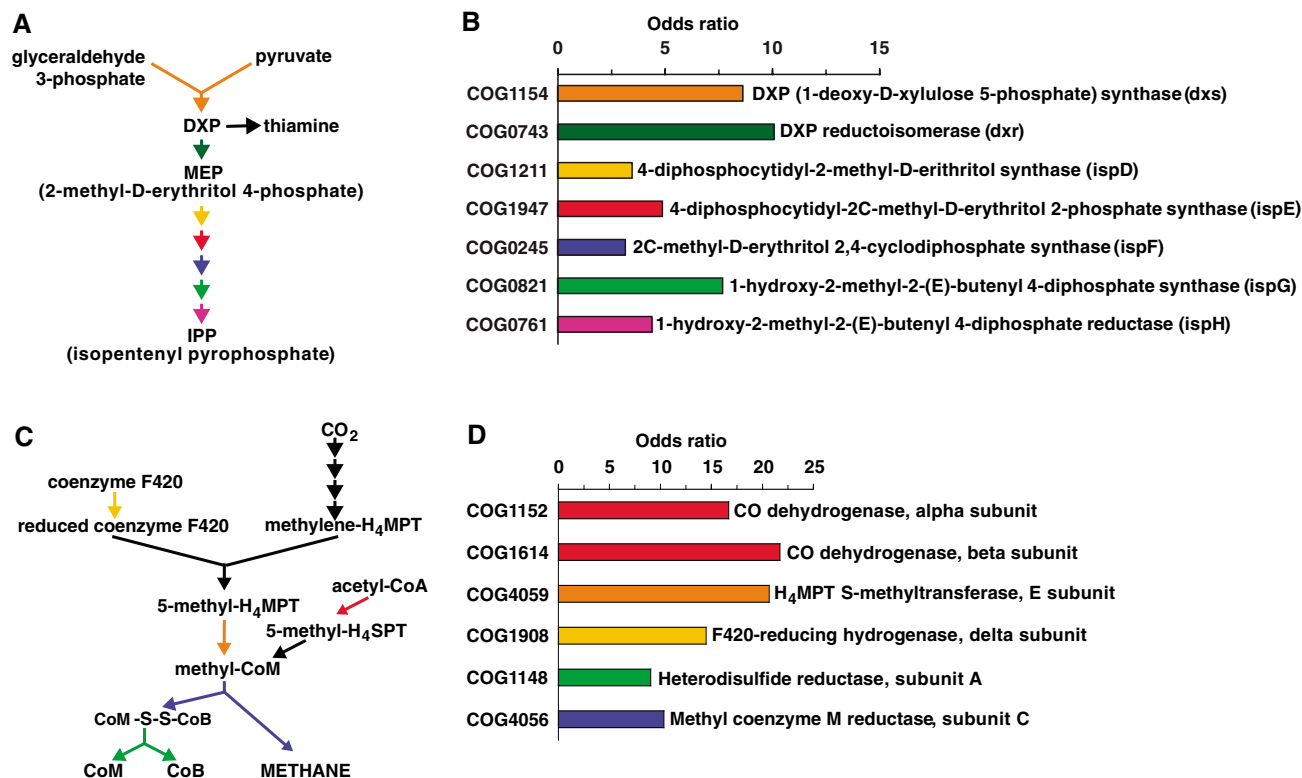


Fig. 4. Isoprenoid biosynthesis via the MEP pathway and methanogenesis are highly enriched in the distal gut microbiome. (A) MEP pathway for isoprenoid biosynthesis. (B) Odds ratio for each COG in the MEP pathway. All enzymes

necessary to convert DXP to IPP and thiamine are enriched ($P < 0.0001$ relative to all sequenced microbes). (C) Location and role of key enzymes in methanogenesis. (D) Odds ratio for each COG highlighted in (C).

sity, and cancer) on the distal gut microbiome of humans living in different environments. Periodic sampling of the distal gut microbiome (and of our other microbial communities) may provide insights into the effects of environmental change on our “microevolution.” The results should provide a broader view of human biology, including new biomarkers for defining our health; new ways for optimizing our personal nutrition; new ways for predicting the bioavailability of orally administered drugs; and new ways to forecast our individual and societal predispositions to disorders such as infections with pathogens, obesity, and misdirected or maladapted host immune responses of the gut.

References and Notes

1. F. Backhed, R. E. Ley, J. L. Sonnenburg, D. A. Peterson, J. I. Gordon, *Science* **307**, 1915 (2005).
2. P. B. Eckburg *et al.*, *Science* **308**, 1635 (2005).
3. R. E. Ley *et al.*, *Proc. Natl. Acad. Sci. U.S.A.* **102**, 11070 (2005).
4. S. K. Mazmanian, C. H. Liu, A. O. Tzianabos, D. L. Kasper, *Cell* **122**, 107 (2005).
5. S. Rakoff-Nahoum, J. Paglino, F. Eslami-Varzaneh, S. Edberg, R. Medzhitov, *Cell* **118**, 229 (2004).
6. F. Backhed *et al.*, *Proc. Natl. Acad. Sci. U.S.A.* **101**, 15718 (2004).
7. J. K. Nicholson, E. Holmes, I. D. Wilson, *Nat. Rev. Microbiol.* **3**, 431 (2005).
8. M. R. Rondon *et al.*, *Appl. Environ. Microbiol.* **66**, 2541 (2000).
9. J. C. Venter *et al.*, *Science* **304**, 66 (2004).
10. G. W. Tyson *et al.*, *Nature* **428**, 25 (2004).
11. Materials and methods are available as supporting material on Science Online.
12. M. A. Schell *et al.*, *Proc. Natl. Acad. Sci. U.S.A.* **99**, 14422 (2002).
13. (<http://gordonlab.wustl.edu/supplemental/Gill/Msmithii/draftgenome/>).
14. A. L. McOrist, M. Jackson, A. R. Bird, *J. Microbiol. Methods* **50**, 131 (2002).
15. M. Kanehisa, S. Goto, S. Kawashima, Y. Okuno, M. Hattori, *Nucleic Acids Res.* **32**, D277 (2004).
16. R. L. Tatusov *et al.*, *BMC Bioinformatics* **4**, 41 (2003).
17. S. G. Tringe *et al.*, *Science* **308**, 554 (2005).
18. (<http://gordonlab.wustl.edu/supplemental/Gill/>).
19. Database available as supporting material on Science Online.
20. URL (<http://afmb.cnrs-mrs.fr/CAZY/>).
21. N. I. McNeil, *Am. J. Clin. Nutr.* **39**, 338 (1984).
22. D. L. Topping, P. M. Clifton, *Physiol. Rev.* **81**, 1031 (2001).
23. A. J. Stams, *Antonie Van Leeuwenhoek* **66**, 271 (1994).
24. J. L. Rychlik, T. May, *Curr. Microbiol.* **40**, 176 (2000).
25. M. Rodriguez-Concepcion, A. Boronat, *Plant Physiol.* **130**, 1079 (2002).
26. J. Pereto, P. Lopez-Garcia, D. Moreira, *Trends Biochem. Sci.* **29**, 469 (2004).
27. D. Umeno, A. V. Tobias, F. H. Arnold, *Microbiol. Mol. Biol. Rev.* **69**, 51 (2005).
28. K. C. Wang, S. Ohnuma, *Biochim. Biophys. Acta* **1529**, 33 (2000).
29. M. Begley *et al.*, *FEBS Lett.* **561**, 99 (2004).
30. J. J. Reiners Jr., R. Clift, P. Mathieu, *Carcinogenesis* **20**, 1561 (1999).
31. C. A. Rice-Evans, N. J. Miller, G. Paganga, *Free Radic. Biol. Med.* **20**, 933 (1996).
32. G. Williamson, G. W. Plumb, Y. Uda, K. R. Price, M. J. Rhodes, *Carcinogenesis* **17**, 2385 (1996).
33. H. Schneider, A. Schwiertz, M. D. Collins, M. Blaut, *Arch. Microbiol.* **171**, 81 (1999).
34. A. K. Mallett, C. A. Bearne, I. R. Rowland, *Appl. Environ. Microbiol.* **46**, 591 (1983).
35. We thank W. Nelson and I. Hance (The Institute for Genomic Research), L. Dethlefsen and E. Bik (Stanford), and D. Leip (Washington University) for their valuable assistance. This work was supported by Defense Advanced Research Projects Agency (DARPA) and the Office of Naval Research grant no. ONR-N00014-02-1-1002 (S.R.G., K.E.N.), the W. M. Keck Foundation (J.I.G.), the Ellison Medical Foundation (D.A.R., J.I.G.), and NIH grants AI51259 (D.A.R.) and DK70977 (J.I.G.). B.S.S. is a recipient of a graduate research fellowship from the NSF (DGE-0202737). This whole-genome shotgun project has been deposited at the DNA Data Bank of Japan (DDBJ), European Molecular Biology Laboratory (EMBL), and GenBank under the project accession AAK00000000 (subject 7) and AAQL00000000 (subject 8). The version described in this paper is the first version, AAK01000000 and AAQL01000000. All near-full-length 16S rDNA sequences were deposited at DDBJ/EMBL/GenBank under the accessions DQ325545 to DQ327606.

Supporting Online Material

www.sciencemag.org/cgi/content/full/312/5778/1355/DC1
Materials and Methods
Figs. S1 and S2
Tables S1 to S8
References

22 December 2005; accepted 5 May 2006
10.1126/science.1124234

REPORTS

Conductance Quantization at a Half-Integer Plateau in a Symmetric GaAs Quantum Wire

R. Crook,* J. Prance, K. J. Thomas, S. J. Chorley, I. Farrer, D. A. Ritchie, M. Pepper, C. G. Smith

We present data from an induced gallium arsenide (GaAs) quantum wire that exhibits an additional conductance plateau at $0.5(2e^2/h)$, where e is the charge of an electron and h is Planck's constant, in zero magnetic field. The plateau was most pronounced when the potential landscape was tuned to be symmetric by using low-temperature scanning-probe techniques. Source-drain energy spectroscopy and temperature response support the hypothesis that the origin of the plateau is the spontaneous spin-polarization of the transport electrons: a ferromagnetic phase. Such devices may have applications in the field of spintronics to either generate or detect a spin-polarized current without the complications associated with external magnetic fields or magnetic materials.

The quantization of conductance in integer multiples of $2e^2/h$ (1, 2) is the signature of one-dimensional (1D) ballistic transport in a quantum wire (3). The factor 2 is a consequence of the spin degeneracy of the

transport electrons. If the degeneracy is lifted, the electrons become spin-polarized and an additional conductance plateau is observed at $0.5(2e^2/h)$. This occurs in a large external magnetic field, typically greater than 5 T, but may also occur in zero magnetic field if exchange interactions favor a parallel-spin ordered ground state, meaning a 1D ferromagnetic phase. Theoretical studies using a 1D Hubbard model (4–7), a density functional theorem (8–10), or a

phenomenological model (11, 12) predict that the ground state can indeed be ferromagnetic over a large range of electron density. However, a zero-field conductance plateau at $0.5(2e^2/h)$ is rarely reported in GaAs quantum wires, indicating that complete and spontaneous spin-polarization is not a robust property in this material system. We report the observation of a pronounced conductance plateau at $0.5(2e^2/h)$, which we refer to as the 0.5 plateau, in a new type of GaAs quantum wire at zero magnetic field.

A conductance structure close to $0.7(2e^2/h)$ is routinely observed in GaAs quantum wires. There are several theories for the origin of this 0.7 structure, and one of the most compelling is a thermally activated state of spontaneous spin-polarized electrons and a ground state with a conductance of $2e^2/h$ (13). This theory is founded on the observed smooth evolution of the 0.7 structure at zero magnetic field into the spin-polarized plateau at $0.5(2e^2/h)$ in high parallel magnetic fields (14). At zero magnetic field, the 0.7 structure has been observed to approach $0.5(2e^2/h)$ with both decreasing (15, 16) and increasing (17) electron density or increasing length (17). In the same work (15), a plateau at $0.5(2e^2/h)$ appearing for low electron densities was reported, and disorder-induced spontaneous

Cavendish Laboratory, 19 JJ Thomson Avenue, Cambridge CB3 0HE, UK.

*To whom correspondence should be addressed. E-mail: rc230@cam.ac.uk

spin polarization suggested as the origin. Unlike all previous observations, the 0.5 plateau reported in this paper was observed in addition to the 0.7 structure. Such coexistence has received theoretical discussion (11).

The sample consists of an 8- μm -wide mesa containing a 2D electron system (2DES) formed at a GaAs-AlGaAs heterojunction 97 nm beneath the surface (18). The device was defined from the mesa by using erasable electrostatic lithography (EEL), where a conductive tip draws patterns of negative charge on the GaAs sample surface to locally deplete the subsurface 2DES and define a quantum device (19). A line of negative charge was drawn across the entire width of the mesa to isolate source and drain regions of the 2DES. Kelvin probe microscopy (KPM) generates images of surface potential and is an effective technique to image charges

previously drawn by EEL (20). KPM was used in this study to identify a narrow section of the charge line. With the tip positioned above this narrow section, the tip was taken to a positive bias to induce a quantum wire (Fig. 1A).

By moving the tip sub-micrometer distances, it was possible to tune the potential landscape in the vicinity of the quantum wire. With the tip positioned within a specific region (discussed later), the 0.5 plateau was observed in addition to plateaus at integer multiples of $2e^2/h$ (Fig. 1B). The 0.5 plateau was stable over the 2-month duration of the experiment, and plots of conductance as a function of tip bias did not exhibit any resonant structures associated with disorder [Supporting Online Material (SOM) Text]. The weak plateau at $0.9(2e^2/h)$ is shown later to have evolved from the 0.7 structure.

To further investigate the 0.5 plateau, we applied a direct current (DC) source-drain bias during measurements. Left-going and right-going transport electrons then have different electrochemical potentials, which allows the quantitative observation of energy gaps in the quantum-wire band structure (21). Figure 1C plots numerically differentiated conductance as a function of source-drain bias and tip bias, where black regions identify plateaus. As the source-drain bias is increased from zero, the transitions between plateaus split, because the chemical potentials of the left-going and right-going electrons cross the same subband at a different tip bias. Crossings between adjacent split transitions occur when the source-drain bias is equal in energy to a subband spacing in the quantum wire. This occurs here at about 3 meV for the transitions to the first and second subbands.

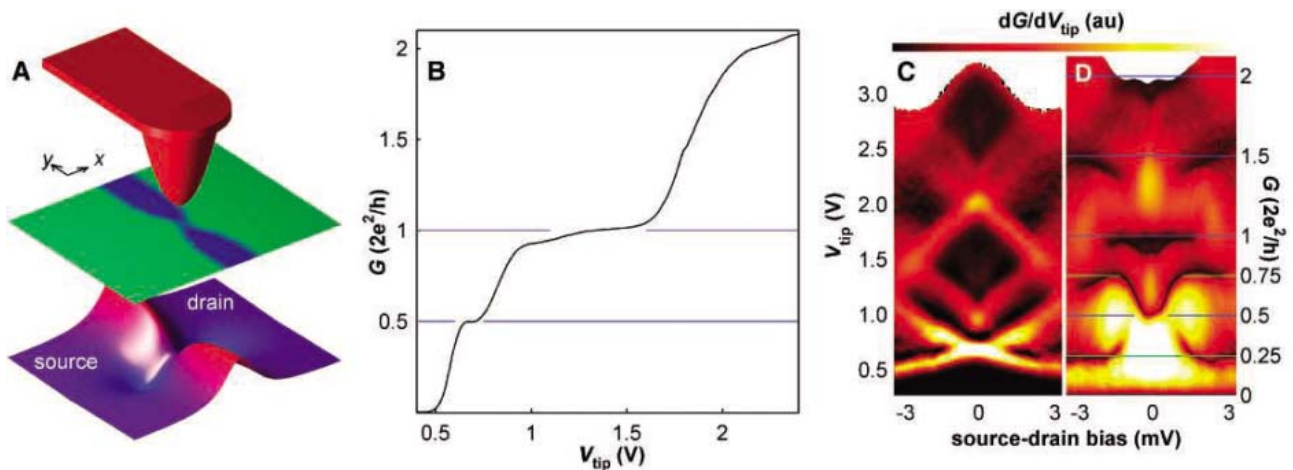


Fig. 1. (A) Experimental setup showing the biased scanning probe tip (top), schematic of the sample surface with charged regions in blue (middle), and the 2DES confining potential with the quantum wire formed at the central saddle (bottom). (B) Plot of device conductance (G) as a

function of tip bias (V_{tip}). (C and D) Plot of conductance numerically differentiated with respect to tip bias as a function of source-drain bias and either tip bias (C) or device conductance (D). All data was taken at 150 mK in zero magnetic field. au, arbitrary units.

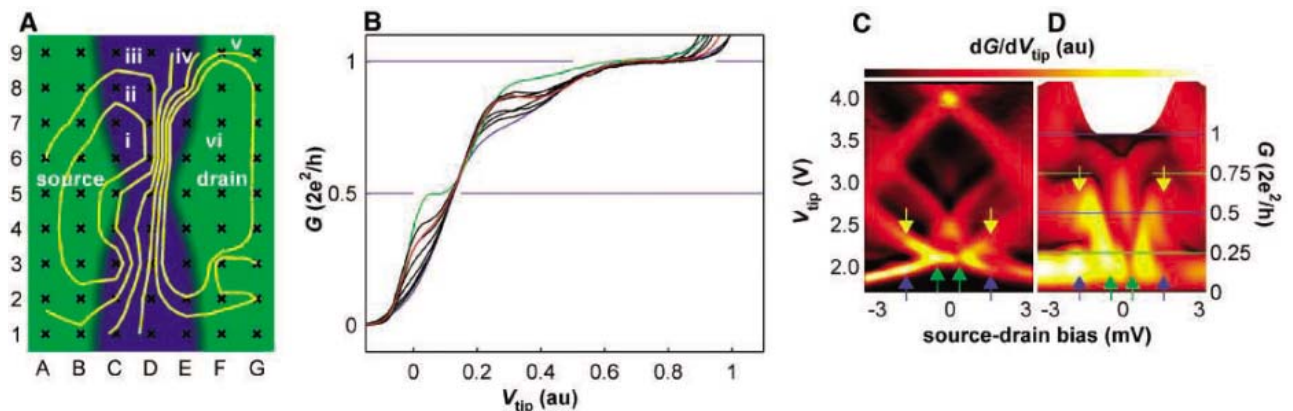


Fig. 2. (A) Coordinates of grid points relative to a schematic of the surface charge. Yellow contour lines separate regions i to vi, which locate tip positions where the conductance of the additional plateau $G = f(2e^2/h)$ is, for region i, $f = 0.45$ to 0.5 ; ii, $f = 0.4$ to 0.45 ; iii, $f = 0.35$ to 0.4 ; iv, $f = 0.30$ to 0.35 ; v, $f = 0.25$ to 0.3 ; and vi, no additional plateau observed. (B) Plots of device conductance as a function of tip bias with the tip positioned at points

C3 (green), B1 (red), F5 (blue), and intermediate points. The plots have been offset and linearly scaled in the x axis. (C and D) Plot of conductance differentiated with respect to tip bias as a function of source-drain bias and either tip bias (C) or device conductance (D) with the tip positioned at B1. Pairs of colored arrows highlight asymmetry. All data were taken at 150 mK in zero magnetic field.

The same numerically differentiated conductance data are plotted in Fig. 1D but as a function of device conductance instead of tip bias. This highlights the evolution of plateau conductance with source-drain bias. A plateau formed between split transitions should have a conductance that is the average of the conductance from left-going and right-going transport electrons. This is clearly seen at a source-drain bias greater than 1 mV, where plateaus exist at $0.25(2e^2/h) = 0.5[0 + 0.5(2e^2/h)]$ and $0.75(2e^2/h) = 0.5[0.5(2e^2/h) + 2e^2/h]$. The smooth evolution of the 0.5 plateau in zero source-drain bias to the plateau at $0.75(2e^2/h)$, rather than isolated plateaus appearing at $0.25(2e^2/h)$ and $0.75(2e^2/h)$, is not understood. However, this exact behavior is also observed in all quantum wires in large magnetic fields orientated parallel to the 2DES (22, 23). The similarity between the plots presented in Fig. 1 and high parallel field measurements supports the hypothesis that spontaneous spin polarization is the origin of the 0.5 plateau in zero magnetic field. From Fig. 1C, the energy between spin-split levels is about 1 meV.

Figure 2A shows a seven-by-nine grid covering a total area of $1 \mu\text{m}$ by $1.3 \mu\text{m}$. At each grid point, the device conductance was recorded as a function of tip bias, and, because the potential landscape depends upon tip position, this experiment can be considered equivalent to measuring 63 different devices. When the tip is positioned within region i, which is identified in Fig. 2A, the 0.5 plateau is pronounced and precisely quantized. The tip was positioned at point C3 in region i for Fig. 1. It is likely that region i is part of a ring where the capacitance between the tip and the quantum wire is constant, and therefore the tip electrostatic perturbation to the potential landscape near the quantum wire is constant. As the tip moves out of region i, the 0.5 plateau becomes less pronounced with a reduced conductance. To highlight this behavior, we present overlaid conductance plots measured at different tip positions (Fig. 2B). Below a conductance of $0.5(2e^2/h)$, the data bunches onto one of two

sides of the data envelope. Under the hypothesis of spin polarization, this is consistent with the existence of two electron spin phases, where the left side of the data envelope corresponds to the spin-polarized phase. At $0.5(2e^2/h)$, all the spin parallel states are occupied and there exists an energy gap to the spin antiparallel states, which accounts for the well-defined plateau at precisely $0.5(2e^2/h)$. The degraded plateau seen below $0.5(2e^2/h)$ may be associated with the same transition between two electron spin phases occurring before all the spin parallel states, in the spin-polarized phase, are fully occupied.

The source-drain energy spectroscopy plots for the tip positioned at point B1 are shown in Fig. 2, C and D. These data are asymmetric in source-drain bias when compared with the data in Fig. 1. The applied voltage is dropped at the entrance and exit of the quantum wire (21), so asymmetry observed in source-drain bias data must imply that asymmetry exists in the quantum wire geometry. Furthermore, plots taken from the seven-by-nine grid are not symmetric about the axis perpendicular to the quantum wire, which implies device asymmetry in the absence of the tip. The plots are roughly symmetric about the axis parallel to the quantum wire because the wire width is small compared with the potential perturbation caused by the tip. The reduced plateau conductance observed at point B1 with zero source-drain bias does not persist to higher source-drain bias, because plateaus near $0.25(2e^2/h)$ and $0.75(2e^2/h)$ are recovered.

The 0.5 plateau is best defined when the tip was positioned at point C3, which is also where the most symmetric source-drain bias data were obtained. We propose that the 0.5 plateau is most pronounced when the potential landscape is tuned to be symmetric. Disorder is inherent in GaAs quantum wires, which will usually cause a level of asymmetry that partly accounts for the infrequent observation of a 0.5 plateau. The strong plateaus at $0.25(2e^2/h)$ and $0.75(2e^2/h)$ seen in both symmetric and asymmetric source-drain bias data suggest that a large source-drain bias overrides the symmetry criterion. This may prove to be a useful bias configura-

tion for operating quantum wires used for spin applications.

With the assumption that the local confining potential is a saddle point of the form $U = (\omega_y^2 y^2 - \omega_x^2 x^2) m^*/2$, where $m^* = 0.067 m_e$ is the effective electron mass in GaAs, the ratio ω_y/ω_x can be calculated from the ratio of the plateau length to the transition length (24). Applied to the conductance plot in Fig. 1B, with the 1D subband spacing deduced from Fig. 1C, the approximate width of the quantum wire is 20 nm and the electron density in the wire is similar to that of the bulk. A further consequence of the unconventional fabrication is the likely existence of regions of electron density higher than the bulk at both ends of the quantum wire due to the positive tip bias, which will increase the screening of disorder in the vicinity of the quantum wire as previously suggested (15). The unusual potential geometry may be a requirement for the 0.5 plateau.

In addition to the 0.5 plateau, a conductance plateau or change in gradient was observed on all the plots between $0.7(2e^2/h)$ and $0.9(2e^2/h)$, which is understood to be the 0.7 structure. The 0.7 structure evolved smoothly as the tip moved over the device, and there is a strong correlation with the 0.5 plateau. When the 0.5 plateau is well defined, the 0.7 structure rises toward $2e^2/h$, and when the 0.5 plateau is not visible the 0.7 structure is at its minimum conductance. It is not clear why this is the case, but this correlation does provide additional weight to the theory that spin polarization plays a central role in the origin of the 0.7 structure. Also note that the 0.7 structure bunches onto either side of the data envelope (Fig. 2B) in a similar fashion to the 0.5 plateau, suggesting that the 0.7 structure is a transition between two different phases associated with electron spin (7, 13, 25). The population of the higher-energy spin-antiparallel states associated with spontaneous spin polarization is a possibility.

Temperature is a useful parameter to help establish the origin of subband structure. In the case of the 0.7 structure, for example, the conductance increases with decreasing temperature, which suggests that thermal activation to a higher energy state is occurring. Increasing temperature is also expected to destroy features whose origin involves an energy gap less than kT . Figure 3 presents plots of device conductance as a function of tip bias, with the tip positioned at points C3, B1, and F5 at various temperatures. When the tip is positioned at point C3, the 0.5 plateau survives to higher temperatures, and by 3 K the 0.5 plateau is better defined than the 1D spin degenerate plateau at $2e^2/h$ (fig. S1). Under the spin polarization hypothesis, this is consistent with a spin energy gap of 1 meV and a Curie temperature greater than 3 K. As the temperature increases, the 0.5 plateau conductance increases slightly, which is the same behavior exhibited by 1D subbands spin-split by large external magnetic fields (26).

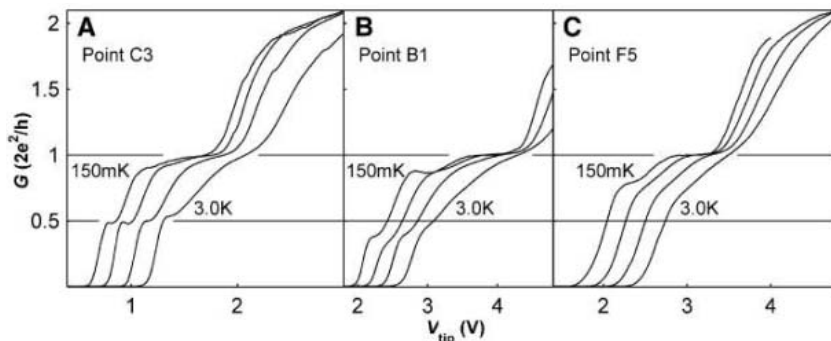


Fig. 3. Plots of device conductance as a function of tip bias at 150 mK, 800 mK, 1.5 K, and 3.0 K with the tip positioned at points C3 (A), B1 (B), and F5 (C) in zero magnetic field. The higher temperature plots have been offset in tip bias for clarity.

The 0.7 structure, which is most clear at point F5, decreases in conductance with increasing temperature. This is consistent with previous observations (13, 14). In perpendicular magnetic fields up to 1.2 T, neither the 0.5 plateau nor the 0.7 structure changed (fig. S1). A parallel magnetic field was not available during these experiments.

Spintronics uses the spin, rather than charge, property of electrons to transport information. Spintronic devices have the potential to operate at higher speeds with higher integration density and lower power consumption compared with conventional charge-based devices (27). Efficient sources and detectors of electron spin are essential spintronic components, but current schemes either are difficult to integrate or require a large external field, which places limitations on other integrated components. In the absence of a magnetic field and magnetic materials, we have presented data that are consistent with spontaneous spin polarization in a GaAs quantum wire. Quantum wires may

therefore be useful sources and detectors of spin and become essential building blocks in spintronic circuits.

References and Notes

- D. A. Wharam *et al.*, *J. Phys. C* **21**, L209 (1988).
- B. J. van Wees *et al.*, *Phys. Rev. Lett.* **60**, 848 (1988).
- T. J. Thornton, M. Pepper, H. Ahmed, D. Andrews, G. J. Davies, *Phys. Rev. Lett.* **56**, 1198 (1986).
- S. Daul, R. M. Noack, *Phys. Rev. B* **58**, 2635 (1998).
- L. Bartosch, M. Kollar, P. Kopietz, *Phys. Rev. B* **67**, 092403 (2003).
- K. Yang, *Phys. Rev. Lett.* **93**, 066401 (2004).
- A. D. Klironomos, J. S. Meyer, K. A. Matveev, *Europhys. Lett.* **74**, 679 (2006).
- A. Gold, L. Calmels, *Philos. Mag. Lett.* **74**, 33 (1996).
- C. K. Wang, K. F. Berggren, *Phys. Rev. B* **57**, 4552 (1998).
- A. Ashok, R. Akis, D. Vasiliska, D. K. Ferry, *Mol. Simulations* **31**, 797 (2005).
- H. Bruus, V. V. Cheianov, K. Flensberg, *Physica E* **10**, 97 (2001).
- D. J. Reilly *et al.*, *Phys. Rev. Lett.* **89**, 246801 (2002).
- A. Kristensen *et al.*, *Phys. Rev. B* **62**, 10950 (2000).
- K. J. Thomas *et al.*, *Phys. Rev. Lett.* **77**, 135 (1996).
- K. J. Thomas *et al.*, *Phys. Rev. B* **61**, R13365 (2000).
- S. Nuttinck *et al.*, *Jpn. J. Appl. Phys.* **39**, L655 (2000).
- D. J. Reilly *et al.*, *Phys. Rev. B* **63**, 121311 (2001).
- Materials and methods are available as supporting material on Science Online.
- R. Crook *et al.*, *Nature* **424**, 751 (2003).
- R. Crook *et al.*, *Physica E*, in press, 10.1016/j.physe.2006.03.061.
- N. K. Patel *et al.*, *Phys. Rev. B* **44**, 13549 (1991).
- K. J. Thomas *et al.*, *Philos. Mag. B* **77**, 1213 (1998).
- S. M. Cronenwett *et al.*, *Phys. Rev. Lett.* **88**, 226805 (2002).
- M. Büttiker, *Phys. Rev. B* **41**, 7906 (1990).
- P. Roche *et al.*, *Phys. Rev. Lett.* **93**, 116602 (2004).
- K. J. Thomas *et al.*, *Physica E* **12**, 708 (2002).
- S. A. Wolf *et al.*, *Science* **294**, 1488 (2001).
- This work was funded by the Engineering and Physical Sciences Research Council, UK. K.J.T. acknowledges support from the Royal Society. We thank A. C. Graham, F. Sfigakis, and V. Tripathi for useful discussions.

Supporting Online Material

www.sciencemag.org/cgi/content/full/312/5778/1359/DC1

Materials and Methods

SOM Text

Fig. S1

21 February 2006; accepted 20 April 2006

10.1126/science.1126445

Atomic-Scale Coupling of Photons to Single-Molecule Junctions

S. W. Wu,* N. Ogawa,* W. Ho†

Spatial resolution at the atomic scale has been achieved in the coupling of light to single molecules adsorbed on a surface. Electron transfer to a single molecule induced by green to near-infrared light in the junction of a scanning tunneling microscope (STM) exhibited spatially varying probability that is confined within the molecule. The mechanism involves photo-induced resonant tunneling in which a photoexcited electron in the STM tip is transferred to the molecule. The coupling of photons to the tunneling process provides a pathway to explore molecular dynamics with the combined capabilities of lasers and the STM.

The combination of optical excitation with ultrahigh spatial resolution would reveal new understanding of nanoscale structures and the elucidation of many light-sensitive, dynamic processes (1–5). To date, techniques available to achieve high spatial resolution with laser illumination are limited by diffraction to about half of the optical wavelength. The introduction of near-field scanning optical microscopes (NSOM), either aperture-based (2) or tip-enhanced (also called apertureless) (3), has extended the spatial resolution beyond the diffraction limit. The aperture-based NSOM has routinely reached a resolution of 50 to 100 nm and potentially down to 10 to 30 nm (2). Apertureless NSOM uses a strongly confined electric field by optically exciting surface plasmons localized at the apex of a sharp

metallic tip; in principle, the highest spatial resolution possible by this technique is on the order of a few nanometers (3).

In contrast, the scanning tunneling microscope (STM) readily provides spatial resolution down to the atomic scale. Thus, if the photons couple to the tunneling electrons, it should be possible to achieve high spectral and temporal sensitivity simultaneously with the spatial resolution of STM. However, efforts in this direction have met with little success because of experimental challenges such as thermal effects from light illumination (6).

Here, we demonstrate the coupling of photons to a single molecule in a double-barrier junction of a STM through a two-step process of photo-induced resonant tunneling (7, 8), in which an electron is photoexcited to a higher level in the tip and then tunnels resonantly to a molecular state. This process is detected statistically by monitoring the result of such electron transfer—generation of a new singly occupied molecular orbital (SOMO). The electron transfer probability vanishes when the tip is positioned outside the electronic

contour of the resonant molecular state and shows spatial variations within the contour.

The experiments were conducted with a home-built ultrahigh-vacuum (UHV) STM at the base temperature of 9.5 K (without laser illumination) (9) with silver (Ag) or tungsten (W) tips (10). To illuminate and align the laser to the junction, a pair of spherical lenses was mounted inside the UHV chamber. The lasers used were frequency-doubled Nd:YAG (532 nm), HeNe (633 nm), and Ti:Sapphire (800 nm). All were in the continuous wave (CW) mode and linearly polarized along the STM tip axis. Upon laser illumination of the junction, the temperature of STM rose linearly with the incident power (~0.65 K/mW). To avoid the temperature drift and fluctuation, a laser stabilizer (Model BEOC-LPC, Brockton Electro-Optics Corp., Brockton, MA) was used just before the laser entered the UHV chamber to reduce the power instability to ~0.1%.

The single-molecule double-barrier junction (schematically shown in Fig. 1A) was defined by positioning the STM tip over an individual molecule adsorbed on a thin (~0.5 nm) insulating alumina film grown on the NiAl(110) surface (11). The two tunnel barriers in the junction are the vacuum gap between the STM tip and the molecule, and the oxide film between the molecule and NiAl. We studied magnesium porphyrine (MgP) (Fig. 1C, inset), a simple metal-porphyrin molecule that is involved in photosynthesis (12), which was thermally sublimed onto the oxidized surface at ~10 K. Because of surface inhomogeneity, different MgP adsorption configurations are present (Fig. 1B).

Here, we focus on one specific type of MgP molecule, such as M₁ and M₂ in Fig. 1B. The direction of the two-lobe structure in the images taken at $V_b > 1.2$ V is always perpendicular to

Department of Physics and Astronomy and Department of Chemistry, University of California, Irvine, CA 92697–4575, USA.

*These authors contributed equally to this work.

†To whom correspondence should be addressed. E-mail: wilsonho@uci.edu

the [001] direction of the underlying NiAl(110), where V_b is the sample bias voltage with respect to the tip. In the absence of laser illumination, the differential tunneling conductance (dI/dV) spectra consistently exhibit stepwise changes and hysteresis. For the molecule shown in Fig. 1C, no states appeared until $V_b = 0.55$ V in the forward scan (ramping V_b up). At $V_b \approx 0.85$ V, the dI/dV signal (as well as the tunneling current) suddenly dropped, indicating that the molecule was switched electronically from one state to the other. In the backward scan, the onset of unoccupied states is shifted up by 0.15 V, and a new occupied molecular state emerged at a threshold of $V_b = -0.45$ V. As the bias was ramped down, the molecule switched back to its original state. This hysteresis behavior could be cycled repeatedly.

The hysteresis, especially the appearance of a new occupied state, indicates that the molecule could be charged at positive bias and discharged at negative bias. The STM images taken at the onset of all of the states further confirm that the molecule with the new occupied state is negatively charged by one extra electron, whereas the one without it is neutral (to be discussed later in the text). The ability to control the molecular charge state is similar to the charging of individual Au atoms adsorbed on an ultrathin NaCl film on a copper surface (13). The ionic relaxation in the alumina, associated with the charging, stabilizes the negative ion, because alumina is even more polar than NaCl (13). In addition, the specific molecular adsorption state is also responsible for this charge transfer phenomenon.

Without laser illumination, the charge state of the molecule cannot be changed when the bias is set within the zero-conductance gap (~ -0.4 V to ~ 0.55 V). However, upon optical excitation in the junction, we observed charging of the molecule that could be controlled by photon energy and flux, sample bias, tip-molecule distance, and position of the tip within the molecule.

To detect and quantify this light-induced charge transfer process, we have adopted an experimental scheme, as shown in Fig. 2A (sequence 1 to 4). In this scheme, the STM feedback was kept on all of the time. We assume that the molecule was initially in its neutral state and set the tunneling parameters at the “parking” condition (V_p and I_p), where the molecule could not be charged with laser illumination except for photon energies larger than ~ 2.1 eV (as discussed below). The STM tip was positioned over the molecule and tracked at the maximum of the topographic image. The bias was stepped to V_c and the tunneling current ramped to I_c . After holding there for a certain time t_{hold} , the tunneling parameters were returned to the parking condition. To probe whether the molecule is charged, the bias was ramped down to sufficiently large

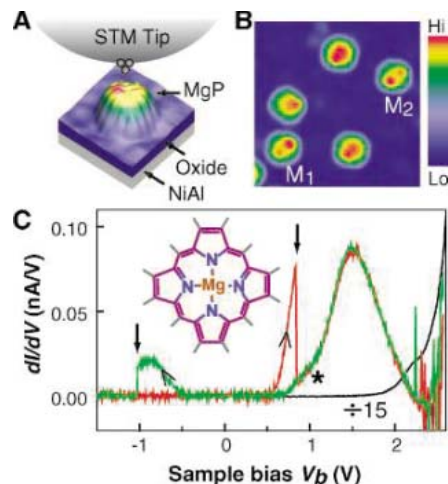


Fig. 1. (A) Schematic of a single-molecule double-barrier junction. (B) STM image showing individual magnesium porphine (MgP) molecules adsorbed on an oxidized NiAl(110) surface. The molecules marked M_1 and M_2 are the type of molecules studied here. The scan size is 10.9 nm by 10.9 nm, $V_b = 1.5$ V. This image and those in the following figures were taken at $|I| = 30$ pA. (C) dI/dV spectra measured over a molecule such as M_1 and M_2 in (B). The forward (red curve) and backward (green curve) scans are indicated by the two arrow heads. The two vertical arrows mark the positions of a sudden change in the dI/dV spectra. In contrast, the dI/dV spectrum (black curve), measured over the bare oxide surface adjacent to the molecule, shows no switching and hysteresis. The dI/dV signal was recorded with the lock-in technique. The tunnel gap was set at $V_b = 1.5$ V and $I = 30$ pA. The bias modulation was 10 mV (rms) at 400 Hz. The inset is the molecular structure of MgP. The asterisk (*) denotes a kink in the dI/dV spectrum because of two overlapping states (schematically shown in Fig. 5 as SUMO and LUMO- β).

negative value (V_d) with $I = I_p$. If the molecule is charged, the STM tip will noticeably retract away from the molecule because of the presence of the newly occupied molecular state. At certain negative bias, the molecule will be discharged. Thus, this probing process also serves as a resetting (discharging) process. In addition, the charging probability away from the tracking position of the molecule could be measured by moving the tip to the desired location just before sequence 2. At the end of sequence 2, the tip was returned to the tracking position as shown in sequence 3. This complete cycle was repeated (three cycles are shown in Fig. 2B) and was under computer control.

The dependence of the charging probability on V_c shows a clear bias threshold (Fig. 3A), and the threshold decreases as the photon energy increases. The linearity of threshold versus photon energy (Fig. 3A, inset) indicates that light couples to the single-molecule junction quantum mechanically. In sharp contrast,

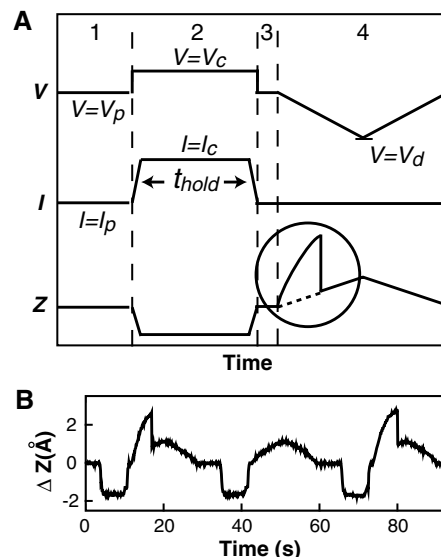


Fig. 2. (A) Experimental scheme (not to scale) used to detect the laser-induced charging probability in the single-molecule junctions. The STM feedback is kept on throughout the entire cycle. Time sequence 1 to 4 represents periods of (1) tracking and optional lateral offset, (2) charging, (3) lateral unoffset (optional), and (4) probing/discharging. The circled area illustrates the difference between charged (solid line) and uncharged (dashed line) molecules. We present results obtained with $V_p = -0.3$ V, $I_p = -30$ pA, and $t_{\text{hold}} = 5$ s. (B) Real-time trace of three successive cycles. The first and third cycles indicate that the molecule was charged by the photons during t_{hold} , whereas the molecule remained uncharged for the second cycle. $V_c = 0.3$ V, $I_c = 50$ pA, and lateral offset distance from the tracking point of the molecule is 8.8 Å.

without laser illumination, the charging probability was zero for $V_c < 0.55$ V, corresponding to the onset of unoccupied states for a neutral molecule. By adjusting the photon flux and the tunnel barrier width, the coupling of photons to the single-molecule junction could be controlled. At low photon flux, the coupling increased approximately linearly and saturated at higher fluxes (Fig. 3B). In addition, the coupling increased monotonically with closer tip-molecule distance, equivalent to the vacuum barrier width, as regulated by the tunneling current I_c (Fig. 3C).

The result in Fig. 3A shows that the sum of the photon energy and the bias threshold is ~ 2.1 V. However, the threshold for charging without laser illumination could be as low as 0.6 V (Fig. 3A). This notable difference suggests that the photons couple to a higher molecular state, the LUMO+1, instead of the LUMO (lowest unoccupied molecular orbital). Thus, the energy difference between LUMO+1 (onset of 2.1 eV) and LUMO (onset of 0.55 eV) for the neutral molecule would be ~ 1.55 eV. This difference is consistent with the 800-nm light observed in the tunneling electron-induced

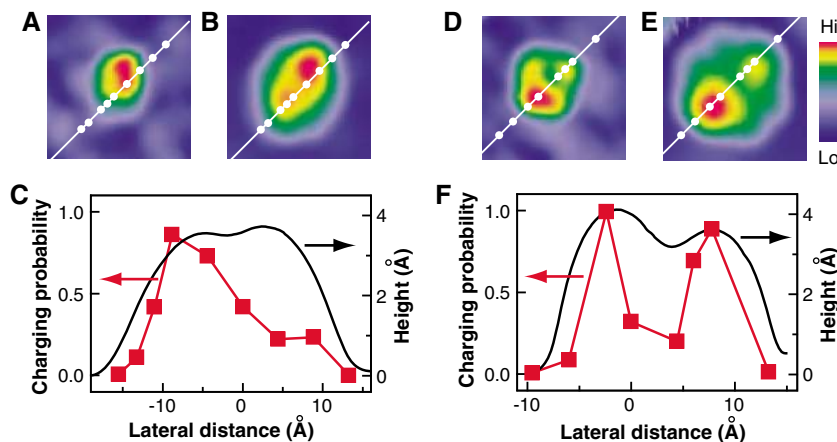
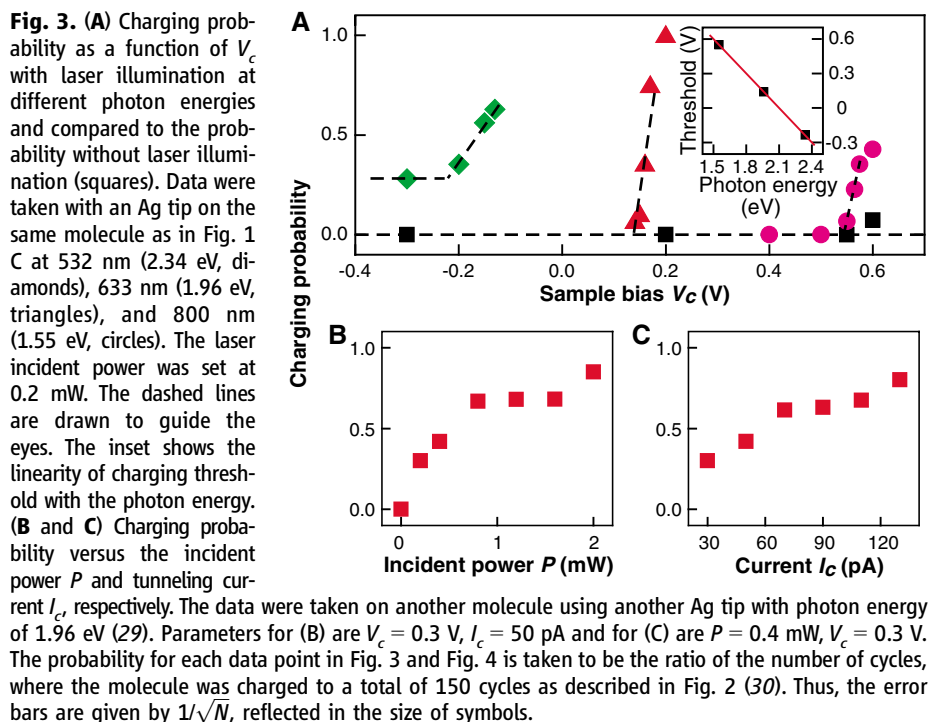


Fig. 4. (A to C) The spatial dependence of the charging probability taken with an Ag tip, $P = 0.4$ mW, $\lambda = 633$ nm, $V_c = 0.3$ V, and $I_c = 50$ pA. (A and B) Images taken at 0.3 V (uncharged, 1.93 Å high), 2.0 V (charged, 4.17 Å high), respectively, without laser illumination. The scan size is 34 Å by 34 Å. (C) The curve connecting the squares represents the charging probability along different parts of the molecule as indicated by the white dots in images (A) and (B). The topographic line cut is taken along the dots from (B). (D to F) show another set of data taken with a W tip, $P = 1.2$ mW, $\lambda = 633$ nm, $V_c = 0.25$ V, and $I_c = 50$ pA. Images (D) and (E) were taken at 0.25 V (uncharged, 2.30 Å high) and 2.0 V (charged, 4.46 Å high), respectively, without laser illumination. The scan size is 23 Å by 23 Å. Given the difference in the laser power and that the charging threshold for the molecule in (A) to (C) is ~ 0.1 V higher than that for the molecule in (D) to (F) (29), the Ag tip is determined to be more efficient than the W tip by a factor of ~ 10 .

fluorescence spectra (10, 14). Density functional theory (DFT) calculation on this molecule shows that the LUMO is doubly degenerate and orthogonal, while the LUMO+1 is nondegenerate (15, 16, 17). The energy separation between them is ~ 1.6 eV (15, 16).

Because the onset of the LUMO+1 for the neutral molecule is ~ 2.1 eV, optical excitation with lower photon energy must be assisted by

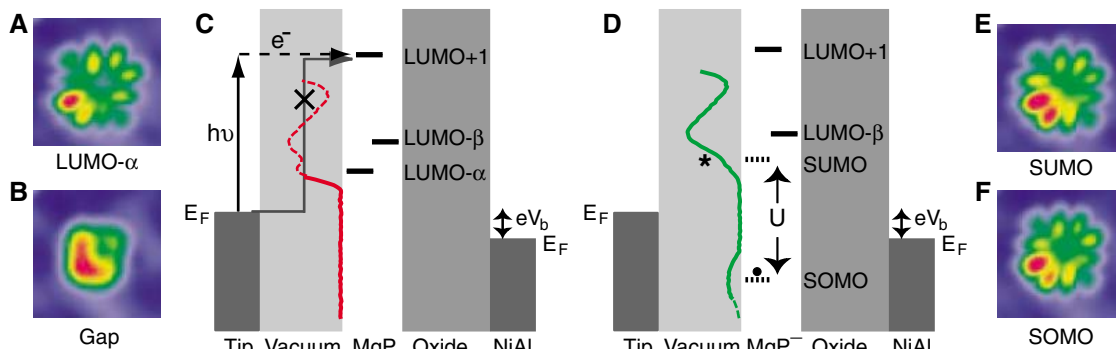
tuning the sample bias to vary the Fermi level of tip relative to LUMO+1 (18). The threshold bias for photo-induced charging is positive for photon energies 1.96 eV and 1.55 eV (Fig. 3A). Thus, the charging process occurred in the tip-molecule junction through the vacuum barrier. In the case of 2.34 eV photons, the photo-induced charging process could also occur in the molecule-substrate junction. Thus, the

charging probability below its threshold is not zero (Fig. 3A). The electron transfer from the substrate to the molecule through the oxide barrier was observed by moving the tip outside the neutral molecule.

The photon coupling strongly depends on the spatial distribution of the molecular state as indicated by the spatial dependence of the charging probability for photon energy of 1.96 eV (Fig. 4). Images taken at V_c for the neutral molecules (before charging), corresponding to the geometry of MgP, are shown in Fig. 4, A and D, whereas Fig. 4, B and E, represent the contour of the molecular electronic states (19). A comparison of the variation of the charging probability and a line cut through the topographic image (Fig. 4, C and F) indicates that the spatial resolution of the photon coupling is as fine as the resolution of the STM images and approximately follows variations in the molecular electronic states. The spatial contrast in charging probability arises from variations in the LUMO+1, whereas the topographic line cut of the images is composed of contributions from all the states integrated below the imaging bias. This spatially dependent data further supports the mechanism of photo-induced electron transfer involving the tip-molecule junction. Combined with the bias-dependent data (Fig. 3A), the possibility of charging arising through local laser thermal heating is ruled out.

The molecular states, in particular LUMO+1, for the neutral molecule could be derived as follows, although they were not directly observed in the dI/dV spectrum because of charging. The STM image (Fig. 5A) taken at the onset of the unoccupied state matches one of the calculated LUMOs, named LUMO- α (15, 16, 17, 19). The image taken at negative bias such as Fig. 5B, is relatively featureless and corresponds to the geometry of MgP (19). Once the molecule is charged, the STM images (Fig. 5, E and F) taken at the onsets of unoccupied and occupied states share the same pattern as the LUMO- α (Fig. 5A), indicating that only one electron is transferred into the LUMO- α of the neutral molecule. The newly occupied state is a SOMO, whereas the previously spin-degenerate state remains as a singly unoccupied molecular state (SUMO). They are separated by a coulomb energy U , as indicated in Fig. 5D. Because the peaks for SUMO and SOMO are not usually observed, a lower bound for U is given by the SOMO onset to the SUMO onset of ~ 1.15 eV (Fig. 1C). Because the molecule is adsorbed on the polar oxide surface, the degeneracy of the LUMOs is most likely split, which is supported by the kink in the dI/dV spectrum (marked by * in Fig. 1C and Fig. 5D). The onset difference between LUMO+1 and SUMO is ~ 1.6 eV (Fig. 1C), indicating that all of the unoccupied states of the charged molecule probably shift up rigidly by 0.15 V, with respect to those of the neutral

Fig. 5. (A and B) Images of a neutral molecule taken at sample bias of 0.57 V and -0.4 V, respectively. **(C)** Energy diagram showing the molecular states of a neutral molecule (MgP). The arrowed solid and dashed lines represent a two-step process of photo-induced resonant tunneling through the vacuum barrier between the STM tip and the molecule. In comparison, the crossed-out process represents a one-step mechanism of photon-assisted resonant tunneling. **(D)** Energy diagram showing the molecular states of a negatively charged molecule (MgP⁻). **(E and F)** Images of the



molecule. These results allow us to roughly project the molecular states of a neutral molecule (dotted line in Fig. 5C). We first fit the dI/dV spectrum before charging for the LUMO- α to a Gaussian. The dI/dV spectrum ($V_b > 0$ portion) for the charged molecule is shifted down 0.15 V and added to half of the fitted LUMO- α Gaussian curve, because a LUMO- α spin state was split off to become a SOMO.

The observed quantum coupling of photons to the single-molecule junction could be explained by photo-induced resonant tunneling, a two-step process involving excited states of the tip (shown in Fig. 5C) (7, 8). This mechanism is feasible because the lifetime of excited electrons in metals [for example, it is ~ 10 fs in Ag (20)] is longer than the traveling time for electron tunneling (sub-fs) (21). Photon-assisted resonant tunneling from the tip directly to the molecule, as sketched in Fig. 5C and described in (22), is not likely, although this one-step mechanism has been observed with photons at microwave (23) and terahertz frequencies (24). In photon-assisted resonant tunneling, photon-assisted discharging directly from the SOMO to the unoccupied state in the tip or the substrate would be expected, but this was not observed. In contrast, to observe the discharging arising from photo-induced resonant tunneling, the photon has to first excite the electron from the SOMO to a higher unoccupied molecular state that depends on the photon energy (25). Furthermore, with the photon energy in the 1 to 2 eV range, the effective tunneling barrier height for photo-induced resonant tunneling is much lower than that for photon-assisted resonant tunneling (8). Thus, the two-step process dominates. However, we have not completely understood the reasons for photo-induced electron transfer to the LUMO+1, instead of the LUMO. One possible reason is that resonant tunneling to the LUMO+1 encounters a lower barrier height in comparison with the LUMO. The excess energy associated with the decay from the LUMO+1 to populate SOMO could be dissipated in the radiative and non-radiative transitions and in the reorganization

energy of the alumina film in the vicinity of the negatively charged molecule (10, 13, 14).

The efficiency of photon coupling depends on the shape and elemental composition of the STM tip. For example, the Ag tip was more efficient than the W tip by a factor of about 10 (Fig. 4). The higher efficiency could be caused by the longer lifetime of excited electrons in the Ag tip than that in the W tip, which would lead to enhanced photo-induced resonant tunneling. In addition, the local electric field enhancement due to surface plasmons (3, 10) could also contribute to the photo-induced electron transfer.

The realization of the coupling of photons to the tunneling process could lead to experiments with chemical sensitivity at a submolecular level, such as the photo-induced current resulting from the intramolecular HOMO-LUMO transition (25) and laser-induced molecular fluorescence between LUMO+1 and LUMO. The use of photons is less destructive toward the molecule and involves different mechanisms compared with processes induced by tunneling electrons alone in the absence of light. Furthermore, the combination of lasers with the STM enables the exploration of molecular dynamics with simultaneous spatial, temporal, and energy resolutions.

References and Notes

- D. M. Adams *et al.*, *J. Phys. Chem. B* **107**, 6668 (2003).
- B. Hecht *et al.*, *J. Chem. Phys.* **112**, 7761 (2000).
- A. Hartschuh, M. R. Beversluis, A. Bouhelier, L. Novotny, *Philos. Trans. R. Soc. London Ser. A* **362**, 807 (2004).
- L. Bartels, F. Wang, D. Möller, E. Knoesel, T. F. Heinz, *Science* **305**, 648 (2004).
- A. Nitzan, M. A. Ratner, *Science* **300**, 1384 (2003).
- S. Grafström, *J. Appl. Phys.* **91**, 1717 (2002).
- S. P. Apell, D. R. Penn, *Phys. Rev. B* **45**, 6757 (1992).
- A. Thon *et al.*, *Appl. Phys. A* **78**, 189 (2004).
- The STM is a variation of the one described in (26).
- X. H. Qiu, G. V. Nazin, W. Ho, *Science* **299**, 542 (2003).
- S. W. Wu, G. V. Nazin, X. Chen, X. H. Qiu, W. Ho, *Phys. Rev. Lett.* **93**, 236802 (2004).
- K. M. Kadish, K. M. Smith, R. Guilard, Eds., *The Porphyrin Handbook* (Academic Press, New York, 2000).
- J. Repp, G. Meyer, F. E. Olsson, M. Persson, *Science* **305**, 493 (2004).
- The tunneling electron-induced fluorescence was observed from the same configuration (tip/vacuum/MgP/oxide/NiAl) but for a different type of molecular adsorption than the one discussed here. The radiative transition from LUMO+1 to LUMO occurs at about 800 nm.
- K. A. Nguyen, R. Pachter, *J. Chem. Phys.* **114**, 10757 (2001).
- We have carried out the DFT calculations on a free, planar MgP by using HyperChem 7.0. The results are identical to those for ZnP.
- D. Spangler, G. M. Maggiora, L. L. Shipman, R. E. Christoffersen, *J. Am. Chem. Soc.* **99**, 7478 (1977).
- In principle, the level of LUMO+1 is not tied to the Fermi levels as a result of the distribution of voltage drops in the double-barrier junction (11). However, because the ratio of the voltage drop is large (~ 7) and the bias applied across the junction is small, the level shift of the LUMO+1 with respect to the Fermi level of the NiAl substrate for different biases is negligible.
- J. Repp, G. Meyer, S. M. Stojković, A. Gourdon, C. Joachim, *Phys. Rev. Lett.* **94**, 026803 (2005).
- B. Lamprecht, A. Leitner, F. R. Aussenegg, *Appl. Phys. B* **64**, 269 (1997).
- R. Wiesendanger, *Scanning Probe Microscopy and Spectroscopy: Methods and Applications* (Cambridge Univ. Press, Cambridge, 1998).
- P. K. Tien, J. P. Gordon, *Phys. Rev.* **129**, 647 (1963).
- T. H. Oosterkamp, L. P. Kouwenhoven, A. E. A. Koolen, N. C. van der Vaart, C. J. P. M. Harmans, *Phys. Rev. Lett.* **78**, 1536 (1997).
- B. J. Keay *et al.*, *Phys. Rev. Lett.* **75**, 4102 (1995).
- M. Galperin, A. Nitzan, *Phys. Rev. Lett.* **95**, 206802 (2005).
- B. C. Stipe, M. A. Rezaei, W. Ho, *Rev. Sci. Instrum.* **70**, 137 (1999).
- J. K. Trautman, J. J. Macklin, L. E. Brus, E. Betzig, *Nature* **369**, 40 (1994).
- X. S. Xie, R. C. Dunn, *Science* **265**, 361 (1994).
- From molecule to molecule, the onset varies (within 0.15 V) for the lowest unoccupied state (LUMO- α) of the neutral molecule. The onset of all the other unoccupied states varies approximately with the LUMO- α .
- Each data point (150 cycles) took about 80 min to measure. The reason for taking 150 cycles is to reduce the data fluctuation due to the blinking effect similar to that observed in (27, 28).
- Supported by the Chemical Science, Geo- and Bioscience Division, Office of Science, U.S. Department of Energy, under grant DE-FG02-04ER1595. The California Institute for Telecommunication and Information Technology at University of California-Irvine provided a fellowship to N.O.

11 January 2006; accepted 21 March 2006

Published online 20 April 2006;

10.1126/science.1124881

Include this information when citing this paper.

Solar Rotation Effects on the Thermospheres of Mars and Earth

Jeffrey M. Forbes,^{1*} Sean Bruinsma,² Frank G. Lemoine³

The responses of Earth's and Mars' thermospheres to the quasi-periodic (27-day) variation of solar flux due to solar rotation were measured contemporaneously, revealing that this response is twice as large for Earth as for Mars. Per typical 20-unit change in 10.7-centimeter radio flux (used as a proxy for extreme ultraviolet flux) reaching each planet, we found temperature changes of 42.0 ± 8.0 kelvin and 19.2 ± 3.6 kelvin for Earth and Mars, respectively. Existing data for Venus indicate values of 3.6 ± 0.6 kelvin. Our observational result constrains comparative planetary thermosphere simulations and may help resolve existing uncertainties in thermal balance processes, particularly CO₂ cooling.

The Sun's atmosphere rotates with a period of about 25 days near the equator and 35 days near the poles. This differential rotation causes magnetic field lines to twist, resulting in the formation of active regions that release enhanced solar energy in various forms, including the extreme ultraviolet (EUV) radiation responsible for heating the hot outermost region of a planetary upper atmosphere, the thermosphere [circa (ca.) ≥ 100 km for Earth, Mars, and Venus]. The rotation of solar active regions produces periodicities in EUV flux emanating from the Sun and subsequently absorbed by planetary thermospheres. Although variations in Mars' ionosphere electron densities due to day-to-day changes in solar flux (1) and even solar flares (2) have recently been discovered, relatively little is known about the response of Mars' neutral thermosphere to short-term solar flux variations.

Planetary thermosphere temperatures are determined by the efficiency with which absorbed radiation is converted to heat, the rates of molecular and eddy heat conduction, and the rate of radiative cooling (3), particularly by CO₂ at 15 μm (4). Excitation of the CO₂ molecule that leads to the 15- μm emission occurs primarily through collisions with atomic oxygen (O). The CO₂ cooling rate therefore increases with the O/CO₂ mixing ratio, which is roughly 0.0001, 0.1, and 1.0 at 150-km altitude in the thermospheres of Earth (5), Mars (4), and Venus (4), respectively. Despite the low mixing ratio for Earth, a doubling of CO₂ is calculated (6) to result in a 50 K reduction in exospheric temperature, that part of the thermosphere temperature profile that is constant with height (above about 250-km altitude for Earth and 150-km altitude for Mars and Venus). CO₂ cooling is a complex process, because local thermodynamic equilibrium (LTE) does not

generally apply. Major uncertainties in the cooling process remain, including the rate of CO₂ excitation by O, k_E .

Laboratory measurements for k_E are not available under planetary thermosphere conditions, so indirect means have been used to estimate k_E (4). Constraining numerical simulations of two or more planetary thermospheres to observational data is a recognized approach for reducing uncertainties in certain common parameters such as k_E (4). This methodology requires measuring the responses of the planetary thermospheres to changes in solar forcing. It is our goal to establish the response of Mars' neutral thermosphere to the quasi-27-day periodicity of EUV fluxes emanating from the Sun and to compare it with Earth's thermosphere response during the same time interval. Comparisons are also made with results previously reported for Venus (4).

The data consist of daily Mars neutral mass densities at 390 km inferred from precise orbit determination of Mars Global Surveyor (MGS) during 1 January to 31 December 2003. In this method, tracking data are used to measure changes in orbital period, and models for radiation pressure, gravity field, and satellite drag coefficient are used to isolate atmospheric density and its drag effect on the orbit. Application of the technique to MGS is described in detail in a study (7)

devoted to development of an empirical drag temperature model (DTM) of Mars' thermosphere, DTM-Mars. DTM-Mars is used to normalize density values to a constant altitude of 390 km. Daily average density values at Earth were obtained from challenging minisatellite payload (CHAMP) satellite accelerometer measurements (8, 9) that were averaged along the orbit and normalized to a constant altitude of 420 km by using the DTM2000 empirical model (10) for the terrestrial thermosphere. The 2003 time period was chosen because of the large quasi-27-day variations in solar flux, the contemporaneous availability of MGS and CHAMP data, and the fact that Mars was relatively close to opposition (see below).

To maintain uniformity with other similar analyses for planetary thermospheres, particularly those for Venus (4), we use the 10.7-cm radio flux (designated F10.7) as a proxy for EUV variability. Because F10.7 is measured at Earth, some assumptions must be made to estimate solar fluxes received at Mars. Corrections must be made for the varying distances of Earth and Mars from the Sun and for the variations in the Earth-Sun-Mars angle as the planets orbit around the Sun. "Opposition" is when the Earth-Sun-Mars angle is 0°, which occurred on 28 August 2003. During 2003, the ratio of Mars' distance from the Sun to that of Earth decreased from 1.64 to 1.50, whereas the Earth-Sun-Mars angle changed from -101.4° (Earth trailing Mars) to $+48.5^\circ$ (Earth leading Mars). The flux from the Sun varies as the inverse of distance squared. We assume that the solar flux at Mars is shifted in time from that observed at Earth by an amount determined by the Earth-Sun-Mars angle and the rotation period of the Sun (assumed to be 27 days). This assumes that the integrated flux from the Earth-facing hemisphere of the Sun does not change during this time interval, although it is known that active regions of the Sun evolve with time. Possible implications of this assumption are noted below. Hereafter, it is understood that F10.7 values quoted in

Table 1. Thermosphere responses of Earth, Mars, and Venus to quasi-27-day variations in solar flux from the Sun. $\Delta\rho$ is the percent change in thermosphere density (390-km altitude for Mars and 420-km altitude for Earth), ΔF is the absolute change in 10.7-cm solar radio flux (F10.7) received at the planet, r is the linear correlation coefficient, and ΔT is the change in exospheric temperature (K).

	$a_1 = \Delta\rho/\Delta F$	r	$\Delta T/\Delta F$	$\Delta T/\Delta F$ ratio to Earth
Earth 2003 (all)	0.63	0.80	1.58	1.00
Days 75–150	0.99	0.91	2.48	1.00
Days 270–365	0.68	0.90	1.70	1.00
Mars 2003 (all)	0.84	0.61	0.47	0.30
Days 75–150	2.05	0.87	1.15	0.46
Days 270–365	1.39	0.88	0.78	0.46
Venus			0.15–0.21	0.062–0.12

¹Department of Aerospace Engineering Sciences, University of Colorado, Boulder, CO 80309, USA. ²Department of Terrestrial and Planetary Geodesy, CNES, 31401 Toulouse, France. ³NASA Goddard Space Flight Center, Greenbelt, MD 20771, USA.

*To whom correspondence should be addressed. E-mail: forbes@colorado.edu

connection with Mars were adjusted to Mars' orbit in the above manner.

In order to isolate the quasi-27-day rotation effect, we processed the time series of daily densities and F10.7 fluxes in the following manner. For the CHAMP data, data points occurring on days when the daily global magnetic index, A_p (11), exceeded 50 were first removed (12). Then 27-day means, shifted forward one day at a time, were applied to each time series, and a set of residuals was determined by subtracting the raw data from the 27-day running means. Lastly, in order to reduce noise in the density data, to isolate the variability associated with solar rotation, and to diminish possible geomagnetic effects in the CHAMP data, we applied a 5-day running mean to the residuals. Below we refer to the latter as "mean residuals." Upper-limit uncertainty estimates for the mean residuals, which include both experimental and geophysical effects, were determined empirically from the noise level of the data. Root mean square (RMS) noise levels were calculated by using the density residuals that remained after filtering out variations with time scales greater than about 10 days, i.e., those variations primarily associated with solar rotation effects. RMS noise levels less than 1% for both Earth and Mars were generally found except after day 270, when Mars RMS levels were near 2%. Uncertainties of order \pm RMS are implied. As shown below, the observed percent density responses are sufficiently large in comparison to support confidence in our results and conclusions. We now provide our numerical results, which are all tabulated in Table 1.

The mean density residuals (expressed in percent with respect to the 27-day mean) at Mars and Earth were compared with their corresponding F10.7 mean residuals (Figs. 1 and 2, respectively). Note the close relationship between variations in density and F10.7, especially when a strong quasi-27-day periodicity is present. Also shown in each figure are two least squares linear fits to the data points of the form $\Delta\rho = a_0 + a_1\Delta F$, where $\Delta\rho$ is the percent change in density with respect to mean density (a_0) over the interval, ΔF is the absolute change in F10.7 flux at the planet, and $a_1 = \Delta\rho/\Delta F$. In one case the fit is performed over the whole year, and in the other the fit is applied over 27-day intervals that are sequentially shifted forward 1 day at a time. When applied over the whole year for Mars, a value of $a_1 = 0.84$ is obtained with a linear correlation coefficient of $r = 0.61$. For Earth we find values of $a_1 = 0.63$ and $r = 0.80$. The lower correlation for Mars compared with Earth may be due, in part, to assumptions made in inferring solar fluxes at Mars from those measured at Earth. However, the running 27-day fits provide marked im-

provements in reproducing the observations during two time periods of enhanced flux variability (days 75 to 150 and 270 to 365) and represent a better measure of the planetary response to short-term solar flux variability. Correlation coefficients for both Earth and Mars during these periods (denoted intervals I and II in the figures) attain correlation coefficients near 0.90, with values of a_1 equaling 0.99 and 0.68 for Earth and 2.05 and 1.39 for Mars.

Comparing the above coefficients, it would appear that Mars's thermosphere is more re-

sponsive to solar flux changes than that of Earth. However, these results do not correspond to the same mean density levels in the two atmospheres. Some normalization of these results is required. Because the thermosphere temperatures in both planetary atmospheres are constant with height above 250 km, we can use an empirical model to relate exospheric temperature changes to density changes in each atmosphere. For this purpose, we used the DTM2000 model for Earth and the DTM-Mars model for Mars and thus obtained the change in exospheric temperature

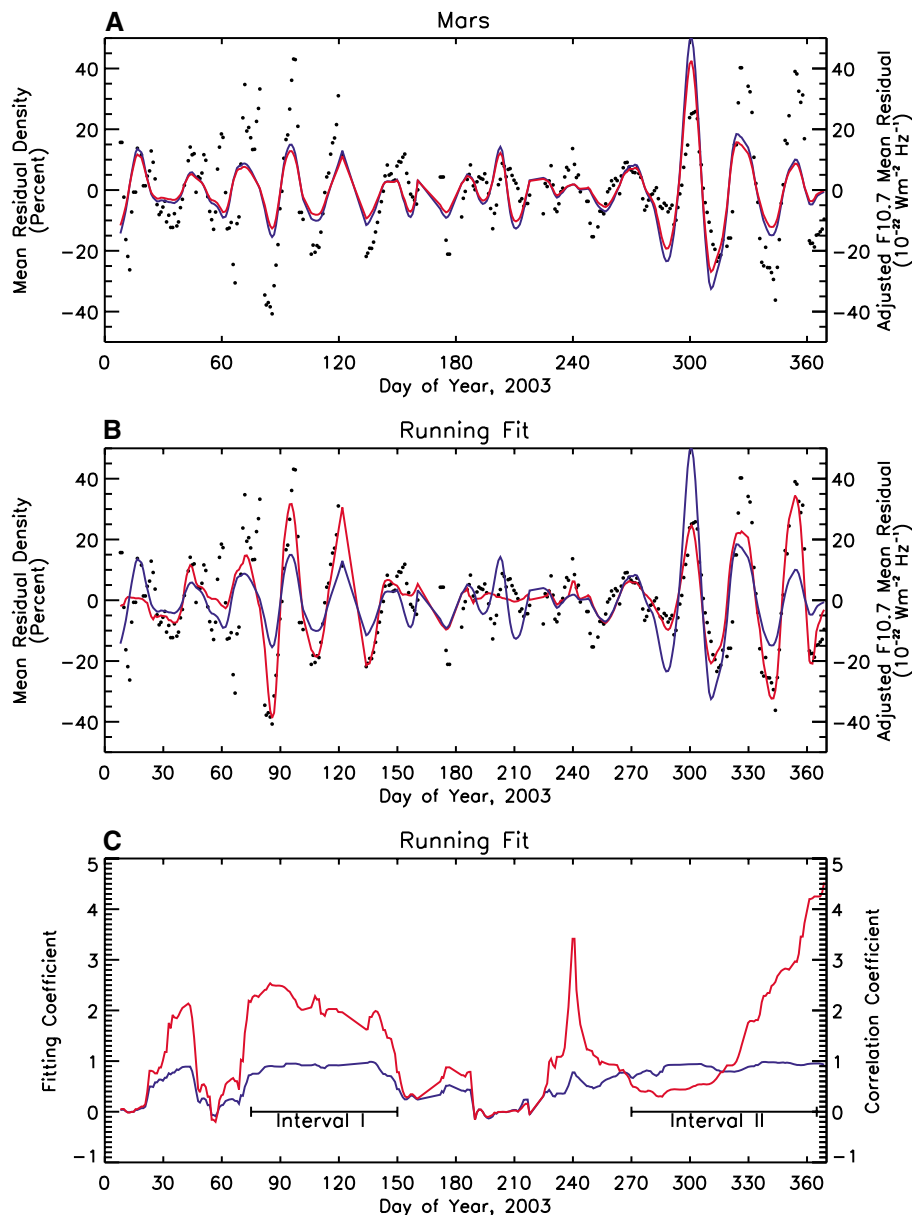


Fig. 1. (A) MGS mean residual densities (percent) at 390 km (dots), F10.7 flux adjusted to Mars' orbit (blue line), and least squares fit of residual densities with respect to adjusted F10.7 (red line) for Earth calendar year 2003. (B) Same as (A), except with 27-day fit slipped forward once per day. (C) Fitting coefficient a_1 (red line) and correlation coefficient r (blue line) versus time for moving 27-day fit. Intervals I and II denote days 75 to 150 and 270 to 365, respectively, when density and F10.7 are most highly correlated (r close to 1.0).

per unit flux received at each planet, $\Delta T/\Delta F$ (Table 1). Also included in Table 1 is the range of values of $\Delta T/\Delta F$ from 0.15 to 0.21 inferred for Venus from analyses of Pioneer Venus neutral mass spectrometer and drag analyses (4, 13–15) and the results for Mars and Venus normalized to those of Earth. Focusing on the two intervals of enhanced solar flux variability, we find that Mars' thermosphere is about 50% as responsive to changes in solar flux, due to rotation of the Sun compared with Earth, but on the order of four to seven times more responsive than Venus. Note that these results are independent of the distance of the planet from the Sun, because we have used absolute changes in solar flux received at the planet in our

analysis. Rather, the range of responses is determined by the different mixing O/CO₂ mixing ratios and the absolute concentrations and distributions of CO₂ in these planetary thermospheres (4).

When interpreting the 27-day effect in Earth's thermosphere, one must be cautious about similar periodicities being introduced in connection with high-speed solar wind streams interacting with the magnetosphere and their subsequent heating effects in the thermosphere. High-speed streams originate in solar coronal holes that also rotate with the Sun. To investigate this possibility, we verified that the mean residual time series for daily mean K_p (16) was uncorrelated ($r = 0.17$) with the CHAMP density residuals.

Further, linear regression analyses of CHAMP densities were performed that included both F10.7 and K_p terms, resulting in an F10.7 coefficient that differed insignificantly from those a_1 values tabulated in Table 1. We conclude that our results for CHAMP represent the solar flux response unaffected by any geomagnetic influence.

Our results should constrain numerical models that strive to simultaneously emulate solar flux influences on the thermospheres of Earth, Mars, and Venus in order to disentangle the relative effects of heating efficiency, CO₂ cooling, and thermal conduction on the thermal and density structures of these planets. Because cooling of Earth's thermosphere due to increases in CO₂ levels over the past 4 decades appears to be occurring (17–19), improved characterization of the CO₂ cooling process will help to understand and predict the fate of our own upper atmosphere to anthropogenic effects (6).

References and Notes

1. P. Withers, M. Mendillo, *Planet. Space Sci.* **53**, 1401 (2005).
2. M. Mendillo, P. Withers, D. Hinson, R. Rishbeth, B. Reinisch, *Science* **311**, 1135 (2006).
3. At low altitudes in planetary atmospheres, CO₂ levels are sufficiently high to trap outgoing infrared radiation, re-emitting it downward to further heat the surface (the so-called greenhouse effect). At high altitudes, e.g., in the thermosphere, CO₂ densities are sufficiently low that infrared radiation is radiated to space, serving as a cooling mechanism.
4. G. M. Keating, S. W. Bougher, *J. Geophys. Res.* **97**, 4189 (1992).
5. R. G. Roble, *AGU Monogr.* **87**, 1 (1995).
6. R. G. Roble, R. E. Dickinson, *Geophys. Res. Lett.* **16**, 1441 (1989).
7. S. Bruinsma, F. G. Lemoine, *J. Geophys. Res.* **107**, 10.1029/2001JE001508 (2002).
8. S. Bruinsma, R. Biancale, *J. Spacecr. Rockets* **40**, 230 (2003).
9. S. Bruinsma, D. Tamagnan, R. Biancale, *Planet. Space Sci.* **52**, 297 (2004).
10. S. Bruinsma, G. Thuillier, *J. Atmos. Solar Terr. Phys.* **65**, 1053 (2003).
11. A_p is a daily measure of magnetic activity in the geospace environment.
12. No perceptible changes in MGS density at Mars occurred on days when $A_p > 50$.
13. K. K. Mahajan, W. T. Kasprzak, L. H. Brace, H. B. Niemann, W. R. Hoegy, *J. Geophys. Res.* **95**, 1091 (1990).
14. G. M. Keating *et al.*, *Adv. Space Res.* **5**, 117 (1985).
15. A. E. Hedin, H. B. Niemann, W. T. Kasprzak, A. Seiff, *J. Geophys. Res.* **88**, 73 (1983).
16. K_p is a 3-hourly measure of magnetic activity in the geospace environment.
17. G. M. Keating, R. H. Tolson, M. S. Bradford, *Geophys. Res. Lett.* **27**, 1523 (2000).
18. J. T. Emmert, J. M. Picone, J. L. Lean, S. H. Knowles, *J. Geophys. Res.* **109**, 10.1029/2003JA010176 (2004).
19. F. A. Marcos, J. O. Wise, M. J. Kendra, N. J. Grossbard, B. R. Bowman, *Geophys. Res. Lett.* **32**, 10.1029/2004GL021269 (2005).
20. This research was supported by the University of Colorado and grant ATM-0208482 from the NSF. The authors thank R. Anderson and X. Zhang for their assistance.

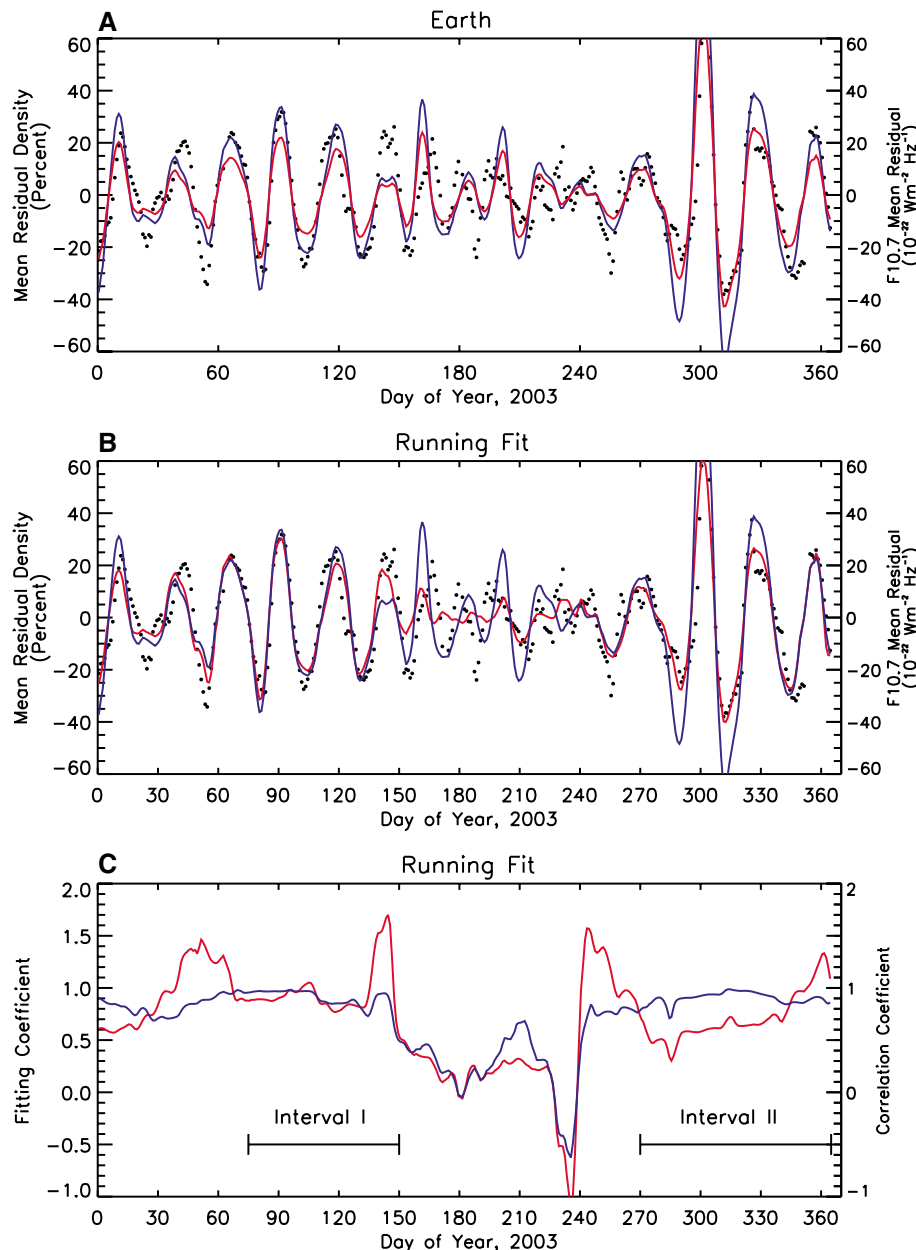


Fig. 2. (A to C) Same as Fig. 1, except for CHAMP densities at 420 km in Earth's atmosphere.

17 February 2006; accepted 20 April 2006
10.1126/science.1126389

Neodymium Isotope Evidence for a Chondritic Composition of the Moon

K. Rankenburg,^{1*} A. D. Brandon,¹ C. R. Neal²

Samarium-neodymium isotope data for six lunar basalts show that the bulk Moon has a $^{142}\text{Nd}/^{144}\text{Nd}$ ratio that is indistinguishable from that of chondritic meteorites but is 20 parts per million less than most samples from Earth. The Sm/Nd formation interval of the lunar mantle from these data is 215^{+23}_{-21} million years after the onset of solar system condensation. Because both Earth and the Moon likely formed in the same region of the solar nebula, Earth should also have a chondritic bulk composition. In order to mass balance the Nd budget, these constraints require that a complementary reservoir with a lower $^{142}\text{Nd}/^{144}\text{Nd}$ value resides in Earth's mantle.

The most widely accepted theory for the formation of the Earth-Moon system proposes a giant impact model, where Earth collided in its later stages of accretion with a body of the approximate size of Mars (1, 2). In this model, the Moon ultimately formed from hot debris generated during this giant impact. Short-lived radioisotope systems such as ^{146}Sm - ^{142}Nd [half-life $t_{1/2} = 103$ million years (My)] are useful in determining the chronology of the events that formed the Earth-Moon system and for determining how these terrestrial bodies evolved after accretion. Recent Sm-Nd data show that chondritic meteorites are on average 20 parts per million (ppm) lower in $^{142}\text{Nd}/^{144}\text{Nd}$ than most terrestrial samples (3). If the bulk silicate Earth (BSE) has an Sm/Nd ratio within the range measured for chondrites, the superchondritic $^{142}\text{Nd}/^{144}\text{Nd}$ ratio of terrestrial materials requires that the silicate Earth experienced a global chemical differentiation during the lifetime of ^{146}Sm (~500 My). If this differentiation event is connected with the formation of the terrestrial depleted upper mantle, then it must have occurred no later than ~30 My after solar system formation (3). If the Moon has superchondritic $^{142}\text{Nd}/^{144}\text{Nd}$ similar to that of Earth's upper mantle, then the giant impact must have occurred into an already differentiated Earth, predominantly sampling the Nd-depleted reservoir. In order to test this hypothesis, we measured Nd-isotope ratios of six lunar basalts that span the compositional range of basaltic lavas from the Moon (4). Although anomalies in ^{142}Nd have been reported previously for lunar samples (5), the uncertainties in these data do not permit an evaluation of whether the bulk Moon is chondritic or instead identical to the terrestrial standard.

Core formation in planetesimals and terrestrial bodies likely occurred within ~30 My after formation of the solar nebula, based on ^{182}Hf - ^{182}W chronometry ($t_{1/2} = 9$ My) (6, 7). Core formation is independently indicated for

¹NASA Johnson Space Center, Mail Code KR, Houston, TX 77058, USA. ²Department of Civil Engineering and Geological Sciences, University of Notre Dame, Notre Dame, IN 46556, USA.

*To whom correspondence should be addressed. E-mail: kai.rankenburg1@jsc.nasa.gov

the impactor (termed Theia), because an undifferentiated projectile could not have produced an iron-poor Moon (8). Estimates for the timing of the giant impact on the basis of tungsten isotopes are model-dependent and range from ~30 My (9, 10) to at least 44 My after the formation of the solar system (11). A later age (≥ 50 My) for the formation of the Moon is more easily reconciled with the lunar initial $^{87}\text{Sr}/^{86}\text{Sr}$ ratio (12). Estimates for the crystallization of the putative lunar magma ocean (LMO), which are indicated by the crystallization age of materials strongly enriched with trace elements as the last remnants of the LMO (termed KREEP for K, potassium; REE, rare earth elements; and P, phosphorus), range from 30 to 50 My based on ^{182}Hf - ^{182}W data (13, 14) to ~250 My based on Sm-Nd data (5). The residual liquid at the end of LMO crystallization is also highly enriched in incompatible, heat-producing radionuclides such as ^{235}U and ^{40}K . This late-stage liquid could have acted as an insulating cover that substantially enhanced the longevity of the LMO (15).

Samarium and neodymium are refractory (i.e., they have high condensation temperatures) and lithophile elements (i.e., they preferentially partition in the silicate phase during core formation). Unlike the ^{182}Hf - ^{182}W system, which is influenced by core formation, the Sm-Nd isotope system is expected to record more reliably anomalies inherited from mantle sources with variable Sm/Nd ratios produced during global differentiation. However, because Earth is a geologically active planet, most variations initially present in

$^{142}\text{Nd}/^{144}\text{Nd}$ and $^{143}\text{Nd}/^{144}\text{Nd}$ from the early decay of ^{146}Sm and ^{147}Sm [$t_{1/2} = 106$ billion years (Gy)], respectively, have been subsequently homogenized. With the exception of only a few old crustal rocks (16, 17), all terrestrial samples have $\epsilon^{142}\text{Nd} = 0$ (18). The lunar samples studied here have crystallization ages of 3150 to 3900 My and preserve a range of present-day $\epsilon^{142}\text{Nd}$ from -0.30 ± 0.07 to $+0.07 \pm 0.05$ (errors are 2σ) when corrected for the effects of neutron irradiation (Fig. 1 and Table 1).

The source region of the low-Ti mare basalts (i.e., Apollo 15 sample 15555 and lunar meteorite LAP 02205) is postulated to consist mainly of olivine and orthopyroxene cumulates, formed early in a crystallizing LMO (19). The high-Ti mare basalt suite (i.e., Apollo 17 samples 70017 and 74275) is derived from Ti-rich mantle sources that contain additional cumulus ilmenite (20). This Ti-rich source may consist of deep mantle cumulates modified by varying degrees of hybridization and/or assimilation of formerly shallow material, swept down by a massive convective overturn of the lunar mantle (21, 22). Alternatively, this source may represent a relatively shallow late-stage cumulate pile containing trapped residual liquid and plagioclase (20).

The origin of the KREEP-rich samples 15386 and SaU 169 is less well constrained. They contain too much MgO to be derived directly from the hypothesized KREEP source that represents the residual liquid of the LMO. The KREEP signature of these basalts likely results from mixing between the KREEP source material and more magnesium-rich magmas derived from deeper mantle sources. Because of the high concentration of incompatible elements in KREEP, it will dominate the trace element and isotopic signature of a hybrid rock, whereas the major element chemistry (such as MgO content) will not be substantially changed.

We modeled the evolution of the lunar mantle for two situations. In the first model (Fig. 2, A and B), we assumed that the Moon formed by a giant impact from material with average chondritic composition with present-day $\epsilon^{143}\text{Nd} = 0$ and $\epsilon^{142}\text{Nd} = -0.2$ (3). The $\epsilon^{143}\text{Nd}$ and $\epsilon^{142}\text{Nd}$ of the evolving lunar mantle were calculated using a two-stage model (4). In

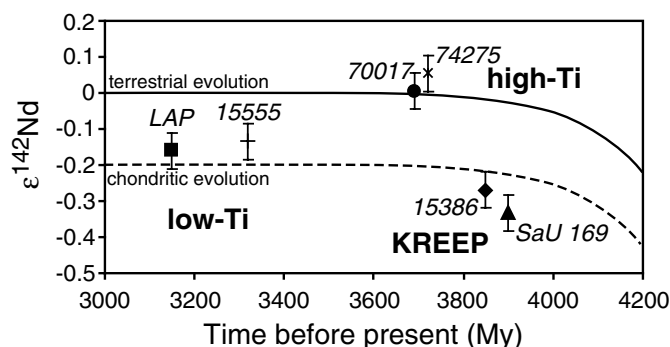


Fig. 1. Crystallization ages of the measured basalts versus their initial $\epsilon^{142}\text{Nd}$. Some lunar data have $\epsilon^{142}\text{Nd}$ values close to the terrestrial value, which has led to the suggestion that the Moon could have formed from a depleted portion of an early differentiated Earth's mantle (3).

the first stage, the LMO has a chondritic $^{147}\text{Sm}/^{144}\text{Nd}$ ratio until it is fractionated at time t_1 by the formation of a suite of contemporaneous lunar mantle rocks. The second stage marks melt extraction from the mantle and crystallization at time t_2 . The $(^{147}\text{Sm}/^{144}\text{Nd})_{t_1}$ ratio is calculated for each basalt source (table S6) from the initial $\epsilon^{143}\text{Nd}$ value ($\epsilon^{143}\text{Nd}_i$) and crystallization ages t_2 of the basalts (Table 1) and by setting t_1 arbitrarily to 50 and 200 My after formation of the solar system at $t_0 = 4567$ My (23). Plotting these values versus the measured present-day $\epsilon^{142}\text{Nd}$ for each time series t_1 forms linear arrays despite their disparate crystallization ages (Fig. 1). This suggests establishment of the sources of these lavas when ^{146}Sm was still alive. Although the choice of 50 or 200 My for the formation of the basalt sources from a chondritic LMO generates differences in the calculated source $^{147}\text{Sm}/^{144}\text{Nd}$ ratios, it does not greatly alter the slope of the best fit lines through the data (Fig. 2A). Self-consistent values of t_0 to t_1 and $(^{147}\text{Sm}/^{144}\text{Nd})_{t_1}$ were calculated for each sample by simultaneously solving equations S1 and S2 (4) for the two unknowns (Table 1). In this way, the combined ^{146}Sm and ^{147}Sm decay schemes constrain the source-formation age and its time-integrated $^{147}\text{Sm}/^{144}\text{Nd}$ ratio for each individual sample (24). An average of the source-formation times t_0 to t_1 (Table 1) was used to iteratively calculate $(^{147}\text{Sm}/^{144}\text{Nd})_{t_1}$ ratios until the slope of the regressed line matched the calculated ^{142}Nd isochron (Fig. 2A). A straightforward interpretation of this best fit solution (Fig. 2B) is that the lunar mantle sources represented by these samples formed at 215^{+23}_{-21} My after solar system formation. Assuming that the Moon formed 30 to 50 My after t_0 , a formation interval for the lunar mantle of $\sim 165^{+23}_{-21}$ to 185^{+23}_{-21} My is derived. This result is in agreement with the 238^{+56}_{-40} My formation interval obtained previously (5). However, our data intersect the chondritic $^{147}\text{Sm}/^{144}\text{Nd}$ ratio at $\epsilon^{142}\text{Nd} = -0.19 \pm 0.02$ [mean squared weighted deviation (MSWD) =

0.99], identical within error to the value of the chondritic uniform reservoir (CHUR) (3). Although this model suggests that a two-stage model is sufficient to explain the formation of the lunar samples represented in this study, it has been speculated that the Moon could have formed from a nonchondritic reservoir (3). Therefore, three- and four-stage models are discussed to constrain the conditions under which an initially nonchondritic bulk Moon could have generated the measured isotopic compositions of the lunar samples.

In the second model (Fig. 2C), the Moon was formed from material that predominantly sampled the Nd-depleted reservoir of an already differentiated Earth and/or impactor. In this case, $\epsilon^{143}\text{Nd}$ and $\epsilon^{142}\text{Nd}$ are calculated using a three-stage model (equations S3 and S4) in which $t_1 = 4537$ My and $(^{147}\text{Sm}/^{144}\text{Nd})_{t_1} = 0.2146$ (3), to yield a modern terrestrial depleted mantle reservoir with $\epsilon^{143}\text{Nd} = +10.7$ and $\epsilon^{142}\text{Nd} = 0$. Parameters t_2 and t_3 are then the times of LMO and basalt crystallization, respectively. Regressing calculated source $^{147}\text{Sm}/^{144}\text{Nd}$ ratios (table S6) versus present-day $\epsilon^{142}\text{Nd}$ yields a best fit $\epsilon^{142}\text{Nd}$ of -0.12 ± 0.02 (MSWD = 1.1) for a bulk Moon with $^{147}\text{Sm}/^{144}\text{Nd} = 0.2146$ (Fig. 2C). However, no calculated ^{142}Nd isochron fits the data in this model, because it also must pass through present-day $\epsilon^{142}\text{Nd} = 0$ (colored lines in Fig. 2C). This also explains the largely different individual source-formation ages calculated from combined $\epsilon^{142}\text{Nd}$ - $\epsilon^{143}\text{Nd}$ chronometry (Table 1). The low-Ti and high-Ti sources yield either unreasonably low (0^{+62} My) or high (761^{+50}_{-358} My) values for the formation interval t_1 to t_0 , respectively.

The datum for 15555, in particular, implies that the Moon has a chondritic mantle with respect to Nd isotopes, because its initial $\epsilon^{143}\text{Nd}$ value is more precisely constrained from an internal isochron (5). For a depleted starting composition, 15555 plots outside the range of possible $\epsilon^{142}\text{Nd}$ - $\epsilon^{143}\text{Nd}$ compositions (Fig. 3). In addition, the Nd isotopic composition of

15555 cannot be interpreted as mixing between KREEP with low $^{147}\text{Sm}/^{144}\text{Nd}$ and depleted lunar mantle with high $^{147}\text{Sm}/^{144}\text{Nd}$ (Fig. 3), because formation of the KREEP source must equal or postdate the formation of the depleted source. To explain these data within the context of an initially depleted Nd isotopic composition for the Moon, a more complicated four-stage model can be constructed, where the depleted starting material is enriched during early differentiation of the LMO [e.g., at 40 My with $(^{147}\text{Sm}/^{144}\text{Nd})_{t_2} = 0.1985$]. Internal differentiation of such a re-enriched LMO at $t_3 = 215$ My with $(^{147}\text{Sm}/^{144}\text{Nd})_{t_3} = 0.217$ could then form a suitable source for sample 15555. However, because of Nd mass-balancing requirements, the additional stage in the model calls for a complementary reservoir of lunar mantle cumulates with, depending on its size, highly depleted Nd isotope compositions. Because such a reservoir is as yet not represented in the lunar sample collection, the hypothesis of an initially depleted Moon is unlikely. If the correlation between $\epsilon^{142}\text{Nd}$ and source $^{147}\text{Sm}/^{144}\text{Nd}$ ratio (Fig. 2B) represents an isochron and not a mixing line, then the age derived from the chondritic model most probably dates the last global lunar mantle re-equilibration. In this context, these Nd isotope data demonstrate that the LMO has a negative present-day $\epsilon^{142}\text{Nd}$ and was not formed entirely from depleted portions of Earth's and/or the impactor's mantle.

The lunar source-formation age of 215^{+23}_{-21} My calculated from Nd isotopes within the context of an initially chondritic Moon is inconsistent with a proposed LMO crystallization age of only 30 to 50 My obtained from ^{182}Hf - ^{182}W systematics (13, 14). For example, low-Ti basalt 15555, used to pinpoint the bulk lunar $^{182}\text{W}/^{184}\text{W}$ (13) provides an Nd source-formation age of 221^{+264}_{-98} My. Moreover, the nonchondritic $^{147}\text{Sm}/^{144}\text{Nd}$ ratio of 0.218 calculated for the 15555 source (Table 1) violates the assumption of an undifferentiated Hf-W ratio (13). Average model ages for KREEP are $4.42 \pm$

Table 1. Nd and Sm isotope data measured in this study. NS, no solution. Crystallization ages and radiometric system from the literature as follows: SaU 169 (Pb-Pb) from (38); 15386 (Sm-Nd) from (5); 70017, 74275 (average of groups B and C from multiple methods) from (39); 15555 (Sm-Nd) from (40). Corr., neutron fluence corrected. Src., source.

Sample	Weight (mg)	$\epsilon^{142}\text{Nd}$	$\epsilon^{143}\text{Nd}$	$\epsilon^{149}\text{Sm}$	$\epsilon^{142}\text{Nd}$ corr.	$\epsilon^{143}\text{Nd}$ corr.	Age (My)	Sm (ppm)	Nd (ppm)	$^{147}\text{Sm}/^{144}\text{Nd}$	$\epsilon^{142}\text{Nd}_i$	$\epsilon^{143}\text{Nd}_i$	t_0 to t_1 CHUR	$^{147}\text{Sm}/^{144}\text{Nd}$ CHUR src.	t_0 to t_1 DLM	$^{147}\text{Sm}/^{144}\text{Nd}$ DLM src.
LAP 02205	43 to 127	-0.18	0.65	-3.5	-0.16	0.68	3150*	5.82	17.9	0.1963	-0.16	1.1*	113^{+50}_{-113}	0.2028	0^{+62}	0.2026
$2\sigma \pm$ ($n = 7$)		0.04	0.03		0.04											
SAU 169	11.98	-0.32	-16.48	-12.5	-0.30	-16.37	3900	61.8	221.5	0.1688	-0.34	-2.5	233^{+353}_{-116}	0.1529	128^{+68}_{-49}	0.1581
$2\sigma \pm$ ($n = 2$)		0.05	0.05		0.07											
15386	22.60	-0.34	-16.35	-32.5	-0.24	-16.06	3850	34.5	122.7	0.1699	-0.27	-1.22*	243^{+50}_{-203}	0.1769	93^{+87}_{-58}	0.1798
$2\sigma \pm$ ($n = 3$)		0.05	0.06		0.07											
74275	54.70	0.06	30.06	-1.9	0.07	30.08	3720	13.1	32.0	0.2470	0.06	5.8	178^{+39}_{-33}	0.2619	372^{+50}_{-114}	0.2757
70017	59.24	0.01	40.64	-1.4	0.02	40.65	3690	5.19	11.7	0.2681	0.01	6.5	232^{+51}_{-39}	0.2726	761^{+50}_{-358}	0.5069
15555	139.90	-0.16	4.71	-5.3	-0.14	4.76	3320	2.70	8.09	0.2017	-0.14	2.88*	221^{+264}_{-98}	0.2177	NS	NS
Allende	1002.30	-0.41	-0.91	-0.6	-0.41	-0.91										

*From internal isochron.

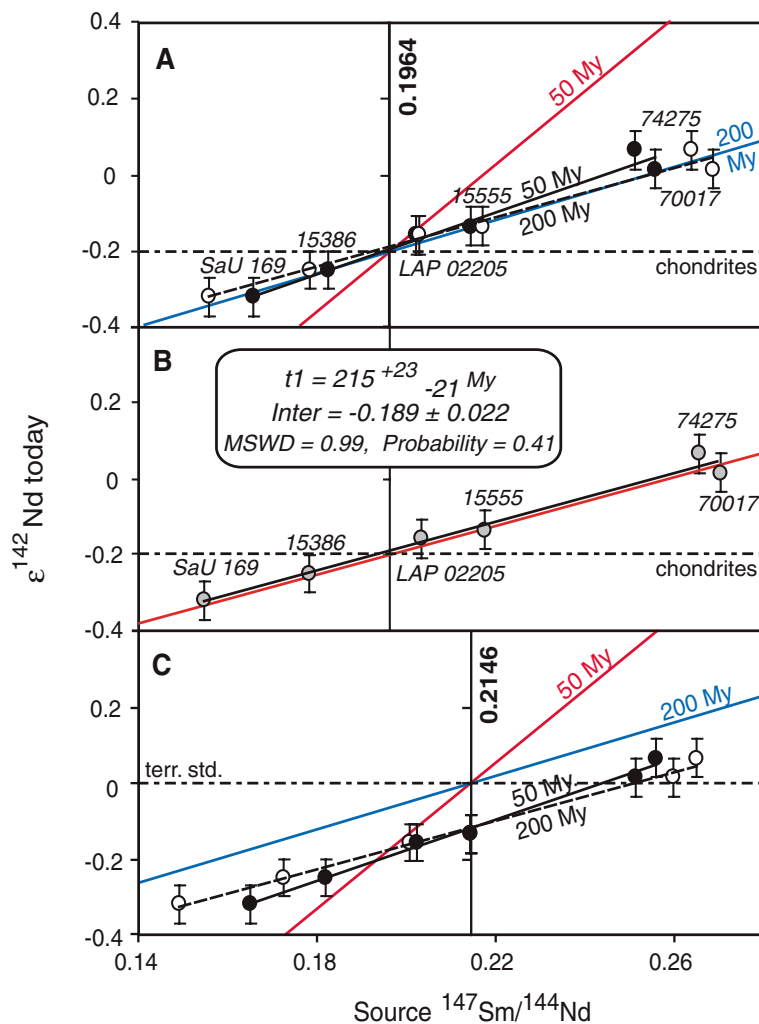
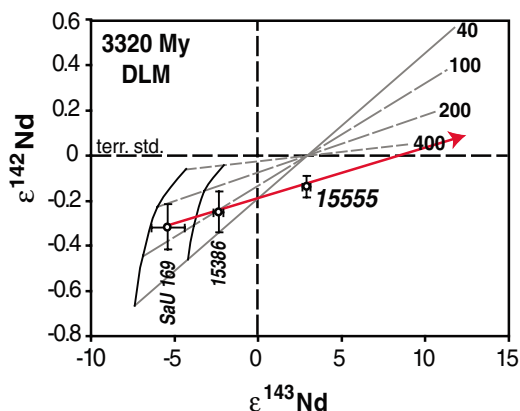


Fig. 2. (A) Illustration of the interaction of $^{147}\text{Sm}/^{144}\text{Nd}$, $\epsilon^{142}\text{Nd}$, and $\epsilon^{143}\text{Nd}$. Source $^{147}\text{Sm}/^{144}\text{Nd}$ ratios for each sample (table S6) plotted versus measured present-day $\epsilon^{142}\text{Nd}$ along with regression lines for each source-formation age (black lines). Also shown are ^{142}Nd -isochrons calculated for reservoirs formed from a chondritic LMO at 50 and 200 My after t_0 (labeled colored lines) using $^{147}\text{Sm}/^{144}\text{Nd} = 0.1964$, $^{146}\text{Sm}/^{144}\text{Sm} = 0.0075$ at 4567 My, and $\lambda^{146}\text{Sm} = 6.74 \times 10^{-9} \text{ year}^{-1}$. (B) A self-consistent model is obtained for $t_1 = 215^{+23}_{-21} \text{ My}$. The present-day bulk lunar $\epsilon^{142}\text{Nd}$ from this model is -0.19 ± 0.02 , similar to that of chondrites (3). (C) Same samples as before, but calculated as three-stage model (4), in which the Moon was formed from a depleted source. The depletion age of 4537 My and $^{147}\text{Sm}/^{144}\text{Nd} = 0.2146$ correspond to a model which forms the terrestrial mid-ocean ridge basalt source with present-day $\epsilon^{142}\text{Nd} = 0$ and $\epsilon^{143}\text{Nd} = 10.69$ (3).

Fig. 3. Snapshot of $^{142,143}\text{Nd}$ isotopic evolution along with isochrons for sources formed from an initially depleted lunar mantle source (DLM) at $t = 40, 100, 200, 400 \text{ My}$ after solar system formation (labeled lines). In this model, low-Ti basalt 15555 plots outside the range of possible $\epsilon^{142}\text{Nd}$ - $\epsilon^{143}\text{Nd}$ compositions. The composition of 15555 cannot be interpreted as mixing between low $^{147}\text{Sm}/^{144}\text{Nd}$ KREEP (15386 and SaU 169 sources) are projected to 3320 My) and depleted high $^{147}\text{Sm}/^{144}\text{Nd}$ lunar mantle, because the formation of the KREEP source must equal or postdate formation of the depleted source; i.e., no mixing line (arrow) can be drawn connecting a KREEP reservoir, sample 15555, and a depleted reservoir that is younger than KREEP.



0.14 (2σ) Gy from ^{87}Rb - ^{87}Sr (25), $\sim 4.42 \text{ Gy}$ from $^{238,235}\text{U}$ - $^{206,207}\text{Pb}$ (26), and $\sim 4.36 \text{ Gy}$ from ^{143}Sm - ^{144}Nd isotope systematics (27) and have been interpreted to represent the final crystallization of the LMO (28). The age presented here overlaps this range and is consistent with other results from Nd isotopes (5).

Models of planetesimal accretion suggest that the impactor formed close to Earth (29), which is in accordance with measured oxygen and chromium isotopes of Earth and the Moon (30, 31). Numerical simulations of the giant impact suggest that $\sim 80\%$ of the lunar mass was derived from the impactor's mantle, the rest from Earth (32). This expectation is difficult to reconcile with a similar nonchondritic lunar and terrestrial $\epsilon^{142}\text{Nd}$, unless the impactor had a similar history of silicate differentiation to Earth (3). Our finding that the Moon was formed from a chondritic reservoir is consistent with other compositional indicators of a chondritic LMO, such as the flat REE patterns inferred for parental liquids of the lunar ferroan anorthosites (FANs) constituting the lunar crust, and superchondritic rather than subchondritic Ba/Sr in FAN plagioclases (33). If Earth and the Moon formed close to each other, it is likely that the bulk Earth also formed with a chondritic $^{147}\text{Sm}/^{144}\text{Nd}$ ratio. Hence, in order to balance the Nd budget of the sampled terrestrial reservoirs having $\epsilon^{142}\text{Nd} = 0$, to obtain a bulk chondritic composition of $\epsilon^{142}\text{Nd} \sim -0.20$, an isolated enriched mantle reservoir must reside somewhere in the present Earth (34–36). Initial differentiation could result from an early formed dense phase with higher compatibility for Nd than Sm, or deep subduction of early-formed crust (33). Such reservoirs are predicted to reside in the interface layer (D'') between Earth's silicate mantle and its metallic core (34–37).

The conclusion that the Moon has $\epsilon^{142}\text{Nd}$ close to the chondritic value does not, however, constrain the relative timing of giant impact and early silicate fractionation on Earth. Assuming that approximately 80% of the Moon-forming material was derived from a chondritic impactor and 20% from a hypothetical depleted Earth reservoir with present-day $\epsilon^{142}\text{Nd} = 0$, the measured lunar $\epsilon^{142}\text{Nd}$ of -0.19 could be achieved if chondrites have an average $\epsilon^{142}\text{Nd}$ of -0.24 , which is well within error limits of measured chondritic values (3).

References and Notes

- W. K. Hartmann, D. R. Davis, *Icarus* **24**, 504 (1975).
- R. M. Canup, *Icarus* **168**, 433 (2004).
- M. Boyet, R. W. Carlson, *Science* **309**, 576 (2005).
- Materials and methods are available as supporting material on Science Online.
- L. E. Nyquist *et al.*, *Geochim. Cosmochim. Acta.* **59**, 2817 (1995).
- T. Kleine, C. Münker, K. Mezger, H. Palme, *Nature* **418**, 952 (2002).
- Q. Yin *et al.*, *Nature* **418**, 949 (2002).
- H. Palme, *Science* **304**, 977 (2004).
- S. B. Jacobsen, Q. Z. Yin, *Proc. Lun. Planet. Sci. Conf.* **34**, 1913 (2003).

10. T. Kleine, K. Mezger, C. Münker, *Proc. Met. Soc.* **66**, 5212 (2003).
11. A. N. Halliday, *Nature* **427**, 505 (2004).
12. A. N. Halliday, D. Pocielli, *Earth Planet. Sci. Lett.* **192**, 545 (2001).
13. T. Kleine, H. Palme, K. Mezger, A. N. Halliday, *Science* **310**, 1671 (2005).
14. C. K. Shearer, H. E. Newsom, *Geochim. Cosmochim. Acta.* **64**, 3599 (2000).
15. P. C. Hess, E. M. Parmentier, *J. Geophys. Res.* **E106**, 28 (2001).
16. G. Caro, B. Bourdon, J.-L. Birck, S. Moorbath, *Geochim. Cosmochim. Acta.* **70**, 164 (2006).
17. M. Boyet et al., *Earth Planet. Sci. Lett.* **214**, 427 (2003).
18. Variations from the terrestrial standard are expressed as $\epsilon^{142}\text{Nd} = \left[\frac{(^{142}\text{Nd}/^{144}\text{Nd})_{\text{sample}}}{(^{142}\text{Nd}/^{144}\text{Nd})_{\text{terr.std}}} - 1 \right] \times 10^4$; variations in $^{143}\text{Nd}/^{144}\text{Nd}$ are expressed as deviations from the evolution of the CHUR as $\epsilon^{143}\text{Nd} = \left[\frac{(^{143}\text{Nd}/^{144}\text{Nd})_{\text{sample}}}{(^{143}\text{Nd}/^{144}\text{Nd})_{\text{CHUR}}} - 1 \right] \times 10^4$.
19. L. T. Elkins-Tanton, N. Chatterjee, T. L. Grove, *Meteor. Planet. Sci.* **38**, 515 (2003).
20. G. A. Snyder, L. A. Taylor, C. R. Neal, *Geochim. Cosmochim. Acta.* **56**, 3809 (1992).
21. A. E. Ringwood, S. E. Kesson, *Proc. Lun. Sci. Conf.* **7**, 1697 (1976).
22. L. T. Elkins-Tanton, J. A. Van Orman, B. H. Hager, T. L. Grove, *Earth Planet. Sci. Lett.* **196**, 239 (2002).
23. Y. Amelin, A. N. Krot, I. D. Hutcheon, A. A. Ulyanov, *Science* **297**, 1678 (2002).
24. C. L. Harper, S. B. Jacobsen, *Nature* **360**, 728 (1992).
25. L. E. Nyquist, C. Y. Shih, *Geochim. Cosmochim. Acta.* **56**, 2213 (1992).
26. F. Tera, G. J. Wasserburg, *Proc. Lun. Sci. Conf.* **5**, 571 (1974).
27. R. W. Carlson, G. W. Lugmair, *Earth Planet. Sci. Lett.* **45**, 123 (1979).
28. G. A. Snyder, L. E. Borg, L. E. Nyquist, L. A. Taylor, in *Origin of the Earth and Moon*, R. M. Canup, K. Righter, Eds. (Univ. Arizona Press, Tucson, 2000), pp. 361–396.
29. G. W. Wetherill, in *Origin of the Moon*, W. K. Hartmann, R. J. Phillips, G. J. Taylor, Eds. (LPI, Houston, TX, 1986), pp. 519–550.
30. U. Wiechert et al., *Science* **294**, 345 (2001).
31. G. W. Lugmair, A. Shukryukov, *Geochim. Cosmochim. Acta.* **62**, 2863 (1998).
32. R. M. Canup, *Annu. Rev. Astron. Astrophys.* **42**, 441 (2004).
33. M. D. Norman, L. E. Borg, L. E. Nyquist, D. E. Bogard, *Meteor. Planet. Sci.* **38**, 645 (2003).
34. I. Tolstikhin, A. W. Hofmann, *Phys. Earth. Planet. Int.* **148**, 109 (2005).
35. T. W. Becker, J. B. Kellogg, R. J. O'Connell, *Earth Planet. Sci. Lett.* **171**, 351 (1999).
36. L. H. Kellogg, B. H. Hager, R. D. Van der Hilst, *Science* **283**, 1881 (1999).
37. G. Caro, B. Bourdon, B. J. Wood, A. Corgne, *Nature* **436**, 246 (2005).
38. E. Gnos et al., *Science* **305**, 657 (2004).
39. J. B. Paces et al., *Geochim. Cosmochim. Acta.* **55**, 2025 (1991).
40. L. E. Nyquist et al., *Proc. Lun. Planet. Sci. Conf.* **22**, 985 (1991).
41. This work was done under a postdoctoral research appointment at NASA managed by the National Research Council, and NASA Cosmochemistry grants to A.D.B. and C.R.N. Sample SaU 169 was kindly provided by B. Hofmann at the Natural History Museum Bern, Switzerland. LAP 02205 and Apollo rocks were supplied by Astromaterials and Research Exploration Science Directorate at NASA-JSC. The comments of S. Berthet, M. Sharma and one anonymous reviewer greatly helped to improve former versions of this paper.

Supporting Online Material

www.sciencemag.org/cgi/content/full/312/5778/1369/DC1

Materials and Methods

SOM Text

Figs. S1 to S11

Tables S1 to S6

References

9 February 2006; accepted 19 April 2006

10.1126/science.1126114

Early Domesticated Fig in the Jordan Valley

Mordechai E. Kislev,^{1*} Anat Hartmann,² Ofer Bar-Yosef³

It is generally accepted that the fig tree was domesticated in the Near East some 6500 years ago. Here we report the discovery of nine carbonized fig fruits and hundreds of drupelets stored in Gilgal I, an early Neolithic village, located in the Lower Jordan Valley, which dates to 11,400 to 11,200 years ago. We suggest that these edible fruits were gathered from parthenocarpic trees grown from intentionally planted branches. Hence, fig trees could have been the first domesticated plant of the Neolithic Revolution, which preceded cereal domestication by about a thousand years.

New archaeobotanic evidence seems to indicate that fig cultivation was widely practiced in the Near East during the 12th millennium before the present (B.P.), nearly a thousand years before the domestication of cereals and legumes. The origin of the common fig (*Ficus carica*) is still an unsettled issue, though some of its major steps have been reconstructed (1–6). Finds include fruit fragments and drupelets from Gilgal I (Fig. 1 and figs. S1 to S3), an early Neolithic site in the Jordan Valley, as well as from a number of other Neolithic sites of similar age (1, 7–11). Figs in these early archaeological sites significantly outnumber any other fruit remains from that period. This successful human initiation was probably due to the simplicity of fig tree propagation, which is achieved by merely cutting and planting branches (12). Small genetic changes in wild figs occurring

at that time considerably improved the fruit's taste. These two characters may explain why the domestication of the fig preceded that of other fruit trees, such as the grape, olive, and date, by almost five millennia (13).

The common fig is a gynodioecious species composed of two sexes: the hermaphroditic inedible caprifig, which is functionally a male fig (*F. carica* var. *caprificus*), and the edible female seed fig (*F. carica* var. *domestica*). The hermaphroditic tree produces both male staminate flowers and female pistillate flowers within each fig syconium, whereas the female variety has only pistillate flowers. There is also a widely grown parthenocarpic variety of

female fig, in which the ovaries develop into drupelets without pollination and fertilization.

The fig tree, whose fertilization is carried out by the symbiotic fig wasp *Blastophaga psenes* (fig. S4), produces three crops during the year: in early summer (June–July), in midsummer-autumn (August–November), and in early spring (March). The polleniferous spring hermaphroditic figs are the main source of wasp-borne pollen, but the syconia of the remaining two crops produce little or no fertile pollen. They function as domiciles in which the short-lived wasps propagate (14).

The syconium is an enclosed inflorescence that transforms into a hollow receptacle. Whereas the syconia of the hermaphroditic caprifig produce minute staminate flowers and pistillate flowers with a short style (2 mm long), the syconia of the female fig tree produce only long-style (3 mm long) pistillate flowers. Style length has a crucial role in the fertilization process, because the minute fig wasp has an ovipositor 2 mm long. After emerging from its native syconium, the flying wasp, coated with pollen, enters through the orifice (ostiole) of a young syconium on a different tree. When meeting the short-style flower in a hermaphroditic tree, the wasp successfully inserts its egg through the style into the flower's ovary. As a result, a larva develops that feeds on the developing tissue and emerges through a hole in

Table 1. Early Neolithic (11,500 to 10,300 years B.P.) fig remains in the Levant.

Site	Region	Calendar years B.P.	Quantity*
Jericho Phase VIIB (7, 21)	Jordan Valley	11,400–10,500	1 + 46
Gilgal I	Jordan Valley	11,400–11,200	9 + 313
Gilgal III	Jordan Valley	11,700–11,260	1 + 30
Netiv Hagdud (8)	Jordan Valley	11,300–10,900	1 + 4913
Gesher (9, 21)	Jordan Valley	11,300	36
Mureybit Phase III (10)	Euphrates Valley	11,400–10,600	1 + 3

*Bold text, fruit fragments; normal text, drupelets.

¹Faculty of Life Sciences, Bar-Ilan University, 52900 Ramat-Gan, Israel. ²Land of Israel Studies and Archaeology Department, Bar-Ilan University, 52900 Ramat-Gan, Israel. ³Department of Anthropology, Peabody Museum, Harvard University, Cambridge, MA 02138, USA.

*To whom correspondence should be addressed. E-mail: kislev@mail.biu.ac.il

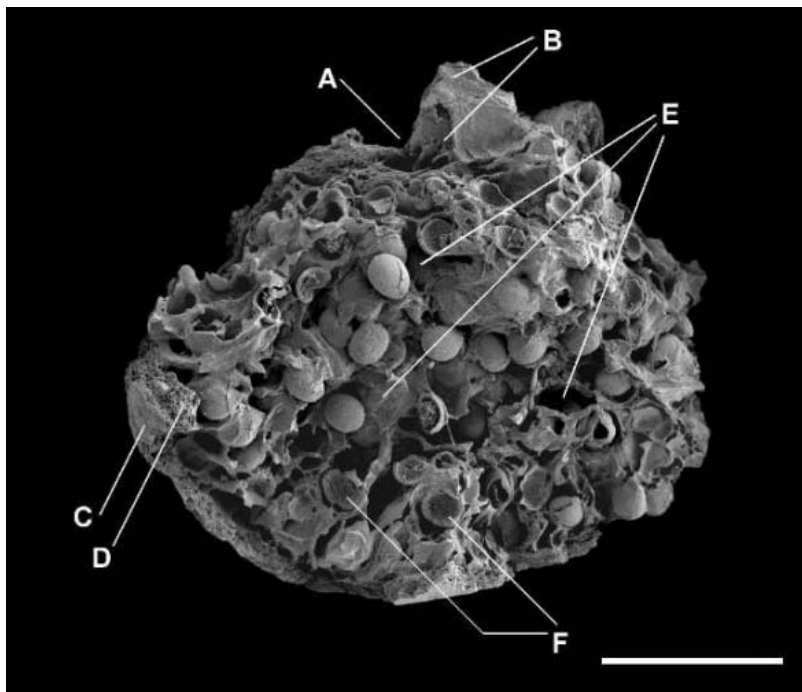


Fig. 1. Carbonized fig fruit (*Ficus carica* var. *domestica*) from Gilgal I, broken lengthwise. Orifice (A) surrounded by scales (B). The fruit skin (C) covers the thin fruit flesh (D) and its inner part (E), which includes the empty drupelets (F). Scale bar, 5 mm. [Panoramic scanning electron microscope micrographs by Y. Langsam]

the wall of the ovary container as an adult male or female (Fig. 2 and fig. S4). But when the wasp enters syconia with the long-style flowers of the female tree, oviposition fails because the ovipositor is too short. The female flowers are nevertheless pollinated and set normal seeds (2, 15).

Sex determination in the common fig appears to be controlled by two closely linked pairs of alleles on an unidentified pair of chromosomes. They are represented as follows: *A* is a dominant allele for the presence of male flowers in the syconium, and *a* is a recessive allele for the suppression of male flowers; *G* is a dominant allele for female flowers with short styles, and *g* is a recessive allele for female flowers with long styles. So, the caprifig homolog is *GA* and genotypes of caprifig trees are *GA/GA* or *GA/ga*. The female homolog is *ga*, and the trees always have the genotype *ga/ga* (3).

Both genetically homozygous (*GA/GA*) and heterozygous (*GA/ga*) hermaphroditic types produce spongy inedible fruits with flowers that turn into wasp-hosted galls (3) (Fig. 2). When caprifig syconia (*GA*) ripen in the spring, they produce wasps and pollen but are unable to produce fertile seeds: the mother wasp entering the young caprifig syconium emerged from a midsummer-autumn syconia crop that does not produce pollen. If, however, the winter-developing caprifigs are fertilized artificially by humans, they produce ripe fruits that are somewhat smaller than those of the unfertilized wasp-populated caprifigs. This results from the considerably smaller intercellular spaces in the flesh of the wasp-free fruit than in the wasp-

inhabited caprifigs (14). Heterozygous wild trees (*GA/ga*) can also generate female fig trees with long functional pistillate flowers (*ga/ga*) that produce fertile seeds (3, 16).

In contrast to seed-producing figs, a second kind of fig tree with edible fruits is a mutant that generates figs with embryoless drupelets by parthenocarpy (development of the ovary without pollination or fertilization). These figs become soft, sweet, and edible because of the persistence of the unfertilized syconia on the tree; this process differs from that in nonparthenocarpic female types, which shed their syconia when unfertilized. This parthenocarpy can be merely vegetative or, in other varieties, can be induced by the stimulus of the female *Blastophaga* inserting her ovipositor into the style of the female flower without oviposition. This stimulation prevents dropping of the fruit, allowing it to develop to maturity. Parthenocarpy, which results from a single dominant mutation *P*, is known to occur in hermaphroditic as well as in female figs (3, 17); it could have also occurred in the predomesticated fig. Because both parthenocarpic hermaphroditic and female fig trees do not set germinative seeds, they are reproductive dead ends unless humans interfere by planting shoots of these parthenocarpic trees.

We found nine carbonized fig fruits as well as 313 single drupelets, dated between 11,400 and 11,200 years B.P., at the early Pre-Pottery Neolithic A (PPNA) Gilgal village site in the Lower Jordan Valley (Fig. 1). The Gilgal figs are rather small, ~18 mm in diameter, but are ripe, with full-sized drupelets: 1.0 to 1.4 mm. The

carbonized figs were not distorted, implying that they were most probably dried purposely for human consumption. They were found broken into large pieces, revealing their flesh, drupelets, and orifice (Fig. 1 and figs. S1 to S3). Dried figs similar in size and structure imported from Iran are found today in the markets of London. However, the Gilgal figs differ from those of *F. pseudosycororus* grown in neighboring regions. Fruits of the latter species are crowded by wasps and are 10 to 15 mm in diameter, even smaller than the Gilgal variety (18).

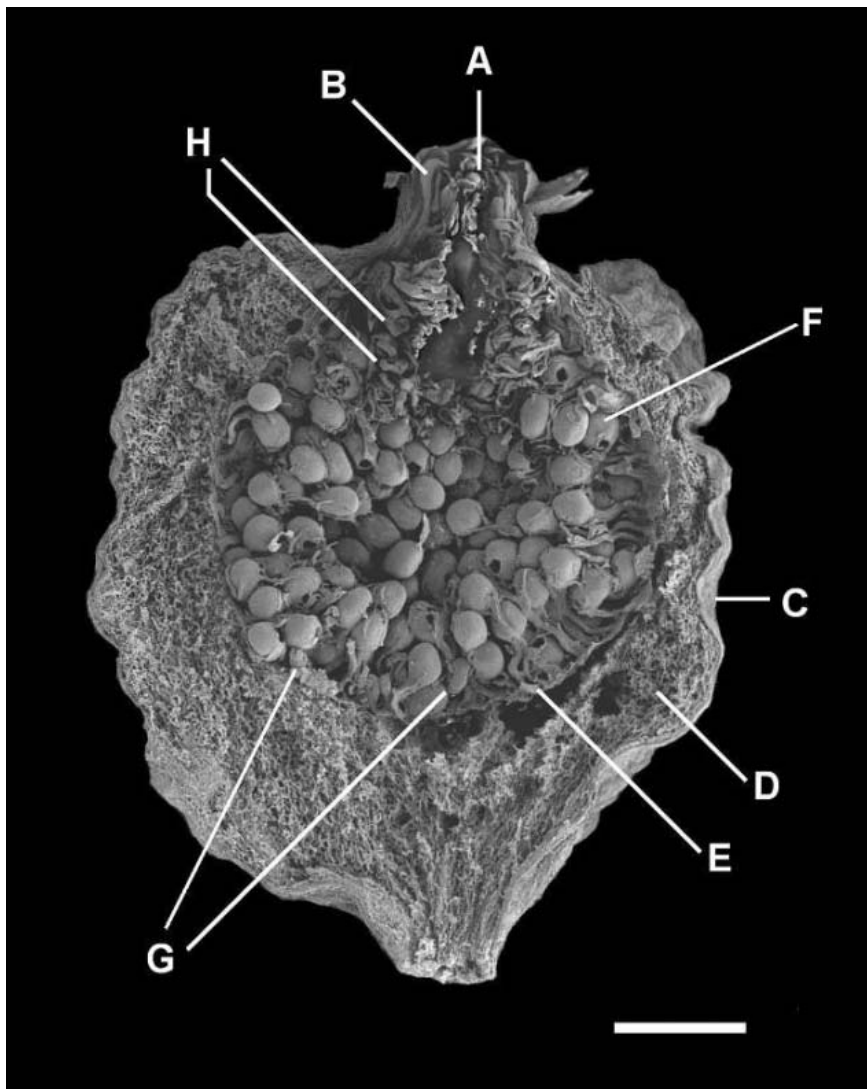
More than 100 of the 313 individual drupelets from ripe fruits were inspected, and most of them were embryoless or had an undeveloped embryo, which reflects parthenocarpy (fig. S3). Such parthenocarpy is observed today in various cultivated fig varieties (fig. S5) (3, 4). It is impossible to distinguish morphologically between fertilized and unfertilized drupelets (19). The small number of drupelets whose cavity seems to be occupied by an embryo (fig. S3) may reflect a natural variation in unfertilized embryos. Alternatively, they might have been fertilized, but their embryo development was arrested before producing full, ripe seed.

The few drupelets that seem to contain an embryo could also be explained by a small number of fertilized drupelets that appeared in a hermaphroditic fig that accidentally produced fruits. This could happen when the wasp population was not large and a single pollen-coated wasp fertilized a small number of short-style female flowers that were not oviposited (4, 13, 20). However, this proposal is unacceptable because no evidence of stamens was observed in the fossil evidence from Gilgal, and not a single drupelet shows any sign of a wasp or wasp exit (compare Fig. 1 to Fig. 2). We therefore conclude that all these remains are of a parthenocarpic variety of *F. carica*.

The large assemblage of parthenocarpic figs uncovered in Gilgal provides early evidence for fig horticulture via vegetative propagation. Once the parthenocarpic mutation occurred, humans must have recognized that the embryoless fruits do not produce new trees, and vegetative fig tree cultivation became a common practice. Additional fig remains are reported from other early Neolithic sites in the Levant (Table 1) (7–10, 21). To confirm our results from Gilgal, we examined several dozen fig drupelets from Netiv Hagdud, an early Neolithic village site that lies 1.5 km west of Gilgal. As was the case in Gilgal, more than 90% lacked embryos, and they are therefore considered to be of the same female variety as at Gilgal. Thus, incipient horticulture by humans commenced with the domestication of fig trees in the Levant at about 11,400 calendar years B.P.

We define domestication in the context of horticulture as a major positive change in the edibility of a wild nonpalatable fruit brought about by a rare genetic event that would disappear without human intervention. In addition, fig trees, whether parthenocarpic or not, are pre-adapted for relatively easy domestication because the cuttings

Fig. 2. Modern hermaphroditic fig fruit (*F. carica* var. *caprificus*) from Kalambaka, Greece, in length section. The orifice (A) is furnished with many scales (B) along its length. The fruit skin (C) covers the spongy fruit flesh (D); the inner part (E) includes many drupelets that exhibit holes through which fig wasps emerged (F). A few wasp males remained within the syconium (G). The stamens (H) are observed below the orifice. Scale bar, 2 mm.



develop roots more easily than those of any other fruit tree (22). Hence, the reported Gilgal figs, stored together with other vegetal staples such as wild barley (*Hordeum spontaneum*), wild oat (*Avena sterilis*), and acorns (*Quercus ithaburensis*), indicate that the subsistence strategy of these early Neolithic farmers was a mixed exploitation of wild plants and initial fig domestication. Apparently, this kind of economy was widely practiced during the second half of the 12th millennium B.P. throughout the Fertile Crescent (23, 24).

References and Notes

- D. Zohary, M. Hopf, *Domestication of Plants in the Old World* (Oxford Univ. Press, New York, ed. 3, 2000).
- G. D. Weiblen, *Am. J. Bot.* **87.9**, 1342 (2000).
- W. B. Storey, in *Advances in Fruit Breeding*, J. Janick, J. N. Moore, Eds. (Purdue Univ. Press, West Lafayette, IN, 1975), pp. 568–589.
- I. J. Condit, *The Fig* (Chronica Botanica, Waltham, MA, 1947).
- J. Galil, *Gard. Bull.* **26**, 303 (1973).
- W. B. Ramirez, *Ann. Mo. Bot. Gard.* **61**, 770 (1974).
- M. Hopf, in *Excavations at Jericho*, K. M. Kenyon, T. A. Holland, Eds. (British School of Archaeology in Jerusalem, London, 1983), vol. 3, pp. 576–610.
- M. E. Kislev, in *An Early Neolithic Village in the Jordan Valley, Part I: The Archaeology of Netiv Hagdud*, O. Bar-Yosef, A. Gopher, Eds. (Peabody Museum of Archaeology and Ethnology, Harvard Univ., Cambridge, MA, 1997), pp. 209–236.
- M. E. Kislev, O. Simchoni, Y. Melamed, in *Gesher: A Pre-Pottery Neolithic A Site in the Central Jordan Valley, Israel. A Final Report*, Y. Garfinkel, D. Dag, Eds. (Ex oriente, Berlin, in press).
- W. van Zeist, J. A. H. Bakker-Heeres, *Palaeohistoria* **26**, 171 [1984 (1986)].
- N. F. Miller, in *Progress in Old World Palaeoethnobotany*, W. van Zeist, K. Wasylikowa, K.-E. Behre, Eds. (Balkema, Rotterdam, 1991), pp. 133–160.
- C. O. Sauer, *Seeds, Spades, Hearths, and Herds* (MIT Press, Cambridge, MA, 1969).
- L. Stager, in *Palestine in the Bronze and Iron Age: Papers in Honour of Olga Tufnell*, J. N. Tubb, Ed. (Institute of Archaeology, London, 1985), pp. 172–188.
- G. Neeman, J. Galil, *New Phytol.* **81**, 375 (1978).
- G. Valdeyron, D. G. Lloyd, *Evolution* **33.2**, 673 (1979).
- T. L. Parrish, H. P. Koelewijn, P. J. van Dijk, *Sex. Plant Reprod.* **17**, 17 (2004).
- W. F. Saleeb, thesis, University of California, Riverside, CA (1965).
- M. Zohary, *Flora Palaestina* (The Israel Academy of Sciences and Humanities, Jerusalem, 1966), vol. 1, pp. 37–38.
- M. Flaishman, personal communication.
- J. Galil, G. Neeman, *New Phytol.* **79**, 163 (1977).
- The full set of data and references for the sites are available as supporting material on Science Online.
- A. Erez, personal communication.
- T. Noy, *Palaeorient* **15.1**, 11 (1989).
- M. E. Kislev, A. Hartmann, T. Noy, in *Gilgal: Early Neolithic Occupation in the Lower Jordan Valley, the Excavations of Tamar Noy*, O. Bar-Yosef, A. Gopher, N. Goring-Morris, Eds. (Brill Academic Publishers, in press).
- We thank D. Zohary, M. A. Flaishman, and S. Lev-Yadun for helpful suggestions. Supported by the Israel Science Foundation, founded by the Israel Academy of Sciences and Humanities (grant no. 903/99); the American School of Prehistoric Research (Peabody Museum, Harvard Univ.); the Israel Museum (Jerusalem); and the Koschitzky Foundation (Land of Israel Studies and Archaeology Department, Bar-Ilan Univ., Israel). We are grateful to A. Gopher (Institute of Archaeology, Tel Aviv University) and N. Goring-Morris (Institute of Archaeology, Hebrew University, Jerusalem) for their help, and E. Boaretto (Kimmel Center, Weizmann Institute of Science) for providing the radiocarbon dates from Gilgal I and III. We thank the Shelby-White-Leon Levi foundation for providing the funds for the final study of the Gilgal finds and the radiocarbon dates.

Supporting Online Material

www.sciencemag.org/cgi/content/full/312/5778/1372/DC1

Figs. S1 to S5

Table S1

References

7 February 2006; accepted 19 April 2006
10.1126/science.1125910

Size Matters More Than Chemistry for Cloud-Nucleating Ability of Aerosol Particles

U. Dusek,¹ G. P. Frank,¹ L. Hildebrandt,^{1,4} J. Curtius,³ J. Schneider,² S. Walter,² D. Chand,¹ F. Drewnick,² S. Hings,² D. Jung,³ S. Borrmann,^{2,3} M. O. Andreae¹

Size-resolved cloud condensation nuclei (CCN) spectra measured for various aerosol types at a non-urban site in Germany showed that CCN concentrations are mainly determined by the aerosol number size distribution. Distinct variations of CCN activation with particle chemical composition were observed but played a secondary role. When the temporal variation of chemical effects on CCN activation is neglected, variation in the size distribution alone explains 84 to 96% of the variation in CCN concentrations. Understanding that particles' ability to act as CCN is largely controlled by aerosol size rather than composition greatly facilitates the treatment of aerosol effects on cloud physics in regional and global models.

The response of cloud characteristics and precipitation processes to increasing anthropogenic aerosol concentrations is one of the largest uncertainties in the current understanding of climate change (1, 2). A major challenge is to determine the ability of aerosols to act as cloud condensation nuclei (CCN) at water vapor supersaturations S (percentage of relative humidity minus 100%) that are relevant for atmospheric conditions. CCN activation of aerosols is therefore being studied intensively in laboratory and field experiments (3–10). To a first approximation, the ability of a particle to act as a CCN at a given S depends on the number of potential solute molecules it contains, which is a function of its size and composition. Thus, knowledge of both particle size distribution and size-resolved particle composition is necessary to predict ambient CCN concentrations (11). Although size distributions can be measured automatically in situ or even remotely, the determination of aerosol chemical composition is much more demanding. Moreover, the effects of organic compounds on CCN activation are not completely understood (12). If the effects of chemical composition on CCN activation could be parameterized for certain regions or aerosol types, this would considerably simplify estimation and modeling of CCN concentrations. It is therefore of great importance to assess the relative contributions of particle size distribution and chemical composition to CCN activity.

Toward this goal, we investigated the CCN activation of aerosols as a function of preselected particle sizes, to separate the effect of particle composition from that of size. This technique is commonly used in the laboratory (3–6) but rarely in the ambient atmosphere

(13, 14). We used a differential mobility analyzer to select a narrow particle size range from the total aerosol population. These particles were passed to a CCN counter (15), which measured the number of activated CCN as a function of S , while a condensation particle counter in parallel determined the total particle concentration (CN) in the selected size fraction. This information was used to derive the CCN/CN ratio at each particle diameter and S . The size-resolved CCN/CN ratio is further referred to as CCN efficiency (16).

The S at which particles of equal size are activated is dependent on particle composition and/or shape. For monodisperse particles, the dependence of the CCN efficiency on S (the CCN spectrum) can therefore serve as an empirical measure of all chemical effects on CCN ac-

tivation, including the effects of slightly soluble organics (17) and of surface active compounds (18). Additionally, possible external mixtures of particles with respect to their CCN properties can be identified (19).

Size-resolved CCN measurements were conducted during the Feldberg Aerosol Characterization Experiment (FACE-2004) field experiment, which took place at the Taunus Observatory (50.2°N, 8.4°E; Kleiner Feldberg, central Germany) from 20 July until 11 August 2004. During the measurement period, diverse air masses were encountered, including aged continental air masses, marine air masses that had moved in rapidly from the North Atlantic, and fresh pollution from the densely populated and industrialized Rhine-Main area, ~20 km to the southeast and southwest of the field site.

Figure 1A shows a representative example of 6-hour averaged CCN efficiencies. At S between 0.25 and 1.5%, the crucial size range for CCN activation is 40 to 120 nm (electrical mobility diameter, d_p). Particles much larger than $d_p = 120$ nm are generally activated at all investigated values of S regardless of their composition, whereas particles <40 nm require unrealistically high S for activation. Between these two extremes, a strong dependence of CCN efficiency on particle size is apparent. Particles with diameters of 40 nm typically require S of up to 1.5% for activation, whereas particles with diameters of 80 nm require S of ~0.5%. The question to be addressed here is whether the effect of particle composition on CCN activation can rival its strong dependence on size.

We illustrate this problem by comparing measurements in air masses representing extremes of chemical compositions encountered

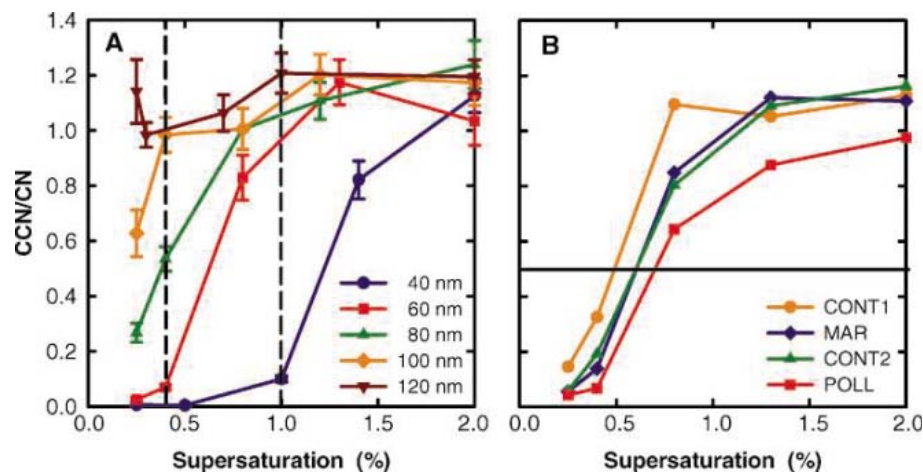


Fig. 1. (A) An example of size-resolved 6-hour averaged CCN spectra for particle diameters between 40 and 120 nm. Sixteen individual spectra have been averaged for each diameter. Error bars correspond to 95% confidence intervals of the mean. Vertical lines indicate the S values of 0.4 and 1% for which CCN size distributions are derived. CCN/CN ratios that are higher than 1 are due to a small bias in the calibration of the sensing volume, which probably changed slightly during the transport of the instrument to the field site. (B) The CCN spectra of particles with $d_p = 60$ nm are compared for different air mass conditions: CONT1 represents aged industrial pollution, MAR aerosol with Atlantic origin and short transport times over land, CONT2 rural continental aerosol, and POLL urban aerosol after a few hours of aging.

¹Department of Biogeochemistry, ²Department of Particle Chemistry, Max Planck Institute for Chemistry, Mainz 55128, Germany. ³Johannes Gutenberg University, Institute for Atmospheric Physics, Mainz 55128, Germany. ⁴California Institute of Technology, Pasadena, CA 91125, USA.

Table 1. Overview of the four air mass cases selected for the case study. The particle chemical composition refers to the size range from $d_p = 0$ to 130 nm, averaged over the respective measurement periods. "Inorg." stands for the mass concentration of NH_4^+ , SO_4^{2-} , and NO_3^- ; "Org." for the mass concentration of

	Time period	Inorg. ($\mu\text{g}/\text{m}^3$)	Org. ($\mu\text{g}/\text{m}^3$)	Inorg./total	Recent pollution	$S = 0.4\%$ cutoff diameter (nm)	Air mass origin
CONT1	7/31 18:00 – 8/1 18:00	1.72	2.38	0.42	No	66	Industrial (Ruhr region)
MAR	7/27 00:00 – 7/28 00:00	0.42	0.86	0.33	No	72.5	Atlantic
CONT2	7/22 00:00 – 7/23 00:00	0.66	1.92	0.26	No	73.6	France
POLL	8/2 12:00 – 8/3 18:00	0.47	2.13	0.18	Yes	83.4	N. Germany and Denmark

during FACE-2004 (Table 1 and Fig. 1B) (16). Two continental cases are considered: CONT1 is characterized by air masses arriving from heavily industrialized regions in the Netherlands and Germany, and CONT2 by air masses from more rural areas in France and southern Belgium. MAR represents marine air masses from the Atlantic, with transport times across Germany of less than 1 day. Local trajectories and wind directions (northwest to east) indicate that in these three cases, the air reached our site after traveling over forested areas for a few hours. Case POLL gives an example of recent pollution during southeasterly wind conditions (from the Frankfurt/Rhine Main area). For back trajectories, see fig. S3.

The composition of the nonrefractory aerosol components was measured by an Aerosol Mass Spectrometer (AMS) (20) in the size range from 40 to 1000 nm (16). In the CCN-relevant size range of $d_p < 130$ nm, the composition was dominated by organic material, followed by ammonium, sulfate, and nitrate. During CONT1, the mass fraction of inorganic ions in this size range was as high as 42%, whereas case POLL contained very little inorganic material, only 18% by mass for particles with $d_p < 130$ nm. The aerosol chemical compositions observed during the campaign span the range that is typical of near-urban to background sites in Europe (21). In the size range of $d_p < 150$ nm, soluble ions rarely make up more than 50% by mass (11, 21). On the other hand, soluble-ion fractions $<15\%$ are mostly found close to sources and in urban areas and increase quickly during atmospheric aging and mixing processes. Typically, about 50% of the organic fraction is also water-soluble and contributes to CCN activity (22).

Figure 1B shows that, in spite of the diverse origins and compositions of the aerosols in these four air mass types, the CCN spectra for a fixed size class (here 60 nm) resemble each other very closely. The S at which 50% of the particles are activated varies by only $\pm 0.1\%$ around the mean value of 0.6% for this size class.

To derive the size distributions of CCN at a given S (for example, at 0.4 and 1%, Fig. 2), the size-resolved CCN spectra (Fig. 1A) are combined with aerosol number size distributions. First, the CCN efficiencies are linearly interpolated to $S = 0.4$ and 1% (dashed lines, Fig. 1A).

organic material; and "Inorg./total" for the mass fraction of inorganic material. The influence of recent pollution from the Frankfurt region was identified by local wind directions from the southeast. The origin of the air mass was determined by 4-day air mass back trajectories [see supporting online material C (16)].

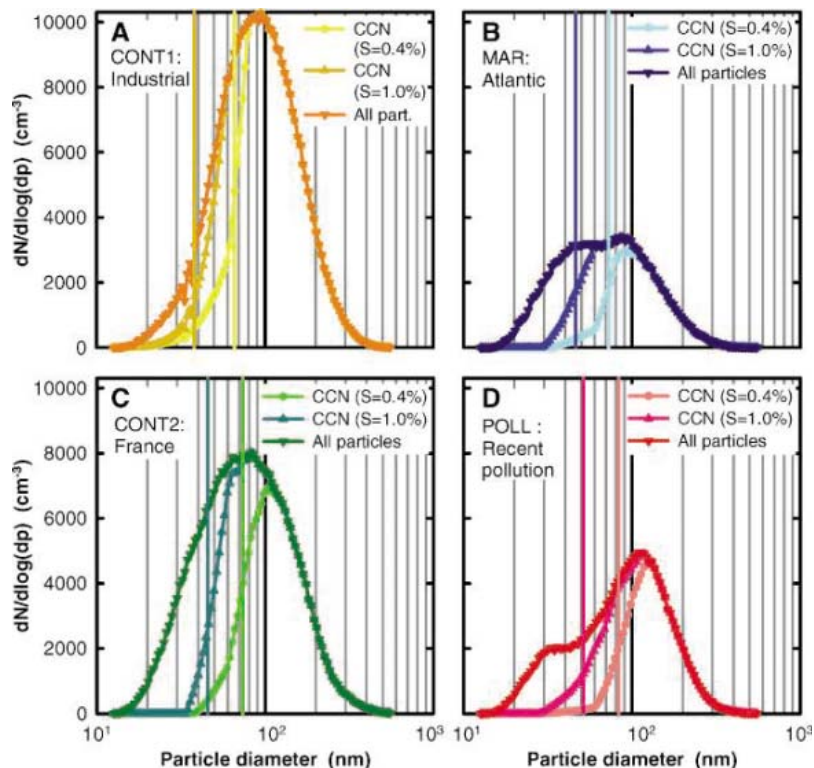


Fig. 2. (A to D) Particle number size distributions and CCN size distributions for the four chosen case studies. The colored vertical lines indicate the respective cutoff diameters: (the diameters where 50% of the particles are activated) at $S = 0.4\%$ and $S = 1.0\%$.

The resulting dependence of CCN efficiency on particle size is then used to derive the CCN size distributions (Fig. 2). For each value of S , the CCN concentration gradually increases toward larger diameters (Fig. 2), instead of showing a sharp cutoff activation diameter, as expected from an internally mixed aerosol. This reflects a certain degree of external mixing in ambient aerosols, as well as the fact that the particles are not exactly monodisperse (23).

We define effective cutoff diameters for each S (indicated as colored vertical lines in Fig. 2) as that diameter where the CCN efficiency reaches 0.5. These effective cutoff diameters are inversely related to the inorganic ion fraction of particles with $d_p < 130$ nm (see Table 1 for $S = 0.4\%$), as would be expected because organic compounds are usually less CCN-active than inorganic salts

(6). However, an increase in inorganic ion content by more than a factor of 2 [reflecting the entire range of composition from fresh pollution (POLL) to aged aerosol (CONT1)] is associated with a decrease in the cutoff diameter of less than 20 nm.

Total CCN concentrations (CCN_{tot}) at a certain S , obtained by integration of the CCN size distributions in Fig. 2, depend both on the total particle concentration and on the fraction of particles activated at the given S , which is a function of both the shape of the size distribution and of particle composition. For example, in CONT1, high CCN efficiency combined with a large modal diameter leads to the highest CCN_{tot} observed during the campaign ($\sim 4500 \text{ cm}^{-3}$ at $S = 0.4\%$). This is considerably higher than in CONT2 ($\sim 3000 \text{ cm}^{-3}$), where both modal diameter and CCN efficiency are lower, whereas total particle concentrations are com-

parable [6300 cm^{-3} (CONT1) versus 5800 cm^{-3} (CONT2)].

We performed sensitivity studies to gain further insight into the roles of total number concentration, shape of the size distribution, and size-resolved CCN efficiencies (that is, particle chemical composition) in determining CCN_{tot} . As a base case, we calculated a time series of 6-hour averaged CCN_{tot} for the entire measurement period, using the measured size distributions and CCN efficiencies. Then we calculated two modified CCN time series: (i) using fixed CCN efficiencies (campaign average) but variable size distributions, and (ii) using a fixed size distribution (campaign average) but variable CCN efficiencies reflecting variable chemical composition (16). A correlation of these modified time series with the base case shows that the size distribution has by far the dominant role in determining CCN_{tot} (Fig. 3, A and B, for $S = 0.4\%$; fig. S4 for $S = 0.25$ and 1.0%). At constant composition and CCN efficiency (case i), variations in the size distribution alone explain from 84% (at $S = 0.25\%$) to 96% (at $S = 1\%$) of the temporal variation in CCN_{tot} . When, on the other hand, a constant mean size distribution (case ii) is assumed, detailed knowledge of the CCN efficiencies is not very helpful in predicting CCN_{tot} ($R^2 \sim 0.3$).

To eliminate the effect of variable total particle concentrations, we investigated how the fraction of particles that can act as CCN (hereafter referred to as the activated fraction) depends on size distribution and CCN efficiencies. For this purpose, we conducted a similar sensitivity study for the activated fraction, calculated as $\text{CCN}_{\text{tot}}/\text{CN10}$, where CN10 denotes the total number concentration of particles $>10 \text{ nm}$ (Fig. 3, C and D, for $S = 0.4\%$; fig. S5 for $S = 0.25$ and $S = 1\%$). The main conclusion remains similar: Variations in the shape of the size distribution explain $\sim 80\%$ of the variation in the activated fraction at S ranging from 0.25 to 1%, whereas variations in the composition (CCN efficiency) explain only 20% ($S = 1\%$) to 63% ($S = 0.25\%$). Figure 3D clearly shows the weak effect that variations in chemical composition have when the size distribution is held constant. The low sensitivity of the activated fraction to CCN efficiency at high S is due to the fact that the activation happens at smaller particle size (Fig. 2), where the size distribution was particularly variable in our measurements. Only at a low S of 0.25% do the CCN efficiencies show some significant correlation with $\text{CCN}_{\text{tot}}/\text{CN10}$. Here, cutoff diameters are near the size mode, which makes the activated fraction relatively sensitive to small changes in composition. However, assuming constant mean CCN efficiencies still gives an adequate prediction of the activated fraction (fig. S5, A and B).

These sensitivity studies confirm that it is more important to know the aerosol number

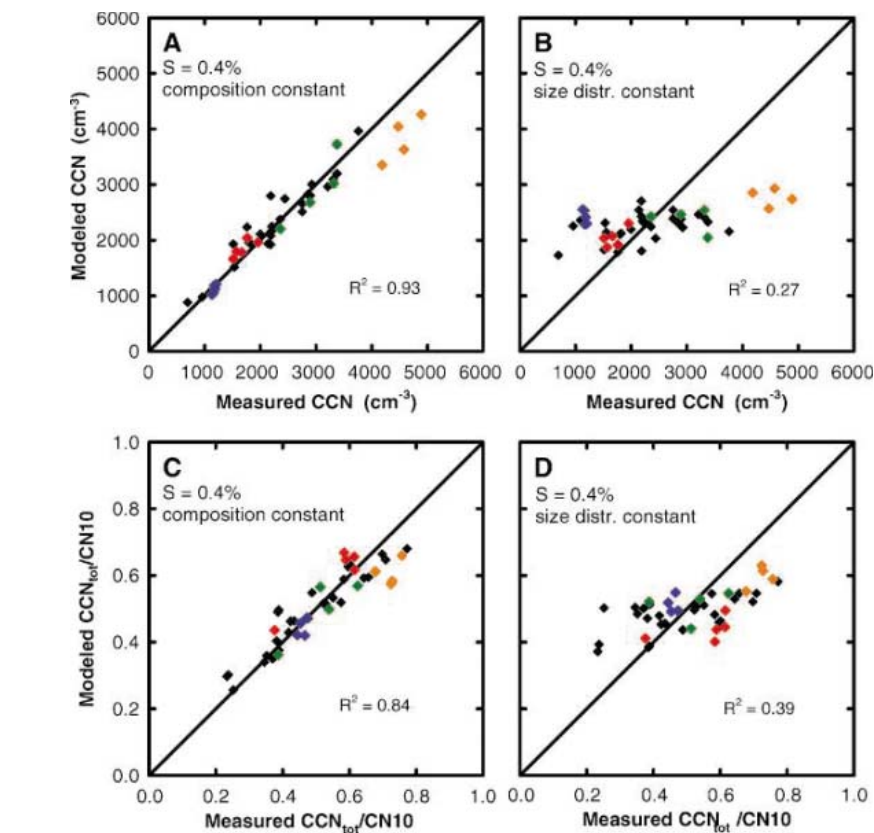


Fig. 3. (A) Correlation of the actual CCN concentration time series with a calculated time series derived using constant mean CCN efficiencies reflecting constant composition. Data points representing high CCN efficiencies tend to lie below the 1:1 line; data points representing low CCN efficiencies tend to lie above the 1:1 line. (B) Correlation of the actual CCN concentration time series with a calculated time series derived using constant mean size distributions but variable composition (CCN efficiencies). (C) same as (A) for activated fractions $\text{CCN}_{\text{tot}}/\text{CN10}$, (D) same as (B) for activated fractions $\text{CCN}_{\text{tot}}/\text{CN10}$. The data points corresponding to the case studies presented in Table 1 and Fig. 2 are marked in the respective colors.

size distribution accurately to achieve a good estimate of CCN_{tot} than to know the detailed particle chemistry or precise size-resolved CCN efficiencies. This result is supported by model studies that suggest that the influence of particle composition on cloud droplet number is moderate (24), even if the effects of realistic mixtures of organic species are considered (25, 26). Our results show that in order to improve our understanding of atmospheric CCN, investigations of CCN activities of specific aerosol components must be complemented by careful studies of the aerosol size distribution and its dependence on atmospheric processes (27).

Although our results are from a continental site in Europe, we expect the primary role of particle size in CCN activation to apply generally. The fundamental reason is that the critical supersaturation (S_c) depends to first approximation on the total number of soluble molecules in the particle. This number depends only linearly on the soluble mass fraction, but to the third power on d_p , making particle size the dominant parameter in controlling S_c . Only in the case of insoluble particles, such as mineral

dust, can adding a trace amount of soluble material reduce S_c drastically (28, 29) and composition can then become dominant. The specific cutoff diameters can vary with aerosol type (for example, there are smaller cutoff diameters for marine aerosol). However, cutoff diameters derived for moderately aged biomass smoke and Amazonian background aerosols are nearly identical to those in our POLL case (30), making our results more generally applicable.

The secondary role of particle composition has great advantages for estimating CCN concentrations from observations and for their parameterization in cloud and climate modeling. With the knowledge of typical size-resolved CCN efficiencies (or cutoff diameters) that are representative of key regions and aerosol types, CCN concentrations can be estimated from observed or modeled size distributions. Establishing a database of such size-resolved CCN efficiencies should be the focus of field studies in different locations. For the purpose of modeling CCN on a global or local scale, more effort should be spent on

accurately predicting particle size distributions than on predicting detailed chemical composition. Although particle chemistry is important to model aerosol growth and transformation processes, the complex effects of particle chemical composition on CCN activation could be parameterized by cutoff diameters depending on location and/or aerosol type without introducing large errors. Assuming a “typical” size distribution (such as for a generalized “continental” aerosol) will lead to much larger errors than assuming a “typical” composition. Our findings also provide a basis for the estimation of CCN abundances over larger time and space scales by remote sensing, because aerosol size distributions are inherently more accessible by remote sensing than particle compositions. Because current sensors are limited, however, in their ability to detect particles in the CCN-relevant size range of 50 to 150 nm, this requires the development of appropriate sensors.

References and Notes

- U. Lohmann, J. Feichter, *Atmos. Chem. Phys.* **5**, 715 (2005).
- M. O. Andreae, C. D. Jones, P. M. Cox, *Nature* **435**, 1187 (2005).
- H. Giebl *et al.*, *J. Aerosol Sci.* **33**, 1623 (2002).
- K. Broekhuizen, P. P. Kumar, J. P. D. Abbatt, *Geophys. Res. Lett.* **31**, L01107 (2004).
- M. Bilde, B. Svenningsson, *Tellus* **56B**, 128 (2004).
- T. M. Raymond, S. P. Pandis, *J. Geophys. Res.* **108**, 4787 (2002).
- P. Y. Chuang *et al.*, *Tellus* **52B**, 843 (2000).
- T. M. VanReken *et al.*, *J. Geophys. Res.* **108**, 4633 (2003).
- G. C. Roberts, M. O. Andreae, J. Zhou, P. Artaxo, *Geophys. Res. Lett.* **28**, 2807 (2001).
- J. R. Snider, J.-L. Brenguier, *Tellus* **52B**, 828 (2000).
- G. McFiggans *et al.*, *Atmos. Chem. Phys. Discuss.* **5**, 8507 (2005).
- R. J. Charlson *et al.*, *Science* **292**, 2025 (2001).
- J. G. Hudson, X. Da, *J. Geophys. Res.* **101** (D2), 4435 (1996).
- J. W. Fitzgerald, W. A. Hoppel, M. A. Vietti, *J. Atmos. Sci.* **39**, 1838 (1982).
- G. P. Frank, U. Dusek, M. O. Andreae, *Atmos. Chem. Phys. Discuss.* **6**, 2151 (2006).
- Materials and methods are available as supporting material on Science Online.
- M. Shulmann, M. C. Jacobson, R. J. Charlson, R. E. Synovec, T. E. Young, *Geophys. Res. Lett.* **23**, 277 (1996).
- M. C. Facchini, M. Mircea, S. Fuzzi, R. J. Charlson, *Nature* **401**, 257 (1999).
- U. Dusek *et al.*, *Geophys. Res. Lett.* **32**, L11802 (2005).
- J. T. Jayne *et al.*, *Aerosol Sci. Technol.* **33**, 49 (2000).
- J. P. Putaud *et al.*, *Atmos. Environ.* **38**, 2579 (2004).
- M. Kanakidou *et al.*, *Atmos. Chem. Phys.* **5**, 1053 (2005).
- G. P. Frank, U. Dusek, M. O. Andreae, *Atmos. Phys. Chem. Discuss.*, in press.
- G. Feingold, *Geophys. Res. Lett.* **30**, 1997 (2003).
- U. Lohmann, K. Broekhuizen, R. Leaitch, N. Schantz, *Geophys. Res. Lett.* **31**, L05108 (2004).
- B. Ervens, G. Feingold, S. M. Kreidenweis, *J. Geophys. Res.* **110**, D18211 (2005).
- D. S. Covert, V. N. Kapustin, T. S. Bates, P. K. Quinn, *J. Geophys. Res.* **101**, 6919 (1996).
- U. Dusek, G. P. Reischl, R. Hitzinger, *Environ. Sci. Technol.* **40**, 1223 (2006).
- Z. Levin, A. Teller, E. Ganor, Y. Yin, *J. Geophys. Res.* **110**, D20202 (2005).
- E. Swietlicki, personal communication.
- We thank H. Bingemer from the University of Frankfurt and the Taunus Observatory team for their help, B. Fay from the German Weather Service for providing trajectory analysis data, and H. Wernli for help with the trajectory interpretation. The Max Planck Society and the University of Mainz are acknowledged for funding the FACE-2004 measurement campaign. We thank the University of Frankfurt for access to the facilities at the Taunus Observatory for the duration of the FACE-2004 campaign. We thank D. Rosenfeld and Z. Levin for valuable comments on the manuscript.

Supporting Online Material

www.sciencemag.org/cgi/content/full/312/5778/1375/DC1

Materials and Methods

Figs. S1 to S5

References

23 January 2006; accepted 14 April 2006

10.1126/science.1125261

A New Genus of African Monkey, *Rungwecebus*: Morphology, Ecology, and Molecular Phylogenetics

Tim R. B. Davenport,^{1*} William T. Stanley,² Eric J. Sargis,³ Daniela W. De Luca,¹ Noah E. Mpunga,¹ Sophy J. Machaga,¹ Link E. Olson⁴

A new species of African monkey, *Lophocebus kipunji*, was described in 2005 based on observations from two sites in Tanzania. We have since obtained a specimen killed by a farmer on Mount Rungwe, the type locality. Detailed molecular phylogenetic analyses of this specimen demonstrate that the genus *Lophocebus* is diphyletic. We provide a description of a new genus of African monkey and of the only preserved specimen of this primate. We also present information on the animal's ecology and conservation.

A previously unknown monkey from southern Tanzania was recently discovered and described as the new species *Lophocebus kipunji*, depicting the holotype and paratype with photographs (1). On 3 August 2005, a subadult male monkey matching the species description of *L. kipunji* (1) was found dead in a trap set by a resident farmer in a

maize field adjacent to the forest on Mount Rungwe in southwestern Tanzania. The specimen was preserved and deposited at the Field Museum of Natural History (FMNH) in Chicago, USA, as a study skin, skull, and partial skeleton (bones from the right fore- and hindlimbs). Muscle tissue was collected for molecular analyses, and the remaining cadaver was preserved in fluid. Although a subadult, the specimen exhibits features differentiating it from any other known primate species (1).

The specimen matches the original description of *L. kipunji* (1) in having black eyelids that do not contrast with the color of the face (fig. S1), a crown with a broad erect crest of hair (figs. S1 and S2), long cheek whiskers (fig. S2), and an off-white distal half of the tail [fig. S2 and supporting online material (SOM) text].

The individual was a subadult on the basis of the presence of deciduous canines and premolars, eruption of only the first molars (SOM text), and the lack of a fused suture between the basioccipital and basisphenoid bones (Fig. 1). Although not fully grown, the skull does exhibit some of the features characteristic of *Lophocebus* compared with *Cercocebus* (2), such as a relatively narrow zygomatic breadth, zygoma that turn smoothly toward the skull at their posterior ends, and upper and lower margins of the mandible divergent anteriorly (Fig. 1). In the postcranium, the long-bone epiphyses are fused to the diaphyses, but many features are not yet fully developed, including those distinguishing the *Lophocebus-Theropithecus-Papio* clade from the *Cercocebus-Mandrillus* clade (3). One postcranial feature, the ratio of scapular width to length, appears to distinguish *L. kipunji* from *Papio*, which has a relatively long and narrow scapula (3).

Mangabeys were once considered to be monophyletic based on their phenotypic similarities (4), and all species were included in *Cercocebus*. After immunological studies (5) and because of cranial differences and a resemblance between *Lophocebus* and *Papio* in some of those features, they were divided into *Cercocebus* and *Lophocebus* (2). Characters that have historically been used to unite mangabeys were discounted as being erroneous observations or convergent similarities (2). It was stated that *Lophocebus*, unlike *Cercocebus*, has dark eyelids that are not lighter than the facial skin, and the deep suborbital fossae of mangabeys may have evolved independently in relation to facial shortening (2). This generic

¹Wildlife Conservation Society, Southern Highlands Conservation Programme, Post Office Box 1475, Mbeya, Tanzania.

²Department of Zoology, Field Museum of Natural History, 1400 South Lake Shore Drive, Chicago, IL 60605, USA.

³Department of Anthropology, Yale University, Post Office Box 208277, New Haven, CT 06520, USA. ⁴University of Alaska Museum, 907 Yukon Drive, Fairbanks, AK 99775, USA.

*To whom correspondence should be addressed. E-mail: tdavenport@wcs.org

division was corroborated by analyses of both mitochondrial and nuclear data (6–9), suggesting that *Cercocebus* is the sister taxon to *Mandrillus*, whereas *Lophocebus* is more closely related to *Papio* and *Theropithecus*, and the deep suborbital fossae represent a homoplastic character that evolved more than once in Papionini, the cercopithecine tribe that includes macaques, mangabeys, baboons, geladas, mandrills, and drills. Recently, several putatively derived postcranial features and one dental character that unite the *Lophocebus-Papio-Theropithecus* clade, as well as one apomorphic postcranial feature shared by *Cercocebus* and *Mandrillus*, were identified (3). Hence, both morphological and molecular evidence indicates that the phenetic similarities shared by *Cercocebus* and *Lophocebus* are not indicative of a close phylogenetic relationship.

To determine the phylogenetic affinities of *L. kipunji*, we conducted maximum likelihood and Bayesian analyses (SOM text) (10) of DNA sequence data obtained from the specimen from Mount Rungwe, including 390 base pairs (bp) of the mitochondrial (mtDNA) 12S ribosomal RNA (rRNA) gene (12S), 686 bp of the mtDNA cytochrome *c* oxidase subunit I gene (COI), 684 bp of the mtDNA cytochrome *c* oxidase subunit II gene (COII), 573 bp of the *y*-linked testis-specific protein gene (TSPY), and 486 bp of the autosomal alpha-1,3-galactosyltransferase pseudogene (α 1,3-GT). Phylogenetic analysis of each individual gene with a diverse sample of homologous cercopithecoid sequences available on GenBank either strongly supported [all three mtDNA genes (e.g., Fig. 2)], weakly supported (α 1,3-GT), or failed to contradict (TSPY) a clade uniting *L. kipunji* with *Papio* (figs. S3 to S8). All single-gene maximum likelihood analyses in which two or more species of *Papio* were included recovered a monophyletic *Papio* as either the sister-taxon to *L. kipunji* (COI and COII) or part of an unresolved trichotomy with *L. kipunji* and *Theropithecus* (12S) (SOM text). No single-gene analysis recovered a monophyletic *Lophocebus*, yet all data sets in which *L. kipunji*, *L. aterrimus*, and *L. albigena* were included (COII, TSPY, and α 1,3-GT) strongly supported a sister taxon relationship between the latter two species (SOM text). We therefore concatenated the 12S sequence for *L. aterrimus* with the remaining sequences for *L. albigena* and performed analyses on two combined data sets, one including all three mtDNA genes (17 taxa, 1732 included positions) and the other including all mtDNA genes and both nuclear genes (9 taxa, 2959 included positions). As with the individual gene analyses, *L. kipunji* was strongly supported as the sister taxon to *Papio* (Figs. 3 and 4).

Despite the compelling molecular evidence that *L. kipunji* is more closely related to *Papio* than it is to its putative congeners, it lacks the diagnostic morphological features required to place it in that genus, such as the long rostrum

or deep mandibular fossae characteristic of *Papio* (as well as *Theropithecus* and *Mandrillus*). Furthermore, although *L. kipunji* possesses deep suborbital fossae on the maxillae, like those of *Lophocebus* and *Cercocebus*, these can easily be distinguished from the deep maxillary fossae present on the rostrum of *Papio* (as well as *Theropithecus* and *Mandrillus*) (Fig. 1). In summary, molecular evidence precludes the inclusion of *L. kipunji* in *Lophocebus* and morphological evidence prohibits its placement in *Papio*, thereby making it necessary to name a new genus.

Rungwecebus Davenport, Stanley, Sargis, De Luca, Mpunga, Machaga, and Olson genus nov.

Lophocebus Palmer, 1903; type species *Presbytis albigena* Gray, 1850.

Lophocebus kipunji Ehardt, Butynski, Jones, and Davenport, 2005.

Holotype. Adult male in photograph taken in the type locality at 9°07'S 33°44'E (1).

Paratype. Adult in photograph taken in Ndundulu Forest Reserve at 07°48'45"S 36°31'05"E, Udzungwa Mountains, Tanzania (1).

Specimen examined. FMNH 187122. Subadult male collected on the southwestern slopes of Mount Rungwe, Rungwe District, Mbeya Region, Tanzania, 09°09'50"S 33°37'55"E, 1769 m above sea level (asl).

Type locality. Rungwe-Livingstone (09°07' to 09°11'S and 33°36' to 33°55'E), Southern Highlands, Tanzania.

Diagnosis. Pelage of dorsum light to medium gray-brown, center of ventrum and distal half of tail off-white (fig. S2). Crown with very long, broad, erect crest of hair (fig. S1). Eyelids black, not contrasting with color of face (fig. S1). Tail longer than body, mainly curled up and backward at rest and during locomotion (fig. S2). Adults emit a distinctive, loud, low-pitched “honk-bark” (1). Predominantly arboreal. Found only at high altitudes (1300 up to 2450 m asl) and low-temperature tolerant.

Measurements. Head-body length of adult males in the Rungwe-Livingstone population estimated at 85 to 90 cm. Adult male body weight estimated at 10 to 16 kg (1). Measurements of preserved subadult male (taken before preservation) include total length, 894 mm; head and body length, 370 mm; tail length, 499 mm; hindfoot length (nail included), 128 mm; ear length, 35 mm; and mass, approximately 4000 g.

Etymology. The genus name acknowledges Mount Rungwe, where this monkey was first observed and which is home to the largest known population of the genus. Because of the demonstrated polyphyly of “mangabeys” and the ambiguity that common name now carries, we suggest the common name of members of this genus to be “kipunji.”

Distribution. Known to occur in about 70 km² of Rungwe-Livingstone in the Southern



Fig. 1. Skull of *Rungwecebus kipunji* (FMNH 187122). Photographs show lateral (A) and anterior (B) views of the cranium and mandible and occlusal views of the cranium (C) and mandible (D).

Highlands, Tanzania, from 1750 up to 2450 m asl and from about 3 km² of Ndundulu Forest Reserve, Tanzania, from 1300 to 1750 m asl.

Habitat. From pristine submontane forest in Ndundulu to degraded montane and upper montane forest in Rungwe-Livingstone.

Rungwecebus differs from mangabeys, baboons, and geladas (11) as follows: (i) *Rungwecebus* is more closely related to *Papio* than to *Lophocebus*, *Theropithecus*, *Cercocebus*, or *Mandrillus* based on molecular evidence. (ii) *Rungwecebus* differs from the semiterrestrial *Cercocebus* (2) in being predominantly arboreal and having noncontrasting eyelids (fig. S1). (iii) *Rungwecebus* differs from *Lophocebus* (12, 13) in having a light to medium gray-brown pelage, an off-white center of ventrum and distal half of tail, and crown with very long, broad, erect crest of hair (fig. S1). *Rungwecebus* usually holds its tail curled up and backward (fig. S2), but very rarely vertical

or arched forward. *Rungwecebus* gives a distinctive “honk-bark” when conspecific groups meet (1) and when threatened. The “honk-bark” bears some structural similarity with the *Papio* “roar-grunt” (14), but *Rungwecebus* does not emit the “whoop-gobble” loud-call characteristic of *Lophocebus* and *Cercocebus torquatus atys* (15, 16). (iv) *Rungwecebus* differs from *Papio* and *Theropithecus* in that it lacks the long rostrum and deep mandibular fossae characteristic of these genera (and *Mandrillus*). *Rungwecebus* possesses deep suborbital fossae on the maxillae similar to those of *Lophocebus* and *Cercocebus*, but these are distinct from the deep maxillary fossae present on the rostrum of *Papio* and *Theropithecus* (and *Mandrillus*). *Rungwecebus* is smaller in body size and more arboreal than *Papio* and *Theropithecus*.

Rungwecebus kipunji is endemic to Tanzania and known only from the Rungwe-Livingstone

forest in the Southern Highlands and the Ndundulu Forest in the Udzungwa Mountains. The remote and unexplored nature of these forests and the cryptic nature of the animal may explain why the kipunji has remained undetected for so long. Recent discoveries in Ndundulu have revealed other vertebrates that show ancient and geographically distant affinities with taxa in western Africa or Asia (17, 18). Furthermore, *Rungwecebus* demonstrates the critical biogeographical importance of Tanzania’s Southern Highlands relative to the Eastern Arc Mountains.

Social groups comprise several adult males and females. In three focal groups studied (SOM text), there was a maximum of two infants per group, but there is no evidence that solitary animals occur. Group size estimates are from 30 to 36 individuals with a mean of 32.33 (SE 1.86; $n = 3$), larger than usually found in *Lophocebus* (13). Home range estimates were from 0.24 to 0.99 km² with a mean of 0.54 km² (SE 0.132; $n = 5$). To date, we have recorded at least 16 groups across Rungwe-Livingstone. In Ndundulu, only three groups are known (1).

R. kipunji is primarily arboreal but has been observed coming to the ground in both Ndundulu and Rungwe-Livingstone to avoid intragroup conflict and predation, as well as to

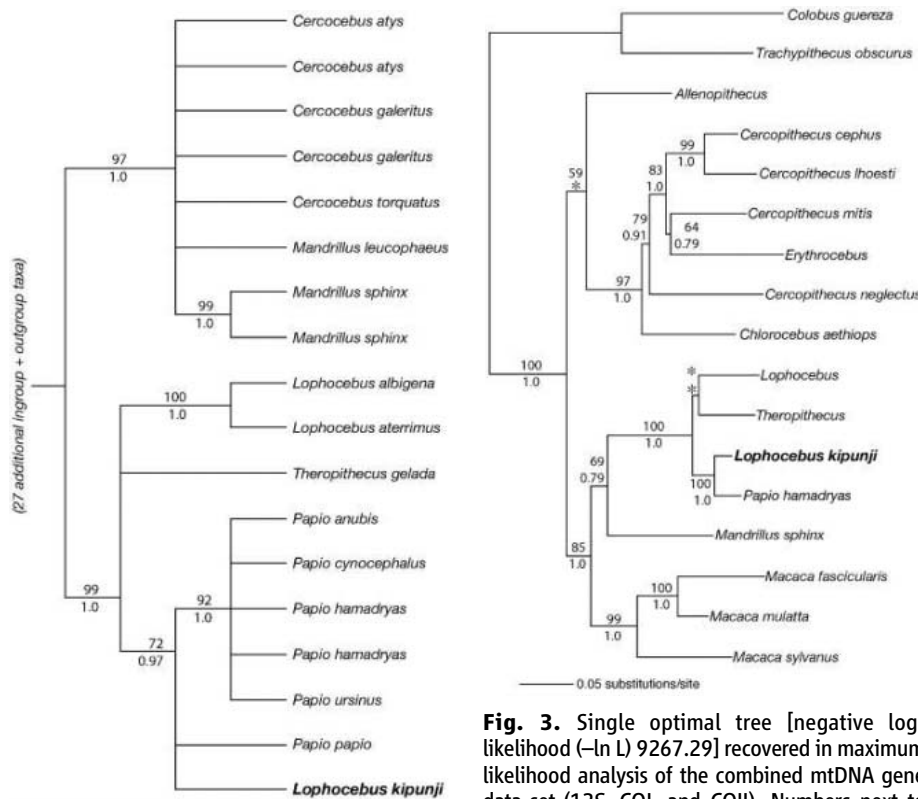


Fig. 2. Phylogenetic relationships among *Cercocebus*, *Mandrillus*, *Theropithecus*, *Papio*, and *Lophocebus* (sensu lato) as recovered in maximum likelihood analysis of the mtDNA COII gene. Numbers next to select nodes represent likelihood bootstrap proportions (top) and Bayesian posterior probabilities (bottom). Nodes receiving <70% bootstrap support and posterior probabilities <0.95 have been collapsed. An additional 31 sequences representing 27 species-level taxa were included in the analysis but have been trimmed from this figure. Entire tree and additional information are available in the SOM text.

Fig. 3. Single optimal tree [negative log-likelihood (–ln L) 9267.29] recovered in maximum likelihood analysis of the combined mtDNA gene data set (12S, COI, and COII). Numbers next to each node as in Fig. 2. Asterisks indicate nodes not recovered in ≥50% of the bootstrap replicates or with posterior probabilities of ≤0.5. Based on evidence from single-gene analyses that *L. aterrimus* and *L. albigena* are each other’s closest relative, the 12S sequence from the former was concatenated with the remaining sequences available for the latter. Tree was rooted with the two colobine sequences shown. Tree resulting from ML search constrained to recover a monophyletic *Lophocebus* (sensu lato) was a significantly poorer fit to the data ($P = 0.02$, Shimodaira-Hasegawa test). Additional information is available in the SOM text.

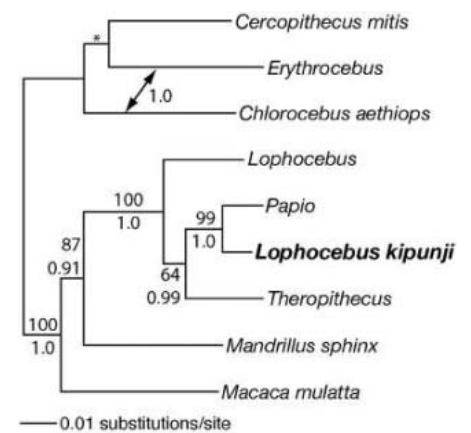


Fig. 4. Single optimal tree (–ln L 8427.57) recovered in maximum likelihood analysis of the combined mtDNA plus nuclear DNA data set (12S, COI, COII, α 1.3-GT, and TSPY). Numbers and asterisk as in Fig. 2. Sequences from *Lophocebus albigena* and *L. aterrimus* were concatenated as in Fig. 3, and the mtDNA sequences available for *Papio hamadryas* were concatenated with the nuclear sequences published for *P. anubis*. Arrow indicates the grouping of *Erythrocebus* with *Chlorocebus aethiops* strongly supported in Bayesian analysis of this data set, which may represent a rooting artifact. Tree was rooted with the three Cercopithecini figured and cannot be rerooted to recover a monophyletic *Lophocebus* (sensu lato). Tree resulting from maximum likelihood search constrained to recover a monophyletic *Lophocebus* (sensu lato) was a significantly poorer fit to the data ($P = 0.002$, Shimodaira-Hasegawa test). Additional information is available in the SOM text.

feed. In Rungwe-Livingstone, they also descend to cross degraded forest patches. The referred specimen was caught in a trap on the ground set by a farmer for crop-raiding primates and had corn in its mouth. *Lophocebus* species, however, are almost entirely arboreal, rarely descending to the ground or raiding crops (2). The main predators of *R. kipunji* are crowned eagles, *Stephanoaetus coronatus*, and possibly leopards, *Panthera pardus* (19). The kipunji is also widely hunted by humans on Mount Rungwe (19) as retribution for and prevention against the raiding of maize, beans, and sweet potato crops. It is also taken as a bycatch when hunting Sykes' monkeys (*Cercopithecus mitis*), and kipunji meat is sometimes eaten by the residents of Rungwe District.

The kipunji's omnivorous diet includes young and mature leaves, shoots, flowers, bark, ripe and unripe fruits, lichen, moss, and invertebrates. In Rungwe-Livingstone, groups form polyspecific associations with *Angola colobus*, *Colobus angolensis*, and *C. mitis*, especially in early mornings and late afternoons, when the three species often sleep in neighboring trees.

Formal assessment for the IUCN Red List of Threatened Animals is ongoing; *R. kipunji* will probably be designated as "critically endangered." In Rungwe-Livingstone, logging, charcoal-making, poaching, and unmanaged resource extraction are common (1, 19, 20). Although Ndundulu Forest Reserve is largely undisturbed, *R. kipunji* is present in very low numbers and the reasons for this remain unclear (20). The target for the genus must be the con-

servation and management of Mount Rungwe and the Bujingijila Forest Corridor that connects Mount Rungwe to Livingstone (19, 20). Without intervention, both forests will be further fragmented. Any hunting of the kipunji or loss of its vulnerable habitat, with the latter probably increasing the frequency of the former, will further threaten this new genus.

References and Notes

1. T. Jones *et al.*, *Science* **308**, 1161 (2005).
2. C. P. Groves, *Primates* **19**, 1 (1978).
3. J. G. Fleagle, W. S. McGraw, *J. Hum. Evol.* **42**, 267 (2002).
4. E. Schwarz, *Ann. Mag. Nat. Hist.* **10**, 664 (1928).
5. J. E. Cronin, V. M. Sarich, *Nature* **260**, 700 (1976).
6. T. R. Disotell, *Am. J. Phys. Anthropol.* **94**, 47 (1994).
7. E. E. Harris, *J. Hum. Evol.* **38**, 235 (2000).
8. S. L. Page, C.-H. Chiu, M. Goodman, *Mol. Phylogenet. Evol.* **13**, 348 (1999).
9. S. L. Page, M. Goodman, *Mol. Phylogenet. Evol.* **18**, 14 (2001).
10. Materials and methods are available as supporting material on Science Online.
11. P. Grubb *et al.*, *Int. J. Primatol.* **24**, 1301 (2003).
12. C. P. Groves, *Primate Taxonomy* (Smithsonian Institution Press, Washington, DC, 2001).
13. J. Kingdon, *The Kingdon Field Guide to African Mammals* (Academic Press, London, 1997).
14. R. W. Byrne, *Behaviour* **78**, 283 (1981).
15. P. M. Waser, in *Primate Communication*, T. Snowdon, C. H. Brown, M. R. Peterson, Eds. (Cambridge Univ. Press, Cambridge, 1982), pp. 117–143.
16. F. Range, J. Fischer, *Ethology* **110**, 301 (2004).
17. W. T. Stanley, M. A. Rogers, R. Hutterer, *J. Zool.* **265**, 269 (2005).
18. L. Dinesen *et al.*, *Ibis* **136**, 2 (1994).
19. T. R. B. Davenport, *Afr. Geogr.* **13**, 56 (2005).
20. T. R. B. Davenport, T. Jones, *Arc J.* **18**, 1 (2005).
21. T.R.B.D. directed the project that produced the discovery and obtained the specimen. T.R.B.D., N.E.M., S.J.M., and

D.W.D. located, observed, and collected all behavioral and ecological data; T.R.B.D., W.T.S., E.J.S., and L.E.O. wrote the paper with editorial input from D.W.D., N.E.M., and S.J.M. W.T.S. and E.J.S. conducted the morphological analysis; L.E.O. conducted all molecular analyses. M. Snapp, R. Banasiak, and M. Schulenberg provided assistance with analysis, specimen preparation, and figures. T. Roberts and M. Alfaro advised us on phylogenetic methodology. K. Hildebrandt assisted with lab work, which was funded by the University of Alaska Museum. DNA sequencing was conducted in the University of Alaska Fairbanks Institute of Arctic Biology (UAF-IAB) Core Facility for Nucleic Acid Analysis with support from NSF Experimental Program to Stimulate Competitive Research grant EPS-0346770. Analyses were conducted on the UAF-IAB Bioinformatics Cluster supported by NIH grant RR-16466-01, NSF grant EPS-0092040, the Alaska IDeA Networks for Biomedical Research Excellence program, and the University of Alaska Foundation. R. Phillips, M. Fungo, W. Mwalwengele, O. Mwaipungu, M. Haruna, A. Mwaambo, S. Kimiti, and G. Picton Phillips provided logistical, field, and Geographic Information Systems support. J. Fooden, A. Gardner, and T. Jones offered valuable advice. Fieldwork was funded by the Wildlife Conservation Society. We are grateful to Tanzania National Parks, Tanzania Wildlife Research Institute, and the Rungwe District Council, and we thank the anonymous reviewers for their helpful comments on earlier versions of this manuscript.

Supporting Online Material

www.sciencemag.org/cgi/content/full/1125631/DC1
Materials and Methods
SOM Text
Figs. S1 to S8
Table S1
References

31 January 2006; accepted 26 April 2006
Published online 11 May 2006;
10.1126/science.1125631
Include this information when citing this paper.

Checkpoint Proteins Control Survival of the Postmitotic Cells in *Caenorhabditis elegans*

Anders Olsen, Maithili C. Vantipalli, Gordon J. Lithgow*

Checkpoints are evolutionarily conserved signaling mechanisms that arrest cell division and alter cellular stress resistance in response to DNA damage or stalled replication forks. To study the consequences of loss of checkpoint functions in whole animals, checkpoint genes were inactivated in the nematode *C. elegans*. We show that checkpoint proteins are not only essential for normal development but also determine adult somatic maintenance. Checkpoint proteins play a role in the survival of postmitotic adult cells.

Many DNA damage checkpoint and repair proteins are essential for development. We identified a checkpoint gene in a genetic screen for whole-organism stress resistance. The predicted

protein, CID-1, has homology to poly(A)⁺ polymerase (PAP) domain proteins (fig. S1), including the fission yeast *Schizosaccharomyces pombe* S-M checkpoint protein caffeine-induced death (Cid) protein-1 (I-3). In *C. elegans*, we observed that worms carrying the *cid-1(rf34::Tc4)* mutation or worms with reduced expression of *cid-1* by RNA interference (RNAi) were highly thermotolerant (Fig. 1, A and B, and table S1).

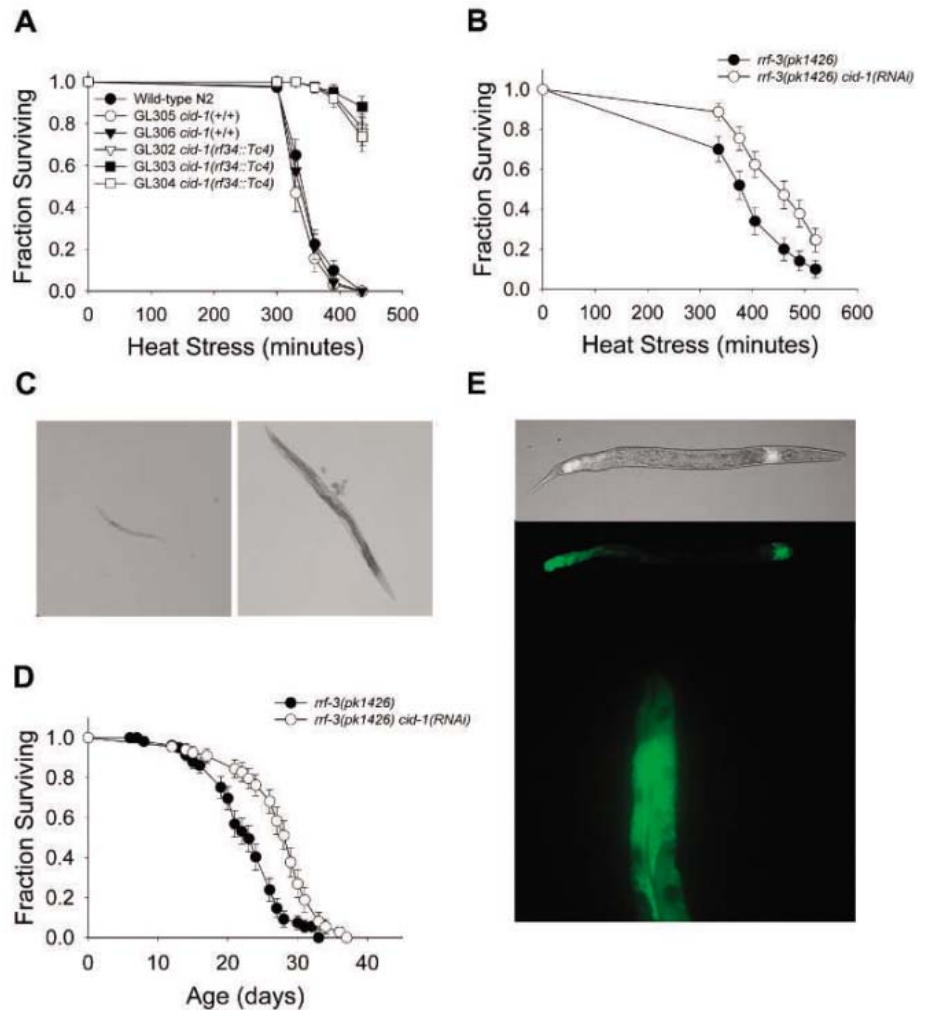
It was not obvious why checkpoint proteins would affect organismal stress resistance in *C. elegans* where the soma is composed of nondividing cells. Consequently, we further investigated the extent to which *cid-1* determined cell survival in worms and whether it was related to checkpoint functions.

The ribonucleotide reductase inhibitor hydroxyurea (HU) causes stalled replication forks. Wild-type worms had arrested development in the presence of HU, but *cid-1(rf34::Tc4)* mutants and *cid-1(RNAi)* worms developed into adults (Fig. 1C). This is consistent with *C. elegans* CID-1 having a checkpoint function. It is also required for normal development, as *cid-1* mutants had shorter, thicker gonads with fewer proliferating and developing germ cells. The worms contained disorganized embryos, produced fewer offspring, and took 24 hours longer to develop into reproductive adults compared with wild-type worms (fig. S2 and table S2). Of *cid-1(rf34::Tc4)* adult worms examined, 20 to 40% developed a protruding vulval defect that blocked egg laying and resulted in premature death.

The Buck Institute, 8001 Redwood Boulevard, Novato, CA 94945, USA.

*To whom correspondence should be addressed. E-mail: glithgow@buckinstitute.org

Fig. 1. CID-1 regulates stress resistance. **(A)** Longitudinal thermotolerance assay of *cid-1(rf34::Tc4)* mutant lines. (+/+) indicates wild-type *cid-1* gene. **(B)** Longitudinal thermotolerance assay of *rrf-3(pk1426) cid-1(RNAi)* worms. The *rrf-3(pk1426)* mutation renders worms more sensitive to RNAi. The complete thermotolerance data can be found in table S1. **(C)** HU-resistance assay. (Left) Wild-type N2 worms showed arrested development at the L1/L2 stage when eggs were placed on HU plates. (Right) *cid-1(rf34::Tc4)* mutants develop into fertile adults at the same concentration of HU. **(D)** Life span of *rrf-3(pk1426) cid-1(RNAi)* worms at 20°C. **(E)** Transgenic worms expressing a *CID-1::GFP* gene fusion. (Top) Composite fluorescent and bright-field micrographs and corresponding fluorescent micrographs of the fusion protein localized to the first layer of intestinal cells (Int 1) and to posterior intestinal cells. (Bottom) A high-resolution fluorescent micrograph of the fusion protein localized to the cytoplasm of the posterior intestinal cells.



Because a number of genes that limit *C. elegans*'s life span also regulate stress resistance (4), CID-1 could play a role in somatic maintenance during normal aging. Although most *cid-1(rf34::Tc4)* mutant worms exhibited premature nonsenescent deaths resulting from their developmental abnormalities, we observed a significant increase in the life span of *cid-1(RNAi)* worms (Fig. 1D and table S3).

In *C. elegans*, heat shock proteins (HSPs) influence survival (5, 6). Therefore, we tested whether *cid-1(RNAi)* worms had altered *hsp* gene expression. *cid-1* RNAi induced expression of *hsp-4*, which encodes a predicted homolog of the mammalian endoplasmic reticulum chaperone BiP and also increases expression of the Mn superoxide dismutase *sod-3* specifically in vulval tissues (Fig. 2). Although the *hsp-4* chaperone is induced by the unfolded protein response (UPR), expression of another UPR-associated chaperone, HSP-16 (7, 8), was not up-regulated (Fig. 2). In addition, RNAi of *hsp-4* resulted in sick, short-lived adults. Thus, *hsp-4* is required for normal

survival and is regulated by *cid-1*, independent of the UPR (table S3). Both *hsp-4* and *cid-1* are expressed in the postmitotic intestinal cells (Fig. 1E and Fig. 2) during development and adulthood, consistent with a role on postmitotic cell survival.

We wished to determine whether other checkpoint proteins affect organismal survival. In *S. pombe*, cell-cycle progression requires activation of a cyclin-dependent kinase (Cdk) complex by the phosphatase Cdc25, which is regulated by several kinases including the serine-threonine kinase Chk1 (9). In *C. elegans*, *cid-1* interacts genetically with *chk-1* and members of the *cdc-25* gene family. *chk-1* is active in the S-M and DNA repair checkpoints (10) and is a DNA-replication checkpoint coupling cell-cycle length to asymmetric cell division of the two-cell embryo (11). *chk-1* and *cid-1* interacted genetically to determine normal embryonic development, and *cid-1* and *cdc-25.1* interacted to determine normal hermaphrodite self-fertility (fig. S3).

The offspring of worms treated with *chk-1* RNAi are viable but sterile (fig. S3). In char-

acterizing the somatic maintenance of these offspring, we observed that *chk-1* RNAi caused large increases in organismal resistance to thermal stress (Fig. 3A and table S1). In addition, the life span of *chk-1(RNAi)* worms increased by 15 to 25% (Fig. 4, A to C, and table S3). *chk-1* RNAi also induced *hsp-4* expression (Fig. 2).

To examine the temporal requirements for CHK-1 regulation of stress responses, we used the CHK-1 chemical inhibitor UCN-01. When worms were treated throughout development, their growth was arrested before they reached adulthood. However, treatment of young adults resulted in a dose-dependent increase in thermotolerance (Fig. 3F). Therefore, inhibition of CHK-1 function during adulthood is sufficient to confer increased somatic maintenance.

After the molt into an adult worm, cell division is confined to the germ line (12). Therefore, CHK-1 could influence somatic maintenance through its action in the germline stem cells. Ablation of germline precursor cells leads to organismal stress resistance and life-span extension through

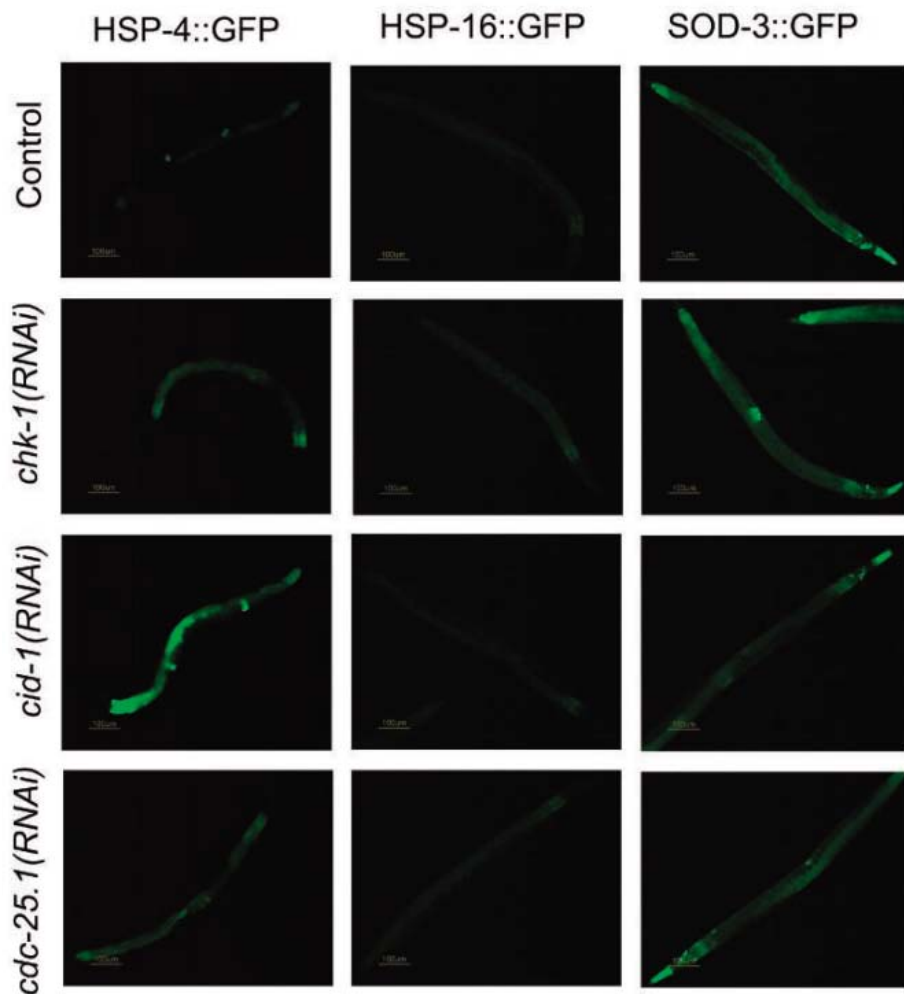


Fig. 2. Checkpoint protein regulation of stress genes in postmitotic cells. **(Left)** Expression pattern of *hsp-4::GFP* in control, *chk-1(RNAi)*, *cdc-25.1(RNAi)*, and *cid-1(RNAi)* worms. Elevated levels of *hsp-4::GFP* were observed in the intestine, particularly in the first layer of intestinal cells, when either component of the pathway was inactivated. **(Middle)** Expression pattern of *hsp-16::GFP* in control, *chk-1(RNAi)*, *cdc-25.1(RNAi)*, and *cid-1(RNAi)* worms. **(Right)** Expression pattern of *sod-3::GFP* in control, *chk-1(RNAi)*, *cdc-25.1(RNAi)*, and *cid-1(RNAi)* worms. Inactivation of *cid-1/chk-1/cdc-25.1* results in elevated levels of *sod-3::GFP* in the vulva. The pictures are representative of results observed in three independent experiments.

a mechanism requiring the forkhead (FOXO) transcription factor DAF-16 and also the nuclear hormone receptor DAF-12 (13–16). Thermotolerance of *chk-1(RNAi)* worms was not dependent on DAF-16 or DAF-12 (Fig. 3, A and B, and table S1). Likewise, life-span extension caused by RNAi of *chk-1* was observed in both *daf-16* and *daf-12* mutant backgrounds (Fig. 4, A and B, and table S3). The magnitude of life-span extension was smaller in the *daf-12* mutant worms, which suggests that the effect of the checkpoint proteins may be partially dependent on cycling germ cells. Exposure to stress or germline ablation causes DAF-16 translocation from the cytoplasm to the nucleus (16–18). We examined the localization of a green fluorescent protein reporter, DAF-16::GFP, in *chk-1(RNAi)* worms and observed DAF-16 in the cytoplasm of intestinal cells (fig. S4). However, after a heat stress, RNAi of *chk-1* did not block translocation of DAF-16 to the nucleus, which suggested that CHK-1 activity is independent of DAF-16. *chk-1* RNAi also extended the life span of an already long-lived

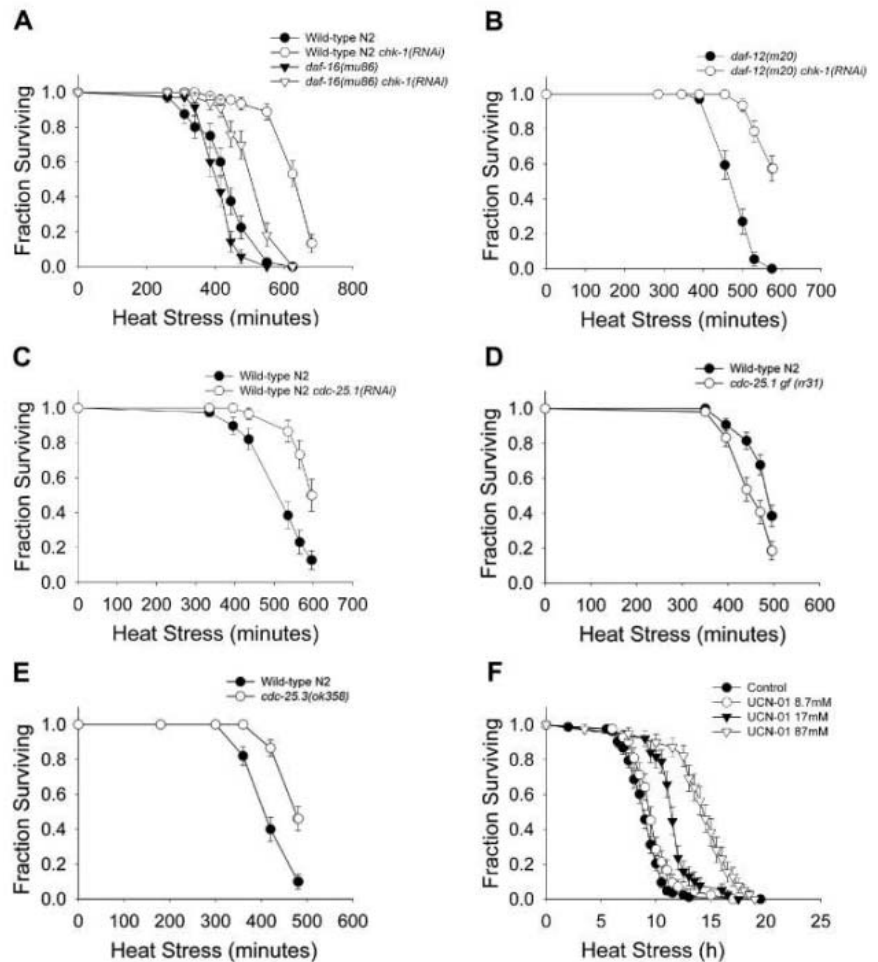
insulin receptor–like mutant *daf-2(e1368)* (19, 20) (Fig. 4C). Taken together, these results suggest CHK-1 regulates somatic maintenance through processes different from the previously described germline signal and the insulin signaling pathway.

Because *cid-1* genetically interacts with *cdc-25.1*, the generality of checkpoint proteins influencing survival was examined. In mammalian cells, CHK-1 targets CDC25A for degradation by phosphorylation in response to DNA damage (21). There are four Cdc25 homologs in *C. elegans*, with the *cdc-25.1* gene predominantly expressed in the germ line (22), where it is required for proliferation (23). Inactivation of *cdc-25.1* causes embryonic lethality, with some surviving embryos developing into sterile adults with abnormal germ lines. Sterile *chk-1(RNAi)* worms were similar in appearance to worms with inactivated *cdc-25.1* (24) (fig. S3). RNAi of *cdc-25.1* resulted in increased thermotolerance and life-span extension (Figs. 3C and 4D). In addition, worms carrying a *cdc-25.1* gain-of-function mutation were thermosensitive (Fig. 3D and

table S1) and short-lived (Fig. 4E and table S3). Inactivation of isoforms *cdc-25.2* and *cdc-25.3* by RNAi also conferred increased thermotolerance, whereas loss of *cdc-25.4* had no effect (table S1). *cdc-25.3(RNAi)* worms had significantly increased life span (table S3) and, like *cid-1(RNAi)* worms, increased expression of *hsp-4* in the intestine and *sod-3* in the vulva (Fig. 4). A *cdc-25.3* knockout (KO) mutant displayed both significantly increased thermotolerance (Fig. 3E) and 40% extended life span (Fig. 4F and table S3). The *cdc-25.3* KO mutants also exhibited many of the phenotypes resulting from lack of *cid-1* and *chk-1* gene products, including delayed development and reduced fertility, which suggests that these genes act in either a single or functionally related pathway. Thus, at least three *cdc-25* genes, *chk-1*, and *cid-1* affect survival, consistent with the general notion that checkpoint proteins have a role of somatic maintenance.

The separation between postmitotic soma and mitotic germ line in *C. elegans* has provided an opportunity to study the roles of

Fig. 3. Inactivation of *chk-1* and *cdc-25* confers organismal stress resistance. Longitudinal thermotolerance assays. **(A)** Thermotolerance of wild-type N2 and *daf-16(mu86)* mutant worms treated with *chk-1* RNAi. **(B)** Thermotolerance of *daf-12(m20)* *chk-1(RNAi)* worms. **(C)** Thermotolerance of *cdc-25.1(RNAi)* worms. **(D)** Thermosensitivity of *cdc-25.1(rr31)*; *rfls1* gain-of-function mutant worms. **(E)** Thermotolerance of *cdc-25.3(ok358)* mutant worms. **(F)** Thermotolerance of wild-type N2 worms treated with UCN-01 during adulthood. Our thermotolerance data can be found in table S1.



checkpoint functions in postmitotic cells in a whole organism. Because postmitotic tissues do not form tumors in *C. elegans*, the effects of checkpoint proteins on acute stress survival and normal life span have been uncovered. The notion that checkpoint proteins function in postmitotic cells suggests a checkpoint surveillance function that is unrelated to the decision to undergo cell division but still regulates cell survival. Checkpoints act as tumor suppressor pathways in mammals in part by promoting cellular senescence. A role in normal aging has been hypothesized; mice with hyperactive p53 exhibit signs of accelerated aging consistent with a trade-off between checkpoint fidelity and tissue regeneration (25, 26), and decreasing p53 activity in fruit fly neurons extends life span (27). This is consistent with the prediction that reduced checkpoint competence leads to reduced rates of tissue aging (28). Our observation indicates that postmitotic cell survival is also regulated by checkpoint proteins, and thus, a trade-off between checkpoint function and cellular maintenance is likely in both mitotic and postmitotic tissues. This

prompts the question whether specific alleles of checkpoint proteins in humans may place individuals at risk for some cancers but protect them against other age-associated diseases. It also appears critical that neurons are maintained in a noncycling, terminally differentiated state to avoid apoptosis. Checkpoint proteins are likely to have a role in maintaining neurons in a postmitotic state; they may also influence intrinsic resistance to stress.

References and Notes

1. S. W. Wang, T. Toda, R. MacCallum, A. L. Harris, C. Norbury, *Mol. Cell Biol.* **20**, 3234 (2000).
2. S. Saitoh *et al.*, *Cell* **109**, 563 (2002).
3. L. Wang, C. R. Eckmann, L. C. Kadyk, M. Wickens, J. Kimble, *Nature* **419**, 312 (2002).
4. C. Kenyon, *Cell* **120**, 449 (2005).
5. G. A. Walker, G. J. Lithgow, *Aging Cell* **2**, 131 (2003).
6. K. Yokoyama *et al.*, *FEBS Lett.* **516**, 53 (2002).
7. M. Calton *et al.*, *Nature* **415**, 92 (2002).
8. F. Urano *et al.*, *J. Cell Biol.* **158**, 639 (2002).
9. J. Melo, D. Toczyski, *Curr. Opin. Cell Biol.* **14**, 237 (2002).
10. N. Kalogeropoulos, C. Christoforou, A. J. Green, S. Gill, N. R. Ashcroft, *Cell Cycle* **3**, 1196 (2004).
11. M. Brauchle, K. Baumer, P. Goczny, *Curr. Biol.* **13**, 819 (2003).
12. J. E. Sulston, H. R. Horvitz, *Dev. Biol.* **56**, 110 (1977).

13. S. Ogg *et al.*, *Nature* **389**, 994 (1997).
14. K. Lin, J. B. Dorman, A. Rodan, C. Kenyon, *Science* **278**, 1319 (1997).
15. H. Hsin, C. Kenyon, *Nature* **399**, 362 (1999).
16. K. Lin, H. Hsin, N. Libina, C. Kenyon, *Nat. Genet.* **28**, 139 (2001).
17. S. T. Henderson, T. E. Johnson, *Curr. Biol.* **11**, 1975 (2001).
18. N. Libina, J. R. Berman, C. Kenyon, *Cell* **115**, 489 (2003).
19. C. Kenyon, J. Chang, E. Gensch, A. Rudner, R. Tabtiang, *Nature* **366**, 461 (1993).
20. K. D. Kimura, H. A. Tissenbaum, Y. Liu, G. Ruvkun, *Science* **277**, 942 (1997).
21. N. Mailand *et al.*, *Science* **288**, 1425 (2000).
22. N. R. Ashcroft, M. Srayko, M. E. Kosinski, P. E. Mains, A. Golden, *Dev. Biol.* **206**, 15 (1999).
23. N. Ashcroft, A. Golden, *Genesis* **33**, 1 (2002).
24. C. Clucas, J. Cabello, I. Bussing, R. Schnabel, I. L. Johnston, *EMBO J.* **21**, 665 (2002).
25. S. D. Tyner *et al.*, *Nature* **415**, 45 (2002).
26. B. Maier *et al.*, *Genes Dev.* **18**, 306 (2004).
27. J. H. Bauer, P. C. Poon, H. Glatt-Deeley, J. M. Abrams, S. L. Helfand, *Curr. Biol.* **15**, 2063 (2005).
28. D. Wodarz, *Oncogene* **23**, 7799 (2004).
29. We thank M. Benedetti and A. Foster for help with the UCN-01 thermotolerance assays; M. Lund and the members of the Lithgow Laboratory, the Kapahi Laboratory, J. Campisi, C. Benz, and D. Bhaumik for helpful discussions; and J. Ahringer and the Medical Research Council gene service for providing the RNAi library. UCN-01 was made available from the Drug Synthesis and Chemistry Branch, Developmental Therapeutics Program,

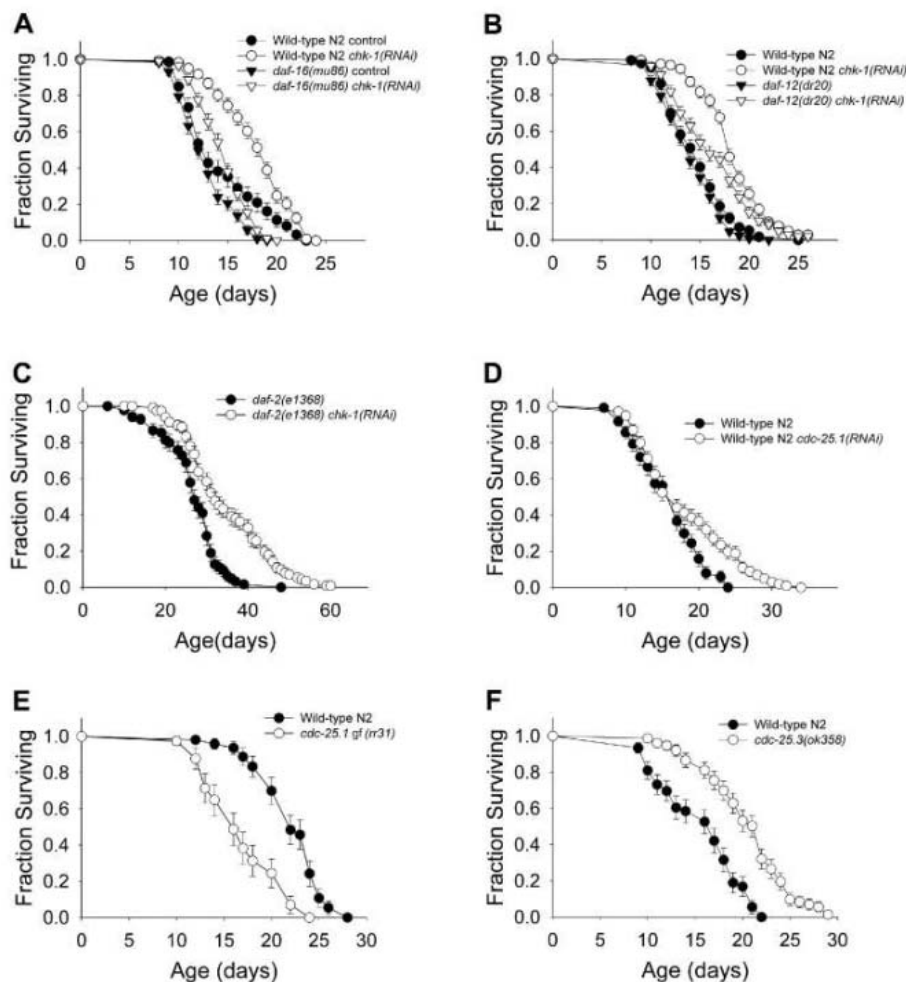


Fig. 4. Inactivation of *chk-1* and *cdc-25* confers increased life span independent of germline signal. **(A)** Life span of wild-type N2 and *daf-16(mu86)* mutant worms treated with *chk-1* RNAi at 25°C. **(B)** Life span of *chk-1* RNAi treated wild-type N2 and *daf-12(m20)* mutant worms at 25°C. **(C)** Life span of *chk-1* RNAi treated *daf-2(e1368)* mutant worms at 20°C. **(D)** Life span of *cdc-25.1(RNAi)* worms at 25°C. **(E)** Life span of *cdc-25.1(rr31)*; *rmls1* gf mutant worms at 20°C. **(F)** Life span of *cdc-25.3(ok358)* mutant worms at 25°C. All the survival data can be found in table S3.

National Cancer Institute. A.O. was supported by the Danish Research Academy and the Danish Cancer Society. G.J.L. was supported by NIH AG21069, AG22868, and NS050789-01; the Ellison Medical Foundation; the Glenn Foundation for Medical Research; the Biotechnology and Biological Sciences Research Council, Science of Ageing

Initiative; and the Herbert Simon Family Medical Foundation.

Supporting Online Material

www.sciencemag.org/cgi/content/full/312/5778/1381/DC1
Materials and Methods

Figs. S1 to S4
Tables S1 to S3
References and Notes

17 January 2006; accepted 10 April 2006
10.1126/science.1124981

Juvenile Hormone Is Required to Couple Imaginal Disc Formation with Nutrition in Insects

J. W. Truman,^{1*} K. Hiruma,² J. P. Allee,³ S. G. B. MacWhinnie,³ D. T. Champlin,³ L. M. Riddiford¹

In starved larvae of the tobacco hornworm moth *Manduca sexta*, larval and imaginal tissues stop growing, the former because they lack nutrient-dependent signals but the latter because of suppression by juvenile hormone. Without juvenile hormone, imaginal discs form and grow despite severe starvation. This hormone inhibits the intrinsic signaling needed for disc morphogenesis and does so independently of ecdysteroid action. Starvation and juvenile hormone treatments allowed the separation of intrinsic and nutrient-dependent aspects of disc growth and showed that both aspects must occur during the early phases of disc morphogenesis to ensure normal growth leading to typical-sized adults.

Research on growth control in insects has largely concentrated on imaginal discs because such structures determine the

size and morphology of the adult (*I*). Imaginal disc growth has both extrinsic and intrinsic components (2, 3). Extrinsic components link growth

to nutritional state via endocrine factors [such as the insulin-like peptides and ecdysone (4–7)], whereas intrinsic components associate growth with local morphogens (such as *wingless* and *dpp*) that establish patterns directing morphogenetic growth (2). Besides possessing growth-promoting factors, insects have a potential growth-inhibiting factor, the juvenile hormone (JH). JH is a sesquiterpene hormone that is released from the corpora allata (CA) and is responsible for directing the action of the ecdysteroid molting hormones ecdysone and 20-hydroxyecdysone. JH is characterized as a “status quo” hormone (8) because, in its presence, ecdysteroids cause molt-

¹Department of Biology, University of Washington, Seattle, WA 98195–1800, USA. ²Faculty of Agriculture and Life Sciences, Hirosaki University, Hirosaki 036–8561, Japan. ³Department of Biological Sciences, University of Southern Maine, Portland, ME 04103, USA.

*To whom correspondence should be addressed. E-mail: jwt@u.washington.edu

ing larvae to repeat the most recent stage. However, the association of JH with growth control has generally been ascribed to this modulation of ecdysteroid action because the disappearance of JH in the last larval stage initiates the endocrine changes that cause metamorphosis (9).

The concepts of imaginal disc growth and morphogenesis are based on highly derived “early-forming” discs, such as those of *Drosophila* and the wing discs of Lepidoptera, such as *Manduca sexta*. The cells for these discs are set apart from the larval tissues during embryogenesis. They play no functional role in the larva but grow in concert with it and begin morphogenesis late in larval life (1, 10). In contrast, an ancestral strategy of disc formation is seen in the development of lepidopteran eye, leg, and antennal discs (11, 12).

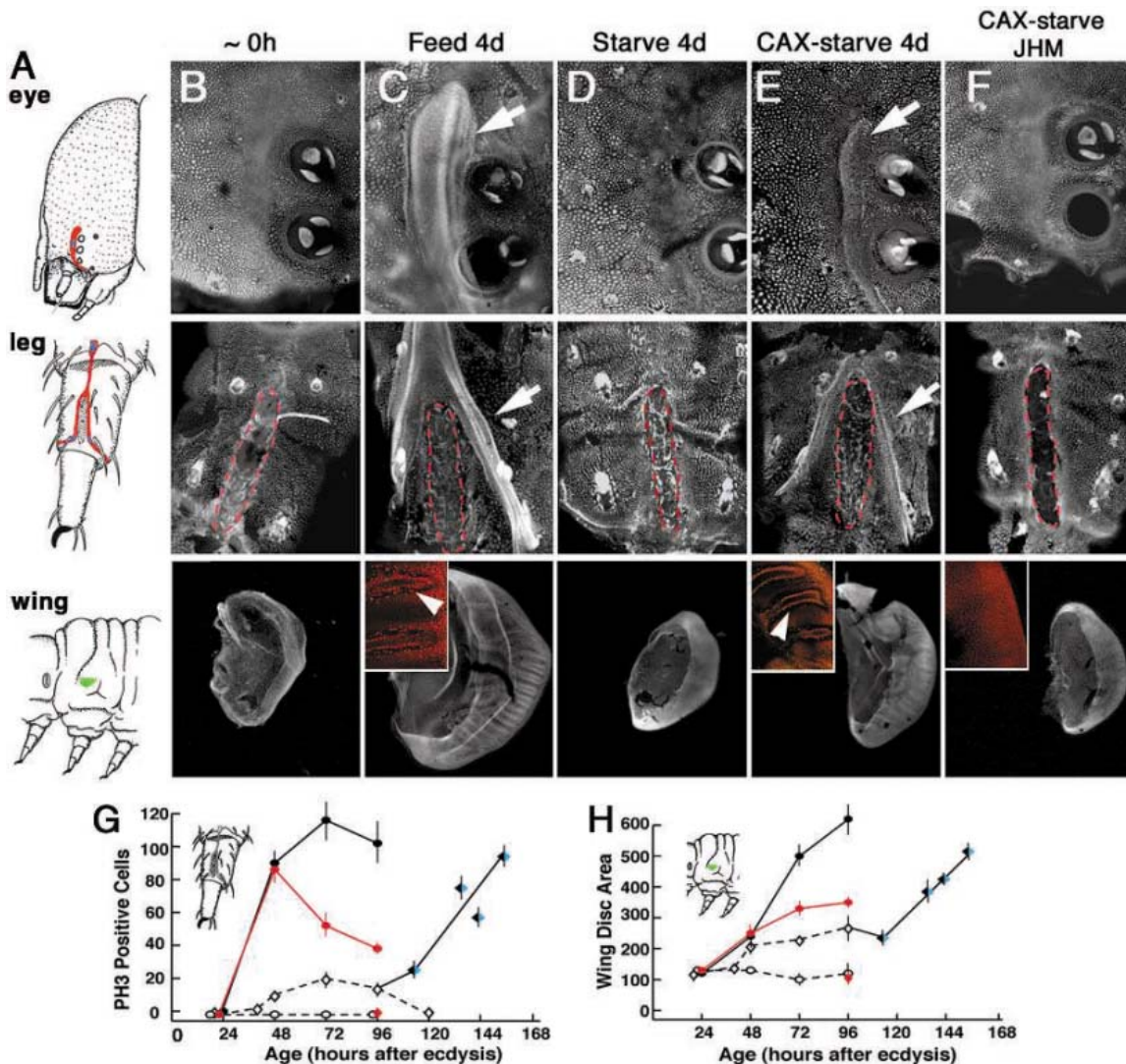
These are “late-forming” discs that arise from the primordia (Fig. 1A, red), which are fields of diploid cells that contribute to the larval body but retain the embryonic potential to form an imaginal disc (11–15). Early in the last larval stage, cells at discrete sites in each primordium (Fig. 1A, blue) begin to transform, becoming columnar and starting to invaginate. Cellular morphogenesis and proliferation then spread from the sites through the primordium, forming a prominent invaginated disc by the start of metamorphosis 3 days later (Fig. 1C). The formation and growth of these late-forming discs depended on feeding and did not occur when last-stage larvae were starved (16, 17) (Fig. 1D). Starvation also results in elevated levels of JH (18) rather than the JH decline typical of the last larval stage. When this JH increase was prevented by the

removal of the CA, we found that the discs formed and grew despite starvation (Fig. 1, E and G).

The earliest known manifestation of the commitment to metamorphosis is the appearance of the *broad* transcription factor, a member of the Broad complex, Tramtrak, and Bric à brac/Pox virus and zinc finger (BTB/POZ) family (17, 19, 20). *Broad-Z2* transcripts appeared in the leg primordium of feeding last-stage larvae by 12 hours after ecdysis and increased through 48 hours (Fig. 2A). *Broad* transcripts did not appear in starved larvae unless the larvae were also lacking their CA. Both the *broad-Z2* expression (Fig. 2B) and disc formation and growth (Fig. 1, F and G) seen in starved allatectomised (CAX) larvae were completely suppressed by treatment with pyriproxifen, a stable JH mimic (JHM).

Fig. 1. Interaction of hormone and nutrient manipulations on imaginal disc organization and growth in larval *Manduca sexta*.

(A) Drawings showing the location of the eye and leg primordia (red) and wing imaginal discs (green) at the onset of the last larval stage. Blue shows the sites that start the disc transformation. (B to F) Propidium iodide–stained projections of confocal Z-stacks showing the state of the primordia and discs after different treatments. (B) At the start of the last instar (0 h, 0 hours), the primordia were quiescent and the wing disc was small. (C) After 4 days of feeding (4d), the primordia formed invaginated discs (arrows) and the wing disc grew and established the wing veins (inset, arrowhead). (D) Larvae starved for 4 days showed neither eye nor leg disc formation nor wing disc growth. (E) Larvae lacking their CA (CAX) and starved for 4 days showed wing disc growth and vein formation (inset, arrowhead), and both the eye and leg discs formed (arrows). (F) Treatment of starved-CAX larvae with JHM (pyriproxifen, 10 μg per larva) suppressed disc formation and wing disc growth and vein formation (inset). The red dashed line in the legs in (B) to (F) shows the muscle insertion on the dorsal distal tibia. (G and H) Quantification of the effects of hormone and nutrient manipulations on (G) proliferation in the tibial portion of the leg disc and (H) growth of the early-forming wing disc. Cell division was assessed by the number of phosphohistone H3 (PH3)–



positive cells (those in mitosis), and growth was assessed by the dorsal area (total pixels × 100) of the wing disc. Circles indicate intact larvae that were fed normal diet (black), fed diet and treated with 10 μg of pyriproxifen per larva (red), or starved (open). Diamonds indicate CAX larvae that were starved (open), starved and treated with pyriproxifen (red), or fed a normal diet after 4 days of starvation (black/blue diamonds). Symbols are the average (±SEM) for four to five preparations.

An early-forming disc, the wing disc, showed similar growth responses to starvation and JH. During the last instar, the wing discs increased markedly in area and also established the sites of the future veins (Fig. 1C, inset) (21). Neither response occurred in starved larvae (Fig. 1, D and H) unless the larvae lacked their CA (Fig. 1, E and H). The wing disc growth and morphogenesis seen in starved CAX larvae were both blocked by treatment with JHM (Fig. 1F).

Because the developmental effects of JH are normally attributed to its modulating the actions of ecdysteroids (9), we used *in vivo* body ligations to test the involvement of ecdysteroids in disc formation and growth. Neck ligation decapitated the larva and deprived the thorax of cephalic endocrine factors, including JH. Decapitated larvae showed the formation and growth of leg (Fig. 3A) and wing discs (not shown in the figure) similar to that seen in starved CAX larvae, and the development of both discs was suppressed by JHM

(Fig. 3B). A ligature applied behind the second thoracic segment additionally isolated the T3 primordia from ecdysteroids coming from the prothoracic glands in the anterior thorax. Nevertheless, the ecdysteroid-free portions posterior to the ligature still showed the organization and growth of their T3 discs (Fig. 3C). Therefore, ecdysteroids are not required for the formation and early proliferation of the discs.

The growth suppression that accompanies starvation is generally attributed to the lack of growth-promoting factors (such as insulin-related peptides) (22, 23). Therefore, JH could be acting systemically to suppress the release of such factors. We tested for systemic versus local effects of JH by topically applying JHM to a single leg of neck-ligated larvae [see the supporting online material (SOM)]. The treated leg showed no disc formation (Fig. 3E), whereas the remaining legs formed their discs normally (Fig. 3D). *In vitro* experiments also supported the direct action of JH in suppressing the organization and growth of the late-forming discs. Pieces of the fourth instar head cuticle that contained the eye primordium formed an eye disc when cultured without pyriproxifen, but disc formation and proliferation were blocked by the addition of JHM. The median effective dose for the suppression of disc proliferation was about 10^{-10} M pyriproxifen (fig. S1A). *In vivo* studies showed that JHM could act within 8 to 12 hours to suppress proliferation in discs that were just starting to form (fig. S1B).

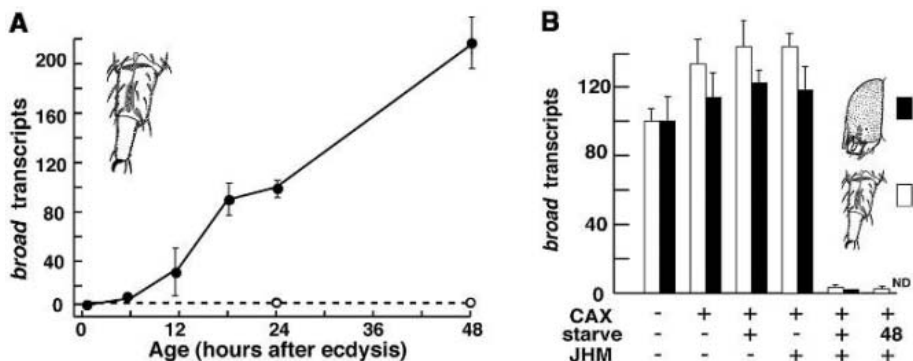
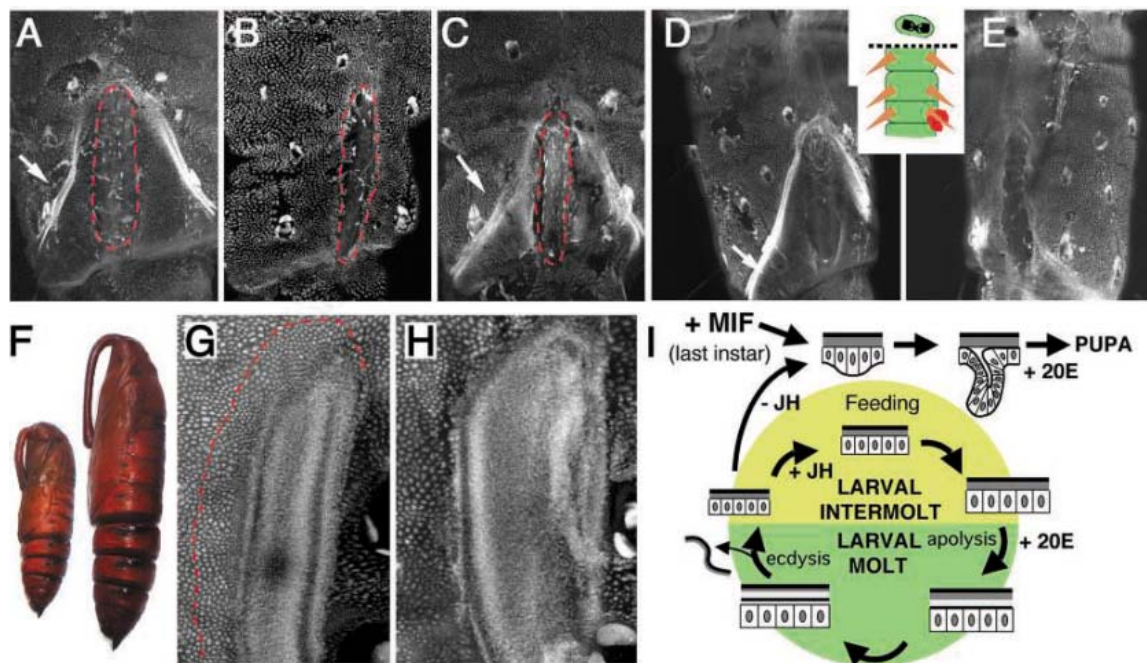


Fig. 2. Interaction of JHM and nutrient manipulations on the expression of the *broad* gene in small pieces of larval epidermis containing the leg or eye primordium. The levels of *broad-Z2* mRNA were determined by reverse transcription polymerase chain reaction and referenced to levels in fed larvae at 24 hours after ecdysis. (A) The time course of *broad-Z2* appearance in the leg primordium of fed (solid circles) or starved (open circles) larvae. (B) The effects of feeding, CA removal (CAX), and treatment with pyriproxifen (JHM) on *broad-Z2* expression in the leg and eye primordia. Values are at 24 hours after ecdysis except where indicated and are the average (\pm SEM) of three determinations per point.

Fig. 3. The effects of treatment with pyriproxifen (JHM) on disc formation and growth. (A and B) Newly ecdysed last-stage larvae that were decapitated by neck ligation showed well-formed leg disc invaginations (arrow) by 4 days after ligation (A), but this morphogenesis was inhibited by treatment with 10 μ g of pyriproxifen (B). (C) Ligation behind segment T2 to remove the influence of the prothoracic glands also resulted in disc formation (arrow). The red dashed lines in the legs in (A) to (C) show the muscle insertion landmark. (D and E) Localized treatment of one leg of a decapitated larva with pyriproxifen by covering it with wax impregnated with JHM suppressed disc formation in the treated leg (E) while the contralateral disc formed normally (D), as indicated by the arrow. (F) Pupae formed from larvae that were starved for 4 days and then fed ad libitum until metamorphosis. Left, CAX individual; right, control. (G and H) The dorsal region of the pre-wandering eye imaginal disc in a normally fed individual (H) and a CAX larva that had been



starved for 4 days and then fed for 60 hours (G). In the latter, the growing eye disc failed to incorporate the small cells in the dorsal and anterior regions of the eye primordium (included in the red dashed line). (I) Scheme summarizing the role of JH in regulating the growth of adult primordia during larval life. 20E, 20-hydroxyecdysone. (A) to (E), (G), and (H) show propidium iodide-stained projections from confocal Z-stacks.

Although the onset of metamorphosis is usually explained in terms of the loss of JH, there is clearly another factor involved. JHM treatment suppressed disc formation and growth in starved CAX larvae but not in larvae that were feeding (Fig. 1G) (16, 17). Similarly, treatment with JHM suppressed *broad-Z2* induction in the primordia of starved CAX larvae but not in feeding larvae (Fig. 2B). This failure of JHM to suppress disc formation in feeding last-stage larvae cannot be explained by the enhanced clearance of the applied hormone, because topical treatment of the leg primordia with JHM was also ineffective in feeding larvae. Therefore, nutritional cues apparently result in the release of a metamorphosis-initiating factor (MIF) that overrides the suppression of disc formation by JH (16, 17). The release of a MIF in response to feeding appears to be unique to the last larval stage, because JH also inhibits disc formation in earlier larval instars but feeding does not overcome this suppression. The endocrine interactions during the last larval stage are known to be species-specific (24, 25), and although a MIF is an additional player in this interaction, its nature is unknown.

Although feeding overrides JH suppression of disc formation in the last instar, there are still JH-sensitive aspects of subsequent disc growth. *Manduca* larvae treated with JHM early in the last instar neither molted nor metamorphosed and grew to monstrous sizes (over 18 g) (26). In such larvae, leg disc proliferation and wing disc growth were normal through the first 2 days but then both processes declined markedly (Fig. 1, G and H). The growing discs started to differentiate on day 2, as demonstrated by the establishment of veins in wing discs (21) (Fig. 1C, inset), but this early differentiation was abnormal in feeding larvae treated with JHM. Hence, JH appears to affect two aspects of disc growth: the initial formation and growth of the disc and the subsequent differentiation of the simple disc epithelium into a complex structure. Nutrient-dependent factors can overcome the first aspect of JH suppression but apparently not the second.

The discs that grew in the starved CAX larvae illustrate the growth potential of the primordium in the absence of additional nutritional input. We have termed this type of growth, which is due to intrinsic signaling within the primordium, "morphogenetic growth." Morphogenetic growth sets the lower size limits for discs that form from their respective primordia. These discs may correspond to the tiny discs formed in *chico* mutants of *Drosophila* that cannot respond to nutrient-related cues because of a mutation in the insulin-signaling pathway (27). The size difference between these discs and those formed by normally fed individuals is the extrinsic contribution of "nutrient-dependent growth." Normally, intrinsic and extrinsic components act cooperatively during the early portion of the last instar as larvae are feeding. The use of CAX larvae, however, permitted us to examine disc growth when these two components were separated in time.

CAX larvae that were starved for 4 days and then given food formed severely stunted pupae as compared to the pupae of similarly treated intact larvae (Fig. 3F; see the SOM). The dramatic size difference reflected the size of imaginal discs made by CAX larvae versus those formed by intact larvae. For example, in normal feeding larvae, all cells of the eye primordium had been incorporated into the eye disc by the start of metamorphosis (Fig. 3H). The mature discs of the CAX larvae, in contrast, were bordered on their anterior and dorsal margins by small cells that were part of the eye primordium (Fig. 3G), and these boundaries were similar to those established by the end of starvation (Fig. 1E). We think that, in normal feeding larvae, the recruitment of cells into the forming disc spreads rapidly through the primordium because of the coexistence of nutrient-dependent and morphogenic signaling. In the starved CAX larvae, in contrast, the lack of the nutrient-dependent component resulted in slower recruitment, leaving many primordium cells outside of the nascent disc at the end of starvation. Because the disc boundaries moved little, if at all, in the CAX larvae during subsequent feeding, there appears to be a limited temporal window for the recruitment of cells into the nascent disc. This window had closed by the end of the starvation period, with only a fraction of the competent cells having been recruited into the disc. When nutrient-dependent mechanisms were subsequently invoked by feeding, no more recruitment of cells was possible and growth was confined to the smaller disc that contributed to a stunted pupa. Whereas recent emphasis on the study of disc growth and size focuses on nutrient-dependent mechanisms working through the insulin-like peptides (4), our study shows that these extrinsic signals must work in concert with intrinsic control systems for normal growth to occur. These intrinsic mechanisms seem especially important early in disc growth, and their occurrence in the absence of nutrition results in stunted pupae despite the subsequent access of larvae to abundant high-quality food. This finding may have parallels to human conditions in which early infant malnutrition results in long-term effects on growth, including stunting and obesity (28).

JH has long been known to be active at the start of molts to modulate ecdysteroid action (9). Here we have shown that JH is also necessary throughout the intermolt periods (Fig. 3I) to allow the isomorphic growth of the primordia together with that of the larva as a whole, while suppressing morphogenetic signaling systems that would transform the primordia into imaginal discs. This larval action of JH in suppressing morphogenesis is an extension of that seen in embryos of more basal insects, in which premature exposure to JH suppresses embryonic patterning and induces precocious terminal differentiation (12, 29). Hence, an ancient developmental role of this hormone appears to be in switching tissues between programs of growth and/or morphogenesis. JH-

like molecules occur in taxa other than the insects (30, 31), where they likely have similar developmental roles. Molecules with such actions might be exploited as antitumor agents in the future.

References and Notes

1. D. Fristrom, J. W. Fristrom, in *The Development of Drosophila melanogaster*, M. Bate, A. Martinez-Arias, Eds. (Cold Spring Harbor Laboratory Press, Plainview, NY, 1993), pp. 843–897.
2. S. J. Day, P. A. Lawrence, *Development* **127**, 2977 (2000).
3. L. A. Johnston *et al.*, *Cell* **98**, 779 (1999).
4. S. Oldham, E. Hafen, *Trends Cell Biol.* **13**, 79 (2003).
5. H. F. Nijhout, L. W. Grunert, *Proc. Natl. Acad. Sci. U.S.A.* **99**, 15446 (2002).
6. C. Mirth, J. W. Truman, L. M. Riddiford, *Curr. Biol.* **15**, 1796 (2005).
7. J. Colombani *et al.*, *Science* **310**, 667 (2005).
8. C. M. Williams, *Biol. Bull.* **121**, 572 (1961).
9. L. M. Riddiford, *Adv. Insect Physiol.* **24**, 211 (1994).
10. S. M. Cohen, in *The Development of Drosophila melanogaster*, M. Bate, A. Martinez-Arias, Eds. (Cold Spring Harbor Laboratory Press, Plainview, NY, 1993), pp. 747–841.
11. P. Svacha, *Dev. Biol.* **154**, 101 (1992).
12. J. W. Truman, L. M. Riddiford, *Nature* **401**, 447 (1999).
13. D. T. Champlin, J. W. Truman, *Development* **125**, 2009 (1998).
14. C. I. Miles, R. Booker, *Dev. Biol.* **155**, 147 (1993).
15. K. Tanaka, J. W. Truman, *Dev. Genes Evol.* **215**, 78 (2005).
16. J. P. Allee, C. L. Pelletier, E. K. Fergusson, D. T. Champlin, *J. Insect Physiol.*, in press.
17. S. G. MacWhinnie *et al.*, *Dev. Biol.* **285**, 285 (2005).
18. B. Cymborowski *et al.*, *J. Insect Physiol.* **28**, 129 (1982).
19. B. Zhou, K. Hiruma, T. Shinoda, L. M. Riddiford, *Dev. Biol.* **203**, 233 (1998).
20. B. Zhou, L. M. Riddiford, *Dev. Biol.* **231**, 125 (2001).
21. J. B. Nardi, T. A. Hardt, S. M. Magee-Adams, D. L. Osterbur, *Tissue Cell* **17**, 473 (1985).
22. E. J. Rutifson, S. K. Kim, R. Nusse, *Science* **296**, 1118 (2002).
23. T. Ikeya, M. Galic, P. Belawat, K. Nairz, E. Hafen, *Curr. Biol.* **12**, 1293 (2002).
24. H. F. Nijhout, *Biol. Bull.* **149**, 214 (1975).
25. H. F. Nijhout, *Dev. Biol.* **261**, 1 (2003).
26. M. Hatakoshi, I. Nakayama, L. M. Riddiford, *J. Insect Physiol.* **34**, 373 (1988).
27. R. Bohni *et al.*, *Cell* **97**, 865 (1999).
28. A. L. Sawaya, P. A. Martins, L. P. Grillo, T. T. Florencio, *Nutr. Rev.* **62**, S127 (2004).
29. D. F. Erezylmaz, L. M. Riddiford, J. W. Truman, *Dev. Genes Evol.* **214**, 313 (2004).
30. L. I. Gilbert, N. A. Granger, R. M. Roe, *Insect Biochem. Mol. Biol.* **30**, 617 (2000).
31. W. Biggers, H. Laufer, *Arch. Insect Biochem. Physiol.* **32**, 475 (1996).
32. We thank K. Tanaka for helpful comments on the manuscript. This study was initiated at the Friday Harbor Marine Laboratories. Research was supported by grants from NSF (IBN 0212072 to D.T.C.; IBN 0344933 to L.M.R.; and IBN 9904959 to J.W.T. and L.M.R.), the National Research Initiative of the U.S. Department of Agriculture Cooperative State Research, Education, and Extension Service (2001-35302-10918 to L.M.R.), the Bioscience Research Institute of Southern Maine (D.T.C.), the Japan Society for the Promotion of Science (17380033 to K.H.), and the Program for Promotion of Basic Research Activities for Innovative Bioscience (2600050015 to K.H.).

Supporting Online Material

www.sciencemag.org/cgi/content/full/312/5778/1385/DC1
Materials and Methods
SOM Text
Fig. S1
References

9 December 2005; accepted 27 March 2006
10.1126/science.1123652

Onset and Progression in Inherited ALS Determined by Motor Neurons and Microglia

S verine Boill e,^{1*} Koji Yamanaka,^{1*†} Christian S. Lobsiger,¹ Neal G. Copeland,² Nancy A. Jenkins,² George Kassiotis,^{3‡} George Kollias,³ Don W. Cleveland^{1†}

Dominant mutations in superoxide dismutase cause amyotrophic lateral sclerosis (ALS), a progressive paralytic disease characterized by loss of motor neurons. With the use of mice carrying a deletable mutant gene, expression within motor neurons was shown to be a primary determinant of disease onset and of an early phase of disease progression. Diminishing the mutant levels in microglia had little effect on the early disease phase but sharply slowed later disease progression. Onset and progression thus represent distinct disease phases defined by mutant action within different cell types to generate non-cell-autonomous killing of motor neurons; these findings validate therapies, including cell replacement, targeted to the non-neuronal cells.

Amyotrophic lateral sclerosis (ALS) is an adult-onset neurodegenerative disease that selectively kills upper and lower motor neurons. Dominant mutations in the gene encoding the ubiquitously expressed superoxide dismutase (SOD1) are the most prominent known causes of inherited ALS (1). Several hypotheses to explain motor neuron degeneration have been proposed, including mitochondrial dysfunction, protein aggregate formation, excitotoxicity, axonal transport malfunction, mutant-derived oxidative damage, lack of growth factors, and inflammation (2). Ubiquitous expression of mutant SOD1 in rodents leads to a progressive selective degeneration of motor neurons because of an acquired toxic property or properties (3–5). However, the contribution of damage mediated by mutant SOD1 to disease onset and progression in specific cell types of the spinal cord is not established. Expression of mutated SOD1 selectively in either motor neurons (6, 7) or astrocytes (8) has failed to cause ALS-like disease in mice. Although reducing SOD1 mutant accumulation within motor neurons by viral-delivered small interfering RNA can slow disease onset (9, 10), disease progression was not affected except in one case in which it was accelerated (10). Indeed, analyses of chimeric mice composed of mixtures of normal and SOD1 mutant-expressing cells have offered evidence that motor neuron death is non-cell-autonomous, with normal

non-motor-neuronal cells having the ability to reduce or eliminate toxicity to mutant-expressing motor neurons (11).

Fig. 1. Selective Cre-mediated gene inactivation shows that mutant SOD1 action within motor neurons is a primary determinant of an early disease phase. (A and B) Mutant SOD1 levels in motor axons of *LoxSOD1^{G37R}* mice in the (A) absence or (B) presence of *Isl1-Cre* expression. L5 ventral root sections were stained simultaneously with antibodies to (green) human SOD1 and (red) myelin basic protein. Insets show magnified images of boxed regions. (C and D) Histograms of relative intensities of mutant SOD1 fluorescence in each L5 motor axon measured from three (C) *LoxSOD1^{G37R}* or (D) *LoxSOD1^{G37R}/Isl1Cre⁺* mice. (E) Total accumulated mutant SOD1 levels measured as relative total fluorescence intensity in motor axons from entire L5 roots in each animal ($n = 3$ for each genotype). (F to H) Ages of (F) disease onset, (G) progression through an early disease phase (to 10% weight loss), and (H) disease end stage of (red) *LoxSOD1^{G37R}/Isl1Cre⁺* mice and (blue) *LoxSOD1^{G37R}* littermates. Insets show ventral root motor axons (stained with toluidine blue) in *LoxSOD1^{G37R}* mice at (F) onset, (G) early disease, and (H) end stage. (I and J) Duration of (I) an early disease phase (from onset to 10% weight loss) and (J) a later disease phase (from 10% weight loss to end stage) for (red) *LoxSOD1^{G37R}/Isl1Cre⁺* and (blue) *LoxSOD1^{G37R}* littermates. Scale bars in (A), (B), and (F) to (H), 50 μ m.

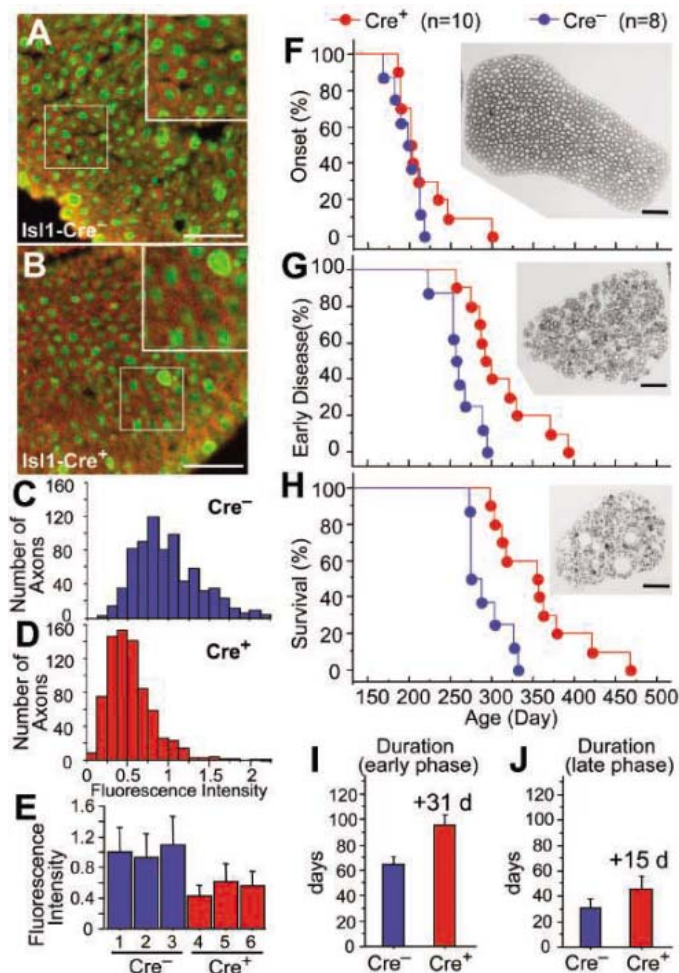
¹Ludwig Institute for Cancer Research and Departments of Medicine and Neuroscience, University of California at San Diego, 9500 Gilman Drive, La Jolla, CA 92093, USA. ²Mouse Cancer Genetics Program, National Cancer Institute–Frederick Cancer Research and Development Center, Frederick, MD 21702, USA. ³Institute of Immunology, Biomedical Sciences Research Center Alexander Fleming, 166 72 Vari, Greece.

*These authors contributed equally to this work.

†To whom correspondence should be addressed. E-mail: dcleveland@ucsd.edu (D.W.C.); kyamanaka@ucsd.edu (K.Y.)

‡Present address: Division of Immunoregulation, National Institute for Medical Research, The Ridgeway, Mill Hill, London NW7 1AA, UK.

To identify which cell types are damaged by mutant SOD1 and how this damage might influence the initiation and propagation of the course of the disease, transgenic mice (*LoxSOD1^{G37R}*) were generated that carried a mutant human SOD1^{G37R} gene flanked at both ends by 34-base pair LoxP sequences allowing recognition and regulated deletion by the Cre recombinase (fig. S1A) (12). Mice developed fatal progressive motor neuron disease, including progressive weight loss from denervation-induced muscle atrophy and paralysis that was essentially indistinguishable from that seen in previously described SOD1^{G37R} lines (5). The *LoxSOD1^{G37R}* line with highest mutant accumulation reached end-stage disease most rapidly (between 8.5 and 11 months), which was accompanied by the death of 55% of spinal motor neurons (fig. S1, B to F) (12). No human SOD1 protein was expressed in any progeny from the *LoxSOD1^{G37R}* females that also carried a transgene encoding the Cre recombinase in their



oocytes (13), demonstrating efficient *in vivo* gene removal in the presence of Cre (fig. S1, G and H) (12).

To examine the contribution to the disease of mutant SOD1 toxicity within motor neurons, *LoxSOD1^{G37R}* mice were mated to mice carrying a Cre-encoding sequence under control of the promoter from the *Islet-1* transcription factor (14). Cre recombinase in this line is expressed in the nervous system exclusively in progenitors of motor and dorsal root ganglion neurons and was sufficient to substantially reduce mutant SOD1 accumulation in most motor axons of L5 motor roots and lumbar motor neurons of presymptomatic *Is1-Cre⁺/LoxSOD1^{G37R}* animals (Fig. 1, A to E, and fig. S2) (12).

A simple objective measure of the earliest onset of disease was defined by the peak of the weight curve (12, 15). This age coincides with initial axonal retraction from neuromuscular synapses but occurs before substantial axonal degeneration or loss proximally in motor roots emerging from the spinal cord (Fig. 1F, inset). An early stage of disease, accompanied by hindlimb weakness and obvious axonal degeneration (Fig. 1G, inset), was defined to be the period from onset until denervation-induced muscle atrophy decreased maximal weight by 10%. Reduction of *SOD1^{G37R}* in motor neurons slowed disease onset in a minority of *LoxSOD1^{G37R}/Is1Cre⁺* mice, yielding an average delay of 18 days

(*Is1Cre⁺*, 216 ± 11.2 days; *Is1Cre⁻*, 198 ± 6.1 days) (Fig. 1F). Progression from onset through early disease was delayed in all of the mice, with a mean extension of 31 days (*Is1Cre⁺*, 95 days; *Is1Cre⁻*, 64 days) (Fig. 1, G and I); there was also a more modest slowing of later disease progression, with a mean extension of 15 days (Fig. 1J). Overall survival was extended by 64 days (*Is1Cre⁺*, 357.5 ± 17.2 days; *Is1Cre⁻*, 293.5 ± 8.7 days) (Fig. 1H).

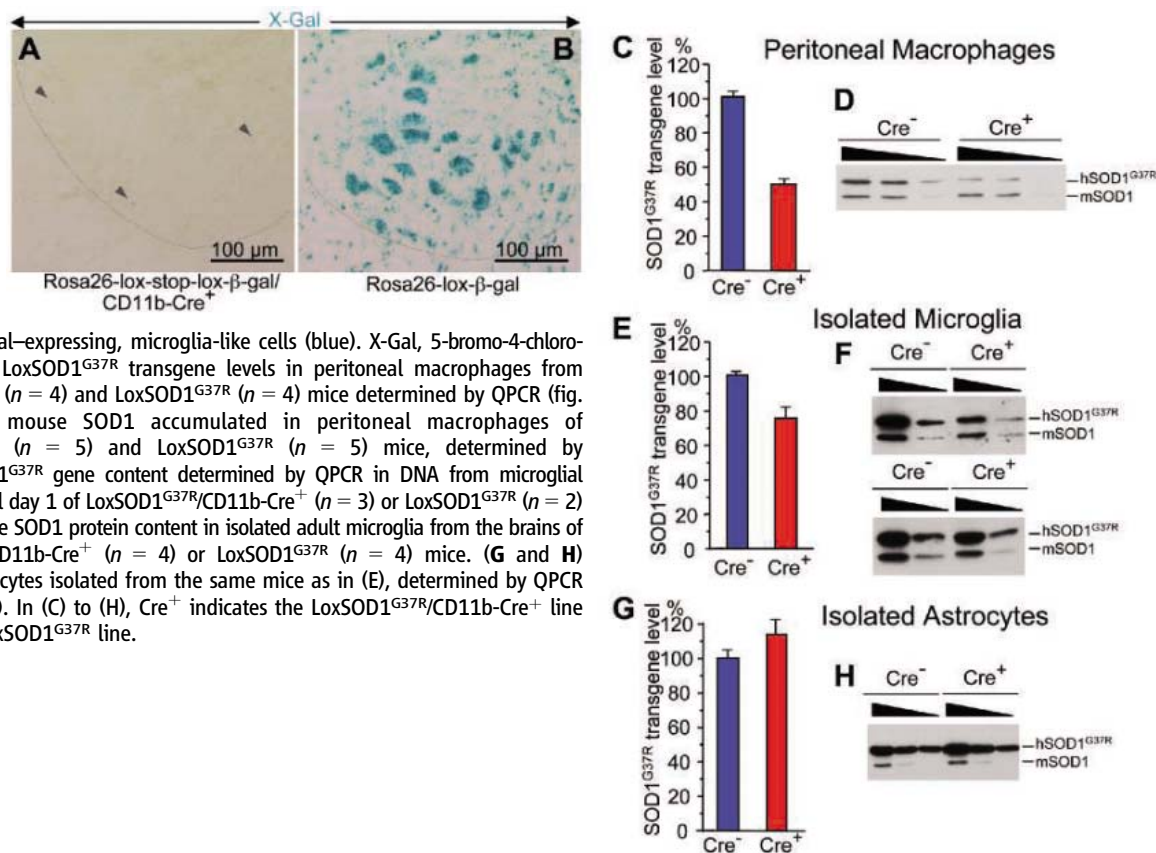
Microglia are the resident immune cells of the central nervous system and are the primary mediators of neuroinflammation (16). In the normal adult nervous system, these cells exist in a resting state and are characterized by a small cell body and fine ramified processes. However, neuronal damage can rapidly activate the release of cytotoxic and inflammatory mediators, including oxygen radicals, nitric oxide, and cytokines, that affect neighboring neurons and astrocytes (16, 17); in ALS, strong activation and proliferation of microglia occur in regions of motor neuron loss (18, 19). Minocycline, an antibiotic that can inhibit microglial activation (20), extends the survival of *SOD1* mutant mice (21–23), as does the inhibition of cyclooxygenase 2 (COX-2) (24), a key enzyme in prostaglandin synthesis. Both findings have raised the possibility of direct microglial involvement in ALS.

To test the role of the SOD1 mutant acting within microglia, we generated mice expressing Cre selectively in these cells using the promoter

for CD11b (25), an integrin expressed exclusively in the myeloid lineage (26) (fig. S3A) (12). Cell-type specificity of Cre expression was verified by mating those mice to the *Rosa26* mouse line that ubiquitously expresses a β-galactosidase (β-Gal) transgene that can be translated into functional β-Gal only if Cre-mediated recombination removes a premature translation terminator (27). Peritoneal macrophages and microglial cells expressed β-Gal in *Rosa26/CD11b-Cre⁺* mice, whereas no cells of either type expressed β-Gal in animals without the *CD11b-Cre* gene (fig. S3, B and D to G) (12). Although both neurons and astrocytes from *Rosa26* mice showed high levels of β-Gal activity after germline Cre expression (Fig. 2B), only small microglia-like cells expressed β-Gal in mice with the *CD11b*-encoded Cre and no β-Gal expression was detectable in neurons or astrocytes (Fig. 2A).

CD11b-Cre expression significantly diminished *SOD1^{G37R}* accumulation in peritoneal macrophages of *LoxSOD1^{G37R}* animals (Fig. 2, C and D; *n* = 4 or 5 per group). Quantitative real-time fluorescence polymerase chain reaction (QPCR), capable of distinguishing as small as a 20% difference in human SOD1 transgene DNA number (fig. S3C) (12), confirmed that macrophages from *CD11b-Cre⁺* animals retained only half of the mutant *SOD1^{G37R}* genes as did the *Cre⁻* animals (Fig. 2C; *n* = 4 per group). Microglia, purified from 1-day-old *LoxSOD1^{G37R}/CD11b-Cre⁺* mice or their *Cre⁻*

Fig. 2. *CD11b-Cre*-directed excision of *SOD1^{G37R}* exclusively in macrophage and microglial lineages. (A and B) β-Gal activity in lumbar spinal cord sections of (A) *Rosa26/CD11b-Cre⁺* mice or (B) *Rosa26* mice after systemic Cre-mediated gene excision. Arrowheads point to small, β-Gal-expressing, microglia-like cells (blue). X-Gal, 5-bromo-4-chloro-3-indolyl-β-galactoside. (C) *LoxSOD1^{G37R}* transgene levels in peritoneal macrophages from *LoxSOD1^{G37R}/CD11b-Cre⁺* (*n* = 4) and *LoxSOD1^{G37R}* (*n* = 4) mice determined by QPCR (fig. S3C). (D) Human and mouse SOD1 accumulated in peritoneal macrophages of *LoxSOD1^{G37R}/CD11b-Cre⁺* (*n* = 5) and *LoxSOD1^{G37R}* (*n* = 5) mice, determined by immunoblotting. (E) *SOD1^{G37R}* gene content determined by QPCR in DNA from microglial cells isolated from postnatal day 1 of *LoxSOD1^{G37R}/CD11b-Cre⁺* (*n* = 3) or *LoxSOD1^{G37R}* (*n* = 2) mice. (F) Human and mouse SOD1 protein content in isolated adult microglia from the brains of 7-week-old *LoxSOD1^{G37R}/CD11b-Cre⁺* (*n* = 4) or *LoxSOD1^{G37R}* (*n* = 4) mice. (G and H) *SOD1^{G37R}* content in astrocytes isolated from the same mice as in (E), determined by QPCR (G) or immunoblotting (H). In (C) to (H), *Cre⁺* indicates the *LoxSOD1^{G37R}/CD11b-Cre⁺* line and *Cre⁻* indicates the *LoxSOD1^{G37R}* line.



littermates and then cultured for 2 weeks, showed a 25% Cre-dependent decrease in the SOD1^{G37R} transgene levels (Fig. 2E). A similar reduction in mutant SOD1 was seen in adult microglia (Fig. 2F). Mutant SOD1 transgene content was unchanged in purified astrocytes (Fig. 2, G and H).

Microglial activation begins at or before disease onset in mutant SOD1 mice (21, 28, 29), with the number of activated cells escalating during progression, as measured with antibodies to CD11b or Iba1 (Fig. 3, A to C). No differences in microglia (Fig. 3, D to F) or astrocyte (Fig. 3, G to I) activation were observed in disease-matched LoxSOD1^{G37R}/CD11b-Cre⁺ and LoxSOD1^{G37R} mice. Nevertheless, lowering mutant SOD1 expression within microglia significantly extended the survival of LoxSOD1^{G37R}

mice, with a longer mean survival of 99 days relative to the cohort of LoxSOD1^{G37R} littermates (Fig. 3J). Half of the Cre-expressing cohort survived more than 100 days past the mean survival of LoxSOD1^{G37R} mice, and most of this extension was derived from slowing disease progression after onset. Indeed, although early disease progression was unchanged (Fig. 3K), the progression of later disease in CD11b-Cre⁺ mice was slowed by an average of 75 days (Fig. 3L). This slowing of later disease may derive in part from gene inactivation not just in microglia but also in peripheral macrophages or their progenitors and/or from the migration of those cells into the central nervous system after initial damage to motor neurons.

The potential for different mechanisms underlying disease initiation and progression has

previously been proposed in human ALS from observations of disease spread from an initially affected region. Our use of partial, selective gene inactivation offers direct evidence for mutant SOD1 damage within different cell types to underlie an initiating phase of disease caused by mutant SOD1 damage within motor neurons, and a mechanistically divergent later phase encompassing the progression to complete paralysis that is linked to the inflammatory response of microglia and mutant toxicity within these cells. These findings have important implications for the development of successful therapies for mutant SOD1-mediated as well as sporadic ALS. Although the mechanistic linkage between familial and sporadic ALS has not been unambiguously established, the two forms of disease are clinically indistinguishable, affect the same neurons, are characterized by ubiquitinated aggregates as hallmarks, display a loss of astrocytic glutamate transporters, and are accompanied by microgliosis and astrogliosis (2). In our study, limiting mutant damage to microglia robustly slowed the disease's course, even when all motor neurons were expressing high levels of a SOD1 mutant. Thus, although the initiation of the disease requires damage to motor neurons and probably to additional cell types, disease therapy might be successful by targeting only a single non-neuronal cell type.

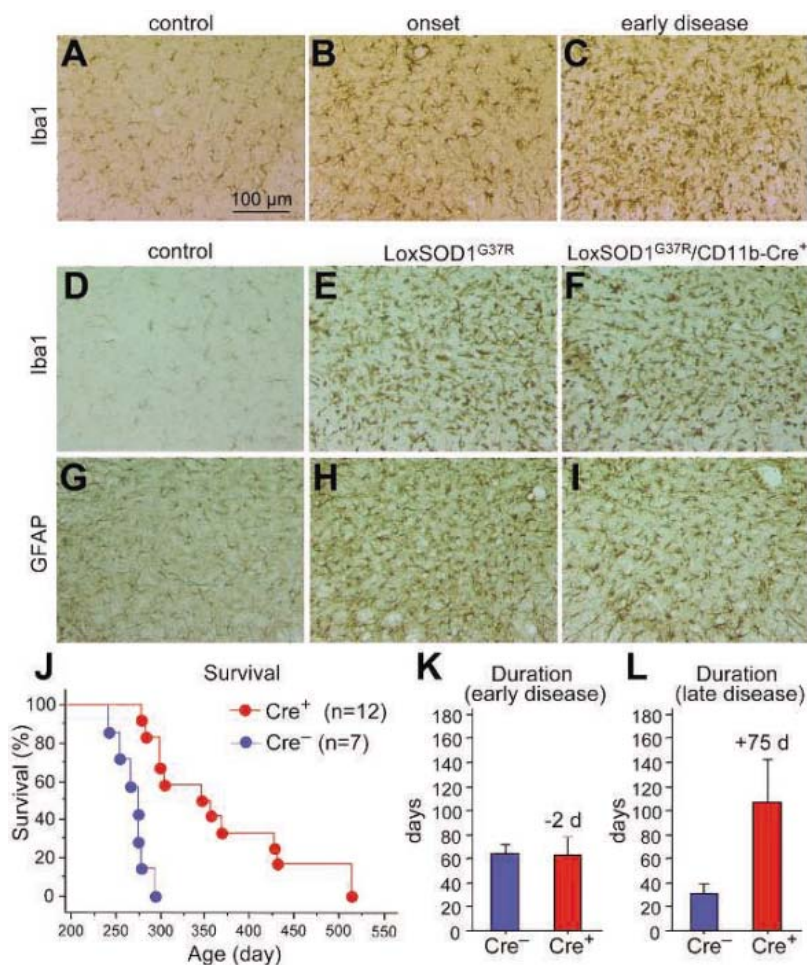


Fig. 3. Selective gene excision shows that mutant SOD1 action within the microglial and macrophage lineages is a primary determinant of a late phase of disease progression. (A to C) Microglial activation in the lumbar spinal cord of a LoxSOD1^{G37R} mouse at (B) disease onset and (C) an early disease stage (defined as 10% weight loss) compared to (A) that in an age-matched normal littermate. (D to F) Microglial activation in the lumbar spinal cord of (D) a normal mouse and of disease-matched (E) LoxSOD1^{G37R} or (F) LoxSOD1^{G37R}/CD11b-Cre⁺ mice, detected with antibodies to Iba1. (G to I) Astrocytes in the lumbar spinal cord of the same mice as in (D) to (F), detected with antibodies to glial fibrillary acidic protein (GFAP). (J) Survival times of LoxSOD1^{G37R}/CD11b-Cre⁺ (Cre⁺) and littermate LoxSOD1^{G37R} (Cre⁻) mice. (K and L) Disease duration of LoxSOD1^{G37R}/CD11b-Cre⁺ mice compared to LoxSOD1^{G37R} mice for (K) an early phase or (L) a late phase of disease.

References and Notes

1. D. R. Rosen *et al.*, *Nature* **362**, 59 (1993).
2. L. I. Bruijn, T. M. Miller, D. W. Cleveland, *Annu. Rev. Neurosci.* **27**, 723 (2004).
3. L. I. Bruijn *et al.*, *Neuron* **18**, 327 (1997).
4. M. E. Gurney *et al.*, *Science* **264**, 1772 (1994).
5. P. C. Wong *et al.*, *Neuron* **14**, 1105 (1995).
6. M. M. Lino, C. Schneider, P. Caroni, *J. Neurosci.* **22**, 4825 (2002).
7. A. Pramatarova, J. Laganier, J. Roussel, K. Brisebois, G. A. Rouleau, *J. Neurosci.* **21**, 3369 (2001).
8. Y. H. Gong, A. S. Parsadanian, A. Andreeva, W. D. Snider, J. L. Elliott, *J. Neurosci.* **20**, 660 (2000).
9. T. M. Miller *et al.*, *Ann. Neurol.* **57**, 773 (2005).
10. G. S. Ralph *et al.*, *Nat. Med.* **11**, 429 (2005).
11. A. M. Clement *et al.*, *Science* **302**, 113 (2003).
12. See supporting material on Science Online.
13. M. Lewandowski, K. M. Wassarman, G. R. Martin, *Curr. Biol.* **7**, 148 (1997).
14. S. Srinivas *et al.*, *BMC Dev. Biol.* **1** (2001); available at www.biomedcentral.com/1471-213X/1/4.
15. J. Liu, L. A. Shinobu, C. M. Ward, D. Young, D. W. Cleveland, *J. Neurochem.* **93**, 875 (2005).
16. G. W. Kreutzberg, *Trends Neurosci.* **19**, 312 (1996).
17. U. K. Hanisch, *Glia* **40**, 140 (2002).
18. J. S. Henkel *et al.*, *Ann. Neurol.* **55**, 221 (2004).
19. T. Kawamata, H. Akiyama, T. Yamada, P. L. McGeer, *Am. J. Pathol.* **140**, 691 (1992).
20. J. Yrjanheikki *et al.*, *Proc. Natl. Acad. Sci. U.S.A.* **96**, 13496 (1999).
21. J. Kriz, M. D. Nguyen, J. P. Julien, *Neurobiol. Dis.* **10**, 268 (2002).
22. L. Van Den Bosch, P. Tilkin, G. Lemmens, W. Robberecht, *Neuroreport* **13**, 1067 (2002).
23. S. Zhu *et al.*, *Nature* **417**, 74 (2002).
24. D. B. Drachman *et al.*, *Ann. Neurol.* **52**, 771 (2002).
25. D. D. Hickstein, D. M. Baker, K. A. Gollahon, A. L. Back, *Proc. Natl. Acad. Sci. U.S.A.* **89**, 2105 (1992).
26. A. Mazzone, G. Ricevuti, *Haematologica* **80**, 161 (1995).

27. P. Soriano, *Nat. Genet.* **21**, 70 (1999).
 28. M. E. Alexianu, M. Kozovska, S. H. Appel, *Neurology* **57**, 1282 (2001).
 29. E. D. Hall, J. A. Oostveen, M. E. Gurney, *Glia* **23**, 249 (1998).
 30. We gratefully acknowledge D.S. Howland (Molecular Genetics, Wyeth Research, Princeton, NJ 08543-8000) for the QPCR protocol; M. Mallat (U495, IFR70, INSERM UPMC, Paris, France) and V. Zujovic (UMR 546, INSERM UPMC, Paris, France) for advice on microglial cell culture; D. Swing for pronuclear injection; J. Folmer for tissue

sections; and T. Jessel, G. Martin, and P. Soriano for *Islet1-Cre*, *ZP3-Cre*, and *Rosa26* reporter mice, respectively. This work was supported by grants from NIH (NS 27036), the Center for ALS Research at Johns Hopkins, the ALS Association, and the European Commission (LSHG-CT-2005-005203). S.B. is a recipient of a Fondation pour la Recherche Medicale fellowship and an INSERM fellowship. K.Y. is a recipient of a Uehara Memorial Foundation fellowship and a Development grant from the Muscular Dystrophy Association.

Supporting Online Material

www.sciencemag.org/cgi/content/full/312/5778/1389/DC1
 Materials and Methods
 SOM Text
 Figs. S1 to S3
 References

6 December 2005; accepted 27 April 2006
 10.1126/science.1123511

An SNP Caused Loss of Seed Shattering During Rice Domestication

Saeko Konishi,^{1*} Takeshi Izawa,^{2*} Shao Yang Lin,^{1†} Kaworu Ebana,² Yoshimichi Fukuta,³ Takuji Sasaki,² Masahiro Yano^{2‡}

Loss of seed shattering was a key event in the domestication of major cereals. We revealed that the *qSH1* gene, a major quantitative trait locus of seed shattering in rice, encodes a BEL1-type homeobox gene and demonstrated that a single-nucleotide polymorphism (SNP) in the 5' regulatory region of the *qSH1* gene caused loss of seed shattering owing to the absence of abscission layer formation. Haplotype analysis and association analysis in various rice collections revealed that the SNP was highly associated with shattering among *japonica* subspecies of rice, implying that it was a target of artificial selection during rice domestication.

Cultivation of major cereals likely started about 10,000 years ago (1–4). During this domestication, ancient humans subjected several key events to selection. These included increase in the number of

seeds, improvement of fertility, change in plant architecture, change in seed shape, adaptation of flowering time to local areas, loss of seed color, and loss of seed shattering.

Recent studies in rice have revealed that several independent domestication events might have occurred to establish cultivated rice (3, 5–7). The archaeological record reveals that *japonica* rice, a subspecies of *Oryza sativa*, was bred about 10,000 years ago in the upstream regions of the Yangtze River in southwest China (3, 8, 9).

The loss of seed-shattering habit is thought to be one of the most important events in rice domestication, because the “easy-to-shatter” trait in wild relatives results in severe reduction in yield. Over the course of human history, distinct grain-threshing systems have been developed in several different eras in local areas of the world, in accordance with the degree of seed shattering. In current rice-breeding programs, this seed-shattering habit is still a target, especially in the construction of new *indica* (another subspecies of *O. sativa*) cultivars. Thus, seed-shattering habit is one of

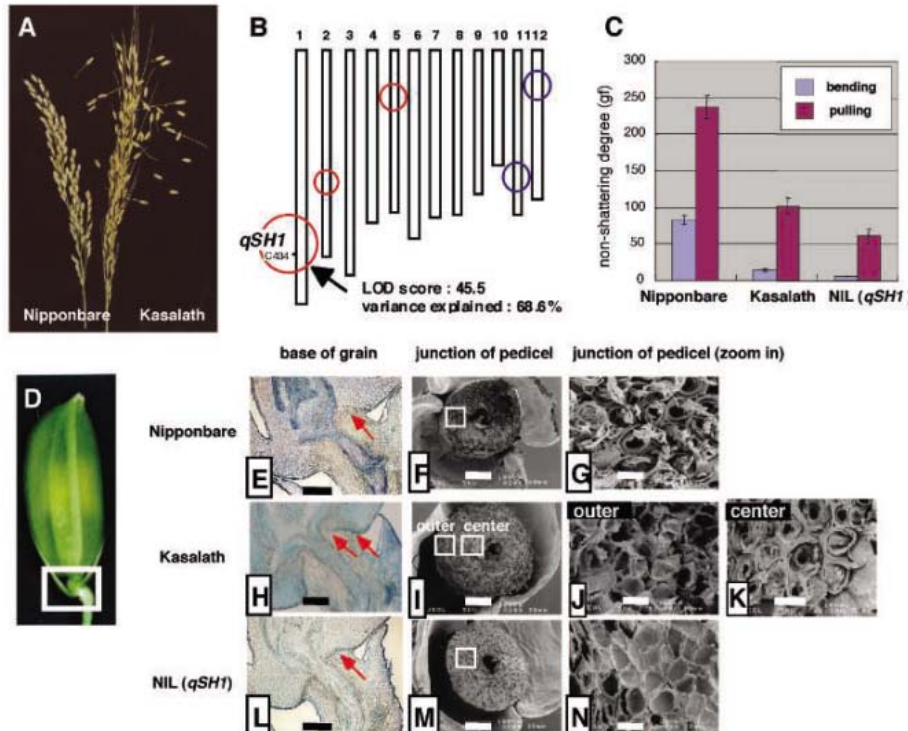


Fig. 1. *qSH1* is required for formation of the abscission layer at the base of the rice grain. (A) Seed-shattering habits of rice panicles. Photos taken after grabbing rice panicles. (Left) Nonshattering-type cultivar, Nipponbare. (Right) Shattering-type cultivar, Kasalath, in which the seed has shattered. (B) Chromosomal locations of QTLs for seed-shattering degree, based on an F₂ population from a cross between Nipponbare and Kasalath. Positions of circles indicate positions of QTLs, and circle size indicates the relative contribution of each QTL. Red circles, Nipponbare alleles contributing to non-shattering habit; blue circles, Kasalath alleles contributing to nonshattering. *qSH1* is marked on chromosome 1 with the nearest DNA marker (C434). (C) Non-seed-shattering habits of Nipponbare, Kasalath, and NIL(*qSH1*). Breaking tensile strength upon detachment of seeds from the pedicels by bending and pulling was measured (10). Increase in value indicates loss of shattering. NIL(*qSH1*), a nearly isogenic line carrying a Kasalath fragment at the *qSH1* locus in the Nipponbare background, as shown in fig. S1A. (D) Photo of a rice grain. White box indicates position of abscission layer formation. (E to G) Nipponbare. (H to K) Kasalath. (L to N) NIL(*qSH1*). (E), (H), and (L) Longitudinal sections of positions corresponding to white box in (D). Arrows point to the partial abscission layer of Kasalath in (H), the complete abscission layer of NIL(*qSH1*) in (L), and the corresponding region of Nipponbare in (E). (F), (I), and (M) Scanning electron microscope (SEM) photos of pedicel junctions after detachment of seeds. (G), (J), (K), and (N) Close-up SEM photos corresponding to white boxes in (F), (I), and (M). (G) Broken and rough surface of Nipponbare when forcibly detached. (N) Peeled-off and smooth surface of NIL(*qSH1*) upon spontaneous detachment. In Kasalath, rough center surface (K) and smooth outer surface (J) are observed. Scale bars: 500 μm in (E), (H), and (L); 100 μm in (F), (I), and (M); 10 μm in (G), (J), (K), and (N).

(F), (I), and (M) Scanning electron microscope (SEM) photos of pedicel junctions after detachment of seeds. (G), (J), (K), and (N) Close-up SEM photos corresponding to white boxes in (F), (I), and (M). (G) Broken and rough surface of Nipponbare when forcibly detached. (N) Peeled-off and smooth surface of NIL(*qSH1*) upon spontaneous detachment. In Kasalath, rough center surface (K) and smooth outer surface (J) are observed. Scale bars: 500 μm in (E), (H), and (L); 100 μm in (F), (I), and (M); 10 μm in (G), (J), (K), and (N).

the most important agronomic traits in rice cultivation and breeding.

It is difficult to obtain shattering-related mutants and reveal the underlying molecular mechanisms, because most rice cultivars have somehow lost the seed-shattering habit. We therefore used natural variations in seed shattering among cultivars. Generally, *indica* cultivars exhibit relatively strong seed shattering, whereas some *japonica* cultivars do not exhibit it at all (Fig. 1A). We first performed a QTL (quantitative

¹Institute of the Society for Techno-Innovation of Agriculture, Forestry, and Fisheries, 446-1 Ippaizuka, Kamiyokoba Tsukuba, Ibaraki 305-0854, Japan. ²National Institute of Agrobiological Sciences, 2-1-2 Kannondai, Tsukuba, Ibaraki 305-8602, Japan. ³Japan International Research Center for Agricultural Sciences, Tsukuba, Ibaraki 305-8686, Japan.

*These authors contributed equally to this work. †Present address: Honda Research Institute Japan Co., Ltd., Kisarazu, Chiba, 292-0818 Japan. ‡To whom correspondence should be addressed. E-mail: myano@nias.affrc.go.jp

trait locus) analysis between a shattering-type *indica* cultivar, Kasalath, and a nonshattering-type *japonica* cultivar, Nipponbare. The seed-shattering degree (breaking tensile strength) of each grain was measured (10), and the average value was scored for QTL analysis.

Five QTLs were detected on five chromosomes of rice in an F₂ population of a cross between Kasalath and Nipponbare (Fig. 1B). Nipponbare alleles at three QTLs on chromosomes 1, 2, and 5, and Kasalath alleles at two other QTLs on chromosomes 11 and 12, all contributed to shattering reduction, suggesting that loss of seed shattering may occur independently in *japonica* and *indica*.

The QTL with the largest effect, termed QTL of seed shattering in chromosome 1 (*qSH1*), explained 68.6% of the total phenotypic variation in the population (Fig. 1B). We therefore made a near-isogenic line (NIL) (fig. S1A) that contained a short chromosomal

segment from Kasalath at the *qSH1* region in a Nipponbare genetic background. The NIL exhibited the formation of a complete abscission layer between pedicel and spikelet at the base of the rice seed (Fig. 1, D and L to N) and had a stronger seed-shattering phenotype than either Kasalath or Nipponbare (Fig. 1C). In contrast, no abscission layer was observed in Nipponbare at all (Fig. 1, E to G). This indicated that a mutation in the *qSH1* gene alone resulted in complete loss of the abscission layer in the Nipponbare genetic background and that the Kasalath allele of *qSH1* could rescue it. Kasalath could form a partial abscission layer only at the peripheries in the transverse plane (Fig. 1, H to K), perhaps because of the presence of the minor QTLs (Fig. 1B).

A large-scale linkage analysis of 10,388 plants segregating at the *qSH1* region (fig. S1, B and C) was performed for the fine mapping of *qSH1*. We finally succeeded in mapping the

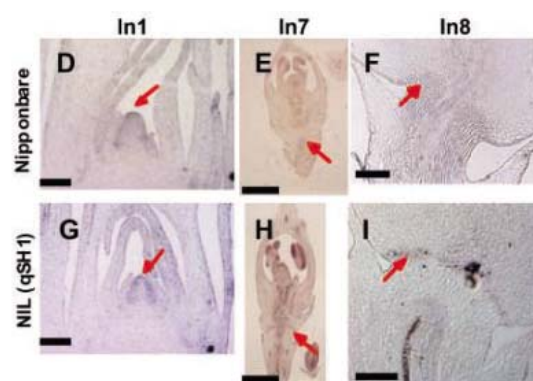
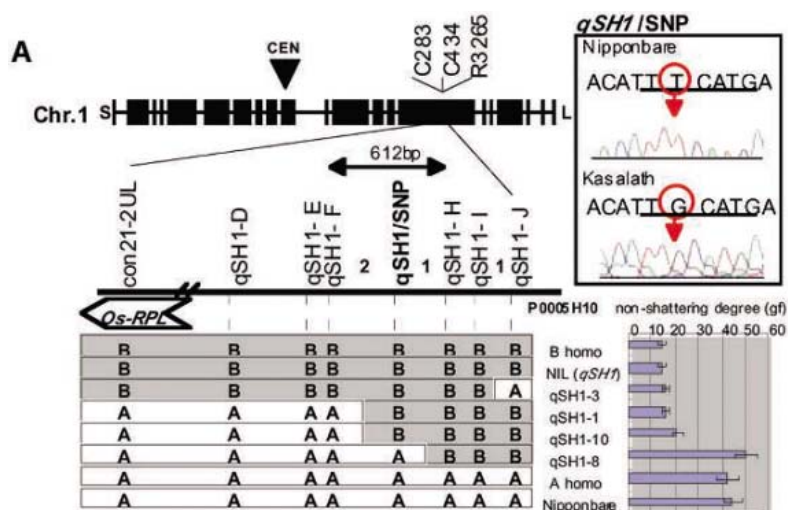
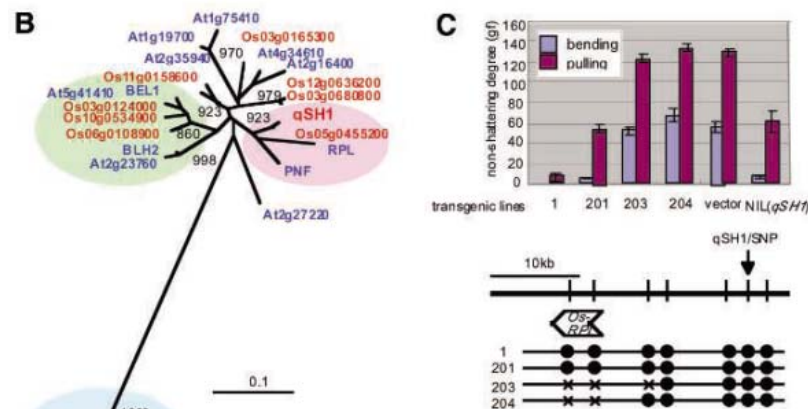


Fig. 2. Fine mapping, identification of FNP, cloning of *qSH1*, and *qSH1* expression. (A) Top left: C434 was the nearest marker to *qSH1* upon the rough mapping. Markers C283 and R3265 were used to select recombinants near the *qSH1* locus. (Bottom) Graphical genotypes of four selected recombinant homozygous lines and their non-shattering degrees. B and A are homozygous for Kasalath and Nipponbare, respectively. NIL(*qSH1*), B homo, A homo, and Nipponbare are control lines. (Top right) The single SNP in the 612-bp region. The typical RY repeat position is underlined. (B) Neighbor-joining phylogenetic tree of BEL1-type homeobox genes found in *Arabidopsis* and rice genomes. STM and OSH1 are outgroups. The region contains only the homeobox domains used for generating the tree (figs. S2C and S6). Rice and *Arabidopsis* genes are in red and blue type, respectively. (C) Complementation test for *qSH1* gene. A 26-kb Kasalath fragment (TAC9) in TAC vector, pYLTAC7 (30), was transformed into Nipponbare. (Top) Nonshattering degrees of T0 plants were measured. (Bottom) Dots and crosses indicate DNA markers used to confirm the transformed and nontransformed parts, respectively, of the 26-kb



fragment in each line. Lines 203 and 204 were partly transformed, because these lines lost the ORF region upon transformation. (D) to (I) In situ analysis of *qSH1* expression. An 870-bp fragment hybridized specifically to the *qSH1*, not to a paralog in Fig. 2B, was used as a probe for this analysis. *qSH1* expression was detected at shoot

apical meristems in both Nipponbare (D) and NIL(*qSH1*) (G) upon floral transition (stage In1) (16). At the flower-formation stage, *qSH1* expression was detected at the anther regions in both NIL(*qSH1*) and Nipponbare (E, H) and at the provisional abscission layer position only in NIL(*qSH1*) (H for stage In7, I for stage In8) and not in Nipponbare (E for stage In7, F for stage In8). Scale bars: 100 μm in (D), (F), (G), and (I); 200 μm in (E), and (H). Arrows point to the meristems in (D) and (G) and to the (provisional) abscission layers in (E), (F), (H), and (I).

functional natural variation in 612 bp between the flanking markers *qSH1-F* and *qSH1-H* and found only one single-nucleotide polymorphism (SNP) within this region (Fig. 2A). We confirmed this result using several recombinant homozygous plants in the progeny (Fig. 2A). Gene prediction for the *qSH1* region in both Nipponbare (11) and Kasalath genome sequences showed no distinct open reading frame (ORF) in the SNP region. However, located 12 kb away from the SNP, we found one ORF (locus ID Os01g0848400 in the Rice Annotation Project DataBase) for a rice ortholog of the *Arabidopsis REPLUMLESS (RPL)* (12, 13) gene (Fig. 2B and fig. S2). The *RPL* gene encodes a BEL1-type homeobox (14, 15) and is involved in the formation of a dehiscence zone (or abscission layer) alongside the valve in the *Arabidopsis* fruit (silique). Because the fruit originates from the carpels in *Arabidopsis*, the botanical origin of the dehiscence zone in *Arabidopsis* fruit does

not correspond to that of the abscission layer in rice seeds. However, it was still possible that this *RPL* ortholog was the *qSH1* gene. To confirm this, we introduced ten 10- to 26-kb Kasalath genomic fragments scanning the predicted ORF and the SNP regions into the nonshattering Nipponbare cultivar (Fig. 2C and figs. S3 and S7). Only transgenic lines that contained the Kasalath fragment with both the ORF and the SNP exhibited complete seed shattering, although one fragment (termed sub51), which contained a full ORF region but not the SNP, partly complemented the phenotype (fig. S3). The other fragments were not able to complement it, even if they contained the entire ORF region or the SNP region. These results indicated that both the ORF and the SNP regions were required for full shattering function.

In situ hybridization analysis revealed that in the NIL the ORF was expressed at the inflorescence meristem in the stage of rachis

meristem establishment [inflorescence stage 1 (In1)] (16) (Fig. 2G). It was also expressed at both the anther region and the provisional abscission layer at the base of the spikelet in the stage of floral organ differentiation (In7) (Fig. 2H) and in the stage of rapid elongation of the rachis and branches (In8) (Fig. 2I). The abscission layer was not yet observable in In7. On the other hand, in Nipponbare, the ORF was expressed in the same way as in the NIL (Fig. 2, D to F), except that it was not expressed at the provisional abscission layer in either In7 or In8 (Fig. 2, E and F).

These results, together with the complementation results, led us to conclude that this *RPL* ortholog was the *qSH1* gene and that the identified SNP affected only the spatial mRNA expression pattern of *qSH1* at the abscission layer. A quantitative RT-PCR for RNA samples of developing panicles supported this conclusion (fig. S8). Consistently, a *cis*-element search re-

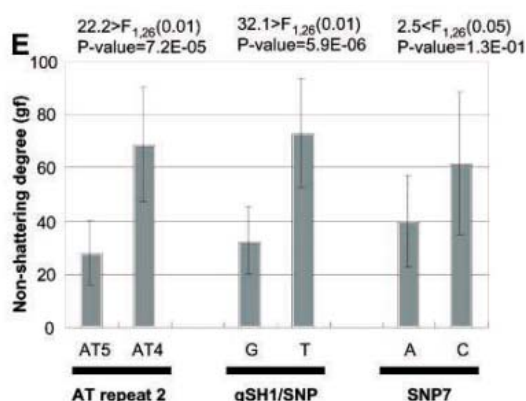
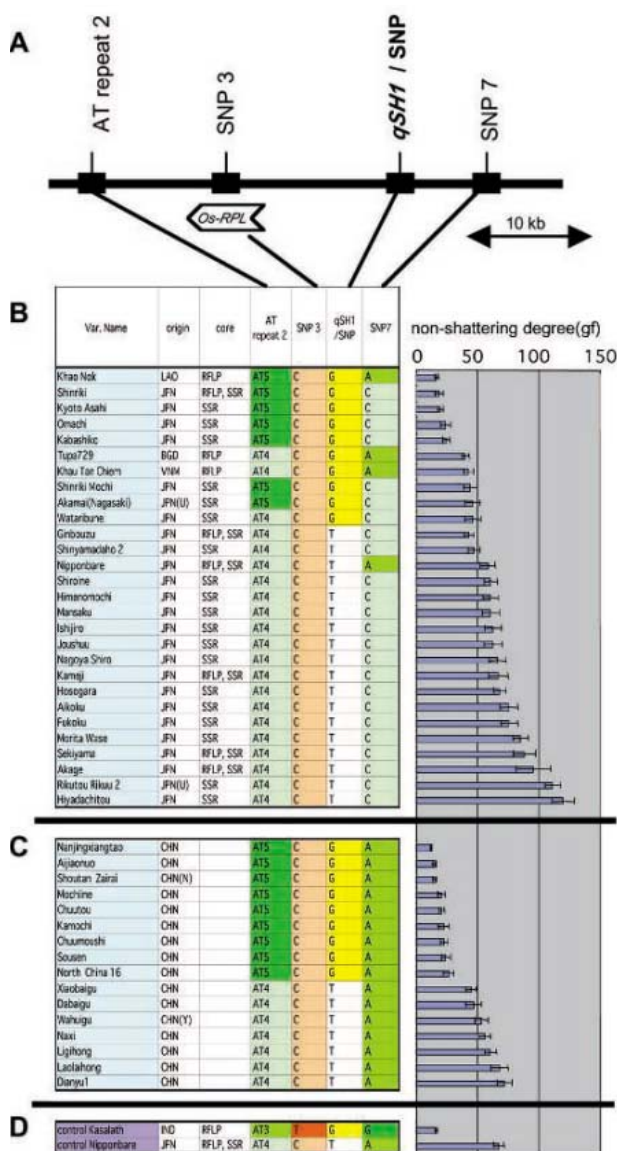


Fig. 3. Association of *qSH1* haplotypes with degree of shattering. (A) The four genomic regions with DNA polymorphisms at the *qSH1* locus are shown as thick black rectangles. *Japonica* has two subgroups, *tropical japonica* and *temperate japonica* (28). Only polymorphisms found in the population of *temperate japonica* cultivars are presented in (B), (C), and (D), with the exception of SNP3. SNP3 is present to show the lack of polymorphism at this site in all *japonica* cultivars tested, although the SNP3 found in Kasalath caused one amino acid change in *qSH1*, which was the sole amino acid change found between the ORFs of Nipponbare and Kasalath (fig. S5). SNP3 was not a target for human selection during rice cultivation. (B) Cultivars in *temperate japonica* core collections selected by genome-wide RFLP (27) and/or SSR (simple repeat sequence) analysis. U, upland-type cultivars. (C) *Temperate japonica* cultivars of Chinese origin. N and Y, North and Yunnan, respectively. These cultivars were assigned to *temperate japonica* by genome-wide RFLP analysis. No indications of RFLP and/or SSR in the core column mean the cultivars were not selected as core collections. (D) Nipponbare and Kasalath controls. At right in (B), (C), and (D), nonshattering degrees were also examined. (E) Statistical analysis of the association of seed shattering with genotype. ANOVA analysis was done with data shown in (B). AT repeat 2 and *qSH1/SNP*, but not SNP7, showed significant associations with seed shattering in *temperate japonica* cultivars. Standard errors are also shown in the graph.

vealed that the Kasalath *qSH1* allele contained a typical RY-repeat (17) that was a binding site of the *ABI3* (*VPI*)-type (18, 19) transcription factor at the SNP site (Fig. 2A and fig. S4). Therefore, the change in the transcriptional control of key genes such as *RPL* and *qSH1* could explain the difference in abscission layer formation between rice and *Arabidopsis*. Several genes downstream of *RPL* have been identified, such as *SHPI2* genes (20) belonging to the *AG*-clade MADS box genes in *Arabidopsis*. Phylogenetic analysis has revealed that *SHP* genes evolved after the eu-dicots separated from the common ancestors of eu-dicot and monocot plants (21), and all the *Arabidopsis AG*-clade MADS box genes are expressed in the carpel regions (22). In addition, it has been recently shown that two *AG* orthologs have evolutionally conserved functions with *AG* in rice (23). Thus, it is very likely that no functionally related ortholog of *SHPI2* exists in the rice genome. Therefore, it is also possible that *qSH1* expression may lead to formation of the abscission layer at the base of the seed by a mechanism distinct from that of dehiscence zone formation in *Arabidopsis* fruit.

Hence, we believe that, like the *RPL* in *Arabidopsis* (24), *qSH1* may have pleiotropic functions in the spikelet development and plant architecture of rice, as well as in abscission layer formation. Therefore, null or severe muta-

tions in the ORF may cause serious defects in rice development to establish it as a cultivar. This type of SNP, which caused loss of *qSH1* mRNA expression only at the abscission layer, could be survived during rice domestication. Similarly, it has been proposed that several maize domestication genes contain critical polymorphisms that have resulted from prehistoric artificial selection in the 5' regulatory regions, although the functional nucleotide polymorphisms have not yet been identified (25, 26).

To address how the SNP in *qSH1* prevailed during rice domestication, we next analyzed rice core collections (27) (Fig. 3, A and B). The results revealed that the SNP was highly associated with the degree of seed shattering among *temperate japonica* rice cultivars (a subgroup of *japonica*) (28) and implied that this SNP had been a target of artificial selection for nonshattering habit during rice domestication (Fig. 3E). All tested *indica* cultivars exhibited strong seed shattering; this result was consistent with the fact that they all contained the functional SNP (fig. S5C). Other QTLs need to be considered to explain the differences among *tropical japonica* cultivars (the other subgroup of *japonica*) (fig. S5D).

Rice cultivation likely started about 10,000 years ago; paddy-style rice cultivation is believed to have started in the Yangtze River re-

gion of China about 7000 years ago and to have been imported into Japan about 3000 years ago (3, 8). We therefore analyzed rice cultivars of Chinese origin (Fig. 3C) and found that the nonshattering SNP at *qSH1* might have been used in ancient China 3,000 to 10,000 years ago, most likely about 7,000 years ago upon the establishment of paddy-style rice cultivation.

Crop domestication might have proceeded during relatively short periods (less than 10,000 years) through the occurrence of nucleotide polymorphisms, such as by spontaneous mutation, recombination, and fixation in populations. Because rice is a self-pollinated plant, such newly occurring nucleotide polymorphisms would have easily become fixed in individuals. If such individuals propagated and contributed to the establishment of cultivated rice, we should be able to follow step by step the haplotype changes that occurred during rice domestication. Therefore, we examined the haplotypes around the *qSH1* gene in the rice collections (Fig. 4A). The identified SNP was likely to be assigned as a mutation that occurred in early domesticates of *japonica* subspecies (Fig. 4B) but not as a preexisting natural variation. In the hypothetical process of evolution of *qSH1*, the SNP distribution clearly revealed a strong selection by ancient humans for the SNP during rice domestication (Fig. 4B). In addition, the

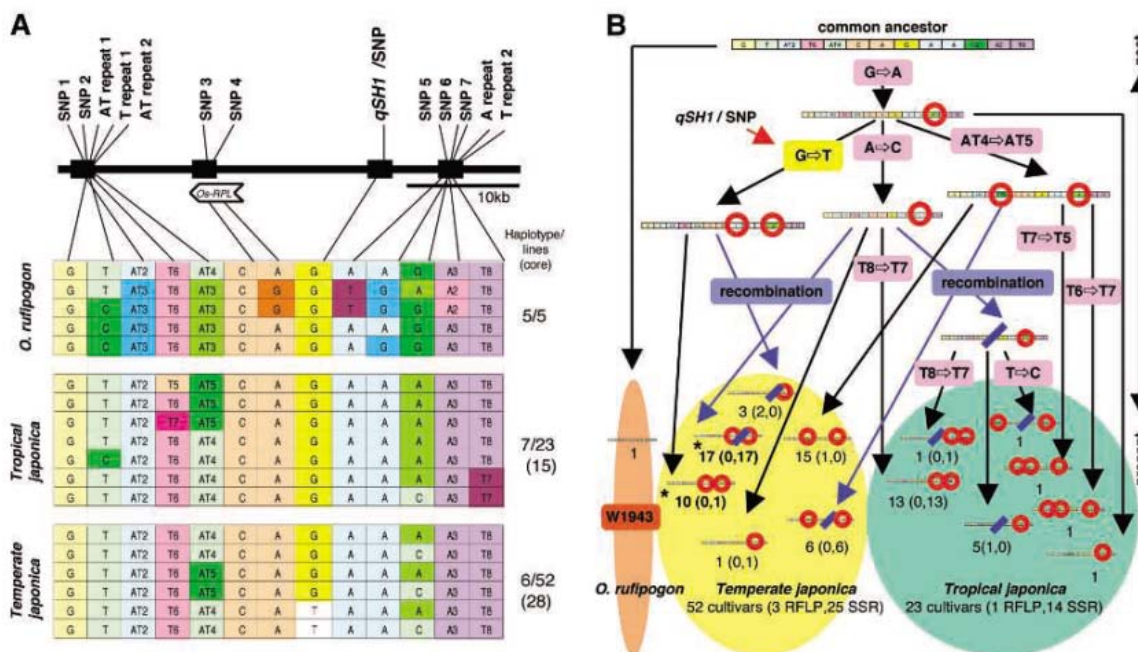


Fig. 4. Haplotypes at *qSH1* and hypothetical evolutionary process in *japonica*. **(A)** Eight SNPs (including the *qSH1*/SNP) and five SSRs from four genomic fragments were examined. On the basis of the results in 80 lines (including 43 cultivars from core collections), 18 haplotypes found at *qSH1* were presented (fig. S5). Results including the *indica* cultivars are shown only in fig. S5; we did not examine accurate haplotypes of some *indica* cultivars because of a lack of PCR amplification fragments. **(B)** Hypothetical process of evolution at *qSH1* during *japonica* rice domestication. Nine mutations and two recombination events are enough to

explain the natural variations at *qSH1* in *japonica*. Among 75 cultivars tested (52 *temperate japonica* and 23 *tropical japonica*), 27 contained the nonshattering T allele at *qSH1*/SNP but represented only two haplotypes (asterisks) among 13 haplotypes found in the 75 cultivars, suggesting strong selection by humans during domestication. Numbers under haplotypes indicate corresponding numbers of rice accessions. Numbers of accessions in RFLP and SSR core collections, in that order, are indicated in parentheses. Red circles highlight the mutation position in the haplotypes.

estimated haplotype of the common ancestor at the *qSH1* locus was found in a wild rice accession, W1943 (Fig. 4B), which is closely related to the *japonica* subspecies (6). We could therefore follow how domestication proceeded at the level of DNA sequence change, from ancestors to cultivated rice. Many agronomic traits are related to domestication events and could have been the targets of artificial selection during domestication. Therefore, this type of evolutionary analysis may give us some insights into the domestication process and could reveal practical, useful allele information for future breeding in cereals (29). For instance, introgression of the Nipponbare *qSH1* allele into *indica* cultivars would reduce the seed-shattering degree and could improve yield.

References and Notes

1. S. D. Tanksley, S. R. McCouch, *Science* **277**, 1063 (1997).
2. F. Salamini, H. Ozkan, A. Brandolini, P. R. Schafer, W. Martin, *Nat. Rev. Genet.* **3**, 429 (2002).
3. G. S. Khush, *Plant Mol. Biol.* **35**, 25 (1997).
4. J. Doebley, *Annu. Rev. Genet.* **38**, 37 (2004).
5. D. A. Vaughan, H. Morishima, K. Kadowaki, *Curr. Opin. Plant Biol.* **6**, 139 (2003).
6. C. Cheng *et al.*, *Mol. Biol. Evol.* **20**, 67 (2003).
7. C. Vitte, T. Ishii, F. Lamy, D. Brar, O. Panaud, *Mol. Genet. Genomics* **272**, 504 (2004).
8. Y. I. Sato, S. X. Tang, L. U. Yang, L. H. Tang, *Rice Genet. News* **8**, 76 (1991).
9. R. S. MacNeish, S. G. Cuunar, A. Zhao, J. Libby, Second Ann. Rep. Sino-American Jianxi Origin of Rice Project (SAJOR), 80 pp. (1998).
10. T. Ichikawa, T. Sugiyama, H. Takahashi, S. Miyahara, *JARQ* **24**, 37 (1990).
11. IRGSP (International Rice Genome Sequencing Project), *Nature* **436**, 793 (2005).
12. A. H. Roeder, C. Ferrandiz, M. F. Yanofsky, *Curr. Biol.* **13**, 1630 (2003).
13. J. R. Dinneny, M. F. Yanofsky, *Bioessays* **27**, 42 (2005).
14. L. Reiser *et al.*, *Cell* **83**, 735 (1995).
15. M. Ito, Y. Sato, M. Matsuoka, *Int. Rev. Cytol.* **218**, 1 (2002).
16. J. Itoh *et al.*, *Plant Cell Physiol.* **46**, 23 (2005).
17. H. Baumlein, I. Nagy, R. Villarreal, D. Inze, U. Wobus, *Plant J.* **2**, 233 (1992).
18. M. Suzuki, C. Y. Kao, D. R. McCarty, *Plant Cell* **9**, 799 (1997).
19. I. Ezcurra, P. Wycliffe, L. Nehlin, M. Ellerstrom, L. Rask, *Plant J.* **24**, 57 (2000).
20. S. J. Liljegen *et al.*, *Nature* **404**, 766 (2000).
21. E. M. Kramer, M. A. Jaramillo, V. S. Di Stilio, *Genetics* **166**, 1011 (2004).
22. A. Pinyopich *et al.*, *Nature* **424**, 85 (2003).
23. T. Yamaguchi *et al.*, *Plant Cell* **18**, 15 (2005).
24. H. M. Smith, B. C. Campbell, S. Hake, *Curr. Biol.* **14**, 812 (2004).
25. R. M. Clark, E. Linton, J. Messing, J. F. Doebley, *Proc. Natl. Acad. Sci. U.S.A.* **101**, 700 (2004).
26. H. Wang *et al.*, *Nature* **436**, 714 (2005).
27. Y. Kojima, K. Ebana, S. Fukuoka, T. Nagamine, M. Kawase, *Breed. Sci.* **55**, 431 (2005).
28. A. J. Garriss, T. H. Tai, J. Coburn, S. Kresovich, S. McCouch, *Genetics* **169**, 1631 (1995).
29. G. S. Khush, *Nat. Rev. Genet.* **2**, 815 (2001).
30. Y. G. Liu *et al.*, *Proc. Natl. Acad. Sci. U.S.A.* **96**, 6535 (1999).
31. We thank T. Murakami for assistance with histology; T. Inoue and K. Tsuchihara for technical help with SEM; J. Kyozuka, T. Kurakawa, and A. Tagiri for assistance with *in situ* analysis; and K. Shu, F. Aota, and R. Matsuzaki for technical assistance. This work was supported in part by the Mutant Panel Project of the Ministry of Agriculture, Forestry and Fisheries (MAFF) of Japan to M.Y. (MP1113a) and in part by the Diversified Genome Project of MAFF to S.K. and T.I. (GD2008). Data have been deposited into GenBank with accession numbers AB071330 to AB071333.

Supporting Online Material

www.sciencemag.org/cgi/content/full/1126410/DC1
Materials and Methods
Figs. S1 to S8
References

21 February 2006; accepted 6 April 2006
Published online 13 April 2006;
10.1126/science.1126410
Include this information when citing this paper.

Outer Membrane Active Transport: Structure of the BtuB:TonB Complex

David D. Shultis,¹ Michael D. Purdy,¹ Christian N. Banchs,² Michael C. Wiener^{1,2*}

In Gram-negative bacteria, the import of essential micronutrients across the outer membrane requires a transporter, an electrochemical gradient of protons across the inner membrane, and an inner membrane protein complex (ExbB, ExbD, TonB) that couples the proton-motive force to the outer membrane transporter. The inner membrane protein TonB binds directly to a conserved region, called the Ton-box, of the transporter. We solved the structure of the cobalamin transporter BtuB in complex with the C-terminal domain of TonB. In contrast to its conformations in the absence of TonB, the Ton-box forms a β strand that is recruited to the existing β sheet of TonB, which is consistent with a mechanical pulling model of transport.

In addition to an inner (plasma) membrane, Gram-negative bacteria have an outer membrane that affords additional environmental protection to the organism. Porins, which are β barrel proteins that typically function as diffusion pores, permit passive transport across the outer membrane of molecules with molecular weights \sim 600 daltons or less (1). However, bacteria, like other organisms, also require molecules that are larger and/or are present in the extracellular milieu at low concentration. Specifically, Gram-negative bacteria require iron, which is often taken up in the form of iron-siderophore complexes (2), as well as other organometallic compounds such as cobalamins (e.g., cyanocobalamin, vitamin B₁₂)

(3). Because a reduction of iron uptake correlates with a decrease in bacterial virulence (4), these transport systems are an attractive target for antibacterial drug discovery.

The uptake of scarce nutrients across the outer membrane is performed by a specialized active transport system that requires three components: specialized outer membrane transport proteins, an inner membrane multiprotein complex, and the inner membrane proton-motive force (pmf) to drive active transport (5). The outer membrane transporters have a common architecture of a 22-stranded β barrel situated in the membrane, long extracellular loops, short periplasmic turns, and a distinctive luminal domain (6). This luminal domain, composed of the N-terminal portion of the transporter, forms a globular-like domain that occludes the barrel. The inner membrane protein complex consists of the proteins ExbB, ExbD, and TonB. ExbB and ExbD are homologous to the MotA and MotB “stator” proteins

of the bacterial flagellar motor (7). The protein TonB—which has a single putative transmembrane helix, a proline-rich linker region, and a periplasmic C-terminal domain—couples the inner membrane pmf to the outer membrane transporter. Multiple structures of the mixed α helical/ β sheet C-terminal domain of TonB have been determined (8). TonB-dependent outer membrane transporters have a conserved motif, the Ton-box (9, 10), that interacts with TonB during the active transport cycle. Deletion (or certain mutations) of the Ton-box abrogate transport but do not affect substrate binding (3). The molecular mechanism of TonB-dependent outer membrane active transport is not known. Conformational change of the luminal domain to open a permeation path for substrate must occur, but whether the domain remains within the barrel or undergoes partial or full removal is not known. The presence of protein components in both bacterial membranes is suggestive of an “action-at-a-distance” mechanical pulling model, but compelling experimental evidence is lacking. In order to obtain additional information on the nature of TonB-dependent outer membrane active transport, we solved the structure of the C-terminal domain of TonB in complex with the cobalamin transporter BtuB.

BtuB and a C-terminal domain of TonB (residues 147 to 239) from *Escherichia coli*, were separately expressed and purified; the complex was made by combining BtuB and TonB in a molar ratio of \sim 1:5 in the presence of the substrate cyanocobalamin (vitamin B₁₂) and excess calcium. The structure was solved to 2.1 Å by molecular replacement using the structure of substrate-bound BtuB [Protein Data Bank (PDB) accession number 1NQJ] (11) as the

¹Department of Molecular Physiology and Biological Physics, and ²Interdisciplinary Graduate Program in Biophysics, University of Virginia, Charlottesville, VA 22908, USA.

*To whom correspondence should be addressed. E-mail: mwienner@virginia.edu

search model; the final crystallographic R and free-R factors are 0.192 and 0.251, respectively (12). The structure that we obtained is a 1:1

complex of BtuB:TonB (Fig. 1, A and B, and fig. S1). TonB is bound to the bottom (i.e., periplasmic-facing side) of BtuB, and covers

approximately one-half of the bottom surface of BtuB (Fig. 1A). Compared with BtuB alone, the major structural changes of BtuB in the complex

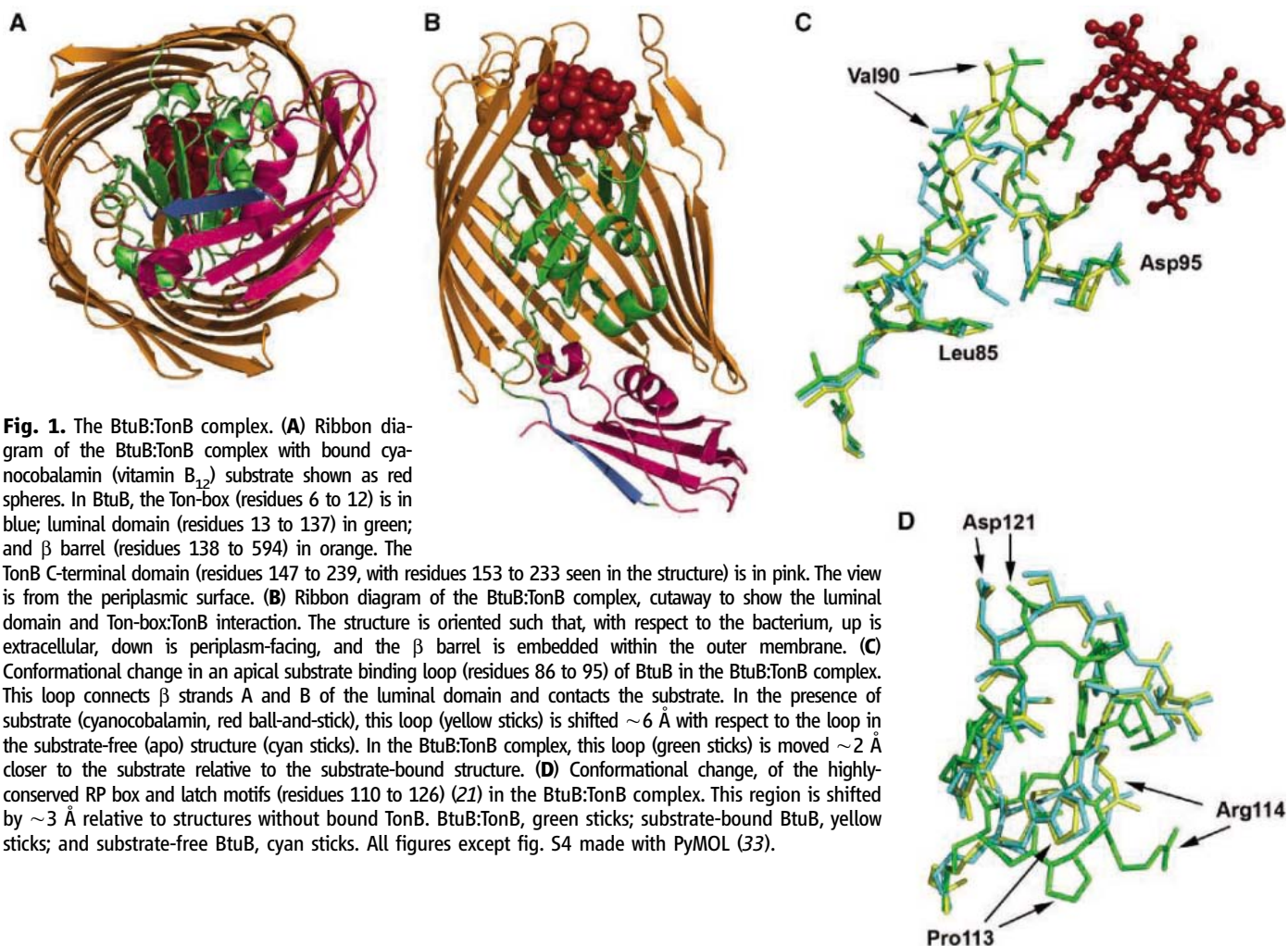
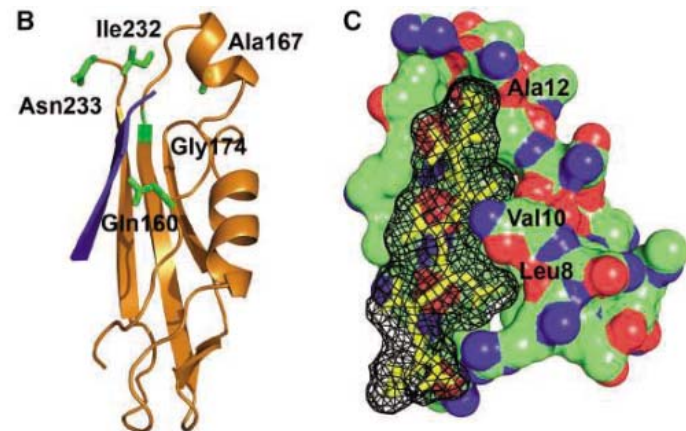


Fig. 2. Ton-box:TonB interactions and properties. **(A)** Ton-box:TonB cysteine-scanning cross-linking data mapped onto the structure. The Ton-box of BtuB (Asp⁶, Thr⁷, Leu⁸, Val⁹, Val¹⁰, Thr¹¹, and Ala¹²) is shown as blue sticks; TonB residues Arg¹⁵⁸, Asn¹⁵⁹, Gln¹⁶⁰, Pro¹⁶¹, Gln¹⁶², Tyr¹⁶³, and Pro¹⁶⁴ are shown as green sticks. Dashed lines depict disulfide crosslinks observed between BtuB and TonB (16); solid lines depict disulfide crosslinks observed between FecA and TonB (17) (with the residues of the FecA Ton-box aligned with the BtuB Ton-box). The salt-bridge between TonB Arg¹⁵⁸ and Ton-box Asp⁶ can be seen. **(B)** NMR chemical-shift data obtained from Ton-box peptide binding to TonB (15), mapped onto the structure. The Ton-box of BtuB (Asp⁶, Thr⁷, Leu⁸, Val⁹, Val¹⁰, Thr¹¹, and Ala¹²) is shown in blue ribbon; TonB is



shown in orange ribbon. The residues (Gln¹⁶⁰, Ala¹⁶⁷, Gly¹⁷⁴, Ile²³², and Asn²³³) present in our structure that displayed the five largest chemical shifts are shown as green side-chain sticks (except for Gly¹⁷⁴, where the backbone is colored green). **(C)** Packing of the Ton-box with TonB. The Ton-box (yellow sticks with black mesh) packs within a crevice formed by a β strand and coil of TonB (surface representation).

are in the conformations of its Ton-box (residues 6 to 12) and the residues (13 to 21) linking it with the luminal domain. The Ton-box in BtuB and other transporters has been observed to be ordered (but lacking regular secondary structure), or to be disordered (6). In the complex, the Ton-box of BtuB is recruited to form a parallel β strand with the three-stranded β sheet of TonB (Fig. 1B). A charged residue in TonB, Arg¹⁵⁸, makes a salt bridge with Asp⁶ of the Ton-box. The Ton-box:TonB interaction is similar to that observed between the C-terminal domain of the bacterial periplasmic-spanning protein TolA and the bacteriophage g3p protein (fig. S3) (12, 13). The structure of TonB in the complex is very similar to those determined by x-ray crystallography (PDB accession number 1UO7) (14) and solution nuclear magnetic resonance (NMR)

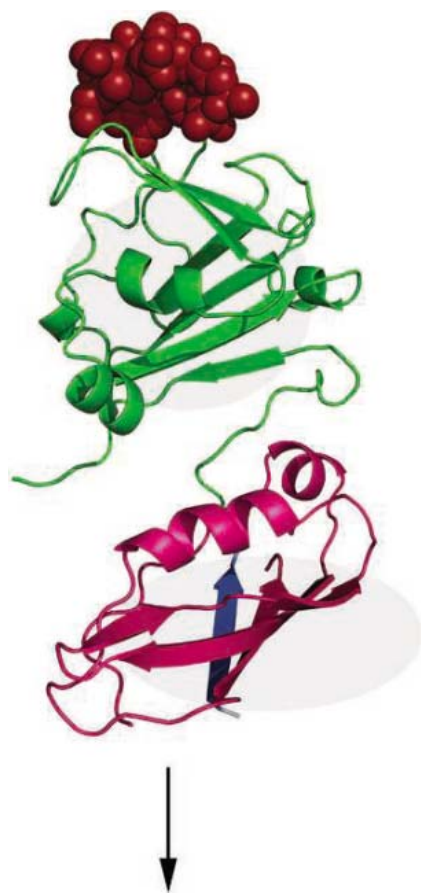


Fig. 3. Dissimilar orientations of the β sheet cores of the luminal domain of BtuB and of the Ton-box:TonB domain. The luminal domain is shown in green; TonB is shown in pink; the Ton-box of BtuB is shown in blue; the bound cyanocobalamin substrate is shown as red spheres. The black arrow, pointing into the periplasmic space and toward the plasma membrane in the bacterial cell, indicates the approximate direction in which intact TonB might exert a pulling force during the transport cycle. The luminal domain β sheet is oriented such that a small force applied in the indicated direction, roughly perpendicular to the β strands, might suffice to affect substantial conformational change.

spectroscopy (PDB accession number 1XX3) (15), with root mean square deviation of common α carbons of 0.8 and 1.1 Å, respectively (fig. S2). The BtuB:TonB interface has an area of 1481 Å²; the Ton-box:TonB interface contributes 542 Å² (36%). In addition to the Ton-box and its linker (and some extracellular loops shifted by crystal contacts), the largest structural changes are in one of the apical loops (residues 82 to 95) that bind the substrate (Fig. 1C) and in a portion of the luminal domain (residues 110 to 126) that interacts with the interior of the β barrel (Fig. 1D).

Cysteine-scanning crosslinking studies of interactions between TonB and BtuB (16), and between TonB and the ferric citrate transporter FecA (17), have identified pairwise interactions between these proteins. The structure of the complex is consistent with these interactions (Fig. 2A). In the TonB:BtuB crosslinking experiments, TonB-Gln¹⁶⁰ interacts strongly with BtuB-Leu⁸ and -Val¹⁰; TonB-Gln¹⁶² with BtuB-Leu⁸ and -Ala¹²; and TonB-Tyr¹⁶³ with BtuB-Ala¹². Mapping the FecA Ton-box to BtuB indicates that crosslinking occurs most strongly at TonB-Gln¹⁶⁰ with BtuB-Asp⁶, -Leu⁸, and -Val¹⁰, and TonB-Gln¹⁶² with BtuB-Asp⁶, -Val⁹, and -Val¹⁰. A solution NMR study (15) characterized the chemical shift changes in TonB when Ton-box peptides bound to it; the largest changes (in those residues that are present in our structure) are in TonB residues Gln¹⁶⁰, Ala¹⁶⁷, Gly¹⁷⁴, Ile²³², and Asn²³³. The structure of the complex is consistent with these interactions (Fig. 2B). A surface representation of the TonB:Ton-box region of the structure illustrates additional constraints on the Ton-box sequence (Fig. 2C). In the Ton-box:TonB parallel β sheet, formed by BtuB residues 6 to 12 and TonB residues 226 to 232, the even-numbered residues of the Ton-box participate in hydrogen bonding whereas the odd-numbered residues do not. Proline cannot form interstrand hydrogen bonds; therefore, its substitution at even positions would be deleterious to parallel β sheet formation, whereas odd-position substitution would be tolerated. This prediction rationalizes a series of proline-substitution loss-of-function mutations characterized in BtuB (18). L8P (where Leu⁸ is replaced by Pro) and V10P are nonfunctional; T7P, V9P, and T11P mutants have wild-type activity (19). The existence of TonB gain-of-function mutants Q160K and Q160L (20), which compensate for the nonfunctional BtuB L8P mutation, suggests that transport can occur with a destabilized Ton-box:TonB β sheet if compensated by other Ton-box:TonB interactions (12).

The core of the luminal domain of TonB-dependent transporters is a four-stranded β sheet. In a previous publication (21), we noted the resemblance of this core domain to that used in single-molecule mechanical unfolding experiments. In particular, in these experiments there is a marked anisotropy in the amount of force required to unfold the β sheet; perpendicular to the β strands of the sheet requires negligible force

and parallel requires much greater force (22, 23). The orientation of the luminal domain core suggested that only a very modest pulling force by TonB would suffice to affect its large conformational change or (partial or full) unfolding. The Ton-box:TonB complex is a four-stranded β sheet core; however, its orientation is rotated nearly 90° with respect to the luminal domain core (Fig. 3). Thus, a (much) larger force might be necessary to disrupt its interstrand interaction. We speculate that if TonB functions by application of a pulling force during the transport cycle, then conformational change of the luminal domain would occur before disengagement of TonB from the transporter. Clearly, such a hypothesis requires verification by multiple experimental approaches.

Binding of TonB to the outer membrane transporter leads to a mechanical pulling force or some other type of interaction that drives active transport. As the N-terminal luminal domain of the transporter occludes the channel, conformational rearrangement must occur to allow vectorial substrate transport through the lumen of the β barrel. The luminal domain, through alteration of its size and shape, may remain within the β barrel and expose a permeation pathway; alternatively, the luminal domain may exit the β barrel (possibly by an unfolding process) (24). Two studies on disulfide linking of luminal and β barrel domains in the hydroxamate transporter FhuA (25, 26) are consistent with a “partial unfolding model” of transport. In Endriß *et al.* (25), disulfide formation between residue 27 (at the N terminus) and residue 533 of the β barrel yields a mutant lacking transport activity. Conversely, Eisenhauer *et al.* (26) observe that mutants containing disulfides between residues 109 and 356, or between residues 112 and 383, still transport substrate. Approximately 80 residues of the luminal domain (N terminus, two β strands, and a long linker domain between them) separate the TonB:transporter interaction from where the luminal domain is tethered to the barrel. We interpret these results to indicate that affixing the luminal domain at (or near) its N terminus to the β barrel prevents any conformational change via TonB interaction. However, partial unfolding (or some other conformational change) in a portion of the luminal domain through TonB interaction is sufficient for substrate transport. The degree of unfolding required may be a function of the size of the substrate, which ranges from several hundred to more than a thousand daltons.

The structure of the BtuB:TonB complex provides a structural rationalization for the conservation of the Ton-box in TonB-dependent outer membrane transporters. Given that TonB binds to approximately one-half of the periplasmic surface of BtuB, our structure does not sterically exclude the possibility of two TonB molecules binding to the transporter during the transport cycle. TonB dimerization has been observed *in vivo* (27, 28), and a 2:1 complex of TonB and the ferricrocin transporter FhuA has been characterized *in vitro* (29). However, a

second coincident TonB could not use the Ton-box in binding, so its affinity would be much lower (as has been observed). Binding of the substrate to the transporter likely induces an order-to-disorder transition in the Ton-box (8), and this disordered Ton-box is the recognition element for TonB. Because the TonB-transporter interaction is transient (i.e., TonB may interact serially with multiple outer membrane transporters to perform multiple transport cycles), the presence of disorder (high entropy) of the Ton-box is a useful strategy for obtaining high specificity without high affinity (30). The disordered Ton-box may be useful for sweeping out a larger volume within the periplasm, thus increasing the probability of encountering TonB. The conserved salt bridge between the Ton-box and TonB may be critical for longer range electrostatic attraction and nucleation of β strand formation of the Ton-box. Lastly, the structure of this complex, particularly the Ton-box:TonB region, may be useful in structure-based lead compound discovery for novel antibacterials. The addition of Ton-box peptides to media inhibits bacterial growth (31), and the expression of periplasmic domains of TonB inhibits transporter function (32). Both of these results indicate that disruption of the physiological TonB:Ton-box interface may provide a drug-discovery paradigm.

References and Notes

- H. Nikaido, *Science* **264**, 382 (1994).
- V. Braun, M. Braun, *FEBS Lett.* **529**, 78 (2002).

- R. J. Kadner, *Mol. Microbiol.* **4**, 2027 (1990).
- V. Braun, *Contrib. Microbiol.* **12**, 210 (2005).
- K. Postle, R. J. Kadner, *Mol. Microbiol.* **49**, 869 (2003).
- A. D. Ferguson, J. Deisenhofer, *Cell* **116**, 15 (2004).
- Y. F. Zhai, W. Heijne, M. H. Saier Jr., *Biochim. Biophys. Acta* **1614**, 201 (2003).
- M. C. Wiener, *Curr. Opin. Struct. Biol.* **15**, 394 (2005).
- M. D. Lundrigan, R. J. Kadner, *J. Biol. Chem.* **261**, 10797 (1986).
- E. Schramm, J. Mende, V. Braun, R. M. Kamp, *J. Bacteriol.* **169**, 3350 (1987).
- D. P. Chimento, A. K. Mohanty, R. J. Kadner, M. C. Wiener, *Nat. Struct. Biol.* **10**, 394 (2003).
- Materials and methods are available as supporting materials on Science Online.
- J. Lubkowski, F. Hennecke, A. Plückthun, A. Wlodawer, *Structure* **7**, 711 (1999).
- J. Ködding *et al.*, *J. Biol. Chem.* **280**, 3022 (2005).
- R. S. Peacock, A. M. Weljie, S. P. Howard, F. D. Price, H. J. Vogel, *J. Mol. Biol.* **345**, 1185 (2005).
- N. Cadieux, R. J. Kadner, *Proc. Natl. Acad. Sci. U.S.A.* **96**, 10673 (1999).
- M. Ogierman, V. Braun, *J. Bacteriol.* **185**, 1870 (2003).
- N. Cadieux, C. Bradbeer, R. J. Kadner, *J. Bacteriol.* **182**, 5954 (2000).
- Single-letter abbreviations for the amino acid residues are as follows: K, Lys; L, Leu; P, Pro; Q, Gln; T, Thr; and V, Val.
- K. J. Heller, R. J. Kadner, K. Gunther, *Gene* **64**, 147 (1988).
- D. P. Chimento, R. J. Kadner, M. C. Wiener, *Proteins* **59**, 240 (2005).
- D. Brockwell *et al.*, *Nat. Struct. Biol.* **10**, 731 (2003).
- M. Carrion-Vazquez *et al.*, *Nat. Struct. Biol.* **10**, 738 (2003).
- P. E. Klebba, *Front. Biosci.* **8**, 1422 (2003).
- F. Endriß, M. Braun, H. Killmann, V. Braun, *J. Bacteriol.* **185**, 4683 (2003).
- H. A. Eisenhauer, S. Shames, P. D. Pawelek, J. W. Coulton, *J. Biol. Chem.* **280**, 30574 (2005).
- J. Ghosh, K. Postle, *Mol. Microbiol.* **55**, 276 (2005).
- A. Sauter, S. P. Howard, V. Braun, *J. Bacteriol.* **185**, 5747 (2003).
- C. Khursigara, G. Crescenzo, P. Pawlek, J. W. Coulton, *J. Biol. Chem.* **279**, 7405 (2004).
- H. J. Dyson, P. E. Wright, *Nat. Rev. Mol. Cell Biol.* **6**, 197 (2005).
- M. Tuckman, M. S. Osburne, *J. Bacteriol.* **174**, 320 (1992).
- S. P. Howard, C. Herrmann, C. W. Stratilo, V. Braun, *J. Bacteriol.* **183**, 5885 (2001).
- W. L. DeLano, *The PyMOL Molecular Graphics System* (DeLano Scientific, San Carlos, CA, USA, 2002); available at www.pymol.org.
- This work supported by NIH grants DK59999 (to D.D.S., M.D.P., C.N.B., and M.C.W.) and GM002055 (to D.D.S.). Data were collected at Southeastern Regional Collaborative Access Team (SER-CAT) 22-ID beamline at the Advanced Photon Source, Argonne National Laboratory. Use of the Advanced Photon Source was supported by the U.S. Department of Energy, Office of Science, Office of Basic Energy Sciences, under contract no. W-31-109-Eng-38. Coordinates and structure factors (accession number 2GSK) will be submitted to the Protein Data Bank. We thank P. Loll, R. Nakamoto, and E. Perozo for critical reading of the manuscript. This paper is dedicated to the memory of Professor Robert J. Kadner.

Supporting Online Material

www.sciencemag.org/cgi/content/full/312/5778/1396/DC1

Materials and Methods

SOM Text

Figs. S1 to S6

Table S1

References

21 March 2006; accepted 1 May 2006

10.1126/science.1127694

Structure of TonB in Complex with FhuA, *E. coli* Outer Membrane Receptor

Peter D. Pawelek,¹ Nathalie Croteau,¹ Christopher Ng-Thow-Hing,¹ Cezar M. Khursigara,¹ Natalia Moiseeva,² Marc Allaire,² James W. Coulton^{1*}

The cytoplasmic membrane protein TonB spans the periplasm of the Gram-negative bacterial cell envelope, contacts cognate outer membrane receptors, and facilitates siderophore transport. The outer membrane receptor FhuA from *Escherichia coli* mediates TonB-dependent import of ferrichrome. We report the 3.3 angstrom resolution crystal structure of the TonB carboxyl-terminal domain in complex with FhuA. TonB contacts stabilize FhuA's amino-terminal residues, including those of the consensus Ton box sequence that form an interprotein β sheet with TonB through strand exchange. The highly conserved TonB residue arginine-166 is oriented to form multiple contacts with the FhuA cork, the globular domain enclosed by the β barrel.

Iron is an essential element in bacteria for a number of redox processes (1). It is highly insoluble in its ferric (Fe^{3+}) form at physiological pH. To overcome the low bioavailability of Fe^{3+} , Gram-negative bacteria have

evolved strategies for high-affinity Fe^{3+} uptake. One well-characterized strategy involves transduction of energy from the cytoplasmic membrane (CM) to the outer membrane (OM), resulting in active transport of Fe^{3+} chelated to molecules known as siderophores. Central to this process, the CM-anchored energy-transducing protein TonB spans the periplasm and contacts OM-embedded receptors that bind metal-chelated siderophores. TonB, through uncharacterized conformational changes, transduces energy from

the CM's proton motive force to the receptor and facilitates siderophore transport into the periplasm. Existing structural data that describe key protein components of the siderophore transport cycle highlight outstanding questions regarding the overall molecular mechanism (2).

The CM protein TonB is composed of three domains. An N-terminal domain (residues 1 to 33) is anchored to the CM and makes contacts with proteins ExbB and ExbD to form an energy-transducing complex. A C-terminal domain (residues 155 to 239) directly contacts receptors in the OM. An intermediate domain (residues 34 to 154) contains a region of alternating Pro-Glu and Pro-Lys repeats located between residues 66 and 100. There is currently no known structure for the entire TonB protein. However, three structures have been reported for the TonB C-terminal domain. Its oligomeric states are variable and correlate with lengths of the recombinant constructs used to obtain the structures: a tightly interwoven dimer, residues 155 to 239 (3); a loose dimer, residues 148 to 239 (4); and a monomer, residues 103 to 239 (5). The monomeric C-terminal domain consists of two α helices positioned on the same face of a four-stranded antiparallel β sheet, strand $\beta 4$ being located at the C terminus of TonB.

The OM receptor FhuA is the *Escherichia coli* transporter of the hydroxamate siderophore

¹Department of Microbiology and Immunology, McGill University, 3775 University Street, Montreal, Quebec, H3A 2B4, Canada. ²National Synchrotron Light Source, Brookhaven National Laboratory, Upton, NY 11973-5000, USA.

*To whom correspondence should be addressed. E-mail: james.coulton@mcgill.ca

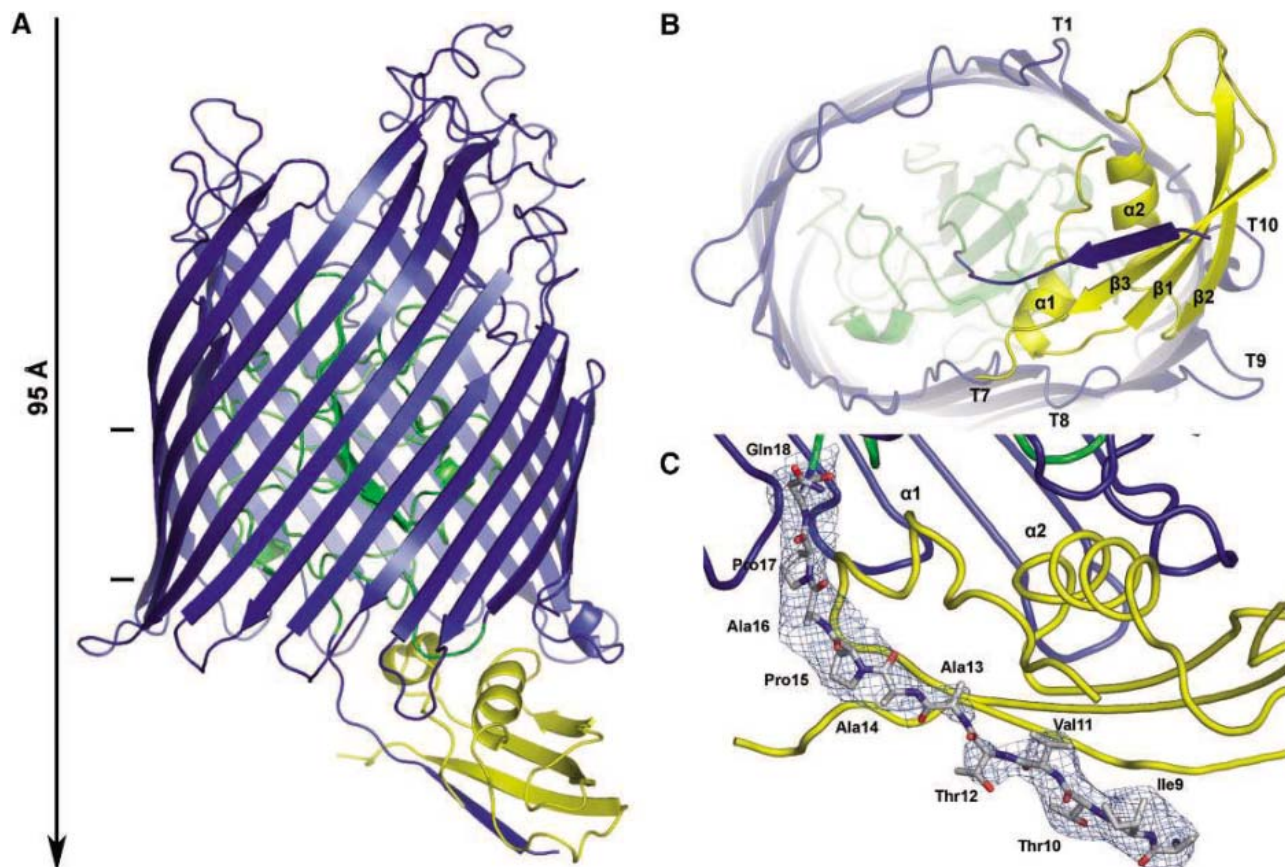


Fig. 1. Overall structure of the TonB-FhuA complex. **(A)** Cartoon representation of TonB residues 158 to 235 complexed to FhuA. β strands are indicated as flat arrows; helices are indicated as flat coils. View is along a plane parallel to the OM. Horizontal bars delineate approximate OM boundaries. Arrow indicates direction toward periplasm. TonB is bound at the periplasmic face of FhuA. The FhuA cork domain (residues 19 to 160) is colored green; remaining residues (8 to 18; 161 to 725) are colored blue. TonB residues are colored yellow. **(B)** View of the TonB-FhuA complex along the longitudinal axis of the FhuA barrel, looking down on the periplasm-exposed surface of the complex. TonB secondary-structure

elements ($\alpha 1$, $\alpha 2$, $\beta 1$, $\beta 2$, $\beta 3$) are labeled. FhuA periplasmic turns 1, and 7 to 10 (T1, T7, T8, T9, T10), are also labeled for reference. **(C)** Electron density (blue) from a simulated-annealing composite omit $2F_{\text{obs}} - F_{\text{calc}}$ electron density map contoured at 1σ showing the extension of electron density from FhuA Ile⁹ to Gln¹⁸. FhuA residues between 8 and 18 are shown as sticks and colored by atom (carbon, white; nitrogen, blue; oxygen, red). FhuA cork domain residues (19 to 160) are shown as a green coil. FhuA barrel domain residues (161 to 725) are shown as a blue coil. TonB is shown as a yellow coil. TonB helices $\alpha 1$ and $\alpha 2$ are labeled for reference.

ferrichrome. Structurally homologous TonB-dependent OM receptors include the *E. coli* transporters of cobalamin (BtuB) (6), ferric citrate (FecA) (7), and ferric enterobactin (FepA) (8). The crystal structure of FhuA demonstrates (9, 10) a porin-like protein, with a 22-stranded C-terminal β barrel domain that encloses a globular N-terminal cork domain. Ferrichrome binds to the receptor via extracellular loops and apical regions of the cork domain. The cork domain occludes the lumen of the barrel, preventing passive diffusion of ferrichrome. Characteristic of TonB-dependent OM receptors, FhuA possesses an N-terminal consensus sequence termed the Ton box ($^8\text{TITVTA}^{13}$) that was not visible in the reported three-dimensional structures of FhuA.

We crystallized a purified complex of TonB (residues 33 to 239) and FhuA (residues 1 to 725) and collected data on a single TonB-FhuA crystal (11). The TonB-FhuA crystal structure consists of one protomer of TonB in complex with one protomer of FhuA (Fig. 1). The model was refined at

a resolution of 3.3 Å to $R_{\text{cryst}} = 28.4\%$ and $R_{\text{free}} = 32.9\%$ (table S1). The overall folds of the FhuA and TonB protomers are in agreement with previously reported structural data. The N-terminal globular cork domain (residues 19 to 160) of FhuA is enclosed by the C-terminal β -barrel domain (residues 161 to 725). The cork domain possesses a four-stranded β sheet between residues 47 and 154. The barrel domain is composed of 22 antiparallel β strands. The β strands terminate in 11 long loops on one face of the barrel and 10 short turns on the other face (Fig. 1A). Given the membrane topology of FhuA, the loops and turns are exposed to the extracellular environment and periplasm, respectively. A molecule of ferricrocin was observed bound to FhuA in a position not much different from that observed for the ligand-loaded FhuA structure 1QFF.

TonB residues 158 to 235 were observed in the TonB-FhuA structure (see supporting online text). The fold of the TonB protomer consists of a three-stranded β sheet ($\beta 1$ - $\beta 2$ between residues

174 and 197, $\beta 3$ between residues 223 and 231), a short helix $\alpha 1$ (residues 165 to 170), and a longer helix $\alpha 2$ (residues 203 to 210) (Fig. 1B). TonB interacts with the periplasm-exposed face of FhuA such that TonB helices $\alpha 1$ and $\alpha 2$ are oriented toward FhuA, with the TonB β sheet (composed of $\beta 1$ to $\beta 3$) distal to the FhuA barrel (Fig. 1A). The TonB protomer occupies approximately one-half of the periplasm-exposed surface area of FhuA and occludes the barrel lumen from the edge containing periplasmic turns 8 to 10 to a boundary delineated by a straight line between periplasmic turns 1 and 7 (Fig. 1B). Inspection of the TonB-FhuA structure relative to FhuA 1QFF revealed minor structural rearrangements [root mean square deviation (RMSD) = 0.23 Å] upon TonB binding. Structural changes proximal to the bound TonB are localized to the periplasmic turns of the FhuA barrel as well as the periplasm-exposed loop at the C terminus of the cork domain (fig. S1). Larger structural changes were observed in TonB upon complex-

Fig. 2. Interactions of the FhuA Ton box with the C-terminal domain of TonB. **(A)** The interprotein β sheet formed between the FhuA Ton box and the central β sheet of the TonB C-terminal domain. TonB and FhuA residues are shown as sticks. Coloring as in Fig. 1C. TonB strands $\beta 1$ to $\beta 3$ are labeled. FhuA periplasmic turns 8 and 9 (T8, T9) are also labeled for reference. **(B)** View along the plane of the interprotein β sheet showing potential hydrogen bonding between two rotamers of TonB Gln¹⁶⁰ and the main-chain carbonyl oxygen atom of FhuA Thr¹². FhuA residues are shown as sticks and are colored as in (A). TonB is shown as a yellow coil. Rotamers ("a" and "b") of TonB

Gln¹⁶⁰ are shown as sticks colored by atom (carbon, green; nitrogen, blue; oxygen, red). TonB strands $\beta 1$ to $\beta 3$ are labeled. **(C)** Superposition of the TonB-FhuA crystal structure (TonB, yellow coil; FhuA, blue coil) and monomeric C-terminal TonB (PDB code 1XX3; pink coil). The Ton box and N terminus of FhuA, and the C terminus of TonB, from the crystal structure are labeled. FhuA periplasmic turns 7, 8, 9, and 10 (T7, T8, T9, T10) are also marked for reference. Yellow arrow indicates direction toward the C terminus of FhuA-complexed TonB. Pink arrow indicates direction toward the C terminus of monomeric TonB.

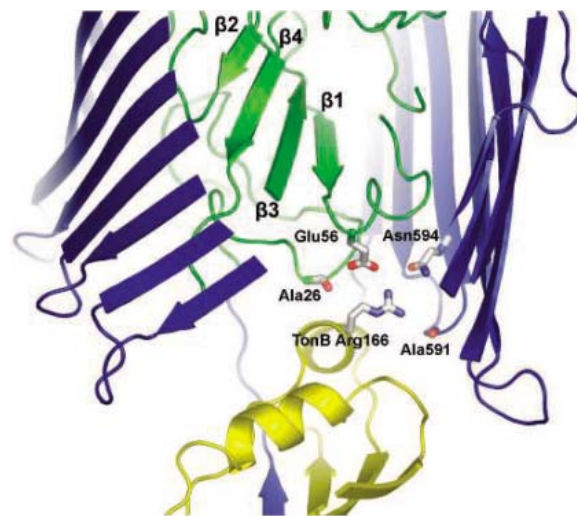
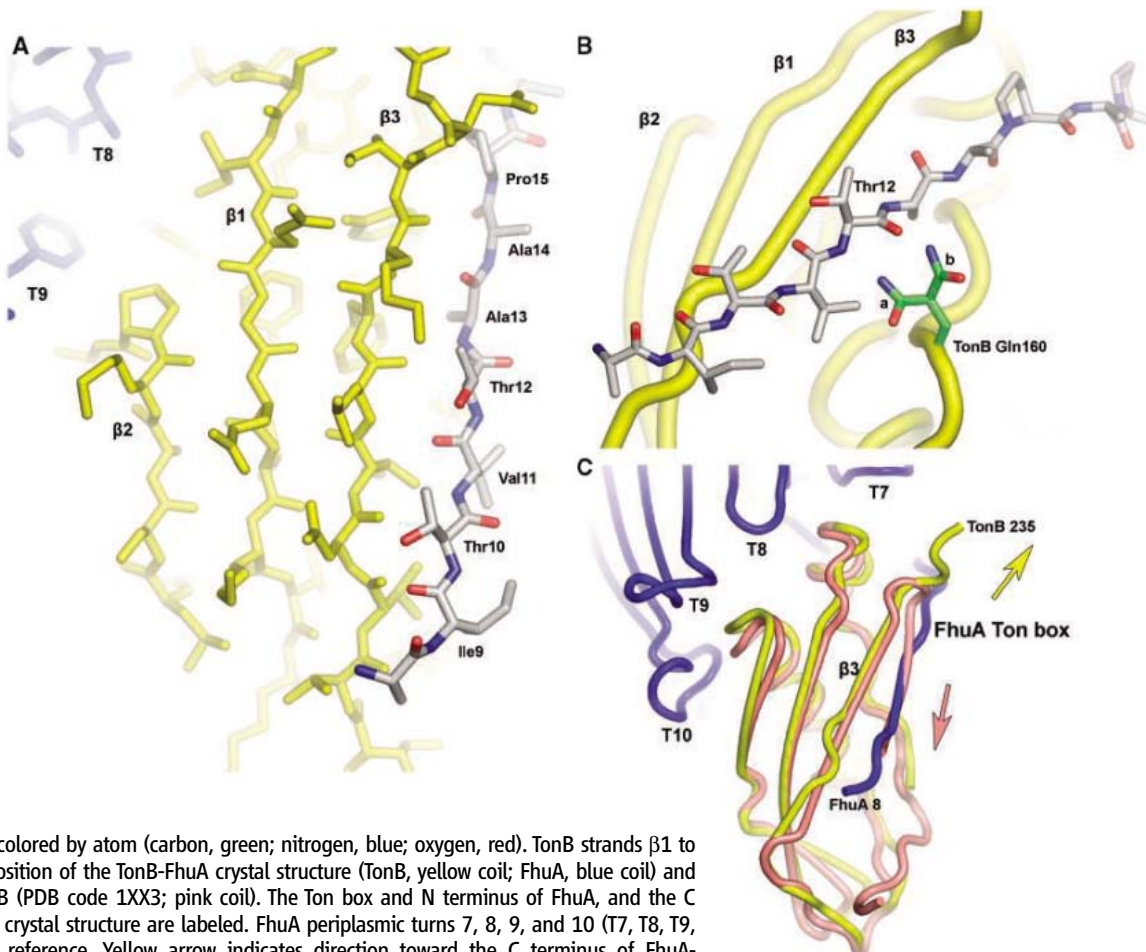
ation with FhuA. The overall $C\alpha$ - $C\alpha$ RMSD between FhuA-complexed TonB and TonB 1U07 is 0.93 Å. The largest main-chain deviations are localized mainly to the C terminus from residues Ile²³² to Thr²³⁵. The $C\alpha$ - $C\alpha$ deviation relative to 1U07 at TonB Ile²³² is 2.0 Å, whereas at Thr²³⁵ the $C\alpha$ - $C\alpha$ deviation is 3.5 Å.

We observed extensive and continuous electron density N-terminal to FhuA Glu¹⁹ and extending toward TonB. This unambiguous electron density allowed us to build FhuA residues 9 to 18 into the model, encompassing five of the six residues in the conserved FhuA Ton box consensus (Fig. 1C). The FhuA Ton box forms a parallel β interaction with $\beta 3$ of the TonB C-terminal domain, extending the β sheet. FhuA residues Ile⁹, Thr¹⁰, Val¹¹, and Ala¹³ interact with TonB residues Val²²⁵, Val²²⁶, Leu²²⁹, and Lys²³¹, respectively (table S2). These interactions result in the formation of an interprotein β sheet with TonB $\beta 1$ to $\beta 3$ (Fig. 2A). The side chain of TonB Gln¹⁶⁰, a residue previously shown to interact with the Ton box, was not visible in the electron density; a specific mode of interaction between this residue and the FhuA Ton box was not immediately apparent. However, sampling of the preferred side-chain rotamers at TonB residue 160 suggests a potential interaction with the FhuA Ton box via a hydrogen bond with the

Fig. 3. Residues from the FhuA cork and barrel domains interacting with TonB Arg¹⁶⁶. Cut-away view showing FhuA and TonB protomers in cartoon representation; β strands are shown as flat arrows, helices as flat coils. The FhuA cork domain (residues 19 to 160) is colored green; the remaining FhuA residues are colored blue. TonB is colored yellow. TonB Arg¹⁶⁶ and interacting FhuA residues (Ala²⁶, Glu⁵⁶, Ala⁵⁹¹, and Asn⁵⁹⁴) are shown as sticks colored by atoms (as in Fig. 1C). Strands of the central β sheet of the FhuA cork domain ($\beta 1$ to $\beta 4$) are labeled.

main-chain carbonyl oxygen atom of Thr¹² (Fig. 2B). The residue immediately N-terminal to FhuA Thr¹² is a position of conserved hydrophobicity. In FhuA this position is occupied by a valine residue. Multiple alignment of the Ton box regions of related TonB-dependent OM receptors (BtuB, FecA, FepA; fig. S2, red) reveals this position to be invariably occupied by valine. The hydrophobic environment at this position may

contribute to the observed instability of TonB Gln¹⁶⁰. The TonB-FhuA interprotein β sheet positions TonB $\alpha 1$ and $\alpha 2$, the two helices of the TonB C-terminal domain, such that they are oriented toward the periplasmic face of FhuA (Fig. 1C). The recently solved nuclear magnetic resonance structure of monomeric TonB (5) indicates that the C terminus of the protein folds back to form the fourth strand ($\beta 4$) of the central β sheet of



the C-terminal TonB domain. We do not observe TonB $\beta 4$ in our structure. Instead, the C terminus of TonB extends away from the complex, such that the FhuA Ton box forms a parallel β interaction with TonB $\beta 3$ (Fig. 2C). This observation clearly demonstrates that the complexation of TonB to FhuA occurs via strand exchange.

Our in vitro surface plasmon resonance studies (12, 13) indicated that TonB-FhuA complexation involves a kinetically limiting conformational rearrangement. The present structure showing exchange of TonB $\beta 4$ with the FhuA Ton box corroborates these biophysical observations and suggests that formation of the interprotein β sheet is the initial committed step of TonB-FhuA complexation. The complex that we observe in this structure is likely the 1:1 high-affinity complex identified by biophysical methods. Interactions between a FhuA Ton box peptide and residues from TonB $\beta 3$ and $\beta 4$ were recently reported (5). Ton box residues may therefore form low-affinity encounter interactions with TonB $\beta 3$ and $\beta 4$ before formation of the stable interprotein β sheet. TonB Gln¹⁶⁰ likely participates in these encounter interactions, perhaps facilitating displacement of TonB $\beta 4$. A cysteine cross-linking study (14) mapped a complex network of interactions between TonB residues 159 and 164 such that each TonB residue interacted with multiple residues in the BtuB Ton box. This is consistent with TonB residues at or near Gln¹⁶⁰ being involved in multiple transient encounter interactions before high-affinity complex formation.

The TonB-FhuA interface has a mean interfacial accessible surface area (Δ ASA) (15) of 1299 Å². The calculated shape correlation statistic (S_c) for this interface is 0.60, indicating that it has a surface complementarity similar to that observed for cork-barrel interfaces of TonB-dependent OM receptors (16). The TonB-FhuA interface is composed of a network of 17-residue pairs bound by hydrophilic interactions (table S2). All pairs were observed to have well-defined electron density for both FhuA and TonB side chains. Within this interface, a single electrostatic interaction occurs between FhuA cork residue Glu⁵⁶ and TonB Arg¹⁶⁶, located on TonB $\alpha 1$ (Fig. 3). A hydrogen bond is also formed between TonB Arg¹⁶⁶ and the main-chain carbonyl oxygen atom of FhuA Ala²⁶, located in the switch helix region. Ferrichrome binding to FhuA was previously observed to result in a 17.3 Å translocation of the FhuA N terminus and unwinding of the switch helix (9). Therefore, it appears that unwinding of the FhuA switch helix upon ligand binding occurs in order to stabilize FhuA interactions with TonB Arg¹⁶⁶. FhuA barrel residues Ala⁵⁹¹ and Asn⁵⁹⁴, located in or near periplasmic turn 8, also form hydrogen bonds with TonB Arg¹⁶⁶.

What does the crystal structure of the TonB-FhuA complex tell us about interactions of TonB with a cognate OM receptor and the transport of metal-chelated siderophore? Given our structural data, combined with findings from previous studies

of TonB interactions with OM receptors in vitro and in vivo, we propose that the interprotein β sheet formed between the receptor Ton box and the TonB C-terminal domain is required to position TonB helix $\alpha 1$ proximal to the receptor cork domain. In the TonB-FhuA structure, this results in TonB Arg¹⁶⁶ forming an electrostatic interaction with FhuA cork residue Glu⁵⁶. Both TonB Arg¹⁶⁶ (17) and FhuA Glu⁵⁶ located in the TEE motif (16) are highly conserved residues, predicting functional importance of this TonB-FhuA ionic interaction. Molecular dynamics simulations of FhuA have suggested that cork domain solvation may lower the energy barrier for active transport of ferrichrome (18). It has recently been proposed that hydration of the central β sheet of the cork domain may render it prone to disruption by TonB through transmission of a relatively small force perpendicularly applied to the β strands of the cork domain (16). Given its position proximal to the central β sheet of the FhuA cork domain, TonB Arg¹⁶⁶ is positioned to mediate a mechanical shearing or pulling force applied in trans to the central β sheet of the cork domain, resulting in its disruption. Localized unfolding of the cork domain would allow siderophore translocation into the periplasm, facilitating subsequent steps of the siderophore transport cycle.

References and Notes

1. C. Wandersman, P. Deleplaire, *Annu. Rev. Microbiol.* **58**, 611 (2004).
2. A. D. Ferguson, J. Deisenhofer, *Cell* **116**, 15 (2004).
3. C. Chang, A. Mooser, A. Plückthun, A. Wlodawer, *J. Biol. Chem.* **276**, 27535 (2001).
4. J. Ködding *et al.*, *J. Biol. Chem.* **280**, 3022 (2005).
5. R. S. Peacock, A. M. Weljie, S. P. Howard, F. D. Price, H. J. Vogel, *J. Mol. Biol.* **345**, 1185 (2005).
6. D. P. Chimento, A. K. Mohanty, R. J. Kadner, M. C. Wiener, *Nat. Struct. Biol.* **10**, 394 (2003).
7. A. D. Ferguson *et al.*, *Science* **295**, 1715 (2002).
8. S. K. Buchanan *et al.*, *Nat. Struct. Biol.* **6**, 56 (1999).
9. A. D. Ferguson, E. Hofmann, J. W. Coulton, K. Diederichs, W. Welte, *Science* **282**, 2215 (1998).

10. K. P. Locher *et al.*, *Cell* **95**, 771 (1998).
11. Materials and methods are available as supporting information on Science Online.
12. C. M. Khursigara, G. De Crescenzo, P. D. Pawelek, J. W. Coulton, *Biochemistry* **44**, 3441 (2005).
13. C. M. Khursigara, G. De Crescenzo, P. D. Pawelek, J. W. Coulton, *Protein Sci.* **14**, 1266 (2005).
14. N. Cadieux, C. Bradbeer, R. J. Kadner, *J. Bacteriol.* **182**, 5954 (2000).
15. S. Jones, J. M. Thornton, *Proc. Natl. Acad. Sci. U.S.A.* **93**, 13 (1996).
16. D. P. Chimento, R. J. Kadner, M. C. Wiener, *Proteins* **59**, 240 (2005).
17. R. A. Larsen *et al.*, *J. Bacteriol.* **178**, 1363 (1996).
18. J. D. Faraldo-Gómez, G. R. Smith, M. S. Sansom, *Biophys. J.* **85**, 1406 (2003).
19. We thank A. Berghuis (McGill University, Montreal, Quebec) and M. Cygler (Biotechnology Research Institute, National Research Council, Montreal, Quebec) for access to home source x-rays and for helpful discussions. F. Rotella and S. L. Ginell at the Advanced Photon Source, beamline 19-ID, assisted with data collection. Use of the Argonne National Laboratory Structural Biology Center beamlines at the Advanced Photon Source was supported by the U.S. Department of Energy, Office of Biological and Environmental Research, under Contract No. W-31-109-ENG-38. We acknowledge the suggestions of K. Diederichs (Universität Konstanz, Germany) concerning site-directed mutagenesis to improve crystal contacts of FhuA. Critical reviews of this manuscript were provided by A. Berghuis, H. Le Moual, and B. Nagar, all at McGill University; J. A. Kashul edited the document. This work was supported by operating grant MOP-14133 (to J.W.C.) from the Canadian Institutes of Health Research. Infrastructure from Canada Foundation for Innovation was awarded to the Montreal Integrated Genomics Group for Research on Infectious Pathogens. Coordinates and structure factors have been deposited in the Protein Data Bank (PDB) with the accession code 2GRX.

Supporting Online Material

www.sciencemag.org/cgi/content/full/312/5778/1399/DC1
Materials and Methods
SOM Text
Figs. S1 and S2
Tables S1 and S2
References

29 March 2006; accepted 27 April 2006
10.1126/science.1128057

From Disorder to Order in Marching Locusts

J. Buhl,^{1,2*} D. J. T. Sumpter,¹ I. D. Couzin,^{1,3} J. J. Hale,¹ E. Despland,^{1†}
E. R. Miller,¹ S. J. Simpson^{1,2}

Recent models from theoretical physics have predicted that mass-migrating animal groups may share group-level properties, irrespective of the type of animals in the group. One key prediction is that as the density of animals in the group increases, a rapid transition occurs from disordered movement of individuals within the group to highly aligned collective motion. Understanding such a transition is crucial to the control of mobile swarming insect pests such as the desert locust. We confirmed the prediction of a rapid transition from disordered to ordered movement and identified a critical density for the onset of coordinated marching in locust nymphs. We also demonstrated a dynamic instability in motion at densities typical of locusts in the field, in which groups can switch direction without external perturbation, potentially facilitating the rapid transfer of directional information.

Despite the huge differences in the scales of animal aggregations and the cognitive abilities of group

members, the similarities in the patterns that such groups produce have suggested that general principles may underlie col-

lective motion. One approach has been to model grouping individuals as self-propelled particles (SPPs), with each “particle” adjusting its speed and/or direction in response to near neighbors (1–6). A recent model by Vicsek and collaborators (1) stands out because of its small number of underlying assumptions and the strength of the universal features that it predicts. A central prediction of this model is that as the density of animals in the group increases, a rapid transition occurs from disordered movement of individuals within the group to highly aligned collective motion (Fig. 1). Because SPP models underlie many theoretical predictions about how groups form complex patterns (7–10), avoid predators (11, 12), forage (8, 13), and make decisions (14), confirming the existence of such a transition in real animals has fundamental implications for understanding all aspects of collective motion.

The desert locust, *Schistocerca gregaria*, has a devastating social and economic impact on humans. Before taking flight as adults, wingless juveniles (also called nymphs or hoppers) form coordinated “marching bands” that can extend over many kilometers (15). The key to effective management of locust outbreaks is

early control and detection of bands, because the control of flying adult swarms is costly and ineffective (16). The first stage in band formation is a change among resident locusts from the harmless, non-band-forming “solitarious” phase to the actively aggregating, band-forming “gregarious” phase (17–19).

Previous work has investigated which combinations of locust population density, vegetation abundance, and vegetation distribution will trigger such gregarization (20–23). Locust aggregations will build into major outbreaks only if locally gregarized populations remain together and move collectively into neighboring areas of habitat, where they can recruit further locusts to the growing band. Unless such cohesive movement occurs, local aggregations will disband and individuals will return to the solitarious phase. Hence, it is vital to predict the onset of collective motion. Within bands, individuals align their directions of travel with those of near neighbors (15, 24). Although it has been shown in the laboratory that marching begins only at high locust density (25, 26), these experiments did not measure how alignment increases with density. A detailed quantitative understanding of the onset of collective motion is therefore essential if we are to understand how, when, and where coordinated bands will form, resulting in improved control measures (27).

The average density of marching bands in the field is 50 locusts/m², with a typical range of 20 to 120 locusts/m² (28), equivalent to 20 locusts in our experiments. We performed experiments on different numbers of third-instar locusts,

ranging from 5 to 120 insects (densities of 12.3 to 295 locusts/m²), in a ring-shaped arena (29). We recorded the locusts’ motion for 8 hours with a digital camera placed above the setup and connected to a computer that captured five images/s (see movie S1 for an example). Movies were processed with tracking software that computed the position and orientation of each locust. For each locust, we calculated its angular coordinates relative to the center of the arena on two consecutive camera images. The orientation χ of a locust was defined as the smallest angle between one line drawn between the locust’s two consecutive positions and a second line drawn from the center of the arena to the locust’s first position. This relationship can be described as $\chi = \arcsin[\sin(\theta - \alpha)]$, where α is the angle of the direction of movement and θ is the angle with the center of the arena. For each camera image, or time step t , we calculated the instantaneous alignment Φ^t as the average of the orientation for all moving locusts, normalized as follows

$$\Phi^t = \frac{2}{m\pi} \sum_{i=1}^m \chi_i^t$$

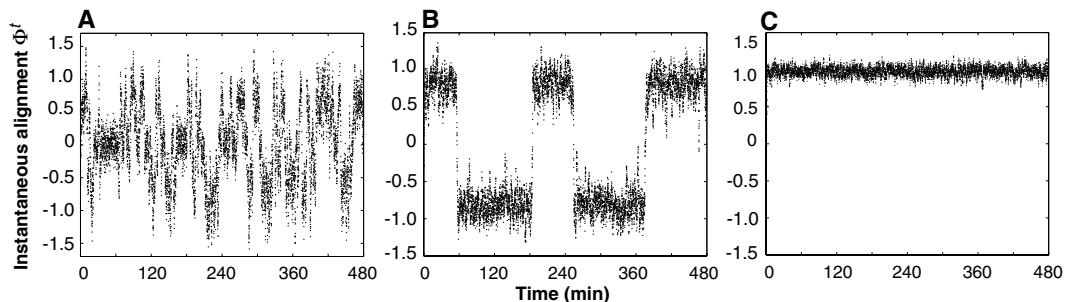
where m is the total number of moving locusts, and i is the i th locust. Thus, values of the alignment close to the extreme values of 1 and -1 indicate the alignment of all locusts in the same direction, whereas values close to zero indicate an absence of any collective alignment. Because locust direction was not influenced by immobile individuals,

¹Department of Zoology, University of Oxford, South Parks Road, Oxford OX1 3PS, UK. ²School of Biological Sciences, Heydon-Laurence Building, A08, University of Sydney, New South Wales 2006, Australia. ³Department of Ecology and Evolutionary Biology, Princeton University, Princeton, NJ 08544–1003, USA.

*To whom correspondence should be addressed. E-mail: jbuhl@usyd.edu.au

†Present address: Biology Department, Concordia University, 7141 Sherbrooke West, Montréal, Québec H4B 1R6, Canada.

Fig. 1. Characteristic output of the model for the dynamics of Φ^t over time and with 3 (A), 11 (B), and 47 (C) individuals. The Vicsek *et al.* SPP model (1) consists of a set of pointwise particles moving synchronously and interacting locally by trying to align with their neighbors (1, 4). We used a variant of the one-dimensional version of their SPP model (30), where N particles move along a line of length L at a discrete time step $\Delta t = 1$. Each particle is characterized by its position x_i and a dimensionless velocity u_i and is updated as follows: $x_i(t + 1) = x_i(t) + v_0 u_i(t)$, $u_i(t + 1) = \alpha u_i(t) + (1 - \alpha)G(\langle u(t) \rangle_i) + \xi_i$, where $\langle u \rangle_i$ denotes the average velocity of all other particles, excluding particle i , within an interaction range $[x_i - \Delta, x_i + \Delta]$. The term α determines the relative weight that the particle assigns to its own velocity and to that of its neighbors in deciding its velocity. For locusts, α corresponds to a directional inertia when walking in the absence of conspecifics. ξ_i is a noise term, randomly chosen with a uniform probability from the interval $[-\eta/2, \eta/2]$. The function G represents the adjustment of a particle velocity to the velocity of its neighbors, implemented as follows



$$G(u) = \begin{cases} (u + 1)/2 & \text{for } u > 0 \\ (u - 1)/2 & \text{for } u < 0 \end{cases}$$

Simulations were run by applying random initial conditions and periodic boundaries. The parameters were set to mimic the walking speed and interaction range of locusts in an arena (see SOM). $T = 8000$ time steps (8 hours), $L = 36$ (251.3 cm), $v_0 = 1$ (1.9 cm/s), $\Delta = 2$ (13.9 cm), $\alpha = 0.66$. The noise term $\eta = 0.8$ was set by trial and error. We used the average velocity $\Phi^t = \langle u(t) \rangle$ as the measure of the order in the system to compare the simulations to the alignment measured experimentally.

and changes of direction occurred mainly as a response to moving neighbors [see the supporting online material (SOM) for details], we considered only the number of moving locusts when calculating densities.

Coordinated marching behavior depended strongly on locust density (Fig. 2). At low densities (2 to 7 moving locusts on average, equating to 5.3 to 17.2 locusts/m²), there was a low incidence of alignment among individuals; in trials where alignment did occur, it did so only sporadically and after long initial periods of disordered motion. Intermediate densities (10 to 25 moving locusts; 24.6 to 61.5 locusts/m²) were characterized by long periods of collective rotational motion with rapid spontaneous changes in direction. At densities above 73.8 locusts/m² (30 or more moving locusts), spontaneous changes in direction did not occur within the time scale of the observations, and the locusts quickly adopted a common and persistent rotational direction (movie S1).

The dynamics of our experiment (Fig. 2, A to C) and that of the SPP model (Fig. 1, A to C) were very similar. To test whether the transition from disordered to ordered marching observed in our experiments was consistent with the predictions of the SPP model, we compared, for different densities, the average Φ^f over the entire experiment with that predicted by an SPP model with parameter values consistent with the behavior of locust

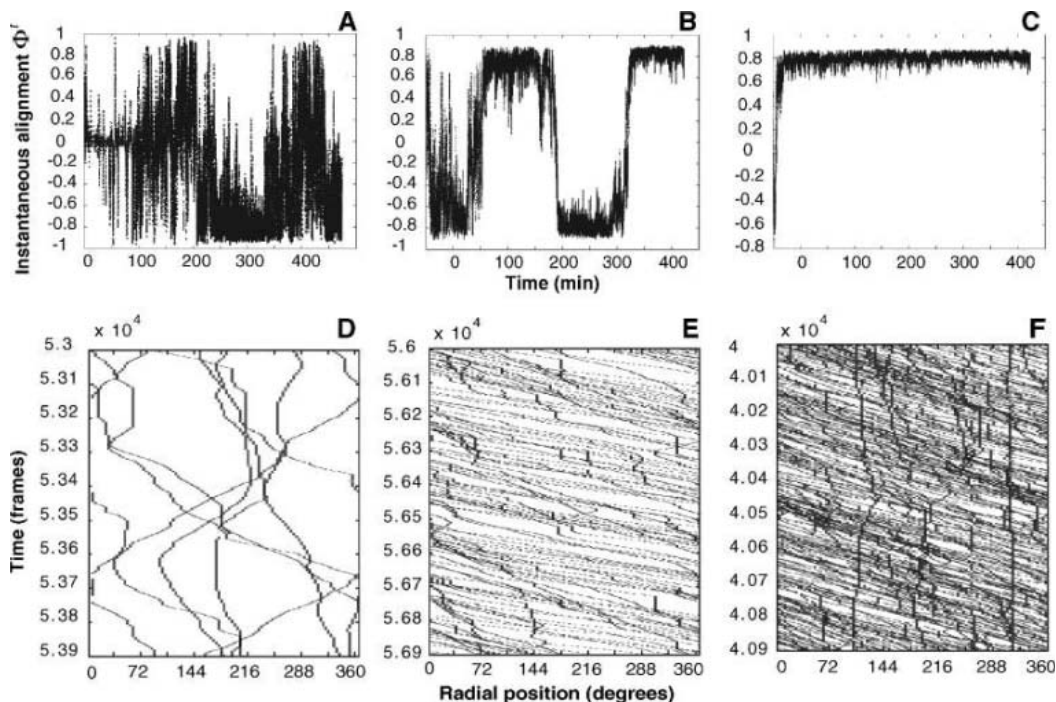
nymphs (Fig. 3, A and D). The mean alignments were very consistent with the distribution of alignment predicted by the model. As density increased, the spread of the alignment changed from a flat distribution to having two well-defined peaks. Rather than being limited to our particular parameterization, such a transition is characteristic of the output of SPP models over a wide range of parameter values (1, 4, 30).

As density increased, the dynamical behavior of the group also exhibited marked changes. The time during which the locusts were aligned increased with increasing density (Spearman's $\rho = 0.782$, $n = 51$, $P < 0.001$) and rapidly saturated at a value corresponding to the total time of the experiment (Fig. 3, B and E). The frequency with which the locusts collectively changed direction decreased with increasing density (Spearman's $\rho = -0.722$, $n = 51$, $P < 0.001$) until it reached a value of zero (Fig. 3, C and F). These two quantities did not saturate at the same densities. Although 10 or more moving locusts (24.6 locusts/m²) were in the ordered phase almost all of the time, it was not until there were at least 30 moving locusts (73.8 locusts/m²) that directional changes dropped to nearly zero. Between these densities, the group was almost always aligned while several directional changes still occurred, indicating that these shifts happened rapidly and without loss in group cohesion. This intermittency in align-

ment is also characteristic of the output of SPP models (31).

At a global level, the behavior of locust groups was fully consistent with the predictions of the SPP model, but did we get the same outcome for different reasons? Detailed observations of the behavior of individual locusts indicate that the mechanisms operating at the level of individual insects are consistent with the core assumptions of the model. The central assumptions of the SPP model are that (i) insects adjust their direction to align with neighbors within an interaction range and (ii) individual behavior does not change with changes in group density. Regarding (i), we observed clear evidence of alignment and chose the interaction range on the basis of detailed analyses of the behavior of locusts in the arena (see SOM). Concerning (ii), we found that the interaction distance did not change with density; the interaction range was 7.58 ± 4.22 SD for the low-density (5 locusts) and 6.24 ± 2.9 SD for the intermediate-density (20 locusts) experiments (two-sample Kolmogorov-Smirnov test: $D^* = 0.09$, $n_1 = 118$, $n_2 = 108$, $P = 0.38$) (see SOM). Similarly, the proportion of active insects, although varying slightly between experimental trials for similar densities, was not related to density (Spearman's $\rho = 0.025$, $n = 51$, $P = 0.862$). As previously reported (25), any given locust spent about half of its time in an active state; the mean proportion of active insects across the group was 0.51 ± 0.11 SD.

Fig. 2. Change in Φ^f over time for three different densities: (A) 7 (or 3.47 moving on average), (B) 20 (or 12.05 moving on average), and (C) 60 (or 47.35 moving on average) locusts. (D to F) Corresponding samples of time-space plots (3 min), where the x axis represents the individuals' angular coordinates relative to the center of the arena, and the y axis represents time.



Inactive insects did not affect the behavior of moving locusts (see SOM). Although there was a significant positive correlation between the mean walking speed of locusts and the number of locusts in the arena (Spearman's $\rho = 0.430$, $n = 51$, $P = 0.002$), it represented only a slight increase (5 locusts, 3.11 ± 0.1 cm/s; 30 locusts, 3.46 ± 0.06 cm/s; 60 to 120 locusts, 3.8 ± 0.08 cm/s). It is known that solitary locusts (those

reared in isolation) increase their activity levels when first exposed to crowding (22). This response is part of the process of behavioral gregarization, which is completed in individuals within a few hours of experiencing crowded conditions (18, 19). Our experiments showed that, within a wide range of densities, once a locust is gregarious there are no further marked changes in its activity.

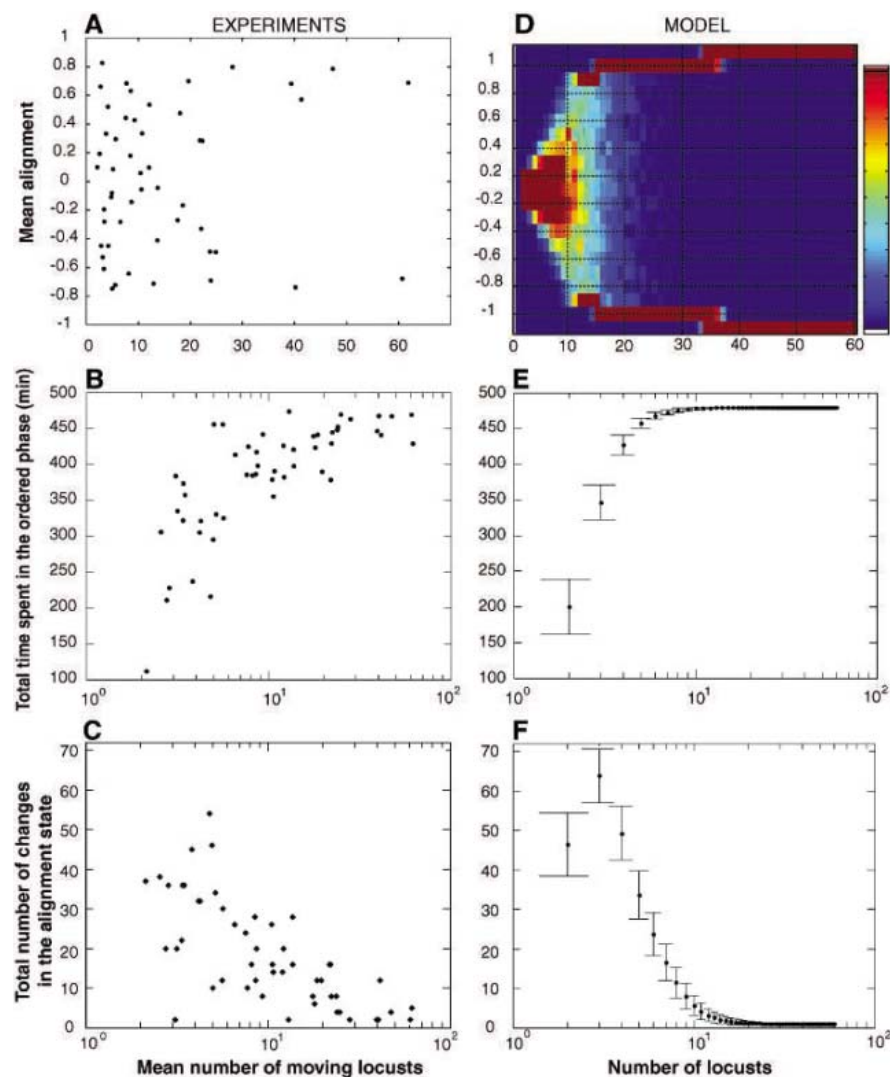


Fig. 3. Changes in alignment with density in experiments (A to C) and the model (D to F). The relation between the number of moving locusts and the mean alignment is shown for the experiments (A) and for simulations (D). Each point in (A) represents one experimental trial, whereas each colored column in (D) shows the distribution of the results obtained for 1000 simulations. To analyze the changes between aligned/unaligned states over time, we considered that locusts belonged to one of three categories: unaligned (alignment value between -0.3 and 0.3), aligned in the counterclockwise direction (alignment value >0.3), or aligned in the clockwise direction (alignment value <-0.3). To remove stochastic noise, the alignment state was only considered to have changed if it persisted for 1 min (16 time steps in the simulation) or more. The relation between the average number of moving locusts and the mean total time spent in the aligned state [(B) and (E)] and the mean number of changes in the alignment state [(C) and (F)] are displayed on a semi-log scale. Error bars, standard deviation.

Both the SPP model and our experiments exhibited dynamic instability, in which changes in direction are sudden and spontaneous, rapidly spreading through the entire group. Such sudden directional changes of locust hoppers and other similar insects such as the Mormon cricket occur in the field (32). Our experiments show that these changes can be independent of external conditions and are likely to be an inherent property of moving groups. These instabilities may have important implications for how directional information is transferred within these groups. For example, if only a subset of a swarm becomes aware of the direction toward a resource, this may facilitate the change in direction over a much greater length scale (14), allowing collective motion along weak environmental gradients that do not elicit responses in individuals alone (13). We predict that at densities of 25 to 60 locusts/m², locust bands are maximally sensitive to such changes in direction. It is unclear, however, whether individual locusts regulate their local density to this level, thereby optimizing their collective access to information about the environment.

We have revealed a critical density at which marching locusts will spontaneously and suddenly adopt directed collective motion. The lower size range of a marching band as defined by the Food and Agriculture Organization of the United Nations (FAO), at 20 locusts/m² (28), corresponds to 8 locusts in our experiments. Because alignment rapidly increases with density around this level, the FAO's definition corresponds to a threshold density for cohesive marching. In our experiments, groups of two to seven moving locusts were only weakly aligned, whereas slightly larger groups changed direction rapidly and in unison. In the field, small increases in density beyond this threshold will cause a sudden transition to a highly unpredictable collective motion, making control measures difficult to implement. Our data and model also suggest that predicting the motion of very high densities of locusts is easier than predicting that of intermediate densities. The small number of directional changes at high densities, observed during the 8 hours of our experiments, was similar to the field observation of "gregarious inertia" that lasts for days (24).

We cannot assume that all of the collective behavior seen in our laboratory experiments translates directly to that observed in the field. However, the wealth of mathematical and simulation-

based understanding of SPP models provides us with tools for performing such scaling. For example, additional rules such as attraction (33) explain how a moving group maintains cohesion in a nonbounded space. In combination with our understanding of the role of the environment in behavioral phase change (20), SPP models could now form the basis of prediction to improve control of locust outbreaks.

References and Notes

1. T. Vicsek, A. Czirók, E. Ben-Jacob, I. Cohen, O. Shochet, *Phys. Rev. Lett.* **75**, 1226 (1995).
2. A. Okubo, *Adv. Biophys.* **22**, 1 (1986).
3. C. W. Reynolds, *Comput. Graphics* **21**, 25 (1987).
4. A. Czirók, H. Stanley, T. Vicsek, *J. Phys. A* **30**, 1375 (1997).
5. J. Toner, Y. Tu, *Phys. Rev. E* **58**, 4828 (1998).
6. G. Grégoire, H. Chaté, *Phys. Rev. Lett.* **92**, 025702 (2004).
7. I. D. Couzin, J. Krause, R. James, G. D. Ruxton, N. R. Franks, *J. Theor. Biol.* **218**, 1 (2002).
8. J. L. Deneubourg, S. Goss, *Ethol. Ecol. Evol.* **1**, 295 (1989).
9. S. Gueron, S. A. Levin, D. I. Rubenstein, *J. Theor. Biol.* **182**, 85 (1996).
10. I. Couzin, J. Krause, *Adv. Stud. Behav.* **32**, 1 (2003).
11. W. D. Hamilton, *J. Theor. Biol.* **31**, 295 (1971).
12. J. Parrish, L. Edelstein-Keshet, *Science* **284**, 99 (1999).
13. D. Grunbaum, *Evol. Ecol.* **12**, 503 (1998).
14. I. D. Couzin, J. Krause, N. R. Franks, S. A. Levin, *Nature* **433**, 513 (2005).
15. B. P. Uvarov, *Grasshopper and Locust: a Handbook of General Acridology. Vol. II: Behaviour, Ecology, Biogeography, Population Dynamics* (Cambridge Univ. Press, Cambridge, 1977).
16. M. Enserink, *Science* **306**, 1880 (2004).
17. S. J. Simpson, E. Despland, B. F. Hägele, T. Dodgson, *Proc. Natl. Acad. Sci. U.S.A.* **98**, 3895 (2001).
18. S. J. Simpson, A. R. McCaffery, B. F. Hägele, *Biol. Rev.* **74**, 461 (1999).
19. S. M. Rogers *et al.*, *J. Exp. Biol.* **206**, 3991 (2003).
20. M. Collett, E. Despland, S. J. Simpson, D. C. Krakauer, *Proc. Natl. Acad. Sci. U.S.A.* **95**, 13052 (1998).
21. E. Despland, S. J. Simpson, *Physiol. Entomol.* **25**, 74 (2000).
22. E. Despland, M. Collett, S. J. Simpson, *Oikos* **88**, 652 (2000).
23. E. Despland, J. Rosenberg, S. J. Simpson, *Ecography* **27**, 381 (2004).
24. J. S. Kennedy, *Trans. R. Entomol. Soc. London* **95**, 247 (1945).
25. P. E. Ellis, *Anti-Locust Bull.* **7**, 1 (1951).
26. P. E. Ellis, *Behaviour* **20**, 282 (1961).
27. S. J. Simpson, G. A. Sword, A. De Loof, *J. Orthoptera Res.*, in press.
28. P. M. Symmons, K. Cressman, *Desert Locust Guidelines* (FAO, Rome, 2001; www.fao.org/ag/locusts/common/ecg/347_en_DLG1e.pdf).
29. Materials and methods are available as supporting material on Science Online.
30. A. Czirók, A. Barabási, T. Vicsek, *Phys. Rev. Lett.* **82**, 209 (1999).
31. C. Huepe, M. Aldana, *Phys. Rev. Lett.* **92**, 168701 (2004).
32. P. Lorch, G. Sword, D. Gwynne, G. Anderson, *Ecol. Entomol.* **30**, 548 (2005).
33. G. Grégoire, H. Chaté, Y. Tu, *Physica D* **181**, 157 (2003).
34. We thank T. Dodgson and M. Klapwijk for rearing the locusts and for their invaluable technical expertise, and two anonymous referees for their helpful comments and suggestions. The authors acknowledge support from the Engineering and Physical Sciences Research Council grant GR/S04765/01 (I.D.C., J.B., D.J.T.S., and S.J.S.), the Royal Society (I.D.C., D.J.T.S., and E.D.), Natural Environment Research Council (J.H.), National Sciences and Engineering Research Council Canada (E.D.), the Australian Research Council Federation Fellowship Scheme (S.J.S.), and the ARC Discovery grant DP0664709 (J.B. and S.J.S.).

Supporting Online Material

www.sciencemag.org/cgi/content/full/312/5778/1402/DC1

Materials and Methods

Fig. S1

Table S1

References

Movie S1

19 January 2006; accepted 19 April 2006

10.1126/science.1125142



Solvent Containment System

Vaplock Closed Systems for solvent containment minimize leaks, spills, and vapor escape from solvent waste and supply containers. A comprehensive line of bottle caps and check valves provide an effective means of sealed solvent delivery, and safety containers with manifolds and carbon filters collect solvent wastes with minimal vapor release. The product line is designed for ease of use and adaptability, and conforms to a broad array of standard laboratory solvent containers.

Bio-Chem Valve For information 973-263-3001 www.bio-chemvalve.com

FT-IR Imaging System

The Spectrum Spotlight 300 FT-IR (Fourier transform infrared) Imaging System enables rapid extraction and analysis of data on molecular composition from a wide range of materials, from pharmaceutical tablets to diseased human tissues to forensic evidence to complex chemical materials. The system's speed, spatial resolution, spectral range, and superior signal-to-noise ratio add up to high quality chemical imaging data. It features solid-state white-light illumination; automated focus, stage movement, and illumination; and a duet detector design containing a single element microscopy and array imaging detector.

Perkin-Elmer For information call 781-237-5100 www.perkinelmer.com

DNA and RNA Recovery

GELase Agarose Gel-Digesting Preparation contains a unique β -agarose digesting enzyme for simple, quantitative recovery of intact DNA and RNA from low-melting-point agarose gels following electrophoresis in TAE, TBE, MOPS, and phosphate electrophoresis buffers. GELase preparation digests the carbohydrate backbone of molten agarose, releasing small, soluble oligosaccharides. The nucleic acid can be used in the digested gel solution or precipitated using ammonium acetate/ethanol. The gel digestion products are alcohol-soluble.

Epicentre Biotechnologies For information 800-284-8474 www.EpiBio.com

Potentiostat

The BioStat System is a high-performance, cost-effective, multi-mode potentiostat that is compatible with virtually any electrochemical sensor or electrode. The BioStat System brings to every laboratory modern digital signal processing technology in a compact, affordable package

that offers sensitivity, dynamic range, and flexibility similar to that of larger, more expensive units. The system allows precise amperometric or potentiometric measurements to be made independently on up to four channels, with the system handling signals of either polarity, employing either 2- or 3-electrode configurations. Total electrical isolation of each channel ensures independent recording with low noise.

ESA Biosciences For information 978-250-7000 www.esainc.com

Centrifugal Evaporator

Model HT-4X centrifugal concentrator can accelerate lyophilization of water and water mixtures. Lyophilization traditionally is a lengthy, multi-stage process; however, the new Lyospeed process combines Genevac's high performance centrifugal evaporation technology with sample lyophilization to deliver a major advance in preparing heat-sensitive samples from aqueous solutions. Drawing on proprietary SampleGuard and Dri-Pure technology, the HT-4X can protect samples that would bump in a traditional freeze drier. Developed for laboratories in which sample purity and speed are important, the HT-4X offers speed of evaporation, shorter condenser defrost time, powerful software, and the flexibility to accommodate a wider range of sample formats than any system in its class, according to the manufacturer. An innovative built-in dual-chamber refrigerated condenser, which combines a powerful cryopump and solvent recovery system together with powerful infrared lamps, accelerates the speed of evaporation, even for high boiling-point solvents. Efficient chamber cooling between runs protects thermally sensitive samples when run immediately after higher boiling point solvents. The system also offers an auto-defrosting option.

Genevac For information +44-1473-240000 www.genevac.com

Bioimaging Certified Reagents

A collection of antibody reagents has been tested and certified for their utility in automated bioimaging and microscopy applications. To be "Bioimaging Certified," each antibody must pass a number of tests that include exceeding a threshold of signal intensity over background in commonly used cell lines, working with widely used fixation and permeabilization methods, and localizing to the appropriate region within the cell following stimulation. The collection of reagents includes antibodies for research in apoptosis, cell cycle, signal transduction, phosphorylation, cancer, neuroscience, and other areas of biological interest. These monoclonal reagents are optimal for use in high-content applications in which reproducibility is essential.

BD Biosciences For information 800-245-2614 www.bdbiosciences.com/imaging

For more information visit **Product-Info**, **Science's new online product index** at <http://science.labvelocity.com>

From the pages of Product-Info, you can:

- Quickly find and request free information on products and services found in the pages of *Science*.
- Ask vendors to contact you with more information.
- Link directly to vendors' Web sites.

Newly offered instrumentation, apparatus, and laboratory materials of interest to researchers in all disciplines in academic, industrial, and government organizations are featured in this space. Emphasis is given to purpose, chief characteristics, and availability of products and materials. Endorsement by *Science* or AAAS of any products or materials mentioned is not implied. Additional information may be obtained from the manufacturer or supplier by visiting www.science.labvelocity.com on the Web, where you can request that the information be sent to you by e-mail, fax, mail, or telephone.

Classified Advertising



Get the Experts
Behind You.

For full advertising details, go to www.sciencecareers.org and click on For Advertisers, or call one of our representatives.

United States & Canada

E-mail: advertise@sciencecareers.org
Fax: 202-289-6742

JILL DOWNING

(CT, DE, DC, FL, GA, MD, ME, MA,
NH, NJ, NY, NC, PA, RI, SC, VT, VA)
Phone: 631-580-2445

KRISTINE VON ZEDLITZ

(AK, AZ, CA, CO, HI, ID, IA, KS, MT, NE,
NV, NM, ND, OR, SD, TX, UT, WA, WY)
Phone: 415-956-2531

KATHLEEN CLARK

Employment: AR, IL, LA, MN, MO, OK, WI
Canada; Graduate Programs; Meetings &
Announcements (U.S., Canada, Caribbean,
Central and South America)
Phone: 510-271-8349

EMNET TESFAYE

(Display Ads: AL, IN, KY, MI, MS, OH, TN, WV;
Line Ads)
Phone: 202-326-6740

GABRIELLE BOGUSLAWSKI

(U.S. Recruitment Advertising Sales Director)
Phone: 718-491-1607

Europe & International

E-mail: ads@science-int.co.uk
Fax: +44 (0) 1223-326-532

TRACY HOLMES

Phone: +44 (0) 1223-326-525

HELEN MORONEY

Phone: +44 (0) 1223-326-528

CHRISTINA HARRISON

Phone: +44 (0) 1223-326-510

SVITLANA BARNES

Phone: +44 (0) 1223-326-527

JASON HANNAFORD

Phone: +81 (0) 52-789-1860

To subscribe to Science:

In U.S./Canada call 202-326-6417 or 1-800-731-4939
In the rest of the world call +44 (0) 1223-326-515

Science makes every effort to screen its ads for offensive and/or discriminatory language in accordance with U.S. and non-U.S. law. Since we are an international journal, you may see ads from non-U.S. countries that request applications from specific demographic groups. Since U.S. law does not apply to other countries we try to accommodate recruiting practices of other countries. However, we encourage our readers to alert us to any ads that they feel are discriminatory or offensive.



POSITIONS OPEN

TENURE-TRACK FACULTY POSITIONS
Emory University
School of Medicine

The Department of Pathology and Laboratory Medicine, in conjunction with the Emory Vaccine Center, invites applications for two Tenure-Track Faculty positions (rank commensurate with candidate's experience) available immediately in the broad field of infectious diseases research with an interest in developing a program on chronic viral diseases. Appointments could be affiliated with one or more departments of the School of Medicine depending upon the interests of the candidate. Emory University School of Medicine has committed substantial resources and laboratory space to expand their program on Infectious Diseases Pathogenesis with a mandate to expand an existing cadre of accomplished interactive scientists. The candidate should possess a Ph.D., M.D., M.D./Ph.D. or D.V.M. degree and have a solid background in one of the specialties within the broad field of infectious diseases, a first-rate publication record, and a strong track record or potential to develop an active independent research program and to generate independent extramural funding. The successful candidate will be expected to form close and substantive ties with other Faculty members in both the basic science and clinical departments.

Interested candidates should send a letter of inquiry and three letters of reference by regular mail or e-mail to:

Dr. A.A. Ansari, Professor
Emory University School of Medicine
Department of Pathology and Laboratory Medicine
Woodruff Memorial Research Building
101 Woodruff Circle, Room 2309
Atlanta, GA 30322

E-mail: pathaaa@emory.edu

Emory University is an Equal Opportunity/Affirmative Action Employer. Women and minority candidates are strongly encouraged to apply.

FACULTY POSITIONS

Kunming Institute of Botany and
Institute of Tibetan Plateau Research at Kunming

Kunming Institute of Botany, Chinese Academy of Sciences located in the biodiversity-rich province of Yunnan in southwest China and Institute of Tibetan Plateau Research at Kunming, is a newly-established joint research Center co-managed by Kunming Institute of Botany and Institute of Tibetan Plateau Research, Chinese Academy of Sciences. The two institutions invite applications for faculty positions at the **PROFESSOR** or **ASSOCIATE PROFESSOR** rank. The Institutes possess excellent infrastructure for molecular phylogeny and phytochemistry researches, with substantial support for the establishment of a new germplasm bank of wild species and new facilities of eco-environment studies in the Tibetan plateau, in an atmosphere that encourages innovation and provides a highly supportive learning environment for young scientists. Positions are open to develop independent research programs in areas including seed biology, plant genomics, functional genomics, global change biology, molecular ecology, biomass energy, pharmaceutical bioassay, and chemical biology and chemical ecology. Candidates must have a Ph.D. or equivalent training, with significant postdoctoral research accomplishments or similar experience. Startup funds, annual operating funds, competitive salary, and housing benefits will be provided. Please submit a cover letter outlining research plans, curriculum vitae, and the contact details of three references to: **Ms. Zeng Yan-mei, Kunming Institute of Botany, Chinese Academy of Sciences, 610 Longquan Road, Kunming, Yunnan 650204, China. E-mail: zengyangmei@mail.kib.ac.cn; telephone: 0086-871-5223169.** Other positions such as Postdoctoral Fellows and Research Assistants/Associates are also open. Please visit our website: <http://www.kib.ac.cn>.

POSITIONS OPEN

FACULTY POSITIONS, VIROLOGY AND BACTERIAL PATHOGENESIS. The Department of Microbiology at University of Texas (UT) Southwestern Medical Center is seeking new Faculty at the **ASSISTANT** or **ASSOCIATE PROFESSOR** (tenure track) levels. Faculty will be expected to develop front-rank, competitive, independent research programs in their chosen fields and contribute to the teaching of medical and graduate students. For virology candidates, emphasis on one or more aspects of the viral life cycle (host-pathogen interactions, viral pathogenesis, disruption of viral replication, command of host cell processes, viral immunology, et cetera) is desirable to complement existing strengths in HCV, West Nile virus, HIV/SIV, and viral oncogenesis, but research on any virus of medical relevance is of interest. For bacterial pathogenesis, areas of particular interest include STDs, emerging/re-emerging pathogens, cellular microbiology, host-pathogen interactions, select agents, and opportunistic infections, but all outstanding candidates are encouraged to apply. Attractive startup packages, including competitive salaries and new laboratory space, are available to conduct research in an expanding, dynamic environment. For exceptional Assistant Professor candidates, an Endowed Scholars Program offers startup funds of \$700,000 (plus \$300,000 towards salary) over a four-year period. Candidates should have a Ph.D. and/or M.D. degree with at least three years of postdoctoral experience and an exceptional publication record. Candidates please forward curriculum vitae, three letters of recommendation, two or three representative publications, and a brief summary of future research to: **Dr. Michael V. Norgard, Chair, Department of Microbiology, University of Texas Southwestern Medical Center, 6000 Harry Hines Boulevard, Dallas, TX 75235-9048 (fax: 214-648-5905; e-mail: michael.norgard@utsouthwestern.edu).** UT Southwestern is an Equal Opportunity university.

POSITIONS AVAILABLE

The Danforth Center

Plant Biochemistry/Bioenergy from Plants

The Donald Danforth Plant Science Center anticipates the addition of one or more **PRINCIPAL INVESTIGATORS** that focus on enhancing production and recovery of energy-rich components from plant materials. Research projects will complement current strengths in biochemistry and metabolic engineering of plants for primary and secondary metabolism at the Danforth Center as described at **website: <http://www.danforthcenter.org>**. Preference given to applicants with multidisciplinary research programs, ongoing research support, and proof of scientific productivity. Opportunity for adjunct academic appointment at area universities. Level of appointment and salary will reflect prior experience. Applicants should submit curriculum vitae, reprints of three significant publications, and description of future research to: **Ms. Billie Broeker, Director of Human Resources, Ref: Plants, Donald Danforth Plant Science Center, 975 North Warson Road, St. Louis, MO 63132, or by e-mail: bcbroeker@danforthcenter.org, with Plants in the subject line.**

Equal Opportunity Employer/Affirmative Action Employer, Minorities/Females/Persons with Disabilities/Veterans.

CHIEF MEDICAL OFFICER

Highly intelligent individual with exceptional communication skills sought by prominent Manhattan family to research and coordinate family medical and healthcare issues. Act as liaison with leading medical researchers and consultants in academia and industry, with full responsibility for technical, financial, and administrative functions. Considerable weight given to evidence of unusual academic or other intellectual distinction. Ph.D. or M.D. required, clinical experience a plus but not essential. Possible entrepreneurial opportunities involving delivery of ultrahigh-end medical care to other, similar families. Full-time position. Excellent compensation with significant upside potential and management possibilities. Resume to e-mail: fmc4@spssfind.com.



The European
Commission

The European Commission, Directorate General Joint Research Centre (JRC), is seeking to recruit (m/f):

DIRECTOR

FOR INSTITUTIONAL AND SCIENTIFIC RELATIONS IN BRUSSELS (COM/2006/10023)

DIRECTOR

OF THE INSTITUTE FOR ENERGY IN PETTEN (COM/2006/10027)

Official Journal C 124 A – 25 May 2006

We are the Joint Research Centre. Our mission is to provide customer-driven scientific and technical support for the conception, development, implementation and monitoring of EU policies. JRC comprises 7 research institutes spread across 5 sites in Europe. We have a staff of 2,650 people and an operating budget of € 300 million per annum. Our core competence areas are food, chemical products and health; environment and sustainability; nuclear safety and security; and horizontal activities such as reference materials and measurements, techno-economic foresight, public security and anti-fraud.

• Director for Institutional and Scientific Relations in Brussels (COM/2006/10023)

We propose: the Directorate for Institutional and Scientific Relations fosters relations between the JRC and its external stakeholders, other research organisations, the European Parliament and Council, the Member States. It coordinates the relations with the JRC Board of Governors. It defines and monitors action plans to integrate new Member States, Candidate countries and Associated countries in the activity of the JRC. The Directorate is responsible for JRC's internal and external communication including public relations and relations with the press. It is intended that it will also become responsible for the co-ordination of the JRC's scientific work programme, including its preparation, and for ensuring the quality of JRC research and services to its customers. The Directorate is also responsible for the management of the intellectual property of the Community and the promotion of technology transfer of JRC's knowledge. The Directorate has about 50 staff and a budget of € 2 million.

• Director of the Institute for Energy in Petten (COM/2006/10027)

We propose: the position as Director of the Institute for Energy (IE). IE provides scientific and technical support to community policies related to energy. IE has a staff of about 200 and a yearly budget of ca. € 30 million. IE carries out research in the fields of clean and sustainable energy spanning both nuclear and non-nuclear domains. Activities encompass: nuclear safety in the enlarged EU, including support to TACIS (technical assistance for the Commonwealth of Independent States) and PHARE (Poland, Hungary aid for the reconstruction of the economy); new nuclear energy systems; thermal treatment of waste and biomass/biofuel; waste incineration; emission mitigation from power plants; clean energy sources. State-of-the-art facilities for performance testing of fuel cells and hydrogen storage have been inaugurated in 2005. Research is also being carried out at the Commission-owned neutron research reactor on site. There are very active cooperations with partners in the EU and beyond.

The position combines the management of specialised research and service provision to the EU policy makers in a field which has taken on renewed importance on the EU agenda. The Director will be expected to provide strategic orientation for and co-ordination of energy-related research and services across the whole of the JRC.

We look for candidates who should have: • a scientific background and a high level of knowledge of science and technology issues dealt with by the JRC; experience in a scientific or customer area relevant to JRC would be an advantage; • motivation to lead a dynamic Directorate and its support to the overall JRC goals; • proven experience to steer the programming and management of human, financial and scientific resources of the Directorate; • the necessary leadership capacity to manage highly specialised research teams; • a good knowledge of Community policies and Institutions; • very good negotiation and communication skills; • the capacity to interact convincingly with high level stakeholders and press; • an excellent knowledge of English.

To be eligible candidates must: • be a citizen of the 10 new EU Member States; • hold a university degree that gives access to undertake doctoral studies; • have at least 12 years' postgraduate professional experience at a level to which the qualifications referred to above give admission, including at least 6 years at a senior management level; • have a thorough knowledge of one of the official languages of the EU and an adequate knowledge of another of these.

The Director will be selected and appointed by the Commission according to its selection and recruitment procedures. Salaries and conditions of employment are those laid down in the Staff Regulations for AD14 grade officials of the European Communities. The Commission applies an equal opportunities policy. Full job descriptions, selection criteria and application details can be found at http://europa.eu.int/comm/dgs/personnel_administration/working_senior_mgt_en.htm

The closing date for registration is 26 June 2006.

On-line registration will not be possible after 12.00 noon Brussels time.



<http://europa.eu.int>

ScienceCareers.org

FEATURED EMPLOYER



Fogarty International Center National Institutes of Health

The Fogarty International Center (FIC), the international component of the NIH, addresses global health challenges through innovative and collaborative research and training programs and supports and advances the NIH mission through international partnerships. This position is located in the Division of International Training and Research responsible for managing research and training grants and fellowships awarded by FIC. Grants support a diverse array of projects in infectious diseases, including HIV/AIDS, TB and malaria, chronic diseases including those related to mental health, injury and tobacco use, and the supporting disciplines of global health, including environmental sciences, population science, economics, bioethics and informatics. A growing number of these grants are highly interdisciplinary and include social and behavioral sciences.

FIC is looking for a behavioral or social scientist who will identify and administer extramural research and training awards in an array of global health relevant fields, including psychology, sociology, economics, anthropology, and health systems. Broad research experience, including experience in developing countries, strong communication and organizational skills are important. In addition to his/her own portfolio of grants, the candidate will work with existing program officers to strengthen the behavioral and social sciences linkages among the various extramural programs and other FIC divisions.

The vacancy announcement contains application procedures and lists all mandatory information, which you must submit with your application. To obtain the announcement which will be available on **05/01/2006**, and posted under #FIC-06-119716, you may visit the OPM website <http://www.usajobs.opm.gov/>. Applications and all supporting documentations must be received by **7/7/2006**.

Postdoctoral, Research and Clinical Fellowships at the National Institutes of Health

www.training.nih.gov/pdopenings

www.training.nih.gov/clinopenings

Train at the bench, the bedside, or both

Office of Intramural Training and Education
Bethesda, Maryland 20892-0240
800.445.8283



Postdoctoral Training Opportunity in the Genetics of Type 2 Diabetes National Human Genome Research Institute

A postdoctoral training position is available in the Genome Technology Branch of the National Human Genome Research Institute. The position is located in the laboratory of Francis S. Collins, M.D., Ph.D., whose research includes work on the genetics of type 2 diabetes. Current studies in the lab focus on this disorder, in collaboration with clinical researchers in Finland, diabetes physiology experts at USC, and the statistical genetics expertise of Mike Boehnke's group at the University of Michigan. Referred to as FUSION (Finland-United States Investigation of NIDDM), this project now represents one of the largest and most powerful studies of type 2 diabetes in the world. Candidates should have or be close to obtaining a Ph.D., M.D., or M.D./Ph.D degree with a focus in human genetics, genomics, molecular biology, or computational biology. Expertise in genotyping, haplotyping, and association analysis is highly desirable, as are skills in gene transfer, gene expression, functional genomics, proteomics, and/or animal models.

The intramural research program is located on the Bethesda campus and offers a wide array of training opportunities for scientists early in their careers. The funding for this position is stable and offers the trainee wide latitude in the design and pursuit of their research questions. Access to extensive core facilities including a transgenic mouse core facility, human clinical-translational research at the NIH clinical center, and others, allows a postdoc to accomplish a great deal in a short time. The Washington DC area provides innumerable opportunities for cultural enrichment as well.

Please send a curriculum vitae, a letter of interest, and names of three potential referees to **Francis Collins** at fc23a@nih.gov or to the address below.

Francis Collins, M.D., Ph.D., Director, NHGRI, Senior Investigator, Genome Technology Branch, Building 31, Room 4B09, 31 Center Drive, Bethesda, MD 20892.



RAPID ACCESS TO PREVENTIVE INTERVENTION DEVELOPMENT "RAPID" PROGRAM

National Cancer Institute

The National Cancer Institute announces the ongoing initiative: Rapid Access to Preventive Intervention Development (RAPID). RAPID will make available to academic investigators the preclinical and early clinical drug development contract resources of NCI's Division of Cancer Prevention. In some instances resources will be provided to the investigator. The goal of RAPID is the rapid movement of novel molecules and concepts from the laboratory to the clinic for clinical trials of efficacy. RAPID will assist investigators who submit successful requests by providing any (or all) of the pre-clinical and phase 1 clinical developmental requirements for phase 2 clinical efficacy trials. These include, for example, preclinical pharmacology, toxicology, and efficacy studies; bulk supply, GMP manufacturing, and formulation; and regulatory and IND support and phase 1 clinical studies. Suitable types of agents for RAPID may range from single chemical or biological entities to defined complex mixtures with the potential to prevent, reverse, or delay carcinogenesis. For more detailed information, visit the web site, <http://cancer.gov/prevention/RAPID>

Requests for RAPID resources are to be submitted as described in the web site. Written requests will be evaluated by a specially constituted RAPID panel, consisting of outside experts from academia and industry. Requests must be received on or before **November 1, 2006**. Applications should be submitted directly to the office listed below. Inquiries are encouraged, and the opportunity to clarify issues or questions is welcome. Please contact:

RAPID Program Official, Executive Plaza North, Room 2117, 6130 Executive Blvd., Bethesda, MD 20892, Rockville, MD 20852 (for express/courier service), Telephone: (301) 435-5011, Email: kapetani@mail.nih.gov, Or Telephone: (301) 594-0459, Email: je94h@nih.gov, Fax: (301) 402-0553.



WWW.NIH.GOV

Scientific and Clinical Director

The National Center for Complementary and Alternative Medicine (NCCAM) seeks an accomplished, innovative neuroscientist and clinician to fill three pivotal roles: as Scientific Director and Clinical Director of its Intramural Research Program (IRP) and as Senior Investigator responsible for developing a new research program in mind-body medicine. This individual will report to the NCCAM Director and will be a member of the NCCAM leadership.

As Scientific Director, you will articulate and implement a vision and oversee research infrastructure for highly unified and mutually supportive laboratory and clinical programs in the conduct of bench-to-bedside and bedside-to-bench research related to CAM therapies.

As Clinical Director, you will chart a course and allocate resources for clinical research; recruit and oversee the activities of clinical staff and fellows; ensure appropriate design and conduct of clinical research protocols; and facilitate the integration of CAM practices into the training programs and delivery of care throughout the NIH Clinical Center.

As Senior Investigator, you will have substantial committed resources to create a cutting-edge program of clinically oriented laboratory research and clinical studies that exploit neuroscience disciplines to define the nature, mechanisms of action, safety, and efficacy of diverse CAM modalities that affect actions and interactions linking mind, body, and behavior.

This exceptional opportunity is available to a U.S. citizen, resident alien, or nonresident alien with valid employment authorization who is an accomplished neuroscientist with a U.S. medical license; a demonstrated record of senior-level management of a large, nationally recognized research program; a commitment to both basic and clinical research; and leadership skills that equip him/her to forge team efforts with colleagues within intramural programs across NIH.

Salary and benefits are commensurate with experience. Qualified individuals are encouraged to email their CV, bibliography, list of three references, and cover letter outlining their relevant experience and vision for leading the NCCAM IRP to:

nccamdirector-r@mail.nih.gov

Subject Line: Scientific and Clinical Director Search

Application Deadline: July 14, 2006

Email receipt of applications and inquiries is preferred; however, candidates needing reasonable accommodation may fax application materials to 301-402-4741.

NIH and DHHS are Equal Opportunity Employers



Interview/Hire the World's Best Scientists

Reach innovative young scientists at the forefront of their fields

Attend the Job Fair for Postdoctoral, Research, and Clinical Fellows

Date: October 19, 2006

Time: 10:30 am - 3:00 pm

Place: Natcher Conference Center
National Institutes of Health
Bethesda, MD

Access 3800 doctoral scientists and clinicians in training at the NIH

Register by September 15th at:
www.training.nih.gov/jobfair

Office of Intramural Training and Education

NIH is dedicated to building a diverse community in its training and employment programs.





U.S. Environmental Protection Agency
Office of Research and Development

HIGH-LEVEL
CAREER OPPORTUNITIES
IN
MICROBIOLOGY

EPA's Office of Research and Development (ORD) is seeking internationally recognized scientists to fill two positions: one in the National Exposure Research Laboratory (NERL) <http://www.epa.gov/nerl/> and another in the National Center for Environmental Assessment (NCEA) <http://www.epa.gov/ncea/>. Both positions are located in Cincinnati, Ohio.

ORD plans to fill these positions using EPA's Title 42 Authority, which offers up to 5-year renewable term appointments at highly competitive, market-based salaries. The positions are part of a larger EPA effort to use state-of-the-science approaches and technologies in its mission of protecting human health and the environment. The ideal candidates will have a doctoral level degree in a pertinent science discipline and extensive specialized experience. For more information about the two organizations and their respective job announcements, please refer to their websites as listed above.

Positions and major duties include:

NERL-06-42-04 Research Microbiologist

- Establishing and conducting a research program to address critical needs related to the assessment of exposure to microbiological hazards in water. An area of particular relevance to NERL is the development of innovative approaches for reliable concentration, detection and characterization of pathogens of concern to EPA. Other areas of research could involve studies to support the assessment of pathogenicity and the development of quantitative models of microbial risk.

NCEA-06-42-05 Microbial Risk Assessor

- Developing and implementing ORD's research agenda for microbial risk assessment, particularly (1) characterizing environmental exposures of humans to pathogenic microorganisms, (2) characterizing infectivity, virulence, and transmissibility of environmental microbial agents, and (3) characterizing both individual and population susceptibility to diseases caused by environmental microorganisms.
- Overseeing the conduct of microbial risk assessments which are of significant strategic importance to EPA risk management and rule-making decisions.

Responsibilities for both positions include providing leadership of ORD's microbiology research program, serving as a senior spokesperson/representative, identifying collaborative opportunities with outside organizations, and playing a vital role in the leadership of a proposed virtual EPA Institute for Environmental Microbiology.

Salary and Benefits: Salary is up to \$200,000 per annum, dependent upon qualifications, experience, and other factors. The selected applicant will be eligible for full benefits including health and life insurance, retirement, and vacation and sick leave.

How to Apply: Send the following information: (a) a vision statement (1-2 pages) including your research goals and how they relate to the duties of the position for which you are applying; (b) curriculum vitae; (c) the names of three references; (d) citizenship status; and (e) compensation requirements. **Candidates must reference the specific vacancy number(s) of the position(s) for which they are applying.**

Applications should be mailed to the attention of: **Ms. Dorothy Carr, U.S. EPA, MD-C639-02, RTP, NC 27711** or sent via email to title42@epa.gov by **June 16, 2006**. For additional information, **Ms. Carr** can also be reached at **(800) 433-9633**. Technical questions pertaining to vacancy **NERL-06-42-04** may be addressed to **Dr. Al Dufour** at **(513) 569-7330**. Technical questions regarding vacancy **NCEA-06-42-05** may be addressed to **Dr. Glenn Suter** at **(513) 569-7808**.

The U.S. EPA is an Equal Opportunity Employer.



DEPARTMENT HEAD
Department of Wildlife
and Fisheries Sciences

Applications are invited for the position of Professor and Head to provide dynamic statewide leadership for the Department of Wildlife and Fisheries Sciences, the Department of Wildlife and Fisheries Sciences, which has programs in wildlife conservation, ecology and evolutionary biology, and aquaculture are nationally recognized. As an administrative unit of the College of Agriculture and Life Sciences, the Texas Agricultural Experiment Station and Texas Cooperative Extension, the Department has a diverse and dynamic mission with faculty and staff engaged in teaching, research, and extension at several locations throughout the state, nation, and world.

Texas A&M University, the Land Grant Institution for the state, is a research intensive university committed to adding 400 faculty members over a 4-year period and strengthening its diversity. The Department recently has expanded its programs and faculty offering new leadership opportunities for the successful candidate.

For the full position announcement, please visit <http://wfsc.tamu.edu/>

The deadline for applications is July 1, 2006 or until a suitable candidate is selected.

Texas A&M University is an Equal Opportunity Employer.

POSTDOCTORAL FELLOWSHIP PROGRAM

NATIONAL SPACE BIOMEDICAL RESEARCH INSTITUTE



The National Space Biomedical Research Institute (NSBRI) is soliciting applications for its Postdoctoral Fellowship Program.

Two-year Fellowships are available in any U.S. laboratory carrying out space-related biomedical or biotechnological research that supports NSBRI's mission and objectives.

Applicants must submit proposals with the support of a mentor and institution, and all proposals will be evaluated by a peer-review panel. *The Program is open to U.S. citizens, permanent residents, or persons with pre-existing visas obtained through their sponsoring institutions that permit postdoctoral training for the project's duration.*

Detailed program and application submission information is available on the NSBRI website at www.nsbri.org/Announcements/rfp06-01.html. Letters of intent and applications must be submitted through NSBRI's electronic proposal submission system. *Letters of intent are due June 22, 2006, and the application deadline is July 20, 2006.*

Questions to: Sonia Rahmati Clayton, Ph.D., Program Coordinator, NSBRI Postdoctoral Fellowship Program, telephone: 713-798-8229, email: postdoc@www.nsbri.org.

The Beatson Institute for Cancer Research in Glasgow is one of Europe's leading research centres. It is core funded by Cancer Research UK and supports cutting edge research into the molecular mechanisms of cancer development. The Beatson Institute provides an outstanding research environment, underpinned by state of the art core services and advanced technologies. A new research facility - to be completed later this year - will allow significant expansion of the Institute over the next few years.

We are now inviting applications for Group Leader positions from outstanding scientists with a focus in cancer research, a commitment to excellence, and a strong record in their field. We welcome applicants from all relevant areas of research, but we are especially interested in scientists with research programmes in:-

- Regulation of cancer cell death and survival
- Regulation of cancer cell migration and invasion
- Regulation of cancer cell proliferation and growth

We offer both tenure track (starting salary from £40,000 pa) and tenured (starting salary c £55,000 pa) positions - depending on previous experience - and substantial, core funding with space for expansion on external grants. We provide a supportive and collaborative environment for scientists with an aspiration to conduct world-class basic, translational or clinical research.

To learn more about the Beatson Institute and Glasgow, or to contact us informally, please visit our website at www.beatson.gla.ac.uk. You can also write directly to Prof. Karen Vousden (Director) by Email at k.vousden@beatson.gla.ac.uk

To submit an application please include a CV, a brief description of research achievements and future proposals and the names of three referees. Recruitment is on-going and there is no formal closing date.



INSTITUT PASTEUR KOREA

PROGRAM LEADER Medicinal Chemistry

The newly established Institut Pasteur Korea (IPK) seeks a proven leader to build and manage a medicinal chemistry program. Institut Pasteur Korea has an international and highly interdisciplinary faculty reaching from biological disease models to drug discovery. IPK emphasises visual based high content screens in conjunction with imaging approaches to screen models of infectious and chronic disease.

The candidate will set up and manage the medicinal chemistry activities including Hit-to-Lead and Lead optimisation. This involves participation in choice of chemical libraries, in silico analysis (chemical space, scaffolds identification), participation in hit triage in collaboration with the screening group, selection of the chemical series to pursue, to design and to synthesise molecules to support our drug discovery effort. The position will give the candidate the opportunity to actively shape drug discovery at IPK.

Applicants for the Program Leader position should have a Ph.D. in Medicinal Chemistry (or related field) with a proven ability to manage drug development projects. Previous experience in team management would be appreciated. Excellent communication skills and the ability to direct an interdisciplinary program in close interaction with the biology groups will be essential.

IPK is a not-for-profit organisation located in Seoul, and is part of the international network of Pasteur Institutes. The working language is English. IPK offers generous support compensation, and substantial relocation package. Salary is commensurate with experience.

A Curriculum Vitae and letter describing previous experience should be submitted electronically to: recruit@pasteur.or.kr. We will only be able to contact those candidates who we will invite for interviews.

UIC UNIVERSITY OF ILLINOIS
AT CHICAGO

**Cancer Center Director and Chief of Hematology/Oncology
College of Medicine, University of Illinois at Chicago**

The University of Illinois at Chicago (UIC) is recruiting a Cancer Center Director who will also serve as Chief for the Section of Hematology/Oncology in the Department of Medicine although the recruitment to the Cancer Center Director position is not limited to a Hematologist/Oncologist. The candidate should be a nationally known physician-scientist with a strong record of grant supported research. Rank will be determined based on the candidate's credentials and experience. The successful candidate will possess the leadership skills needed to advance multidisciplinary and translational cancer research and cancer care among the six health sciences colleges at the University of Illinois Medical Center. The successful candidate will collaborate with deans and department heads across the health sciences colleges to recruit academic clinicians, translational and clinical investigators, and laboratory-based scientists to foster the career development of future leaders in cancer research. The Cancer Center Director will function as the chief executive officer of a university-wide organization that integrates clinical care and cancer research and therefore must have strong skills in communication, consensus-building, and the ability to nurture interdisciplinary programs.

For fullest consideration, applicants should submit a letter of application and CV by **July 1, 2006** to:

**Ms. Lillye A. Hart
Associate Dean for Administration
UIC College of Medicine
1853 West Polk Street (M/C 784)
Chicago, Illinois 60612**

*UIC is an Affirmative Action/Equal Opportunity Employer.
Women and minorities are encouraged to apply.*

**Careers in
Biotechnology &
Pharmaceuticals 2**

Advertising Supplement



Get the
experts
behind
you.

Be sure to read this
plement
devoted to opportunities
in biotechnology &
pharmaceuticals in the
upcoming **16 June issue**
of **Science**.

You can also
read it online on
www.sciencecareers.org.

To advertise in this
issue, please contact:

U.S. Daryl Anderson
phone: 202-326-6543
e-mail: danderso@aaas.org

Europe and International
Tracy Holmes
phone: +44 (0) 1223 326 500
e-mail: ads@science-int.co.uk

Japan Jason Hannaford
phone: +81 (0) 52 789-1860
e-mail: jhannaford@sciencemag.jp

The Coca-Cola Company

The Coca-Cola Company exists to benefit and refresh everyone it touches. Founded in 1886, our Company is the world's leading manufacturer, marketer, and distributor of nonalcoholic beverage concentrates and syrups, used to produce nearly 400 beverage brands. Our corporate headquarters are in Atlanta, with local operations in over 200 countries around the world. We are currently expanding our strategic research capabilities in the area of human taste. The Company presently has the following opportunities for scientists at the Corporate Headquarters in Atlanta, Georgia:

Cell Biologist/Biochemist (Job No. 6381)

Suitable candidates will have a PhD and relevant post-doctoral and/or industrial experience. Appropriate areas of expertise include cell biology, biochemistry, pharmacology, or cellular physiology. Sub-areas of training might include cell signaling, receptor/ion channel biology, protein trafficking, cellular imaging, or membrane biology. Experience in mammalian cell culture is desirable. The primary responsibilities of the position include: (1) to perform at-the-bench research related to programmatic goals, and (2) to contribute intellectually to research and innovation efforts. Although research activity will be focused, the individual is expected to function with minimal supervision.

Molecular Biologist/Cell Biologist (Job No. 6380)

Suitable candidates will have a PhD and relevant post-doctoral and/or industrial experience. Appropriate areas of expertise include molecular genetics/biology, biochemistry, or molecular neuroscience. Sub-areas of training might include gene expression analysis, manipulation of mammalian/eukaryotic gene expression, or neuronal cell signaling. Experience in mammalian cell culture is desirable. The primary responsibilities of the position include: (1) to perform at-the-bench research related to programmatic goals, and (2) to contribute intellectually to research and innovation efforts. Although research activity will be focused, the individual is expected to function with minimal supervision.

The Coca-Cola Company offers a competitive salary, excellent benefits and an opportunity to work in an exciting interdisciplinary team environment. All candidates must be eligible to work in the US without sponsorship. For consideration, please visit our website at <http://www.coca-cola.com>, follow the links for Careers, North America and submit a resume to the job number referenced above.

ScienceCareers.org

We know science

AAAS

SCIENTIFIC PROGRAMME OFFICER



Science Foundation Ireland (SFI)
Ref: SFI 05-06

Science Foundation Ireland (SFI), the National Foundation for Excellence in Scientific Research, was established under the Industrial Development (Science Foundation Ireland) Act 2003 to undertake and support strategic research of world class status in key areas of scientific endeavour which would underpin economic development, particularly the areas of Biotechnology and Information and Communications Technologies (ICT).

Applications are invited for the position of Scientific Programme Officer, in the following directorates:

- BioSciences and BioEngineering
- Information and Communications Technology
- Frontier Engineering and Scientific (FES) Research – this Directorate has responsibility for the operation of general science and engineering grants programme, European Union Framework and other international programmes liaison and integration; the Mathematics Initiative and for integrative work with other SFI directorates.

This position is located in Wilton Park House, Wilton Place, Dublin 2, Ireland.

Candidates must have:

- Ph.D. in a relevant field. The preferred areas for the FES Directorate are Chemistry, Physics, Engineering, Geological Sciences, Mathematics, Environmental Science or Ecology.
- Proven track record with *at least* 5 years experience beyond the Ph.D. in the academic or private sector, in the conduct of active quality scientific research and the management of such research in ICT, BIO or FES.

A full detailed job description is available on the SFI website at www.sfi.ie under 'about SFI' and 'Jobs'.

From the recruitment process an appointment may be made on a full-time or part-time contract basis. In addition a panel may be formed for 12 months, from which future Scientific Programme Officer posts may be appointed.

If you wish to be considered for this position, please email your CV, quoting the job reference number SFI-05-06, to siobhan.smith@sfi.ie or send it to:

Science Foundation Ireland,
FAO: Siobhán Smith, Human Resources,
Wilton Park House, Wilton Place,
Dublin 2, Ireland

The closing date for receipt of applications is
June 16th 2006.

SFI is an equal opportunities employer.

R&D &
YOU & US

PGRD

Pfizer Global Research & Development

Imagine a career that touches the lives of people everywhere. Imagine an opportunity to reach beyond your area of expertise to make an impact on something greater than the bottom line. Imagine playing a key role in some of the most critical issues facing health care today. This is your career at Pfizer – a career unlike any other. We have multiple postdoctoral opportunities at our state-of-the-art research facility in La Jolla, CA.

Postdoctoral Opportunities

Ideal applicants should hold a recent Ph.D. degree and be willing to work in a multidisciplinary environment. More experienced candidates interested in a focused second postdoc will have an advantage. Positions are for one year and may be extended to two years.

Qualified candidates can join us in one of the following areas:

Cell Biology/Signaling

Req # 056152 – Cancer Stem Cells

Req # 056150 – Chemosensitivity to targeted cancer drugs

Req # 056158 – Novel targets for insulin sensitization

Biochemistry

Req # 056155 – Mechanistic studies of allosteric regulation of glucokinase

Req # 056156 – Expression, characterization and mechanistic studies of Hepatitis C viral enzymes

Protein NMR

Req # 056160 – NMR studies of protein interfaces

Virology

Req # 056157 – Characterization of novel target

HIV-1 inhibitors

Req # 056149 – In vitro infectious replication of HCV

Ophthalmology

Req # 056151 – Neuroprotective effects of glaucoma drugs

We offer competitive compensation, full benefits and talented professional colleagues...some of the best and brightest in the research field today. Submit your resume today at: www.pfizer.com/careers and search by the appropriate **Req number**.

Pfizer is proud to be an Equal Opportunity Employer and welcomes applications from people with different experiences, backgrounds and ethnicities.



Expect More From Your Career.®

www.pfizer.com/careers

FACULTY POSITIONS - MICROBIOLOGY University of Connecticut-Storrs

The Department of Molecular and Cell Biology at the University of Connecticut invites applications for two tenure-track positions at the **ASSISTANT or ASSOCIATE PROFESSOR** levels in the areas of (1) *Functional Genomics of Complex Communities*, (2) *Molecular Evolution of Microbial Systems* or (3) *Genetics of Microbe/Host Interactions*. We seek investigators using genome-wide approaches to investigate: gene expression and functions of microbes in complex environments, the evolution of metabolic pathways or regulatory networks, the roles of horizontal gene transfer in evolution, the effects of host associations on the evolution of bacteria and their host, or the coordination of microbe physiology with that of the host. Successful applicants are expected to establish a productive research program, teach undergraduate microbiology and contribute to graduate courses. Start date: **Fall 2007**. Applicants must have postdoctoral experience and an outstanding research record. UConn boasts strong research in microbial symbiosis, evolution, genomics, and ecology (www.microbiology.uconn.edu).

The University of Connecticut, rated first among public universities in New England, is located in northeastern Connecticut with easy access to Boston and New York City.

Submit a CV, a concise statement of research and teaching interests, and three letters of recommendation to:

**Microbiology Search Committee Chair
Department of Molecular and Cell Biology U-3125
University of Connecticut
Storrs, CT 06269**

Review of applications will begin **June 21, 2006** and continue until the positions are filled. The Department's web page is www.mcb.uconn.edu.

We encourage applications from underrepresented groups including minorities, women, and people with disabilities.



Center for Immunology & Microbial Disease Albany Medical College

Faculty Position

The Center for Immunology & Microbial Disease at Albany Medical College invites applications for a tenure-track faculty position from individuals who have a doctoral degree, postdoctoral experience, and demonstrated research productivity. The successful candidate will be expected to establish an independent, extramurally-funded research program and participate in the teaching of medical and graduate students. The basic science departments at Albany Medical College are organized as interdisciplinary research centers and the Center for Immunology & Microbial Disease has a focus on microbial pathogenesis and immune defense, particularly as related to bioterror agents and emerging infections. Faculty at the Albany Medical College receive competitive salaries, attractive start-up packages, and access to the Center's ABSL-3/BSL-3, Microbiology and Immunology Core Labs. In addition, we have established a close relationship with the New York State Department of Health Wadsworth Laboratories, providing a diverse environment that is rich in infectious disease expertise. Albany Medical College is located in a mid-sized city within the upstate New York Capital Region, and has easy access to Boston, New York City, and the Adirondack Mountains.

Applicants should send their curriculum vitae, a statement of research plans, and three letters of reference to:

**Dennis W. Metzger, Ph.D.
Professor, Theobald Smith Alumni Chair and Director
Center for Immunology & Microbial Disease
Albany Medical College
47 New Scotland Avenue, MC-151
Albany, NY 12208**

For further information about the Center, visit
www.amc.edu/Academic/Research/imd.htm

*An Equal Opportunity/Affirmative Action Employer.
Women and minorities are encouraged to apply.*

CLINICAL CYTOGENETICIST

The Department of Hematopathology at **The University of Texas M. D. Anderson Cancer Center** is seeking a candidate for the position of Clinical Cytogeneticist for the Clinical Cytogenetics Laboratory. Candidates must possess a Ph.D. and/or M.D. degree and must be board-eligible/certified by the ABMG in Clinical Cytogenetics.

The successful applicant will have a strong commitment to diagnostic cancer cytogenetics and clinical research. Primary responsibilities will include review of cytogenetic cases and reports, and development and monitoring of test protocols. Opportunities for clinical research within the department and throughout the institution are numerous, and the applicant will be expected to interact closely with the clinical faculty and staff. Additional responsibilities will include teaching residents, fellows, and undergraduate students in the Allied Health Science programs. The salary, title and level of appointment will be dependent on academic qualifications and experience.

Interested applicants should submit a current C.V. and the names of three references to:

**Lynne Abruzzo, M.D., Ph.D.
The University of Texas M. D. Anderson Cancer Center
Department of Hematopathology
1515 Holcombe Blvd., Box 072
Houston, TX 77030
Fax: 713-745-0736
E-mail: labruzzo@mdanderson.org**

THE UNIVERSITY OF TEXAS
**MD ANDERSON
CANCER CENTER**
Making Cancer History®

M. D. Anderson Cancer Center is an equal opportunity employer and does not discriminate on the basis of race, color, national origin, gender, sexual orientation, age, religion, disability or veteran status except where such distinction is required by law. All positions at The University of Texas M.D. Anderson Cancer Center are security sensitive and subject to examination of criminal history record information.
Smoke-free and drug-free environment.

Challenging Opportunity to do Global Research from India

The Center for Genomic Application (TCGA) is the first public-private partnership and symbolizes the current revolution in India's biotechnology industry (Nature, July 28, 2005). TCGA is a partnership between TCG Lifesciences and Institute of Genomics and Integrative Biology (IGIB) in the areas of genomic and proteomic research in India. We focus on broad areas relating to biomedical sciences, functional genomics and bioinformatics. Our state-of-the-art research center is located in New Delhi, India. We invite you to know more about us through our website www.tcgaresearch.org

Requirements

- **Group Leaders** with 5-10 years of post-doctoral experience, industry experience desirable.
- **Senior Research Scientists** with 3-6 years of post-doctoral experience, industry experience desirable.
- **Research Scientists** with 1-4 years of post-doctoral experience, industry experience desirable.
- **Research Associates** with a PhD.

Qualifications

- PhDs from reputed institutes with good academic credentials in Molecular Biology, Disease Genomics, Microbiology, Bioinformatics, Cell Biology, Life sciences, Chemistry-Biology Interface and Drug Development.
- Excellent leadership qualities, communication and interpersonal skills
- The candidates should possess good skills and hands-on experience in various genomics, functional genomics, bio-informatics, proteomics and associated fields.

Send in your detailed resume
to career@tcgaresearch.org
or fax to +91-11-51708321
with attention to **HR Head**



Dwan Research Endowed Chair in Pediatric Cardiology
University of Minnesota Department of Pediatrics
University of Minnesota Children's Hospital

The Division of Cardiology in the Department of Pediatrics at the University of Minnesota Medical School and the University of Minnesota Children's Hospital, Fairview are seeking a scientist (M.D. M.D./Ph.D. or Ph.D.) for the Paul F. Dwan Endowed Chair in Pediatric Cardiology. The Chair holder should have independent research funding, national recognition in cardiology research, and demonstrated abilities in research mentorship. The Dwan Chair consists of \$3.5 million in endowment that generates \$175,000 per year in discretionary income for research support. There is an additional \$1.5 million for research start up funds and/or recruitments as well as outstanding laboratory space.

The Department of Pediatrics at the University of Minnesota has 105 full time faculty and over \$16.9 million in NIH grants in 2005, ranking it among the best in the United States. The University of Minnesota Children's Hospital has 207 beds and a very active clinical cardiology and cardiothoracic surgery services, including heart and lung transplantation. The new University of Minnesota Children's Hospital is scheduled for completion in 2010.

Please send curriculum vitae to:

John R. Schreiber, M.D.
Head, Department of Pediatrics
University of Minnesota Medical School
420 Delaware St. SE
Minneapolis, MN 55455
Telephone: 612-624-3113
E-mail: jrs@umn.edu

*The University of Minnesota is an Equal Opportunity
Educator and Employer.*



Professor of Tumour Biology Ref: ABM0107/S
INSTITUTE OF CANCER THERAPEUTICS

We are looking to recruit, to a personal chair, an expert in cancer biology of international standing with a proven track record in research relating to tumour initiation and/or progression. Expertise in the molecular basis of tumour angiogenesis, metastasis or resistance mechanisms all would be appropriate. You will build an independent team within the Institute of Cancer Therapeutics but also want to contribute to the output of the existing cancer medicines discovery team. The Institute has close links with the Leeds-Bradford Medical School and Cancer Research Unit at Leeds University. It is also designated as the Leeds-Bradford Key Cancer Centre and NTRAC/Experimental cancer medicine (ECMC) Centre to provide PKPD support to early phase clinical trials.

The mission of the research at the Institute of Cancer is to conduct the highest possible quality research and development that will enable the progress of cancer medicines from design to clinical application for the benefit of patients. The Institute of Cancer Therapeutics is RAE 5 rated and has major support from Cancer Research UK, Yorkshire Cancer Research, UK research councils and Pharmaceutical and Biotechnology organisations. In August 2006 the team will relocate to a new 2600m² floor space building to support our expansion in tumour biology, pharmacology, medicinal chemistry, drug analysis and proteomics.

Further information regarding the activity of the Institute can be found at www.cancer.brad.ac.uk

Closing Pdate: P30th June 2006. Phterviews Pwill Pbe Pheld: Pw/cP17th July 2006.

How to apply: jobs@bradford.ac.uk tel: 01274 233091
(minicom: 01274 235807). For more information see
www.bradford.ac.uk/jobs

Applications submitted by agencies will not be considered.

Confronting Inequality : Celebrating Diversity

The **Department of Biological Sciences** at **San José State University** seeks applicants for **THREE TENURE TRACK POSITIONS** to start on January 23, 2007.

ASSISTANT PROFESSOR
Anatomy

Applicants must have a Ph.D. degree in the anatomical or physiological sciences and experience in cadaver-based anatomy. Ability to teach courses in histology, embryology and/or neuroanatomy is desirable. The successful candidate will participate in teaching anatomy and physiology courses for non-majors and may teach in courses for biology majors and graduate students. **Please include Job Opening ID (JOID) #12169 on all correspondence.**

ASSISTANT/ASSOCIATE PROFESSOR
Immunology

Applicants must possess a Ph.D. in immunology. Preference will be given to applicants with post-doctoral experience. Duties will include coordinating and teaching an upper division lecture and laboratory course in immunology, a graduate level immunologic techniques course, and coordinating the use of cell culture and flow cytometry facilities. Depending on the candidate's area of expertise, other possible assignments might include courses in flow cytometry, virology and laboratories in microbiology or cell biology. **Please include Job Opening ID (JOID) #12388 on all correspondence.**

ASSISTANT/ASSOCIATE PROFESSOR
Molecular Biology

Applicants must possess a Ph.D. in Molecular Cell Biology or closely related discipline. Preference will be given to applicants with post-doctoral experience. Teaching duties will include core introductory Cell Biology for all biological sciences majors and graduate lecture and laboratory methods courses in molecular biology. The successful candidate will also have the opportunity to develop courses in their area of expertise that may include cell and molecular biology, virology, genetics, and evolutionary biology. **Please include Job Opening ID (JOID) #12389 on all correspondence.**

FOR ALL THREE POSITIONS: Applicants must have a proven record or potential for excellence in teaching. The successful candidate must address the needs of a student population of great diversity – in age, cultural background, ethnicity, primary language and academic preparation. Applicants must have research experience and publications in their discipline. The successful candidate must have the ability to establish an extramurally funded research program involving undergraduates and M.S. graduate students. Research collaborations with other department faculty are encouraged. Opportunities for external collaboration include nearby biotechnology companies, Bay Area universities, Moss Landing Marine Labs and NASA Ames Research Center. For more details see <http://www.fa.sjsu.edu/employment/employment.htm>.

FOR CONSIDERATION for one of these positions, send hard copies of a letter of application, curriculum vitae, official university graduate and undergraduate transcripts, a statement of teaching interests/philosophy and research interests, and at least three original letters of reference with contact information to the respective search committee at the **Department of Biological Sciences, San José State University, One Washington Square, San José, CA 95192-0100.**

- **Anatomy and Physiology Search Committee.** Please include Job Opening ID (JOID) #12169 on all correspondence.
- **Immunology Search Committee.** Please include Job Opening ID (JOID) #12388 on all correspondence.
- **Molecular Biologist Search Committee.** Please include Job Opening ID (JOID) #12389 on all correspondence.

Review of applications will commence on **July 15, 2006** and continue until positions are filled. Website: <http://www.sjsu.edu/depts/Biology>.

*SJSU is an Equal Opportunity/Affirmative Action Employer
committed to the core values of inclusion, civility, and respect
for each individual.*

Max-Planck-Institut für
Eisenforschung GmbH



The Max-Planck-Institut für Eisenforschung in
Düsseldorf will establish a new scientific group for

Steel Metallurgy

and is therefore looking for a new head of the research group. Candidates with an excellent background in metallurgy / material science should have a good expertise in hot metal processing or powder metallurgy and should be willing to interact strongly with experimental groups in the area of material characterization, thermodynamics and also with industrial partners. Excellent working conditions are guaranteed. For further information please contact Prof. Pyzalla (Tel +49 211 6792 217 pyzalla@mpie.de).

The Max Planck Society is an equal opportunities employer. Women are encouraged to apply.

Please send your application to:

**Max-Planck-Institut für Eisenforschung
GmbH**

Prof. Dr. Anke R. Pyzalla

Max-Planck-Str. 1 • 40237 Düsseldorf

Further information about the Institute can be found on the
website: <http://www.mpie.de>

Université McGill University
Faculty of Medicine/Faculté de médecine



Chair Department of Anatomy and Cell Biology

The Faculty of Medicine at McGill University is inviting applications for the position of Chair, Department of Anatomy and Cell Biology.

The Department of Anatomy and Cell Biology has a strong tradition of excellence in research and teaching. It consists of 16 full-time academic staff members, 4 part-time appointees, 11 adjunct professors and 12 associate members and is well supported by CIHR, NSERC, NIH and other funding agencies. It offers a dynamic research environment with extensive inter-departmental and multi-disciplinary research collaboration. Opportunities exist to develop existing areas and build new areas of strength through recruitment. The Department participates in teaching at all levels (406 students: 369 undergraduate; 9 MSc and 19 PhD, 9 other graduate students and postdoctoral fellows), as well as to medical students. Further details can be found at: <http://www.mcgill.ca/anatomy/>.

A commitment to research with an international reputation in the field of anatomy and cell biology broadly defined at the systems, cellular or molecular levels are essential attributes. The successful applicant will have completed a doctoral degree, will have senior academic experience with proven administrative and teaching skills.

Interested applicants should send electronically their curriculum vitae, including a list of publications, a statement of interest, as well as names, addresses and emails of three references indicating 'Chair, Anatomy and Cell Biology' to: danielle.lepage@mcgill.ca; c/o Dean Abraham Fuks, Faculty of Medicine, McGill University, 3605 de la Montagne, Montreal, QC H3G 2M1, CANADA. The deadline for submission is August 31, 2006.

Candidates would benefit from a working knowledge of both official languages. All qualified candidates are encouraged to apply, however, in accordance with Canadian immigration requirements, priority will be given to Canadian citizens and permanent residents of Canada. McGill University is committed to equity in employment.

CARNEGIE INSTITUTION

At the Frontiers of Science

Director The Geophysical Laboratory Carnegie Institution of Washington

The Carnegie Institution of Washington seeks applications by mid-career scientists to serve as the Director (and Staff Member) of the Geophysical Laboratory. The Director of Carnegie's Geophysical Laboratory will head an organization that is a leader in high-pressure mineralogy and physics, in the developing science of astrobiology, and in petrology. The Department was founded a century ago with the benefit of an endowment by Andrew Carnegie and is recognized for its continuing significant contributions to Earth and material sciences. See www.ciw.edu.

The successful candidate must have an internationally recognized record of research accomplishments in geochemistry, geophysics, geobiology, or planetology, and must possess proven managerial abilities. The successful candidate will be expected to assume leadership of the Geophysical Laboratory on July 1, 2007. Please send an e-mail letter of intent to the chair of the search committee, **W. Gary Ernst** (ernst@geo.stanford.edu), on or before **July 15, 2006**.

The Carnegie Institution of Washington is an Equal Opportunity Employer, and especially encourages applications from women and minorities.

Looking for a JOB?

- Job Postings
- Job Alerts
- Resume/CV Database
- Career Advice
- Career Forum

NEW

ScienceCareers.org

We know science



Science Careers Forum

ScienceCareers.org has partnered with moderator Dave Jensen and three well-respected advisers who, along with your peers, will field career related questions.

Visit
ScienceCareers.org and
start an online dialogue.

ScienceCareers.org

We know science





Neurobiology Faculty Positions Tenure Track - Open Rank

Virginia Commonwealth University

- The Department of Anatomy and Neurobiology on the Medical College of Virginia Campus of Virginia Commonwealth University invites applications for **four tenure-track positions at all ranks**.
- The Department has 17 full-time Neuroscience faculty whose research is supported by \$5 million in extramural funding.
- The Department currently has over 30 Doctoral and Master's degree students.
- The Department maintains a full-service imaging facility with confocal and multi-photon laser scanning microscopes, state-of-the-art TEM and SEM facilities, stereology and image analysis.
- The Department maintains a fully equipped and staffed molecular biology core facility.
- The available positions offer attractive salaries that are fully supported by Institutional funds. In addition, attractive start-up packages and appropriate laboratory space will be provided.

The Department seeks exceptional investigators pursuing innovative questions relevant to the Department's research strengths in cellular neuroscience and CNS injury and repair. Applicants should have a Ph.D., M.D., or D.D.S., with an outstanding research record. The level of appointment will be determined by a combination of experience and funding. Successful candidates will be expected to maintain an externally funded research program and to participate in graduate or professional teaching, as well as pre- and postdoctoral training. The ideal candidate will have experience that complements the department's teaching missions in either Neuroscience, Histology or Gross Anatomy. Review of applications will begin August, 2006 and continue until filled.

Departmental website: <http://views.vcu.edu/ana>

Virginia Commonwealth University is an Equal Opportunity/Affirmative Action Employer. Women, minorities, and persons with disabilities are encouraged to apply.



AREAS OF RESEARCH INTEREST

Cellular Neuroscience

Positions are available for individuals conducting research on neuronal and glial cell biology in normal and pathological conditions.

CNS Trauma and Repair

Positions are available for individuals conducting contemporary research on the pathobiology and/or the therapeutic management of traumatic brain injury.

Interested candidates should send curriculum vitae, letter of intent including research outline and the name, address, telephone number, fax number and email address of three references.

Electronic submissions preferred to: anatrecurit@vcu.edu.

Mailing address:

John W. Bigbee, Ph.D.
Chair, Faculty Search Committee
Virginia Commonwealth University
Department of Anatomy and Neurobiology
P.O. Box 980709
Richmond, VA 23298-0709



where
LEADERSHIP DRIVES EXCELLENCE

The Skirball Institute of Biomolecular Medicine, New York University School of Medicine seeks a Bioinformatics Programmer to organize and direct staff in computing applications in the RNAi Facility at NYU School of Medicine.

BIOINFORMATICS PROGRAMMER

Candidate will be responsible for developing and designing a web-interface for a Functional Genomics facility at the NYU School of Medicine; monitoring project status, identifying and resolving problems which may impact the project results; maintaining software and hardware; working with departmental leadership on developing and implementing policies; consulting with departmental leadership regarding application alternatives, security, software usage, capacity planning, training, recovery and backup procedures. Individual should be able to seamlessly interface biology with computational skills, plus all related duties.

Individual should possess BS/MS in Biology with an additional degree in computer science, computational biology, bioinformatics, or several years' professional programming experience. Experience with multiple programming languages, mainly Perl, C, HTML and SQL; additional experience with C++, Java, Python is preferred. Must have experience with web development including CGI scripting and HTML, database development and design. MCSE Certification on Windows 2002/2003.

Applicants should send their CV, with a list of three references to: Nan McKeown, HR Coordinator, Email: mckeown@saturn.med.nyu.edu, NYU School of Medicine, Skirball Institute of Biomolecular Medicine -3rd Fl Admin., 540First Ave., New York, New York 10016. EOE

www.nyumc.org



SCOTT & WHITE



College of Medicine
The Texas A&M University System
Health Science Center

Pediatric Hematology-Oncologist

The Section of Pediatric Hematology/Oncology at **Scott and White Clinic** and the **Texas A&M University System Health Science Center College of Medicine** (TAMUS HSC-COM) are seeking a clinician scientist with current research grants for a faculty position in a rapidly growing program. The candidate should be BE/BC in pediatric oncology and committed to an academic career. The successful candidates will join and enhance ongoing efforts in basic and translational research, with an institutional commitment to building a world-class experimental therapeutics program. An outstanding start-up package includes high quality laboratory space, excellent benefits and competitive salaries commensurate with academic qualifications. The position guarantees 75% protected time for research activities.

Scott & White Clinic is a 500+ physician directed multi-specialty group practice that is the leading provider of cancer care in Central Texas. Scott and White Clinic and the 486 bed tertiary Scott & White Memorial Hospital is the main clinical teaching facility for TAMUS HSC-COM. Outstanding clinical practice and laboratory facilities on campus that perform state of the art molecular and cellular biology research, flow cytometry, genomics and biostatistics are in place to support the research effort.

Please contact: **Don Wilson, M.D. Professor and Chairman, Department of Pediatrics, Scott & White, 2401 S. 31st, Temple, TX 76508. (800)725-3627 dwilson@swmail.sw.org Fax (254) 724-4974.**

For more information about Scott & White, please visit www.sw.org For Texas A&M www.tamhsc.edu. Scott & White is an equal opportunity employer.

CONFERENCE

cancer conference
ncri
national cancer research institute



Second NCRI Cancer Conference
International Convention Centre, Birmingham, UK
8 – 11 October 2006

Registration for the Second NCRI Cancer Conference is now open.

Earlybird registration closes on Monday 31 July 2006.

Final deadline for registration is Sunday 10 September 2006.

Plenary Speakers: Leslie Bernstein, Chris Boshoff, Harry Burns, Titia de Lange, Elizabeth Eisenhauer, Tariq Enver, Lesley Fallowfield, Richard Gilbertson, Gerard Hastings, Ken Hillan, Tyler Jacks, Scott Lowe, Gillies McKenna, Tom Smith, Fiona Watt.

NCRI Cancer Conference Secretariat P.O. Box 49709 61 Lincoln's Inn Fields London WC2A 3WZ United Kingdom
t: +44 (0)20 7269 3420 e:ncriconference@ncri.org.uk www.ncri.org.uk/ncriconference/

Parallel Sessions: Cancer Cell Biology: Cancer genetics, Chemical biology in relation to cancer, DNA repair, Epigenetics and methylation, High throughput SNP screening for the identification of cancer genes, Infection and cancer, NCRI Informatics, Radiobiology, Stem cells in cancer, The immune system: a barrier to cancer?, Tissue banks, Tumour cell migration and invasion Clinical: Advances in upper GI cancer, Breast cancer, Colorectal cancer, Future directions in oncology imaging, Haemato-oncology, Imaging, Lung cancer, Ovarian cancer, Paediatric oncology – Clinical trials, Paediatric oncology – Translational biology, Primary care, Prostate cancer Epidemiology and Prevention: Behaviour change, Chemoprevention, Diet and cancer NCRI Clinical Studies Groups: Details to be confirmed Patients and The Public: Demonstrating value: patients in cancer research, Research information for patients and the public, Survivorship Supportive and Palliative Care: Addressing patients' care needs through nurse-led research, Places of care near the end of life, Psychological approaches to reducing cancer risk and increasing survival Therapeutic Development: Drug development: target validation and biomarkers, Immunotherapy, Targeting DNA damage and repair for new drug discovery

CONFERENCE

[SBMC 2006] Conference
on Systems Biology
of Mammalian Cells

Call for abstracts | deadline: 15.06.2006

Cellular behavior and cell fate decisions are the result of the coordinated activation and deactivation of multiple signaling pathways. What causes the purposeful behavior of mammalian cells? An answer can be provided by quantitative mathematical models for example of the interactions of signaling pathways or of the interactions of transcription factors and their target sequences. For this purpose research approaches in Systems Biology bring together the expertise of experimental and theoretical scientists. The Conference is the definitive venue for you to present your latest work in this exciting new field of research - register now!

12.07-14.07.2006
Heidelberg | Germany
Convention Center
www.sbcm06.de

AWARDS

The Jacob P. Waletzky Memorial Award
for
Innovative Research in Drug Addiction
and Alcoholism

The Society for Neuroscience is pleased to announce the Call for Nominations for the Jacob P. Waletzky Memorial Award. This prize is awarded each year at the SfN annual meeting to a young scientist who has received an advanced degree of either a PhD or MD within the past fifteen years, and who has done research or plans to do research in the area of substance abuse and the brain and nervous system. The award is \$25,000.

Nomination packages should include the following:

- An essay of not more than 500-words describing the future goals and direction of their planned research in the area of substance abuse and the brain and nervous system.
- Up to 3 letters of recommendation. Only one letter can be from the applicant's institution and only one can be from a current or former mentor (graduate student or postdoctoral advisor). The third letter should be from an individual who has not worked with the applicant. No individual may recommend more than one applicant.
- Supporting documents, such as curriculum vitae and a list of all publications and abstracts authored or co-authored by the applicant.

A selection committee will review all applications and select the awardee. Because of potential conflicts of interest issues, members of the Award Committee cannot serve as nominators nor should they write letters of support.

Nomination packages for The Jacob P. Waletzky Memorial Award should be submitted to: **Attn: Waletzky Award, Society for Neuroscience, 1121 14th St. NW, Suite 1010, Washington, DC 20005, or awards@sfn.org.**

**Deadline for Nomination Packages:
WEDNESDAY, JUNE 28, 2006**

IBC's 11th Annual World Congress



DRUG DISCOVERY TECHNOLOGY[®] & Development

Conference: August 7-10, 2006 • Exhibition: August 8-10, 2006 • World Trade Center Boston/Seaport Hotel • Boston, MA

Science Subscribers
Register Early and Save
See website for details

Keynote Speakers



Andrew C. von Eschenbach, M.D.
Acting Commissioner, FDA
and Director, National Cancer Institute



Steven M. Paul, M.D.
Executive Vice President, Science and
Technology, President, Lilly Research
Laboratories, Eli Lilly and Company



Peter B. Corr, Ph.D.
Senior Vice President, Science & Technology
Pfizer Inc



Susan Hockfield, Ph.D.
President
Massachusetts Institute of Technology

Providing Coverage of the Most Vital Topics in Drug Discovery and Development

More Sessions than Ever Before ... Six Dedicated Conferences

- Targeting Disease and Evaluating Disease-Relevant Targets
- Lead Discovery and Lead Optimization
- Discovery to Development: Case Studies, Safety, PK/PD and Pharmacogenomics
- Biomarkers: Utility, Validation and Applications from Discovery to Clinic
- R&D Strategies and Business Alliances
- The Interface between Drug Discovery and Informatics

Plus! 7 In-Depth, Focused Pre-Conference Workshops

200+
Speakers

Plus! The Top Ten Reasons You Can't Afford to Miss this Event

- 1** Discover new approaches for targeting disease and next generation target prioritization techniques including the re-emergence of genetics approaches
- 2** Gain insights to reduce cost and attrition, improve innovation, implement new R&D models and develop productive alliances from the perspective of 60+ thought leaders
- 3** Improve your lead discovery and optimization efforts by attending 14 case studies, and hear about innovative chemistry techniques, compound collection strategies and the latest in fragment-based approaches from 30+ speakers
- 4** Hear cutting-edge biomarker applications from 35+ leading voices and get the latest updates on the FDA's pharmacogenomics guidance and biomarker validation
- 5** Find out which approaches to safety and PK/PD are adding value and how pharmacogenomics and personalized medicine are being applied from discovery to clinic
- 6** Bridge the gap between Science and Informatics in your company and learn how to put your scientific data to use. Attend the informatics sessions featuring 40+ speakers, 5 interactive panel discussions and new exciting debates
- 7** Evaluate over 300 exhibit booths showcasing the latest technologies, products and services in drug discovery and development....all under one roof
- 8** Participate in 16 thought provoking panels on cost reduction, the role of Asia & Eastern Europe, VC funding, strategic alliances dos and don'ts and more...
- 9** Network with 4000+ attendees by taking advantage of DDT Event Connect...the on-line networking tool that lets you set up meetings before the event
- 10** Learn from 200+ speakers, 150+ poster presentations covering all facets of drug discovery and development

VIP CODE: 3200SADM

Presidential Sponsor



Executive Sponsors



Executive Support Sponsors



Sponsoring Publication



Association Sponsor



Organized by



To Register: Call (800) 390-4078 • Fax: (941) 365-0104 • Email: reg@ibcusa.com

www.drugdisc.com

POSITIONS OPEN

ASSISTANT CURATOR

The Field Museum, Department of Geology
Chicago, Illinois

The Field Museum's Department of Geology seeks a broadly interested, productive colleague with an innovative specimen-based research program in paleomammalogy or paleobotany. Special areas of interest include systematics, phylogenetics, morphologic evolution, biogeography, biostratigraphy and faunistics, and paleoecology. The successful candidate will have a Ph.D., a significant record of scientific achievement, and is expected to build a strong research program with a field component. The position entails the curation of a major fossil mammals or fossil plants collection. Curators participate in a wide range of public learning programs (including exhibits, mentoring, and informal education), institutional advancement, administrative and service activities. Participation in undergraduate and graduate education at area universities is also strongly encouraged.

The search is targeted at the Assistant Curator level. Please include: curriculum vitae; statement of research objectives; and copies of relevant publications. Direct applications to, and arrange for three letters of reference to be sent to:

Search Committee, Department of Geology
The Field Museum
1400 South Lake Shore Drive
Chicago, IL 60605-2496

Please ensure that all of the listed items except copies of publications are also sent as e-mail attachments, such as PDFs or word documents (the preferred application is Microsoft Word, although WordPerfect is also acceptable). E-mail address for this search is **e-mail: klawson@fieldmuseum.org**.

Deadline for applications is September 15, 2006. Consideration of applications will begin October 1, 2006.

RESEARCH FACULTY POSITION

The Department of Urology at the University of Pittsburgh seeks tenure-track Faculty at the **ASSISTANT PROFESSOR** level in the area of prostate and urologic cancer. The successful candidate will also participate at the Prostate and Urologic Cancer Program of the University of Pittsburgh Cancer Institute. Candidates must possess a Ph.D. and/or M.D. degree with productive postdoctoral training in the area of cancer biology or related fields. Successful applicants will be expected to develop a vigorous research program with the potential for extramural funding. We offer competitive academic salary, fringe benefits, and state-of-the-art facilities for both basic and translational research. Positions available until filled. Applicants should send a letter describing their research interest, curriculum vitae, and the names of at least three persons from whom references can be obtained to: **Vinnette Sommariva, University of Pittsburgh School of Medicine, Department of Urology, Shadyside Medical Center, 5200 Centre Avenue, Suite G40, Pittsburgh, PA 15232.** *The University of Pittsburgh is an Affirmative Action, Equal Opportunity Employer.*

TERRESTRIAL ANIMAL ECOLOGIST

The Smithsonian Environmental Research Center (SERC), Edgewater, Maryland, seeks a broadly trained Animal Ecologist for a federal career-track position. Applicant's research should focus on animals in terrestrial habitats, including uplands and/or wetlands, and may consider plant-animal interactions. Successful candidate is expected to develop a grant-funded research program that includes focal work in the Chesapeake Bay region exploiting SERC's long-term study site in the Rhode River watershed of Maryland, and collaborative team-based research. Announcement: 06JW-6144. See website: **http://www.serc.si.edu/opportunities/employment.jsp**. *Women and underrepresented minorities are encouraged to apply. Equal Opportunity Employer.*

POSITIONS OPEN

BIOINFORMATICS SCIENTIST
Biotechnology/Bioservices Center
University of Connecticut

The University of Connecticut seeks a Bioinformatics Scientist (Academic Assistant II/III) to serve the biological science community by working within a newly formed Bioinformatics Facility in the Biotechnology/Bioservices Center. The Bioinformatics Facility consists of a 17-node Apple Workgroup Cluster that uses Sun Grid Engine for its distributed resource management and runs Bioteam's iNquiry as a portal to over 170 applications. Qualifications include a M.S. or Ph.D. in bioinformatics and experience or the equivalent skills to handle problems in genomics, gene and protein expression analysis, database mining, molecular modeling and programming, and structure-function domain analysis. Highly desirable are two years of post-M.S. work experience. The successful candidate will have an excellent command of verbal and written communication skills and must use them effectively. Salary commensurate with qualifications. A detailed description of this position can be found at website: **http://www.biotech.uconn.edu/bf/bioinfrm.pdf**. This position is subject to annual renewal up to six years and becomes eligible for three-year appointments thereafter.

Screening of candidates will begin June 26, 2006. Interested candidates should submit a cover letter, curriculum vitae, and have three letters from professional references sent to: **Sue Levesque, Biotechnology/Bioservices Center, University of Connecticut, 91 N. Eagleville Road, Unit 3149, Storrs, CT 06269-3149**. Submissions without this information will not be considered. *The University of Connecticut actively solicits applications from minorities, women, and people with disabilities.*

MOLECULAR AND CELLULAR
NEUROSCIENCE RESEARCH

POSTDOCTORAL RESEARCH ASSOCIATE sought to join multidisciplinary molecular and cellular neuroscience group in studies of nicotinic acetylcholine receptors. Investigations encompass molecular genetic, protein chemical, electrophysiological, immunological, and pharmacological approaches in a unique and dynamic institution. Send curriculum vitae, names and addresses of three references, and brief statement of research experience, interests, and career objectives to: **R.J. Lukas, Ph.D., Division of Neurobiology, Barrow Neurological Institute, St. Joseph's Hospital and Medical Center, 350 West Thomas Road, Phoenix, AZ 85013.** E-mail: **rjluks@chw.edu**. *Affirmative Action/Equal Opportunity Employer.*

POSTDOCTORAL POSITION

**Children's Hospital, Harvard Medical School
Boston, United States of America**

A Postdoctoral Position is available to investigate T cell immunity to Streptococcus pneumoniae. Projects center cellular immunity elicited by experimental vaccines. Candidates should have, or soon expect to receive, a Ph.D. with a strong background in immunology. Experience with pneumococcus desirable but not essential. Please submit a letter of interest, curriculum vitae, and names and contact information of three references to: **Richard Malley, M.D., Assistant Professor of Pediatrics, Children's Hospital, Division of Infectious Diseases, Enders 861.3, 300 Longwood Avenue, Boston, MA 02115.** E-mail: **richard.malley@childrens.harvard.edu**.

NIH training grant-supported **POSTDOCTORAL POSITION** to investigate differentiation and function of $\gamma\delta$ T cells in tumor immunity and memory response is available at Yale School of Medicine. Candidates should have a Ph.D. or M.D./Ph.D. degree in immunology and/or molecular biology. *Must be U.S. citizen or permanent resident.* Please submit curriculum vitae and names of three references to: **Dr. Zhinan Yin (e-mail: zhinan.yin@yale.edu)**.

POSITIONS OPEN

TWO POSTDOCTORAL FELLOWS. One Fellow will solve structural problems in catalytic antibody biology. Experience in protein crystallography, computer structure modeling, and protein isolation is required. Molecular biology experience is helpful. The second Fellow will isolate high turnover, high specificity catalytic antibodies to HCV E2, amyloid beta peptides and HIV gp120 using phage library, EBV/hybridoma and mammalian cell vector methods. Requires experimental dexterity and decision-making skills in DNA, RNA, and protein manipulation. Both positions require scholarly, rigorous approach and ability to work in a milestone-driven, collaborative/interdisciplinary group. For research objectives and rationale, see reviews in *Immunol. Letters* **103:8, 2006** and *Springer Semin Immunopathol* **26:485, 2005** and references therein. Salary \$40,000 to \$50,000 a year, based on accomplishments. Send curriculum vitae, reference letters, and explanation of your interest in the position to **e-mail: laura.nixon@uth.tmc.edu**. **Chemical Immunology Research Center, Department of Pathology, University of Texas Houston Medical School, 6431 Fannin, MSB 2.246, Houston, TX 77030.** *The University of Texas Health Science Center at Houston is an Equal Opportunity/Affirmative Action Employer. Minorities/Females/Persons with Disabilities/Veterans.*

POSTDOCTORAL POSITIONS available to study complement-dependent innate (inflammation) and adaptive immune responses. Areas of investigation include autoimmune disease, ischemic disease, organ transplantation, and central nervous system (CNS) injury. A background in immunology is required and experience in molecular biological techniques would be an advantage for some projects. Send curriculum vitae and names of three references to: **Stephen Tomlinson, Ph.D., Medical University of South Carolina, Department of Microbiology and Immunology, BSB-201, 173 Ashley Avenue, Charleston, SC 29403.** E-mail (preferred): **tomlinss@muscc.edu**.

MARKETPLACE


Diverse Small Molecules
Ready for Screening

<p>High Quality & Drug-Like</p> <p>Pre-Plated in DMSO</p> <p>Very Competitively Priced</p> <p>Upwards of 200,000 Compounds</p>	<p>ChemBridge Corporation</p>  <p>Website: www.chembridge.com Email: sales@chembridge.com</p> <p>Toll Free: (800) 980-CHEM Tel: (858) 451-7400</p>
--	--

<p>Widely Recognized Original & Guaranteed</p>	<p>KlenTaq1</p>	<p>8¢/u Truncated Taq DNA Polymerase Withstand 99°C</p>
<p>US Pat #5,436,149 Call: Ab Peptides Fax: 314•968•8988</p>	<p>e-mail: abpeps@msn.com 1•800•383•3362 www.abpeps.com</p>	

Software for the Molecular Biologist for

Pathogen Detection
Microarrays
Standard PCR
Real Time RT-qPCR
Plasmid Maps



www.PremierBiosoft.com 650-856-2703

Believe it!

DNA Sequencing for **\$2.50** per reaction.

- Read length up to 900 bases.
- High quality electropherograms.
- Fast turnaround.
- Plasmid and PCR purification available.



A T G G C A T A G A C T A T T C A G G G C C G A T C
151 147 143 139 135 131

\$2.50
per reaction!

POLYMORPHIC
Polymorphic DNA Technologies, Inc.SM

www.polymorphicdna.com
info@polymorphicdna.com

1125 Atlantic Ave., Ste. 102
Alameda, CA 94501

For research use only. © Polymorphic DNA Technologies, 2005

Polymorphic exclusively uses ABI 3730XL sequencers.
Data delivered via secure FTP, email or CD.
No charge for standard sequencing primers.
384 sample minimum order.
96 well plates only—no tubes.

888.362.0888

For more information please visit
www.polymorphicdna.com